



Predictive Models to Aid in Design of Membrane Systems for Organic Micropollutant Removal

WaterReuse Research Foundation

Predictive Models to Aid in Design of Membrane Systems for Organic Micropollutant Removal

About the WaterReuse Research Foundation

The mission of the WaterReuse Research Foundation is to conduct and promote applied research on the reclamation, recycling, reuse, and desalination of water. The Foundation's research advances the science of water reuse and supports communities across the United States and abroad in their efforts to create new sources of high-quality water through reclamation, recycling, reuse, and desalination while protecting public health and the environment.

The Foundation sponsors research on all aspects of water reuse, including emerging chemical contaminants, microbiological agents, treatment technologies, salinity management and desalination, public perception and acceptance, economics, and marketing. The Foundation's research informs the public of the safety of reclaimed water and provides water professionals with the tools and knowledge to meet their commitment of increasing reliability and quality.

The Foundation's funding partners include the Bureau of Reclamation, the California State Water Resources Control Board, the California Energy Commission, and the California Department of Water Resources. Funding is also provided by the Foundation's subscribers, water and wastewater agencies, and other interested organizations.

Predictive Models to Aid in Design of Membrane Systems for Organic Micropollutant Removal

Jörg E. Drewes, Ph.D.
Christopher L. Bellona, Ph.D.
Mark Eberhart, Ph.D.
Colorado School of Mines

Shankar Chellam, Ph.D.
University of Houston

Cosponsors

Bureau of Reclamation
California State Water Resources Control Board
Orange County Water District (CA)



WaterReuse Research Foundation
Alexandria, VA



Disclaimer

This report was sponsored by the WateReuse Research Foundation and cosponsored by the Bureau of Reclamation, the California State Water Resources Control Board, and Orange County Water District. The Foundation, its Board Members, and the project cosponsors assume no responsibility for the content of this publication or for the opinions or statements of facts expressed in the report. The mention of trade names of commercial products does not represent or imply the approval or endorsement of the WateReuse Research Foundation, its Board Members, or the cosponsors. This report is published solely for informational purposes.

For more information, contact:

WateReuse Research Foundation
1199 North Fairfax Street, Suite 410
Alexandria, VA 22314
703-548-0880
703-548-5085 (fax)
www.WateReuse.org/Foundation

© Copyright 2013 by the WateReuse Research Foundation. All rights reserved. Permission to reproduce must be obtained from the WateReuse Research Foundation.

WateReuse Research Foundation Project Number: WRRF-06-009
WateReuse Research Foundation Product Number: 06-009-1

ISBN: 973-1-934183-95-3
Library of Congress Control Number: 2013955863

Printed in the United States of America

Printed on Recycled Paper

Contents

List of Figures	ix
List of Tables	xvi
Acronyms.....	xviii
Foreword.....	xxi
Acknowledgments	xxii
Executive Summary	xxiii
Chapter 1. Introduction.....	1
1.1 Background.....	1
1.2 Objectives	1
Chapter 2. Review of Modeling Solute Rejection in High-Pressure Membranes	3
2.1 Introduction.....	3
2.1.1 Differences Among Membranes	3
2.1.2 Solute Transport through RO and NF	3
2.2 Observations of Rejection at Pilot- and Full-Scale Membrane Installation.....	4
2.3 Calculating Rejection.....	8
2.3.1 Concentration Polarization	8
2.3.2 Rejection.....	9
2.4 Mechanisms and Understanding Rejection (Size Exclusion)	11
2.5 Rejection of Solutes with Membrane Interactions.....	19
2.5.1 Adsorption and Partitioning Through Membrane Materials	20
2.5.2 Electric/Donnan and Dielectric Exclusion of Charged Solutes.....	26
2.6 Modeling	29
2.6.1 Solution–Diffusion Model	30
2.6.2 Hydrodynamic Model.....	32
2.6.3 Phenomenological Model and Pore Size Distribution Approach.....	34
2.6.4 Extended Nernst–Planck Equation.....	36
2.6.5 Other Mass Transfer Models.....	37
2.6.6 Quantitative Structure Activity Relationship Models	38
2.6.7 Empirical Models	39
2.7 Operational Impacts on Rejection.....	42
2.7.1 Recovery.....	42
2.7.2 Permeate Flux.....	43
2.7.3 Differential Element Approach	45
2.8 Summary of Factors that Affect Rejection	47
2.8.1 Membrane Reproducibility.....	47
2.8.2 Rejection Equilibrium	47

2.8.3	Temperature	48
2.8.4	Feed Water Chemistry.....	48
2.8.5	Conclusions and Major Findings.....	50
Chapter 3. Materials and Methods		53
3.1	Choosing Trace Organic Chemicals for Study	53
3.1.1	Selection Method to Develop Model Development and Validation Compounds.....	53
3.1.2	Sources of Descriptor Data.....	58
3.1.3	Statistical Methods	60
3.2	Analytical Methods for Bulk Parameter and Trace Organic Chemicals	61
3.2.1	Physicochemical Parameters	61
3.2.2	Bulk Parameters	62
3.2.3	HPLC-DAD.....	62
3.2.4	HPLC-RID	62
3.2.5	LC/MS-MS.....	63
3.2.6	GC-ECD	64
3.3	Experimental Methods.....	65
3.3.1	Bench-Scale Systems	65
3.3.2	Pilot-Scale Membrane System	71
3.3.3	Full-Scale Sampling Campaign at Orange County Water District.....	72
3.3.4	Challenges	73
Chapter 4. Bench-Scale Rejection Database		77
4.1	Bench-Scale Experiments to Augment Rejection Database.....	77
4.1.1	Rejection of Solutes with Expected Behavior.....	77
4.1.2	Rejection of Solutes Exhibiting Adsorptive Effects During Recycle Experiments	88
4.1.3	Rejection of Solutes Exhibiting Adsorptive Effects During Flow-Through Experiments.....	92
4.2	Rejection Databases for NF-270 and ESPA2 Membranes	99
Chapter 5. Modeling of Solute Rejection at Bench Scale.....		101
5.1	Introduction	101
5.2	Quantitative Structure Property Relationship Model	101
5.2.1	QSPR Development for NF-270 Membrane	101
5.2.2	QSPR Development for ESPA2 Membrane.....	109
5.3	Phenomenological Model	112
5.3.1	Phenomenological Model for NF-270 Nanofiltration Membrane.....	112
5.3.2	Phenomenological Model for ESPA2 Membrane	133
5.4	Hydrodynamic Model	137
5.4.1	Model Theory.....	137
5.4.2	Determination of NF-270 Membrane Pore Size.....	139

5.5. Solution–Diffusion Model	144
5.5.1 Bench-Scale Modeling.....	145
5.5.2 Correlation of Mass Transfer Coefficients with Molecular Descriptors.....	150
5.5.3 Conclusions.....	152
5.6 Empirical Models—Rejection Diagram.....	152
5.6.1 Optimization using the NF-270 Membrane Rejection Database	152
5.6.2 Application of Updated Rejection Diagram to the ESPA2 Membrane Rejection Database.....	157
Chapter 6. Validation of Rejection Models at Pilot Scale	159
6.1 Introduction.....	159
6.2 Pilot-Scale Rejection Experiments Using Nanofiltration Membranes and Rejection Modeling Using QSPR and Empirical Models.....	159
6.2.1 Comparing Bench- and Pilot-Scale Nanofiltration Testing	159
6.2.2 QSPR Model To Describe Pilot-Scale Nanofiltration Rejection Data	163
6.2.3 Application of Empirical Rejection Diagram to NF-270 Membrane	165
6.3 Pilot-Scale Rejection Experiments Using Nanofiltration Membranes and the Phenomenological Pilot-Scale Model.....	167
6.3.1 Introduction.....	167
6.3.2 Model Theory	167
6.3.3 NF-4040 Bench-Scale Results and Model Evaluation.....	170
6.3.4 Pilot-Scale Model Development.....	174
6.3.5 Model Development and Validation—Pilot Testing of NF-270 Membrane	184
6.3.6 Predicting Rejection Using Previously Developed QSPR Approach	192
6.4 Pilot-Scale Rejection Experiments Using the ESPA2 Reverse Osmosis Membrane.....	194
6.4.1 Experimental Conditions	194
6.4.2 Analytical Results.....	195
6.4.3 QSPR Model ESPA2 Membrane.....	200
6.4.4 Application of Rejection Diagram to ESPA2 Membrane.....	202
6.4.5 Phenomenological Model for ESPA2 Membrane.....	203
Chapter 7. Validation of Rejection Models at Full Scale	205
7.1 Full-Scale Sampling Campaign	205
7.2 Quantitative Structure Property Relationship Model.....	208
7.3 Phenomenological Model	209
7.4 Rejection Diagram	215
Chapter 8. Conclusions and Recommendations.....	219
8.1 Conclusions.....	219
8.1.1 Summary of Project Results	219
8.1.2 Literature Review	219
8.1.3 Organic Solute Selection	220
8.1.4 Bench-Scale Experimentation.....	221

8.1.5 Bench-Scale Modeling	223
8.1.6 Pilot-Scale Model Development	224
8.1.7 Full-Scale Rejection and Model Development.....	224
8.2 Recommendations	225
8.3 Future Research Needs	225
References	227
Appendix A: Supplemental Information	241
Appendix B: Equations Employed	249
Appendix C: Quality Control of Bench-Scale Experiments.....	253
Appendix D: Correlation Matrix for Descriptors	257
Appendix E: NF-270 Membrane Experimental Bench-Scale Rejection Diagrams.....	261
Appendix F: ESPA2 Membrane Experimental Bench-Scale Rejection Diagrams.....	281

Figures

2.1	Feed, permeate and rejection concentrations for NDMA, chloroform, and TCAA by the TFC-HR and ESPA2 membranes at full scale and the TMG10 and NF-90 membranes at pilot scale	7
2.2	Rejection of phenacetine, TCEP, TCPP, and TDCPP by 11 commercially available RO, LPRO, and NF membranes	12
2.3	Rejection of sugars and alcohols as a function of molecular weight and molecular width.....	13
2.4	Reflection coefficient (real or observed rejection at infinite pressure, ~17-bar driving pressure during this study) of aliphatic sugars and alcohols for the NF-4040 membrane on bench scale (SEPA cell) at 19 °C and pH 6.3	13
2.5	Reflection coefficient (real or observed rejection at infinite pressure, ~17-bar driving pressure during this study) of aliphatic sugars and alcohols for the NF-90 membrane on bench scale (SEPA cell) at 19 °C and pH 6.3	14
2.6	Experimental data for estradiol, estrone, testosterone, and progesterone for 2 NF membranes as compared to predicted retention as calculated by the hydrodynamic model	14
2.7	Rejection of pesticides versus molecular weight	15
2.8	Molecular size parameters as determined for a nonspherical molecule	18
2.9	Hydrogen bond formation of trichlorophenol with the carbonyl group of a polyamide chain	21
2.10	Relationship between Taft numbers and solute rejection.....	22
2.11	Rejection as a function of Log P (Log K_{ow}) for organic solutes where $MW < MWCO$	23
2.12	Log P (Log K_{ow}) versus rejection for 4 membranes	24
2.13	Summarized laboratory-scale candidate membrane rejection of nonionic (neutral) trace organic compounds.....	28
2.14	Spiked feed and permeate concentrations and subsequent rejection values of ionic trace organic contaminants during pilot-scale testing of the NF-4040.....	29
2.15	Modeling the MTC for salts based on the charge number of the salt	31
2.16	Equations for the hydrodynamic model	32
2.17	Rejection of phenacetine and acetaminophen by NF membrane	33
2.18	Equations for the phenomenological and pore size distribution model.....	35
2.19	Modified rejection diagram including three mechanisms of rejection, steric exclusion, adsorption, and electrostatic exclusion	40
2.20	Rejection of a model solute as a function of recovery	42
2.21	Rejection of total organic halide precursors by several membranes versus feed water recovery.....	43
2.22	Rejection of four nitrosamine compounds by NF-4040 membrane installed on a pilot-scale membrane unit.....	44
2.23	Rejection of NaCl and permeate flux versus recovery.....	45

3.1	Range of molecular weight for compounds included in model development and validation compared with the total number of compounds considered	56
3.2	Range of Log D (pH=6) for compounds included in model development and validation compared with the total number of compounds considered	57
3.3	Range of dipole moments for compounds included in model development and validation compared with the total number of compounds considered	57
3.4	SEPA II membrane testing unit employing flat-sheet membrane	65
3.5	Bench-scale membrane testing unit process flow diagram.....	66
3.6	Rejection of BDCM by NF-270 membrane in recirculation experiments.....	67
3.7	Once-through experimental apparatus at Colorado School of Mines.....	68
3.8	Schematic of pilot-scale membrane unit and sampling locations.....	71
3.9	CSM's pilot-scale membrane skid.....	72
3.10	OCWD's RO membrane gallery.....	72
3.11	OCWD's RO membrane elements within pressure vessels.....	72
3.12	Rejection of acetaminophen by NF membrane (Dow/Filmtec) obtained in different configurations	74
3.13	Rejection of neutral organic solutes by NF-270 membrane (Dow/Filmtec) obtained in different configurations.....	75
4.1	Average bench-scale intrinsic and observed rejection over a range of permeate fluxes for acetaminophen for NF-270 membrane.....	78
4.2	Intrinsic and observed rejection as a function of permeate flux for NDMA for ESPA2 membrane	79
4.3	Intrinsic and observed rejection for estriol as a function of permeate flux for NF-270 membrane.....	79
4.4	Intrinsic and observed rejection as a function of permeate flux for ciprofloxacin for ESPA2 membrane	80
4.5	Intrinsic and observed rejection of benzyl alcohol as a function of permeate flux for NF-270 membrane.....	81
4.6	Observed rejection as a function of flux for ethanol, glycerol, and glucose for NF-270 membrane	83
4.7	Observed rejection as a function of flux for ethanol, glycerol, and glucose for ESPA2 membrane.....	83
4.8	Observed rejection as a function of permeate flux for resorcinol, 1-naphthalenemethanol and caffeine for NF-270 membrane.....	84
4.9	Observed rejection as a function of permeate flux for NDMA, NMEA, and NPYR for ESPA2 membrane	84
4.10	Observed rejection for HN compounds (molecular weight) at 12 gfd for NF-270 membrane 24 h after startup.....	85
4.11	Observed rejection for HN compounds (molecular weight) at 12 gfd for ESPA2 membrane 24 h after startup	85
4.12	Observed rejection for compounds that are HoN (molecular weight, Log K_{ow}) at 12 gfd for NF-270 membrane 24 h after startup.....	86

4.13	Observed rejection for ionic compounds at 12 gfd: negatively charged (HCN), positively charged (HCP), and zwitterions (HCNP) as a function of molecular weight for NF-270 membrane	87
4.14	Observed rejection for ionic compounds at 12 gfd: negatively charged (HCN), positively charged (HCP), and zwitterions (HCNP), as a function of molecular weight (ESPA2 membrane)	87
4.15	Observed rejection of negatively charged and neutral compounds with similar molecular weights for NF-270 membrane	88
4.16	Observed rejection as a function of permeate flux for 2-naphthol and triethylene glycol for NF-270 membrane	90
4.17	Observed rejection for triclosan and 4-n-nonylphenol as a function of permeate flux for NF-270 membrane	90
4.18	Observed rejection for neutral compounds as a function of Log D (pH = 6) at 12 gfd for NF-270 membrane 24 h after startup	92
4.19	Rejection of THMs over time by NF-270 membrane at a flux of 12 gfd	94
4.20	Rejection of THMs over time by ESPA2 membrane at a flux of 12 gfd	94
4.21	Concentration of THMs in permeate stream of deionized water experiment	96
4.22	Concentration of THMs in final permeate sample from deionized water experiment plotted by molecular mass	96
4.23	Rejection of THMs over time by NF-270 membrane at flux of 30 gfd	97
4.24	Rejection of THMs over time by NF-270 membrane at flux of 6 gfd	98
5.1	QSPR (volume, FOSA, E_{HOMO}) for neutral compounds developed from bench-scale NF-270 membrane data	107
5.2	QSPR (Stokes, FOSA, IP) for neutral compounds developed from bench-scale NF-270 membrane data	108
5.3	QSPR (volume, FOSA, E_{HOMO}) for F-270 membrane applied to validation compounds	108
5.4	QSPR (Stokes, FOSA, IP) for NF-270 membrane applied to validation compounds	109
5.5	QSPR (FOSA, E_{HOMO} , SASA) for neutral compounds developed from bench-scale ESPA2 membrane rejection data described as Log removal	112
5.6	QSPR (FOSA, E_{HOMO} , SASA) for ESPA2 membrane applied to validation compounds	112
5.7	Sample phenomenological fits of intrinsic rejection versus permeate flux	115
5.8	Comparison of molecular weight and phenomenological coefficients for major classes of compounds investigated	117
5.9	Correlations between Log P_s and molecular size descriptors for all neutral compounds	118
5.10	Correlations between HN Log P_s and molecular size descriptors	119
5.11	Correlations between Log P_s and molecular descriptors for HoN compounds	120
5.12	Experimental vs predicted Log P_s values for neutral compounds that exhibited minimal solute–membrane interactions	121

5.13	Log-normal cumulative density function fits for sugars, alcohols, urea, and uracil (left) and all neutral organic compounds with resulting pore size average and deviation values	122
5.14	Carbamazepine rejection versus permeate flux with predicted rejection	123
5.15	NPYR rejection versus permeate flux with predicted rejection.....	124
5.16	MTBE rejection versus permeate flux with predicted rejection	125
5.17	Dilantin rejection versus permeate flux with predicted rejection	126
5.18	Fenofibrate rejection versus permeate flux with predicted rejection.....	127
5.19	Isobutylparaben rejection versus permeate flux with predicted rejection	128
5.20	LOO model correlations with experimental 12-gfd rejection data	129
5.21	Correlation between phenomenological model coefficients and Stokes radius for ionic compounds (HCN, HCP, HCNP).....	130
5.22	Experimental versus predicted Log P_s values for ionic compounds at pH 6.3 (HCN, HCP, HCNP).....	130
5.23	Experimental versus predicted Log P_s values for HCP and HCNP compounds at pH 6.3	131
5.24	Experimental rejection with predicted phenomenological model predictions for baclofen, ciprofloxacin, diltiazem and imiquimod	132
5.25	Examples of phenomenological model fits of ESPA2 rejection data.....	134
5.26	Distribution of reflection coefficients and Log P_s values for ionic compounds with ESPA2 membrane	136
5.27	Distribution of reflection coefficients and Log P_s values for nonionic compounds with ESPA2 membrane	136
5.28	Cumulative Log-normal density function fit of reflection coefficient data and Log P_s correlation with diffusion coefficient for sugars, alcohols, urea, and uracil for ESPA2 membrane	137
5.29	Correlation between Log P_s and diffusion coefficient for all nonionic solutes	137
5.30	Determination of membrane permeability constant (L_p) using permeate flux data from all NF-270 rejection experiments.....	139
5.31	NF-270 membrane pore size determination using sugar, alcohols, and urea.	140
5.32	Sample hydrodynamic model fits of intrinsic rejection vs permeate flux data.....	141
5.33	NF-270 membrane pore size determination using all nonionic organic solutes	142
5.34	Sample hydrodynamic model fits of intrinsic rejection when incorporating δ/A_k into the Peclet number	143
5.35	Thickness-to-porosity ratio (δ/A_k) versus Stokes radius for all nonionic solutes evaluated.....	144
5.36	Plot produced by the MATLAB model for solution–diffusion showing rejection versus flux in LMH for alanine, 1,4-butanediol, NDMA, and urea	149
5.37	Correlation between Wilke–Chang diffusion coefficient and solution–diffusion MTCs (K_s) for neutral compounds	151
5.38	Correlation between Stokes radius (nm) and solution–diffusion MTCs (K_s) for neutral compounds	152
5.39	Experimental NF-270 rejection as a function of predicted rejection values based on the qualitative rejection diagram.....	154

5.40	Experimental rejection data as a function of r_s/r_p compared to the hydrodynamic model	155
5.41	Modified solute rejection diagram	156
5.42	Experimental NF-270 membrane rejection as a function of rejection predicted by updated rejection diagram	157
5.43	Experimental ESPA2 rejection compared to predicted rejection from updated rejection diagram	157
6.1	Bench-scale rejection for caffeine and acetaminophen as a function of permeate flux (primary x axis) and recovery (secondary x axis) for NF-270 membrane	161
6.2	Pilot-scale rejection for caffeine and acetaminophen as a function of recovery (primary x axis) and permeate flux (secondary x axis) for NF-270 membrane.....	161
6.3	Pilot-scale rejection at 12 gfd compared to 12-gfd bench-scale rejection for NF-270 membrane	162
6.4	Observed rejection as function of time for triclocarban at pilot scale for NF-270 membrane	162
6.5	Pilot-scale rejection at 12 gfd compared to 12-gfd bench-scale rejection for ESPA2 membrane	163
6.6	Developed QSPR (Stokes, FOSA, IP) applied to neutral NF-270 membrane pilot-scale data	164
6.7	Rejection diagram applied to NF-270 membrane pilot-scale data	165
6.8	Intrinsic rejection and phenomenological model fits for acetaminophen, caffeine, and phenacetine.	171
6.9	Observed rejection of acetaminophen and phenacetine versus permeate flux (J_v) at different feed water concentrations	172
6.10	Bench-scale rejection of acetaminophen by membrane specimens extracted from two separate spiral-wound elements versus experimental run time	173
6.11	Acetaminophen rejection versus permeate flux rate for membranes extracted from three spiral-wound membrane elements.....	174
6.12	Rejection of acetaminophen and caffeine versus recovery for constant feed flow rate and variable feed flow rate experiments	175
6.13	Caffeine concentrations in feed, intraconcentrate, and concentrate samples as a function of recovery	176
6.14	Caffeine concentrations in permeate as a function of recovery	176
6.15	Rejection of caffeine from two experiments with model fit; 1st-stage, 2nd-stage, and combined permeate concentrations with model fit; 1st intrastage, 1st-stage concentrate, 2nd intrastage, and 2nd-stage concentrate with model fit.....	178
6.16	Rejection of acetaminophen with model fit; 1st-stage, 2nd-stage, and combined permeate concentrations with model fit; 1st interstage, 1st-stage concentrate, 2nd interstage, and 2nd-stage concentrate with model fit	180
6.17	Rejection of DEET with model fit; 1st-stage, 2nd-stage, and combined permeate concentrations with model fit; 1st interstage, 1st-stage concentrate, 2nd interstage, and 2nd-stage concentrate with model fit.....	181

6.18	Rejection of phenacetine with model fit; 1st-stage, 2nd-stage, and combined permeate concentrations with model fit; 1st interstage, 1st-stage concentrate, 2nd interstage, and 2nd-stage concentrate with model fit.....	182
6.19	Rejection of thiabendazole with model fit; 1st-stage, 2nd-stage, and combined permeate concentrations with model fit; 1st interstage, 1st-stage concentrate, 2nd interstage, and 2nd-stage concentrate with model fit.....	183
6.20	Rejection of phenacetine versus recovery at three feed flow rates.....	184
6.21	Ranges of pharmaceutically active compounds and a pesticide (atrazine), personal care products (DEET, propylparaben, triclocarban, triclosan), a plasticizer (TCEP), and a pharmaceutically active compound (meprobamate).....	186
6.22	Rejection of organic contaminants by NF-270 over a period of 500 h.....	186
6.23	Rejection of inorganic constituents and bulk carbon by NF-270 over a period of 500 h.....	187
6.24	Meprobamate rejection, permeate concentrations, and concentrate concentrations as function of system recovery (20-gpm feed flow rate).....	188
6.25	Carbamazepine rejection, permeate concentrations, and concentrate concentrations as function of system recovery (20-gpm feed flow rate).....	189
6.26	Rejection of organic contaminants quantified in feed and permeate samples after 24 h and for three sampling campaigns performed over 1500 h of testing of NF-270 membrane at 85% recovery and feed flow rate of 22 gpm.....	190
6.27	Rejection values for atenolol, ketoprofen, and TCEP at 22-gpm feed flow rate.....	191
6.28	Rejection of contaminants at 16- and 22-gpm feed flow rate and 85% recovery during pilot-scale testing and modeled rejection at 22 and 16 gpm.....	192
6.29	Observed and predicted DEET rejection values and observed and predicted permeate and concentrate concentrations.....	193
6.30	Feed water concentrations of nine compounds detected over the course of the multiday, pilot-scale experiment.....	196
6.31	Rejection versus recovery for well-removed compounds in ESPA2 membrane pilot-scale experiment.....	197
6.32	Rejection versus recovery for poorly removed compounds in ESPA2 membrane pilot-scale experiment.....	198
6.33	1st-stage, 2nd-stage, and combined permeate concentrations of cimetidine for the three recovery set-points tested in the pilot-scale experiment with ESPA2 membranes.....	198
6.34	1st-stage, 2nd-stage, and combined permeate propylparaben concentrations for the three recovery set-points tested in the pilot-scale experiment with ESPA2 membranes.....	199
6.35	Rejection versus recovery for urea in ESPA2 membrane pilot-scale experiment.....	200
6.36	Rejection versus recovery for glycerol in ESPA2 membrane pilot-scale experiment.....	200
6.37	Experimental rejection for the ESPA2 membrane pilot scale compared to predicted rejection using the QSPR.....	201
6.38	ESPA2 membrane pilot-scale rejection compared to the rejection predicted from the updated rejection diagram.....	202
6.39	Pilot-scale rejection of organic solutes with phenomenological model fits using coefficients derived from bench-scale experiments.....	204

7.1	Feed concentration of organic compounds quantified in OCWD's RO feed water	205
7.2	ESPA2 membrane permeate concentrations for five compounds	207
7.3	Experimental full-scale ESPA2 membrane rejection compared to QSPR predicted rejection	208
7.4	Rejection of atenolol, atenolol permeate concentrations, and concentrate concentrations	211
7.5	Rejection of DEET, DEET permeate concentrations, and concentrate concentrations	212
7.6	Rejection of benzophenone , benzophenone permeate concentrations, and concentrate concentrations	213
7.7	Rejection of meprobamate, meprobamate permeate concentrations, and concentrate concentrations	214
7.8	Rejection of TCEP, TCEP permeate concentrations, and concentrate concentrations	215
7.9	Experimental ESPA2 full-scale rejection compared to rejection predicted by updated rejection diagram	216

Tables

2.1	Compounds Detected in Full- and Pilot-Scale RO Permeate Samples.....	6
2.2	LaBas Molar Volume Increments.....	17
2.3	Possible Outcomes or Categories of the Modified Rejection Diagram	41
3.1	List of Compound Designations and Comparison of Original Compound List with Final Compound List.....	54
3.2	Compound List Used for Model Development and Model Validation.....	55
3.3	List of Molecular Descriptors Used for Modeling Approaches with Selected Programs Utilized to Obtain Descriptors and Descriptions.....	59
3.4	Theoretical Detection Limit for LC/MS-MS Method.....	64
3.5	Feed Concentration Measurements Taken Throughout Three Recirculation Experiments with BDCM	68
3.6	Feed Concentration Measurements Taken Throughout Two Once-Through Experiments with BDCM	69
4.1	Compounds that Exhibit Adsorptive Effects Including Their Molecular Weight and Log D at pH 6	91
5.1	Molecular Descriptors Separated into Different Categories on the Basis of Their Properties	102
5.2	Parameters Significant to a 3-Parameter Correlation for All Neutral Compounds in Experimental Database	104
5.3	Parameters Significantly Correlated to Rejection Listed with Significant Statistics...	105
5.4	Parameters Significantly Correlated to Rejection Listed with Significant Statistics...	106
5.5	Results from the LOO Cross-Validation for QSPR Internal Validation.....	107
5.6	Parameters Significant to a 3-Parameter Correlation for All Neutral Compounds in Experimental Database	110
5.7	Parameters Significantly Correlated to Rejection Listed with Significant Statistics...	111
5.8	List of Compounds Not Fitting with Phenomenological Model.....	113
5.9	List of Compounds with Less-than-Optimal Phenomenological Model Fits	114
5.10	Phenomenological Model Coefficients for All Organic Compounds (NF-270 Membrane).....	116
5.11	Phenomenological Model Coefficients for All Organic Compounds (ESPA2 Membrane).....	135
5.12	Sample Data Table Used for Solution–Diffusion Modeling Program	146
5.13	Solution–Diffusion Model MTCs for All Compounds Processed with ESPA2 Membrane	147
5.14	List of Compounds that Demonstrate High “Modelability” with Solution–Diffusion Model.....	150

6.1	NF-270 Membrane Pilot-Scale Rejection, Predicted QSPR Rejection, and Percentage Difference from Experimental Pilot-Scale Data.....	164
6.2	Pilot-Scale Rejection and Predicted Rejection from Rejection Diagram for Experimental NF-270 Pilot-Scale Data.....	166
6.3	Average Bulk Wastewater Quality for Major Constituents	185
6.4	Compounds Detected in All Samples from Pilot-Scale Experiment with ESPA2 Membranes by Using LC/MS-MS Method.....	195
6.5	ESPA2 Pilot-Scale Rejection, Predicted QSPR Rejection, and Percentage Difference from Experimental Pilot-Scale Data	201
6.6	Bench- and Pilot-Scale Rejection, Predicted Rejection from Rejection Diagram, and Percentage Difference from Experimental Pilot-Scale Data for ESPA2 Membrane	203
7.1	Rejection Values for Sampling Campaign Performed at OCWD’s Full-Scale RO Facility.....	206
7.2	ESPA2 Membrane Full-Scale Rejection, Predicted QSPR Rejection, and Percentage Difference from Experimental Full-Scale Data	209
7.3	ESPA2 Membrane Full-Scale Rejection, Rejection Predicted from Rejection Diagram, Predicted Rejection Ranges, and Percentage Difference from Experimental Full-Scale Data	217

Acronyms

AHTN	7-acetyl-1,1,3,4,4,6-hexamethyl tetrahydronaphthalene
ALK	alkalinity
BHA	butylated hydroxyanisole
BOD	biochemical oxygen demand
BPA	bisphenol A
CDPH	California Department of Public Health
COD	chemical oxygen demand
COL	color
COND	conductivity
CSDLAC	County Sanitation Districts of Los Angeles County
CSM	Colorado School of Mines
DBPs	disinfection by-products
DOC	dissolved organic carbon
DSPM	Donnan steric pore model
E _{HOMO}	highest energy occupied molecular orbital that contains an electron
E _{LUMO}	lowest energy occupied molecular orbital that does not contain an electron
E1	estrone
E2	17 β -estradiol
E3	estriol
EAT	estrogens, androgens, thyroids
EDC	endocrine disrupting compounds
EDTA	ethylenediaminetetraacetic acid
EE2	17 α -ethynylestradiol
EfOM	effluent organic matter
EPA	Environmental Protection Agency
ESI	electrospray ionization
FDA	Food and Drug Administration
FISA	hydrophilic component of the total solvent accessible surface area
FOSA	hydrophobic component of the total solvent accessible surface area
GC/MS	gas chromatography with mass spectroscopy
GC/MS-MS	gas chromatography with tandem mass spectroscopy
gfd	gallons per square foot and day
HAAs	haloacetic acids
HCNP	hydrophilic negatively and positively charged
HCP	hydrophobic positively charged
HN	hydrophilic neutral; Log K_{ow} < 2

HHoN	hydrophilic/hydrophobic neutral; $\text{Log } K_{ow} > 2$ and $\text{Log } K_{ow} < 3$
HoN	hydrophobic neutral; $\text{Log } K_{ow} > 3$
HPLC	high-performance liquid chromatography
IMS	integrated membrane system
IP	ionization potential
IR	infrared
LC/MS-MS	high-performance liquid chromatography with tandem mass spectroscopy
LMH	liters per square meter and hour
LOD	limit of detection
LOQ	limit of quantification
LPRO	low-pressure RO
MBR	membrane bioreactor
MDL	method detection limit
MF	microfiltration
MTC	mass transfer coefficient
MWCO	molecular weight cutoff
NDMA	<i>N</i> -nitrosodimethylamine
NF	nanofiltration
NOM	natural organic matter
OCWD	Orange County Water District
OTNE	(1-[1,2,3,4,5,6,7,8-octahydro-2,3,8,8-tetramethyl-2-naphthalenyl]ethanone)
PFBBBr	pentafluorobenzyl bromide
PhAC	pharmaceutically active compounds
PISA	π bonds
POC	particulate organic carbon
PPCPs	pharmaceuticals and personal care products
PSD	Pore size distribution
RMSE	root mean squared error
RO	reverse osmosis
SASA	solvent accessible surface area
SAT	soil-aquifer treatment
SCADA	supervisory control and data acquisition
SFPM	surface force pore model
SM	standard methods
SMZ	sulfamethoxazole
SNWA	Southern Nevada Water Authority
SPE	solid-phase extraction
SUVA	specific UV absorbance

TCEP	Tris(2-chloroethyl)phosphate
TCPP	Tris(1,3-dichloroisopropyl)phosphate
TDCPP	Tris(1,3-dichloro-2-propyl)phosphate
TDS	total dissolved solids
THMs	trihalomethanes
TOC	total organic carbon
UF	ultrafiltration
UV	UV light
UVA	UV light absorbance
WPSA	weakly polar surface area
WRRF	WateReuse Research Foundation

Foreword

The WateReuse Research Foundation, a nonprofit corporation, sponsors research that advances the science of water reclamation, recycling, reuse, and desalination. The Foundation funds projects that meet the water reuse and desalination research needs of water and wastewater agencies and the public. The goal of the Foundation's research is to ensure that water reuse and desalination projects provide high-quality water, protect public health, and improve the environment.

An Operating Plan guides the Foundation's research program. Under the plan, a research agenda of high-priority topics is maintained. The agenda is developed in cooperation with the water reuse and desalination communities including water professionals, academics, and Foundation subscribers. The Foundation's research focuses on a broad range of water reuse research topics including:

- Definition of and addressing emerging contaminants
- Public perceptions of the benefits and risks of water reuse
- Management practices related to indirect potable reuse
- Groundwater recharge and aquifer storage and recovery
- Evaluation and methods for managing salinity and desalination
- Economics and marketing of water reuse

The Operating Plan outlines the role of the Foundation's Research Advisory Committee (RAC), Project Advisory Committees (PACs), and Foundation staff. The RAC sets priorities, recommends projects for funding, and provides advice and recommendations on the Foundation's research agenda and other related efforts. PACs are convened for each project and provide technical review and oversight. The Foundation's RAC and PACs consist of experts in their fields and provide the Foundation with an independent review, which ensures the credibility of the Foundation's research results. The Foundation's Project Managers facilitate the efforts of the RAC and PACs and provide overall management of projects.

High-pressure membrane processes, such as reverse osmosis (RO) and nanofiltration (NF), are becoming increasingly widespread in water treatment, industrial processes and wastewater reclamation/reuse applications where a high product water recovery is desired. The overall goal of this project is to develop models that can be used, a priori, to predict the rejection of a wide variety of organic compounds by NF and RO membranes. The objectives of this research project were to (a) evaluate molecular modeling approaches and determine method-independent and reliable molecular descriptors for the development of quantitative structure activity relationship models, (b) identify, develop, and optimize membrane modeling strategies and develop models that can be employed to predict the rejection of organic solutes, and (c) evaluate the efficiency that membranes employed on full-scale removal of trace organic chemicals and to successfully predict the removal rates with the developed model(s).

Richard Nagel
Chair
WateReuse Research Foundation

G. Wade Miller
Executive Director
WateReuse Research Foundation

Acknowledgments

This project was funded by the WateReuse Research Foundation in cooperation with the United States Bureau of Reclamation, California State Water Resources Control Board (CA), the Orange County Water District (CA), and the Southern Nevada Water Authority (NV).

This study would not have been possible without the insights, efforts, and dedication of many individuals and organizations. These include the members of the research team and PAC members (as identified); the WateReuse Research Foundation's project managers, Anna Durden, Caroline Sherony, Jimena Pinzon, and Julie Minton; our technical advisor, Dr. Harry Ridgway, many key individuals at the participating utilities and related organizations; and the outstanding staff, especially Monte DiPalma, of the Advanced Water Technology Center (AQWATEC) at the Colorado School of Mines.

The research team thanks the WateReuse Research Foundation for funding this research project, as well as the following organizations for their in-kind contributions: Orange County Water District and the Southern Nevada Water Authority.

Principal Investigator

Jörg E. Drewes, Ph.D., *Colorado School of Mines*

Co-Principal Investigator and Project Manager

Christopher L. Bellona, Ph.D., *Colorado School of Mines*

Co-Principal Investigators

Mark Eberhart, Ph.D., *Colorado School of Mines*

Shankar Chellam, Ph.D., *University of Houston*

Research Project Team

David Ball, *Colorado School of Mines*

Karen Budgell, *Colorado School of Mines*

Travis Jones, Ph.D., *Colorado School of Mines*

Kate Spangler, *Colorado School of Mines*

Dean Heil, Ph.D., *Colorado School of Mines*

Shane Snyder, Ph.D., *Southern Nevada Water Authority*

Brett Vanderford, *Southern Nevada Water Authority*

Gary Amy, Ph.D., *UNESCO-IHE, The Netherlands*

Project Advisory Committee

Frank Leitz, *Bureau of Reclamation*

Joan Oppenheimer, *MWH*

Donald Phipps, Ph.D., *Orange County Water District*

Executive Summary

Project Background

One possible solution for securing additional drinking water sources is the reclamation of wastewater effluents using high-pressure membranes such as reverse osmosis (RO) and nanofiltration (NF) membranes, which is being implemented in the United States and explored in Australia. Past laboratory research projects have demonstrated that a limitation of RO and NF is the incomplete removal of various organic solutes, such as certain disinfection by-products, pharmaceutical residues, personal care products, household chemicals, and emerging disinfection by-products (Nghiem et al., 2004; Drewes et al., 2005; Xu et al., 2006; Snyder et al., 2006). Uncertainty regarding the rejection of certain solutes, coupled with the increasing number of detections of trace organic chemicals at the parts-per-trillion level in impaired water sources, justifies the development of modeling approaches that can adequately predict—a priori—the removal of contaminants by RO and NF membranes. A successful predictive model would eliminate the need to conduct pilot-scale evaluation of trace organic contaminant removal, eliminate uncertainty regarding permeate water quality, and promote the implementation of water reuse projects employing membrane treatment.

Project Objectives

The objectives of this project were (a) to evaluate molecular modeling approaches and determine method-independent and reliable molecular descriptors for the development of quantitative structure activity relationship (QSAR) models, (b) to identify, develop, and optimize membrane modeling strategies and develop models that can be employed to predict the rejection of organic solutes, and (c) to evaluate the efficiency that membranes employed on full-scale removal of trace organic chemicals and to successfully predict the removal rates with the developed model(s). The research study consisted of three major phases. The project was initiated with the development of a roadmap for membrane rejection modeling, including a comprehensive literature review and the determination and calculation of reliable, accurate, and relevant molecular descriptors for a wide range of trace organic chemicals. The second phase of the project addressed the construction and optimization of viable membrane rejection models and their validation. Evaluation and validation of the membrane rejection models were conducted by using pilot- and full-scale units or facilities.

This research was performed by a team of faculty, scientists, and graduate students from the Colorado School of Mines and the University of Houston. The study was supported by researchers at the Southern Nevada Water Authority and UNESCO-IHE. It was funded by the WateReuse Research Foundation, Bureau of Reclamation, California State Water Resources Control Board, the Orange County Water District, and the Southern Nevada Water Authority.

Study Findings

Numerous possible approaches for describing solute mass transfer through high-pressure membranes have been proposed in the past. Therefore, there is a strong need to summarize the current knowledge base regarding trace organic solute removal and the mathematical description of their rejection. Current limitations in predicting the rejection of organic chemicals during water reuse applications exist because an understanding of viable modeling

approaches is lacking; many past modeling approaches utilized unrealistic experimental setups and produced data that are inappropriate for predicting rejection on larger scales. In addition, modeling membrane treatment is an inherently difficult problem because of system complexities and numerous factors affecting rejection. Information gained through a comprehensive literature review was used to develop a representative list of organic solutes for experimentation, an experimental protocol for measuring rejection, and a list of pertinent modeling strategies for NF and RO membranes.

For this study, 270 organic solutes were initially selected for model development and model validation. The list of compounds was compiled from a variety of sources and yielded a relatively diverse set of organic solutes based on properties (e.g., size, charge, hydrophobicity/hydrophilicity, etc.), relevance to membrane treatment (e.g., functional groups affecting rejection and likelihood of permeation), and environmental relevance (e.g., EPA Candidate Contaminant List and recent advancements in emerging contaminant research, human health, and environmental relevance). After removal of compounds that caused analytical and experimental issues (e.g., high volatilization, instability, and poor solubility), a shorter list of 137 compounds was generated for model development and validation. Compounds were categorized by expected rejection mechanism based on charge and hydrophobicity. Six different categories were developed: hydrophilic neutral (HN; less than 0.01% charged at pH 6.5; Log Kow < 2), hydrophilic/hydrophobic neutral (HHoN; less than 0.01% charged at pH 6.5; Log Kow > 2 and Log Kow < 3), hydrophobic neutral (HoN; less than 0.01% charged at pH 6.5; Log Kow > 3), hydrophilic negatively charged (HCN; greater than 50% negatively charged at pH 6.5), hydrophilic positively charged (HCP; greater than 50% positively charged at pH 6.5), and hydrophilic negatively and positively charged (HCNP; having both positive and negative charge at pH 6.5).

For each rejection mechanism subgroup, principal component analysis and k-means clustering/discriminate analysis were performed to further group similar compounds on the basis of molecular properties calculated and compiled from various sources (e.g., Syracuse Research Corporation, ACD Labs, Schrödinger, and Hyperchem). This selection process yielded a group of 134 compounds for model development and validation. On the basis of further analysis, this final list of compounds retained much of the diversity of the full list on the basis of criteria outlined previously (e.g., properties, rejection mechanisms, classes of compounds, environmental relevance, etc.). The list was then randomized with the 33 top compounds selected for the validation set and the remaining 101 selected for the model development set.

Several criteria were used to develop an experimental protocol to measure organic solute rejection at bench scale under conditions that allowed the development of a rejection database for the select solutes. This database provided the basis for subsequent rejection model developments. For each compound, replicate experiments were conducted by using flat-sheet membrane material cut from a spiral-wound element. During experimentation, concentration polarization was minimized by maintaining recovery below 1.5%. Short-term rejection was evaluated at five permeate flux set-points spanning a range from 3 to 60 gal per sq ft and day (gfd). Longer-term rejection to study potential interactions between solutes and membranes was evaluated by operating the SEPA system at flux of 12 gfd for approximately 24 h. Feed and permeate samples were collected in replicate, and solute concentration was quantified by a variety of analytical methods including total organic carbon analysis, refractive index detection, liquid chromatography diode-array detection, gas chromatography electron capture detection, and liquid chromatography with tandem mass spectroscopy detection. By characterization of the hydrodynamic conditions of the testing system, intrinsic rejection (i.e.,

rejection in the absence of concentration polarization) was calculated for each compound by using feed and permeate concentrations. The rejection-versus-flux data were used to populate a database consisting of rejection data and solute properties, which was subsequently used for model development.

Because of the large number of experiments planned, two different membranes were employed during the study. The NF-270 membrane from Dow/Filmtec was selected as the representative NF membrane because this membrane had been applied in previous pilot-scale studies using reclaimed water and exhibited excellent rejection performance for organic solutes, low fouling propensities, and a significantly higher specific flux than conventional RO membranes (Bellona and Drewes, 2007; Bellona et al., 2008). The ESPA2 membrane from Hydranautics was selected as the representative low-pressure RO membrane because this membrane is employed at several full-scale water reclamation facilities.

Numerous possible modeling approaches for describing solute mass transfer through high-pressure membranes were identified. Several approaches were characterized as impractical for describing rejection at larger-scale membrane applications, including the Donnan steric pore and surface force pore models. Modeling approaches evaluated during this study included quantitative structure property relationships (QSPRs), empirical models, the hydrodynamic model, the phenomenological model, and the solution–diffusion model.

A significant portion of this study evaluated rejection at pilot scale under carefully controlled laboratory experiments and in the field at a water reclamation facility. This approach provided valuable information on comparing and upscaling bench-scale experimental rejection results to larger membrane systems. Findings from these studies suggest that bench-scale rejection results can be used to describe the rejection at a large scale; however, the hydrodynamic conditions and flux and concentration gradients for a large-scale system need to be characterized. The differential element approach combined with the phenomenological model was an effective modeling approach to describe rejection at pilot scale. Bench-scale-derived phenomenological model coefficients could be used to estimate pilot-scale permeate concentrations and rejection. QSPRs and the rejection diagram approach developed with bench-scale rejection data could estimate rejection at pilot scale.

Recommendations

Different modeling approaches were evaluated during the course of the study to develop a broadly applicable model to predict the rejection of trace organic chemicals by NF and RO membranes. Although modeling approaches were developed that can estimate rejection at bench, pilot-, and full-scale installations, developing accurate models for the thousands of potential organic contaminants is difficult for a number of previously discussed reasons. The research team found that bench-scale results can be used to describe the rejection of organic solutes at larger scales; however, changes in membrane performance over time from compaction and fouling to aging are difficult to incorporate into modeling approaches. These issues aside, there are different modeling approaches that can be adopted on the basis of the level of effort required for development. They are listed in order of increasing complexity:

1. The rejection diagram is a simple and effective approach for describing the range of rejection for a wide variety of organic solutes as it requires few, easily determined solute descriptors. The rejection diagrams (Figure 5.4.1) were developed and tested during the course of this study for one RO-type membrane and one NF-type membrane.

2. A utility looking to develop a transport model to describe the rejection of organic solutes would be advised to sacrifice an (fouled) element from its system and to run experiments (rejection as a function of permeate flux) with organic solutes spanning a range of size, charge, and hydrophobicity. For nonionic solutes, simple correlations can be developed between the reflection coefficient and permeability coefficient and a solute size descriptor. For ionic compounds, the measured range of reflection and permeability coefficients should be sufficient to estimate the range of rejection for these compounds. A simple mass balance model can be developed for a full-scale membrane system by using bench-scale-derived phenomenological coefficients.
3. The major issue with QSPR models is that they are dependent on the conditions used to develop the rejection data and require a large number of rejection data to generate statistically significant correlations. The solute selection method employed during this study proved to be a good approach for selecting solutes for QSPR development.

Future Research Needs

A number of research questions were raised during the completion of this study that should be studied further to understand the transport of organic compounds through NF and RO membranes. These include

- Understanding the solute properties that result in adsorption and partitioning through membrane materials and developing modeling approaches for these compounds
- Quantifying the time it takes to reach rejection equilibrium conditions for a broad range of solutes with strong membrane interactions
- Quantifying the effect of membrane compaction and fouling on the rejection of organic solutes
- Identifying membrane-specific descriptors that affect solute mass transport
- Integrating membrane-specific descriptors into rejection models

Chapter 1

Introduction

1.1 Background

High-pressure membrane processes, such as reverse osmosis (RO) and nanofiltration (NF), are becoming increasingly widespread in water treatment, industrial processes, and wastewater reclamation/reuse applications where a high product water recovery is desired. For example, Bartels et al. (2008) reported that the capacity of global high-pressure membrane applications for water reclamation over the past 30 years increased from approximately 150,000-m³/day in 1977 to approximately 900,000-m³/day in 2008.

For drinking water augmentation projects in the United States, Singapore, and Australia that use reclaimed water, treatment using an integrated membrane system (IMS), such as microfiltration (MF) pretreatment followed by RO, is the industry standard. Facilities employing RO for water reclamation include the West Basin Water Recycling Facility (El Segundo, CA), Scottsdale Water Campus (Scottsdale, AZ), Leo J. Vander Lans Plant (Orange County, CA), Terminal Island Treatment Plant (Long Beach, CA), Groundwater Replenishment System (Orange County, CA), and several installations in Singapore and Australia. Past research projects have demonstrated that a limitation of RO and NF is the incomplete removal of various organic solutes, such as certain disinfection by-products, pharmaceutically active compounds, household chemicals, chlorinated flame retardants, steroid hormones, and pesticides (Nghiem et al., 2004; Drewes et al., 2005; Xu et al., 2006; Snyder et al., 2007). Uncertainty regarding the rejection of certain solutes, coupled with the increasing number of detections of emerging trace organic chemicals at the part-per-trillion level in impaired water sources, justifies the development of modeling approaches that can adequately predict—a priori—the removal of contaminants by RO and NF membranes. A successful predictive model would eliminate the need to conduct pilot-scale evaluations of trace organic contaminant removal, eliminate uncertainty regarding permeate water quality, and promote the implementation of water reuse projects employing membrane treatment.

1.2 Objectives

The overall goal of this project is to develop models that can be used, a priori, to predict the rejection of a wide variety of organic compounds by NF and RO membranes. The objectives of this research project were (a) to evaluate molecular modeling approaches and determine method independent and reliable molecular descriptors for the development of quantitative structure activity relationship (QSAR) models, (b) to identify, develop, and optimize membrane modeling strategies and develop models that can be employed to predict the rejection of organic solutes, and (c) to evaluate the efficiency at which membranes employed at full scale remove trace organic chemicals and to successfully predict the removal rates with the developed model(s). The research study consisted of three major phases. The project was initiated with the development of a roadmap for membrane rejection modeling, including a comprehensive literature review and the determination and calculation of reliable, accurate, and relevant molecular descriptors for a wide range of trace organic chemicals. The second phase of the project addressed the development, optimization, and validation of viable membrane rejection models. Evaluation and validation of the membrane rejection models were conducted at pilot- and full-scale membrane installations.

This research was performed by a team of faculty, scientists, and graduate students from the Colorado School of Mines and the University of Houston. The study was supported by researchers at the Southern Nevada Water Authority and UNESCO-IHE. The research was funded by the WateReuse Research Foundation, U.S. Bureau of Reclamation, California State Water Resources Control Board, the Orange County Water District, and the Southern Nevada Water Authority.

Chapter 2

Review of Modeling Solute Rejection in High-Pressure Membranes

2.1 Introduction

The goal of this literature review is to identify the factors that affect rejection and identify the most promising modeling approaches for the development of predictive models for organic solutes. This topic is very broad and is complex and is constantly expanding. Therefore, any review on this subject matter should be considered a work in progress, but the review provided in this chapter represents the current state-of-the-art of solute rejection and modeling approaches in high-pressure membranes.

2.1.1 Differences Among Membranes

Differences among thin-film composite RO membranes, low-pressure RO (LPRO) membranes, and NF membranes are subtle and often debatable. The nomenclature used to describe a particular membrane is often based upon the application for which the membrane was designed. Membranes designed for applications in which monovalent salt-free permeate is desired (i.e., seawater desalination and brackish water treatment) are most often termed seawater RO elements, brackish water RO elements, and/or low-pressure brackish water elements. These membranes hinder the diffusive transport of solutes through the membrane, are capable of rejecting >99% of monovalent salts, and will be termed RO membranes for this study (Zhao and Taylor, 2004; Zhao et al., 2005).

LPRO (<200 psi) membranes designed for high monovalent salt removal (>98%) and low-molecular-weight organic removal (<100 Da) are loosely termed LPRO membranes. Although it is debatable whether LPRO membranes have discrete pores or operate solely through diffusive transport limitations, it has been shown that solute removal involves a combination of steric and electric exclusion and is likely a combination of both diffusive and convective limitations (Ozaki and Li, 2002; Košutić and Kunst, 2002; Tsuru et al., 1991a).

NF membranes span a wide range of properties and are indistinguishable from ultra-LPRO (ULPRO) membranes if they reject monovalent salts well and are indistinguishable from certain ultrafiltration (UF) membranes if they moderately reject low-molecular-weight organics (<300 Da) and divalent cations. Generally, NF membranes are considered to operate at lower pressures than ULPRO membranes (~100 psi), are considered to have pores in the 1-nm range (although this is debatable), efficiently remove divalent cations and most organic solutes, and pass monovalent salts and organics smaller than the membrane pore size (Bowen and Mukhtar, 1996; Nghiem et al., 2005). It has been shown that NF membranes remove solutes through steric and electrostatic exclusion from pores (Bowen and Mukhtar, 1996; Hagemeyer and Gimbel, 1998; Bandini and Vezzani, 2003; Bellona and Drewes, 2005).

2.1.2 Solute Transport through RO and NF

There is still controversy regarding pore structures in NF and RO membranes. Wijmans and Baker (1995) published a review on the solution-diffusion model in which they discuss the controversy surrounding whether transport through RO membranes should be described by

pore-flow or solution–diffusion models. According to the researchers, “Both models were proposed in the 19th century, but the pore-flow model, because it was closer to normal physical experience, was more popular until the mid-1940s...the transport mechanism in reverse osmosis membranes was a hotly debated issue in the 1960s and early 1970s. By 1980, however, the proponents of solution–diffusion had carried the day; currently only a few die-hard pore-flow modelers use this approach to rationalize reverse osmosis.” Wijmans and Baker (1995) attempted to clarify the difference between solute diffusion limiting membranes and membranes where solute transport is partially due to pore-flow phenomena: “The transition between a pore-flow and a solution–diffusion mechanism seems to occur with membranes having very small pores. Membranes that reject sucrose and raffinose but pass all micro-ions are clearly pore-flow membranes...Presumably, the transition is in the nanofiltration range, with membranes having good rejection of monovalent ions in the 20–50% range.”

How important are pore structure and solute transport when selecting models to describe solute rejection for a particular membrane? Solution–diffusion models are applicable to dense membranes where permeating solutes first dissolve into the membrane and diffuse through the membrane material following a concentration gradient (Wijmans and Baker, 1995; AWWA, 2007). For these membranes, dissolved solutes have very low permeability as compared to water. For membranes with high water flux at low pressure that allow some solutes to a degree similar to that of water, pore-flow models may be more applicable. However, whether pore-flow models apply to low-pressure RO membranes is unclear. Early RO models included terms for convection, which led to much of the mass transport controversy reported by Wijmans and Baker (see Dresner, 1971; Spiegler and Kedem, 1966). Does the ability of small polar molecules, such as *N*-nitrosodimethylamine (NDMA) and boron, to freely permeate commercially available LPRO membranes (examples are ESPA2 from Hydranautics and the TFC-HR from Koch Industries) and to a somewhat lesser extent desalination RO membranes, mean that RO membranes have pores? It is quite easy to find literature supporting both pore flow and diffusion as transport mechanisms for RO membranes (Dresner, 1971; Spiegler and Kedem, 1966; Kargol, 2001; Kim et al., 2007). However, it appears that most researchers agree that solute transport through RO membranes occurs by diffusion through the membrane polymer.

For NF membranes, it appears that most researchers acknowledge that solute transport through NF membranes occurs by convection and diffusion. NF modeling approaches developed in the 1990s used a ratio of solute size to effective pore size to develop convective hindrance factors based on the work reported by Deen (1987). Using atomic force microscopy, researchers have worked to defend the idea that NF and to a lesser extent RO had discernible pores in the 1-nm range (Bowen et al., 1997).

2.2 Observations of Rejection at Pilot- and Full-Scale Membrane Installations

Past laboratory research projects have demonstrated that a limitation of RO and NF is the incomplete removal of various organic solutes, such as certain disinfection by-products, pharmaceutically active compounds, chlorinated flame retardants, steroid hormones, and pesticides (Nghiem et al., 2004; Drewes et al., 2005; Xu et al., 2006, Snyder et al., 2007). However, there is some question whether these laboratory-scale studies indicate that RO membranes operating at full scale have incomplete rejection of organic compounds of

concern. Recently, studies have been conducted investigating the rejection of a variety of organic contaminants by RO and NF membranes at full-scale membrane installations (Drewes et al., 2007; Snyder et al., 2007). A summary of the organic compounds that have been found to permeate RO membranes operating at water reuse facilities (full-scale and pilot-scale data) is presented in Table 2.1. Most of the compounds that are quantified in feed water are not detected in membrane permeates or, when they are, are at low concentrations. However, it was discovered at a full-scale reclamation plant employing RO treatment that trace organics such as 1,4-dioxane and NDMA were present in product water at concentrations greater than the California Department of Public Health (CDPH) action limit.

Drewes et al. (2008) investigated 12 commercially available RO and NF membranes in rejecting a wide variety of organic contaminants on a laboratory-scale testing unit employing two spiral-wound 4040 membrane elements. One of the major findings was that nonionic organic contaminants are often incompletely removed, even by RO membranes with greater than 99% monovalent salt rejection. In addition, although RO and NF membranes operating at full scale at the West Basin Water Recycling Plant (WBWRP, El Segundo, CA) were observed to adequately reject negatively charged organic solutes such as trichloroacetic acid (TCAA), the removal of low-nonionic-molecular-weight organic chemicals, such as NDMA, and of solutes with strong membrane affinity, such as chloroform, was marginal during pilot- and full-scale investigations (Figure 2.1). These results highlight that the properties of an organic solute often determine rejection and that there may not be one membrane modeling approach that can incorporate all of the factors driving rejection, including solute and membrane properties and operational conditions.

Table 2.1. Compounds Detected in Full- and Pilot-Scale RO Permeate Samples

Compound	Concn (ng/L)	Citation	Scale	Membrane	Membrane Type
1,4-Dioxane	NA	Drewes et al., 2008	Full	TFC-HR, ESPA2	RO
Bisphenol A	25	Drewes et al., 2008	Pilot	TMG10, NF-90	RO and NF
Caffeine	1.2–52	Snyder et al., 2007	Pilot and full	TFC-HR, ESPA2	RO
Chloroform	2–5 (*10 ³)	Drewes et al., 2008	Pilot and full	TFC-HR, ESPA2, TMG10	RO
Diethyl- <i>m</i> -toulamideDEET	2	Snyder et al., 2007	Full	Saehan FL	RO
Galaxolide	11	Snyder et al., 2007	Full	ESPA2	RO
Gemfibrozil	2	Snyder et al., 2007	Full	ESPA2	RO
Ibuprofen	4–27	Drewes et al., 2008	Pilot	TMG10	RO
Iopromide	1.1–72	Snyder et al., 2007	Pilot	TFC-HR	RO
Meprobamate	1	Snyder et al., 2007	Pilot	Saehan RE-FRM	RO
Naproxen	1	Drewes et al., 2008	Pilot	TMG10	RO
NDMA	20–40	Drewes et al., 2008	Full	ESPA2	RO
Oxybenzone	6	Snyder et al., 2007	Full	ESPA2	RO
Pentoxifylline	45	Snyder et al., 2007	Pilot	TFC-HR	RO
Sulfamethoxazole	1–2	Snyder et al., 2007	Pilot	Saehan FL	RO
Tris(2-chloroethyl)phosphate	2–30	Snyder et al., 2007	Pilot and full	ESPA2, Saehan RE-FRM, Osmonics AK	RO

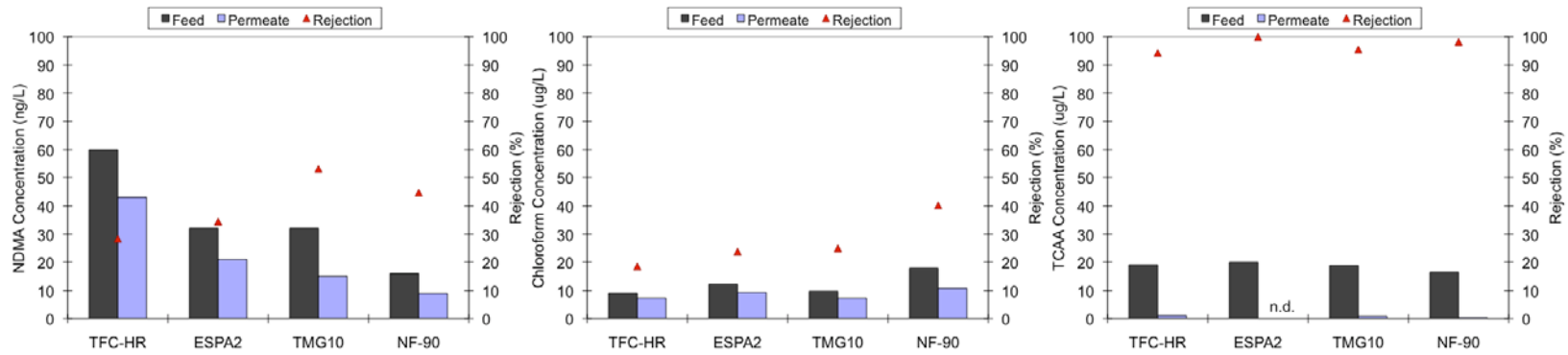


Figure 2.1. Feed, permeate and rejection concentrations for NDMA (left), chloroform (middle), and TCAA (right) by the TFC-HR and ESPA2 membranes at full scale and the TMG10 and NF-90 membranes at pilot scale.

2.3 Calculating Rejection

2.3.1 Concentration Polarization

The accumulation of retained solutes at the membrane surface as water crosses the membrane is termed concentration polarization. The film model has been used to describe concentration polarization and describes the film caused by concentration polarization as a one-dimensional film in which longitudinal transport is negligible (Hofman et al., 2007). During membrane operation, it is assumed that equilibrium is reached where convective transport of solutes towards the membrane is balanced by back diffusion into the bulk solution (Hofman et al., 2007). The degree of concentration polarization (often expressed as β) is based on the film model and can be calculated by:

$$\beta = \frac{c_m}{c_f} = \exp\left(\frac{J_w}{k_m}\right) \quad (2.1)$$

where c_m and c_f are the concentration of the solute at the membrane and in the bulk solution, respectively, J_w is the convective flux, and k_m is the local mass transfer coefficient (MTC) on the brine or feed side. The local MTC can be calculated by a Sherwood equation developed by Schock and Miquel (1987) for spacer-filled channels (Hofman et al., 2007):

$$Sh = 0.065 \cdot Re^{0.875} \cdot Sc^{0.25} \quad (2.2)$$

where Re is the Reynolds number, Sc is the Schmidt number, and Sh is the Sherwood number, which is given by the following equation:

$$Sh = \frac{k_m d_h}{D_s} \quad (2.3)$$

where d_h is the hydraulic diameter and D_s is the bulk diffusivity (meters²/seconds⁻¹). Sutzkover et al. (2000) later redefined the constants in Equation 2.2 for their specific membrane system, and the constants should be determined for each membrane system being investigated. The Schmidt number is defined as

$$Sc = \frac{\eta}{\rho D_{i,\infty}} \quad (2.4)$$

with η the viscosity of the bulk solution and $D_{i,\infty}$ the diffusion coefficient at infinite dilution. The Reynolds number is defined as

$$Re = \frac{\rho v d_h}{\eta} \quad (2.5)$$

For a cross-flow spiral-wound membrane module, the cross-flow velocity v can be calculated by

$$v = \frac{Q_f}{nLh_{sp}\varepsilon} \quad (2.6)$$

where Q_f is the feed flow rate, n is the number of membrane leaves, L is the length of the element, h_{sp} is the thickness of the spacer, and ε is the feed spacer porosity. The hydraulic diameter for a spiral-wound element is determined by

$$d_h = \frac{4\varepsilon}{\frac{2}{h_{sp}} + (1-\varepsilon) \cdot S_{vsp}} \quad (2.7)$$

where S_{vsp} is the specific surface of the spacer. Schock and Miquel (1987) found that S_{vsp} could be calculated as $4/d_f$, where d_f is the thickness of the filaments in the spacer. The porosity can be calculated by using the average filament thickness and mesh size of the spacer:

$$\varepsilon = \frac{1 - V_{sp}}{V_{Tot}} \quad (2.8)$$

where V_{sp} is the total volume of the spacer and V_{Tot} is the total channel volume.

2.3.2 Rejection

For membrane applications where the percent removal of a solute in the feed water is desired, removal is commonly expressed as rejection, which is calculated by the following equation:

$$R(\%) = \left(1 - \frac{C_p}{C_f}\right) * 100 \quad (2.9)$$

where R is rejection expressed as a percentage, C_p is the permeate concentration, and C_f is the feed concentration. The experimental determination of rejection can be complicated by a number of factors, including concentration polarization, changes in concentration along full-scale membrane elements employed in a multiple-element pressure vessel, and adsorption of a solute to a membrane. Therefore, more information about solute removal is often desired, especially for modeling exercises where concentration gradients and solute flux across a membrane are needed.

There are different methods by which to calculate rejection, including the general equation given earlier. The feed water concentration, however, differs from the actual concentration at the membrane surface, especially when concentration polarization effects are noticeable; therefore, rejection should be calculated accordingly (Bouranene et al., 2007; Bowen et al., 1998). The intrinsic or real rejection, R_{int} , is rejection when taking into account the concentration at the membrane surface. Observed rejection (R_{obs}) can be related to intrinsic

rejection (R_{int}) by the following equations (Bouranene et al., 2007; Sutzkover et al., 2000; Nghiem et al., 2004):

$$R_{obs} = \frac{R_{int} \exp(-J_v / K)}{1 + R_{int} (\exp(-J_v / K)) - 1} \quad (2.10)$$

or

$$R_{int} = \frac{R_{obs} \exp(J_v / K)}{1 - R_{obs} (1 - \exp(J_v / K))} \quad (2.11)$$

and

$$\ln\left(\frac{1 - R_{int}}{R_{int}}\right) = \ln\left(\frac{1 - R_{obs}}{R_{obs}}\right) - \left(\frac{J_v}{K}\right) \quad (2.12)$$

where J_v is the permeate flux rate and K is the MTC for back diffusion (previously expressed as k_m). K can be calculated by using either of the two following equations:

$$K = \frac{(J_v)_{salt}}{\ln\left\{\frac{\Delta P}{\pi_b - \pi_p} * \left[1 - \frac{(J_v)_{salt}}{(J_v)_{water}}\right]\right\}} \quad (2.13)$$

or

$$Sh = \frac{K \cdot d_h}{D_{i,\infty}} = 0.20 \cdot Re^{0.91} \cdot Sc^{0.25} \quad (2.14)$$

where π_b and π_p are the osmotic pressures of the bulk and permeate solutions, respectively, ΔP is the applied pressure, Sh is the Sherwood number, Re is the Reynolds number, Sc is the Schmidt number, d_h is the hydraulic diameter, and $D_{i,\infty}$ is the diffusion coefficient of a solute at infinite dilution. Sutzkover et al. (2000) developed Equation 2.13 as a simple technique for determining the MTC and the concentration polarization of an RO membrane system.

Through experimentation with a spiral-wound RO module, the researchers were able to develop Equation 2.14, which was found to be similar to the Deissler correlation (i.e., $Sh = 0.023Re^{0.875} Sc^{0.25}$). However, because this correlation was developed for a specific spiral-wound module, for different membrane configurations, it may be necessary to calculate K from experiments and Equation 2.13.

When one is evaluating larger membrane systems such as full-scale treatment trains, the feed water concentration can change considerably (six times the initial feed concentration, depending on the recovery of the system) along a pressure vessel, making it difficult to calculate rejection. In this case, the rejection of a feed water component is the feed/brine average rejection value, which is used to compare systems that are operated under different conditions and is given by Equation 2.15.

$$\text{Rejection (Feed/Brine Concentrations)} = \frac{C_f * \left(\frac{\ln\left(\frac{1}{1 - \text{Recovery}}\right)}{\text{Recovery}} \right) - C_p}{C_f * \left(\frac{\ln\left(\frac{1}{1 - \text{Recovery}}\right)}{\text{Recovery}} \right)} \quad (2.15)$$

This value takes into account the increased concentrations of a component at the surface of a downstream membrane in a system of a certain recovery and offers a more useful comparison for two systems operated at different recoveries. Solution–diffusion models, where the permeate concentration model output is dependent upon the feed water concentration, have been modified to account for the effect of hydrodynamic conditions, such as concentration polarization on rejection (Zhao et al., 2005).

2.4 Mechanisms and Understanding Rejection (Size Exclusion)

There have been numerous studies of the effect of size on the rejection of solutes by RO and NF membranes. The underlying principle is that membranes exclude large solutes from the permeate side (size exclusion) but that, depending on the membrane, small molecules are incompletely removed. Size exclusion is generally referred to as a convective flux phenomenon where small solutes could permeate through a membrane pore or void space (see Kiso et al., 2001a); however, because small molecules are expected to diffuse at higher rates, size exclusion is also a diffusion phenomenon. As a general summary, molecular size does not always correlate with rejection and finding a good-sized parameter is not always easy. The following sections discuss molecular size parameters, the effect of size on rejection, and size exclusion modeling approaches.

In the past decade, numerous papers have reported (in one way or another) on the correlation between the size of an organic solute and rejection. Describing the size of a solute is nontrivial as illustrated by the number of attempts to correlate rejection of nonionic solutes to their size (Braeken et al., 2005; Kiso et al., 1992; Van der Bruggen et al., 1999). There have been a number of studies that have attempted this correlation and therefore a number of different means of describing the size of a molecule. In many cases, however, the rejection of organic solutes is somewhat independent of molecular size and depends on other factors. These factors will be discussed in the next section.

The rejection of uncharged organic compounds is largely dependent on the size of a solute and the molecular weight cutoff (MWCO) or effective pore size of a membrane (Bellona et al., 2004). To illustrate, Figure 2.2 presents the rejection of four organic solutes (phenacetine, TCEP [Tris(2-chloroethyl)phosphate], TCPP [Tris(1,3-dichloroisopropyl)phosphate], and TDCPP [Tris(1,3-dichloro-2-propyl)phosphate]) by 11 commercially available NF, LPRO, and RO membranes. For the low-molecular-weight compound phenacetine, rejection was highly variable among the membranes tested, with the NF membranes exhibiting between 40 and 70% rejection and the RO membranes exhibiting between 70 and 95% rejection. There have been many attempts to correlate rejection with different solute size descriptors, which are discussed in the following sections.

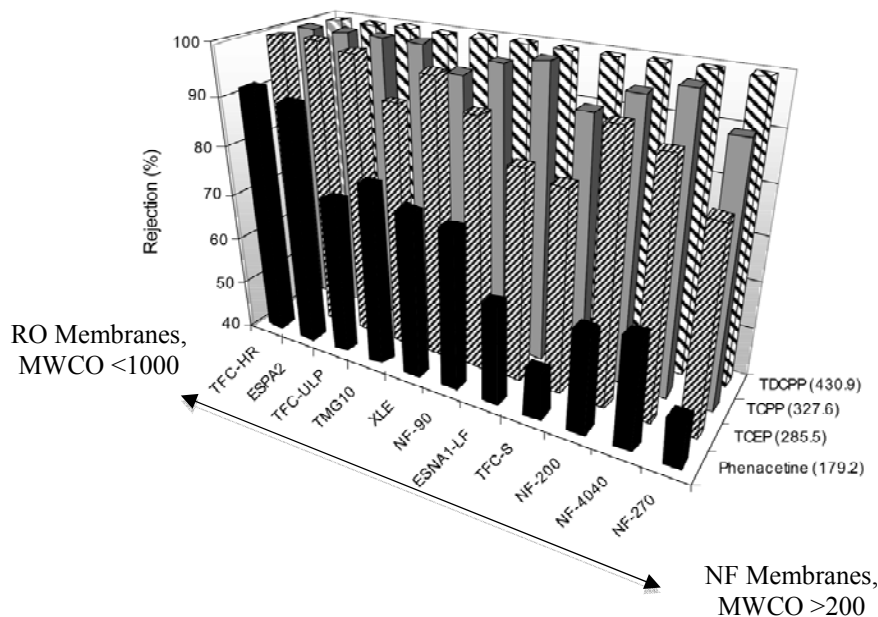


Figure 2.2. Rejection of phenacetine, TCEP, TCP, and TDCPP by 11 commercially available RO, LPRO, and NF membranes.

Notes: Laboratory experiments performed with 4040 spiral-wound element testing unit, 16-gfd flux, 20% recovery, and ~500-ng/L feed concentration (Bellona et al., 2008).
gfd = gallons per square foot and day.

Molecular Weight. The simplest, yet one of the most insufficient, measures of a solute's size, is the molecular weight or molar mass of a solute of interest. Ozaki and Li (2002) reported that, for ULPRO membranes, the rejection of noncharged and nonpolar compounds could be predicted by using the molecular weight of the compound. Researchers (Van der Bruggen and Vandecasteele, 2002; Van der Bruggen et al., 1999; Schutte, 2003) have also proposed that the molecular weight of a noncharged compound can be a useful predictor of rejection and for calculation of reflection coefficients (rejection at infinite pressure). Other studies confirmed that the molecular weight of a solute with characteristics other than noncharged and hydrophilic is a rather poor predictor of rejection (Kiso et al., 1992; Kiso et al., 1996). Because steric hindrance may be an important driving factor in the rejection of molecules by NF membranes, a quantification of the molecular size (and geometry) of a solute, coupled with the pore size of a membrane, might be a better descriptor of the rejection than is MWCO, molecular weight, or desalting degree.

Kiso et al. (2001a) reported that, for two NF membranes (MWCO > 500 Da), rejection of sugar and alcohols increased as molecular weight increased. In addition, the researchers found that, for these NF membranes, molecular size parameters (e.g., radius, length, and diameter) were only slightly better than molecular weight in predicting the rejection of compounds for which steric hindrance is the main driving factor in rejection. However, when examining NF membranes with MWCOs of <250 Da, Kiso et al. (2001b) reported that molecular size parameters were significantly better descriptors for rejection when size exclusion was the dominant mechanism (Figure 2.3).

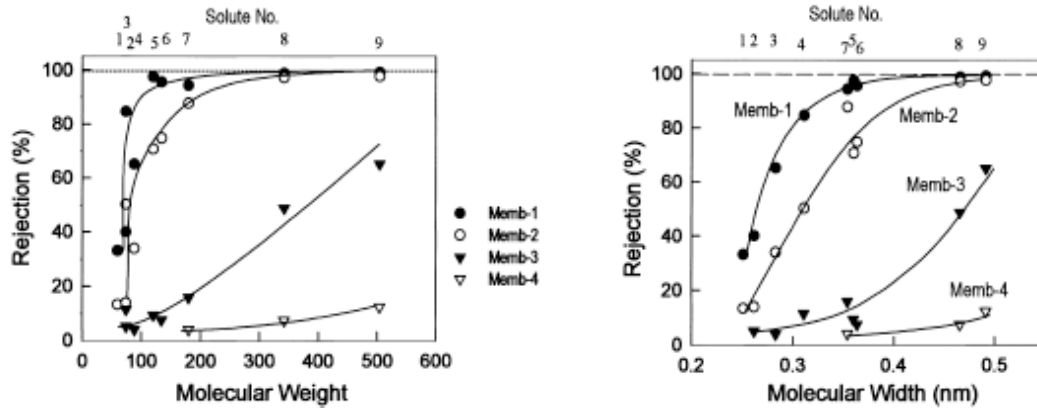


Figure 2.3. Rejection of sugars and alcohols as a function of molecular weight and molecular width.

Source: Kiso et al., 2001b

Past research has illustrated that the rejection of a limited class of compounds, mainly aliphatic alcohols and sugars, can be described well by molecular weight (Kiso et al., 2001b; Bellona, 2007). Figures 2.4 and 2.5 summarize the reflection coefficient for nine aliphatic compounds determined for the NF-4040 and NF-90 membranes and the model fit utilizing the cumulative density function. The reflection coefficient (σ) is defined as rejection at infinite pressure where convective transport dominates (Van der Bruggen and Vandecasteele, 2002). In general, the cumulative density function developed by using the molecular weight of a solute and MWCO of a membrane was found to adequately describe the reflection coefficient for these compounds.

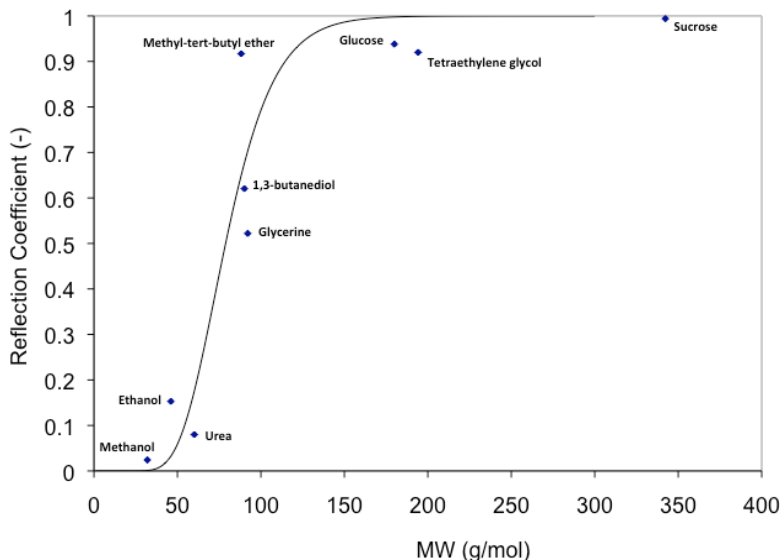


Figure 2.4. Reflection coefficient (real or observed rejection at infinite pressure, ~17-bar driving pressure during this study) of aliphatic sugars and alcohols for the NF-4040 membrane on bench scale (SEPA cell) at 19 °C and pH 6.3.

Note: The model line fit was developed by using the cumulative density function as proposed by Van der Bruggen and Vandecasteele (2002). The MWCO was found to be 190 Da.

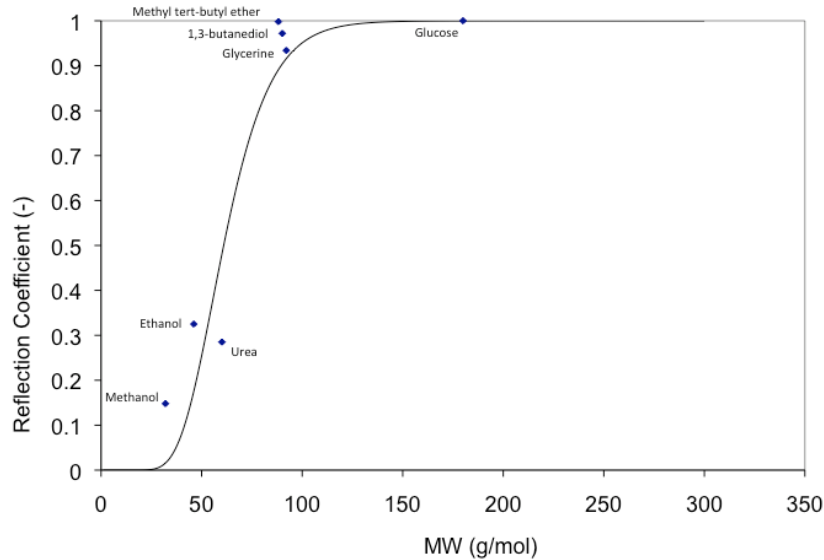


Figure 2.5. Reflection coefficient (real or observed rejection at infinite pressure, ~17-bar driving pressure during this study) of aliphatic sugars and alcohols for the NF-90 membrane on bench scale (SEPA cell) at 19 °C and pH 6.3.

Note: The model line fit was developed by using the cumulative density function as proposed by Van der Bruggen and Vandecasteele (2002). The MWCO was found to be 90 g/mol.

However, as pointed out by numerous researchers, molecular weight often fails to be an accurate descriptor for the rejection for a large number of compounds (Bellona, 2007; Kiso et al., 2001b; Nghiem et al., 2004). Nghiem et al. (2004) found that steroid hormones are rejected less often than would be expected on the basis of their molecular weights (Figure 2.6). Kiso et al. (2001b) found that molecular weight poorly describes the level of rejection for pesticides (Figure 2.7). A study funded by the Water Research Foundation determined that molecular weight was a poor descriptor for the rejection of phenyl urea pesticides (Hofman et al., 2007). Other size parameters have therefore been examined.

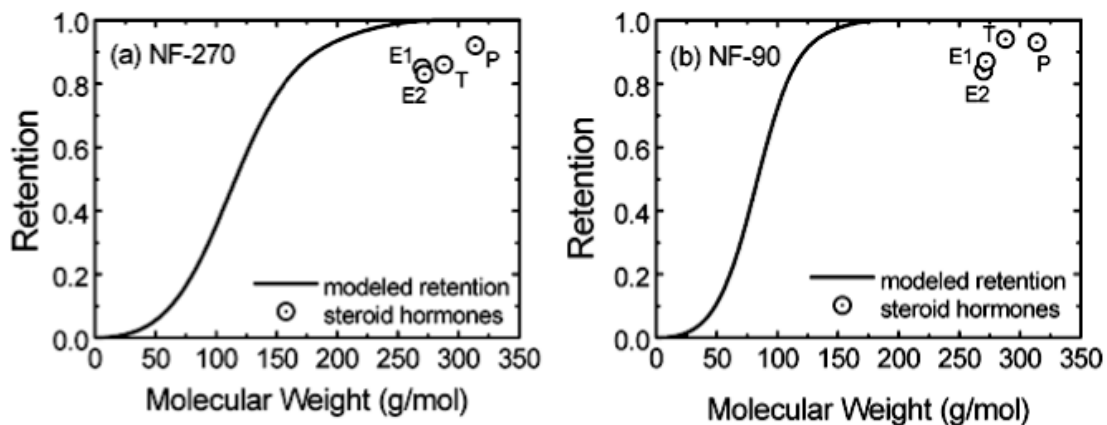


Figure 2.6. Experimental data for estradiol, estrone, testosterone, and progesterone for 2 NF membranes as compared to predicted retention as calculated by the hydrodynamic model.

Source: Nghiem et al., 2004.

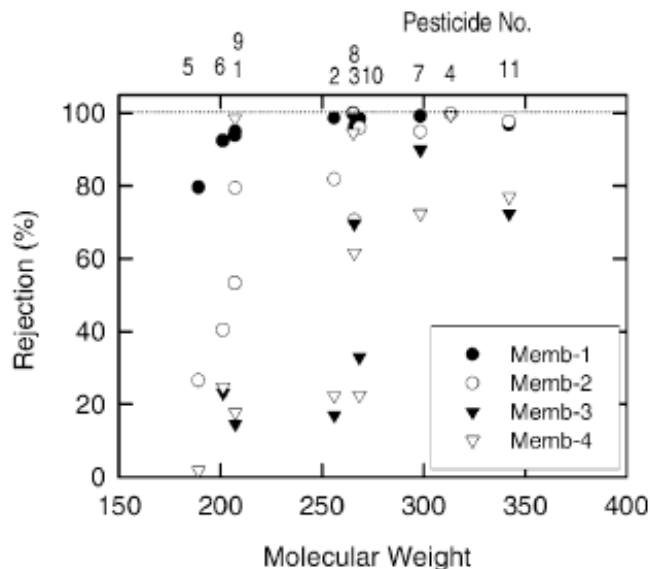


Figure 2.7. Rejection of pesticides versus molecular weight.

Source: Kiso et al., 2001b.

Molecular Size. The molecular weight of a compound is easy to determine but does not provide any information on the geometry of a molecule. To evaluate the effect of size on the rejection of certain solutes by NF, researchers have attempted to develop an easy yet effective way to describe the molecular characteristics of a molecule. Berg et al. (1997) determined that molecular structure, such as the number of methyl groups, may be an important parameter for predicting the rejection of noncharged molecules. Noncharged compounds with a higher number of methyl groups were reportedly rejected at higher levels than ones with lower numbers of methyl groups. Several studies confirmed that molecular size parameters, such as molecular width, Stokes radii, and molecular mean size (MMS), have been shown to be better predictors of steric hindrance effects upon the rejection of solutes by NF membranes than MW (Ozaki and Li, 2002; Berg et al., 1997; Kiso et al., 1992 and 2002; Bowen and Welfoot, 2002; Van der Bruggen et al., 1998; Kiso et al., 2001b). The Stokes radius has been used in molecular biology to characterize the size of proteins based on elution times through a chromatographic column. The Stokes radius according to Kiso et al. (1992) is determined by using the Stokes–Einstein equation:

$$r_s = \frac{kT}{6\pi\eta D_s} \quad (2.16)$$

where r_s is the molecular radius or Stokes radii (meters), D_s is the diffusion coefficient of the organic compound in water (meters²-seconds⁻¹), k is the Boltzmann constant (Joule-Kelvin⁻¹), T is the absolute temperature (Kelvin) and μ is viscosity of water (N-seconds-meters⁻²).

Calculating Diffusion Coefficients for Stokes Radius Calculation

Cussler (1997) reported that the most common basis for calculation of diffusion coefficients of solutes in liquids is given by the Stokes–Einstein equation (Equation 2.16) but that it is only accurate to 20%. The main limitation to the Stokes–Einstein equation is that it was developed for a system given by a rigid sphere in a solvent and that, when solutes become small or on the order of the size of water, the equation becomes increasingly less accurate

(Cussler, 1997). Because of this limitation, investigators have developed empirical correlations to obtain diffusion coefficients for small solutes. These include the Wilke–Chang correlation and Hayduk–Laudie correlation among the number of developed correlations. The diffusion coefficient can be calculated by the Wilke–Chang correlation given by

$$D_s = \frac{7.4 \times 10^{-8} (\phi M)^{0.5} T}{\eta_0 V_s^{0.6}} \quad D_s = \frac{7.4 \times 10^{-8} (\phi M)^{0.5} T}{\mu V_s^{0.6}} \quad (2.17)$$

where D_s is the diffusion coefficient, ϕ is an association factor for hydrogen bonding (set at 2.26 for water as the solvent), and M is the molecular weight of the solvent (grams/mole), T is the temperature, μ is viscosity of water (Newton-seconds-meters⁻²), and V_s is the molar volume of the solute. Delgado (2007) experimentally determined the diffusion coefficients of 2-naphthol, benzoic acid, salicylic acid, camphor, and cinnamic acid in water as a function of temperature and found that the Wilke–Chang correlation was an accurate means to predict diffusion coefficients.

Another method that has been favored for membrane applications is the Hayduk–Laudie correlation, which is given by

$$D_s = 13.26 \times 10^{-5} \cdot \mu^{-1.14} \cdot V_s^{-0.589} \quad (2.18)$$

Although these empirical correlations may lead to more-accurate diffusion coefficients, the molar volume of a solute must be determined, which can lead to another source of error depending on the method used. The most commonly used method is the La Bas molar volume method, which assigns molar volumes to atoms, ring structures, and functional groups. The LaBas molar volume is an estimated property according to the equation:

$$V'_B = \sum_i n_i \Delta V'_{B,i} \quad (2.19)$$

where $V'_{B,i}$ is the molar volume assigned to each substituent group and n represents the equivalent concentration. A list of the molar volumes assigned to various substituent groups is presented in Table 2.2.

Table 2.2. LaBas Molar Volume Increments

Atom	DV' _{B,i} (10 ⁶ m ³ /mol)	Atom	DV' _{B,i} (10 ⁶ m ³ /mol)
C	14.8	Br	27.0
H	3.7	Cl in R-CHCl-R'	24.6
O (except as below)	7.4	Cl in RCl	21.6
Carbonyl	7.4	F	8.7
Aldehyde, ketone	7.4	I	37.0
Methyl ether	9.9	S	25.6
Ethyl ester	9.9	P	27.0
Higher esters	9.9	Ring	
Higher ethers	9.9	3-membered	-6.0
Acids (-OH)	11.0	4-membered	-8.6
Joined to S, P, N	8.3	5-membered	-11.5
N Double bonded	15.6	6-membered	-15.0
Primary amine	10.5	Napthalene	-30.0
Secondary amine	12.0	Anthracene	-47.5

Source: Table adapted from Hofman et al., 2007.

Other Size Descriptors. Kiso et al. (2001a) reported that “the Stokes radius is a commonly used factor for the evaluation of the steric hindrance; however, the diffusivities to estimate Stokes radius cannot be obtained for many organic solutes.” In addition, the Stokes radius is based on the assumption that molecules are spherical and rigid, which is not always correct. Because Stokes radius calculations can be difficult for some molecules, other measures of molecular size have been developed.

STERIMOL parameters are used for determining the size of a molecule by utilizing molecular shape descriptors such as length and width (Kiso et al., 1992 and 2001a). Two studies by Kiso et al. (2000 and 2001a) compared the molecular widths of molecules calculated by using STERIMOL with the Stokes radius of the same molecules and reported a high correlation between the two. STERIMOL parameters consist of five measurements for a molecule; one length (L) measurement and four width measurements (B1 to B4) (Kiso et al., 2001a). Figure 2.8 demonstrates how these values are determined. The molecular length (L) is determined as the greatest distance between two atoms of the molecule and forms the L axis. The area of the rectangle (S) is the minimum area enclosed perpendicular to the L axis. Molecular width is defined as half the square root of the area of the rectangle. MMS is defined as half the length of the rectangle that has the same volume as a cylinder that encompasses the molecule lengthwise (Kiso et al., 2001a). Originally intended for pharmaceutical development, STERIMOL parameters have been applied in QSAR studies to assess the toxicological relevance of organic compounds (Verma and Hansch, 2007. Kiso et al. (1992) first applied STERIMOL parameters to organic solute removal with cellulose acetate RO membranes.

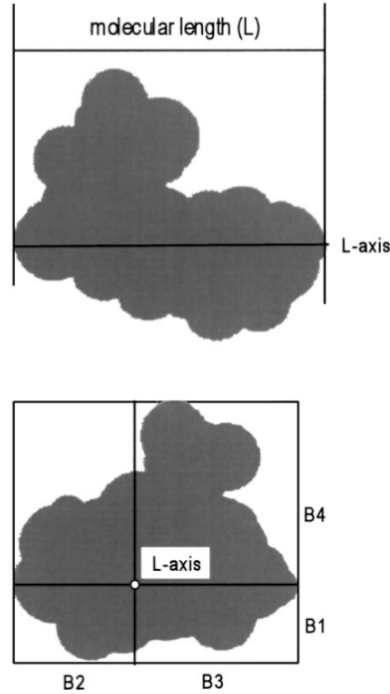


Figure 2.8. Molecular size parameters as determined for a nonspherical molecule.

Source: Kiso et al., 2001a

Another molecular size quantification developed in a manner similar to that of molecular width is the MMS (sometimes designated as W) of a molecule. The MMS is calculated by taking half of the length of the edge of the cube encompassing the molecule (Kiso et al., 2001b). Kiso et al. (2001b) demonstrated that MMS correlated better than molecular width with Stokes radii and could also be an effective measurement of molecular size. In their study, the molecular width and MMS were calculated for a variety of alcohols and saccharides and were evaluated as predictors for the rejection of these compounds by four NF membranes. For two other membranes examined in this study ($MWCO < 250$ Da), molecular width was found to be a better descriptor than MMS and especially better than molecular weight for the effects of steric hindrance on the rejection of alcohols and saccharides. Molecular width appeared to be a better predictor for rejection, especially for the tighter NF membranes.

Recently, a study performed by Zheng et al. (2009) compared different molecular size descriptors to the rejection of nonionic organic compounds. The researchers developed a new size descriptor, calculated mean size, which is a length parameter calculated with the smallest volume taken up by a molecule. The calculated mean size is determined by calculating the area and length of a molecule in three perpendicular planes and taking the cube root of the smallest volume obtained:

$$d_c = \sqrt[3]{\min\{S_{xy}L_z, S_{xz}L_y, S_{yz}L_x\}} \quad (2.20)$$

where S is the area of a molecule, L is length and d_c is the calculated mean size. The authors found that the calculated mean size was a significant improvement over the Stokes radius, molecular width, and molecular length as a descriptor for rejection.

Taylor et al. (2000) determined the molecular structure of pesticides with the Hyperchem software package. The free energy between the intramolecular interaction of the polymer and functional groups was used to calculate the structure, theoretical length, and volume of the pesticides. The pesticide length depended upon the orientation of view or view angle and represented the cross-sectional diameter due to structural rotation. The pesticide volume was defined as the volume of the rotated pesticide molecule. Taylor et al. (2000) concluded that, in conjunction with pore size distribution of a membrane, pesticide size and orientation determined the range of pesticide rejection by RO and NF membranes.

Recent research conducted by Bellona (2007) compared the MMS, Stokes radius, molecular width, and size parameters (length and width) calculated from molecular modeling software as size parameters for use in modeling exercises. The Stokes radius was found to be the best size descriptor for modeling steric exclusion for compounds spanning a wide range of sizes. Because the range of MMS and of molecular width was relatively narrow for the compounds evaluated, the model output (rejection) for all of the compounds was narrower than experimental rejection was found to be. In contrast, the Stokes radius was found to better represent the different sizes exhibited by the molecules and therefore the model output was more accurate (Bellona, 2007).

2.5 Rejection of Solutes with Membrane Interactions

As pointed out in the previous section, for neutral compounds, size often fails as a parameter to describe rejection. In many cases, the rejection of an organic solute is less than would be expected based on the size, and researchers have reported that certain compounds can adsorb to and partition through membrane materials (Kim et al., 2007; Nghiem et al., 2004; Williams et al., 1999). Besides the work of Williams et al. (1999), Matsuura and Sourirajan (1971), and a few others, very little work has been performed to determine the nature of these interactions and to find molecular descriptors to describe the strength of adsorption and propensity for lower-than-expected rejection (based on size). For example, researchers continue to compare rejection to a compound's partitioning coefficient $\text{Log } K_{ow}$ value (Braeken et al., 2005; Agenson et al., 2003), although there is an abundance of work demonstrating that only in certain cases does $\text{Log } K_{ow}$ correlate with rejection. Researchers such as Williams et al. (1999) have pointed out that there are likely two types of adsorption (i.e., specific and nonspecific) that have different impacts on rejection. Nonspecific adsorption arises as a result of hydrophobic or nonpolar compounds' preference for a membrane (often called lipophilicity), although specific adsorption refers to the ability of a molecule to form hydrogen bonds with the membrane sites that facilitate the transfer of water.

Although partitioning coefficients such as the $\text{Log } K_{ow}$ describes the tendency (or thermodynamic favorability) of a molecule to remain in water (as opposed to a lipophilic solvent such as octane,) they do not necessarily describe whether a solute can interact with membrane polymers. For example, Braeken et al. (2005) reported that, for compounds with molecular weight below the MWCO of a membrane, the greater the $\text{Log } K_{ow}$, the lower the rejection. However, other researchers have clearly demonstrated that compounds such as benzene with a relatively high $\text{Log } K_{ow}$ value (~ 2.2) are often significantly better rejected than solutes with smaller values such as phenol (~ 1.4). Additionally, because size is still a major factor in the rejection of these compounds, finding one descriptor to describe solute-membrane interactions and subsequently rejection is extremely difficult.

On the basis of past work, it appears that nonionic compounds with strong membrane interactions are the most likely to permeate a membrane. Therefore, elucidating the

mechanism by which these compounds can adsorb to membrane materials is integral to developing modeling approaches. On the basis of past research, it appears that it may be more important to identify the functional groups that result in membrane interactions than to correlate rejection to partitioning coefficients. Understanding how these interactions occur and where they occur on or in the membrane may assist in identifying more meaningful descriptors for solute–membrane interactions (McCallum et al., 2008).

2.5.1 Adsorption and Partitioning Through Membrane Materials

Williams et al. (1999) performed a study to investigate the adsorption of organic compounds to an RO membrane and quantify the subsequent effect on permeate flux rates. The researchers found that phenols and substituted phenols adsorbed strongly to membrane materials and significantly decreased the permeate flux of the membrane. Benzene was found to adsorb to membrane materials but had a very marginal effect on flux. The researchers hypothesized that the phenolic compounds specifically adsorb to the active sites of the membrane designed to transport water, which decreases the permeate flux (Figure 2.9). Benzene, which is nonpolar, adsorbed to the membrane, but the interaction was hydrophobic in nature as characterized by minimal permeate flux loss.

Ahmad and Tan (2004) reported results similar to those of the Williams et al. (1999) study for chlorophenol, nitrophenol, and phenol. The researchers found that, during experiments with these compounds, permeate flux declined significantly and that rejection was extremely low. They reported that the characteristics of a strong solute–membrane affinity system include a decrease in rejection when permeate flux increases, lower flux than that shown by pure water and that is not caused by osmotic effects, lower-than-expected rejection, possible negative rejection, and an increase in rejection with increasing feed water concentrations. The researchers state that “solute separation in reverse osmosis is generally governed by the hydrogen bonding ability of an organic molecule.”

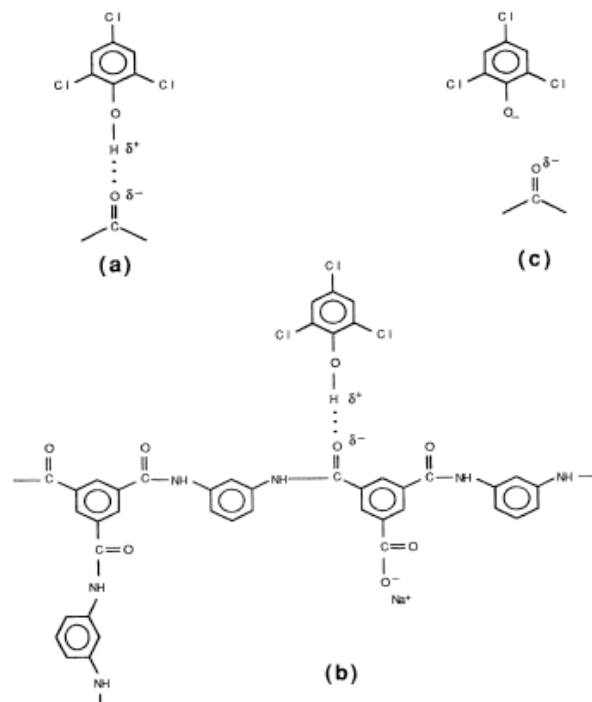


Figure 2.9. Hydrogen bond formation of trichlorophenol with the carbonyl group of a polyamide chain.

Source: Williams et al., 1999.

Hammett and Taft numbers have been proposed as steric parameters that can be used to describe molecular interactions with membrane polymer structures. Although the Hammett equation accounts for how field, inductive, and resonance effects influence reaction rates, the Taft equation also describes the steric effects of a substituent. On the basis of hydrogen bonding theory illustrated in Figure 2.9, Matsuura and Sourirajan (1971) attempted to develop correlations between rejection and molecular descriptors for a number of organic compounds. They hypothesized that, because Hammett and Taft numbers quantify the degree by which a compound “wants” to donate a proton, they could be used as potential indicators for hydrogen bond formation with the membrane. Matsuura and Sourirajan (1971) found that the more negative Hammett and Taft numbers fit well with greater rejection as these values indicated a decrease in hydrogen bond formation between the solute and membrane (Figure 2.10). Because Taft and Hammett numbers are difficult to calculate for a large number of organic compounds, the researchers eventually used a measure of the stretching of the OH bond in a solute as a measure of the proton donating ability (and hydrogen bond formation ability) of a solute. Generally, this parameter was found to correlate well with the compounds that were studied.

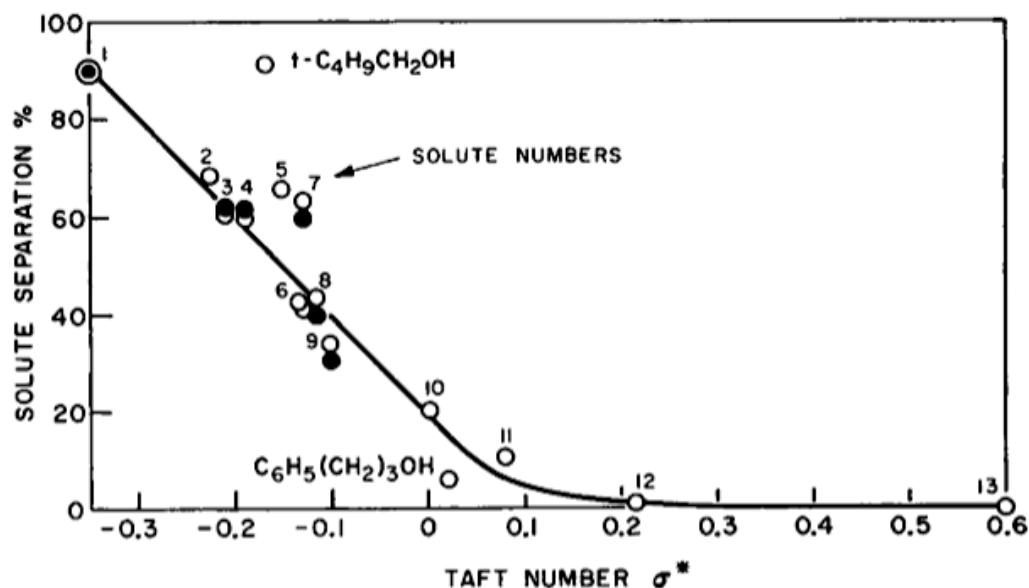


Figure 2.10. Relationship between Taft numbers and solute rejection.

Source: Matsuura and Sourirajan, 1971.

Although it is generally accepted that certain organic solutes interact with specific membrane active layer sites, there has been very little work investigating which types of compounds display this behavior and which ones do not. Nghiem et al. (2004) found that steroid hormones are rejected at lower concentrations than would be expected on the basis of their size. These compounds have aromatic rings with hydroxyl groups attached, which hypothetically make them capable of forming hydrogen bonds with membranes. Other compounds that have exhibited lower rejection than expected include bisphenol A (Nghiem et al., 2009), chloroform (Xu et al., 2006), triclosan (Bellona, 2007), and 2-naphthol (Kimura et al., 2003a). Compounds that have been listed as not adsorbing to membranes include dextrose, dioxane, erythritol, and xylose (Nghiem et al., 2004). In recent studies by Marts (2008) and Bellona (2007), certain aromatic organic compounds including carbamazepine and primidone were found to have behavior very similar to that of sugars and alcohols whose rejection depends mostly on size, although other aromatic organic compounds such as acetaminophen and phenacetine had much lower rejection than expected on the basis of size. Therefore, determining molecular descriptors that indicate whether a solute will interact strongly with the membrane is needed.

The dipole moment of a compound is another descriptor that has been used in studies as a potential indicator of solute-membrane interactions. Dipole moment values are representative of the polarity of a compound. In a study by Van der Bruggen et al. (1999), the dipole moment was found to correlate strongly with rejection of organic solutes. Van der Bruggen et al. (1999) argued that compounds with high dipole moment consistently have lower rejection values due to the interaction of the dipole with the membrane. Although this interaction may occur as Van der Bruggen et al. (1999) described, the rejection data show that compounds with lower dipole values may also have low rejection, suggesting that dipole moment may not be a very successful descriptor.

As previously discussed, a number of researchers have attempted to correlate $\text{Log } K_{ow}$ with rejection with the explanation that hydrophobic compounds adsorb to membranes (Braeken et al., 2005; Braeken et al., 2006; Agenson et al., 2003; Kiso et al., 2000). Braeken et al. (2005)

suggested a linear relationship between $\text{Log } K_{ow}$ and rejection by NF membranes for compounds with molecular weights below the MWCO of two NF membranes, the UTC-20 and the Desal-HL-51. The greater the $\text{Log } K_{ow}$ of the solute, the lower the rejection (Braeken et al., 2005; Figure 2.11). Braeken et al. (2005) indicated that this relationship also exists for compounds with molecular weights greater than the MWCO of the membrane. In a small sample of three compounds with similar molecular weights, estrone ($\text{Log } K_{ow}$: 3.43) and estradiol ($\text{Log } K_{ow}$: 3.94) demonstrated lower rejection values than salicine ($\text{Log } K_{ow}$: -1.41) in 15 h run times. Although $\text{Log } K_{ow}$ may reflect rejection behavior, as compound size increases, the $\text{Log } K_{ow}$ value is less influential in this behavior.

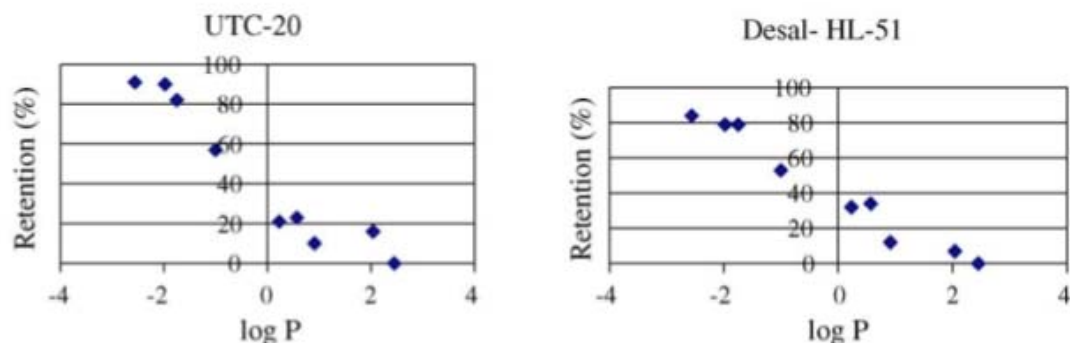


Figure 2.11. Rejection as a function of $\text{Log } P$ ($\text{Log } K_{ow}$) for organic solutes where $\text{MW} < \text{MWCO}$.

Source: Braeken et al., 2005.

Two studies by Kiso et al. (2000 and 2001b) reported on the rejection of hydrophobic pesticides by four flat-sheet Nitto Denko NF membranes (NTR-729HF, NTR-7250, NTR-7450, and NTR-7410). The researchers found that $\text{Log } K_{ow}$ was a good descriptor for the rejection of certain compounds but failed for other compounds (Figure 2.12). Kimura et al. (2003b) found no correlation between partitioning coefficients and the rejection of a number of endocrine disrupting compounds (EDCs) and pharmaceutically active compounds. Bellona (2007) found that the $\text{Log } K_{ow}$ could not be reliably used to determine what compounds are likely to exhibit strong solute-membrane interactions and have low removal. For example, chloroform ($\text{Log } K_{ow} = 2.97$), NDMA (-0.57), triclosan (5), 2-naphthol (2.7), and methylparaben (1.86) all displayed similar rejection by an NF membrane. On the basis of the specific-versus-nonspecific adsorption idea, the $\text{Log } K_{ow}$ does not directly quantify the degree by which a solute can interact with specific sites on a membrane. Although partitioning coefficients are related to polarity of a compound, they are often ambiguous; that is, two or more molecules could have the same $\text{Log } K_{ow}$ value but completely different structures, interactions with membrane materials, and rejection.

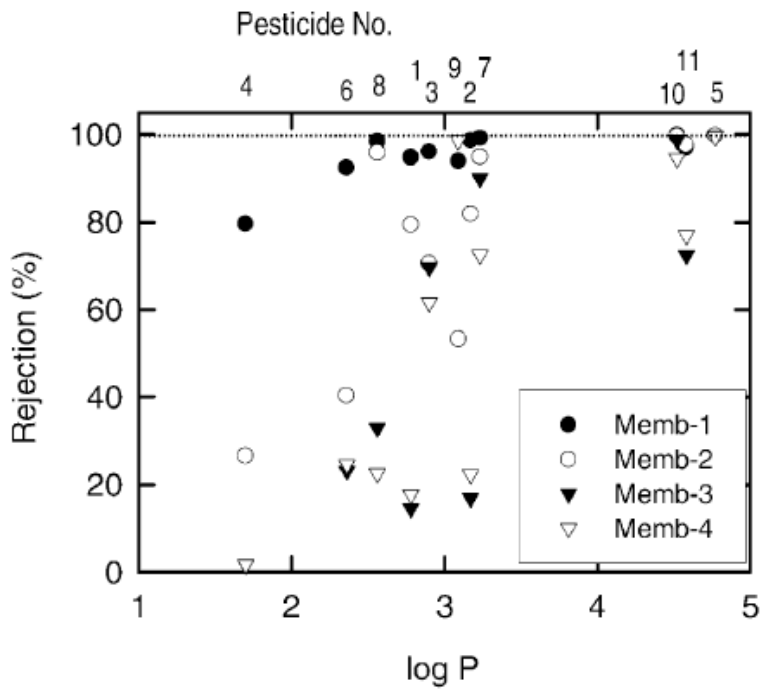
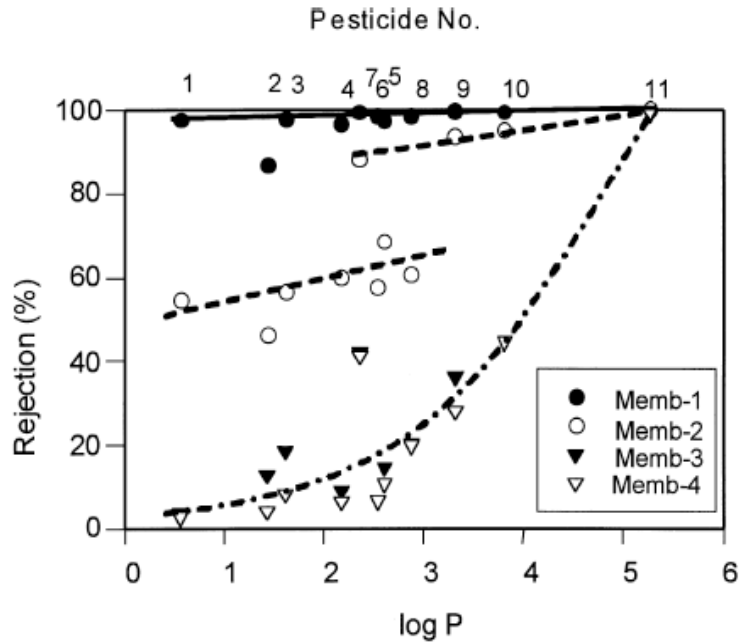


Figure 2.12. Log P (Log K_{ow}) versus rejection for 4 membranes.

Notes: Larger Log K_{ow} values also show higher rejection values that are not characteristic of behavior when using Log K_{ow} as a descriptor.

Source: Top figure: Kiso et al., 2003; bottom: Kiso et al., 2001b.

Similar to the idea behind the work of Matsuura and Sourirajan (1971), it may be more important to determine the relative contribution of functional groups on the adsorption and partitioning phenomenon. Employing compounds with different functional groups, Kiso et al. (2001a) demonstrated that polar groups within the compound had various effects upon the adsorption and that the effect of polar groups on adsorption decreases as follows: $-C(O)O^- > -CO^- > HCON > CH_3CON > -OH- > -O-$. In addition, when $\text{Log } K_{ow}$ values of similar compounds (e.g., monosubstituted benzenes) were compared to rejection, strong correlations were found indicating that specific chemical characteristics of compounds are more important.

According to the preferential sorption capillary flow model, rejection of organic solutes by a membrane is a two-step process (Matsuura and Sourirajan, 1971). First, the solute is adsorbed by the membrane. Subsequently, the solute passes through the membrane by diffusion and/or convection. Breakthrough concentrations are theorized to depend on the size of the compound relative to the pore size of the membrane, and compounds smaller than the pore size have been observed to permeate more freely (Duranceau et al., 1992; Nghiem and Schäfer, 2002; Nghiem et al., 2002a and 2002b; Schäfer et al., 2003). When membrane–solute interactions are strong; however, size exclusion becomes a much less valuable descriptor. Using the Hyperchem molecular modeling software to simulate the optimized molecular shape of each compound, Braeken et al. (2005) calculated the effective molecular diameter to compare compounds of similar molecular size. By comparing the effective diameter to rejection, Braeken et al. (2005) found that molecular size is a poor descriptor of expected rejection for compounds that can interact with membrane materials. For both of the membranes used in the study, UTC-20 (Toray Industries, Inc.) and Desal-HL-51 (Osmonics), xylose with the shortest calculated effective diameter (0.69 nm) had some of the highest rejection values, although compounds with much longer effective diameters, such as benzilidene acetone (0.99 nm) and 3,4-methylnitrophenol (0.82 nm), were among the compounds with the worst rejection.

McCallum et al. (2008) recently identified the site of adsorption to membrane materials to be within the polysulfone support layer. Ruining rejection experiments with the NE-70 membrane and a sample of unfinished NE-70 membrane, just the polysulfone support and nonwoven fabric backing, showed that the normalized concentration profiles of estradiol were nearly identical, suggesting that the polysulfone support layer as opposed to the active layer largely governs the non-steady-state breakthrough phenomenon. This finding stresses the need for a better understanding of both where solute–membrane interactions take place and how different functional groups of a solute may participate in these interactions. For compounds to adsorb to the support layer, however, they must be transported through the active layer, which appears to be governed by specific characteristics of compounds.

Observations from Pilot and Full Scale. Many of the compounds that have been detected in permeate samples during pilot- and full-scale membrane studies at water reuse facilities are nonionic solutes that are expected to have interactions with the membrane polymer because of their relative hydrophobicity and moieties that may cause specific adsorption (Table 2.1). These compounds include bisphenol A, chloroform, galaxolide, iopromide, oxybenzone, and TCEP. Compounds that are nonionic but have not been studied in terms of adsorption but have moieties that may interact with the membrane include diethyl-*m*-toulamide (DEET), caffeine, meprobamate, and pentoxifylline. As will be discussed in the modeling section, the rejection of these compounds is partially a function of their molecular size but also of the degree to which they interact with a membrane. The development of a predictive model, therefore, is hindered by the lack of understanding of the nature of solute–membrane interactions and of ways to quantify them.

2.5.2 Electric/Donnan and Dielectric Exclusion of Charged Solutes

For charged solutes, three removal mechanisms are generally accepted: size exclusion, electrostatic (or Donnan) exclusion, and dielectric exclusion (Bowen et al., 2004; Timmer 2001). Because of the charged nature of membranes, solutes with an opposite charge of the membrane are attracted to neutralize the membrane charge, although solutes with an opposite charge are repelled. This phenomenon is referred to as Donnan exclusion. Dielectric exclusion refers to the idea that water molecules within the membrane structure are polarized, which results in a decreased dielectric constant inside the pore, making it less favorable for charged solutes to enter. As pointed out by Timmer (2001), the mechanisms by which charged membranes remove charged solutes are a point of debate in the scientific community. What is generally accepted, however, is that charged organic solutes are removed at a relatively high level regardless of size (Bellona et al., 2008).

2.5.2.1 *Electrostatic Effects—Literature Review*

Electrostatic interactions between charged solutes and membranes have been frequently reported to be an important rejection mechanism (Tsuru et al., 1991a and 1991b; Wang et al., 2002; Duranceau et al., 1992; Wang et al., 1997; Bowen et al., 2002; Childress and Elimelech, 2000; Xu and Lebrun, 1999). RO and NF membranes are composed of a thin membrane skin that acts as the strainer and a thicker support layer underneath (Braghetta et al., 1997; Wang et al., 1997; Xu and Lebrun, 1999; Ariza et al., 2002). The membrane skin, for most thin-film composite membranes, carries a negative charge to minimize the adsorption of negatively charged foulants present in membrane feed waters and to increase the rejection of dissolved salts (Braghetta et al., 1997; Tsuru et al., 1991a and 1991b; Deshmukh and Childress, 2001; Xu and Lebrun, 1999; Shim et al., 2002). The negative charge on the membrane surface is usually caused by sulfonic and/or carboxylic acid groups that are deprotonated at neutral pH. Membrane surface charge is usually quantified by zeta potential measurements. Studies (Deshmukh and Childress, 2001; Childress and Elimelech, 2000; Xu and Lebrun, 1999; Tanninen and Nystrom, 2002) have determined that pH had an effect on the charge of a membrane because of the disassociation of functional groups. Zeta potentials for most membranes have been observed in many studies to become increasingly more negative as pH is increased and as functional groups deprotonate (Braghetta et al., 1997; Deshmukh and Childress, 2001; Hagemeyer and Gimbel, 1998; Lee et al., 2002; Ariza et al., 2002; Tanninen and Nystrom, 2002; Shim et al., 2002; Yoon et al., 2002).

Dissolved ion rejection by NF and RO membranes is heavily dependent on the membrane surface charge and therefore on feed water chemistry (Wang et al., 1997 and 2002; Hagemeyer and Gimbel, 1998; Childress and Elimelech, 2000; Xu and Lebrun, 1999; Yoon et al., 2002; Seidel et al., 2001; Bellona and Drewes, 2005; Kim et al., 2002). Ozaki et al. (2002) reported that the rejection of heavy metals by ULPRO membranes was positively correlated with the pH of the feed water. Yoon et al. (2002) performed a study investigating the transport of perchlorate through NF and UF membranes and reported that “perchlorate rejection by negatively charged NF and UF membranes was greater than expected based on only steric/size exclusions.” Researchers in this study also reported that the rejection of perchlorate increased with increasing pH and that the diffusive transport coefficient for perchlorate decreased as pH was increased. Increasing the pH increased the negative surface charge of the membrane as confirmed by others (Braghetta et al., 1997; Deshmukh and Childress, 2001; Lee et al., 2002; Tanninen and Nystrom, 2002; Ariza et al., 2002), which resulted in increased electrostatic exclusion of a negatively charged solute by a membrane. Conversely, it was

determined that the presence of counterions (Ca^{2+} and K^+) decreased the rejection of perchlorate.

This last finding is thought to be a result of two mechanisms. One explanation is that increasing ionic strength shields the surface charge of a membrane and is supported by previous studies where ions such as Na^+ , K^+ , Ca^{2+} , and Mg^{2+} in feed water reduced the negative zeta potential of a membrane (Braghetta et al., 1997; Deshmukh and Childress, 2001; Ariza et al., 2002; Shim et al., 2002). A decrease in surface charge would theoretically decrease electrostatic exclusion and the rejection of charged solutes. This is the explanation given by Nghiem et al. (2006) as to why ibuprofen and sulfamethoxazole rejection decreases with increasing ionic strength. Recent research by Bouranene et al. (2007) showed that increasing ionic strength decreases the hydrodynamic radius of organic solutes, which decreases exclusion from size and decreases rejection.

The second explanation is that ions in solution that can permeate a membrane affect the transport of other ions in solution. In 1924, Donnan published his classic paper on the theory of membrane equilibria, which presented an explanation to the “peculiar electrical and other effects which must occur in a system in which two solutions containing electrolytes are separated by a membrane which is freely permeable to most of the ions, but impermeable to at least one of them.” The main factor is that electroneutrality has to be maintained on both sides of a membrane and that, when one charged solute crosses the membrane, an oppositely charged species must cross the membrane. When a divalent ion crosses the membrane, two monovalent ions must cross to conserve electroneutrality. Chellam and Taylor (2001) observed that calcium rejection by two NF membranes increased by a factor of 2 (at all recoveries tested) for a 14-fold increase in sulfate concentrations. Charged functional groups attract ions of the opposite charge, inhibiting them from crossing the membrane (Chellam and Taylor, 2001). Counterions are also retained to preserve electroneutrality, and rejection for the counterion increases substantially. Ozaki et al. (2002) reported that, when divalent cations (Mg^{2+} and Ca^{2+}) were present in the feed water, the rejection of heavy metals decreased. It was hypothesized that the need to preserve electroneutrality across the membrane resulted in a lower rejection of metals. For organic solutes, the hypothesis is that adding salts overwhelms the charge of the membrane and the ability of the membrane to retain counterions, which leads to a breakthrough of both coions and counterions, including the charged organic compounds.

On basis of the previous discussion, it should be noted that operating conditions can have a significant effect on the rejection of charged species because of concentration polarization and “overwhelming” of the membrane charge.

Literature reporting on the effect of membrane surface charge on the rejection of charged organic compounds is not as abundant as studies on inorganic ion rejection. In fractionation experiments, Hu et al. (2003) and Schäfer et al. (2002a) found that low-molecular-weight acids had higher rejections by RO and UF membranes than did larger neutral organics because of electrostatic repulsion. In a study conducted by Berg et al. (1997), it was determined that charged organic solutes were rejected at higher levels than were noncharged organic compounds of the same size. Rejection experiments with the pesticide mecoprop in disassociated and undisassociated forms were performed with five different NF membranes. Mecoprop, in the disassociated form, was rejected at a higher rate than in the nondisassociated form by all five membranes at levels between 10 and 90%. Ozaki and Li (2002) performed a rejection experiment utilizing urea and acetic acid, both having the same molecular weight, at different pH ranges using an LPRO membrane (ES20; Nitto Denko).

Acetic acid is negatively charged at a pH of 4.8, although urea remains noncharged throughout the pH ranges (3–9) tested. Although the rejection of urea decreased slightly from 35 to 28%, the rejection of acetic acid increased from an initial value of 32% in the noncharged form at pH 3 to 100% in the negatively charged form at pH 9. The increase in the rejection of acetic acid as observed by Ozaki and Li (2002) and in mecoprop as reported by Berg et al. (1997) is most likely due to electrostatic repulsion at the membrane surface. The increase in the rejection of acetic acid at pH values above the pK_a for association (pK_a), is most likely caused by the increasing negative charge of the membrane repulsing the negatively charged acetic acid (Ozaki and Li, 2002).

Observations from Pilot and Full Scale. Drewes et al. (2007) investigated the organic compound removal efficiencies of 11 commercially available membranes on a spiral-wound membrane testing unit (Figure 2.13). Although the rejection of uncharged organic solutes was variable and depended on the molecule of interest and the membrane, the rejection of ionic trace organic compounds was greater than 90% for all compounds and membranes tested. As an example, Figure 2.13 presents the rejection of four negatively charged compounds of different size by a variety of RO, LPRO, and NF membranes.

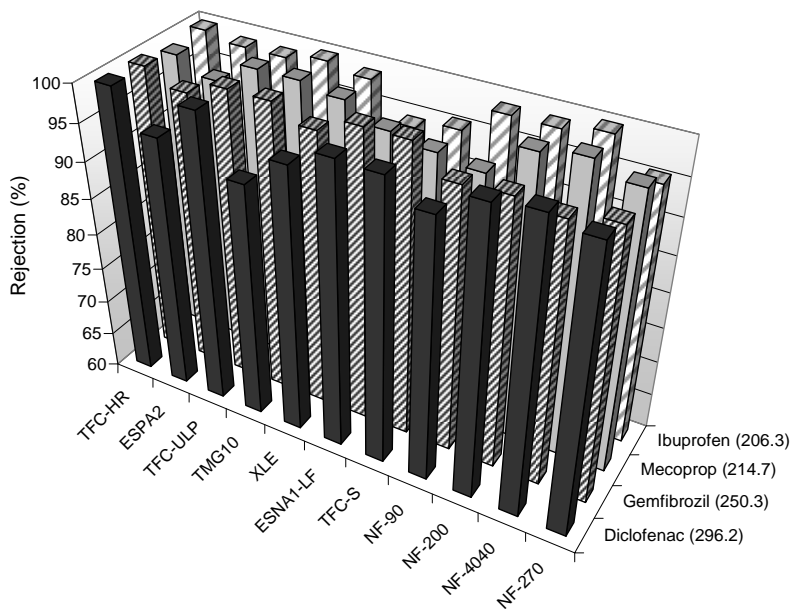


Figure 2.13. Summarized laboratory-scale candidate membrane rejection of nonionic (neutral) trace organic compounds (for 80% recovery and permeate flux rate of 20–24 L/m² h).

During pilot-scale and full-scale testing at two water reuse facilities, spiking experiments were conducted with samples collected for the analysis of a select number of pharmaceuticals and personal care products (PPCPs) and EDCs to determine removal efficiencies. In results similar to those of laboratory-scale testing, even a “loose” NF membrane (NF-4040) rejected >95% of the ionic trace organics that were spiked into the feed water (Figure 2.14).

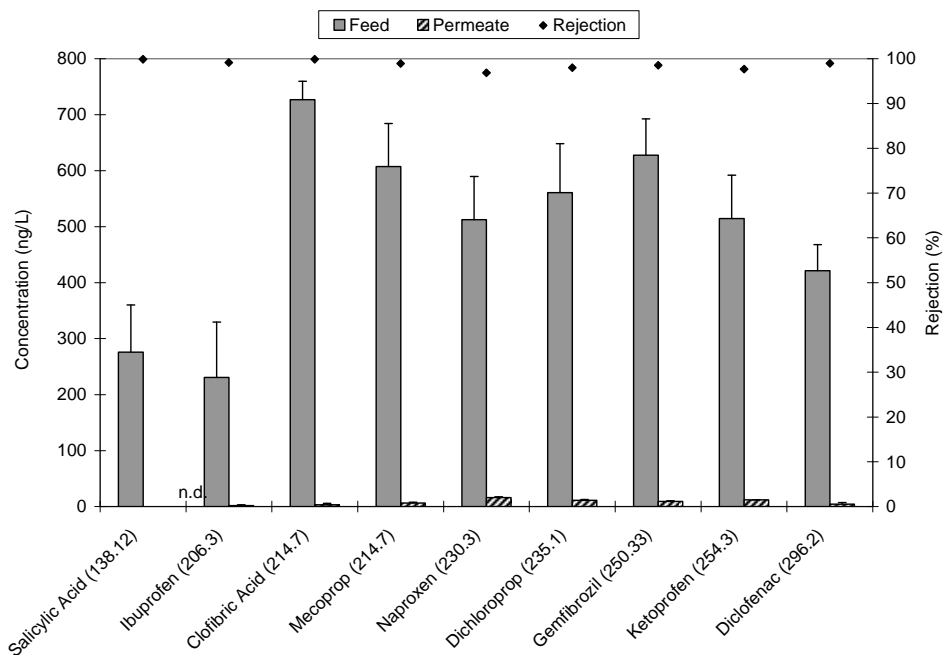


Figure 2.14. Spiked feed and permeate concentrations and subsequent rejection values of ionic trace organic contaminants (negatively charged, molecular weights in parentheses) during pilot-scale testing of the NF-4040 (spiking and sampling occurred at end of testing period).

Source: Bellona and Drewes, 2007.

There have been permeate detections of ionic organic contaminants (Table 2.1); however, the concentrations are generally quite low. From past research, it appears that most negatively charged organic contaminants are well removed regardless of their size. Therefore, developing complex models for these compounds may not be necessary.

2.6 Modeling

There has been considerable work over the last 40 to 50 years on modeling the rejection of charged (mainly salts) solutes by NF and RO membranes. Some of the earliest work was performed by Dresner (1971), Kedem and Katchalsky (1956), and Spiegler and Kedem (1966). More recently, research groups from Japan (Tsuru et al., 1991a; Wang et al., 1997) and the United Kingdom (Bowen) have put considerable effort into developing modeling approaches to describe the permeation of salts. These researchers have approached the problem utilizing fundamentally derived mass transfer models, including the Teorell–Meyers–Sievers (TMS) model, the Space Charge model, and the Extended Nernst–Planck (ENP) model among a few others. Other researchers have modified the surface force pore model (SFPM) (Jain and Gupta, 2004) and the solution–diffusion model (Williams et al., 1999) to account for solute–membrane interactions. The advantage to these models is that they are, for the most part, fundamentally derived. The major disadvantage is that they generally require numerical methods to solve and likely cannot be used as a predictive tool. In addition, many of these approaches would be extremely difficult to use on a larger-scale system than bench scale. The following sections discuss various modeling

approaches, but it is also worth noting that there are numerous other approaches that have been investigated as well.

2.6.1 Solution–Diffusion Model

The solution–diffusion model has been modified numerous times to account for a membrane system’s operational conditions and the mass transfer contribution from convective flux. Wijmans and Baker (1995) provide a good point of departure for the solution–diffusion model and its derivation. The solution–diffusion model defined by Wijmans and Baker (1995) is

$$J_s = \frac{D_j K_j}{\ell} (c_{j0} - c_{j\ell}) \quad (2.21)$$

where J_s is solute flux, D_j is the diffusion coefficient of solute j , K_j is the sorption coefficient of solute j , and ℓ is the membrane thickness. Researchers have modified the solution–diffusion model to account for the dependence of the concentration gradient on recovery (Zhao, 2004; Chellam and Taylor, 2001). The homogenous solution–diffusion model (HSDM) output of permeate concentration as a function of system recovery is given by

$$C_p = \frac{K_s C_f}{K_w (\Delta P - \Delta \Pi) \frac{2 - 2R}{2 - R} + K_s} \quad (2.22)$$

where K_s is solute MTC, K_w is the solvent (water) MTC, C_p is the permeate concentration, R is the system recovery, and ΔP and $\Delta \Pi$ are the driving and osmotic pressure differentials, respectively. Given a membrane system’s ΔP and $\Delta \Pi$, recovery, solvent MTC, and a solute’s MTC, the permeate concentration can be predicted.

Another derivation of the solution–diffusion model is the film theory diffusion model (FTM), which incorporated concentration polarization. The FTM is given by

$$C_p = \frac{C_f K_s e^{\frac{F_w}{k_b}}}{K_w (\Delta P - \Delta \pi) \left(\frac{2 - 2R}{2 - R} \right) + K_s e^{\frac{F_w}{k_b}}} \quad (2.23)$$

where F_w is the water flux through the membrane (often given as J_v) and k_b is the back-diffusion MTC as defined in Equation 2.13 (as K in Equation 2.13). Other modifications to the FTM have included correction terms for the solute MTC that are based on recovery and flux (Zhao, 2004).

The solution–diffusion model assumes that the transport of a solute across a membrane is due to diffusion through the membrane polymer. As discussed previously, it is commonly accepted for NF and a lesser extent for LPRO that mass transport occurs both by diffusion through the membrane material (solid-phase diffusion) as well as diffusion and convection through a membrane pore. The advantage of the solution–diffusion model is that it requires one parameter for a solute, K_s , to predict rejection.

A modified solution–diffusion model to include convective and diffusive hindrance factors was reported by Hofman et al. (2007) to be developed on the basis of work developed by Taylor et al. (1996) and is given by

$$R_i = \frac{1 - K_{c,i}}{1 + \frac{K_{s,i}}{K_w(\Delta P_i - \Delta \Pi_i)} \left(\frac{2 - R}{2(1 - R)} \right) + K_{c,i} \left(\frac{R}{2(1 - R)} \right)} \quad (2.24)$$

where R_i is the rejection of solute species i , $K_{c,i}$ is a convective hindrance factor, $K_{d,i}$ is the coefficient for hindered diffusive transport through pores, R is recovery, and K_s is the solid-phase diffusion parameter. Although this model may be fundamentally sound, in order to apply it, three independent solute MTCs must be known. Hofman et al. (2007) attempted to correlate the MTCs to the ratio between solute and pore size as reported by Deen (1987) and Bowen et al. (2002); however, no model verification was reported.

Over the past 2 decades, a few researchers have used the solution–diffusion modeling approach to model charged solutes, namely, salts (Chellam and Taylor, 2001; Zhao, 2004). To develop a predictive model, the solute MTC needs to be correlated to a solute parameter. Zhao (2004) developed an exponential relationship between the charge number of a salt and the MTC as shown in Figure 2.15. Once the MTC is known, the HSDM can be used.

One advantage to solution–diffusion models, such as the HSDM, is that one solute parameter is needed that could encompass solute properties if correlations can be made between solute properties and MTCs. As pointed out previously, however, the transport of solutes through NF and possibly LPRO membranes is thought to be a combination of diffusion and convection. Solution–diffusion models may be limited to certain RO membranes. For these membranes, the solution–diffusion model will likely be one of the best options because operational conditions such as recovery are considered.

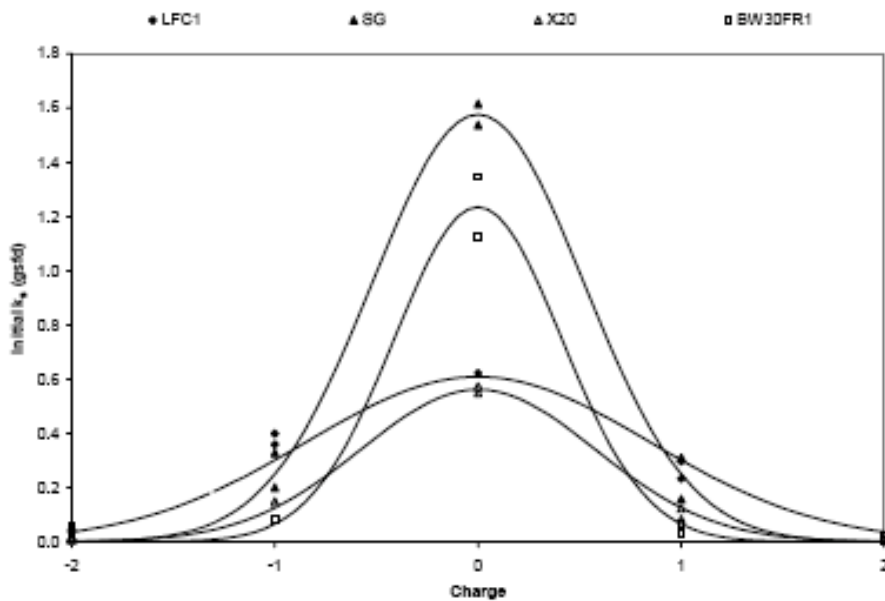


Figure 2.15. Modeling the MTC for salts based on the charge number of the salt.

Source: Zhao, 2004.

2.6.2 Hydrodynamic Model

The hydrodynamic model is commonly used to describe the rejection of uncharged solutes, primarily to characterize the pore size of a given membrane, and detailed descriptions of the derivation and application can be found in numerous publications (Bowen et al., 2004; Santos et al., 2006; Yoon and Lueptow, 2005). The major equations used to employ the hydrodynamic model are presented in Figure 2.16. The model is comprised of two components, hindered convection and hindered diffusion of a solute, to describe the transport of molecules through pore structures considered to be cylinders (Equation 2.25). Partitioning within a membrane pore on the feed and permeate sides of the membrane is given by Equations 2.26a and 2.26b, respectively, where the solute partitioning coefficient (Φ) is a function (Equation 2.27) of the ratio between the hypothetical pore radius and the solute radius (λ , Equation 2.28). By assuming a parabolic profile of the Hagen–Poiseuille type, the solute hindrance factors for convection and diffusion are given by Equations 2.29 and 2.30 (Bowen et al., 1997), although other researchers have proposed other functions to describe solute hindrance (Bouranene et al., 2007; Deen, 1987). Bowen et al. (2002) showed that the introduction of the Peclet number and the inclusion of the Hagen–Poiseuille definition of pore solvent velocity (Equation 2.31) erased the need for the extra fitting parameter, namely, membrane thickness, and allowed for a center line approach for calculating hindrance factors using Equations 2.29 and 2.30. Rearranging and integrating Equation 2.25 yield Equations 2.32 and 2.33, which describe the ratio between the bulk feed and permeate concentrations and rejection, respectively.

Hydrodynamic Model Equations

$$j_i = -K_{i,d} D_{i,m} \frac{dc_i}{dx_i} + K_{i,c} c_i V \quad (2.25)$$

$$c_f = \Phi C_f \quad c_p = \Phi C_p \quad (2.26a, 2.26b)$$

$$\Phi = (1 - \lambda)^2 \quad (2.27)$$

$$\lambda = \frac{r_s}{r_p} \quad (2.28)$$

$$K_c = (2 - \Phi)(1.0 + 0.054\lambda - 0.988\lambda^2 + 0.441\lambda^3) \quad (2.29)$$

$$K_d = 1.0 - 2.3\lambda - 1.154\lambda^2 + 0.224\lambda^3 \quad (2.30)$$

$$Pe = \frac{K_{d,r} \Delta P_c}{8D_p \eta_0} \quad (2.31)$$

$$\frac{C_p}{C_f} = \frac{\Phi K_c}{1 - [1 - \Phi K_c] \exp(-Pe)} \quad (2.32)$$

$$R = 1 - \frac{\Phi K_c}{1 - [1 - \Phi K_c] \exp(-Pe)} \quad (2.33)$$

Figure 2.16. Equations for the hydrodynamic model.

The hydrodynamic model output is mainly dependent upon λ , the ratio between a solute's size and the membrane's pore size. Choosing a size parameter that effectively captures a solute's geometry, therefore, is essential for model development, and numerous studies have attempted to determine the best size parameters that correlate with rejection (see previous discussion on molecular size). The often unsatisfactory result of these rejection/molecular size correlations have been explained by two main schools of thought: (a) that an effective molecular size descriptor is elusive (Santos et al., 2006; Zheng et al., 2009 and/or (b) that physicochemical properties other than size strongly affect rejection (Nghiem et al., 2004). Because the hydrodynamic model requires a chosen molecular size parameter, as a predictive measure, the model output is generally poor when compared to experimental results. As an example, the rejection of two pharmaceutically active compounds, acetaminophen and phenacetine, by the NF membrane as determined experimentally and modeled by using the hydrodynamic model and the Stokes radius is presented in Figure 2.17. In the case of both molecules, rejection is overestimated by the hydrodynamic model, and the output is unsatisfactory as a predictive measurement. The hydrodynamic model fails as a predictive tool either because the Stokes radius is ineffective in describing a solute's size or because physicochemical properties of the solutes and resulting solute–membrane interactions affect rejection or both.

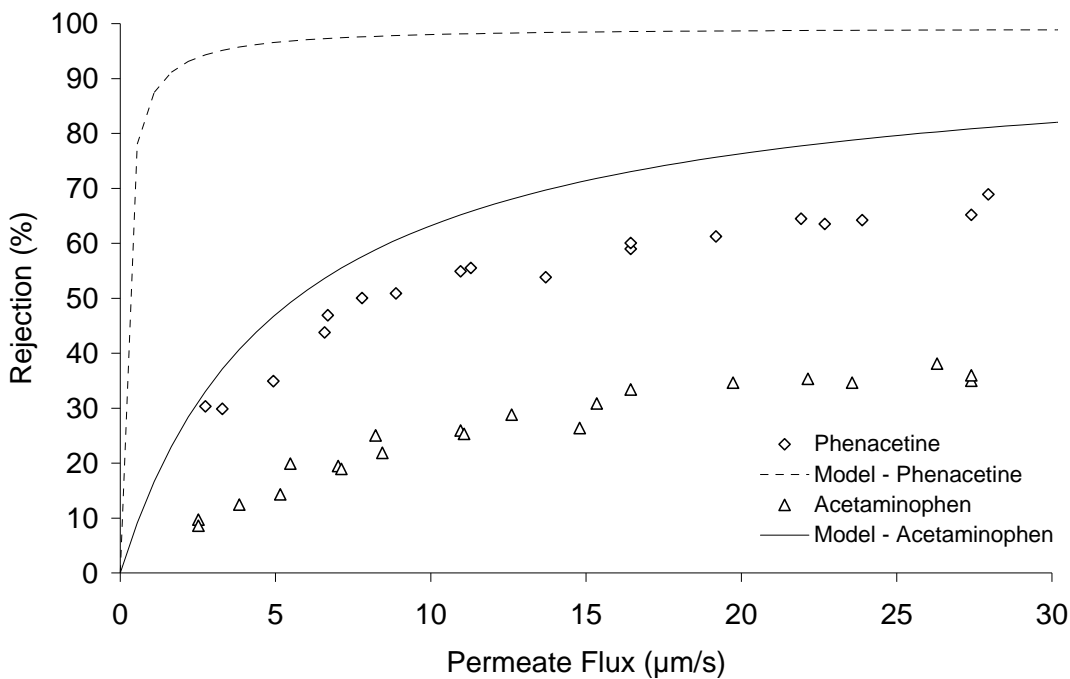


Figure 2.17. Rejection of phenacetine and acetaminophen by NF membrane.

Note: Model lines determined by using the hydrodynamic model and the solute's Stokes radius.

There are many cases where the hydrodynamic model was found to accurately predict the rejection of neutral compounds by NF membranes on the bench scale, but there are many cases where the model significantly overpredicts rejection (Bellona, 2007). It appears that the model can be applied to compounds where size exclusion is the dominant rejection mechanism. However, when solute–membrane interactions become important, size exclusion

models fail. The difficulty in solving this problem is determining, a priori, which compounds are expected to have minimal solute–membrane interactions. It is also worth noting that there has been little work applying these models to pilot- and full-scale systems.

2.6.3 Phenomenological Model and Pore Size Distribution Approach

The main equations for the Spiegler–Kedem, phenomenological, or irreversible thermodynamic model are presented in Figure 2.18. The basic phenomenological transport equation (Equation 2.34) is nearly identical to Equation 2.25 of the hydrodynamic model except that hindrance factors for diffusion and convection are replaced by coefficients that encompass general properties of the solute and membrane. In this way the phenomenological model has been considered a “black box” approach, because the solute permeability (P) and reflection coefficient (σ) are fitting parameters that only generally capture the properties and interactions of a given membrane and solute. In addition, the phenomenological approach has generally been limited to the modeling of solution–diffusion processes because other mechanisms and elements of rejection (i.e., pore size, pore size distribution, and hydrodynamic hindrance) are difficult to capture within the phenomenological coefficients. Van der Bruggen and Vandecasteele (2002) circumvented this problem in the application of the phenomenological model to describe organic solute rejection by NF membranes by calculating the reflection coefficient based on the pore size and pore size distribution of the membrane and the size of a solute.

If one rearranges Equations 2.34 and 2.35, the rejection of a given solute by a given membrane can be calculated by using Equations 2.36 and 2.37. The permeability coefficient (P) for a given solute is related to the diffusion parameter for a particular compound and the thickness of a membrane and through rearranging can be calculated from Equation 2.38, where the diffusion parameter (ρ) is membrane specific (Van der Bruggen and Vandecasteele, 2002). Van der Bruggen and Vandecasteele (2002) applied a Log-normal distribution for the determination of the reflection coefficient using the average pore size of the membrane, the standard deviation of pore size, and solute size. This method assumes that each pore will reject or pass the solute depending on the size of the solute in relation to the pore size (e.g., each pore has a reflection coefficient of 1 or 0). When all the pores in the membrane are combined, the reflection coefficient is the percentage of pores small enough to reject the solute (Kargol, 2001). The reflection coefficient can be expressed in terms of the probability density function [$P(x)$, Equation 2.39] or cumulative density function [$D(x)$, Equation 2.40].

To use the probability or cumulative density function to calculate the reflection coefficient for a given membrane, the parameters average pore size (r) and standard deviation of pore sizes (S_p) must first be known. These parameters are determined by performing rejection experiments for several solutes with different sizes. The reflection coefficient of a given compound is the maximum or limiting rejection at infinite pressure, where only convective transport occurs. Rejection experiments, therefore, are performed at pressures great enough to estimate the reflection coefficient for a number of compounds. Equations 2.39 and 2.40 can then be fitted to the reflection coefficient versus solute size curve by manipulating the average pore size and standard deviation of pore sizes to achieve the best fit.

Phenomenological (Spiegler-Kedem) Model Equations

$$J_v = -P\Delta x \frac{dc}{dx} + (1 - \sigma)J_v c \quad (2.34)$$

$$J_v = L_p (\Delta P - \sigma \Delta \Pi) \quad (2.35)$$

$$R = \frac{\sigma(1 - F)}{1 - \sigma F} \quad (2.36)$$

$$F = \exp\left(-\frac{1 - \sigma}{P} J_v\right) \quad (2.37)$$

$$P_v = \frac{\rho}{d_v} \quad (2.38)$$

Spiegler-Kedem Pore Size Determination

$$P(x) = \frac{1}{S_p \sqrt{2\pi}} \frac{1}{r} \exp\left[-\frac{\left(\ln(r) - \ln(\bar{r})\right)^2}{2S_p^2}\right] \quad (2.39)$$

$$D(x) = \frac{1}{2} \left[1 + \operatorname{erf}\left(\frac{\ln(r) - \ln(\bar{r})}{S_p \sqrt{2}}\right) \right] \quad (2.40)$$

Figure 2.18. Equations for the phenomenological and pore size distribution model.

The greatest difficulty in developing the phenomenological model is determining the reflection coefficient and diffusion parameter for a wide variety of organic solutes. In work performed by Bellona (2007), the diffusion parameter (ρ) was not found to be membrane dependent as was claimed by Van der Bruggen and Vandecasteele (2001). Instead, it appeared that the permeability constant could be calculated directly from a molecule's size by using an empirical regression. In addition, determining the reflection coefficient by using the cumulative density function with a solute's size and the membrane effective pore size was found accurate only for sugars and alcohols. Computing the reflection coefficient for the aromatic compounds studied yielded a model output that overpredicted rejection, similar to the hydrodynamic model.

The phenomenological model presented earlier uses a pore size distribution approach to calculate the reflection coefficient. However, the reflection coefficient could be based on any solute property as long as statistical correlations were developed. This approach is often called a "black box approach" because the diffusion parameter and reflection coefficient incorporate all of the fundamental interactions between the solute and membrane, which are

not considered explicitly. Therefore, the phenomenological model presents a mass transport approach that could be developed into a “hybrid model” that incorporates solute properties other than size into the reflection coefficient (σ) and diffusion or permeability coefficient (P).

2.6.4 Extended Nernst–Planck Equation

The successful implementation of the ENP equation to describe and/or predict the transport of solutes, mostly salts, across a membrane has been detailed in numerous papers (Tsuru et al., 1991a and 1991b; Dresner, 1971; Hagemeyer and Gimbel, 1998; Bowen and Mukhtar, 1996). The ENP equation has been favorably applied to membrane modeling, because it introduces solute transport due to solvent volume flux as well as diffusive transport due to concentration and electrical potential gradients (Dresner, 1971; Tsuru, 1991a; Bowen and Mukhtar, 1996). The ENP equation is given by

$$j_i = -D_{i,p} \frac{dc_i}{dx} - \frac{z_i c_i D_{i,p}}{RT} F \frac{d\Psi}{dx} + K_{i,c} c_i V \quad (2.41)$$

where $D_{i,p}$ is the diffusion coefficient of a solute in a pore, z_i is the valence of the ion, R is the ideal gas constant, T is the temperature, F is the Faraday constant, Ψ is electric potential, $K_{i,c}$ is the hindrance factor for convection, and V is the solute velocity.

The ENP equation coupled with the TMS assumption, which includes electroneutrality equations, null-current conditions, Donnan ion partitioning equations, and volumetric flux equations was used to describe the transport of salts within and through a membrane (Dresner et al., 1971; Tsuru et al., 1991b; Hagemeyer and Gimbel, 1998; Bowen and Mukhtar, 1996). Bowen and Mukhtar (1996) proposed a hybrid model, termed the Donnan steric pore model (DSPM), which allowed for the treatment of a membrane as porous through the use of diffusive and convective hindrance factors. The major advantages of the DSPM are the use of structural and electrical properties of a membrane for use in describing solute transport. Many recent studies investigating the transport of salts through membranes have employed and/or built upon the DSPM, thus demonstrating the applicability of this approach to describe fundamental mass transfer processes during membrane separations (Hagemeyer and Gimbel, 1998; Bowen and Welfoot, 2002a; Bowen et al., 1997; Bowen and Mohammad, 1998; Bandini and Vezzani, 2003; Lee and Lueptow, 2001). The DSPM has also been applied to describe the transport of uncharged solutes through membranes, although the use of the DSPM for this purpose has been generally limited to the characterization of a membrane in terms of pore size (Santos et al., 2006; Bowen et al., 2002; Bowen et al., 1997).

The greatest limitation of the DSPM as pointed out in Bowen et al. (2002) and in Bandini and Vezzani (2003) is the complex fitting procedures that require extensive iterations and experimentation to characterize the membrane. In addition, the DSPM has mainly been used to either (a) describe the separation of salt mixtures by NF and RO membranes or (b) optimize the separation of individual components of salt/organic dye mixtures. In the case of municipal water reclamation projects, where the prediction of ionic and nonionic organic solutes would be greatly beneficial, the utilization of the full DSPM is hindered by its complexity and the limited range for which it has been used.

Recently, Bowen et al. (2002) and Bandini and Vezzani (2003) put forth linearized versions of the DSPM called the linearized DSPM and DSPM&DE, respectively. In both cases the use of electroneutrality conditions and linearized concentration gradients transforms the differential transport equations into a set of algebraic equations that are subsequently shown

to effectively describe the separation of binary and ternary salt mixtures by NF membranes. The separation of a quaternary mixture of salts and organics was later shown to be satisfactorily described by the linearized version of the DSPM (Bowen et al., 2004). The main advantage of the linearized approach is the relative rapidity of the computations required to solve the equations and the inclusion of dielectric exclusion as a rejection mechanism.

2.6.5 Other Mass Transfer Models

There have been a few studies that have used the SFPM and a modified solution–diffusion model to incorporate solute–membrane interactions. Williams et al. (1999) uses a modified solution–diffusion model (steady state) and diffusion–adsorption model (non-steady state) to describe transport of benzene and substituted phenols through RO and NF membranes. The modified solution–diffusion model as described by Williams et al. (1999) is expressed as

$$J_s = \frac{D_{sm} C_{tm}}{\delta} \left(\frac{b_0 C_F}{1 + b_0 C_F} - \frac{b_0 C_P}{1 + b_0 C_P} \right) = B^* \left(\frac{b_0 C_F}{1 + b_0 C_F} - \frac{b_0 C_P}{1 + b_0 C_P} \right) \quad (2.42)$$

where J_s is solute flux, C_F is feed concentration, C_P is permeate concentration, B^* is the solute permeability constant, D is the diffusion coefficient of the solute in the membrane, C_{tm} is the total concentration in the membrane, δ is a distance parameter, and b_o is a coefficient of for concentration polarization. Given that the concentration is changing because of adsorption, the actual concentration gradient (including what is adsorbed to the membrane) needs to be calculated:

$$\frac{dC_c}{dt} = \frac{A_m J_w C_c - A_m J_w C_P - \frac{dQ_{tm}}{dt}}{V_F(1 - r)} \quad (2.43)$$

where Q_{tm}/dt is the total solute adsorbed by the membrane as a function of time (adsorption rate), dC_c/dt is the feed concentration change as a function of time, J_w is water flux, A_m is membrane permeability, and V_F is the molar volume of water. This model was developed to describe the effect of adsorption on flux and can be used to model the initial decline in rejection as solutes adsorb to the membrane. Researchers have shown, however, that equilibrium is reached within 1 to 3 days and that, therefore, other models can be applied to model the steady-state rejection without capturing the nonequilibrium portion of the rejection curve.

Mehdizadeh and Dickson (1991) applied a modified version of the SFPM to describe the rejection of solutes with strong membrane interactions. This approach is basically a system of differential equations describing the forces exerted on a solute by a membrane and the solvent. Jain and Gupta (2004) applied this model to a system composed of sodium and chloride and sodium sulfate and found that the model output was very similar to the phenomenological model described earlier. The SFPM, however, consisted of six independent fitting parameters and required a very sophisticated numerical technique to solve. It should be noted that, because the goal of the project is to develop predictive models for full-scale membrane systems, models requiring numerical techniques to solve may not be appropriate. The advantage to these models is that the fitting parameters represent the

interactions between the solute and membrane, which allows for an investigation into the fundamental aspects of mass transfer.

2.6.6 Quantitative Structure Activity Relationship Models

Although advancements have been made in the science of membrane modeling, additional research is needed to develop quantitative models capable of predicting the removal of solutes with a wide range of molecular structures and physicochemical properties. Previous research has demonstrated that the rejection of nonionic organic solutes can be described by using the ratio between solute size and effective pore size (Van der Bruggen and Vandecasteele, 2002; Nghiem et al., 2004). However, because rejection is also strongly dependent upon solute and membrane properties (e.g., hydrophobicity and polarity) and interactions (e.g., adsorption and hydrogen bonding), this approach is often limited in predictive power (Kiso et al., 1992; Bellona et al., 2004; Ng and Elimelech, 2004). In addition, membrane models based on the ratio between solute and pore size often fail to yield accurate predictions because of the difficulty in selecting an appropriate solute size parameter and/or because a universal determination of solute size does not exist (Oedekoven, 2005; Kiso et al., 1992; Santos et al., 2006).

Although the rejection of a limited number of nonionic organic solutes has been successfully predicted using the hydrodynamic model and phenomenological model, limited work has focused on incorporating solute properties other than molecular size into the model, which would allow for predictions of a broader class of compounds (Van der Bruggen and Vandecasteele, 2002; Nghiem et al., 2004; Bellona et al., 2004).

One method of incorporating molecular properties into the prediction of solute rejection by RO and NF membranes has been the development of QSARs and quantitative structure property relationships (QSPRs). The concept behind QSAR and QSPR analysis is to mathematically quantify the correlations between an activity or property (e.g., reactivity, phase partitioning, and membrane transport) and molecular descriptors. Once a correlation is found, the activity or property can be predicted from molecular descriptors. The first step in a generalized QSAR approach is determining activity data (e.g., rejection) for a number of compounds that are used as a “training set” for QSAR model development. The second step involves the calculation of suitable molecular descriptors for the “training set” that influence the removal mechanisms. The third step is the application of statistical methods (multiple linear regression models, partial least squares [PLS], etc.) to derive correlations between the activity data and the molecular descriptors generated for the training set.

A few studies have investigated the use of QSAR as a tool for predicting the rejection of trace organic contaminants by RO and NF membranes. Agenson et al. (2003) developed a QSAR approach to model the rejection of volatile organic compounds by employing empirical equations incorporating molecular size parameters and octanol–water partitioning coefficients to predict rejection. Rodriguez et al. (2004) examined endocrine disruptors, antibiotics, pesticides, and neuroactive drugs and developed QSAR models for predicting their passage through, adsorption to, and rejection by RO membranes. Recently, this work was published by Libotean et al. (2008).

Although these empirical models are membrane and water matrix dependent and did not incorporate relevant parameters commonly used in membrane models, such as solvent volume flux (including hydraulic pressure gradients and solvent viscosity), membrane pore size, and resulting transport due to convective and diffusive flux, they are relatively simple.

One major limitation to the previously discussed mass transport models is their complexity, especially when considering large-scale systems such as pilot- and full-scale membrane installations. For example, the DSPM used for charged solutes, although fundamentally derived, is generally limited to a ternary system because of the numerical techniques required to solve the equations. This model could never be practically applied to natural waters.

Our research team, therefore, believes that the development of robust QSPR models is needed for simple predictions of the likelihood that a compound could permeate an RO or NF system. Besides the Rodriguez et al. (2004) study, there has been little work developing QSPR models that included solute descriptors other than size, Log K_{ow} , dipole moment, and pK_a . As was previously mentioned, these descriptors often fail to describe rejection. One major goal of this study was to investigate a wide range of descriptors and develop new unambiguous descriptors for membrane QSAR models.

2.6.7 Empirical Models

A simple, yet mostly effective modeling approach developed by Bellona et al. (2004) uses a decision diagram to determine an estimation of rejection based on solute and membrane properties. A revised version of the “rejection diagram” is presented in Figure 2.19. By moving through the diagram, one encounters several possible outcomes or categories in which compounds fit in depending on their properties and the membrane in question. The seven possible categories are presented in Table 2.3. This model has adequately estimated the rejection of a wide range of organic solutes during laboratory, pilot, and full-scale investigations (Drewes et al., 2008) and was independently verified by a group of researchers in The Netherlands (Verliefde et al., 2007). One difficulty in developing the model, however, is incorporating molecular descriptors to rank the strength or overall effect of solute–membrane interactions on rejection. Initially, the Log K_{ow} of a compound was utilized to estimate the rejection of compounds that have been demonstrated to adsorb to membrane materials. Although it validated the model, Log K_{ow} was found not to be a good parameter for this estimation as it does not correlate well with rejection for all compounds that have membrane interactions.

The new version of the model incorporates the Taft (could also be the Hammett constant) parameter or constant, which has been used to describe the strength of hydrogen bonding for organic compounds to membranes (Matsuura and Sourirajan, 1971). The Taft and Hammett constant can be difficult to calculate for a wide variety of organic compounds, however, and finding a molecular descriptor for adsorption is challenging. Therefore, additional research is needed to refine the model in order to make it applicable for a wide variety of organic compounds. Although this modeling approach requires additional work to fully develop, our research team believes that it could be a simple yet effective tool that nonscientists and nonengineers could employ if needed.

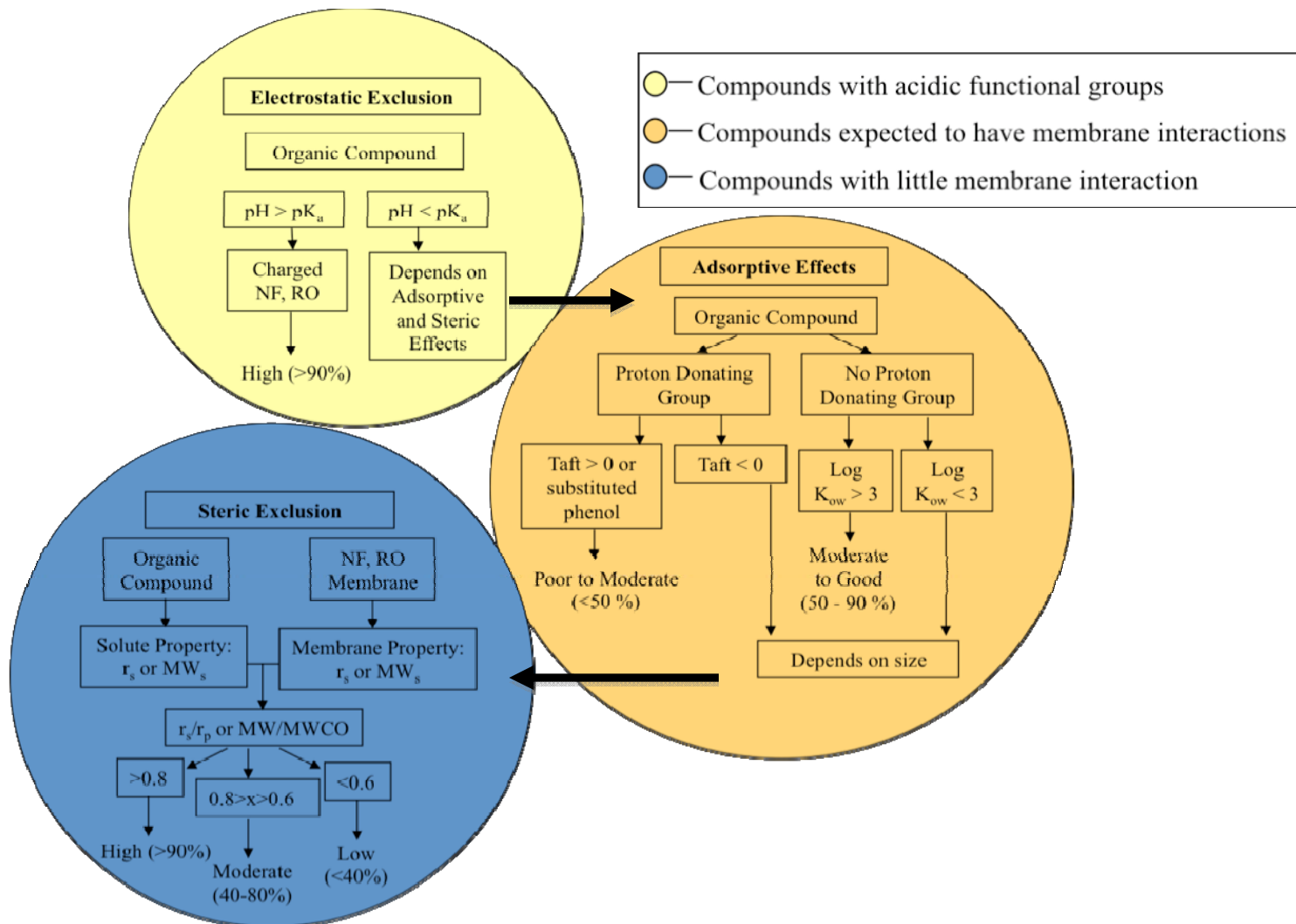


Figure 2.19. Modified rejection diagram including three mechanisms of rejection, steric exclusion, adsorption, and electrostatic exclusion.

Table 2.3. Possible Outcomes or Categories of the Modified Rejection Diagram

Category	Charge	Proton Donating Group	Hydrophobic Interaction	MW	r_s/r_p	Rejection Mechanism	Expected Rejection	
1	pH > pK _a (negative)	NA	Log K _{ow} < 3	NA	NA	Primarily Electrostatic	> 90%	
2	pH < pK _a (uncharged)	Yes	NA	NA	NA	H Bonding Dominates	< 40%	
3		Not substantial	Log K _{ow} > 3	> MWCO	NA	Hydrophobic Interactions Dominate	70 - 90%	
4			Log K _{ow} > 3	< MWCO	NA		< 20%	
5			Log K _{ow} > 3	< MWCO	<0.6	Steric Interactions Dominate	< 40%	
6					~ MWCO		0.8 > x > 0.6	40 - 80%
7					> MWCO		>0.8	> 90%

NA - Not applicable or not important for this compound to estimate rejection

2.7 Operational Impacts on Rejection

2.7.1 Recovery

System recovery is defined as the percentage of the feed stream flow that becomes permeate stream flow:

$$\text{Recovery (\%)} = \frac{Q_p}{Q_f} * 100 \quad (2.44)$$

where Q_p is the permeate stream flow, and Q_f is the feed stream flow. The maximum recovery specified by manufacturers for one spiral-wound element is 15%. For water reuse applications treating wastewater effluents, overall system recoveries are generally between 70 and 85%. When one operates bench-scale flat-sheet experiments, recoveries are generally about 1%. These differences in scale are important because recovery can have a significant impact on observed rejection. Figure 2.20 shows the effect of recovery on the model output (rejection) of the HSDM. Because of concentration polarization, the driving force for diffusion is increased and rejection decreases with increasing recovery. Chellam and Taylor (2001) performed a comprehensive study on the effect of recovery on the rejection of constituents by a number of membranes and found that recovery has a big influence on solutes that are only marginally rejected at low recoveries (Figure 2.21). For most of the constituents of interest, the HSDM was found to accurately describe the effect of recovery on observed rejection. However, in the cases of constituents with low rejection at low recovery, the model was found to be less accurate.

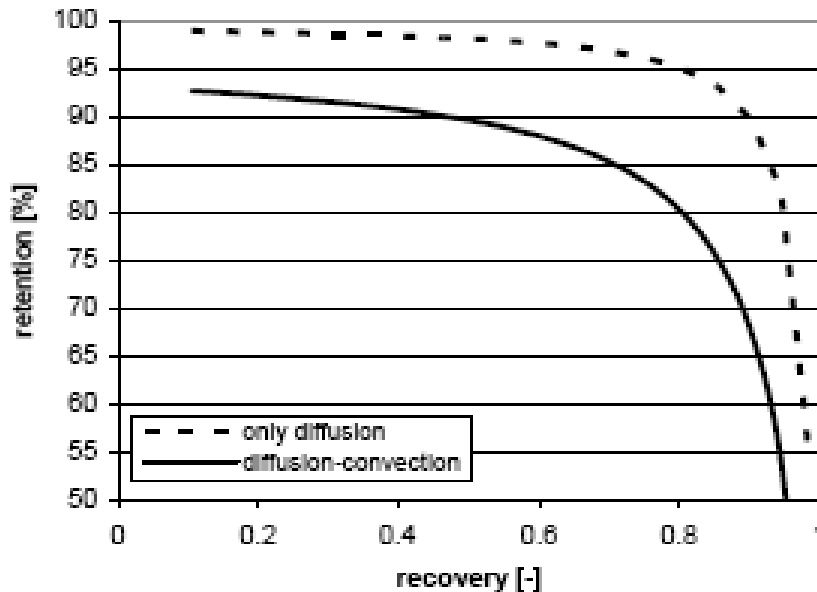


Figure 2.20. Rejection of a model solute as a function of recovery.

Note: A diffusion model and a convection–diffusion model were used to generate the curves.

Source: Hofman et al., 2007.

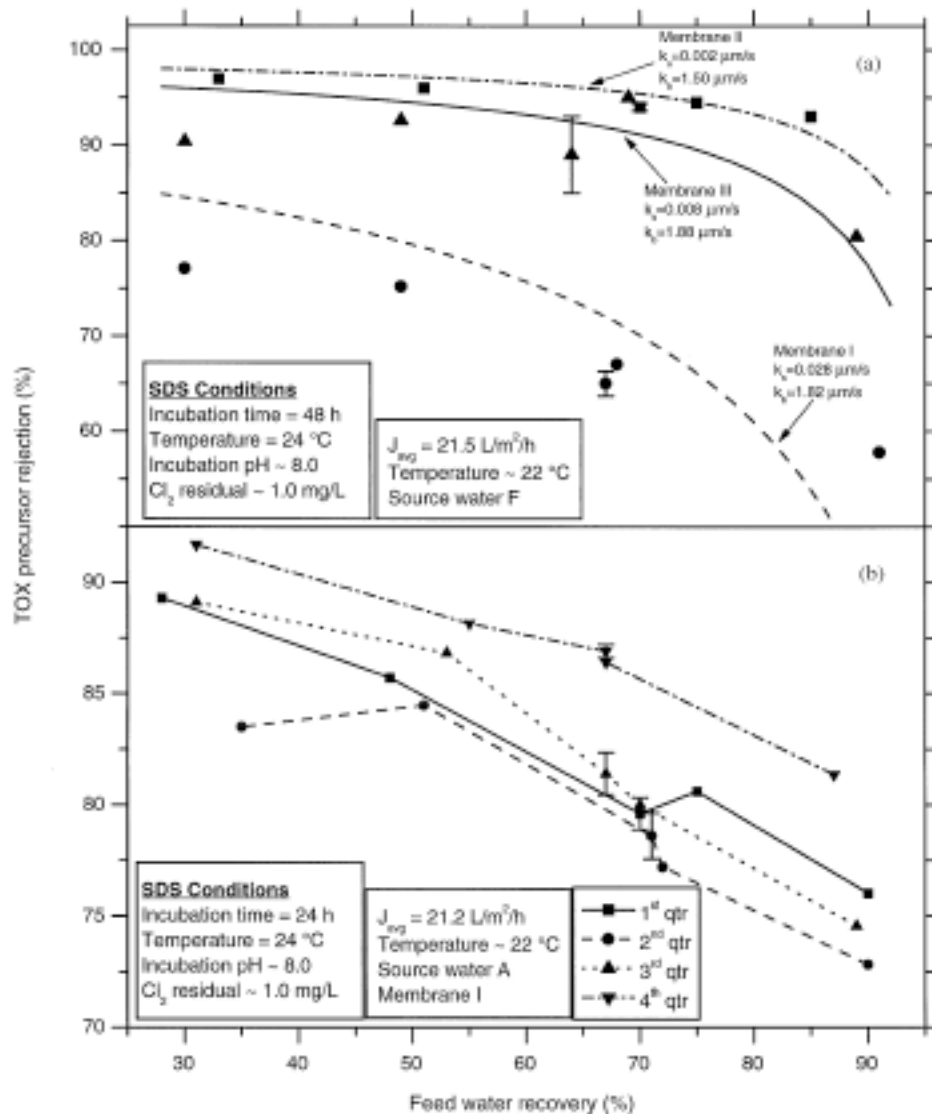


Figure 2.21. Rejection of total organic halide precursors by several membranes versus feed water recovery.

Source: Chellam and Taylor, 2001.

2.7.2 Permeate Flux

From the mass transfer models, it should be apparent that, at a constant recovery, increasing permeate flux decreases the concentration of a solute in the permeate and increases rejection. Figure 2.22 presents the rejection of four nitrosamine compounds as a function of permeate flux during experiments conducted on a pilot-scale membrane unit. During the experiment, recovery was kept constant (approximately 72%) by changing the feed flow.

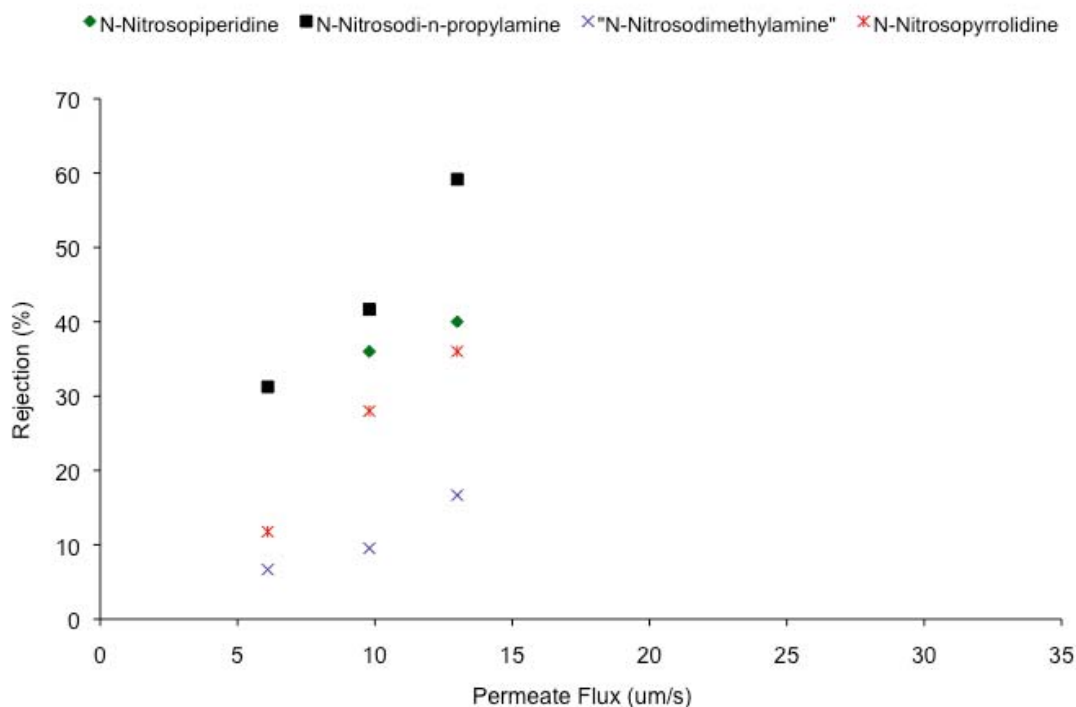


Figure 2.22. Rejection of four nitrosamine compounds by NF-4040 membrane installed on a pilot-scale membrane unit.

Note: Recovery was kept constant (approximately 72%) by increasing the feed flow as the permeate flow rate was increased.

When the feed flow is kept constant and the permeate flux is increased, the increase in recovery eventually adversely affects rejection. Figure 2.23 presents the bench-scale rejection of sodium chloride and permeate flux for an NF membrane as a function of recovery. At low recoveries (less than 1%), increasing permeate flux increased rejection. However, at recoveries greater than 1%, concentration polarization began to affect the observed rejection and eventually negatively impacted the observed rejection.

One of the major issues with many modeling approaches is that they are generally developed by using bench-scale flat-sheet units at very low recovery. In addition, many of the transport models do not account for recovery implicitly and cannot be used to model full-scale systems.

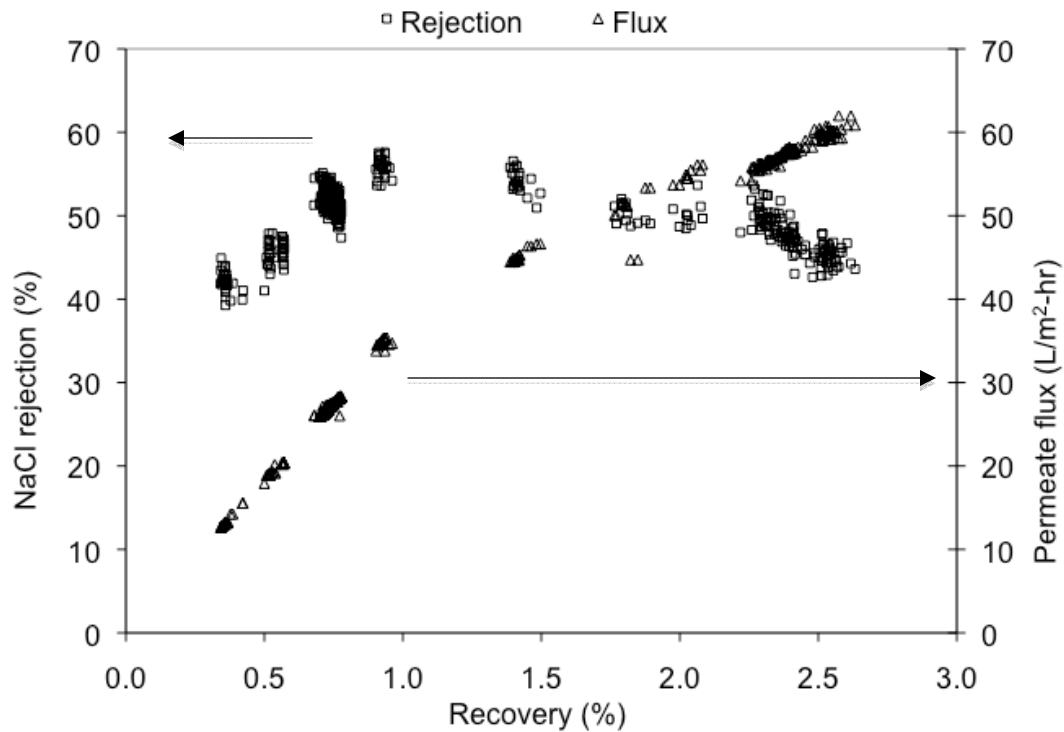


Figure 2.23. Rejection of NaCl and permeate flux versus recovery.

Notes: Increasing the feed pressure decreased the feed flow of the pump, resulting in an increase in recovery. Below a recovery of 1%, increasing permeate flux increased rejection and there was minimal impact from increasing recovery. At higher recovery, concentration polarization effects began to decrease rejection with increased permeate flux.

2.7.3 Differential Element Approach

One of the major limitations of commonly studied modeling approaches is that little attention is given to the fact that, at pilot and full scale, recoveries are relatively high (70–85%) and large concentration gradients exist across membrane treatment trains. The concentration gradient will significantly affect the combined permeate concentration of solutes and needs to be considered for modeling exercises. Sharma and Chellam (2008) recently published a method by which modeling approaches used at bench scale could be used to model systems operated at higher recovery. The approach is termed the differential element approach and is similar to a method used by Zhao (2004). A membrane system is conceptually divided into numerous identical sub-elements that are then modeled as completely mixed reactor. Each sub-element is connected to its immediate neighbor by using appropriate flow and solute mass balances at steady state. The following equations are used for the differential element approach. The flow mass balance is given by

$$Q_f(j) = Q_f(1) - \sum_{k=1}^{j-1} Q_p(k) \quad (2.45)$$

and the solute mass balance given by

$$C_f(j+1) = \frac{Q_f(j)C_f(j) - Q_p(j)C_p(j)}{Q_f(j+1)} \quad (2.46)$$

The permeate flow rate $Q_p(j)$ for each sub-element j can be calculated as

$$Q_p(j) = J_v(j) \frac{A}{n} = L_p [\Delta P - \pi(j)] \frac{A}{n} \quad (2.47)$$

where $J_v(j)$ is the local permeate flux for sub-element j , A is the membrane area, n is the number of sub-elements, L_p is the membrane solvent permeability constant, ΔP is the hydraulic pressure across the membrane, and $\Delta\pi(j)$ is the osmotic pressure difference calculated on the basis of the Van't Hoff equation:

$$\Delta\pi(j) = 2RT [C_m(j) - C_p(j)] \quad (2.48)$$

or other empirical relationships between total dissolved solids and osmotic pressure. For experiments with extremely low feed concentrations, the effect of osmotic pressure on flux is expected to be small. The pressure drop is assumed to be linear across the membrane system, and the following equation can be used to calculate the driving force for permeate flow from each sub-element:

$$\Delta P(j) = \left((P(1) - (j - 0.5)) \frac{P(1) - P(j+1)}{n} \right) \quad (2.49)$$

The permeate ($C_p(j)$) and feed concentrations for each sub-element can be related by using a one-dimensional film theory model like

$$\frac{C_p(j)}{C_f(j)} = \frac{\exp(J_v(j)/k(j))}{\frac{C_m(j) - C_p(j)}{C_p(j)} + \exp(J_v(j)/k(j))} \quad (2.50)$$

The expression

$$\frac{C_m(j) - C_p(j)}{C_p(j)} \quad (2.51)$$

can be calculated from membrane transport models including the solution–diffusion model, the hydrodynamic model, the ENP equation approach, and the phenomenological approach. For these models, parameters related to the membrane and the solute are inputs and the differential element approach is used to model concentration gradient through the system.

Once $C_p(j)$ for each sub-element is determined, the weighted average permeate concentration over the entire element can be calculated by using

$$C_p = \frac{\sum_{j=1}^n Q_p(j) C_p(j)}{\sum_{j=1}^n Q_p(j)} \quad (2.52)$$

2.8 Summary of Factors that Affect Rejection

2.8.1 Membrane Reproducibility

The properties of a membrane can differ considerably across one membrane specimen because of imperfections in membrane-casting techniques. For example, in a study by Hofman et al. (2007), the researchers investigated membrane coupons cut from different areas of the same flat-sheet specimen. The researchers found that salt passage changed considerably depending on the location the sample was taken from on a flat-sheet sample. Near the edges of the membrane sheet, salt passage was found to be the greatest but decreased as the sampling location moved away from the edge of the membrane sheet. The researchers concluded that this effect was due to the equipment used to cast membranes and that the variation could affect model development.

2.8.2 Rejection Equilibrium

A study performed by Hofman et al. (2007) demonstrated that atrazine rejection required 3 or 4 days before equilibrium was reached. The researchers believe that after this time adsorption equilibrium was reached, which stabilized the concentration in the permeate. However, this result was not seen for all solutes that were studied and the rejection of atrazine changed by only 1% over the 3 days. Other studies have demonstrated that, for some solutes, a period on the order of days is needed to establish equilibrium and to reach a steady-state permeate concentration.

Kimura et al. (2003b) reported that the adsorption of hydrophobic compounds to membrane materials may result in overestimated rejection values if experiments are not performed over a long-enough time to reach equilibrium. Synthetic feed waters used during experimentation, with a low solute concentration, may not completely occupy the adsorptive sites of the membrane if experiments are too short. As a result of the higher number of unoccupied membrane adsorptive sites, rejection values are inflated during initial operation of membrane systems. Kimura et al. (2003b) concluded that, until a membrane is saturated with solute, rejection values will be an overestimation when compared to steady-state conditions. The experiments conducted by Kimura et al. (2003b) were terminated after approximately 20 h, and on the basis of the data presented, rejection was not at equilibrium. However, one observation is that these experiments were conducted at a relatively high recovery (5%) and an extremely low feed flow rate (~180 ml/min). It is difficult to extract useful information from these experiments because of the unrealistic operating conditions.

2.8.3 Temperature

The temperature of the feed water has a significant effect on the solvent and solute permeability of membranes. Sharma and Chellam (2005) reported that an increase in feed water temperature changed the pore structure of NF membranes, increasing the pore size and decreasing the pore density. The net outcome of these changes would be greater transport of solutes across a membrane, which has been documented for RO and NF membranes (Sharma and Chellam, 2005). Experiments designed to determine MTCs, effective pore size, and other model parameters should be conducted at various temperatures.

2.8.4 Feed Water Chemistry

There are feed water constituents that have been reported to affect rejection. These factors mainly include organic matter, pH, ionic strength, and membrane fouling.

Organic Matter. Researchers have reported various effects to rejection when organic carbon is added to the feed solution. Nghiem et al. (2002b) reported that the rejection of the steroid estrone by seven of eight membranes was decreased when secondary effluent was added to the deionized feed water. A study by Majewska-Nowak et al. (2002) found that pesticides such as atrazine could adsorb to organic matter present in feed water, increasing rejection as a result of increased size and electrostatic interaction between the organic and the membrane. A more recent study by Jin et al. (2007) found that the rejection of estrone significantly increased when an aromatic hydrophobic acid with phenolic groups was added to the feed water solution. The explanation given was that estrone could form hydrogen bonds with the solute, which either increased the size and thus steric exclusion, or that, because the hydrophobic acid was negatively charged, electrostatic exclusion prevented adsorption of estrone. However, when dextran was added to the deionized water solution, there was no change in the rejection. In a study by Yoon et al. (2005, out of four water matrices studied, the rejection of a wide variety of organic compounds was lowest in the feed water matrix with the highest dissolved organic carbon (DOC) concentration. Obviously, for membrane experiments, deionized water is preferable to natural water for analytic purposes. However, on the basis of past research, it appears that the organic matter matrix can significantly affect rejection.

pH. The pH of a feed water solution changes the surface charge of a membrane and can also affect the charges of species present in the feed water. As was presented in the electrostatic effect section, the rejection of charged species generally increases with increasing pH.

The influence of pH and membrane surface charge on membrane pore structure and on the rejection of uncharged organics as well as on permeate flux is not completely understood. At high pH values (8–10), it has been reported that the rejection of uncharged solutes decreased, although permeate flux increased (Braghetta et al., 1997; Berg et al., 1997). This phenomenon may be the result of an increase in pore size of a membrane caused by the electrostatic repulsion between the acidic functional groups within the membrane (Braghetta et al., 1997; Berg et al., 1997). Other researchers have found little dependence of the rejection of uncharged organics and permeate flux on pH unless ions were present in the feed solution (Ozaki and Li, 2002; Yoon et al., 1998; Boussahel et al., 2002).

Ionic Strength. As previously mentioned in the electrostatic effect section of this review, the ionic strength of a solution, particularly when multivalent ions are present, can significantly

affect the rejection of charged species. For example, Bellona and Drewes (2005) determined calcium additions could significantly reduce the rejection of negatively charged organics for membranes with larger pores because Donnan exclusion effects were minimized. However, diclofenac rejection was minimally affected by additions of sodium chloride, and negatively charged organic solutes are generally well rejected regardless of the matrix.

Braghetta et al. (1997) used the Debye length parameter to quantify the effects of ionic strength on the zeta potential and on the structure of a membrane. Findings of this study and three others revealed that the Debye length was short at higher ionic strengths, the zeta potential was more positive, electrostatic interaction was minimized within the membrane, and the pore radii could shrink (Braghetta et al., 1997; Lee et al., 2002; Bellona and Drewes, 2005; Boussahel et al., 2002; Freger et al., 2000). At low ionic strength when the Debye length is longer and the zeta potential is more negative, pore radii can increase in size to minimize electrostatic repulsion between the negative functional groups (Braghetta et al., 1997; Bellona and Drewes, 2005; Boussahel et al., 2002; Freger et al., 2000). Boussahel et al. (2002) found that calcium additions could increase the rejection of uncharged pesticides by reducing the pore size of certain NF membranes. Schäfer et al. (2002a) found that, although the rejection of dissolved organic carbon by UF membranes was affected little by feed water pH, increasing ionic strength had a significant inverse effect on rejection. It was hypothesized that ionic strength additions could affect the structure of the organic carbon and also could reduce the charge of the membrane, leading to reduced electrostatic interaction and lower rejection. Finally, Bouranene et al. (2007) recently employed a ceramic NF membrane to investigate the effect of increased ionic strength on rejection because ceramic pores are not expected to change in size as a function of ionic strength. The researchers found that increased electrolyte concentrations reduced the rejection of polyethylene glycols and that the trend in decreasing rejection followed the Hofmeister series and is caused by the dehydration of molecules, which reduces their hydrated radius. Like temperature, the effect of ionic strength on rejection may be an important factor to assess when determining model parameters.

Membrane Fouling. The effect of fouling on the rejection of organic solutes has garnered increased attention over the past few years. Membrane fouling is defined as the reduction of membrane performance that is due to reversible and irreversible deposition of solids on the membrane surface and pores. Fouling results in a decline in permeate flux when a system is operating at constant pressure or when an increase in pressure is imposed to achieve constant flux, which increases operational costs. On the basis of what research has been published to date, the overall effect of fouling on rejection is not completely understood.

Three types of experiment have been conducted to investigate the effect of fouling on rejection. The first were methods used to measure small concentrations of trace organic compounds naturally present in wastewater effluent and their rejection in a natural water matrix over time (Bellona and Drewes, 2007; Drewes et al., 2005). In the second method, trace organic contaminants were spiked into the feed solution at the beginning of filtration, and rejection and fouling were measured over time (Ng and Elimelech, 2004). The third method was to pre-foul the membrane with either effluent or a synthetic solution and then to spike trace organic contaminants to determine rejection (Bellona and Drewes, 2007; Nghiem et al., 2008; Xu et al., 2006). The third type of experiment is generally performed at bench scale.

Ng and Elimelech (2004) employed the second method and observed a decrease in trace organic contaminant rejection with fouling using silica colloids. They observed that cake-

enhanced concentration polarization associated with fouling facilitated the transport of small inert organic compounds (ethylene glycol and glycerol) and trace organic contaminants (estradiol and progesterone). Inert organic compounds with a molecular weight higher than the MWCO were minimally affected by fouling, because size exclusion was the dominant removal mechanism. Comerton et al. (2008) found that trace organic contaminants were consistently rejected by an RO membrane but that variable rejection was observed for two NF membranes. Comerton et al. (2008) tested 22 compounds by using wastewater effluent-impacted Lake Ontario water and membrane bioreactor effluent. In general, compounds were more effectively rejected by membranes with a fouling layer, contrary to the study by Ng and Elimelech (2004). Comerton et al. (2008) also suggested a correlation between rejection and hydrophobicity ($\text{Log } K_{ow}$), with more hydrophobic compounds having a higher rejection. The increased organic compound rejection may be attributed to increased adsorption with fouling.

Xu et al. (2006) pre-fouled membrane specimens and performed rejection experiments and found that membrane fouling from wastewater effluent affected trace organic rejection by NF and ULPRO membranes but had a less significant effect on RO membranes. Rejection of primidone, a hydrophilic nonionic compound, was found to remain the same or to decrease with fouling for the membranes tested. Bromoform, chloroform, and trichloroethylene adsorbed more onto fouled membranes than to unfouled membranes, resulting in higher rejection after 50 h of filtration. Nghiem and Hawkes (2007) and Nghiem et al. (2008) investigated the removal of the nonionic organic compounds carbamazepine and bisphenol A with membranes fouled with Sigma-Aldrich humic acid. Rejection was seen to increase with fouling for a loose nanofilter with large pores and was attributed to pore blocking by the foulants. A decrease in rejection was observed with the NF-270 membrane, attributed to cake-enhanced concentration polarization. A slight increase in rejection was observed with a “tight” NF membrane (NF-90) for bisphenol A, and a slight reduction was observed with carbamazepine. The authors indicated that cake enhanced concentration polarization. A slight increase in rejection was observed with a “tight” NF membrane (NF-90) for bisphenol A, and a slight reduction observed with carbamazepine. The authors indicated that cake-enhanced concentration polarization also occurred with the NF-90 membrane; however, because of the small pores, steric exclusion was the dominating effect. Nghiem et al. (2008) also indicated that increased trace organic adsorption could facilitate diffusional transport and lower rejection. Further investigation into the effect of fouling on membrane properties and on solute rejection is needed in order to understand and describe membrane performance during treatment of wastewater effluent.

2.8.5 Conclusions and Major Findings

The intent of this literature review was to summarize the major factors affecting solute removal by NF and RO membranes and to identify strategies for solute rejection modeling. The following conclusions summarize the most important information gained through the literature review:

- The rejection of organic solutes depends on three major mechanisms: size exclusion, electrostatic exclusion, and solute–membrane interactions.
- Charged organic solutes are generally well removed by NF and RO membranes regardless of size; in general, negatively charged solutes exhibited better removal than positively charged solutes.
- Nonionic solutes with solute–membrane interactions are likely to have incomplete removal.

- Although size is a dominant factor in the rejection of nonionic solutes, solute–membrane interactions are an important factor.
- Currently, there is no definitive way to predict which compounds will have strong solute–membrane interactions based on molecular descriptors.
- Other than solute and membrane properties, there are a number of factors that affect rejection, with the most important being operational conditions, feed water temperature and chemistry, and membrane fouling.
- The overall effect of membrane fouling on rejection of organic solutes is not well established.
- Pertinent modeling approaches include mass transfer equations, QSPR models, and empirical models.
- Mass transfer models are advantageous because they integrate operational conditions and to a limited degree solute and membrane properties.
- QSPR models are advantageous because solute properties are easily incorporated.
- Empirical models are advantageous because they are simple to use.
- Models that rely on solute size as input parameters often overpredict rejection because solute–membrane interactions are not included.
- The solution–diffusion model is advantageous because only one solute input parameter is required.
- The phenomenological model is advantageous because of the “black box” nature of the model and possibility of correlating solute properties to the input parameters.
- The differential element approach combined with the phenomenological model can be applied to a full-scale system and could potentially include both operational conditions and solute and membrane properties.
- Adjustments to any model need to be made to account for fouling and for changes in temperature and feed water chemistry. In addition, experimental replication is needed to account for differences between different types of membranes.

Chapter 3

Materials and Methods

3.1 Choosing Trace Organic Compounds for Study

3.1.1 Selection Method to Develop Model Development and Validation Compounds

For this study, 270 organic solutes were initially selected for model development and model validation. The list of compounds was compiled from a variety of sources and yielded a relatively diverse set of organic solutes based on properties (e.g., size, charge, hydrophobicity/hydrophilicity, etc.), relevance to membrane treatment (e.g., functional groups affecting rejection, likelihood of permeation), and environmental relevance (e.g., EPA Candidate Contaminant List, recent advancements in emerging contaminant research, human health, and environmental relevance). After removal of compounds that caused analytical and experimental issues (e.g., high volatilization, instability, and poor solubility), a shorter list of compounds was generated that retained the diversity of the original list for model development and validation.

All compounds were categorized by expected rejection mechanism based on charge and hydrophobicity (Table 3.1). Six different categories were developed: hydrophilic neutral (HN; less than 0.01% charged at pH 6.5; $\text{Log } K_{ow} < 2$), hydrophilic/hydrophobic neutral (HHoN; less than 0.01% charged at pH 6.5; $\text{Log } K_{ow} > 2$ and $\text{Log } K_{ow} < 3$), hydrophobic neutral (HoN; less than 0.01% charged at pH 6.5; $\text{Log } K_{ow} > 3$), hydrophilic negatively charged (HCN; greater than 50% negatively charged at pH 6.5), hydrophilic positively charged (HCP; greater than 50% positively charged at pH 6.5), and hydrophilic negatively and positively charged (HCNP; having both positive and negative charge at pH 6.5). Compounds were grouped by these categories, which yielded 51 HoN compounds, 27 HHoN compounds, 76 HN compounds, 50 HCN compounds, 38 HCP compounds, and 18 HCNP compounds.

For each rejection mechanism subgroup, principal component analysis and *k*-means clustering/discriminate analysis was performed (using XLSTAT) to further group compounds based on molecular properties determined with the Schrödinger software package. These descriptors included $\text{Log } K_{ow}$, solubility, volume, solvent accessible surface area (SASA), hydrophobic surface area (FOSA), hydrophilic surface area (FISA), polar surface area (PISA), weakly PISA (WPSA), polarizability, dipole moment, quantum mechanic (QM) dipole moment, QM energy, solvation energy, and E_{HOMO} and E_{LUMO} energy. For HN, HHoN, HoN, HCN and HCP compounds, five groups were developed, whereas, for HCNP, three groups were developed. Random selection was then used to select, at the least, 33% of the compounds from each grouping (all compounds were selected from groups with only two compounds, 66% were selected from groups with three compounds, and 50% of compounds were selected from groups with four compounds).

Table 3.1. List of Compound Designations and Comparison of Original Compound List with Final Compound List

Designation	Charge Designation ^a	Log K_{ow} ^b	Total No. Initially Considered	No. in Development Set	No. in Validation Set
HCN	>98% negative (acidic group deprotonated)	No restriction	50	19	6
HCP	>98% positive (basic group protonated)	No restriction	38	14	5
HCNP	>50% positive (basic group protonated), >50% negative (acidic group deprotonated), >98% overall net charge	No restriction	18	9	5
HN	>98% uncharged	<2	76	31	5
HHoN		3 > Log K_{ow} ≥ 2	27	12	4
HoN		≥ 3	51	14	6
Other	<98% negative or positive charge	No restriction	10	1	1

^aAt pH 6.5.

^bFor certain compounds, Log K_{ow} differs depending on source making this classification difficult.

This selection process yielded a group consisting of 132 compounds for model development and validation (Table 3.2). According to an in-depth analysis, this final list of compounds retained much of the diversity of the full list based on criteria outlined previously (e.g., properties, rejection mechanisms, classes of compounds, environmental relevance, etc.). The list was then randomized with the 33 top compounds selected for the validation set and the remaining 101 selected for the model development set (Table 3.2). Figures 3.1 through 3.3 present box and whisker plots of key descriptors such as molecular weight, Log D, and dipole moment, respectively, for the original list of compounds compared to the final list used as model development and validation sets.

Table 3.2. Compound List Used for Model Development and Model Validation

Class	Compounds		
HCN (Log K_{ow} < 2)	Acetic acid	Enalapril	Salicylic acid
	Benzoic acid	Furosemide	Sulfacetamide
	Captopril	Gemfibrozil	Sulfadimethoxine ^b
	Chlortetracycline	Ibuprofen	Sulfadioxine
	Clofibric acid	Ketoprofen	Sulfamerazine
	Dibromoacetic acid	Maleic Acid	Sulfamethoxazole
	Dichloroacetic acid	Methotrexate	Sulfasalazine
	Diclofenac	Naproxen	Trichloroacetic acid
	1,4-Dihydroxybenzoic acid		
HCP (Log K_{ow} < 2)	Amitriptyline	Imiquimod	Pseudoephedrine
	Atenolol	Ketoconazole	Ranitidine
	Cimetidine	Metformin	Salbutamol
	Diethylamine	Methylamine	Tamoxifen
	Diltiazem	Metoprolol	Trazodone
	Diphenhydramine	Norfluoxetine	Trimethoprim
	Guanidine		
HCNP (Log K_{ow} < 2)	Alanine	Doxycycline	Oxytetracycline
	Arginine	L-Glutamic acid	Phenylalanine
	Baclofen	Histidine	Serine
	Ciprofloxacin	Lysine	Tyrosine
	Cysteine	Norfloxacin	
HN (Log K_{ow} < 2)	Acetaminophen	Meprobamate	Phenacetine
	Benzyl acetate	Methanol	Primidone
	Benzyl alcohol	Methylparaben	Propylphenazone
	1,4-Butanediol	Methyl-tert-butyl-ether	Resorcinol
	Caffeine	NDMA	Sucralose
	Chloroform	NDMA	Sucrose
	Ethanol	NDMA	Triethylene glycol
	Fluconazole	<i>N</i> -Nitrosomethylethylamine	Tris(1-chloro-2-propyl)phosphate
	2-Fluorophenol		
	Glucose	<i>N</i> -Nitrosomorpholine	TCEP
	Glycerol	<i>N</i> -Nitrosopiperidine	
	Hydrocortisone	<i>N</i> -Nitrosopyrrolidine	Uracil
	Isopropanol	Pentoxifylline	Urea
HHoN (3 > Log K_{ow} > 2)	Atrazine	Diethylphthalate	<i>n</i> -Nitrosodibutylamine
	Bromoform	Dilantin	
	Carbamazepine	Estriol	Propylparaben
	Dibromochloromethane	Methyl salicylate	Thiabendazole
	Dichlorobromomethane	1-Naphthalenemethanol	Warfarin
	DEET	2-Naphthol	

Table 3.2. Compound List Used for Model Development and Model Validation (cont.)

Class	Compounds		
HoN (Log K_{ow} >3)	Benzophenone	Estrone	2-Phenylphenol
	Bisphenol A	Ethinylestradiol	Progesterone
	Butylparaben	Fenofibrate	Testosterone
	Desloratadine	Fluoxetine	Triclocarban
	2,4-Dichlorophenol ^a	n-Nitrosodiphenylamine	Triclosan
	Diethylstilbestrol	4-Nonylphenol	TDCPP
	17 β -Estradiol	Oxybenzone	

Note: Model validation is shaded in gray.

^aOriginally classified other: Reported pK_a values for 2,4-dichlorophenol were 7.89 (SRC Database) and 8.05 (ACD Lab Software), indicating between 97 and 98 nonionic at pH 6.3. As such, this compound was included in the HoN designation for model development.

^bOriginally classified other: Reported pK_a values for sulfadimethoxine are between 5.5 and 5.9, indicating between 72 and 86% negatively charged at pH of 6.3.

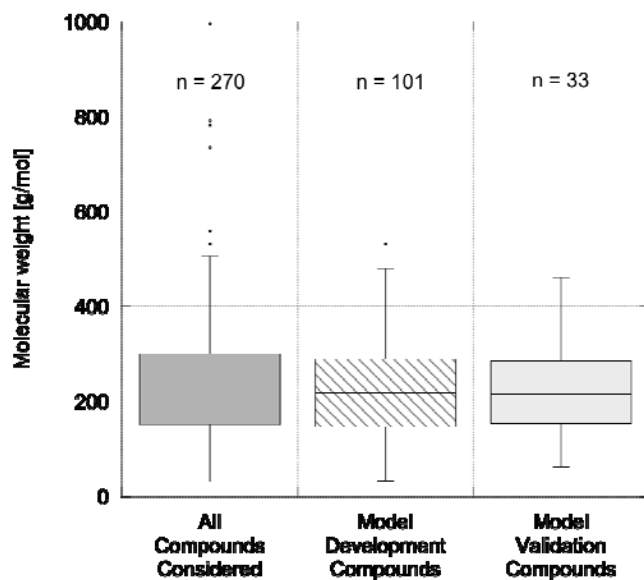


Figure 3.1. Range of molecular weight for compounds included in model development and validation compared with the total number of compounds considered.

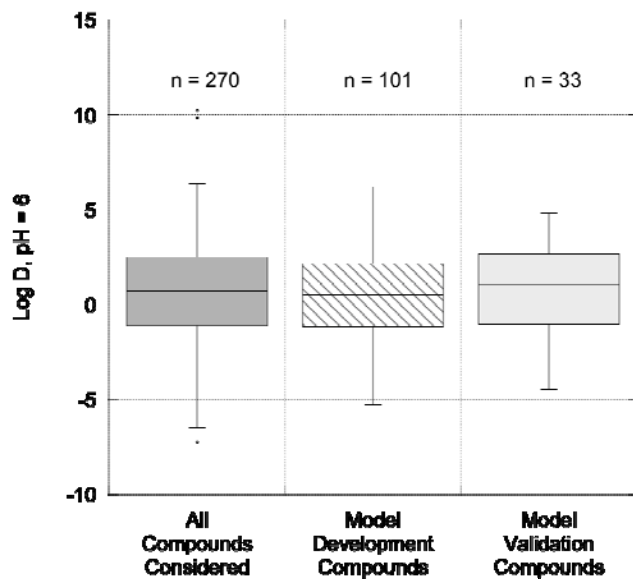


Figure 3.2. Range of Log D (pH = 6) for compounds included in model development and validation compared with the total number of compounds considered.

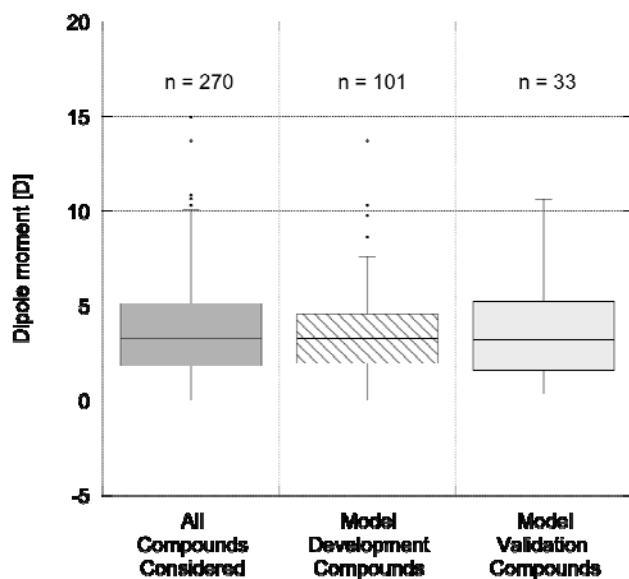


Figure 3.3. Range of dipole moments for compounds included in model development and validation compared with the total number of compounds considered.

3.1.2 Sources of Descriptor Data

Molecular descriptors were obtained and calculated from a variety of sources and programs listed in Table 3.3. Properties that could potentially predict steric interactions include molecular weight, length, width, depth, area, volume, globularity EqDepth, Wilke–Chang diffusion coefficient, Stokes radius, and molecular volume. Globularity (glob) is defined as $S/S_{\text{equivalents}}$, in which $S_{\text{equivalent}}$ is the surface area of a sphere of equivalent volume V . Calculations utilized to obtain the Wilke–Chang diffusion coefficient, Stokes radius, and molecular volume are summarized in Appendix B. Agenson et al. (2003) observed molecular weight and molecular width sterically affected rejection. Yangali-Quintanilla et al. (2010) developed QSPRs incorporating dimension descriptors such as length, width, and EqDepth to predict rejection.

Log K_{ow} , obtained from the SRC Physical Property Database and Schrödinger QikProp (QPlogPo/w), is a measure of the compound's affinity to adsorb to the membrane. Log D values or Log K_{ow} values at a given pH were also calculated by ACD Lab Software. Previous research by Braeken et al. (2005) observed Log K_{ow} can negatively affect rejection; however, research by Kiso et al. (2001b) observed Log K_{ow} has no significant correlation with rejection. The molecular structure, obtained from NIST WebBook, can help gain an understanding of possible solute–membrane interactions. Previous research by Williams et al. (1999) and Matsuura and Sourirajan (1971) revealed interactions between hydroxyl groups and the membrane surface due to possible hydrogen bonding.

The formal charge for each compound can be determined by pK_a and pK_b values at a given pH. The total formal charge at neutral pH was also calculated by Schrödinger LigPrep. Ozaki and Li (2002) observed an increase in rejection as the compound under investigation became negatively charged over a pH range. Verliefe et al. (2007) observed rejection efficiencies greater than 95% for negatively charged compounds and greater than 85% rejection for positively charged compounds due to electrostatic interactions. Libotean et al. (2008), Kimura et al. (2004), and Van der Bruggen et al. (1998) observed that dipole moment, a measure of a compound's uneven distribution of positive and negative charges, had a significant effect on neutral solute rejection because of electrostatic interactions.

Other molecular descriptors that could have an effect on compound rejection and were investigated include polarizability, ionization potential (IP), electron affinity (EA), E_{HOMO} , E_{LUMO} , hydration energy, aqueous solubility, free energy of solvation, and various surface area components. Polarizability is a measure of a compound's electron cloud to be distorted due to an external force, such as a dipole or ion nearby. IP is the amount of energy required to remove an electron from a molecule and become ionic. EA is the energy change that occurs when a molecule gains an electron. E_{HOMO} is the highest-energy molecular orbital that contains an electron, and E_{LUMO} is the lowest-energy molecular orbital that does not contain an electron. Hydration energy is the amount of energy released when 1 mol of a solute is dissolved in a large amount of water, and aqueous solubility is the maximum amount of a compound that can dissolve in water at equilibrium. Free energy of solvation in a solution is the amount of energy released as a solute becomes stable in a solution. The different descriptors for surface area can be used to quantify membrane interactions because it is a measure of the different components of the molecule: FOSA is a measure of saturated hydrocarbons; FISA represents nitrogen, oxygen, and hydrogen attached to heteroatoms; PISA represents π bonds; and WPSA represents halogens, phosphorus, or sulfur.

Table 3.3. List of Molecular Descriptors Used for Modeling Approaches with Selected Programs Utilized to Obtain Descriptors and Descriptions

Program	Molecular Descriptor	Description
NIST Chemistry WebBook	Mol weight	
	Mol formula	
	Mol structure	Listed as no. of -OH, -NH _n , -halogens, aromatic rings, etc.
SRC Physical Property Database	Mol wt	
	Water solubility	mg/L
	Log <i>K</i> _{ow}	Experimental at 25 °C
	p <i>K</i> _a	Experimental at 25 °C
Hyperchem	Length	Largest dimension of molecule in optimal configuration, nm
	Width	Medium dimension of molecule in optimal configuration, nm
	Depth	Smallest dimension of molecule in optimal configuration, nm
	Area	Approximate area, Å ²
	Vol	Å ³
	Hydration energy	Based on the approximate surface area calculation, kcal/mol
	Polarization	Atom-based method, Å ³
ACD Lab Software v.8.14	p <i>K</i> _a	Acid dissociation constant
	p <i>K</i> _b	Base dissociation constant
	Log D	pH 4, 6, 7, 8, 9
	Vol	cm ³ /mol
	PISA	Å ²
Schrödinger - LigPrep	Total Q	Total charge of the molecule
Schrödinger - QikProp	Dipole	Computed dipole moment of the molecule
	SASA	Total SASA
	FOSA	Hydrophobic component of SASA (saturated C and attached H)
	FISA	Hydrophilic component of SASA (N, O, and H on heteroatoms)
	PISA	π (C and attached H) component of the SASA
	WPSA	Weakly polar component of the SASA (halogens, P, and S)
	Vol	Total solvent-accessible volume, Å ³
	Glob	Globularity descriptor (1.0 for a spherical molecule)
	QPpolrz	Predicted polarizability, Å ³
	QPlogPoct	Free energy of solvation in octanol
	QPlogPw	Free energy of solvation in water
	QPlogPo/w	Predicted octanol–water partition coefficient

	QPlogS	Predicted aqueous solubility, Log S.
	CIQPlogS	Conformation independent predicted aqueous solubility
	IP	PM3 calculated IP, eV
	EA	PM3 calculated electron affinity, eV
Calculated	EqDepth	Arithmetic mean of the depth and width, nm
	Diffusion coefficient	Wilke–Chang, m ² /s
	Stokes radius	LaBas Additive Method, nm
	Mol vol	LaBas Additive Method, cm ³ /mol
	E _{HOMO}	Highest Occupied Molecular Orbital, eV; B3LYP Based Method
	E _{LUMO}	Lowest Unoccupied Molecular Orbital, B3LYP Based Method

3.1.3 Statistical Methods

During the course of this study, QSPRs were developed to describe and predict solute rejection and consisted of four parts: experimental database development, molecular descriptor evaluation, multiple linear regressions, and model validation.

Experimental Database Development. Bench-scale database development consisted of compiling average quasi-equilibrium 12-gal-per-sq-ft-and day (gfd) data for each compound tested for the NF-270 and ESPA2 membranes. Compounds selected for these experiments represented the six different categories: HN, HHoN, HoN, HCN, HCP, and HCNP. The data were quality checked before QSPR development continued.

Molecular Descriptor Evaluation. Molecular descriptor evaluation was conducted by using JMP 8.0.2 (SAS Institute, Inc., 2009), a statistical package employing multivariate methods and various modeling techniques. Initial cross-validation calculated a root mean squared error (RMSE) value for each possible multiparameter regression. Cross-validation of all molecular descriptors investigated calculated the optimum numbered parameter regression for QSPR development to be 3. To begin evaluating molecular descriptors, a correlation matrix was developed (presented in Appendix D) to determine which parameters are correlated. PLS with cross-validation was employed to remove any insignificant parameters before QSPR development. PLS determines which molecular descriptors contribute to the variability in rejection. Significant descriptors have a PLS coefficient greater than 0.05 and a variable importance plot (VIP) value above 0.8 (Wold, 1995).

Multiple Linear Regression. Three parameter correlations were developed by using descriptors found to be significant in the PLS evaluation. The significant descriptors employed in each calculation were less than 0.25 correlated with each other (results shown in the correlation matrix). QSPRs were developed in JMP and determined statistically valid by using the following statistical tools. The coefficient of determination, R^2 , should be close to 1 and no less than 0.75.

$$R^2 = \frac{\sum_i^n (y_{pred,i} - \bar{y})^2}{\sum_i^n (y_{obs,i} - \bar{y})^2} \quad (3.1)$$

$$\bar{y} = \frac{1}{n} \sum_i y_{obs,i} \quad (3.2)$$

where $y_{pred,i}$ are the outputs from the regression, \bar{y} is the mean observed value, $y_{obs,i}$ are the corresponding observed values, and n is the number of compounds in the model set. The overall F-ratio determines the overall significance of the model and should be greater than 2.8, where the larger the value, the more significant the correlation.

$$F - ratio = \frac{\sum_i (y_{pred,i} - \bar{y})^2 / DF_{SSR}}{\sum_i (y_{obs,i} - \bar{y})^2 / DF_{SSE}} \quad (3.3)$$

where DF_{SSR} is the degrees of freedom for the regression sum of squares, the number of parameters used in the regression. DF_{SSE} is the degrees of freedom for the error sum of squares, meaning the number of observations minus the number of parameters used in the regression. The p value is the probability that correlation happened by chance. A p value less than 0.05 means there is a 95% chance that the correlation did not happen by chance and that it is significant. A small RMSE indicates a better fit, generally an RMSE of <0.5.

$$RMSE = \sqrt{\frac{\sum_i (y_{pred,i} - y_{obs,i})^2}{n}} \quad (3.4)$$

Model Validation. Significant QSPR models were internally validated by using the leave-one-out (LOO) cross-validation method in which one compound is excluded from the data set and the model correlated with the remaining data. This method was repeated n times for n compounds in the data set. The results from this validation were then combined and a single QSPR was produced, yielding a q^2 value. A q^2 value greater than 0.5 indicates a good fit, and a q^2 value greater than 0.9 indicates an excellent fit (Eriksson et al., 2003). After LOO cross-validation was conducted, the QSPR was externally validated by applying the model to the validation compounds at bench scale.

3.2 Analytical Methods for Bulk Parameters and TORCs

3.2.1 Physicochemical Parameters

3.2.1.1 pH and Conductivity

pH was determined by using a Beckman 260 portable pH meter with combination of a gel-filled electrode (Beckman, Fullerton, CA; Standard Method 4500-H⁺) (Clesceri et al., 1998). Conductivity was determined by using an YSI model 85 multimeter (YSI, Inc., Yellow Springs, OH; Standard Method 2510).

3.2.1.2 Alkalinity

Alkalinity was measured by using the Hach Alkalinity Kit. A 100-mL sample was titrated with 1.6N sulfuric acid to a pH of 4.3 by using the Hach digital titrator model 16900 (Hach, Loveland, CO).

3.2.2 Bulk Parameters

3.2.2.1 Inorganic Anions

Inorganic anions were determined by using a Dionex IS 90 Ion Chromatography system according to Standard Method 4110 B. The anions that were examined are fluoride, bromide, chloride, nitrate, phosphate, and sulfate. Ammonia was measured according to the Hach Nessler Method 8038 adapted from Standard Methods 4500-NH₃ B and C (Clesceri et al., 1998). Metals were determined by using a Perkin-Elmer Elan 6100 inductively coupled plasma mass spectrometry system (Standard Method 3125 B) (Clesceri et al., 1998). This method measured a suite of metals. These metals included Ag, Al, As, B, Ba, Be, Ca, Cd, Co, Cr, Cu, Fe, K, Li, Mg, Mn, Mo, Na, Ni, P, Pb, S, Sb, Sc, Se, Si, Sn, Sr, Ti, U, V, and Zn.

3.2.2.2 TOC/DOC

Total organic carbon (TOC)/DOC was quantified by using a Sievers 5310 TOC analyzer with autosampler (Ionics Instruments, Boulder, CO) according to Standard Method 5310 B (Clesceri et al., 1998). The samples were placed in 17-mL sample vials and were acidified with phosphoric acid. Measurements of TOC are based on calibration with potassium hydrogen phthalate standards. DOC was measured by the same procedure used for TOC, except the sample was prefiltered (0.45- μ m pore size).

3.2.2.3 UV Absorbance and SUVA

UV absorbance (UVA) was analyzed by using a Beckman UV/VIS spectrophotometer with a 1-cm quartz cell (Standard Method 5910 B) (Clesceri et al., 1998). Samples were measured at wavelengths of 200–400 nm. The specific UVA (SUVA) is defined as the ratio between UVA (254 nm) and DOC.

3.2.3 HPLC-DAD

Aromatic organic compounds were quantified by using a Hewlett-Packard 1100 high-performance liquid chromatography (HPLC) system equipped with ultraviolet diode array detection (UV-DAD) and C-18 reversed-phase column and by applying a variety of different methods depending on retention times and compound hydrophobicity. A solution of 340-mg/L monobasic potassium phosphate (KH₂PO₄) and 3.8 mL of H₃PO₄ was used as a buffer. The methods initially utilized eluent concentration ranging from 5% methanol and 95% buffer to 50% methanol and 50% buffer, utilizing a greater initial concentration of methanol for hydrophobic compounds in order for separation to occur. UV optimization occurred prior to HPLC analysis. Samples for UV-DAD analysis were collected in 2-mL autosample vials and were stored at 4 °C pending analysis. Specific compound standards (0.1, 0.5, 1, and 5 mg/L) were run before and after compound analysis for instrument quality check and calibration curve and for signs of compound degradation. Integration of peaks was performed manually. The detection limit for the UV-DAD was 0.1 mg/L.

3.2.4 HPLC-RID

A Hewlett-Packard 1050 HPLC system equipped with a 1047A refractive index detector was used to quantify sugars and alcohols. HPLC-refractive index detection (RID) quantifies concentration by determining the change in refractive index in each sample. Deionized water was utilized as the eluent, and no analytical column was employed for analysis. Compound

samples for UV-RID analysis were collected in 2-mL autosampler vials and were stored at 4 °C pending analysis. Integration of peaks was performed manually. The detection limit for UV-RID analysis was 1 mg/L.

3.2.5 LC/MS-MS

Trace organic compounds were measured by LC with tandem mass spectroscopy (LC/MS-MS) (Table 3.4) as described by Vanderford and Snyder (2006). This method analyzes pharmaceuticals and other trace organic compounds in water by isotope dilution LC/MS-MS. Analytes were extracted by using solid-phase extraction (SPE) followed by LC/MS-MS as described by Vanderford et al. (2003). The surrogate standards [¹³C]-caffeine, [¹³C]-atrazine, [¹³C]-sulfamethazine, carbamazepine-d₁₀, [¹³C]-ibuprofen, [¹³C]-triclosan, and [¹³C₂]-estradiol were spiked into the filtered samples at a concentration of 50 ng/L. Analytes were extracted in batches of six samples by using preconditioned 500-mg hydrophilic-lipophilic balance cartridges. All extractions were performed by using an automated SPE system. The sample was then loaded (15 mL/min) onto the cartridges, after which the cartridges were rinsed with 5 mL of reagent water and then dried with a stream of nitrogen for 60 min. Next, the cartridges were eluted with 5 mL of 10/90 (v/v) methanol/methyl tert-butyl ether (MTBE) followed by 5 mL of methanol into 15-mL calibrated centrifuge tubes. The resulting extract was concentrated with a gentle stream of nitrogen to a volume of 50 µL. Then 20 µL of a 2.5-mg/L solution of internal standards (diazepam-d₅ and testosterone-d₃) was added, and the extract was brought to a final volume of 1 mL by using methanol. The final concentration of the internal standards was 50 µg/L. Detection limits for the target compounds are summarized in Table 3.4.

Table 3.4. Theoretical Detection Limit for LC/MS-MS Method

Compounds	Detection Limit (ng/L)	Compounds	Detection Limit (ng/L)
Acetaminophen	10	<i>N</i> -Nitrosodibutylamine	1000
Amitriptyline	10	NDMA	1000
Atenolol	10	NDMA	1000
Atrazine	10	<i>N</i> -Nitrosodipropylamine	1000
Benzophenone	250	NDMA	1000
Bisphenol A	50	<i>N</i> -Nitrosomorpholine	1000
Caffeine	10	<i>N</i> -Nitrosopiperidine	1000
Carbamazepine	100	<i>N</i> -Nitrosopyrrolidine	1000
DEET	50	<i>N</i> -Nitrosodiphenylamine	1000
Diclofenac	25	4- <i>n</i> -Nonylphenol	250
Dilantin	50	Norfluoxetine	25
Diphenhydramine	100	Oxybenzene	10
17 β -Estradiol	6.25	Primidone	10
Estriol	16	Progesterone	1
Estrone	6.25	Propylparaben	10
Ethinylestradiol	2.5	Sucralose	250
Fluoxetine	10	Sulfamethoxazole	10
Gemfibrozil	10	TCEP	10
Ibuprofen	100	TCPP	25
Ketoprofen	500	TDCPP	100
Meprobamate	10	Testosterone	1
Metformin	100	Triclocarban	10
Methylparaben	10	Triclosan	10
Naproxen	25	Trimethoprim	10

Note: Detection limit determined by the lowest standard concentration that passes the signal-to-noise ratio (7:1).

3.2.6 GC-ECD

Trihalomethanes (THMs) and haloacetic acids were analyzed by gas chromatography coupled with an electron capture detector (GC-ECD) following EPA Methods 524.2 and 552.2, respectively. For EPA Method 551.1, 40 mL of sample solution was collected during the experiments from the appropriate sampling port in a clean 40-mL EPA vial with a TFE-lined screw cap. Once the sample was confirmed to be free of air, the vial was labeled and stored in a refrigerator at 4 °C pending analysis. No sample was ever stored for more than 7 days before extraction. During each extraction, a set of standards was prepared to provide a quality assurance check of the equipment and the procedure and to establish a calibration curve for the run. The set of standards included a series of concentrations designed to provide a calibration curve that included all concentrations in the samples. For sample extraction, 30 mL of the solution was measured into a clean graduated cylinder. The volume remaining in the vial was then wasted, and the 30 mL in the graduated cylinder was poured back into the vial. To each vial 8 g of sodium chloride and 3 mL of MTBE were added, and the vials were

mixed on a vortex mixer for about 30 seconds, or until inspection indicated that all of the sodium chloride had dissolved. This sample was then placed in a rack and allowed to stand and develop an MTBE layer, while the rest of the samples and standards underwent the same procedure. For the extraction procedure, a pasteur pipette was used to extract 2 mL of the top, organic layer. This 2 mL was transferred into the appropriate autosampler vial, which was immediately capped and placed in a rack. After all samples had been extracted, the autosampler vials were placed in a freezer pending analysis. This freezing always occurred within 4 days of extraction. Samples were analyzed by using a GC-ECD. The temperature program included an initial temperature of 35 °C with a 4-min hold time. Subsequently, the temperature was ramped to 180 °C at 30 °C per min. Integration of the chromatographs was performed manually with a consistent technique and operator.

3.3 Experimental Methods

3.3.1 Bench-Scale Systems

3.3.1.1 Recycle Mode

Bench-scale experimentation was conducted by using a cross-flow stainless steel SEPA II (GE Osmonics) membrane-testing unit employing a 140-cm² flat-sheet membrane (Figure 3.4). The cell holder has a channel height of 31 mil, with the active layer of a membrane specimen having a width of 9.5 cm and length of 14.6 cm. A flow diagram illustrating the bench-scale unit is shown in Figure 3.3. A rotary vane pump head was utilized to deliver the feed solution from a temperature-controlled feed container at 1.5 L/min to the flat-sheet cell. A supervisory control and data acquisition (SCADA) system collected output signals from flow, pressure, and temperature sensors and controlled and maintained temperature set-points. A digital analytical balance was utilized to measure the permeate flow rate.



Figure 3.4. SEPA II membrane testing unit employing flat-sheet membrane.

New virgin membrane specimens were used for each experiment to minimize any variability in results. In addition, fouling effects were not considered in generating bench-scale rejection data. Membranes were flushed with 20 L of deionized water at 150 psi prior to rejection

experiments to remove any impurities. Spike solutions were added to the 20-L feed tank to obtain the desired feed concentration, about 700 $\mu\text{g/L}$ for the NF-270 membrane and 3 mg/L for the ESPA2 membrane. Rejection experiments were conducted at a constant feed flow rate, 2 L/min, water temperature of 18 $^{\circ}\text{C}$, and pH of 6.3. The pressure was increased from approximately 10 to 200 psi to obtain five permeate flux rates between 5 and 70 gfd for the NF-270 membrane and between 5 and 40 gfd for the ESPA2 membrane. An additional 12-gfd sample was collected after 18 h to verify that quasi-equilibrium was reached. After 1 h, 250 mL of permeate was collected before sampling to allow the system to equilibrate. Duplicate samples were collected in the appropriate vials, depending on analytical method, from feed and permeate stream. Samples were stored at 4 $^{\circ}\text{C}$ pending analysis. A minimum of two experiments for each set of compounds was performed.

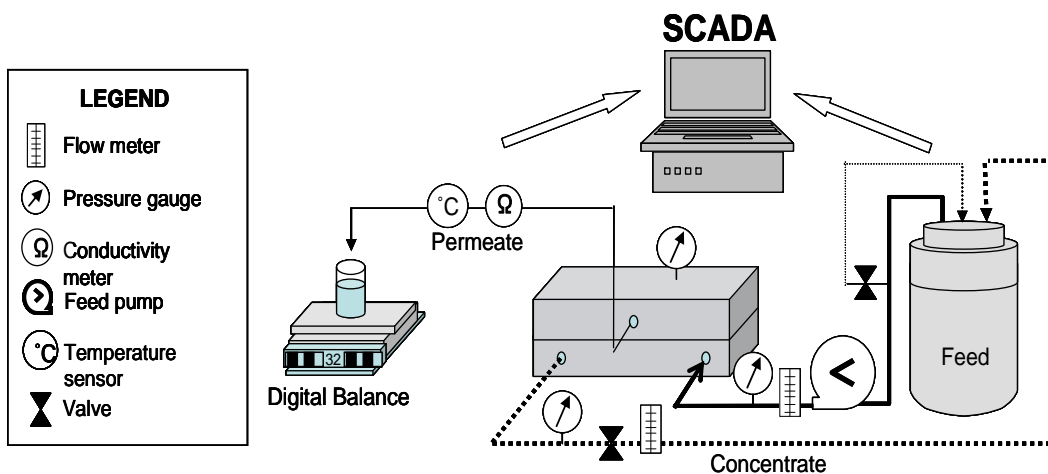


Figure 3.5. Bench-scale membrane testing unit process flow diagram.

3.3.1.2 Once-Through Mode

For the purposes of developing more-accurate rejection models, it is necessary to determine compound-specific rejection for a given system at a state of equilibrium. This situation involves reaching a point in an experiment where permeate and feed concentrations are independent of time. Many compounds tested during our research exhibited stable concentrations relatively quickly. For some compounds, however, feed and permeate concentrations failed to stabilize within the course of a 24-h experiment. Of the compounds considered, THMs displayed the most extreme case of concentration instability. In several experiments the rejection of these compounds dropped below 0, implying a higher concentration in the permeate stream than in the feed stream. Figure 3.6 depicts this rejection decline for bromodichloromethane (BDCM) during a recirculation experiment. This negative rejection was an artifact of the experimental setup and had to be remedied in order to understand the behavior of partitioning compounds like the THMs.

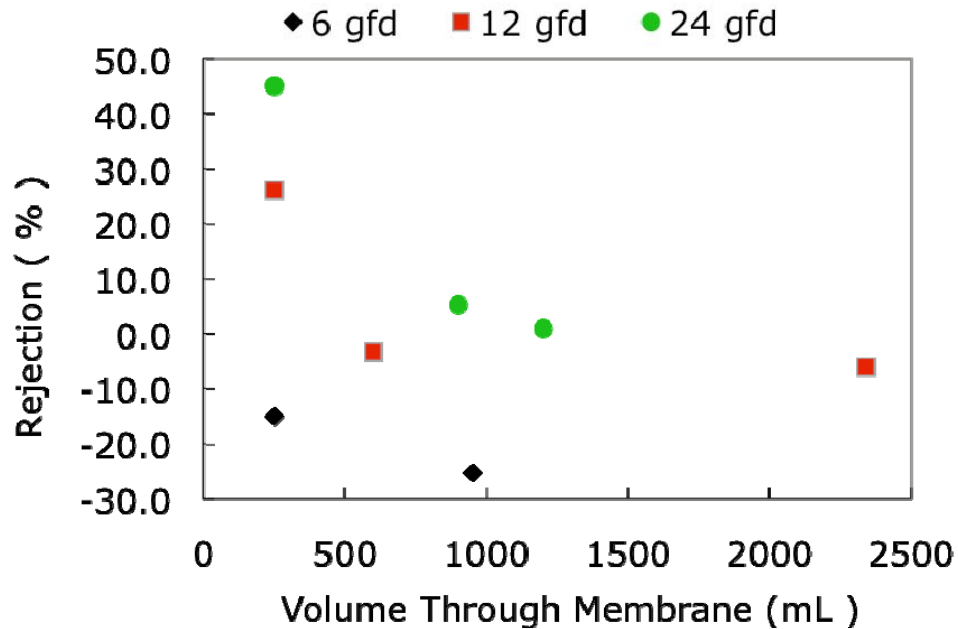


Figure 3.6. Rejection of BDCM by NF-270 membrane in recirculation experiments.

Declining concentration in the feed solution was the main factor that caused negative rejection results in recirculation experiments. An example of the declining feed concentration observed for BDCM in recirculation experiments is shown in Table 3.5. Compound mass from the feed solution was continuously being lost because of adsorption onto various interfaces within the system and into the membrane matrix. Therefore, as the feed solution was recycled, it constantly returned to the feed tank with less mass. Increasing the flux rate increased the mass that was exposed to the membrane. Therefore, the rate of mass lost to the system increased with the increasing flux rate. This phenomenon made it impossible to compare compound rejection behavior against flux even if the concentration decline could be factored out. As a consequence, the team designed a system that eliminated the recirculation aspect of the experiments.

The main objective in designing a new system was to provide a stable feed concentration to the membrane. In order to avoid recycling the feed water, a system was devised that did not require that permeate and concentrate streams be recycled. Two 500-gal tanks connected in parallel were filled with deionized water and were spiked with compounds to be tested. This solution was fed to the membrane cell after which both permeate and concentrate streams were wasted. Figure 3.7 illustrates the system with feed tanks in the background and membrane cell, pump, and computer in front. Experiments run by using this setup will be referred to as “once-through” experiments throughout the report.

Table 3.5. Feed Concentration Measurements Taken Throughout Three Recirculation Experiments with BDCM

Exptl Flux Set-Point	No. of h after Startup	Feed Conc (mg/L)
6 gfd	0.0	176
	5.8	114
	22.2	82
12 gfd	0.0	90
	2.9	92
	7.0	86
	27.3	24
24 gfd	0.0	136
	1.5	118
	5.3	104
	7.0	94



Figure 3.7. Once-through experimental apparatus at Colorado School of Mines.

With a feed flow rate of 1000 mL per min, these experiments could proceed for more than 50 h before the feed water was exhausted. Table 3.6 presents the feed concentration values for BDCM during two once-through experiments. The data in this table revealed a steady decline in feed concentration over time. This same trend was observed for the three other THMs during once-through experiments. It is unclear what mechanism caused these feed concentration declines, but volatilization and partitioning to tank walls are probably responsible for most of the mass loss.

Table 3.6. Feed Concentration Measurements Taken Throughout Two Once-Through Experiments with BDCM

Expt 1		Expt 2	
Time	Feed Conc	Time	Feed Conc
(h after startup)	($\mu\text{g/L}$)	(h after startup)	($\mu\text{g/L}$)
0	504	0	86.8
1	500	1	77.0
2	490	2	84.5
4	474	3.5	72.3
7	456	6	85.1
22	367	7.5	78.9
25	316	9.5	82.5
27	294	24.5	13.1
32	268	26.5	37.4
47	228	29.5	69.3
52	213	32.5	66.9
53	215	33.5	62.0
58	206	50.5	67.3
59	206	51.5	61.9
		55.5	56.2

Although the concentration did steadily decrease throughout the experiments, the decline was not as rapid as observed in the recirculation experiments. In addition, mass loss was decoupled from the flux, which was not the case during recirculation experiments. In spite of the decline, rejection levels did show a stabilizing trend in once-through experiments. This observation leads to the conclusion that the feed concentration decline was slow enough to allow the permeate stream to reach steady state and to reflect a concentration gradient appropriate for that level. Analysis of the results of the THM experiments will be discussed in Section 4.1.3.

3.3.1.3 Estimating Concentration Polarization

The degree of concentration polarization during bench-scale experimentation was determined by employing two different methods, velocity variation method and the flux variation method. These methods are discussed later.

Velocity Variation Method. A series of experiments was conducted on the basis of the velocity variation method adapted from Geraldine and de Pinho (2006) to estimate the intrinsic rejection. Velocity and hydraulic diameter calculations utilized methods from Schock and Miquel (1987). By using the bench-scale flat-sheet setup, caffeine, acetaminophen, 2-naphthol, and resorcinol were separately examined as the feed flow rate was varied from 1 to 7 L/min in increments of 1 L/min at constant permeate flux rate of 55 gfd. Experiments were conducted at constant water temperature (18.5°C) and a pH of 6.3. After 1 h elapsed and 250 mL of permeate was collected to allow the system to equilibrate, sampling was conducted. Duplicate samples were collected in HPLC vials from feed and permeate streams and stored at 4°C pending analysis. A minimum of two experiments for each set of

compounds was conducted in order to confirm results. New flat-sheet membrane specimens were inserted for each velocity set-point. Rejection was quantified by using the HPLC UV-DAD method. The coefficients for the Sherwood equation were calculated and are displayed in Equation 3.5.

$$Sh = 0.225Re^{0.83}Sc^{0.83} = \frac{k_d h}{D_1} \quad (3.5)$$

The concentration at the membrane surface and intrinsic rejection can be calculated by using Equations 3.6 and 3.7, respectively.

$$\beta = \frac{C_m}{C_f} = \exp\left(\frac{Jv}{k}\right) \quad (3.6)$$

$$R_{int} = \frac{R_{obs} \exp(Jv/k)}{1 - R_{obs} \exp(Jv/k)} \quad (3.7)$$

Flux Variation Method. A series of experiments was conducted on the basis of the flux variation method adapted from Sutzkover et al. (2000). Applying the bench-scale flat-sheet membrane system, researchers varied permeate flux rates from 12 to 85 gfd at a constant feed flow rate by using a solution of sodium chloride spiked in deionized water. Experiments were conducted at a constant water temperature (18.5 °C) and pH of 6.3. After 1 h elapsed and 250 mL of permeate was collected, sampling occurred. Duplicate samples were collected from feed and permeate streams and were stored at 4 °C pending analysis. A minimum of two experiments for each set of compounds was conducted in order to confirm results. New flat-sheet membrane specimens were inserted for each flux set-point. Concentrations were quantified by using conductivity measurements. The coefficients for the Sherwood equation were calculated by using Equation 3.8.

$$Sh = 0.16Re^{0.47}Sc^{0.83} = \frac{k_d h}{D_1} \quad (3.8)$$

Method Analysis. The coefficients in the empirical correlations (Equations 3.5 and 3.8) obtained from the two methods described earlier resulted in large deviations between observed and intrinsic rejections, especially at high permeate flux rates. Even though these values were determined by two separate peer-reviewed methods, further analysis was conducted to evaluate whether these coefficients yielded unrealistic intrinsic rejections. It was observed that, at low Reynolds numbers, between 157 and 1090, rejections significantly changed; however, at higher Reynolds numbers, between 1090 and 1557, rejection increased by less than 1%. This finding suggests that the two peer-reviewed methods used to calculate the Sherwood correlation coefficients resulted in an overestimation of intrinsic rejection at high permeate flux rates. Assuming limited rejection was reached at a Reynolds number of 1557, the coefficients were recalculated and yielded new coefficients as presented in Equation 3.9, which were used in this study.

$$Sh = 0.42Re^{0.5}Sc^{0.83} = \frac{k_d h}{D_1} \quad (3.9)$$

3.3.2 Pilot-Scale Membrane System

A pilot-scale NF/RO system at Colorado School of Mines (CSM) was used for controlled spiking studies in tap water to study the rejection of select nitrosamines by NF membranes. The pilot-scale system is a two-stage membrane unit that was designed to mimic a two-stage full-scale treatment system. The unit was built in a four-stage array configuration to minimize space and consists of six pressure vessels, four in the first stage and two in the second stage. The pilot-scale unit requires 21 4040 spiral-wound elements, with 14 elements in the first stage and 7 elements in second stage. The system is equipped with a SCADA system; has a variable speed feed pump; and can be operated at different recoveries, feed flow rates, and permeate flux rates. On the basis of the system's configuration, it requires a feed flow rate between 15 and 25 gpm and therefore was operated in recycle mode, where permeate and concentrate streams were returned to the feed water tank. The system is fed water from two 500-gal feed tanks that are temperature controlled by using an in-house chilled process water stream. The pilot-scale system has multiple sampling locations that allows for samples to be collected from the feed, permeate from each pressure vessel, combined permeate from the first stage, combined permeate from the second stage, total combined permeate, concentrate from pressure vessels, first-stage combined concentrate, and total combined concentrate. A schematic and picture of the pilot-scale unit with sampling locations are presented in Figures 3.8 and 3.9, respectively.

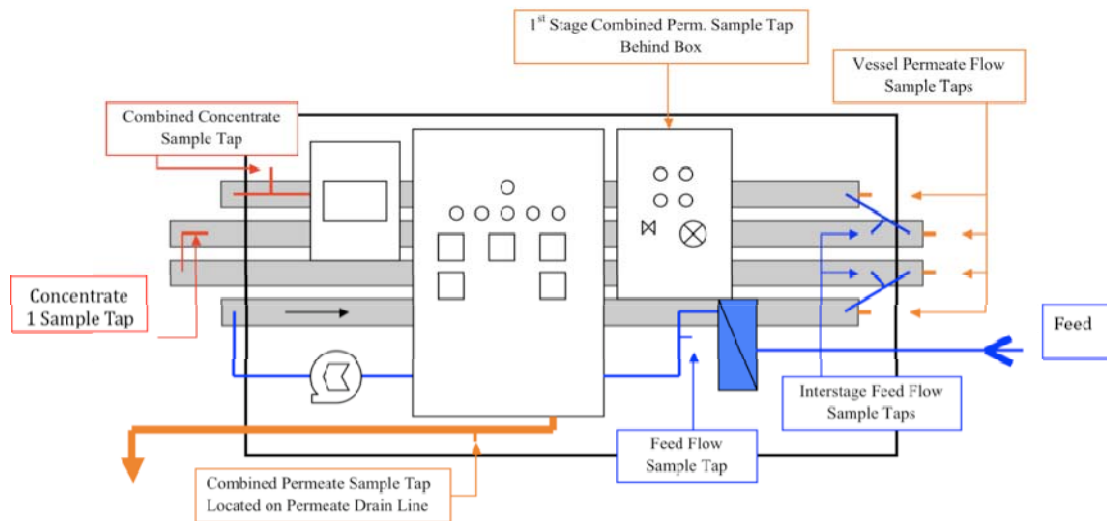


Figure 3.8. Schematic of pilot-scale membrane unit and sampling locations.



Figure 3.9. CSM’s pilot-scale membrane skid.

3.3.3 Full-Scale Sampling Campaign at Orange County Water District

The Orange County Water District (OCWD), CA, Groundwater Replenishment System (GWRS) Advanced Water Purification Facility (AWPF) utilized reclaimed water after primary and secondary treatment. Primary wastewater treatment consists of coagulant addition and sedimentation. Following primary clarification, the primary effluent flow stream was split and oxidized by using two secondary treatment processes: activated sludge and trickling filters. Secondary clarifiers at the activated sludge system and trickling filters produced fully oxidized and clarified secondary effluent. Subsequently, the effluent is pumped to the GWRS AWPF, where it is treated with MF, RO, and UV-peroxide advanced oxidation processes. The secondary treated wastewater was first chloraminated prior to MF. The water was then treated by MF by using Siemens/Memcor submerged hollow-fiber membranes with a maximum nominal pore size of 0.2 μm . The water is then diverted to RO (ESPA2 membranes; Hydranautics, Oceanside, CA) system (Figures 3.10 and 3.11). Upstream of the RO process, the flow was pretreated by adding sulfuric acid for pH adjustment and scaling inhibitor to prevent precipitation of sparingly soluble salts and by 10- μm -pore-size cartridge filtration. The system was designed to operate at pH 6.8, an 85% recovery rate, and at a permeate flux of 12 gfd.



Figure 3.10. OCWD’s RO membrane gallery.



Figure 3.11. OCWD’s RO membrane elements within pressure vessels.

3.3.4 Challenges

Past work developing models to describe the rejection of organic contaminants has generally used flat-sheet membrane configurations for experimentation (Kiso et al., 1996, 2000, 2001a; Kimura et al., 2003a and 2003b). Flat-sheet material can be obtained through two means: the membrane manufacturers provide dry, flat-sheet specimens, or flat-sheet material can be cut out of spiral-wound elements. As was found by a study on modeling organic contaminant removal by KIWA (Hofman et al., 2007), the properties of flat-sheet material can vary significantly throughout a spiral-wound element. These differences can affect rejection performance and ultimately lead to the development of models that are not applicable to large-scale systems with large amounts of membrane area. Because one objective of this project was to develop modeling approaches at bench scale and to upscale the approaches to modeling a pilot-scale system, it was imperative that the flat-sheet material be representative of the membrane properties of an entire large-scale system.

3.4.4.1 Flat-Sheet Specimens

Two years before the start of this project, experiments were conducted to quantify the removal of organic contaminants by the NF membrane (Dow/Filmtec). The NF membrane was obtained in rolls of dry, flat-sheet material from Dow/Filmtec, and rejection of a variety of compounds was determined as a function of permeate flux. During this study, 21 spiral-wound elements (4 in. × 40 in.) were obtained for pilot-scale experiments and multiple spiral-wound elements were later sacrificed for bench-scale experiments. Unfortunately, the results obtained for the rolls of flat-sheet material were not comparable to results obtained by using the membranes cut from spiral-wound membranes (Figure 3.12). For many of the compounds tested, the rejection using the flat-sheet material provided by the manufacturer yielded significantly lower rejection than did flat sheets cut from the spiral-wound elements. Because these experiments were performed under identical conditions at bench scale, possible explanations for this discrepancy include that the manufacturer changed the polymer chemistry during the 2-year period, the roll of flat-sheet material was flawed, the surface of the spiral-wound material was modified by the manufacturer, or the spiral-wound membrane was modified (e.g., compacted) during limited pilot-scale experiments.

Additional membrane–organic solute rejection experiments were conducted with NF-270 membranes obtained in flat-sheet rolls from the manufacturer and also cut from virgin spiral-wound NF-270 modules (4 in. × 40 in.). Similar results were observed (Figure 3.13), with the membranes cut from the spiral-wound elements providing greater rejection for the solutes investigated. Whatever the explanation, the discrepancy highlights a few difficulties associated with developing membrane models. These include the following:

- Models developed from a rejection data set may not be applicable for a data set generated with the same membrane type but different flat-sheet material.
- Manufacturers may alter membrane chemistries and properties, which may significantly affect rejection performance and subsequently the applicability of a previously developed modeling approach.
- Upscaling results obtained at bench scale to larger-scale systems may be difficult because of the large amount of membrane area in large systems and associated variability.

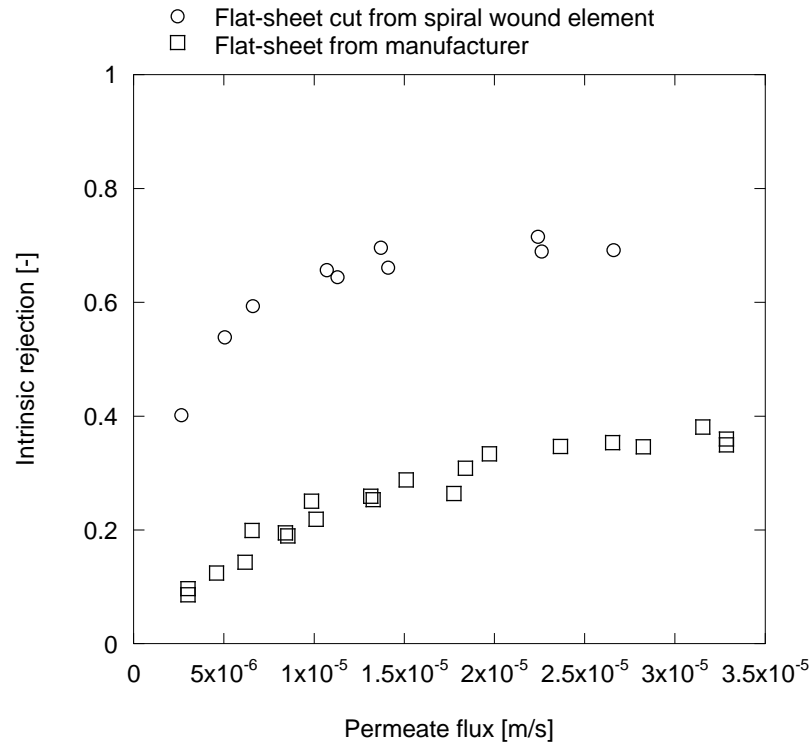


Figure 3.12. Rejection of acetaminophen by NF membrane (Dow/Filmtec) obtained in different configurations.

Note: Experiments were conducted at 18.5 °C.

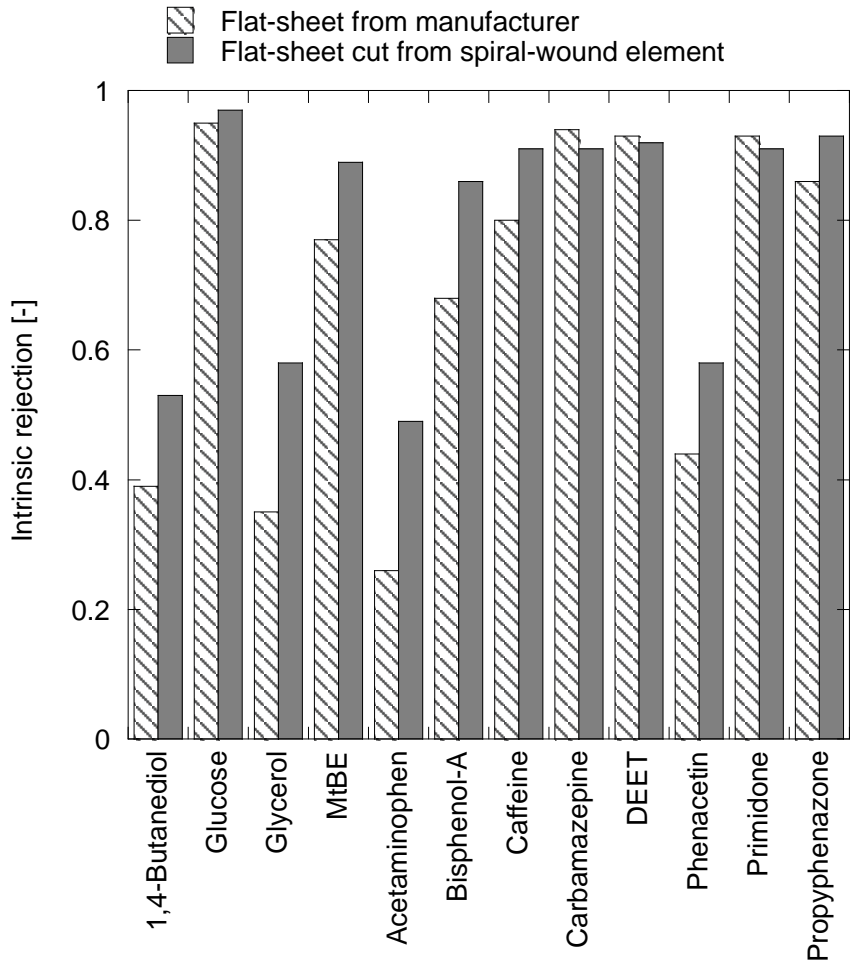


Figure 3.13. Rejection of neutral organic solutes by NF-270 membrane (Dow/Filmtec) obtained in different configurations.

Note: Experiments were conducted at 18.5 °C and a permeate flux rate of 12 gfd.

Chapter 4

Bench-Scale Rejection Database

4.1 Bench-Scale Experiments to Augment Rejection Database

Bench-scale experiments were conducted with selected target compounds (see Table 3.2) to determine their rejection behavior using representative NF and RO membranes. The compounds investigated, listed in Table 3.2, included zwitterions and HN and HoN, neutral, negatively charged, and positively charged substances. The rejection behavior was expressed as percent removal, and solute transport parameters were determined that are specific to certain modeling approaches. This information was compiled in a rejection database that provided the foundation to test and improve various modeling approaches with the aim to mathematically describe and ultimately predict rejection. The NF-270 membrane from Dow/Filmtec was selected as a representative NF membrane because this membrane had been employed in previous pilot-scale studies using reclaimed water and exhibited excellent rejection performance for organic solutes, low fouling propensities, and a significantly lower specific flux than conventional RO membranes (Bellona and Drewes, 2007; Bellona et al., 2008). The ESPA2 membrane from Hydranautics was selected as a representative LPRO membrane because this membrane is employed at several full-scale water reclamation facilities.

The following sections describe the rejection behavior of the target solutes selected for this study. The results of these experiments are presented by considering expected rejection mechanisms and also by highlighting those compounds that exhibited strong solute–membrane interactions. The findings from these experiments were compiled in a rejection database that presented the foundation for rejection modeling approaches for the solute groups described in Chapter 5.

4.1.1 Rejection of Solute with Expected Behavior

4.1.1.1 Solute Rejection Versus Flux for NF and RO Membranes

Observed and intrinsic rejection was calculated for all compounds at each permeate flux rate evaluated for both NF-270 and ESPA2 membranes (figures for all compounds in Appendices E and F for the NF-270 and ESPA2 membranes, respectively). Compounds that have minimal interactions (i.e., adsorptive effects) with the membrane exhibit increased rejection with increased permeate flux for the NF-270 membrane as illustrated with acetaminophen rejection in Figure 4.1. With a small increase in permeate flux, a large increase in rejection was observed. For example, as the permeate flux rate increased from 5 to 12 gfd, acetaminophen rejection increased from 19 to 30%. A similar rejection behavior was observed by Agenson et al. (2003). It is worth noting that average deviation values for flux and rejection (Figure 4.1) were calculated from replicate experiments by using different membrane specimens cut from the same spiral-wound element. Permeate flux average deviations are due to the difficulty in achieving exact permeate flux for replicate experiments. Similar behavior was observed with the ESPA2 membrane, illustrated with NDMA rejection in Figure 4.2. As the permeate flux increased from 4 to 8 gfd, NDMA rejection increased from 35 to 47%.

As discussed in Chapter 2, for the permeate flux range evaluated during the study, the transport of solutes towards the membrane is greater than diffusive transport away from the membrane. Compared to the bulk solution (i.e., feed water) this phenomenon causes an increased concentration of solutes at the membrane surface and is termed concentration polarization (Hofman et al., 2007; Sutzkover et al., 2000). Although observed rejection is linked to the concentration of solutes in the bulk solution, intrinsic rejection (Equation 2.11) is linked to the concentration of the solute at the membrane surface, which allows for the calculation of rejection in the absence of concentration polarization effects. Concentration polarization increases with increased permeate flux; therefore, the difference between observed rejection and intrinsic rejection becomes greater at higher permeate flux (Figures 4.1 and 4.2).

Although the majority of compounds with minimal membrane interactions exhibited increasing rejection with increasing flux, compounds that are highly rejected (greater than 90%) display rejection that does not change significantly with increasing permeate flux. As presented in Figure 4.3, observed and intrinsic rejection for estriol for the NF-270 membrane remains relatively flat with various permeate flux rates. The hydrophobic estriol (Log D = 2.94 at pH 6) with a molecular weight of 288.4 g/mol exhibited rejection greater than 90% and did not exhibit decreasing rejection over time, contradicting the observation from Braeken et al. (2005). Braeken et al. (2005) observed rejection of hydrophobic compounds decreasing over time because of adsorption to the membrane; however, this effect does not seem to apply to all hydrophobic compounds. This phenomenon will be discussed in further detail in Section 4.1.3. It should be noted that the variation between duplicate rejection experiments for estriol was minimal; therefore, error bars are too small to be seen in Figure 4.3.

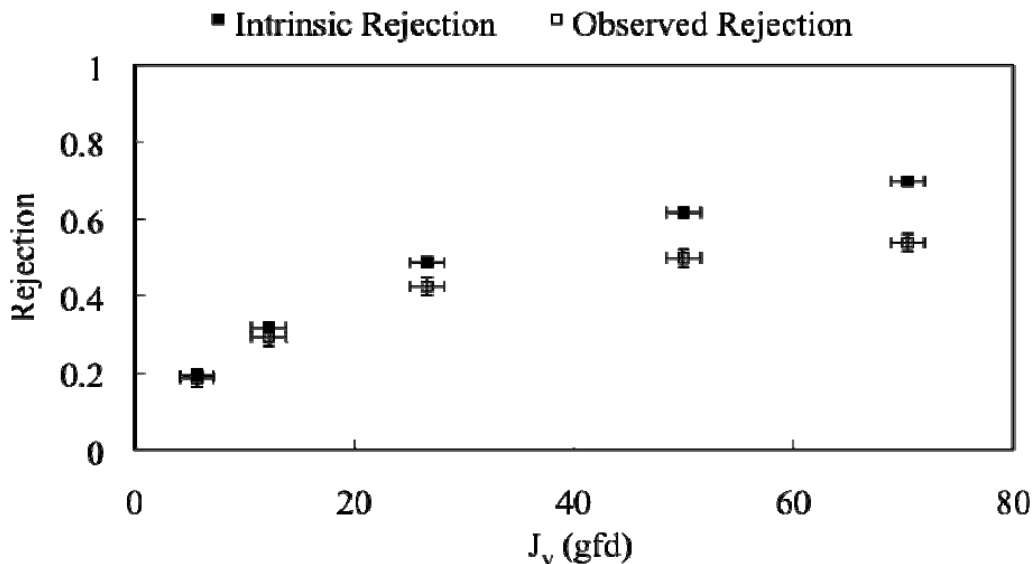


Figure 4.1. Average bench-scale intrinsic and observed rejection over a range of permeate fluxes for acetaminophen for NF-270 membrane.

Note: Error bars represent average deviation values calculated from replicate experiments.

Compounds that exhibit relatively high rejection (greater than 90%) for the ESPA2 membrane also display rejection that does not change significantly with permeate flux.

Presented in Figure 4.4, ciprofloxacin is rejected by 98% independent of permeate flux rate. This was the case for 90% of the compounds tested with the ESPA2 membrane, exhibiting greater than 90% rejection because of the small pores of the ESPA2 membrane.

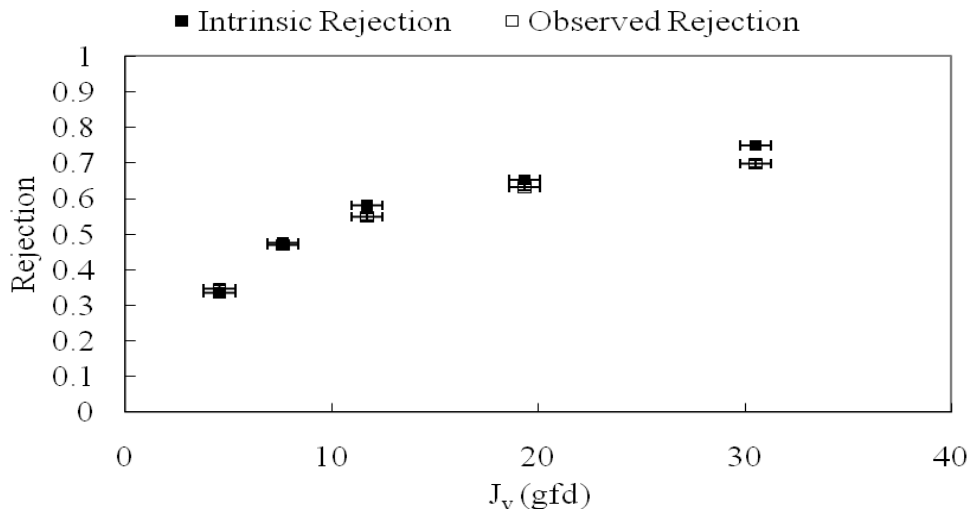


Figure 4.2. Intrinsic and observed rejection as a function of permeate flux for NDMA for ESPA2 membrane.

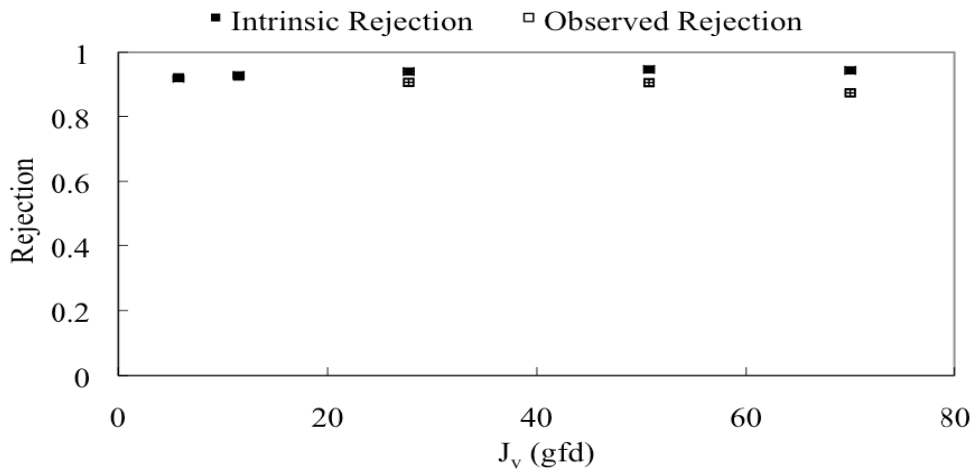


Figure 4.3. Intrinsic and observed rejection for estriol as a function of permeate flux for NF-270 membrane.

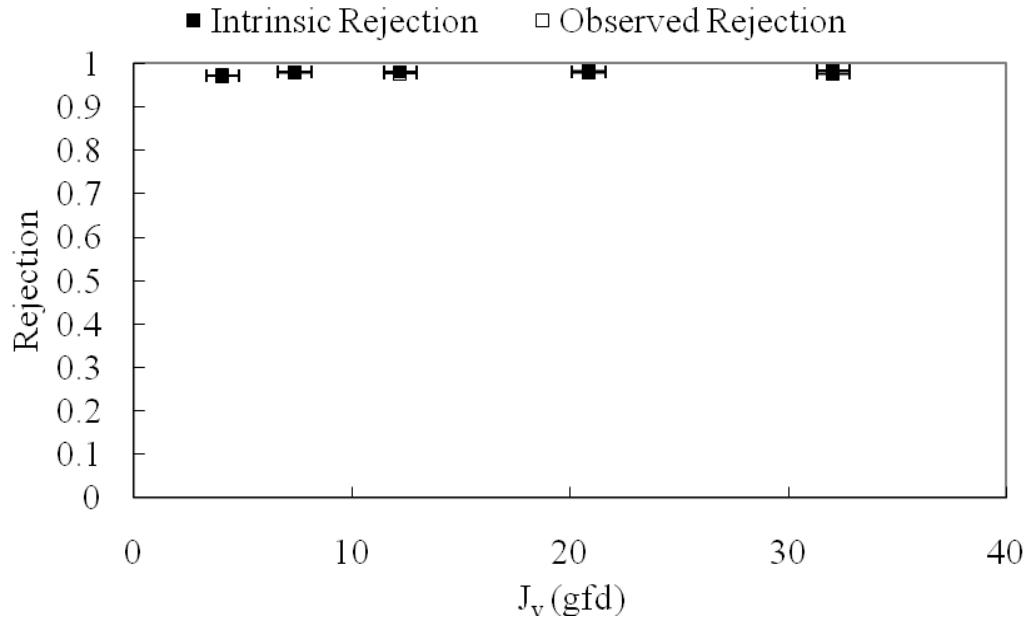


Figure 4.4. Intrinsic and observed rejection as a function of permeate flux for ciprofloxacin for ESPA2 membrane.

Benzyl alcohol exhibited increased rejection with increasing permeate flux for the NF-270 membrane (Figure 4.5); however, initial rejection was observed to be negative, suggesting the concentration in the permeate was higher than the concentration in the feed. Because observed rejection takes into account only the feed and permeate concentration, a large concentration buildup at the membrane surface could result in negative observed rejection. Hydrophilic benzyl alcohol (Log D = 1.01, pH 6) is composed of an aromatic ring with an attached hydroxyl group. Williams et al. (1999) reported that aromatic structures with an attached hydroxyl group have strong affinity to a membrane surface. Matsuura and Sourirajan (1971) also reported this adsorption phenomenon for these types of solutes.

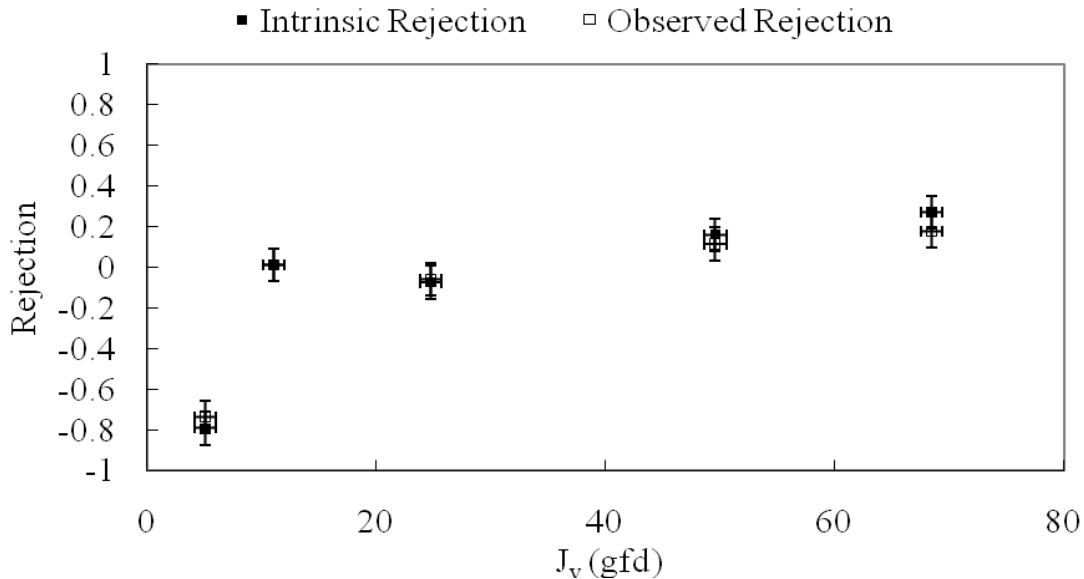


Figure 4.5. Intrinsic and observed rejection of benzyl alcohol as a function of permeate flux for NF-270 membrane.

4.1.1.2 Rejection Due to Steric Exclusion

As discussed previously (see Chapter 2), the rejection of nonionic organic compounds (i.e., HN, HHoN, and HoN) is mainly influenced by steric effects (Agenson et al., 2003; Bellona et al., 2004; Kimura et al., 2004; Van der Bruggen et al., 1999). The observed rejection of ethanol, glycerol, and glucose for the NF-270 membrane is presented in Figure 4.6 as a function of permeate flux rate. These compounds exhibit increasing rejection with increasing permeate flux. Rejection also increases for each compound with increasing molecular weight: glucose (molecular weight of 180 g/mol) exhibits the highest rejection, glycerol exhibits moderate rejection (molecular weight of 92 g/mol), and ethanol (molecular weight of 46 g/mol) exhibits the lowest rejection. This behavior indicates that steric exclusion is the main mechanism determining rejection for these nonionic compounds. Similar behavior, though less pronounced, was observed with the ESPA2 membrane; ethanol, glycerol, and glucose exhibit increasing rejection with increasing molecular weight (Figure 4.7). These compounds exhibit the same behavior through both membranes; however, compounds rejected by the ESPA2 membrane exhibit greater rejection than did those rejected by the NF-270 membrane, which is likely because the ESPA2 membrane has smaller pores.

Rejection due to steric effects for the NF-270 membrane is also illustrated in Figure 4.8 for caffeine (molecular weight of 194.2 g/mol) exhibiting the highest rejection, 1-naphthalenemethanol (molecular weight of 158.2 g/mol) exhibiting moderate rejection, and resorcinol (molecular weight of 110.1 g/mol) exhibiting the lowest rejection. Rejection due to steric effects for the ESPA2 membrane is presented in Figure 4.9 with NDMA, *N*-nitrosomethylethylamine (NMEA), and *N*-nitrosopyrrolidine (NPYR). NPYR (molecular weight of 100.1 g/mol) exhibited the highest rejection, NMEA (molecular weight of 88.1 g/mol) exhibited moderate rejection, and NDMA (molecular weight of 74.1 g/mol) exhibited the lowest rejection. Compound rejection increased with increasing molecular weight. Kimura et al. (2004) and Agenson et al. (2003) also reported increasing rejection with increasing molecular weight for neutral compounds that do not exhibit adsorptive effects.

From findings presented in Figures 4.6 and 4.9, it is revealed that compounds with similar molecular weights are rejected to different degrees by the NF-270 and ESPA2 membranes.

The rejection of select HN compounds at a permeate flux of 12 gfd for the NF-270 membrane (24 h after startup) with increasing molecular weight is presented in Figure 4.10. For these compounds, rejection increased with molecular weight, confirming findings reported by Kimura et al. (2004) and Agenson et al. (2003). In addition to results presented in Figure 4.6, a significant increase in rejection occurred after 180 g/mol, indicating that the MWCO of the NF-270 membrane is approximately 180 g/mol. The rejection of the same HN compounds at a permeate flux of 12 gfd for the ESPA2 (24 h after startup) with increasing molecular weight is presented in Figure 4.11. All compounds are greater than 90% rejected, except for NDMA (molecular weight of 74.1 g/mol). This finding indicates that the “effective MWCO” for the ESPA2 membrane is between 74.1 and 108.1 g/mol, much lower than the MWCO for the NF-270 membrane.

Rejection of HoN compounds at a permeate flux of 12 gfd 24 h after experiment startup is presented in Figure 4.12 for the NF-270 membrane (molecular weight and Log K_{ow} in parentheses). For the relatively hydrophobic compounds (i.e., Log $K_{ow} > 3$), a clear trend of increasing rejection with increasing molecular weight was not observed. Hydrophobic compounds with a molecular weight greater than 314 g/mol, such as progesterone, exhibited high rejection (greater than 90%). However, if one considers molecular weight alone, most of the hydrophobic compounds exhibited lower rejection than what was observed for the hydrophilic compounds. For example, the relatively hydrophilic compound TCEP (Log D of 0.48 at pH 6), with a molecular weight of 285.5 g/mol, exhibited 80% rejection, although triclosan (Log D of 5.17 at pH 6), with a molecular weight of 289.5 g/mol, had only 50% rejection. Lower-than-expected rejection of hydrophobic compounds with molecular weights greater than the MWCO of a membrane was also reported by Agenson et al. (2003). This finding indicates that, for these compounds, additional solute–membrane interactions besides steric exclusion may be important.

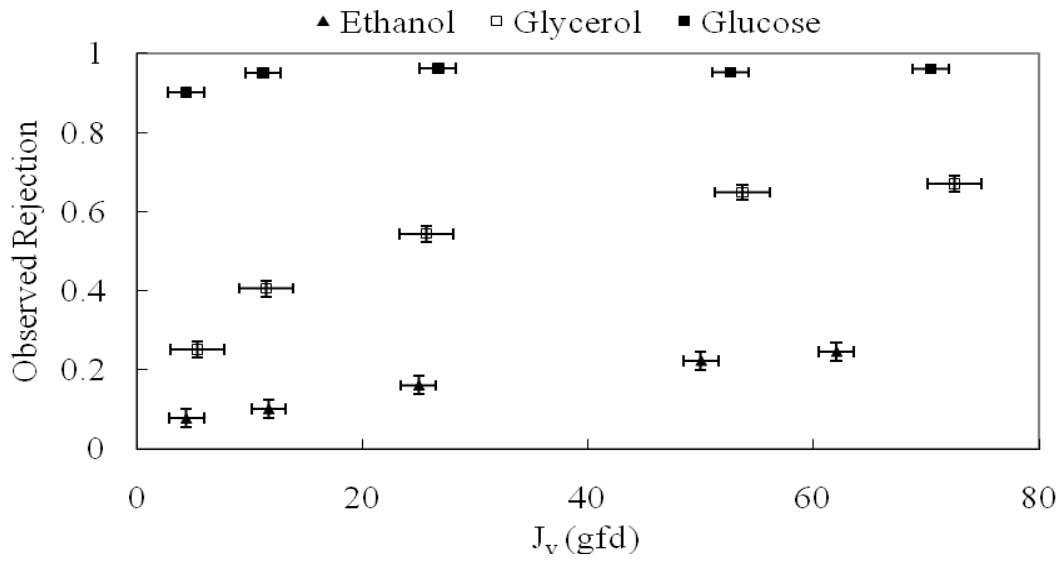


Figure 4.6. Observed rejection as a function of flux for ethanol, glycerol, and glucose for NF-270 membrane.

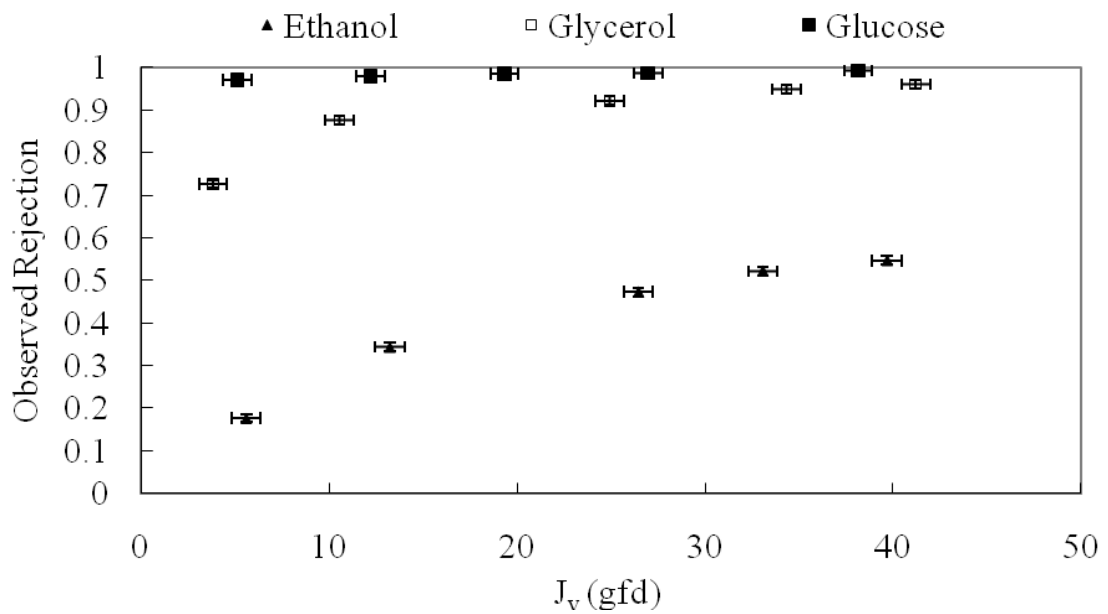


Figure 4.7. Observed rejection as a function of flux for ethanol, glycerol, and glucose for ESPA2 membrane.

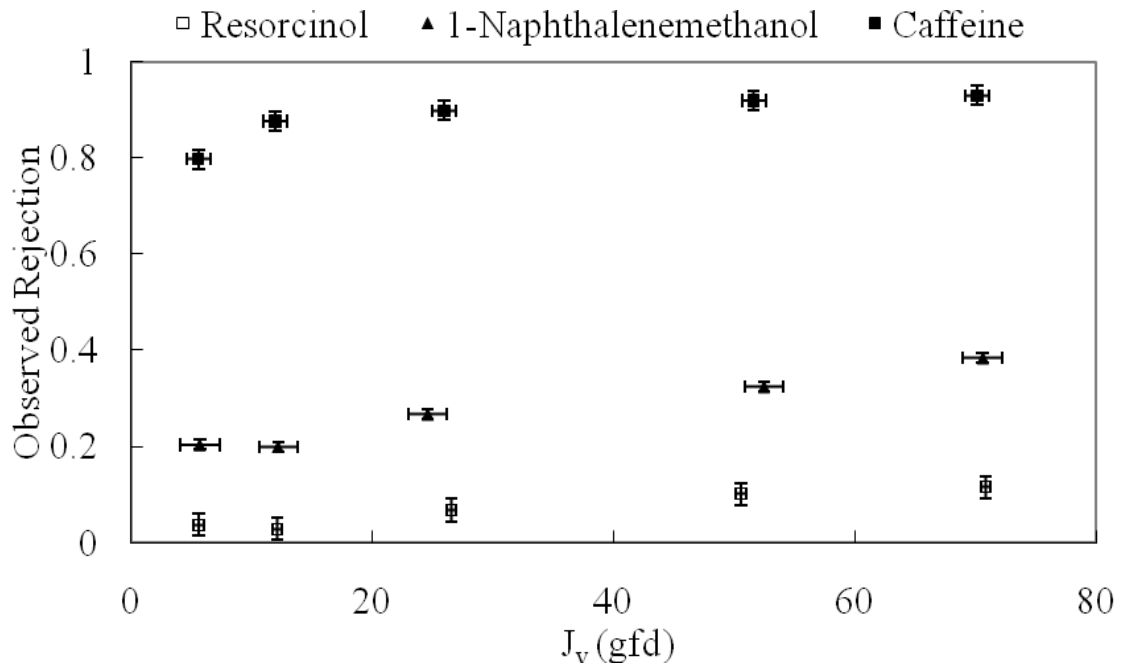


Figure 4.8. Observed rejection as a function of permeate flux for resorcinol, 1-naphthalenemethanol, and caffeine for NF-270 membrane.

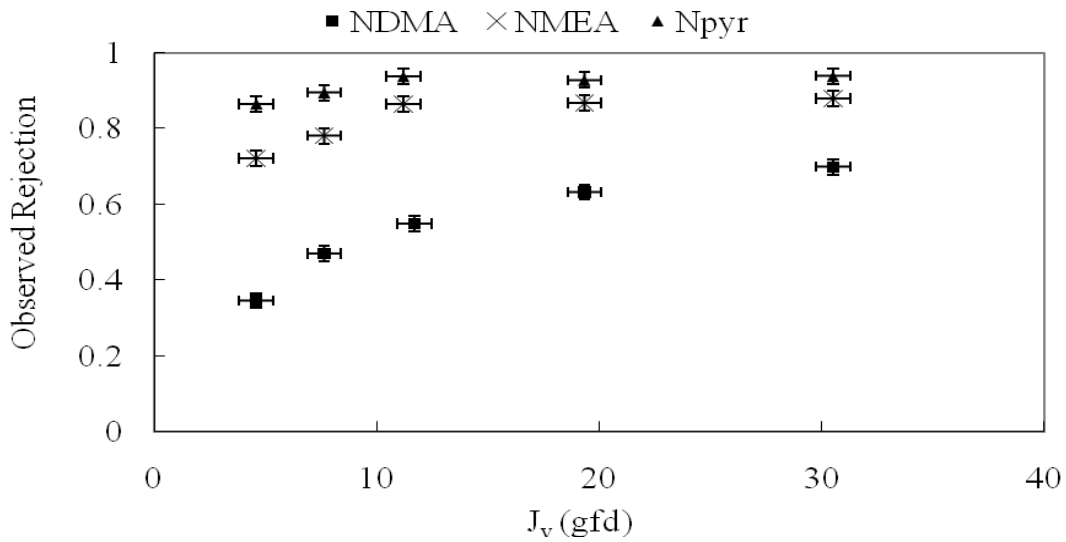


Figure 4.9. Observed rejection as a function of permeate flux for NDMA, NMEA, and NPYR for ESPA2 membrane.

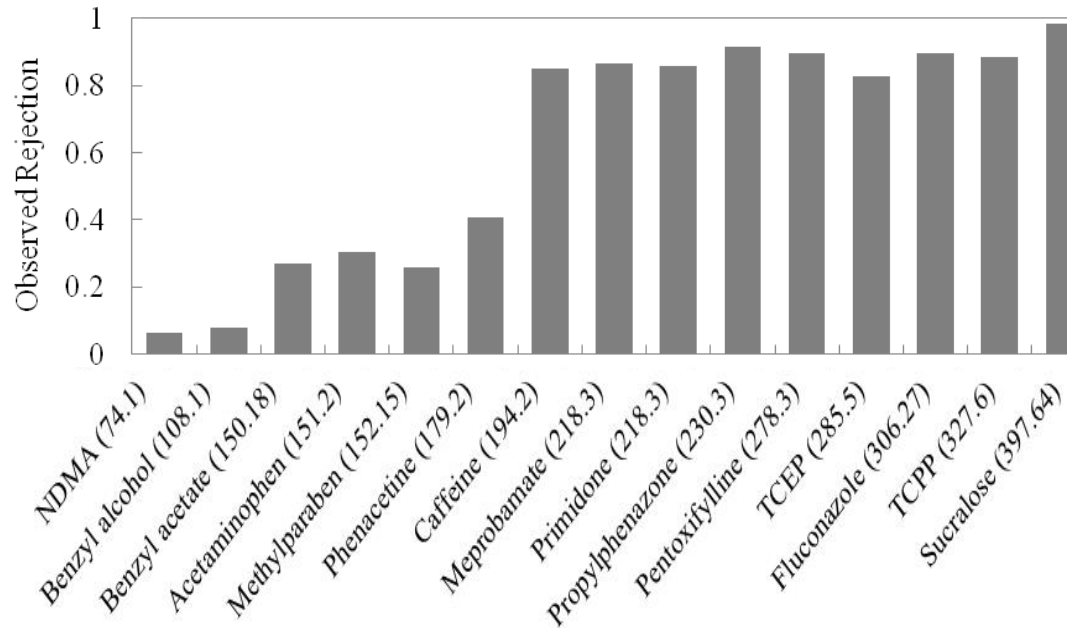


Figure 4.10. Observed rejection for HN compounds (molecular weight) at 12 gfd for NF-270 membrane 24 h after startup.

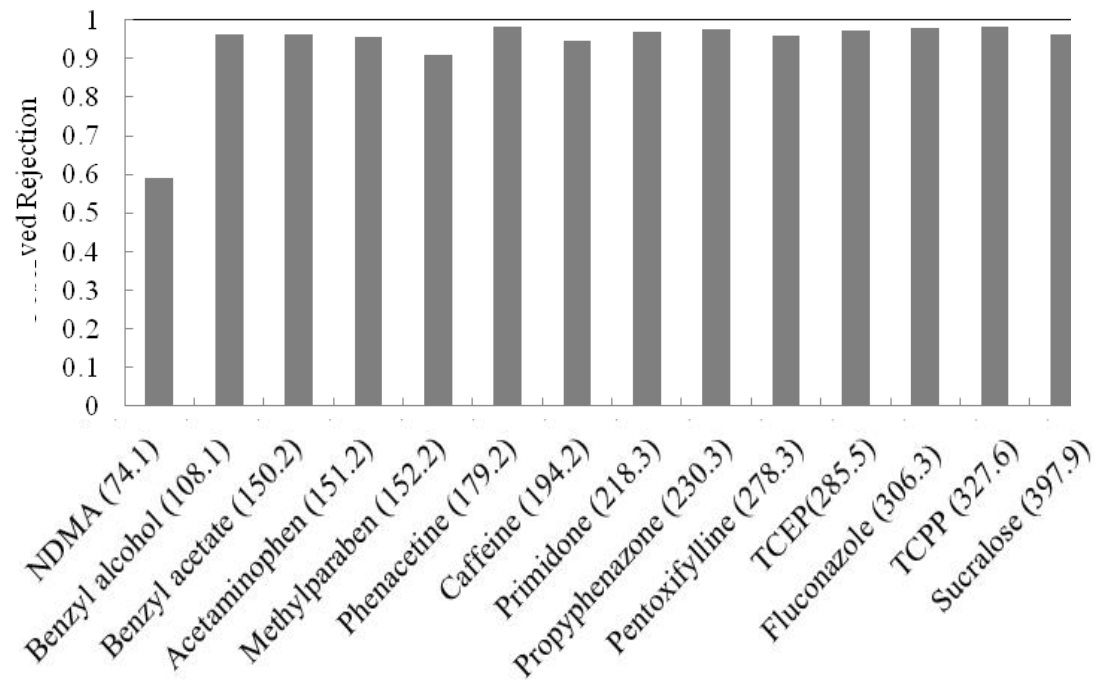


Figure 4.11. Observed rejection for HN compounds (molecular weight) at 12 gfd for ESPA2 membrane 24 h after startup.

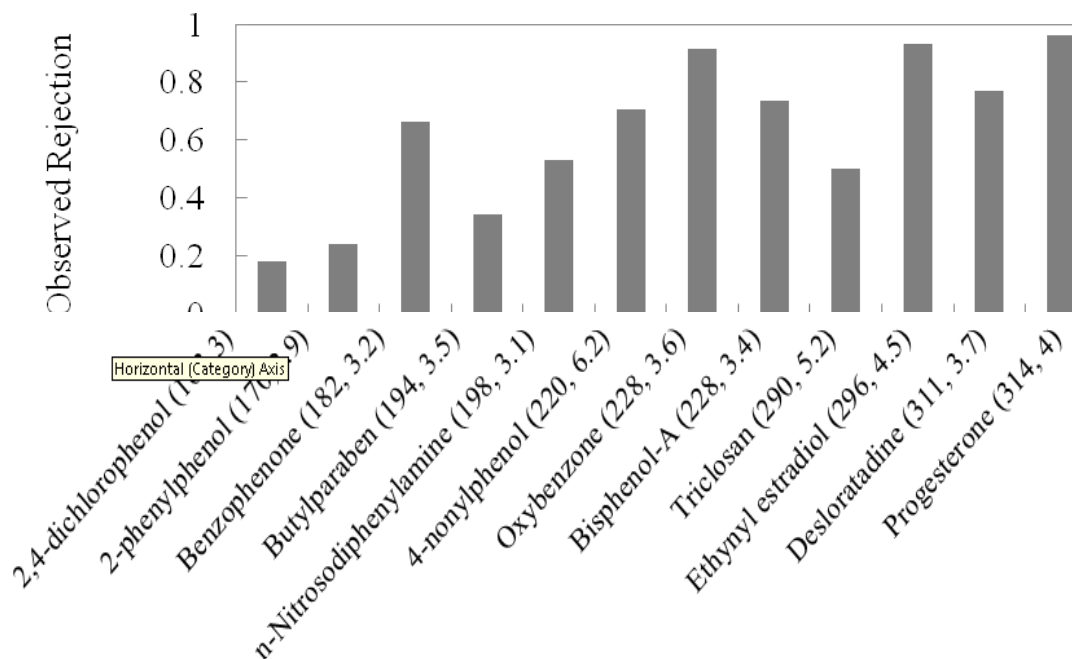


Figure 4.12. Observed rejection for compounds that are HoN (molecular weight, Log K_{ow}) at 12 gfd for NF-270 membrane 24 h after startup.

4.1.1.3 Electrostatic Exclusion

High removal (greater than 80%) was observed for the majority of the ionic compounds (i.e., HCN, HCP, HCNP) for the NF-270 membrane (Figure 4.13). All ionic compounds exhibited greater than 80% removal for the ESPA2 membrane (Figure 4.14). Negatively charged compounds are mainly rejected because of the electrostatic repulsion from the negatively charged membrane surface, exhibiting greater than 85% rejection for the NF-270 membrane and greater than 95% rejection for the ESPA2 membrane. The zwitterion compounds (HCNP) exhibited behavior similar to that of the negatively charged compounds, with most exhibiting rejection greater than 80% for both membranes. Removal rates for the positively charged compounds (HCP) were variable and ranged from 60 to >99% for the NF-270 membrane and 80 to 100% for the ESPA2 membrane. The lower-than-expected rejection for positively charged compounds was also reported by Verliefde et al. (2007). Positively charged compounds are hypothesized to be attracted to the negatively charged membrane surface, allowing for permeation through the membrane after a concentration layer builds. The concentration layer of positively charged compounds at the membrane surface can also result in lower observed rejection because observed rejection takes into account only the feed and permeate concentrations. However, low rejection was not observed for all positively charged compounds, as some were rejected close to >99%. Verliefde et al. (2007) observed higher rejection of compounds with an increase in compound concentration and theorized shielding effects were the cause. Positively charged compounds can shield the negatively charged membrane surface, leading to a lower concentration of positively charged compounds at the membrane surface and, therefore, result in higher observed rejection.

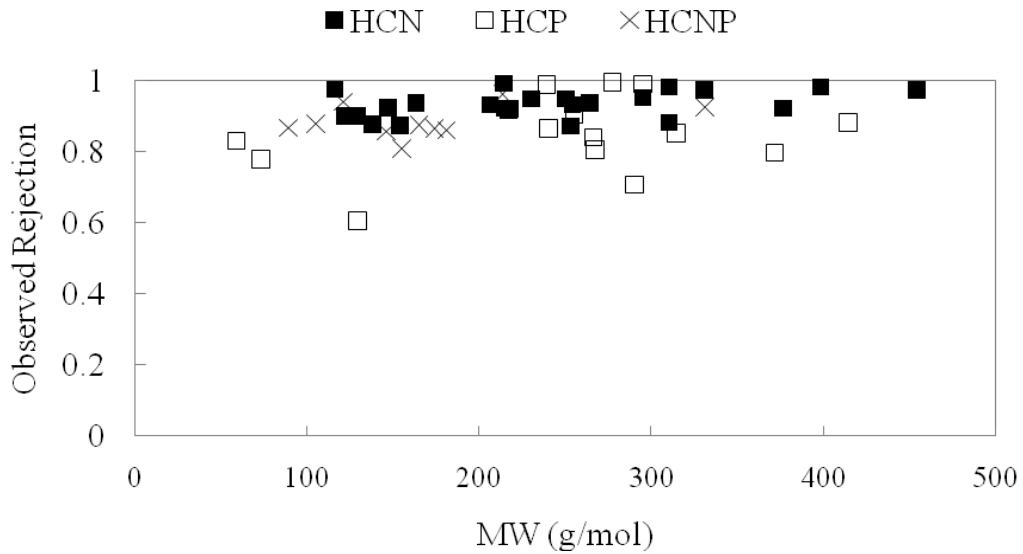


Figure 4.13. Observed rejection for ionic compounds at 12 gfd: negatively charged (HCN), positively charged (HCP), and zwitterions (HCNP) as a function of molecular weight for NF-270 membrane.

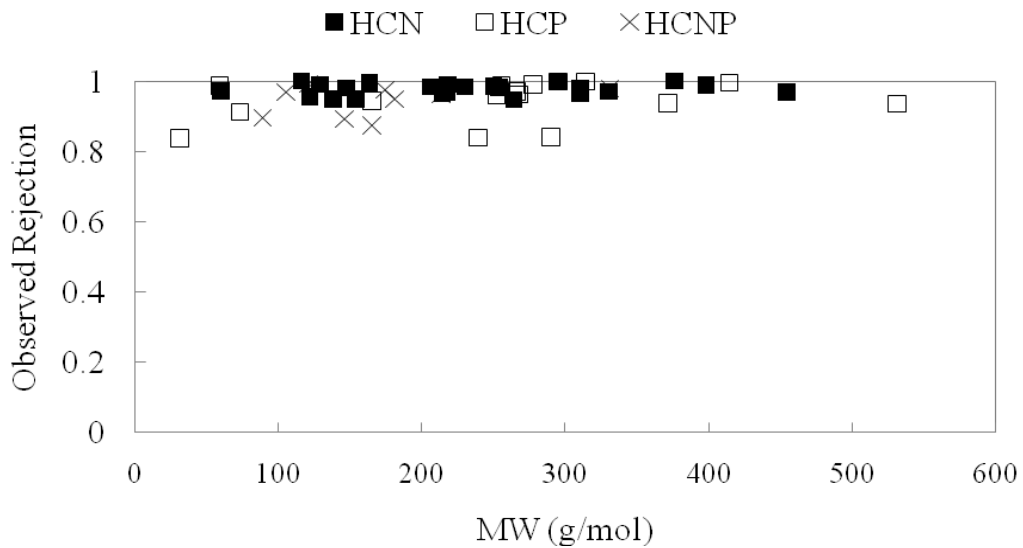


Figure 4.14. Observed rejection for ionic compounds at 12 gfd: negatively charged (HCN), positively charged (HCP), and zwitterions (HCNP) as a function of molecular weight (ESPA2 membrane).

Negatively charged compounds exhibited greater rejection based on their size, presumably because of electrostatic interactions with the membrane. For example, negatively charged compounds displayed greater rejection for the NF-270 membrane than did nonionic compounds of similar molecular weight (Figure 4.15). The rejection of negatively charged solutes still slightly increased with increasing molecular weight, indicating that steric

exclusion might still affect rejection for these compounds. Ozaki and Li (2002) also observed negatively charged compounds exhibiting higher rejection than did nonionic compounds.

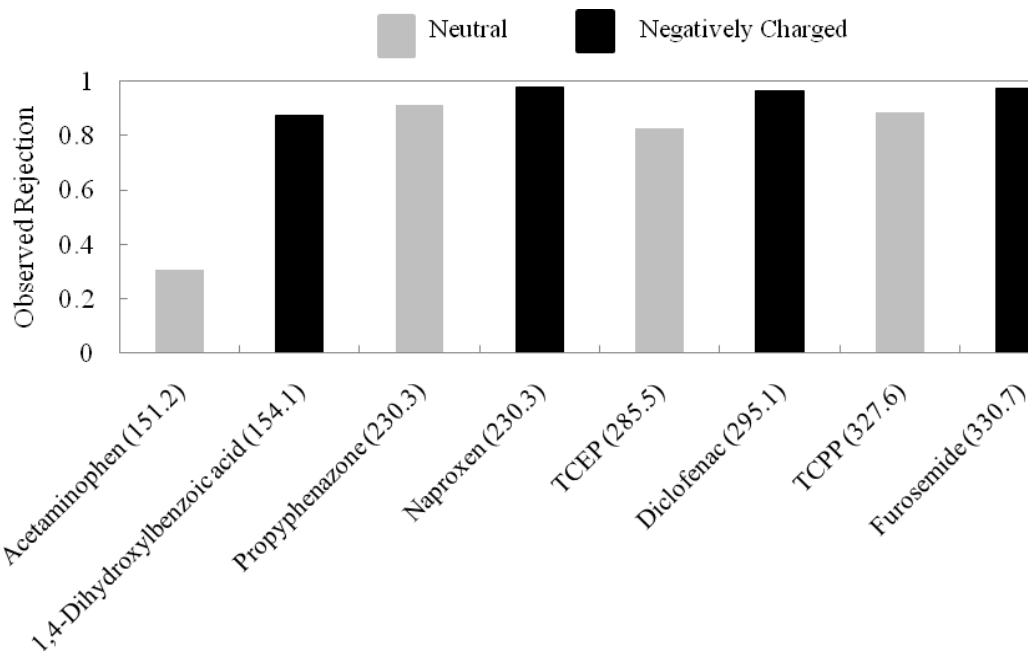


Figure 4.15 Observed rejection of negatively charged and neutral compounds with similar molecular weights for NF-270 membrane.

4.1.2 Rejection of Solutes Exhibiting Adsorptive Effects During Recycle Experiments

During bench-scale rejection experiments, compounds with adsorptive interactions behaved differently from compounds that are rejected solely by steric interactions for the NF-270 membrane. Adsorptive effects were not observed for the ESPA2 membrane because of the high rejection (greater than 90%) exhibited for the majority of the compounds independent of permeate flux. Adsorptive effects from using NF-270 membrane are presented in Figure 4.16 for the rejection of two nonionic compounds with similar molecular weights, 2-naphthol (molecular weight = 144.2 g/mol) and triethylene glycol (molecular weight = 150.2 g/mol). Observed rejection values are presented over the range of permeate fluxes evaluated with a sampling order of 5, 28, 50, 70, and 12 gfd with an additional 12-gfd sample collected 18 h after the first 12-gfd sample. Because of steric effects, these two compounds were expected to be similarly removed. However, 2-naphthol with a Log D of 2.71 had significantly lower rejection than triethylene glycol with a Log D of -1.87 (Figure 4.16) and also exhibited decreased rejection over time, which is likely due to adsorption (i.e., rejection decreases as the membrane becomes saturated). Braeken et al. (2005) observed a similar behavior for 3,4-methylnitrophenol, where rejection decreased significantly over time. Because 3,4-methylnitrophenol and 2-naphthol do not behave like triethylene glycol, different modeling approaches may be required to describe rejection of compounds exhibiting adsorptive effects.

Compounds exhibiting adsorptive effects can also exhibit different behavior with respect to adsorptive effects among each other. Rejection efficiencies for two HoN compounds, triclosan (Log D of 5.17 and molecular weight of 289.5 g/mol) and 4-*n*-nonylphenol (Log D of 6.17 and molecular weight of 220.4 g/mol), are plotted as a function of permeate flux in Figure 4.17 for the NF-270 membrane. Both compounds have molecular weights above the MWCO of the NF-270 membrane. Nevertheless, the solutes exhibited different rejection behavior. Observed rejection for 4-*n*-nonylphenol stayed relatively constant at 85% in the first 12-gfd permeate sample; however, a 15% rejection decrease was observed for the second 12-gfd sample collected after 18 h (circled point in Figure 4.17). Triclosan initially exhibited high rejection (98%), but rejection decreased over time (as well as with increasing flux rate). Rejection decreased by 47% from the first 12-gfd sample to the second 12-gfd sample collected 18 h later (circled point in Figure 4.17).

About 15% of compounds of all solutes tested exhibited adsorptive effects when the NF-270 membrane was used, and these are summarized in Table 4.1 with select solute properties (molecular weight and Log D [$\log K_{ow}$ at pH 6]). Two different levels of membrane retention interactions were qualified: moderate and extreme. Compounds with moderate interactions are those with increased rejection and increasing permeate flux but greater than 5% decrease in rejection at 12 gfd after 18 h. Compounds with extreme interactions exhibited decreased rejection over time, and rejection was observed to be independent of permeate flux. Compounds with moderate and extreme interactions were comprised of positively charged compounds and neutral compounds with various molecular weights and log D values. Positively charged compounds could be permeating through the membrane after 18 h because a concentration polarization layer occurred because of electrostatic interactions between the solute and the negatively charged membrane as proposed by Verliefde et al. (2007).

Previous researchers have attempted to predict rejection for compounds exhibiting solute–membrane interactions by correlating Log K_{ow} values with solute rejection (Braeken et al., 2005; Kiso et al., 2001a; Verliefde et al., 2007). Rejection of neutral compounds during NF-270 membrane bench-scale experiments was compared to Log K_{ow} values, and results are presented in Figure 4.18. Based on these results, no correlation was observed. This observation is consistent with findings reported by Kiso et al. (2001a); however, Braeken et al. (2005) and Verliefde et al. (2007) observed a decrease in rejection with increasing Log K_{ow} values. Even though Log K_{ow} does not directly correlate to rejection, compounds with a Log K_{ow} value above 2 tend to adsorb to the membrane material.

Of all solutes tested, 70% of the compounds with adsorptive effects are composed of aromatic rings with an attached proton donating group. Williams et al. (1999) and Matsuura and Sourirajan (1971) also observed these compounds exhibiting adsorptive effects during membrane filtration. These compounds have the ability to form hydrogen bonds with functional groups on the membrane surface, similar to water molecules, which results in adsorption and partitioning through the membrane. Chloroform and bromoform are relatively hydrophobic and also exhibit adsorptive effects, which is consistent with findings observed by Kiso et al. (2001b).

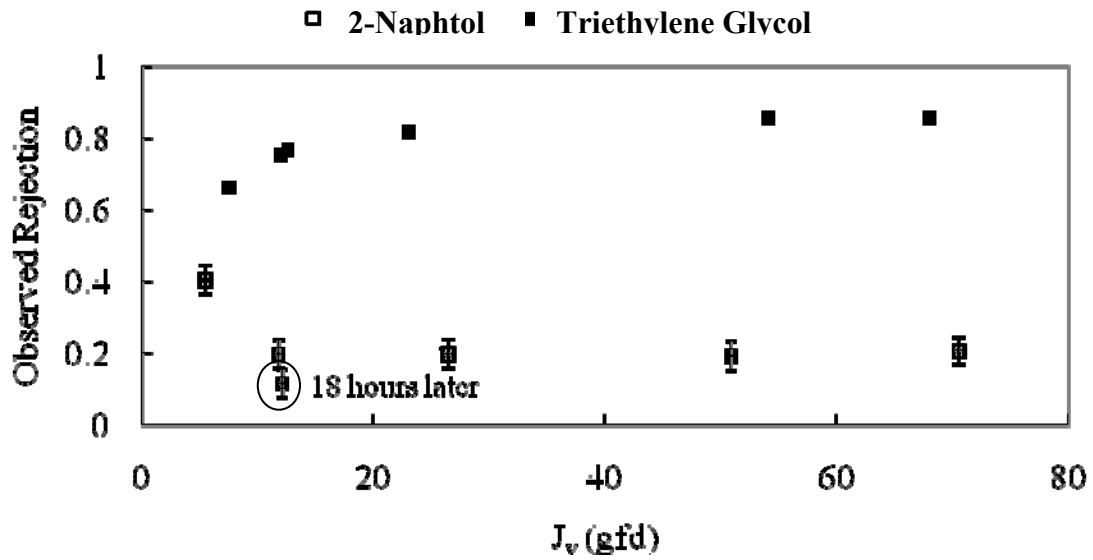


Figure 4.16. Observed rejection as a function of permeate flux for 2-naphthol and triethylene glycol for NF-270 membrane.

Note: The sampling order of permeate flux was 5, 28, 50, 70, 12, and 12 gfd (18 h after the first 12-gfd sample).

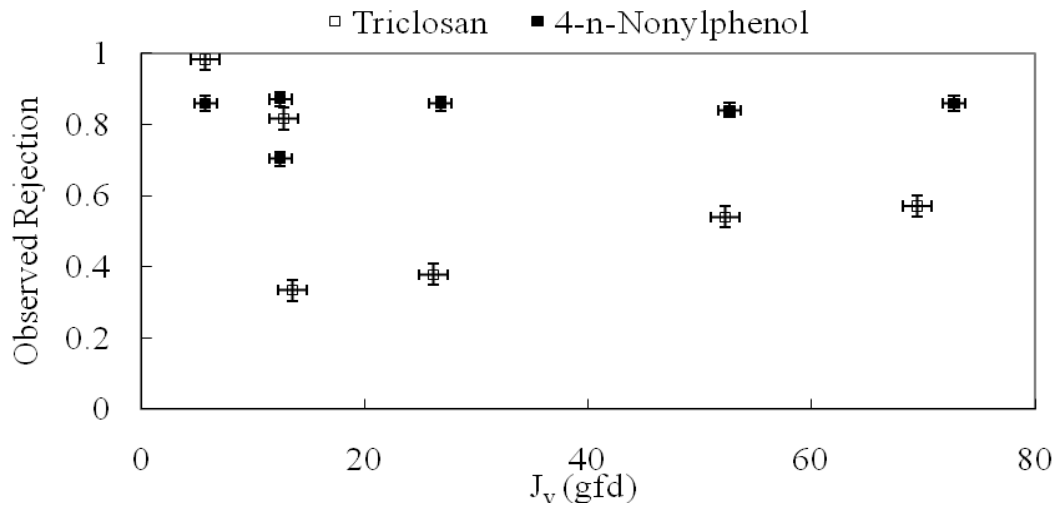


Figure 4.17. Observed rejection for triclosan and 4-n-nonylphenol as a function of permeate flux for NF-270 membrane.

Note: The sampling order of permeate flux was 5, 28, 50, 70, 12, and 12 gfd (18 h after the first 12-gfd sample).

Table 4.1. Compounds that Exhibit Adsorptive Effects Including Their Molecular Weight and Log D at pH 6

Compound Name	Class	Level of Interaction with Membrane	12-gfd Rejection	12-gfd Rejection after 18 h	Mol Wt	Log D(6)
Imiquimod	HCP	Moderate	0.94	0.86	240.3	1.76
Diltiazem	HCP	Moderate	0.97	0.88	414.5	0.92
Trazodone	HCP	Moderate	0.88	0.80	371.9	0.85
Metformin	HCP	Moderate	0.74	0.60	129.2	-4.31
TCP	HoN	Moderate	0.97	0.94	430.9	1.79
<i>N</i> -Nitrosodibutylamine	HHoN	Moderate	0.77	0.69	158.2	2.55
4- <i>n</i> -Nonylphenol	HoN	Moderate	0.87	0.70	220.4	6.19
Oxybenzone	HoN	Moderate	0.97	0.91	228.3	3.63
Estrone	HoN	Moderate	0.94	0.90	270.4	3.69
Resorcinol	HN	Moderate	0.04	0.02	110.1	0.76
Bisphenol A	HoN	Moderate	0.77	0.74	228.3	3.43
Ethinylestradiol	HoN	Moderate	0.96	0.93	296.4	4.52
17 β -Estradiol	HoN	Moderate	0.92	0.89	272.4	4.13
Trimethoprim	HCP	Extreme	0.78	0.71	290.3	-0.42
Chloroform	HN	Extreme	0.54	0.26	119.4	1.76
Bromoform	HHoN	Extreme	0.91	0.41	252.7	2.29
Dibromochloromethane	HHoN	Extreme	0.85	0.21	208.3	2.2
Bromodichloromethane	HHoN	Extreme	0.79	0.15	163.8	2.02
Benzyl acetate	HN	Extreme	0.49	0.27	150.2	1.93
Benzophenone	HoN	Extreme	0.76	0.66	182.2	3.18
<i>n</i> -Nitrosodiphenylamine	HoN	Extreme	0.82	0.53	198.2	3.13
Methylparaben	HN	Extreme	0.30	0.26	152.2	1.86
Benzyl alcohol	HN	Extreme	0.01	0.08	108.1	1.03
Propylparaben	HHoN	Extreme	0.43	0.32	180.2	2.92
2,4-Dichlorophenol	HoN	Extreme	0.36	0.18	163.0	2.99
2-Fluorophenol	HN	Extreme	0.16	0.01	112.1	1.71
2-Phenylphenol	HoN	Extreme	0.33	0.24	170.2	2.94
Triclosan	HoN	Extreme	0.77	0.50	289.5	5.17
2-Naphthol	HHoN	Extreme	0.18	0.09	144.2	2.71

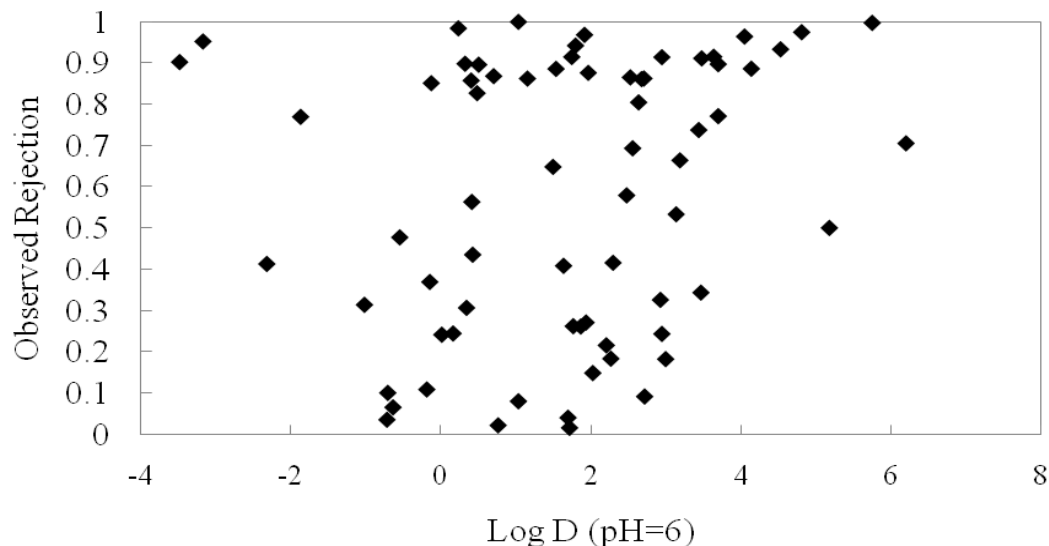


Figure 4.18. Observed rejection for neutral compounds as a function of Log D (pH = 6) at 12 gfd for NF-270 membrane 24 h after startup.

4.1.3 Rejection of Solutes Exhibiting Adsorptive Effects During Once-Through Experiments

Depending on the class of solute, it can take considerable time to reach stable or equilibrium conditions. Given that full-scale membrane applications operate continuously with a single set of membranes for long periods, it is the steady-state rejection, not the initial rejection, that is relevant for performance assessments. Bench-scale rejection experiments with recirculation, discussed in Section 4.1.2, proved to be limited in their ability to demonstrate equilibrium rejection for compounds that reach equilibrium slowly. To solve the problems associated with the recycling experiments, a once-through system was devised. The system was implemented specifically to examine THMs, which are representing extreme examples of delayed equilibrium during membrane experiments. A thorough explanation of the once-through experimental apparatus and of the problems it was designed to resolve is provided in Section 3.3.1.2.

For the THM compounds, equilibrium rejection conditions were not observed during the span of the once-through experiments using the cross-flow apparatus, although it appeared that rejection was stabilizing towards the end of the experiment after 55 h (Figures 4.19 and 4.20). This transient behavior can cause problems in membrane research and operation, because short-term experiments that may fail to adequately characterize long-term rejection of a contaminant are commonly performed. If transient rejection is used to characterize the removal of a constituent by a given membrane, the rejection levels for the compound/membrane pair will be overpredicted (Kimura et al., 2003a). The goal of this project was to develop a representative rejection data set so that rejection values from a full-scale treatment system that has been using the same set of membranes for extended periods could be characterized.

Recent publications have hypothesized that the decline in rejection level occurs although molecules “fill” specific sites within the membrane matrix, of which there are a limited number (Braeken et al., 2005). Steady-state rejection for these compounds is the result of a

membrane reaching a saturation point, after which there is no site to which a molecule can attach and become “stalled.” With the absence of available binding sites, the molecule will diffuse across the membrane without interrupting or replacing another molecule, forcing it into solution (Steinle-Darling and Reinhard, 2008). Although this phenomenon can be observed during simple, yet sufficiently long, bench-scale experiments, the reasons and mechanisms behind it are still poorly understood. It is commonly accepted that uncharged, “moderately” hydrophobic compounds are more prone to these types of interactions (Steinle-Darling and Reinhard, 2008). However, there have been few hypotheses that go beyond this vague generalization and attempt to quantify the specific characteristics that are responsible for this behavior.

Flow-through experiments for THMs depict a clear, declining rejection trend versus time for both membranes evaluated (NF-270 and ESPA2), indicating that these solutes form strong solute–membrane interactions and partition through the membrane. Results presented in Figures 4.19 and 4.20 illustrate THM rejection versus time during two flow-through experiments at a permeate flux of 12 gfd with the NF-270 and the ESPA2 membranes, respectively. Although the trend of decreasing rejection was observed for both membranes, the magnitude of the drop in rejection was dependent upon the type of membrane. With the ESPA2 membrane, rejection of the THMs stabilized near the end of the experiments (at approximately 70%), although rejection by the NF-270 membrane appeared to be decreasing at the termination of the experiment. The higher rejection by the ESPA2 membrane than by the NF-270 membrane was likely associated with a denser polymer matrix that inhibits partitioning and contributes to the high monovalent salt rejection. Neither of the experiments provides conclusive data on final, steady-state rejection values, though the curve does indicate that the end of the transient behavior was nearly achieved by the end of each experiment. More experimental run time would be necessary to provide definitive steady-state rejection values. Unfortunately, in the once-through apparatus, tank capacity limited the ability to run longer experiments.

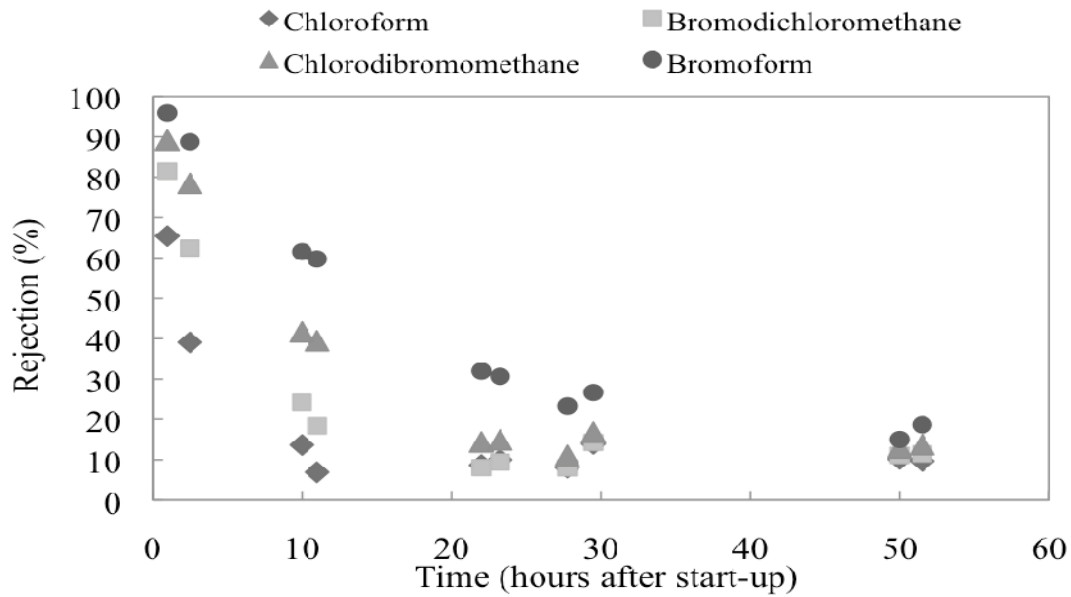


Figure 4.19. Rejection of THMs over time by NF-270 membrane at a flux of 12 gfd.

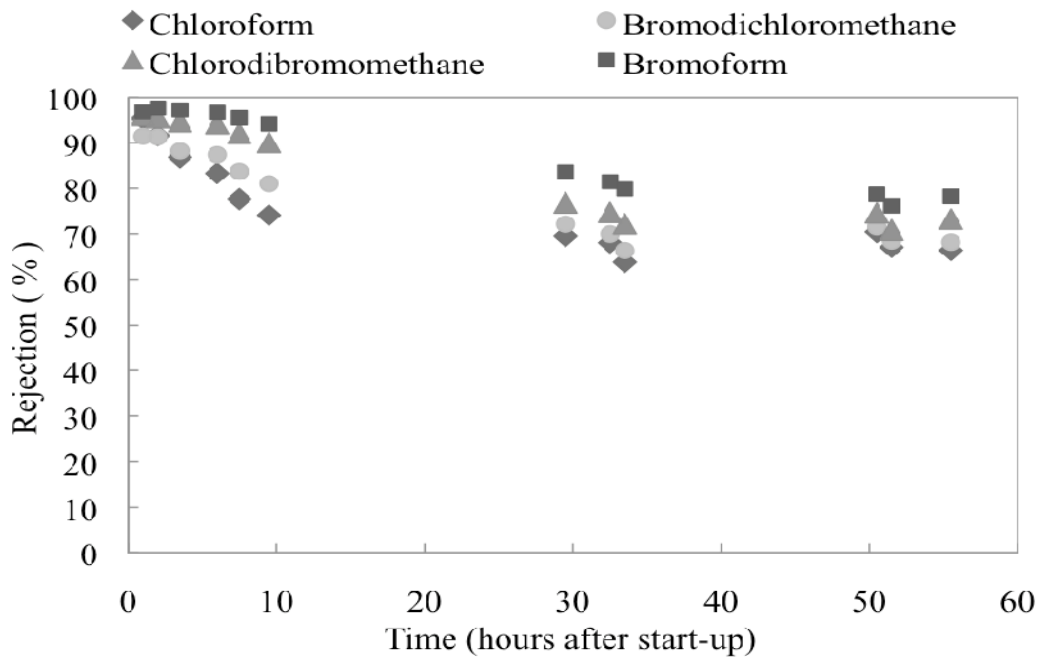


Figure 4.20. Rejection of THMs over time by ESPA2 membrane at a flux of 12 gfd.

The data presented in Figures 4.19 and 4.20 demonstrate the importance of molecular structure in the transient behavior of the THMs. It is evident that the time it takes for rejection levels to drop varied among the different compounds. Bromoform and chloroform were both rejected by the NF-270 membrane at percentages between 10 and 20% at 50 h. However after 10 h, bromoform exhibited a rejection of 60%, although chloroform has already reached its final rejection level near 10%. The trend is less clear from the ESPA2 membrane experimental data, but upon closer inspection, it is obvious that, especially in the early hours, the rejection of chloroform decreased more quickly than that of bromoform. It is evident from these experiments that the larger the solute, the longer it takes for the compound to reach steady state. This observation will be important to consider in the design of future experiments as it adds a complication to the experimental process used in determining steady-state rejection values for various compounds. Larger, heavier partitioning compounds likely require long experimental run times to reach steady state.

By the end of one of the membrane experiments performed with the ESPA2 membrane, the feed water spiked with THMs that had been running through the system for multiple days was replaced with deionized water. Permeate samples were taken at timed intervals and were tested for THM concentrations. Summarized results from this experiment are presented in Figure 4.21. It appeared that there was a great deal of mass accumulated within the membrane, as THMs continue to occur in permeate samples collected for hours after the spiked feed water was replaced with deionized water.

The fact that THM permeate concentration decreased at a greater rate for the smaller solutes provides further evidence of the hindered transport of larger THMs through the membrane. The permeate concentration of each compound in the final sample is plotted against its respective molar mass in Figure 4.22. Although bromoform was quantified at relatively high concentrations in the permeate water at the conclusion of the experiment, the concentration of chloroform almost reached zero. This observation is the opposite of what was observed for rejection experiments; i.e., the same phenomenon that hinders the achievement of steady-state rejection for the larger THMs was likely responsible for the continual leaching of THMs from the membrane. Larger molecules diffuse more slowly through the membrane matrix and therefore desorb at a lower rate.

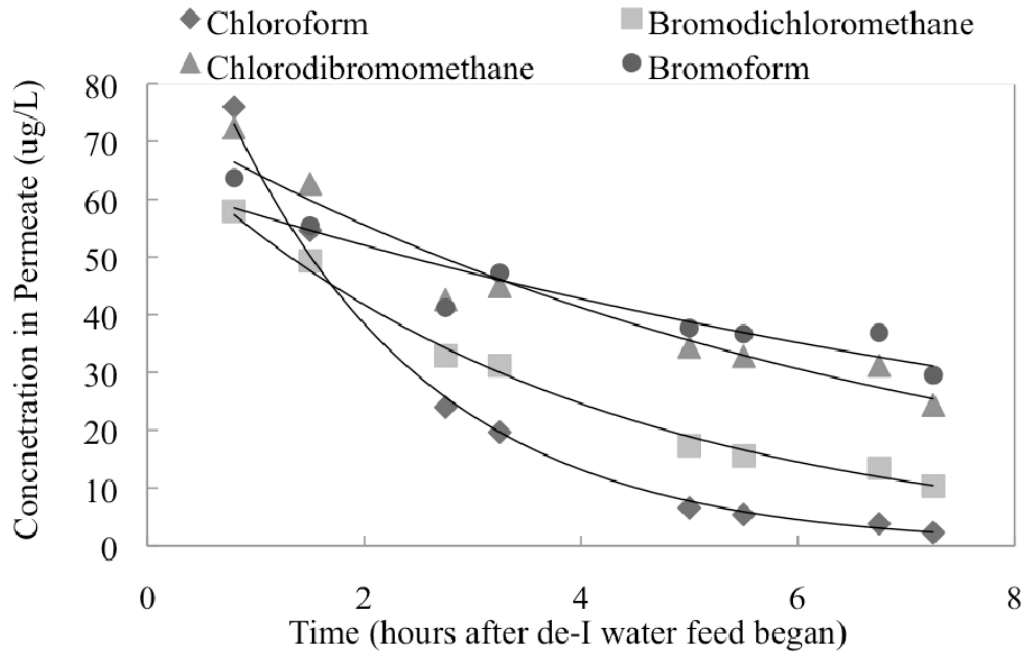


Figure 4.21. Concentration of THMs in permeate stream of deionized water experiment.

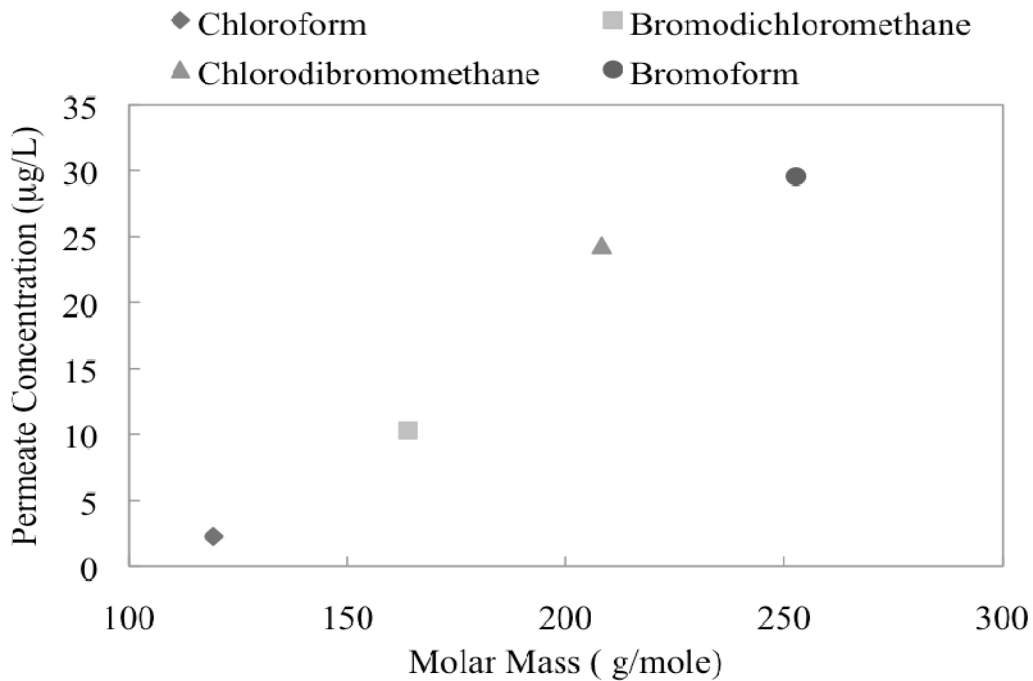


Figure 4.22. Concentration of THMs in final permeate sample from deionized water experiment plotted by molecular mass.

THM rejection by the NF-270 membrane was also examined at various permeate fluxes. Figures 4.23 and 4.24 summarize the rejection of THMs versus time by the NF-270 membrane at 30 and 6 gfd, respectively. In both experiments a sharp decline in rejection was observed at the very end of the experiments. This phenomenon is attributed to a corresponding sharp decline in the feed concentration that occurred at the end of the experiments. Unfortunately, the resolution of the data does not allow for a thorough analysis of the relationship between flux and rejection for THMs. The rejection values over time in the 6- and 30-gfd experiments were very similar to those witnessed during the 12-gfd experiment, making it impossible to generate flux-versus-rejection curves essential to modeling exercises.

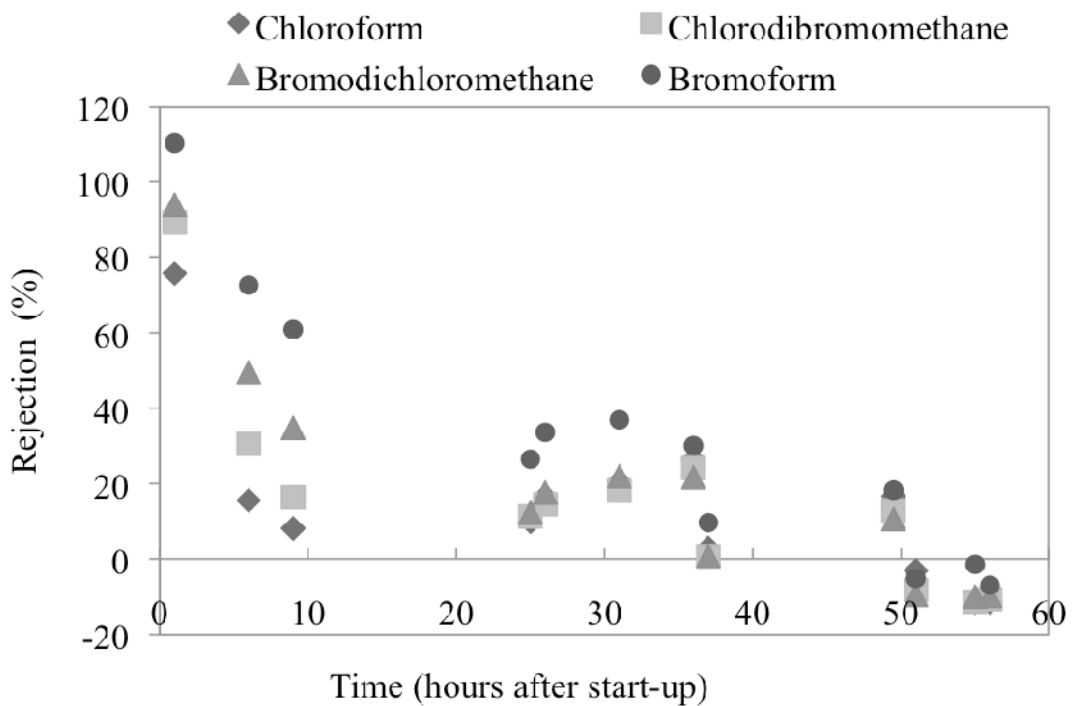


Figure 4.23. Rejection of THMs over time by NF-270 membrane at flux of 30 gfd.

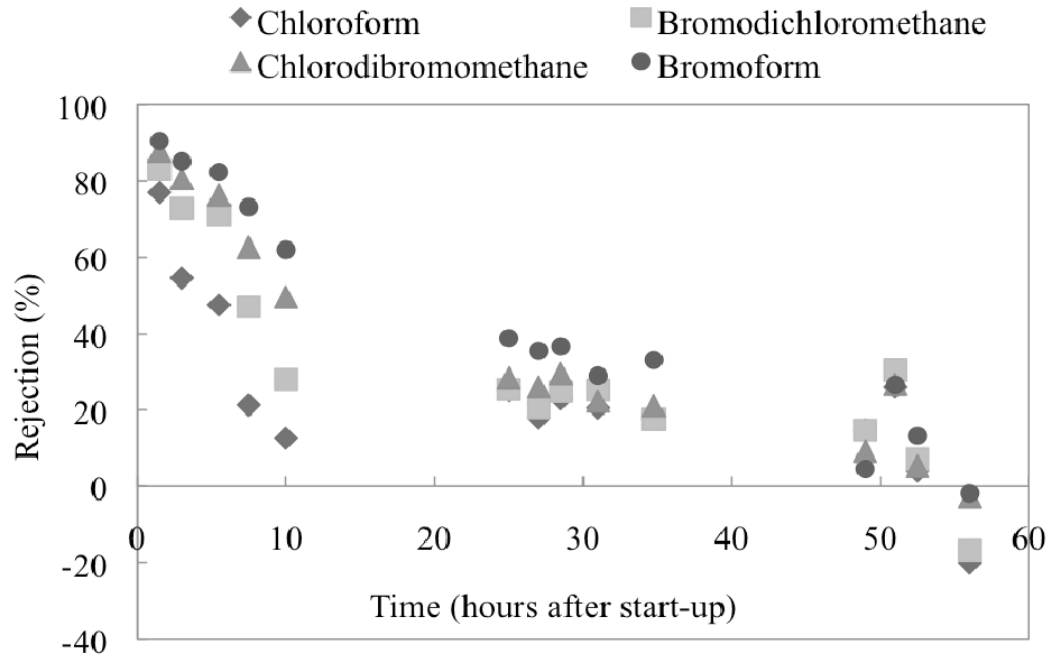


Figure 4.24. Rejection of THMs over time by NF-270 membrane at flux of 6 gfd.

4.1.3.1 Challenges

These investigations revealed that partitioning compounds require complex and resource-intensive experiments to elucidate steady-state rejection values for membrane characterization and modeling purposes. As discussed in Section 3.3.1.2, the original issue that the team reacted to with a modified experimental apparatus was the mass of compound lost into the membranes during recycling experiments. For a flow-through apparatus, the period of transient behavior proved to vary among the THMs and, for the heavier THMs, appeared to exceed the maximum 55 h that the once-through setup could be operated. Given the structural differences among other compounds with solute–membrane interactions, it is probable that their periods of transience will also be unique. This finding points to a need for experimental protocols to be tailored to each specific partitioning compound to extract the relevant rejection values.

Recent research by Steinle-Darling et al. (2010) reveals that the issue of competitive sorption further complicates the study of partitioning compounds in membrane systems. If the theory that there exist specific “sites” to which compounds may sorb is correct, it is likely that the degree of affinity between various molecules and these sites will vary. This variable affinity implies that the different compounds will “compete” to occupy them (Steinle-Darling et al., 2010). Future experiments will need to be designed to incorporate this possibility. It is clear that, if competitive sorption affects partitioning behavior to a large degree, then single-compound (or even several-compound) experiments will not provide data relevant to real-world systems that certainly contain a plethora of compounds in the feed stream.

4.2 Rejection Databases for NF-270 and ESPA2 Membranes

Bench-scale rejection experiments were conducted to evaluate different modeling approaches, as well as the adsorption-partitioning behavior of solutes in membrane systems. For example, the phenomenological model, hydrodynamic model, solution–diffusion model, and SFPM all require evaluating rejection as a function of permeate flux. In addition, to determine which solutes adsorb and partition through membrane materials, 24-h rejection experiments were conducted at an operationally relevant permeate flux (i.e., 12 gfd). Once rejection experiments had been conducted, intrinsic rejection was calculated on the basis of feed-brine channel cross-flow velocity maintained during each experiment. For each membrane evaluated (i.e., NF-270 and ESPA2), Excel databases consisting of rejection data and solute properties were developed to investigate different modeling approaches to describe and predict the rejection of organic solutes. These databases were used in conjunction with Excel, Mathematica (Wolfram Research), MatLab (The Mathworks Inc.), and JMP statistical software (SAS) to evaluate and develop modeling approaches to describe and predict the rejection of organic solutes.

Chapter 5

Modeling of Solute Rejection at Bench Scale

5.1 Introduction

The following sections describe various modeling efforts using the rejection database generated in controlled experiments described in Chapter 4 for the NF-270 and ESPA2 membranes. The modeling approaches examined consist of QSPR, the phenomenological model, the hydrodynamic model, the solution–diffusion model, and empirical models.

5.2 Quantitative Structure Property Relationship Model

Previous research revealed that solutes rejected by electrostatic interactions exhibit high rejection, with negatively charged compounds exhibiting greater than 90% rejection and positively charged compounds exhibiting greater than 75% rejection (Bellona et al., 2008; Verliefde et al., 2007). Neutral compounds are more difficult to predict because of steric interactions and potential adsorptive effects. Membrane properties can vary and lead to different interactions with solutes. Thus, molecular descriptors can differ with respect to expressing the degree of solute rejection for different membranes. Therefore, developing a universal QSPR was not feasible. Instead, a QSPR was developed for each membrane tested (i.e., NF-270 and ESPA2 membrane) as described later.

5.2.1 QSPR Development for the NF-270 Membrane

A QSPR was developed for neutral compounds (i.e., HN, HHoN, and HoN) by utilizing the NF-270 membrane bench-scale database at 12 gfd developed during this study. The NF-270 membrane bench-scale data set includes 77 neutral compounds (64 solutes of the development and 13 solutes of the validation set, respectively) encompassing a wide variety of molecular descriptors, including compounds rejected by adsorptive effects. The goal of this QSPR development was to determine if all neutral compounds can be predicted by using one model. QSPR development consists of four parts: experimental database development, molecular descriptor evaluation, multiple linear regressions, and model validation.

Experimental Database Development. Rejection experiments were conducted for 77 neutral compounds by using the same operating conditions (figures in Appendix E). A database was created with the average quasi-equilibrium (i.e., rejection after 24 h of operation) rejection data generated at a permeate flux of 12 gfd. It is important to note that the bench-scale rejection database was created with virgin membranes. The solutes selected were separated into model development compounds and model validation compounds.

Molecular Descriptor Evaluation. The molecular descriptors for these compounds were separated into different categories based on their properties and possible interactions with the membrane listed in Table 5.1.

Table 5.1. Molecular Descriptors Separated into Different Categories on the Basis of Their Properties^a

Size	Component Surface Area	Electron Distribution	Hydrophobicity	Solubility
Mol wt	SASA (solvent accessible)	E _{HOMO}	Log D (Log K _{ow})	Hydration energy
Length	FOSA (saturated hydrocarbons)	E _{LUMO}	Solvation energy in octanol	Aqueous solubility
Width	FISA (nitrogen and oxygen)	IP	Solvation energy in water	
Depth	PISA (π bonds)	Electron affinity		
Area	WPSA (weakly polar)	Dipole		
Volume	PISA	Polarization		
Stokes radius				
Mol vol				
Diffusion coefficient				
Globularity				

^aDescription of properties listed in Table 3.1.

A wide variety of molecular descriptors were initially evaluated. Size parameters were expected to have a significant effect on the rejection of neutral compounds as observed in previous studies (Agenson et al., 2003; Bellona et al., 2004; Kimura et al., 2004; Van der Bruggen et al., 1999). Component surface area descriptors represent the contribution of different components that could potentially interact with the membrane, such as π bonds or saturated hydrocarbons. Descriptors for electron properties also include the dipole moment, which has been reported to affect neutral compound rejection (Kimura et al., 2004; Libotean et al., 2008; Van der Bruggen et al., 1998). Hydrophobicity descriptors include Log D values. Braeken et al. (2005) and Verliefde et al. (2007) observed that Log D negatively correlated with rejection, although Kiso et al. (2001b) reported no correlation between Log D and solute rejection. Solubility descriptors that could affect solute transport through the membrane include hydration energy and solubility.

To determine which descriptors contribute to the variability in rejection, a PLS evaluation was conducted in JMP 8.0.2. For the PLS evaluation, all of the molecular descriptors were evaluated (Table 5.2). Parameters with the least weight, parameter coefficient less than 0.05, and VIP less than 0.8 were removed from model development (Wold, 1995). Twelve parameters out of the 30 initial parameters were found to significantly affect rejection for the selected compounds.

On the basis of the PLS outcome, size parameters such as Stokes radius, molecular volume, volume, and molecular weight were found to account for a significant portion of variability in the rejection data. All four size parameters have relatively equal weights and a positive effect

on rejection, meaning that, as steric parameters increase, rejection also increases as observed by Agenson et al. (2003), Kimura et al. (2004), and Van der Bruggen et al. (1999). From the PLS evaluation, FOSA and FISA would both have a positive effect on rejection. FOSA is the measure of the solvent accessible surface area of saturated carbons and attached hydrogen, and FISA is the measure of the solvent accessible surface area of nitrogen and oxygen. This finding indicates that aliphatic compounds and compounds containing nitrogen and oxygen atoms would exhibit greater rejection than would aromatic compounds and compounds without oxygen and nitrogen. PISA positively affects solute rejection. Kimura et al. (2004) observed solute rejection to increase with increasing polarity. Both E_{HOMO} and E_{LUMO} were negatively correlated with solute rejection (i.e., the greater the energy in the E_{HOMO} or E_{LUMO} , the less a solute is rejected). E_{HOMO} is the highest-energy molecular orbital that contains an electron, and E_{LUMO} is the lowest-energy molecular orbital that does not contain an electron. This finding indicates that compounds with a larger E_{HOMO} or E_{LUMO} will have a decrease in rejection because the compound is more likely to interact with the membrane polymer. IP and polarization were positively correlated with rejection. This finding indicates that compounds that are less likely to interact with the membrane will have higher rejection. No significant correlation was found with $\text{Log } K_{\text{ow}}$ during the PLS evaluation, indicating that $\text{Log } K_{\text{ow}}$ is not a good descriptor for estimating rejection, contradicting observations from Braeken et al. (2005) and Verliefde et al. (2007).

A correlation matrix was developed in order to avoid using multiple parameters that highly correlate with each other in a QSPR model (full correlation matrix summarized in Appendix D). Uncorrelated parameters were employed in QSPR development in order to capture other solute–membrane interactions besides steric interactions, the main rejection mechanism for neutral compounds. All size parameters were correlated with one another; thus, only one size parameter was used in a given QSPR. Polarizability and SASA also correlated with size parameters; therefore, these size parameters were not used in QSPR models that already contained one size parameter. E_{HOMO} was found to be negatively correlated (-90%) to IP. FOSA was marginally correlated with molecular volume (38%), although PISA, FISA, and E_{LUMO} did not correlate with any other parameters found to be significant during PLS calculations.

Multiple Linear Regressions. A multiple linear regression approach was employed to relate a combination of molecular descriptors to solute rejection. The number of descriptors utilized is important to model development; using too many parameters can result in overfitting and using too few parameters can result in solute behavior not being captured. To determine the optimum number of parameters, initial cross-validation in JMP was utilized. Cross-validation calculated an RMSE value for each possible multiparameter regression. Cross-validation of all molecular descriptors investigated calculated the optimum (lowest RMSE) numbered parameter regression for QSPR development to be 3. On the basis of this finding, QSPR development will consist of a three-parameter regression.

Multiple linear regressions were conducted by using JMP. Regressions were valid and further explored if the statistics met the criteria listed later (see also Section 3.1.3).

$$P < 0.05$$

$$\text{F-ratio} > 2.8$$

$$\text{RMSE} < 0.5$$

$$R^2 > 0.75$$

Table 5.2. Parameters Significant to a 3-Parameter Correlation for All Neutral Compounds in Experimental Database

Category	Molecular Descriptor	PLS Wt	VIP
Size	Stokes radius (nm)	0.072	1.360
	Mol vol (cm ³ /mol)	0.071	1.323
	Vol (Å ³)	0.068	1.356
	MW (g/mol)	0.054	1.247
Component surface area	FOSA (Å ²)	0.125	1.133
	SASA (Å ²)	0.068	1.341
	FISA (Å ²)	0.057	0.835
	PISA (Å ²)	0.050	0.934
Electron distribution	E _{LUMO} (au)	-0.087	0.727
	E _{HOMO} (au)	-0.063	0.824
	IP (eV)	0.084	0.803
	Polarization (Å ³)	0.061	1.290

Every possible three-parameter correlation was explored where all descriptors were uncorrelated with each other. For example, volume and molecular volume, two highly correlated size descriptors, were not used in the same correlation. Out of the 84 correlations examined, nine were found to meet the criteria listed earlier and are listed in Tables 5.3 and 5.4 along with relevant statistical data. The QSPRs contain one size parameter: volume, molecular volume, Stokes radius, or SASA, along with FOSA, PISA, E_{HOMO}, or IP. The developed correlations always contained a size parameter, as steric exclusion is expected to be the main rejection mechanism for nonionic compounds (Agenson et al., 2003; Kimura et al., 2004; Van der Bruggen et al., 1999). Models containing the FOSA parameter were found to be more statistically significant and to provide better fits than models that included the FISA parameter. This finding indicates that the amount of saturated hydrocarbon surface area affects rejection more than the amount of nitrogen and oxygen surface area. PISA positively affected solute rejection, indicating polar compounds will be rejected more than will nonpolar compounds. Kimura et al. (2004) observed increasing rejection with increasing dipole moment for neutral compounds. IP also positively affects rejection. The greater the IP, the less likely a compound will interact with the membrane, therefore increasing rejection. E_{HOMO} negatively affects rejection, indicating that a compound more likely to interact with the membrane polymer will have lower rejection.

Each correlation yielded an R^2 value above 0.8 and RMSE below 0.5, meeting the criteria of R^2 value above 0.75 and RMSE below 0.5. The overall F-ratio was relatively high (61–67.3) where individual F-ratio values ranged from 4.5 to 138, above the criteria of greater than 2.8. As expected, the size parameters obtained the highest F-ratio and the Stokes radius was the most significant size parameter. Each parameter had a P of less than 0.05, indicating a low probability that the parameters are correlated by chance.

It is worth noting that this QSPR modeling approach has limits. If the QSPR predicts rejection to be less than 0, rejection is assumed to be 0. If the QSPR predicts rejection to be greater than 1, rejection is assumed to be 1.

If $\text{Rej} \leq 0$, $\text{Rej} = 0$; If $0 < \text{Rej} < 1$, $\text{Rej} = \text{QSPR}$; If $\text{Rej} \geq 1$, $\text{Rej} = 1$

Table 5.3. Parameters Significantly Correlated to Rejection Listed with Significant Statistics

Parameter 1	Parameter 2	Parameter 3	R^2	Overall F-Ratio	RMSE	Coefficient			
						1	2	3	Intercept
Volume	FOSA	PISA	0.845	62.2	0.397	0.10343	0.04611	0.16315	-26.03
Mol volume	FOSA	E_{HOMO}	0.852	63.35	0.388	0.12029	0.04475	-215.62	-83.25
Stokes	FOSA	PISA	0.848	61.63	0.393	0.36188	0.04366	$\frac{0.26102}{1}$	-18.21
Stokes	FOSA	PISA	0.843	64.1	0.400	221.894	0.04974	0.15899	-40.48
Stokes	FOSA	E_{HOMO}	0.845	63.55	0.397	254.049	0.04961	$\frac{-}{187.971}$	-92.00
SASA	FOSA	IP	0.854	67.32	0.386	263.68	0.04158	7.6937	-122.30
SASA	FOSA	PISA	0.831	61	0.415	0.20931	0.04789	$\frac{0.18414}{8}$	-44.06
SASA	FOSA	E_{HOMO}	0.833	63.36	0.412	0.25056	0.0461	$\frac{-}{259.289}$	-116.78
	PISA	E_{HOMO}	0.833	61.4	0.412	0.25121	0.14851	-228.92	-108.61

Table 5.4. Parameters Significantly Correlated to Rejection Listed with Significant Statistics

Parameter 1	Parameter 2	Parameter 3	F-Ratio			P		
			1	2	3	1	2	3
Volume	FOSA	PISA	94.40	5.32	5.10	<0.0001	0.0252	0.0283
Volume	FOSA	E _{HOMO}	131.96	5.07	5.88	<0.0001	0.0287	0.0189
Mol volume	FOSA	PISA	93.27	4.69	14.06	<0.0001	0.0351	0.0005
Stokes	FOSA	PISA	97.80	6.43	4.94	<0.0001	0.0143	0.0307
Stokes	FOSA	E _{HOMO}	132.40	6.35	4.56	<0.0001	0.0149	0.0376
Stokes	FOSA	IP	138.29	4.53	7.16	<0.0001	0.0383	0.01
SASA	FOSA	PISA	92.12	5.68	6.51	<0.0001	0.0209	0.0137
SASA	FOSA	E _{HOMO}	131.99	5.42	8.26	<0.0001	0.0239	0.0059
SASA	PISA	E _{HOMO}	125.30	4.04	5.97	<0.0001	0.0497	0.018

The two QSPR models with the highest R^2 value and lowest RMSE value are listed in Equations 5.1 and 5.2.

$$Ref(\%) = 0.1203Volume + 0.04475FOSA - 215.62E_{HOMO} - 83.252 \quad (5.1)$$

$$Ref(\%) = 263.68Stokes + 0.4158FOSA + 7.694IP - 122.3 \quad (5.2)$$

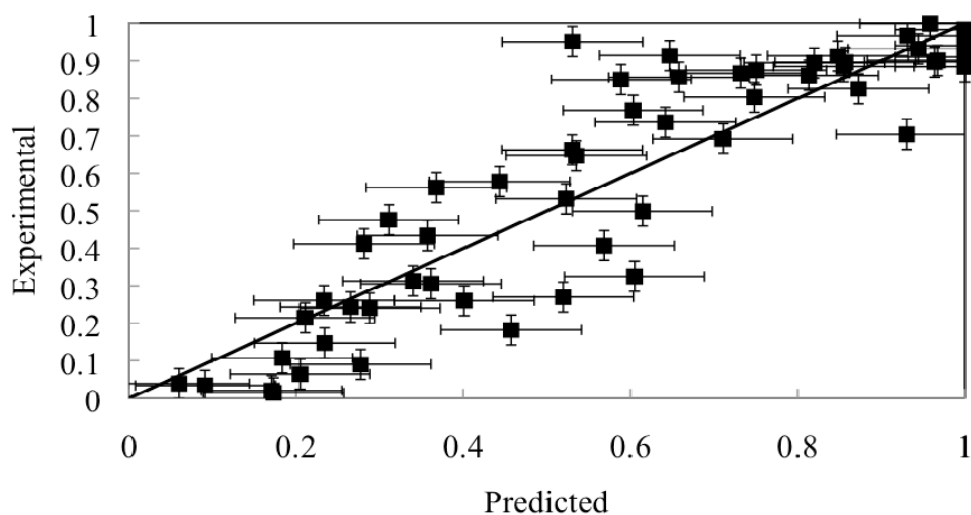
The result of applying Equations 5.1 and 5.2 to the development compounds in the bench-scale database is illustrated in Figure 5.2. The error bars on the figures in the x direction represent the individual 95% confidence intervals and in the y direction represent the experimental deviation. The two QSPR models did yield high R^2 values (0.852 for Equation 5.1 and 0.854 for Equation 5.2); however, there were a few outliers. Compounds containing low FOSA values but not exhibiting adsorptive effects were underpredicted, such as thiabendazole. A low FOSA value usually indicates low removal because aromatic compounds have a greater affinity to adsorb to the membrane than do aliphatic compounds. Compounds that were overpredicted are compounds that exhibit extreme adsorptive effects (i.e., decreasing rejection with increasing permeate flux and time), such as propylparaben and 2-fluorophenol.

Model Validation. All of the models considered significant were internally validated by using the LOO cross-validation method; one compound was excluded from the data set and the model correlated with the remaining data. This method was repeated n times for n compounds in the data set. The results from this validation were then combined, and a single QSPR was produced yielding a q^2 value. A q^2 value greater than 0.5 indicated a good fit, and a q^2 value greater than 0.9 indicated an excellent fit (Eriksson et al., 2003). The results from the internal validation are summarized in Table 5.5. All q^2 values were greater than 0.5, indicating a good fit. The greatest q^2 value was obtained from the QSPR containing volume, FOSA, and E_{HOMO} and Stokes, FOSA, and IP described by Equations 5.1 and 5.2.

Table 5.5. Results from the LOO Cross-Validation for QSPR Internal Validation

Parameter 1	Parameter 2	Parameter 3	q^2
Volume	FOSA	Polar SA	0.802
Volume	FOSA	E_{HOMO}	0.819
Mol volume	FOSA	Polar SA	0.804
Stokes	FOSA	Polar SA	0.795
Stokes	FOSA	E_{HOMO}	0.808
Stokes	FOSA	IP	0.816
SASA	FOSA	Polar SA	0.785
SASA	FOSA	E_{HOMO}	0.798
SASA	Polar SA	E_{HOMO}	0.798

The two QSPR models yielding the highest q^2 value, Equations 5.1 and 5.2, were externally validated by applying the models to the validation compounds for the NF-270 membrane bench-scale data (Table 3.2). Results of this comparison are presented in Figures 5.3 and 5.4. Equation 5.1 (Figure 5.3) yielded an R^2 value of 0.734, and Equation 5.2 (Figure 5.4) yielded an R^2 value of 0.758, suggesting that utilizing Stokes radius, FOSA, and IP was a better fit for this data set consisting of neutral compounds with a wide variety of molecular descriptors and rejection mechanisms including adsorptive effects. Most compounds were predicted within 20%. Compounds that were underpredicted, such as carbamazepine and dilantin, had low FOSA values but did not adsorb to the membrane. Compounds that were overpredicted are the ones that exhibited extreme adsorptive effects, such as 2,4-dichlorophenol and 2-phenylphenol.

**Figure 5.1. QSPR (volume, FOSA, E_{HOMO}) for neutral compounds developed from bench-scale NF-270 membrane data.**

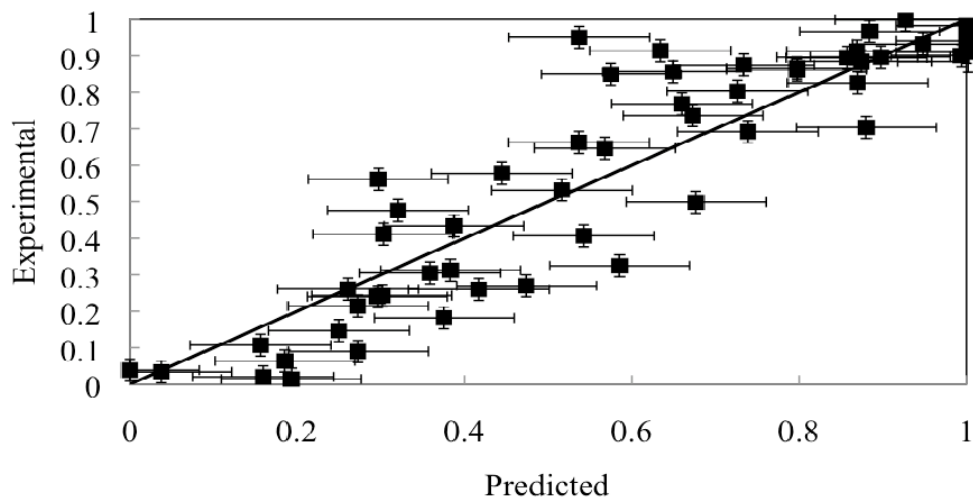


Figure 5.2. QSPR (Stokes, FOSA, IP) for neutral compounds developed from bench-scale NF-270 membrane data.

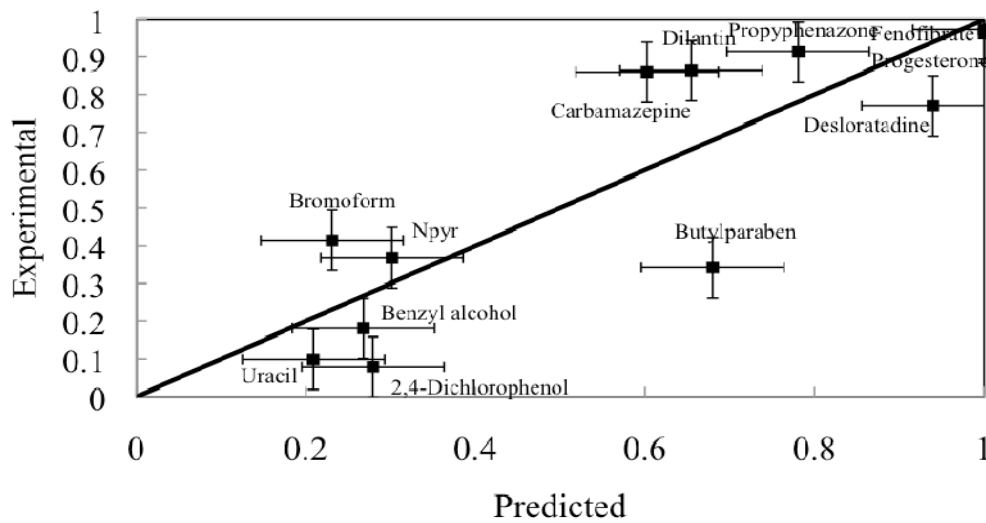


Figure 5.3. QSPR (volume, FOSA, E_{HOMO}) for F-270 membrane applied to validation compounds.

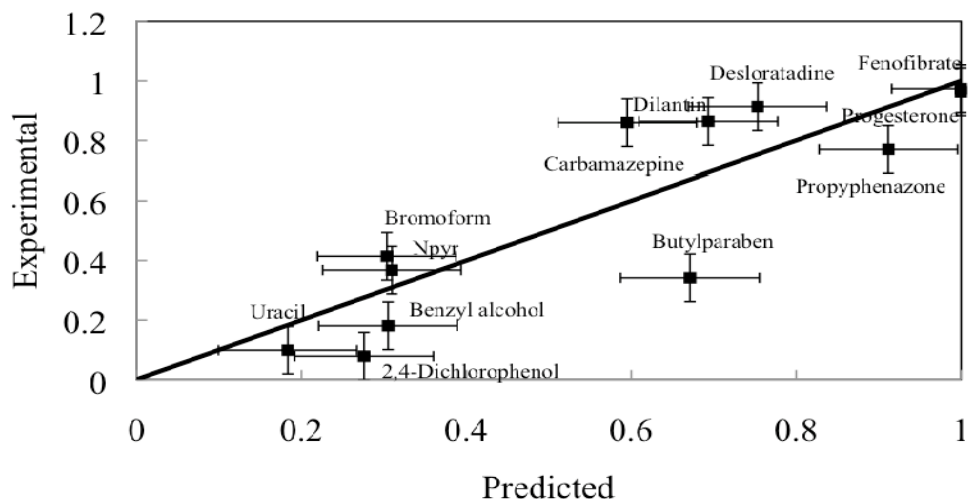


Figure 5.4. QSPR (Stokes, FOSA, IP) for NF-270 membrane applied to validation compounds.

5.2.2 QSPR Development for the ESPA2 Membrane

QSPR development for neutral compounds was also conducted for the ESPA2 membrane by using the same procedure previously applied to the NF-270 membrane data set (Section 5.2.1).

Experimental Database Development. Rejection experiments were conducted for 64 neutral compounds using the same operating conditions (figures in Appendix F). A database was created with the average steady-state (i.e., rejection after 24 h of operation) rejection data generated at a permeate flux rate of 12 gfd by using virgin membranes. For model development, the rejection data were transformed into a Log scale because the majority of compounds were greater than 90% removed. The compounds were then separated into model development compounds and model validation compounds.

Molecular Descriptor Evaluation. The molecular descriptors (Table 5.1) were investigated to determine which descriptors contribute to the variability in rejection by employing a PLS evaluation in JMP 8.0.2. Parameters with the least weight, parameter coefficient less than 0.05, and VIP less than 0.8 were removed from model development (Table 5.6). Ten parameters out of the 30 initial parameters were found to significantly affect rejection for the selected compounds based on the PLS evaluation.

Table 5.6. Parameters Significant to a 3-Parameter Correlation for All Neutral Compounds in Experimental Database

Category	Molecular Descriptor	PLS Wt	VIP
Size	Length (nm)	0.145	1.060
	Width (nm)	0.091	0.987
	Wilke–Chang diffusion coefficient (m ² /s)	-0.234	1.258
	Stokes radius (nm)	0.088	1.132
	Vol (cm ³ /mol)	0.117	1.125
	Vol (Å ³)	0.106	1.146
Component surface area	FOSA (Å ²)	-0.110	0.819
	SASA (Å ²)	0.130	1.170
Electron distribution	E _{HOMO} (au)	0.159	0.881
	IP (eV)	-0.083	1.031

Size parameters were again found to account for a significant portion of variability in the rejection data, which was expected for neutral compounds. All size parameters have a positive effect on rejection, except for the Wilke-Chang diffusion coefficient, which is negatively correlated with size. From the PLS evaluation, FOSA, IP, and E_{HOMO} affect solute rejection with the ESPA2 membrane differently from how they affect it with the NF-270 membrane. FOSA has a negative effect on rejection for the ESPA2 membrane. This finding indicates that aliphatic compounds would have lower rejection than aromatic compounds. Compounds did not show strong adsorptive effects with the ESPA2 membrane because most compounds exhibited higher than 90% rejection. Because the adsorptive effects were not observed, aromatic compounds tend to have higher rejection than aliphatic compounds, given their larger size. IP was negatively correlated with rejection, which indicates compounds that are less likely to interact with the membrane will have lower rejection. E_{HOMO} was positively correlated with solute rejection (i.e., the greater the energy in the E_{HOMO}, the more a solute is rejected). This finding indicates that compounds with a larger E_{HOMO} will have an increase in rejection.

Multiple Linear Regressions. A three-parameter multiple linear regression approach was employed to relate a combination of molecular descriptors to solute rejection by using JMP. Regressions were valid and further explored if the statistics met the criteria previously defined (Section 3.5):

$$P < 0.05$$

$$F\text{-ratio} > 2.8$$

$$RMSE < 0.5$$

$$R^2 > 0.75$$

All combinations of molecular descriptors found to be significant during the PLS evaluation were investigated, and only one correlation was found to be significant, listed in Equation 5.3.

$$Ref(\log Removal) = -1.11 \times 10^{-3} FOSA + 6.207 E_{HOMO} + 4.72 \times 10^{-3} SASA + 1.333 \quad (5.3)$$

This correlation includes FOSA, E_{HOMO} , and SASA and yielded an R^2 value of 0.75 and RMSE of 0.346. The overall F-ratio was relatively high, 43, where individual F-ratios ranged from 5 to 89 and P values were below 0.05, listed in Table 5.7, indicating a low probability that the parameters are correlated by chance. The size descriptor, SASA, obtained the greatest F-ratio and the most significance. This finding was expected because steric exclusion is expected to be the main rejection mechanism for nonionic compounds (Agenson et al., 2003; Kimura et al., 2004; Van der Bruggen et al., 1999).

Table 5.7. Parameters Significantly Correlated to Rejection Listed with Significant Statistics

Parameter 1	Parameter 2	Parameter 3	F-Ratio			P		
			1	2	3	1	2	3
FOSA	E_{HOMO}	SASA	5.134	8.711	89.091	0.028	0.005	<0.0001

Applying the QSPR Equation 5.3 to the development compounds in the ESPA2 bench-scale database revealed results that are illustrated in Figure 5.5 (tables containing QSPR-predicted rejection versus experimental rejection are listed in Appendix F). The error bars on the figures in the x direction represent the individual 95% confidence intervals and in the y direction represent the experimental deviation. The QSPR model does contain a few outliers. Compounds exhibiting a high FOSA value but with a lower rejection based on size were overpredicted, such as ethanol, methanol, and urea. A higher FOSA value usually indicates low removal from the ESPA2 membrane because aromatic compounds usually have a larger volume, indicating compounds rejected by steric interactions.

Model Validation. The model was internally validated by using the LOO cross-validation method, yielding a q^2 value of 0.66 and indicating a good fit (Eriksson et al., 2003). The QSPR model was also externally validated by applying the model to the validation compounds for the ESPA2 membrane bench-scale data (Table 3.2). Results of this comparison are presented in Figure 5.6, and an R^2 value of 0.7414 was yielded. All compounds were predicted within 7%.

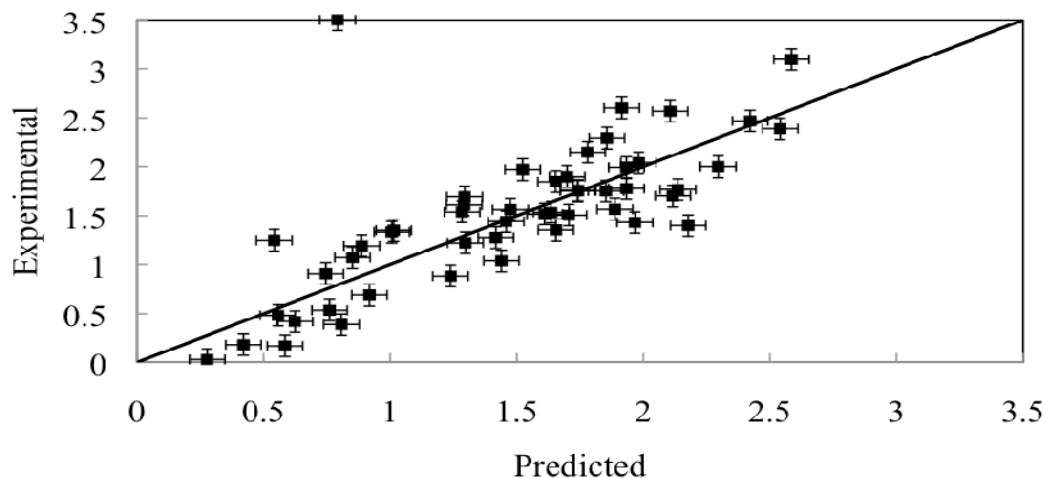


Figure 5.5. QSPR (FOSA, E_{HOMO} , SASA) for neutral compounds developed from bench-scale ESPA2 membrane rejection data described as Log removal.

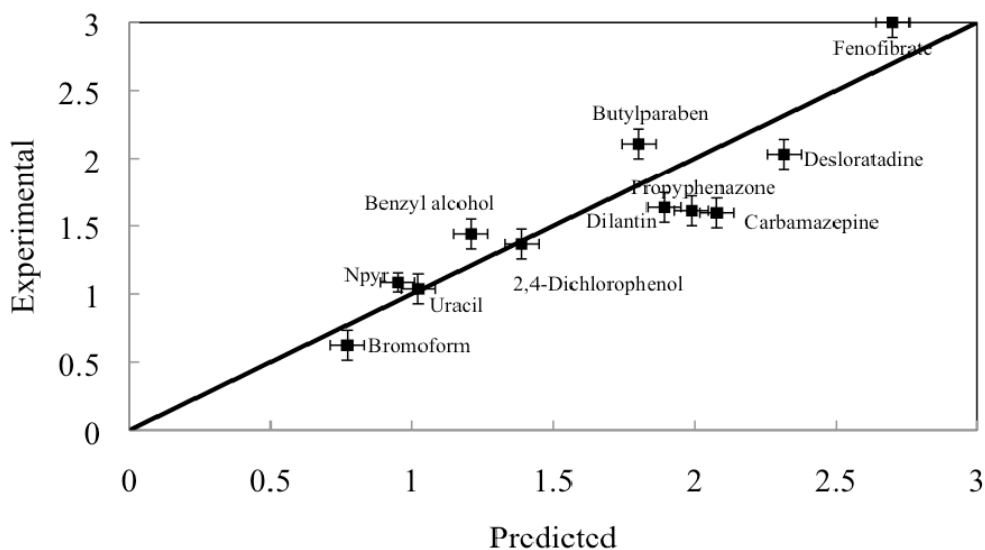


Figure 5.6. QSPR (FOSA, E_{HOMO} , SASA) for ESPA2 membrane applied to validation compounds.

5.3 Phenomenological Model

5.3.1 Phenomenological Model for NF-270 Nanofiltration Membrane

Rejection data for all of the organic solutes analyzed and documented in Chapter 4 were fit with the phenomenological model by manipulating model coefficients (σ , P_s). To achieve the best fit, a nonlinear fitting program in Mathematica (Wolfram Research, Champaign, IL) was used. Fitting the phenomenological model requires increased rejection with increased permeate flux and certain organic compounds studied displayed rejection-versus-flux trends

that cannot be described by the phenomenological model. These compounds generally exhibited rejection trends synonymous with solute–membrane interactions, which included decreasing rejection as a function of experimental run time and decreased rejection with increased permeate flux. In addition, a few compounds exhibited highly variable rejection that may be due to analytical error or degradation in the feed water container or collection vessel. A list of compounds whose rejection data could not be fit with the phenomenological model is provided in Table 5.8. Many of the compounds displaying solute–membrane interactions are phenol-type compounds with hydroxyl groups attached to aromatic rings (e.g., benzyl alcohol, 2,4-dichlorophenol, methylparaben, and 2-naphthol). The THM compounds (i.e., chloroform, bromoform, BDCM, and dibromochloromethane) adsorb strongly to membrane materials and are poorly removed after a matter of hours. These compounds are hypothesized to form hydrogen bonds with the active layer of polyamide/polypiperazine membranes and are difficult to model. Additionally, relatively hydrophobic solutes with carbonyl or ester functional groups (e.g., benzophenone, benzyl acetate, and *N*-nitrosodiphenylamine) were observed to adsorb to membrane material. Somewhat surprisingly, two positively charged compounds, trimethoprim and trazodone, also displayed adsorption behavior and rejection data that could not be described by the phenomenological model.

Table 5.8. List of Compounds Not Fitting with Phenomenological Model

Compound	Class	Log Kow	Notes
Benzophenone	HoN	3.18	Strong interactions with membrane
Benzyl acetate	HN	1.93	
Benzyl alcohol	HN	1.03	
Chlortetracycline	HCN	-2.87	Unstable results, may degrade in feed water
2,4-Dichlorophenol	HoN	3	Strong interactions with membrane
Chloroform	HN	1.76	Very strong interactions with membrane
Bromoform	HHoN	2.29	
Bromodichloromethane	HHoN	2.02	
Dibromochloromethane	HHoN	2.22	
Oxytetracycline	HCN	-4.03	Unstable results, may degrade in feed water
2-Fluorophenol	HN	1.7	Strong interactions with membrane
Methylsalicylate	HHoN	2.23	
Methylparaben	HN	1.86	
2-Naphthol	HHoN	2.71	
2-Phenylphenol	HHoN	2.94	
Triclosan	HoN	5.17	
Trimethoprim	HCP	-0.42	
Trazodone	HCP	0.85	
<i>N</i> -nitrosodiphenylamine	HoN	3.13	

Several compounds exhibited relatively constant rejection versus permeate flux, which can be difficult to describe with the phenomenological model (Table 5.9). Rejection data for these compounds were fit with the phenomenological data; however, suboptimum model fits were obtained. With the exception of norfloxacin (carrying negative and positive charges) and resorcinol (phenolic compound), most of the solutes exhibiting this behavior were relatively hydrophobic with hydroxyl groups attached to aliphatic or aromatic ring structures.

Table 5.9. List of Compounds with Less-than-Optimal Phenomenological Model Fits

Compound	Class	Log Kow	Notes
1-naphthalenemethanol	HHoN	2.26	Flat rejection curve or rejection slightly decreased with increasing permeate flux, minimal (<10%) decrease in rejection over time
Estrone	HoN	3.69	
17-B-estradiol	HoN	4.13	
Ethinylestradiol	HoN	4.52	
Progesterone	HoN	4.04	
Testosterone	HoN	3.47	
Norfloxacin	HCNP	-0.9	
Resorcinol	HN	0.76	Some rejection data points indicate adsorption
Propylparaben	HHoN	2.92	

With the exception of the compounds described earlier, the phenomenological model provided sufficient fits of intrinsic rejection-versus-flux data for HN, HHoN, HoN, HCN, HCP, and HCNP compounds. Several examples of these phenomenological model fits of rejection data are provided in Figure 5.7. This fitting exercise resulted in the characterization of each compound with two model parameters, sigma (σ) and solute permeability (P_s). Sigma is considered limiting rejection and is defined as rejection at infinite flux or the reciprocal of the sieving coefficient. The solute permeability parameter (P_s) controls the shape of the rejection curve at low permeate flux and represents solute diffusion through the membrane. A complete list of phenomenological model parameters for the organic compounds evaluated is provided in Table 5.10.

Once sigma (σ) and solute permeability (P_s) are known for a compound, rejection can be calculated for any permeate flux value, which does not apply to QSPR models. By correlating model parameters with molecular descriptors, model parameters for unknown compounds could potentially be calculated, which would allow the prediction of rejection at any permeate flux. Therefore, once model parameters were determined for the suite of compounds, correlations between model parameters and solute descriptors were developed. To achieve this, compounds were grouped into neutral (HN, HHoN, HoN, and all three grouped together), negatively charged, positively charged, and both positively and negatively charged compound bins. Because the value of solute permeability is very small, the base-10 logarithm of the solute permeability was used to develop correlations.

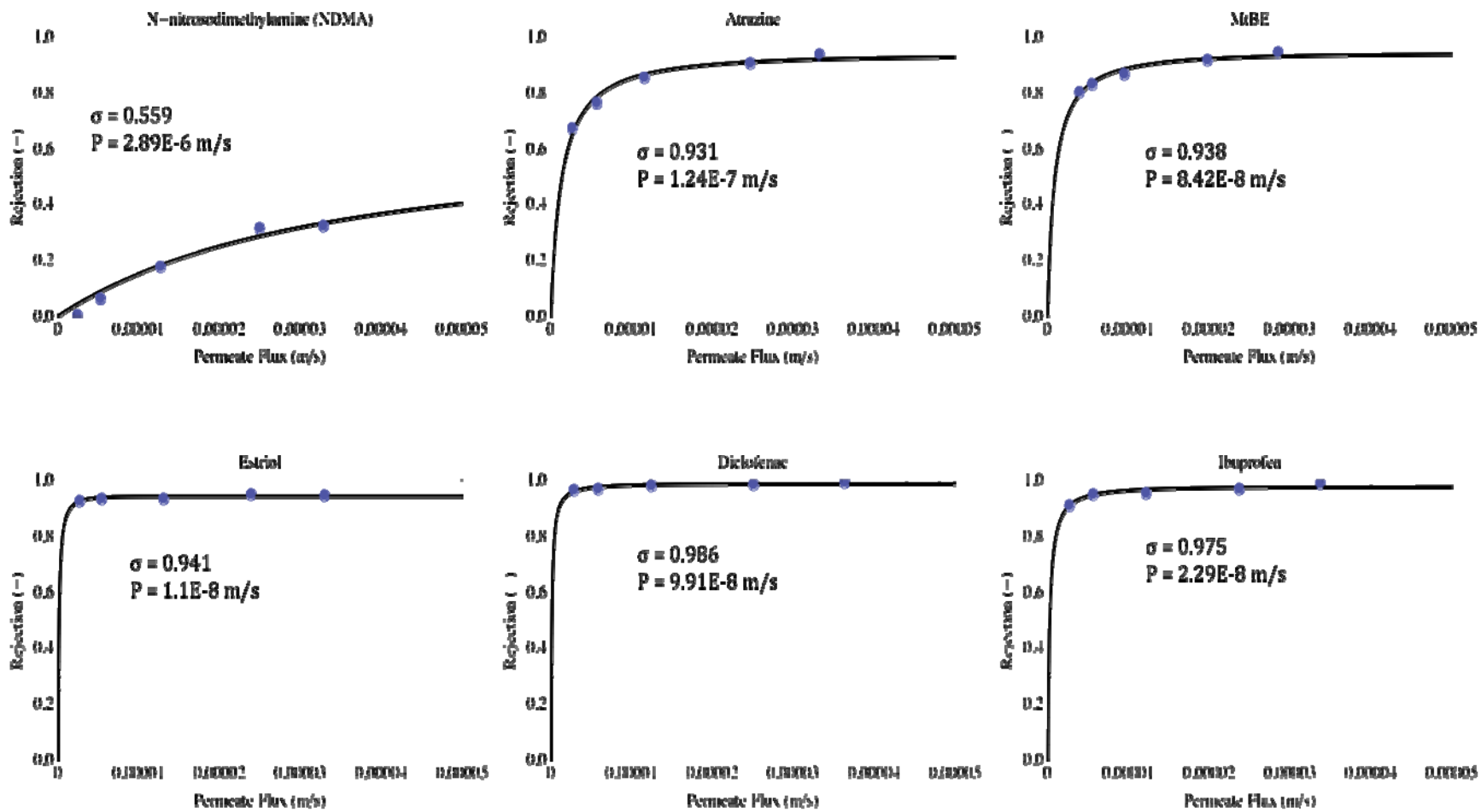


Figure 5.7. Sample phenomenological fits of intrinsic rejection versus permeate flux.

Table 5.10. Phenomenological Model Coefficients for All Organic Compounds (NF-270 Membrane)

Compound	Reflection coefficient (σ)	Permeability coefficient (P) m/s	Compound	Reflection coefficient (σ)	Permeability coefficient (P) m/s	Compound	Reflection coefficient (σ)	Permeability coefficient (P) m/s	Compound	Reflection coefficient (σ)	Permeability coefficient (P) m/s
2,4-Dihydroxybenzoic acid	0.9294	7.522E-07	Alanine	0.9399	6.053E-07	Dilantin	0.9520	1.926E-07	Nitrosomorpholine	0.9461	5.028E-06
Acetic acid	0.8627	5.508E-06	Arginine	0.9112	2.613E-07	Estriol	0.9414	1.095E-07	Pentoxifylline	0.9336	3.722E-07
Benzoic acid	0.9244	2.775E-07	Baclofen	0.9795	5.547E-08	N-nitrosodibutylamine (NDBA)	0.8865	5.533E-07	Phenacetin	0.9315	7.400E-06
Captopril	0.9996	1.419E-06	Cysteine	0.9671	4.350E-07	Propylparaben	0.6855	6.316E-06	Primidone	0.9405	6.588E-07
Ciprofloxacin	0.9832	1.219E-07	Lysine	0.9685	1.247E-06	Thiabendazole	0.9214	5.024E-06	Propyphenazone	0.9575	3.218E-07
Clofibrac acid	0.9582	1.616E-07	Norfloracin	0.6713	1.447E-06	Tyrosine	0.9491	6.493E-07	Rescorcinol	0.3094	3.274E-05
Dibromoacetic acid	0.9449	5.276E-08	Serine	0.9039	5.328E-07	Warfarin	0.9753	3.143E-08	Sucralose	0.9320	2.699E-07
Dichloroacetic acid	0.9382	1.004E-07	Amitriptyline	0.9946	8.919E-09	1-nitrosopiperidine	0.8899	2.920E-06	Sucrose	0.9922	7.774E-08
Diclofenac	0.9861	9.910E-08	Atenolol	0.9320	5.382E-07	1-nitrosopyrrolidine	0.8712	6.943E-06	TCEP	0.9355	7.174E-07
Enalapril	0.9788	3.041E-07	Cimetidine	0.9188	1.277E-06	1,4-Butanediol	0.8333	8.708E-06	TCPP	0.9428	3.087E-08
Gemfibrozil	0.9807	1.163E-07	Diltiazem	0.9650	2.978E-07	Acetaminophen	0.8318	9.669E-06	Triethyleneglycol	0.9401	1.437E-06
Glutamic acid	0.9659	8.337E-07	Guanidine	0.9894	8.399E-07	Caffeine	0.9511	6.665E-07	Uracil	0.7843	2.647E-05
Histidine	0.9057	2.108E-06	Imiquimod	0.9760	4.481E-07	Chlortetracycline	0.8842	3.444E-07	Urea	0.2321	3.675E-05
Ibuprofen	0.9749	2.294E-07	Ketoconazole	0.9953	7.558E-09	Cortisol	0.9852	3.258E-07	17-B-Estradiol	0.9645	2.930E-08
Ketoprofen	0.9910	1.318E-07	Metformin	0.8278	6.411E-07	Ethanol	0.4073	1.585E-05	Bisphenol A	0.9708	2.019E-06
Maleac acid	0.9793	2.073E-07	Metoprolol	0.9353	7.269E-07	Fluconazole	0.9334	3.466E-07	Desloratidine	0.8794	2.206E-07
Methotrexate	0.9801	1.041E-07	Norfluoetine	0.9946	1.509E-08	Furosemide	0.9715	8.767E-08	Diethylstilbesterol	0.9158	1.246E-07
Naproxen	0.9825	4.221E-08	Pseudoephedrine	0.8799	1.026E-06	Glucose	0.9725	1.735E-07	Estrone	0.9752	1.016E-08
Phenylalanine	0.9556	6.360E-07	Ranitidine	0.8981	3.802E-07	Glycerol	0.8546	6.222E-06	Ethinylestradiol	0.9804	9.583E-09
Salicylic acid	0.9800	4.503E-07	Salbutamol	0.9786	5.084E-08	Isopropanol	0.7969	1.375E-05	Fenofibrate	0.9930	1.055E-08
Sulfacetamide	0.9812	8.157E-08	Sulfamethoxazole	0.9578	4.678E-07	Meprobamate	0.9348	4.849E-07	Fluoxetine	0.9951	8.000E-09
Sulfadimethoxine	0.9817	6.978E-08	1-Naphthalenemethanol	0.5611	9.356E-06	Methanol	0.0799	1.634E-05	iso-Butylparaben	0.9226	8.188E-06
Sulfadoxine	0.9465	6.274E-07	Atrazine	0.9310	1.240E-07	MtBE	0.9383	8.417E-07	Nonylphenol	0.9151	2.675E-07
Sulfamerazine	0.9791	2.409E-07	Carbamazepine	0.9428	3.970E-07	N-nitrosodiethylamine (NDEA)	0.8331	4.388E-06	Oxybenzone	0.9816	1.425E-08
Sulfasalazine	0.9887	4.772E-08	DEET	0.9497	4.781E-07	N-nitrosodimethylamine (NDMA)	0.5586	2.894E-05	Progesterone	0.9910	3.634E-08
Trichloroacetic acid	0.9504	2.145E-08	Diethylphthalate	0.9278	4.705E-07	N-nitrosodipropylamine (NDPA)	0.9063	1.408E-06	TDCPP	0.9808	2.540E-08
			Triclocarban	0.9950	8.067E-09	N-nitrosomethylamine (NMEA)	0.8164	1.195E-05	Testosterone	0.9583	3.168E-08

The ranges of phenomenological model coefficients for the different major classes of compounds along with the range of molecular weights are presented in Figure 5.8. With the exception of the HN compounds, sigma values generally fell within a small range, especially for the HCN compounds. The range of sigma values for HN compounds was broader than for the other classes because of the impact of molecular size on rejection. Ranges of the $\text{Log } P_s$ parameter for each compound class were larger than for sigma. On first inspection, it appeared that HCNP compounds exhibited a $\text{Log } P_s$ range different from that of other ionic compounds. However, the HCNP tended to be of less molecular weight, which may explain why $\text{Log } P_s$ values for these compounds tended to be less negative than for other ionic compounds. Significant effort was undertaken to develop correlations between phenomenological model coefficients and molecular descriptors to predict model coefficients for “new” compounds. These efforts are discussed later.

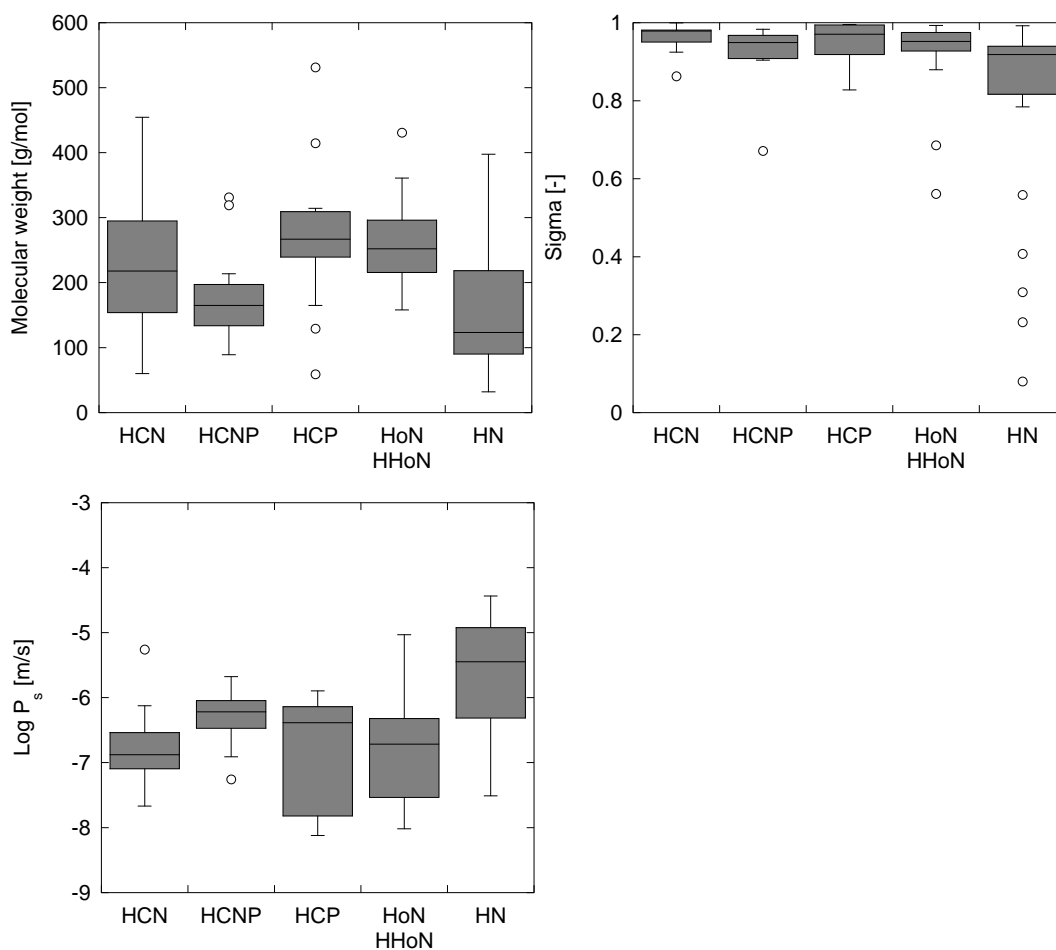


Figure 5.8. Comparison of molecular weight and phenomenological coefficients for the major classes of compounds investigated.

5.3.1.1 Neutral Compounds—Solute Permeability (P_s)

Cross-validation PLS analysis was performed to determine the most important solute descriptors for developing correlations with $\text{Log } P_s$ for all neutral compounds as well as the optimum number of descriptors in a regression. Somewhat surprisingly, the RMSE of the best correlations could not be significantly improved by including more than one descriptor. In addition, solute size descriptors were found to be the most important for describing $\text{Log } P_s$ for all of the neutral organic compounds analyzed. Size descriptors such as molecular volume, Stokes radius, second moment of the charge density (S_x , S_y , and S_z), molecular weight, and surface area descriptors were found to be the most important factors for $\text{Log } P_s$. Examples of correlations developed between $\text{Log } P_s$ and size descriptors are presented in Figure 5.9. Recursive partitioning was also implemented to find the best descriptors for use in multiple linear regressions. Partitioning identified that the best descriptors for a multiple linear correlations would be the equivalent width (square root of width multiplied by depth) and the base-10 logarithm of solubility ($\text{Log } S$). The developed multiple linear regression; however, was not statistically significant (on the basis of t and F values for descriptor coefficients).

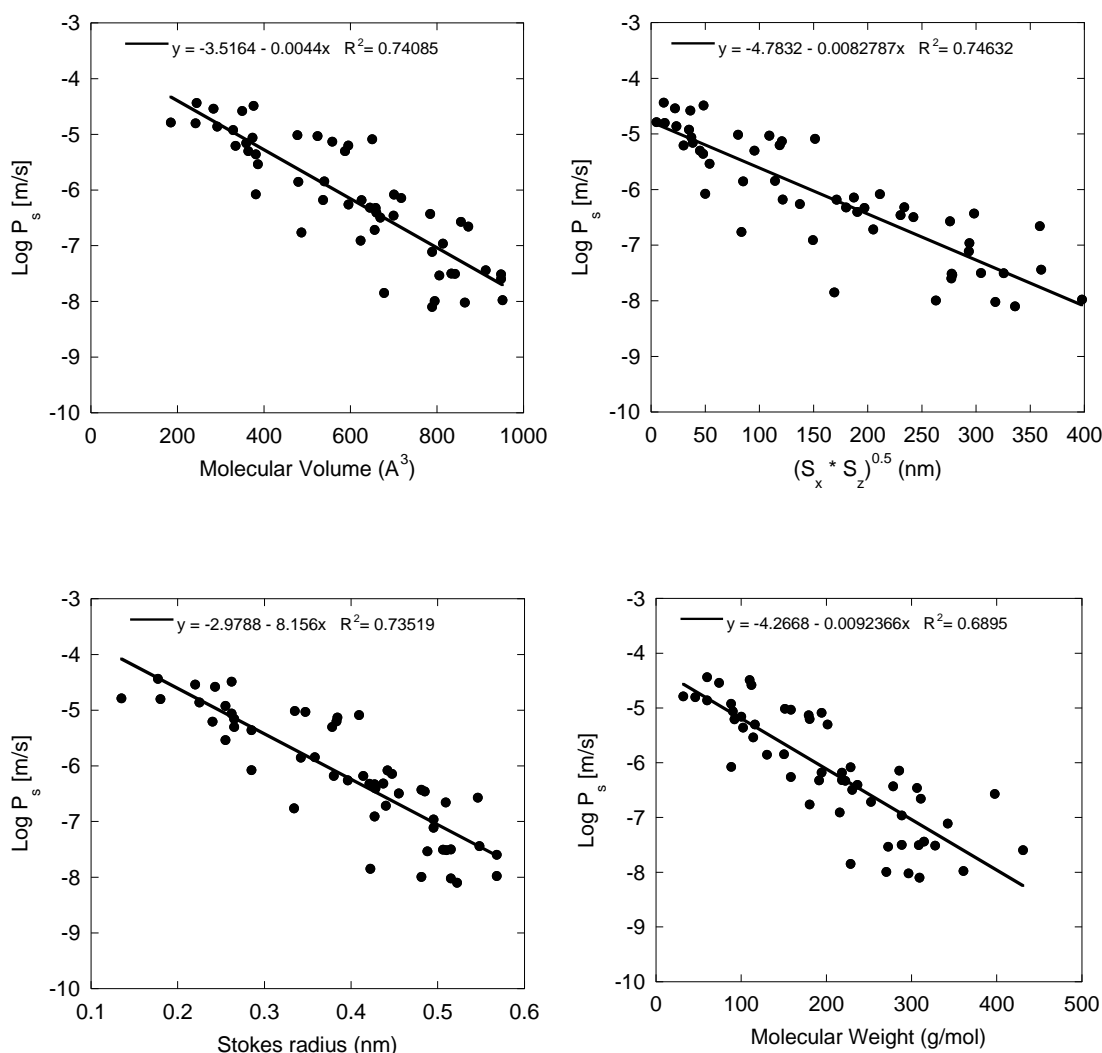


Figure 5.9. Correlations between $\text{Log } P_s$ and molecular size descriptors for all neutral compounds.

For HN compounds (minus the validation compounds), the most important factors determining rejection included molecular volume, Stokes radius, second moment of the z axis charge density (S_z), solvent accessible surface area, depth, diffusion coefficient, and molecular weight. Correlations developed between $\text{Log } P_s$ and molecular volume, S_z , Stokes radius, and molecular weight are provided in Figure 5.10. Molecular volume and S_z provided the best fit of $\text{Log } P_s$ data; however, more-accessible descriptors such as Stokes radius and molecular weight provided statistically significant fits of $\text{Log } P_s$ data (on the basis of the t and F statistic). Recursive partitioning identified depth and diffusion coefficient as the two best parameters for use in multiple linear regression; however, the correlation was not as significant as using molecular volume alone. These results indicate that, for organic solutes with $\text{Log } K_{ow}$ values less than 2 (our definition of HN compounds), molecular size is the most important factor for the rejection of solutes at relatively low permeate flux ranges.

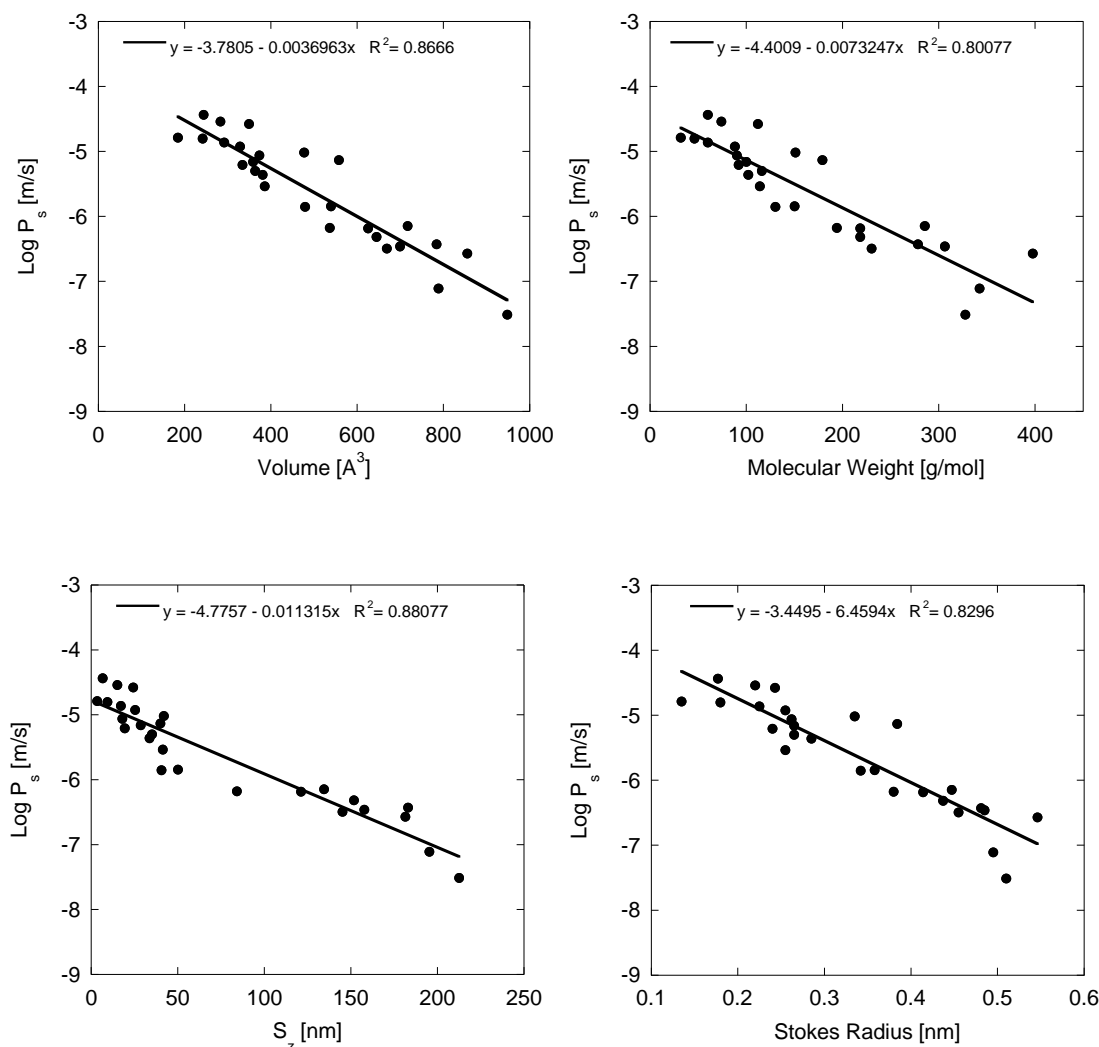


Figure 5.10. Correlations between HN $\text{Log } P_s$ and molecular size descriptors.

The cross-validation PLS analysis was repeated for $\text{Log } P_s$ values for the HoN compounds ($\text{Log } K_{ow} > 3$). The most important factors for the HoN compounds were identified as critical point descriptors (S_x , S_y , and S_z) and solubility; however, bivariate correlations were much less significant than for the HN compounds ($R^2 < 0.4$, Figure 5.11). As was previously mentioned, solutes that interact with membrane materials are not well described by the phenomenological model. Solutes that were identified as having moderate membrane interactions during rejection experiments exhibited relatively “flat” rejection-versus-permeate-flux curves, which was more common among the compounds with $\text{Log } K_{ow}$ values greater than 3 (see Table 5.10). The other compounds that could not be fit with the phenomenological (presented in Table 5.9) model exhibited decreased rejection with increased flux and significant change in rejection over 24 h. On the basis of these observations, the phenomenological model is not a good approach for describing the rejection of hydrophobic compounds ($\text{Log } K_{ow} > 3$) or certain compounds with functional groups that interact with membrane polymers (e.g., phenols). Therefore, compounds displaying solute–membrane interactions will be left out of further phenomenological model development discussion.

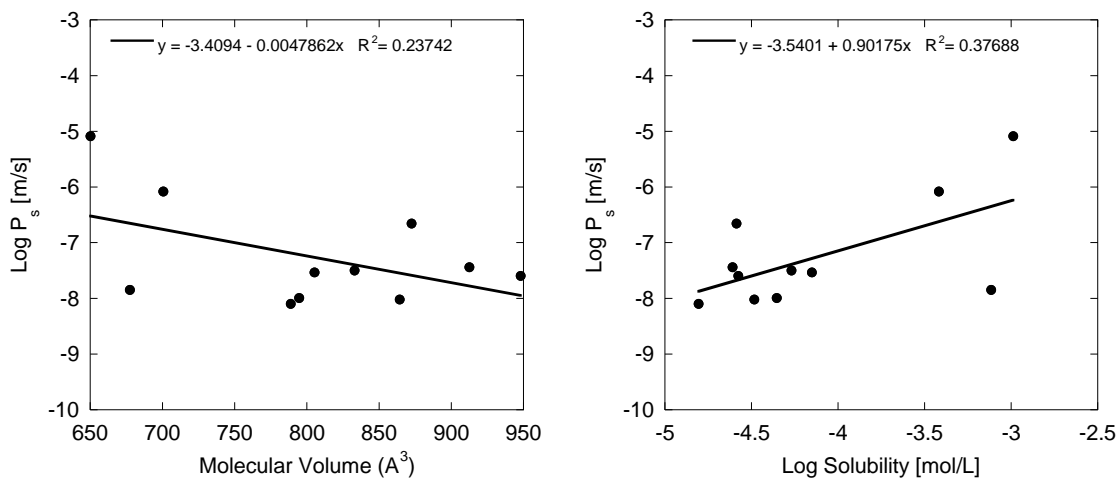


Figure 5.11. Correlations between $\text{Log } P_s$ and molecular descriptors for HoN compounds.

Recursive partitioning was used to identify the best descriptors for multiple linear correlations to calculate $\text{Log } P_s$ for HN, HHoN, and HoN compounds that exhibited minimal solute–membrane interaction. The most statistically significant correlation included depth, $\text{Log } S$, and S_y . This correlation was used to predict $\text{Log } P_s$ for the training set and the correlation between experimental $\text{Log } P_s$ and predicted $\text{Log } P_s$. As a comparison, a correlation was developed by using molecular volume to predict $\text{Log } P_s$. Experimental versus predicted $\text{Log } P_s$ values are presented for both correlations in Figure 5.12.

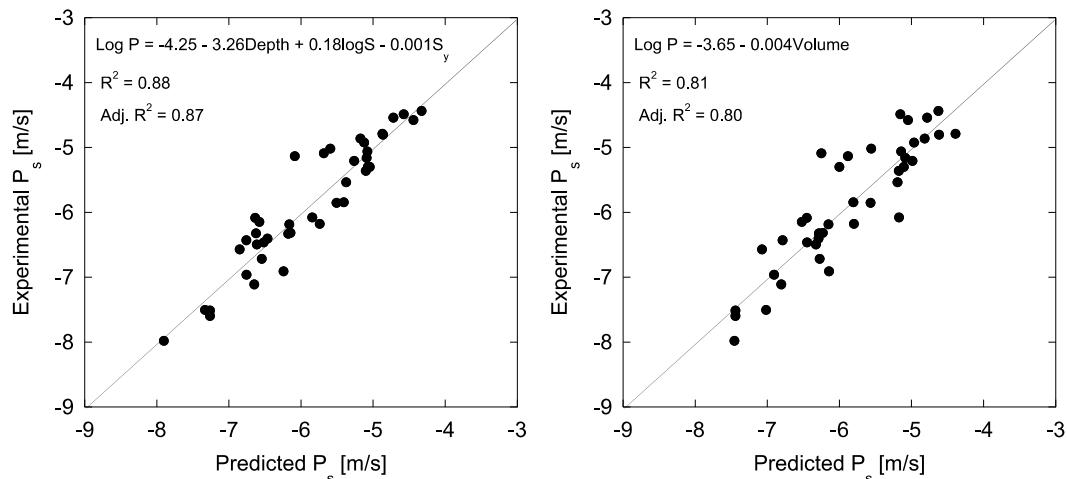


Figure 5.12. Experimental versus predicted $\text{Log } P_s$ values for neutral compounds that exhibited minimal solute–membrane interactions.

5.3.1.2 Neutral Compounds—Sigma (σ)

No statistically significant correlations could be developed between sigma values and molecular descriptors by using common statistical techniques (i.e., recursive partitioning, PLS, multiple linear regression, and bivariate regression). Past studies have used sigma values obtained through phenomenological fitting to determine a monomodal pore size distribution (Van der Bruggen and Vandecasteele, 2002). At infinite flux, solute transport is dominated by convection and diffusion can be assumed to be negligible. Therefore, a sigma value for a given molecule represents the reciprocal of the sieving coefficient—for example, the proportion of pores that are smaller than the given molecule. By running of several molecules of different size, a pore size distribution can be determined from reflection coefficients, which has been demonstrated to fit best with the Log-normal cumulative density function (Van der Bruggen and Vandecasteele, 2002; Bellona and Drewes, 2010).

This exercise was carried out for different groupings of neutral compounds: all neutral compounds and only the aliphatic compounds with little environmental relevance (alcohols, sugars, urea, and uracil). The compounds with minimal environmental relevance were chosen because they span a wide range of molecular size (Stokes radius between 0.1 and 0.6 nm) and exhibited no membrane interaction. Fitting the reflection coefficients for these compounds with the Log-normal cumulative density function resulted in an average pore size of 0.196 nm and standard deviation of pore size of 0.229 nm (Figure 5.13). Using all of the neutral compounds to calculate a pore size distribution yielded a marginally larger average pore size (0.197 nm) and standard deviation of pore size (0.293 nm [Figure 5.13]). A significant number of reflection coefficients for the neutral compounds investigated were overpredicted by the monomodal Log-normal pore size distribution, indicating the Stokes radius is not the best size descriptor for these compounds, the pore size distribution is bimodal, or other molecular properties influence the reflection coefficient. Similar statistical analysis as discussed previously for $\text{Log } P_s$ was carried out for the reflection coefficient; however, no statistically significant correlations were found with descriptors other than size descriptors.

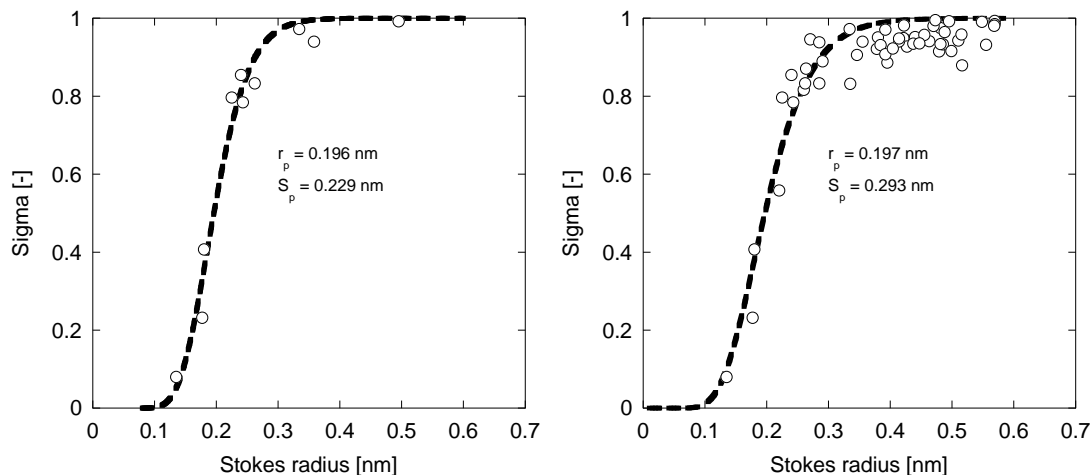


Figure 5.13. Log-normal cumulative density function fits for sugars, alcohols, urea, and uracil (left) and all neutral organic compounds with resulting pore size average and deviation values.

5.3.1.3 Predicting Rejection of Neutral Validation Compounds Using the Phenomenological Model

Several correlations developed in the previous sections were used to predict bench-scale rejection for the neutral validation compounds with minimal solute–membrane interactions: carbamazepine, dilantin, fenofibrate, MTBE, 1-nitrosopyrrolidine, and isobutylparaben (Figures 5.14 through 5.19). With the exception of isobutylparaben, and of MTBE for the volume correlation, this approach provided reasonably good fits of rejection data spanning a wide permeate flux range. For the validation compounds evaluated, adding additional parameters to linear regression to predict $\text{Log } P_s$ only significantly improved the model fit for MTBE. Therefore, it is presumable that, to characterize a given membrane, rejection experiments over a flux range could be run with sugar- and alcohol-type compounds spanning a range of size or pore size distribution (PSD) (e.g., ethanol, isopropanol, urea, glycerol, glucose, and sucrose) and several environmentally relevant compounds with minimal solute–membrane interactions (e.g., NDMA, carbamazepine, caffeine, DEET, and primidone). Similar correlations could be developed between phenomenological coefficients and molecular size to predict the rejection of neutral compounds expected to have minimal solute–membrane interactions. However, precaution should be taken to conduct the experiments so that concentration polarization is minimized.

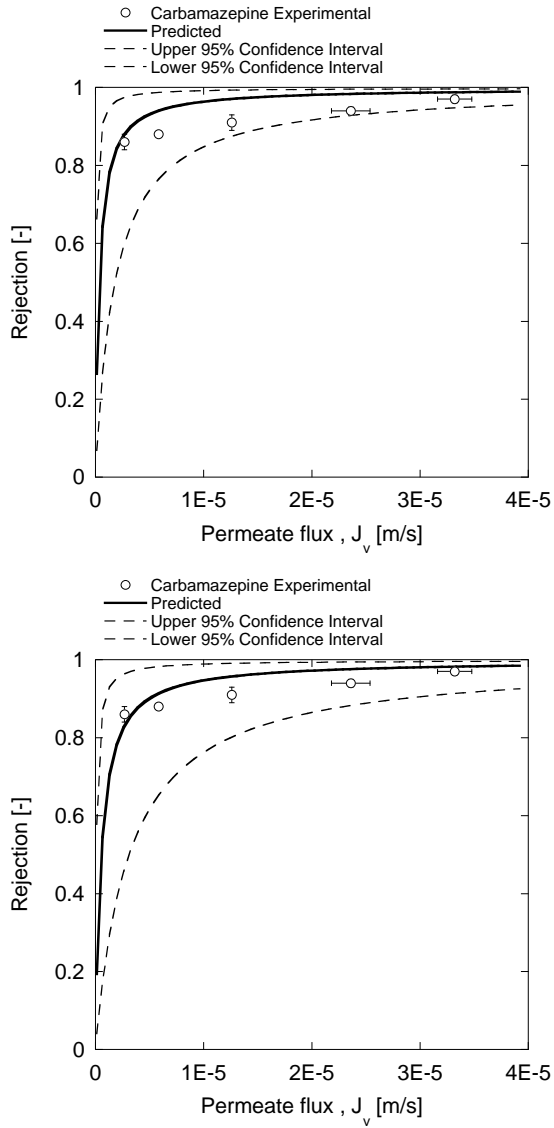


Figure 5.14. Carbamazepine rejection versus permeate flux with predicted rejection.

Top figure: Predicted model used 3-parameter correlation for $\text{Log } P_s$ (Figure 5.12) and sugar and alcohol PSD (Figure 5.13).

Bottom figure: Used 1-parameter correlation for $\text{Log } P_s$ (Figure 5.12) and sugar and alcohol PSD (Figure 5.13).

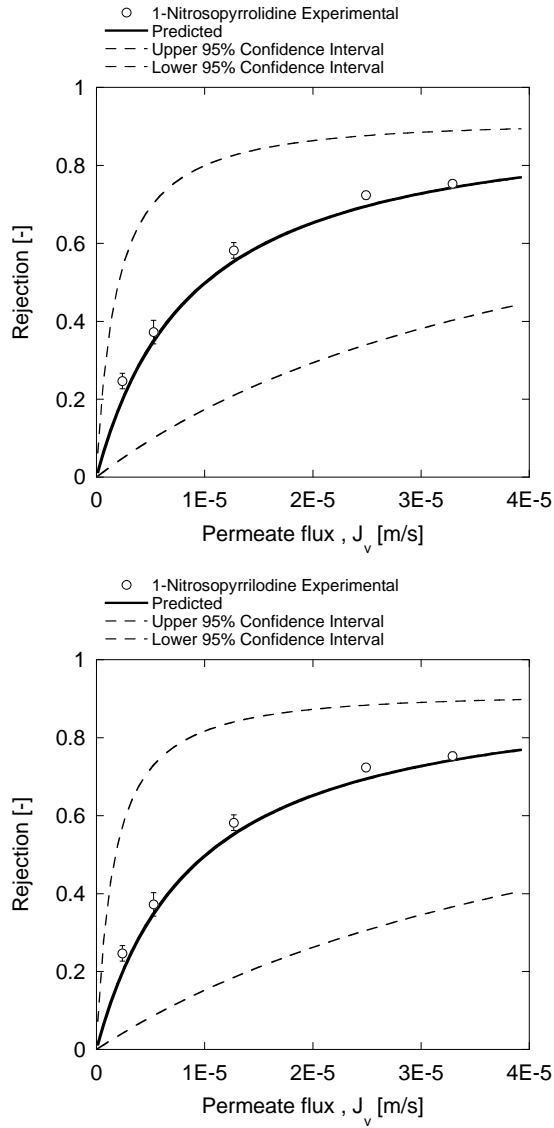


Figure 5.15. NPYR rejection versus permeate flux with predicted rejection.

Top figure: predicted model used 3-parameter correlation for $\text{Log } P_s$ (Figure 5.12) and sugar and alcohol PSD (Figure 5.13).

Bottom figure: used 1-parameter correlation for $\text{Log } P_s$ (Figure 5.12) and sugar and alcohol PSD (Figure 5.13).

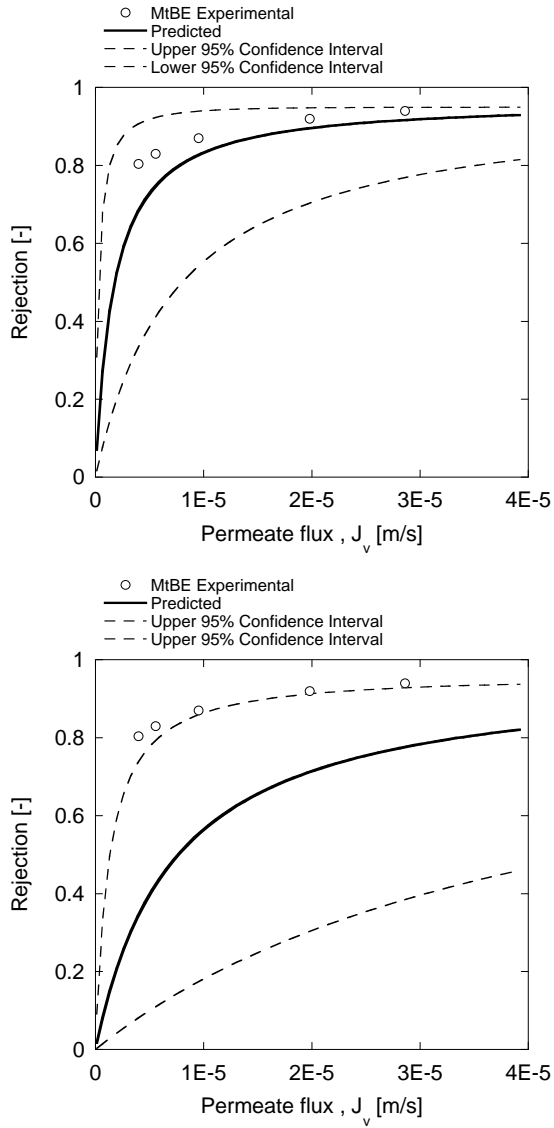


Figure 5.16. MTBE rejection versus permeate flux with predicted rejection.

Top figure: predicted model used 3-parameter correlation for $\text{Log } P_s$ (Figure 5.12) and sugar and alcohol PSD (Figure 5.13).

Bottom figure: used 1-parameter correlation for $\text{Log } P_s$ (Figure 5.12) and sugar and alcohol PSD (Figure 5.13).

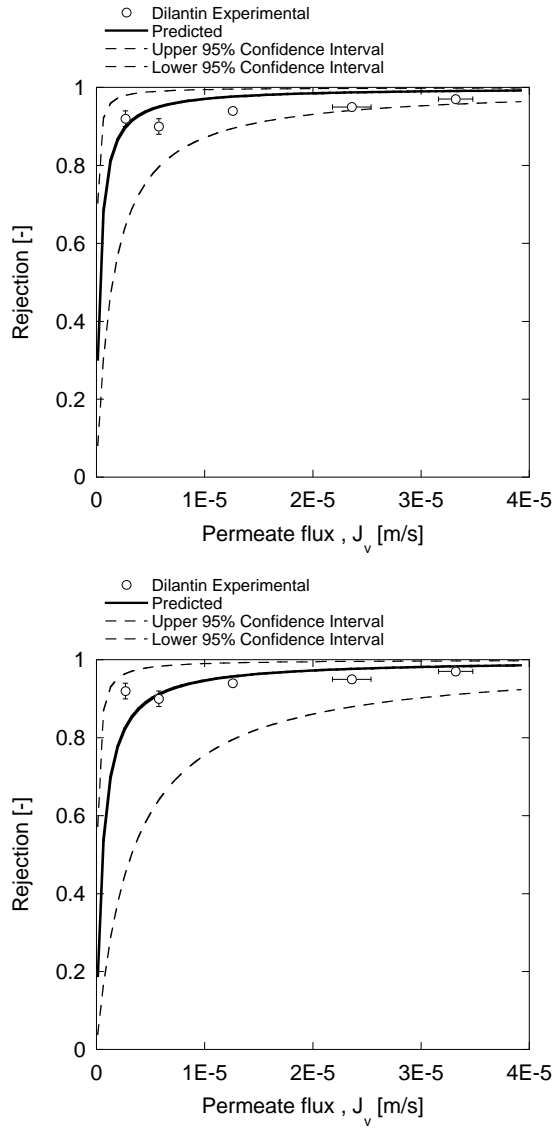


Figure 5.17. Dilantin rejection versus permeate flux with predicted rejection.

Top figure: predicted model used 3-parameter correlation for $\text{Log } P_s$ (Figure 5.12) and sugar and alcohol PSD (Figure 5.13).

Bottom figure: used 1-parameter correlation for $\text{Log } P_s$ (Figure 5.12) and sugar and alcohol PSD (Figure 5.13).

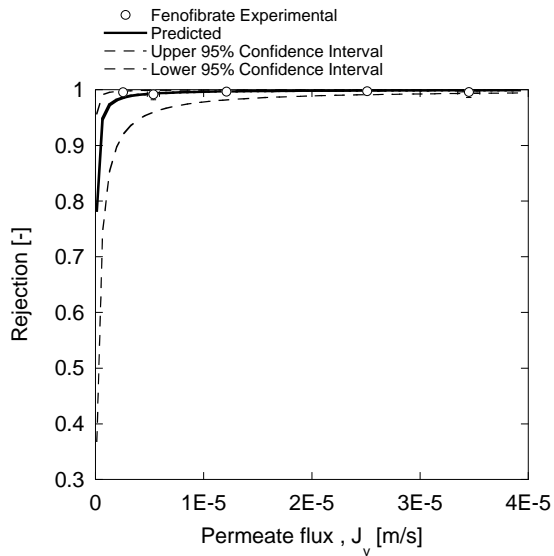
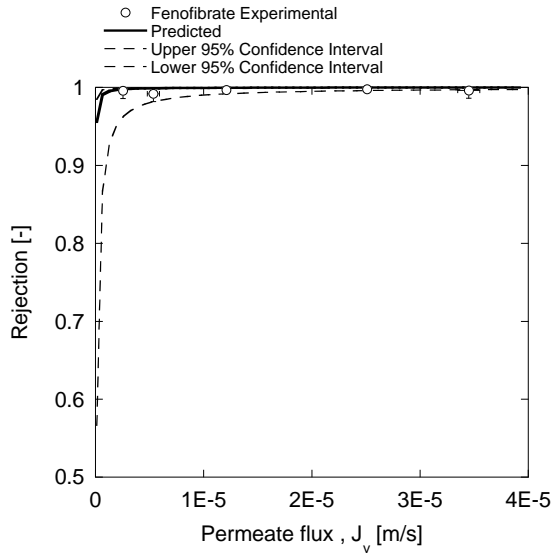


Figure 5.18. Fenofibrate rejection versus permeate flux with predicted rejection.

Top figure: predicted model used 3-parameter correlation for $\text{Log } P_s$ (Figure 5.12) and sugar and alcohol PSD (Figure 5.13).

Bottom figure: used 1-parameter correlation for $\text{Log } P_s$ (Figure 5.12) and sugar and alcohol PSD (Figure 5.13).

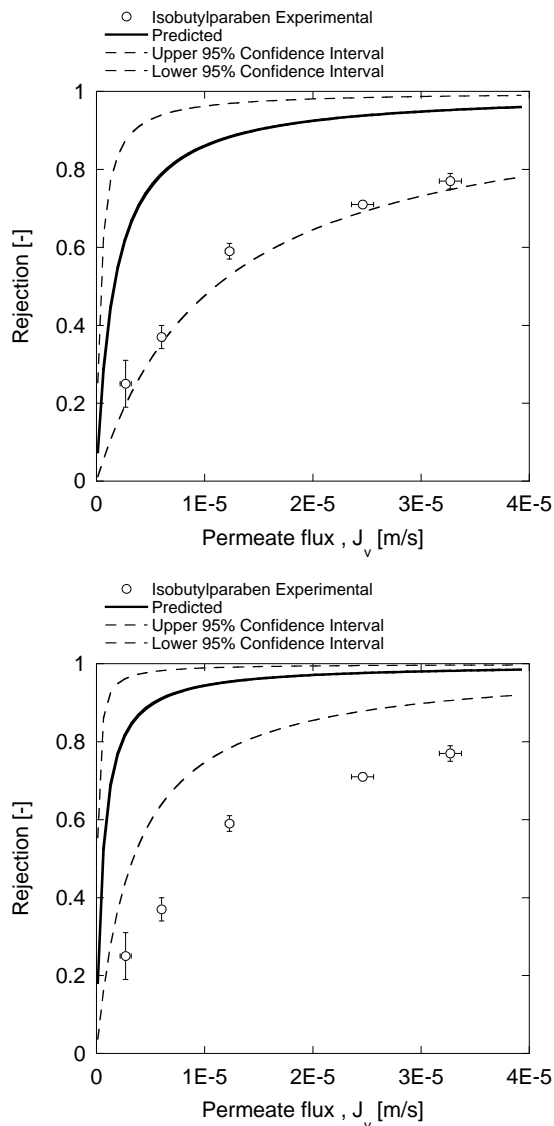


Figure 5.19. Isobutylparaben rejection versus permeate flux with predicted rejection.

Top figure: predicted model used 3-parameter correlation for $\text{Log } P_s$ (Figure 5.12) and sugar and alcohol PSD (Figure 5.13).

Bottom figure: used 1-parameter correlation for $\text{Log } P_s$ (Figure 5.12) and sugar and alcohol PSD (Figure 5.13).

5.3.1.4 LOO Model Validation—Neutral Organic Contaminants

To evaluate the phenomenological-QSPR modeling approach, one compound was kept out of $\text{Log } P_s$ correlation calculations using the three-parameter multiple linear regression model and the multiple regression model using only molecular volume. The reflection coefficient was calculated by using the PSD developed for sugars, alcohols, urea, and uracil discussed previously (Figure 5.13). This approach was used to calculate the rejection at 12-gfd permeate flux for the environmentally relevant neutral compounds that exhibited minimum membrane interactions during experiments (Figure 5.20). Three solutes, acetaminophen,

phenacetine and isobutylparaben, were found to be poorly fit by this approach using both models. Interestingly, these compounds have very similar structures, that is, a benzene ring with two functional groups in the *para* substitution pattern. Isobutylparaben and acetaminophen both have a phenolic moiety attached to the benzene ring, with the only difference being that acetaminophen has an amide group and isobutylparaben has an ester group in the *para* position. Phenacetine does not have a hydroxyl group and instead has an ester group and an amide group in the *para* position. Other similar compounds, such as methylparaben, benzyl acetate, and methyl salicylate, exhibited significant membrane interactions, had lower-than-expected rejection on the basis of size, and could not be described by using the phenomenological approach.

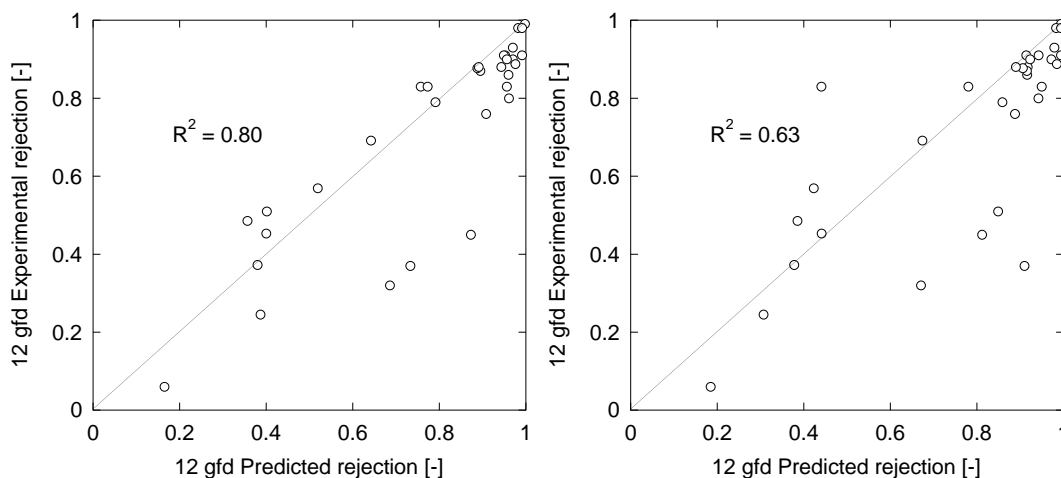


Figure 5.20. LOO model correlations with experimental 12-gfd rejection data.

5.3.1.5 Ionic Compounds—Sigma (σ) and Solute Permeability (P_s)

Sigma and especially Log P_s values for ionic compounds spanned a significantly narrower range than did neutral compounds (Figure 5.8). This finding may partially explain why developing statistically significant correlations between molecular descriptors and phenomenological coefficients was more difficult for ionic compounds than for neutral compounds. As an example, correlations developed between phenomenological model coefficients and size parameters were poor (Stokes radius presented in Figure 5.21). Cross-validation PLS identified the most important descriptors for describing Log P_s as being the number of halogens, WPSA, FOSA, E_{LUMO} , number of six-membered rings, and solubility, respectively. Increasing numbers of halogens and six-membered rings tend to result in more-negative Log P_s values (increased rejection at low permeate flux), although an increase in hydrophobicity tends to make Log P_s values less negative (decreased rejection at low permeate flux).

Recursive partitioning and PLS analysis were used to develop multiple linear regressions for predicting Log P_s for all ionic compounds from molecular descriptors. The multiple linear regression resulting in the best correlation ($R^2 = 0.66$) with statistically significant coefficients (based on t and F-ratios) included the number of halogens, solubility, and E_{LUMO}

and is presented in Figure 5.22. Although significant, this approach did not provide a high degree of predictive power and additional analysis was performed.

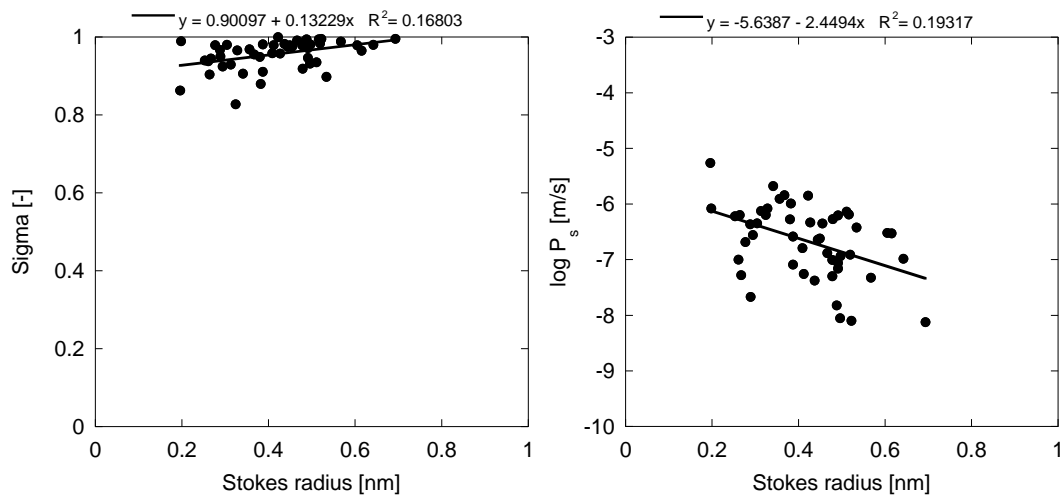


Figure 5.21. Correlation between phenomenological model coefficients and Stokes radius for ionic compounds (HCN, HCP, HCNP).

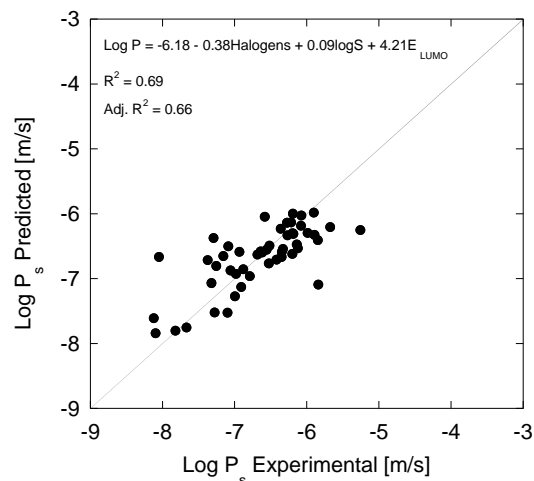


Figure 5.22. Experimental versus predicted $\text{Log } P_s$ values for ionic compounds at pH 6.3 (HCN, HCP, HCNP).

5.3.1.6 Ionic Compounds—HCP and HCNP

Through trial and error and by using PLS analysis, it was observed that HCNP and HCP phenomenological coefficients had correlations with similar descriptors. Therefore, HCNP and HCP compounds were grouped together and were analyzed by using PLS analysis and multiple linear regression. Statistically significant multiple linear regression models were developed to describe $\text{Log } P_s$ by using the number of halogens and a size parameter such as Stokes radius, second moments of inertia, and molecular weight. The two most statistically significant and correlated regressions are presented in Figure 5.23. As previously described, increasing the number of halogens resulted in more-negative $\text{Log } P_s$ values, especially for

HCP compounds (increased rejection at low permeate flux). As expected, increasing molecular size also resulted in a more negative Log P_s value. Two validation compounds for each class of compounds (HCP and HCNP) were subsequently left out of multiple regression development to evaluate this modeling approach. Because second-moment-of-inertia descriptors are difficult to calculate, the regression using molecular weight was used to predict Log P_s for validation compounds. Unfortunately, no significant correlations could be developed between sigma values and molecular descriptors likely because of the small variation in sigma values for HCNP and HCP compounds. The average of HCNP and HCP compound sigma values was used with the standard deviation (plus and minus) for inclusion into the phenomenological model.

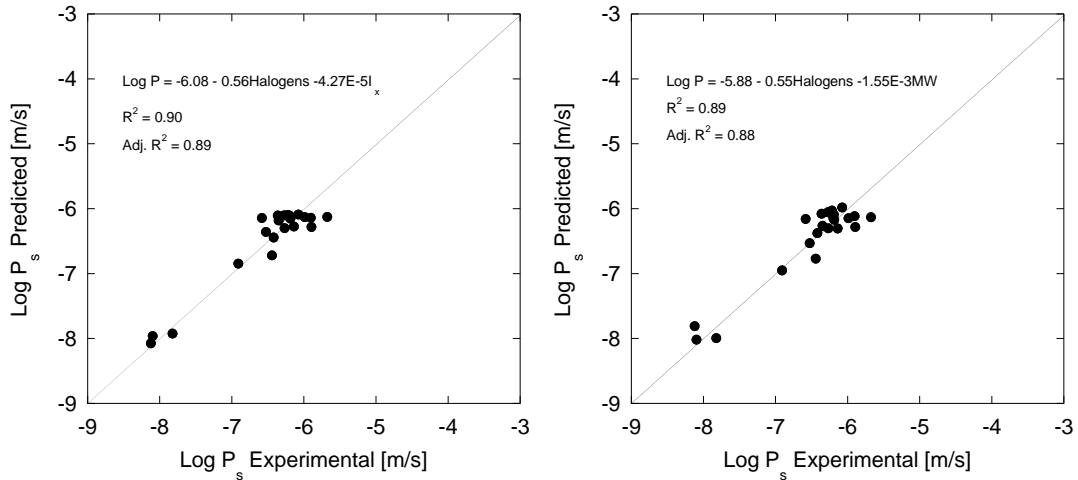


Figure 5.23. Experimental versus predicted Log P_s values for HCP and HCNP compounds at pH 6.3.

The results of the rejection prediction exercise described earlier are presented in Figure 5.24. Because two sigma values were used (average sigma plus or minus standard deviation), a range of rejection was predicted across the permeate flux range investigated. In general, this approach resulted in predicted rejection within the range of experimental values, although baclofen rejection was underestimated at several permeate flux values. On the basis of this analysis, it is possible that several HCNP and HCP compounds could be selected (e.g., ciprofloxacin, lysine, ketoconazole, and metoprolol) to characterize a membrane's rejection of HCNP and HCP compounds.

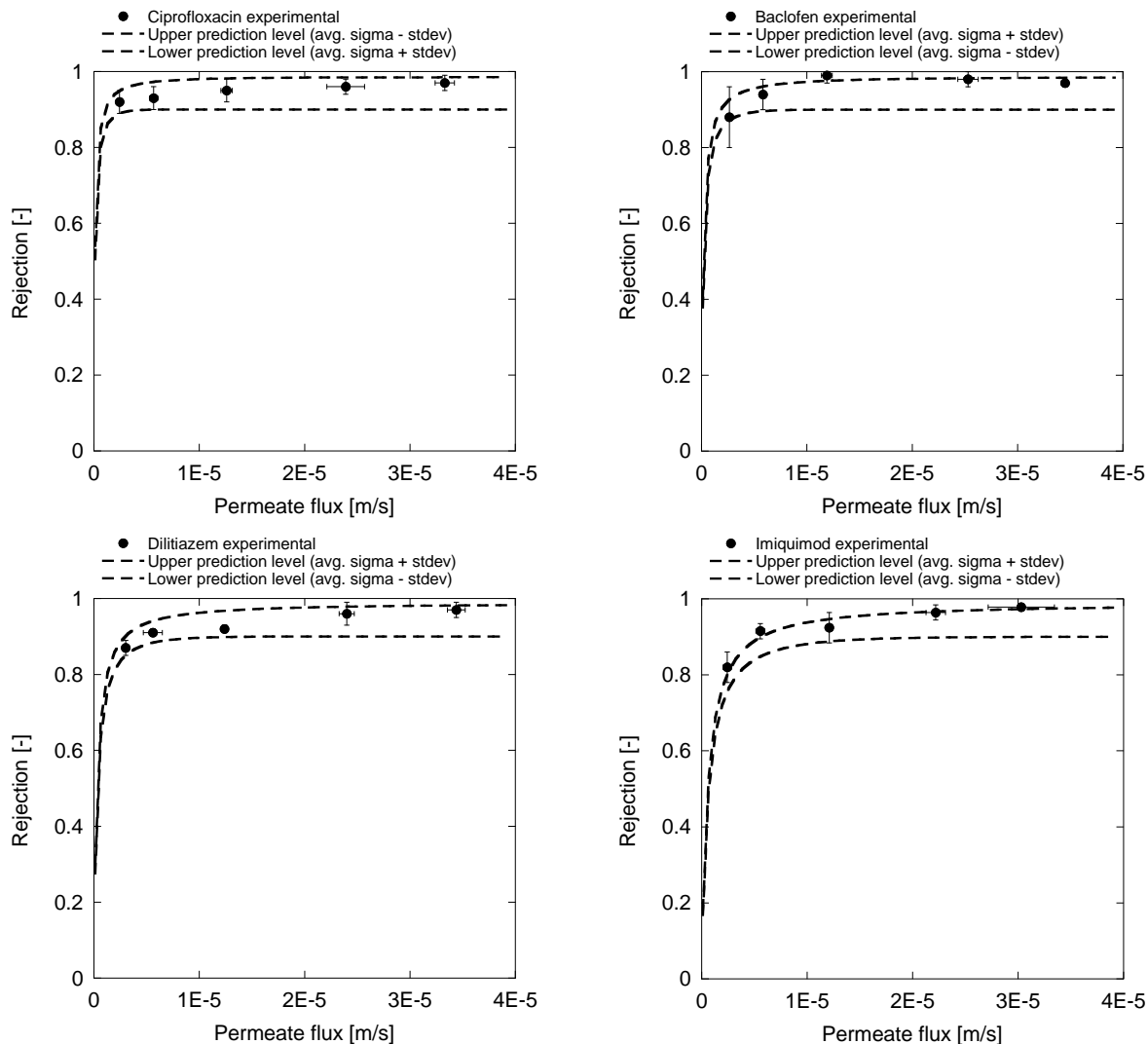


Figure 5.24. Experimental rejection with predicted phenomenological model predictions using the multiple linear regression approach presented in Figure 5.23 for baclofen (upper left, HCNP), ciprofloxacin (upper right, HCNP), diltiazem (lower left, HCP), and imiquimod (lower right, HCP).

Note: Sigma values used were the average of all HCNP and HCP compounds minus the validation compounds (0.945) plus and minus the standard deviation (0.40).

5.3.1.7 Ionic Compounds—HCN

Similar correlations between phenomenological coefficients and molecular descriptors described earlier were explored for HCN compounds. However, no strong correlations could be developed among sigma, $\text{Log } P_s$, and molecular descriptors. One possible explanation for the lack of correlation with descriptors could be the fact that the range of $\text{Log } P_s$ values for HCN compounds was narrow (Figure 5.8). Including either HCNP or HCP compounds only marginally improved the significance of developed multiple linear correlations. Recursive partitioning could be used to develop a modeling approach with good correlations ($R^2 \sim 0.8$) between predicted and experimental $\text{Log } P_s$ values; however, there is no straightforward way to determine the significance of the descriptors used in the model. For example, a recursive

partitioning model for predicting $\text{Log } P_s$ values for all ionic compounds was comprised of eight descriptors in the form of a decision tree. Although the model provided relatively good fits of experimental $\text{Log } P_s$ data, a user would be required to calculate relatively complicated descriptors, such as second moments of the charge density, E_{LUMO} , and surface area descriptors such as FOSA, PISA, and WPSA. It is worth noting that all of the HCN compounds evaluated, with the exception of acetic acid, exhibited greater than 90% rejection by the NF-270 membrane at permeate fluxes equal to or greater than 12 gfd. In addition, all of the HCN compounds considered to be organic contaminants were more than 94% rejected at permeate flux equal to or greater than 12 gfd.

5.3.2 Phenomenological Model for the ESPA2 Membrane

As with the NF-270 membrane, ESPA2 membrane rejection data (for most of the organic solutes evaluated) were fit with the phenomenological model by manipulating model coefficients (σ , P_s). As previously discussed, a number of NF-270 membrane organic solute rejection curves could not be described by the phenomenological model because of hypothesized solute–membrane interactions. This issue was not as pronounced with the ESPA2 membrane, however, and the phenomenological model could be used to describe the rejection of the majority of compounds evaluated. Compounds that could not be described include the THMs (chloroform, bromoform, BDCM, and dibromochloromethane), ketoconazole, trazodone, and trimethoprim. Compounds exhibiting a flat or slightly declining rejection-versus-flux curve resulting in less than optimal fits included 2-phenylphenol and propylparaben. Examples of phenomenological model fits are presented in Figure 5.25, and a list of phenomenological coefficients is presented in Table 5.11.

The ranges of reflection coefficients and solute permeability coefficients for each solute classification is presented in Figures 5.26 and 5.27. The range of ESPA2 membrane reflection coefficients was much narrower than for the NF-270 membrane, as the majority of compounds exhibited rejection greater than 95% at elevated permeate flux. In addition, the ranges of reflection coefficients and solute permeability coefficients for compound classification were relatively similar to one another as the ESPA2 provided high rejection of almost all the solutes evaluated. Notable exceptions included methanol, ethanol, urea, and NDMA because of their small molecules.

Reflection coefficients for sugars, alcohols, urea, and uracil were fit with the Log-normal cumulative Log-normal density function to determine the effective average pore radius and standard deviation of pore radius (Figure 5.28, left). On the basis of this approach, the effective average pore radius was determined to be 0.16 nm, which is approximately 20% smaller than the NF-270 membrane. Analysis by PLS indicated that the most significant descriptor for $\text{Log } P_s$ was a solute's diffusion coefficient, which was significantly correlated with $\text{Log } P_s$ values for the sugars, alcohols, urea, and uracil (Figure 5.28, right). The correlation between $\text{Log } P_s$ and diffusion coefficients for all of the nonionic organic compounds was less significant, and the correlations could not be improved by adding more descriptors to the regression. It is worth noting that, because the ESPA2 membrane provides such high rejection, the reflection coefficient and $\text{Log } P_s$ data were skewed toward reflection coefficients of 1 and negative $\text{Log } P_s$ values between 6 and 8.

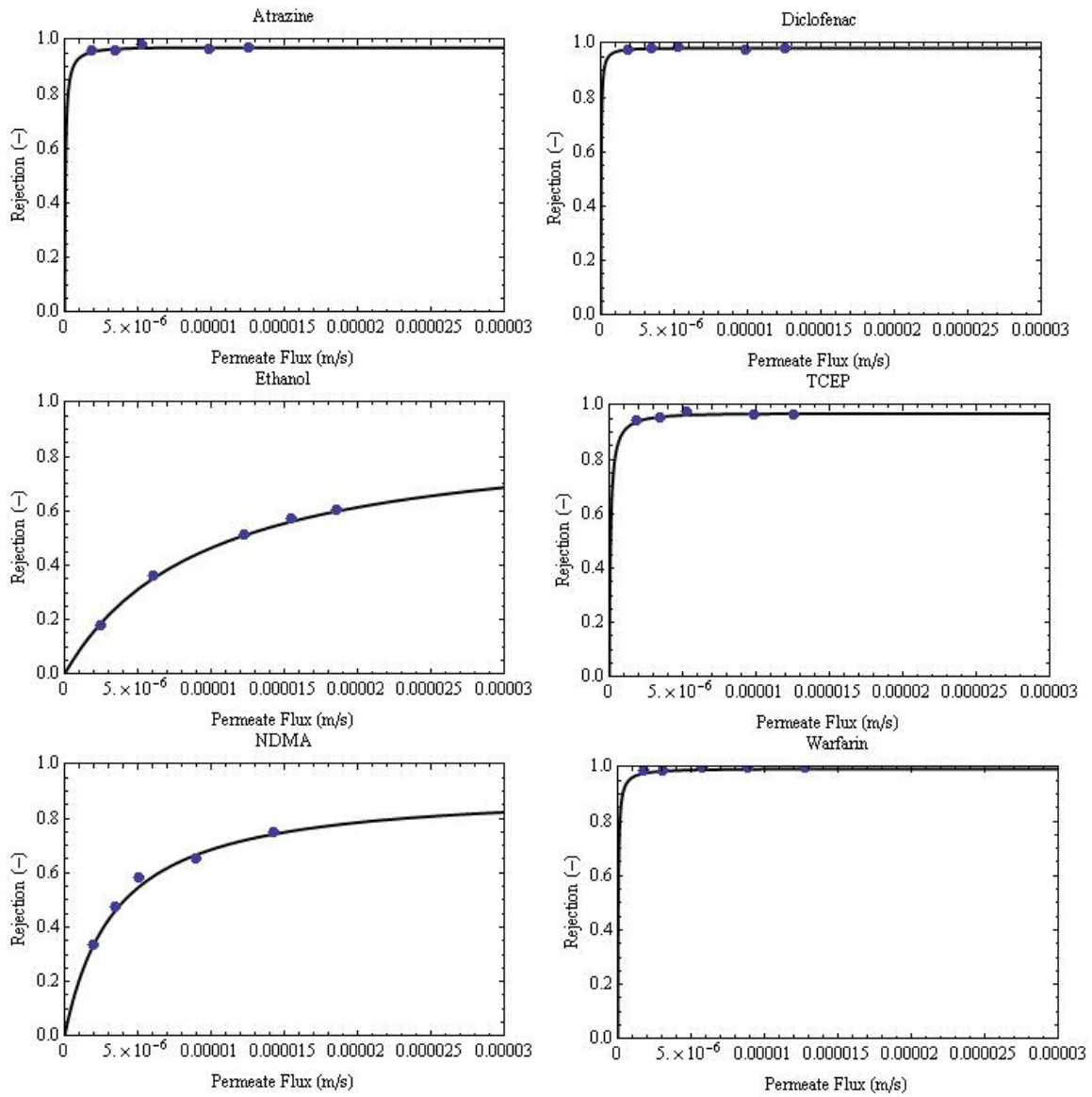


Figure 5.25. Examples of phenomenological model fits of ESPA2 rejection data.

Table 5.11. Phenomenological Model Coefficients for All Organic Compounds (ESPA2 Membrane)

Compound	Reflection coefficient (σ)	Permeability coefficient (P) m/s	Compound	Reflection coefficient (σ)	Permeability coefficient (P) m/s	Compound	Reflection coefficient (σ)	Permeability coefficient (P) m/s	Compound	Reflection coefficient (σ)	Permeability coefficient (P) m/s
Acetic acid	0.9986	7.992E-07	Arginine	0.9847	1.35E-07	Diethylphthalate	0.9884	7.745E-08	Nitrosopiperidine	0.9686	6.755E-08
Benzoic acid	0.9963	2.760E-08	Baclofen	0.9758	1.97E-07	Dilantin	0.9702	5.136E-08	Nitrosopyrrolidine	0.9667	2.861E-07
Captopril	0.9995	7.940E-07	Ciprofloxacin	0.9883	4.81E-08	1-naphthalenemethanol	0.9925	8.319E-08	Pentoxifylline	0.9813	2.071E-07
Chlortetracycline	0.9461	8.825E-08	Cysteine	0.9897	6.31E-08	2-naphtol	0.9920	2.543E-08	Phenacetin	0.9926	5.124E-08
Clofibrin acid	0.9718	9.619E-08	Lysine	0.9992	1.58E-06	N-nitrosodibutylamine	0.9855	8.639E-09	Primidone	0.9543	7.287E-08
Dibromoacetic acid	0.9877	2.396E-08	Phenylalanine	0.9545	6.33E-07	Propylparaben	0.9464	1.951E-08	Propyphenazone	0.9848	6.626E-08
Dichloroacetic acid	0.9860	7.524E-09	Serine	0.9750	9.15E-08	Thiabendazole	0.9800	8.733E-08	Resorcinol	0.9993	2.096E-07
Diclofenac	0.9813	2.176E-08	Tyrosine	0.9734	1.54E-07	Warfarin	0.9932	3.607E-08	Sucralose	0.9525	7.571E-08
Dihydroxybenzoic acid	0.9556	6.361E-08	Amtriptyline	0.9963	1.41E-08	Acetaminophen	0.9444	2.369E-07	Sucrose	0.9897	3.855E-08
Furosemide	0.9789	7.064E-08	Atenolol	0.8271	3.20E-07	Benzyl alcohol	0.9944	3.130E-07	TCCP	0.9802	1.512E-08
Gemfibrozil	0.9783	2.519E-08	Cimetidine	0.9993	4.25E-07	Butanediol	0.9755	4.235E-07	TCEP	0.9682	8.579E-08
Glutamic acid	0.9755	1.187E-07	Diltiazem	0.9950	2.48E-08	Ethanol	0.8380	8.825E-06	Triethylene glycol	0.9936	3.076E-07
Ibuprofen	0.9884	5.337E-08	Diphenylhydramine	0.9959	1.56E-08	Fluconazole	0.9924	7.324E-08	Uracil	0.9787	8.471E-07
Ketoprofen	0.9721	2.724E-08	Fluoxetine	0.9963	1.43E-08	2-fluorophenol	0.9196	2.004E-07	Urea	0.8696	9.334E-06
Methotrexate	0.9799	4.143E-08	Guanidine	0.9997	1.59E-06	Glucose	0.9922	6.734E-08	Caffeine	0.9512	1.799E-07
Naproxen	0.9746	2.006E-08	Ketoconazole	0.9664	1.30E-08	Glycerin	0.9907	6.409E-07	Bisphenol-A	0.9528	4.170E-08
Salicylic acid	0.9500	2.487E-07	Metoprolol	0.9940	3.41E-08	Isopropanol	0.9576	3.010E-07	Butylparaben	0.9934	5.472E-08
Sulfacetamide	0.9761	1.693E-07	Norfluoxetine	0.9964	1.42E-08	Methanol	0.1049	9.759E-06	N-nitrosodiphenylamine	0.9947	1.217E-08
Sulfadimethoxine	0.9773	1.343E-07	Pseudoephedrine	0.9686	1.10E-07	Methylparaben	0.8469	7.690E-07	Nonylphenol	0.9895	3.944E-08
Sulfadoxin	0.9913	7.288E-08	Ranitidine	0.9967	2.48E-08	MtBE	0.9944	7.942E-08	Oxybenzone	0.9898	3.749E-08
Sulfamerazine	0.9696	1.679E-07	Salbutamol	0.8431	2.42E-07	N-nitrosodiethylamine	0.9564	1.540E-07	2-phenylphenol	0.9529	1.884E-08
Sulfamethoxazole	0.9695	3.474E-08	Tamoxifen	0.9967	1.86E-08	N-nitrosodimethylamine	0.8705	3.293E-06	TDCPP	0.9913	3.355E-08
Sulfasalazine	0.9947	3.008E-08	Atrazine	0.9702	5.46E-08	N-nitrosodipropylamine	0.9775	5.532E-08	Triclocarban	0.9952	1.713E-08
Trichloroacetic acid	0.9920	2.130E-08	Carbamazepine	0.9698	5.69E-08	N-nitrosomethylethylamine	0.9560	7.424E-07	Triclosan	0.9948	1.932E-08
Alanine	0.9625	8.518E-07	DEET	0.9635	1.05E-07	Nitrosomorpholine	0.9589	1.337E-07	Desloratidine	0.9914	3.591E-08

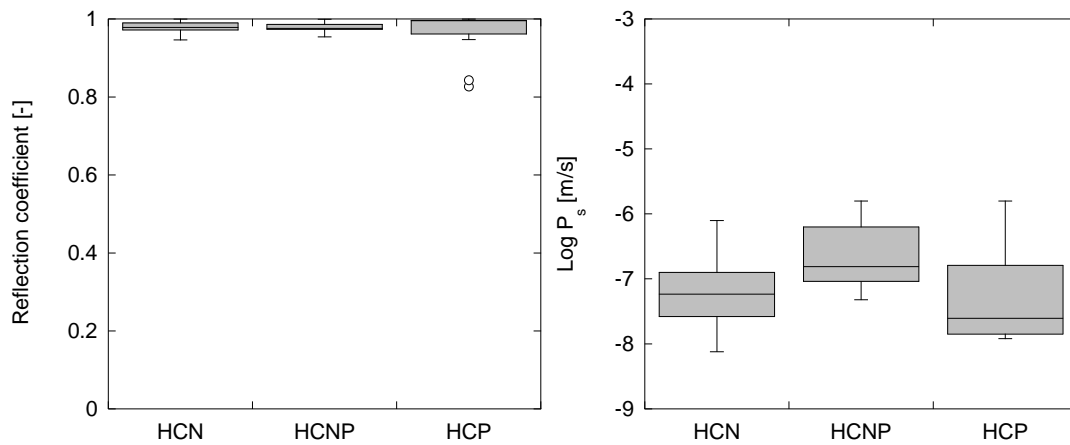


Figure 5.26. Distribution of reflection coefficients (left) and $\text{Log } P_s$ values (right) for ionic compounds with ESPA2 membrane.

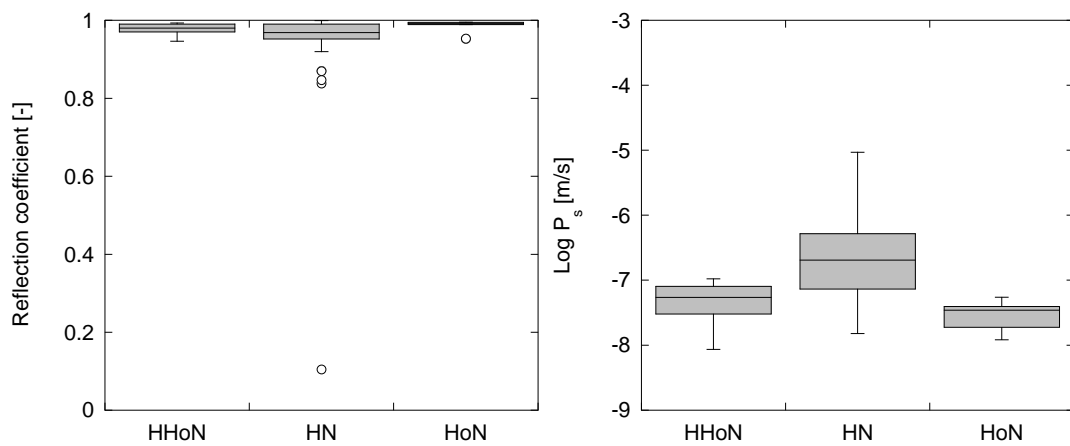


Figure 5.27. Distribution of reflection coefficients (left) and $\text{Log } P_s$ values (right) for nonionic compounds with ESPA2 membrane.

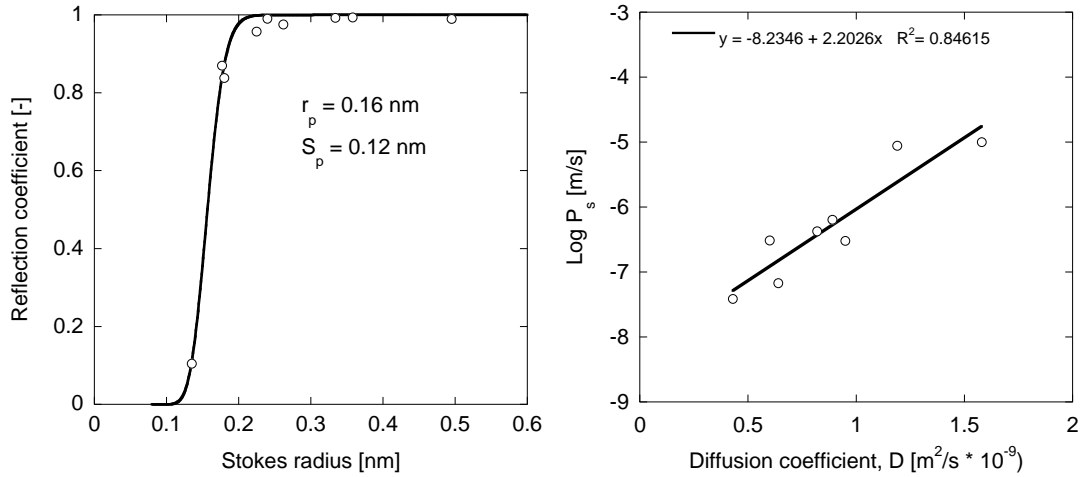


Figure 5.28. Cumulative Log-normal density function fit of reflection coefficient data (left) and $\text{Log } P_s$ correlation with diffusion coefficient (right) for sugars, alcohols, urea, and uracil for ESPA2 membrane.

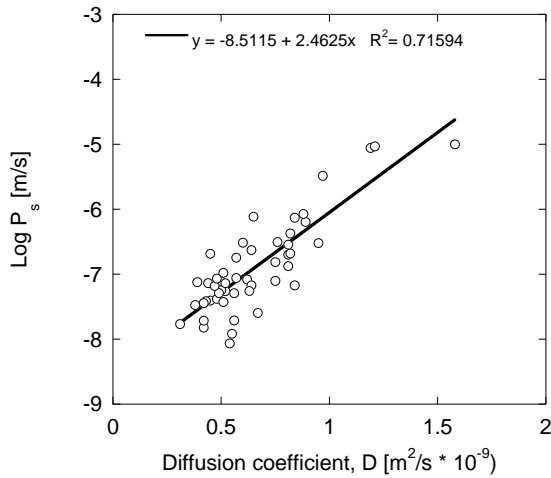


Figure 5.29. Correlation between $\text{Log } P_s$ and diffusion coefficient for all nonionic solutes.

5.4 Hydrodynamic Model

5.4.1 Model Theory

The hydrodynamic modeling approach assumes that NF membranes are composed of a bundle of cylindrical pores with the same radius and that the transport or flux of a nonionic solute within a pore is due to hindered convection and diffusion:

$$J_s = -K_d D_\infty \frac{dc}{dx} + K_c c J_v \quad (5.1)$$

where $K_{i,c}$ and $K_{i,d}$ are hindrance coefficients. The average solute flux is obtained by integrating Equation 5.1 over the length of the pore and relating the pore concentration to the external feed and permeate solute concentration through solute partitioning expressions ($c_m = \Phi C_m$, $c_p = \Phi C_p$). The solute steric hindrance (λ) is defined as the ratio between the solute radius and the characterized average pore radius:

$$\lambda = \frac{r_s}{r_p} \quad (5.2)$$

If one assumes a parabolic profile of the Hagen–Poiseuille type (Bowen and Mohammad, 1998), the solute hindrance factors for convection and diffusion are given as

$$K_c = A + B\lambda + C\lambda^2 + D\lambda^3 \quad (5.3)$$

$$K_d = E + F\lambda + G\lambda^2 + H\lambda^3 \quad (5.4)$$

For the case of $0 < \lambda \leq 0.8$, the coefficients in Equations 5.3 and 5.4 are defined as

$A = 1.0$, $B = 0.054$, $C = -0.988$, $D = 0.441$, $E = 1.0$, $F = -2.30$, $G = 1.154$, and $H = 0.224$

For the case of $0.8 < \lambda \leq 1.0$ the coefficients are defined as

$A = -8.830$, $B = 19.348$, $C = -12.518$, $D = 0$, $E = -0.105$, $F = 0.318$, $G = -0.213$, and $H = 0$

For relatively narrow and long pores with fully developed velocity profiles, Deen (1987) reported that Equation 5.3 should be multiplied by $(2-\phi)$ where

$$\Phi = (1 - \lambda)^2 \quad (5.5)$$

As it is speculative to assume the nature of the pore structure of NF membranes, Equation 5.5 was used in combination with Equation 5.3 to determine the convective hindrance factor (K_c). By rearrangement and integration of Equation 5.1 and introduction of the Peclet number, the ratio between the bulk permeate and feed solute concentrations, rejection can be defined as

$$R = 1 - \frac{\Phi K_c}{1 - [1 - \Phi K_c] \exp(-Pe)} \quad (5.6)$$

As has been reported by Bowen et al. (1998), the Peclet number can be described as

$$Pe = \frac{K_c r_p^w J_v}{8 D_p \eta_0 L_p} = \frac{K_c r_p^w \Delta P}{8 D_p \eta_0} \quad (5.7)$$

This representation of the Peclet number eliminates the need to characterize the thickness-to-porosity ratio of a membrane, which is discussed later. The rejection of an uncharged solute (Equation 5.6), therefore, is a function of pore radius, solute size and diffusivity, and permeate flux. Past modeling efforts have defined the Peclet number as

$$Pe = \frac{K_c J_v}{K_d D_p} \left(\frac{\delta}{A_k} \right) \quad (5.8)$$

where the term δ/A_k is the membrane thickness-to-porosity ratio. This term has been neglected by introducing the Hagen–Poiseuille model

$$\left(\frac{\delta}{A_k} \right) = \frac{1}{L_p} \left(\frac{r_p^2}{8\eta} \right) \quad (5.9)$$

and substituting into Equation 5.8 to get the middle term in Equation 5.7. One limitation to using Equation 5.9 to calculate the Peclet number is that an additional fitting parameter is introduced, which must be determined for each solute. If one uses Equation 5.7 to calculate the Peclet number, δ/A_k is neglected and rejection is mostly a function of solute size, membrane pore size, and permeate flux. The use of Equations 5.7 and 5.8 is discussed in the following section.

5.4.2 Determination of NF-270 Pore Size

Initially, an attempt was made to use an average membrane permeability constant determined through permeate flux and pressure data generated for all rejection experiments (~200) in Peclet number determination. The result of this exercise is presented in Figure 5.30.

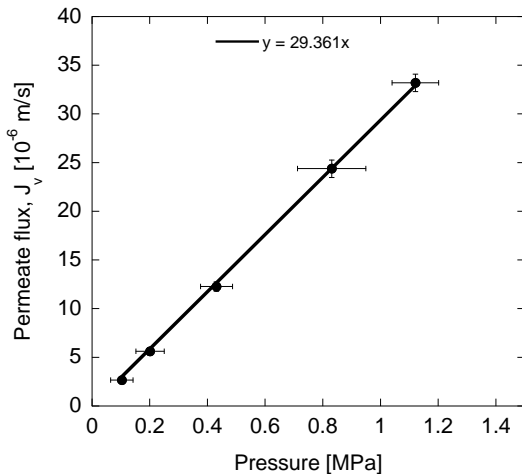


Figure 5.30. Determination of membrane permeability constant (L_p) using permeate flux data from all NF-270 rejection experiments ($n \approx 200$).

For each of the permeate flux set-points, actual permeate flux and pressure were averaged and the standard deviation calculated. Fitting the average permeate flux-versus-pressure curve resulted in a very good correlation; however, standard deviations of pressure were relatively large. Therefore, during calculations of the Peclet number for modeling rejection of a given solute, the membrane permeability was calculated from each individual experiment.

Intrinsic rejection-versus-permeate-flux curves for sugars (glucose and sucrose), alcohols (1,4-butanediol, ethanol, isopropanol, glycerol, and triethyleneglycol) and urea were fit with the hydrodynamic model by manipulating the membrane pore radius (r_p) to minimize the error between modeled and experimental rejection values. The resulting pore radius

compared with each solute's Stokes radius is presented in Figure 5.31. Because the two largest compounds, glucose and sucrose, were not completely rejected by the NF-270 membrane, the pore radii for these compounds are significantly longer than for the other compounds. Although this result indicates that the membrane pore radius depends on the solute used to characterize the membrane, this approach was investigated further as a method to predict the rejection of nonionic organic solutes.

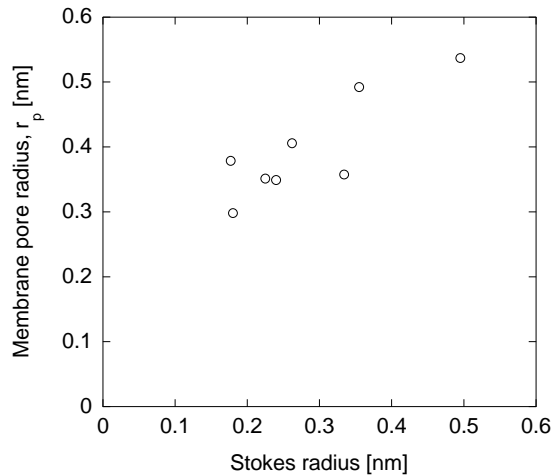


Figure 5.31. NF-270 membrane pore size determination using sugar, alcohols, and urea.

The use of the hydrodynamic model for the purpose of predicting the rejection of nonionic organic solutes would require a determination of an average pore radius for use in the model. For example, the average value for the sugar, alcohols, and urea was determined to be 0.4 nm. The same exercise was repeated for all of the nonionic solutes evaluated during the course of this study, whereby a new membrane pore radius was calculated to achieve the best fit of rejection data. Several examples of hydrodynamic model fits are presented in Figure 5.32. In general, the hydrodynamic model provided good fits of experimental data, although the shape of rejection curves was not always well described by this approach.

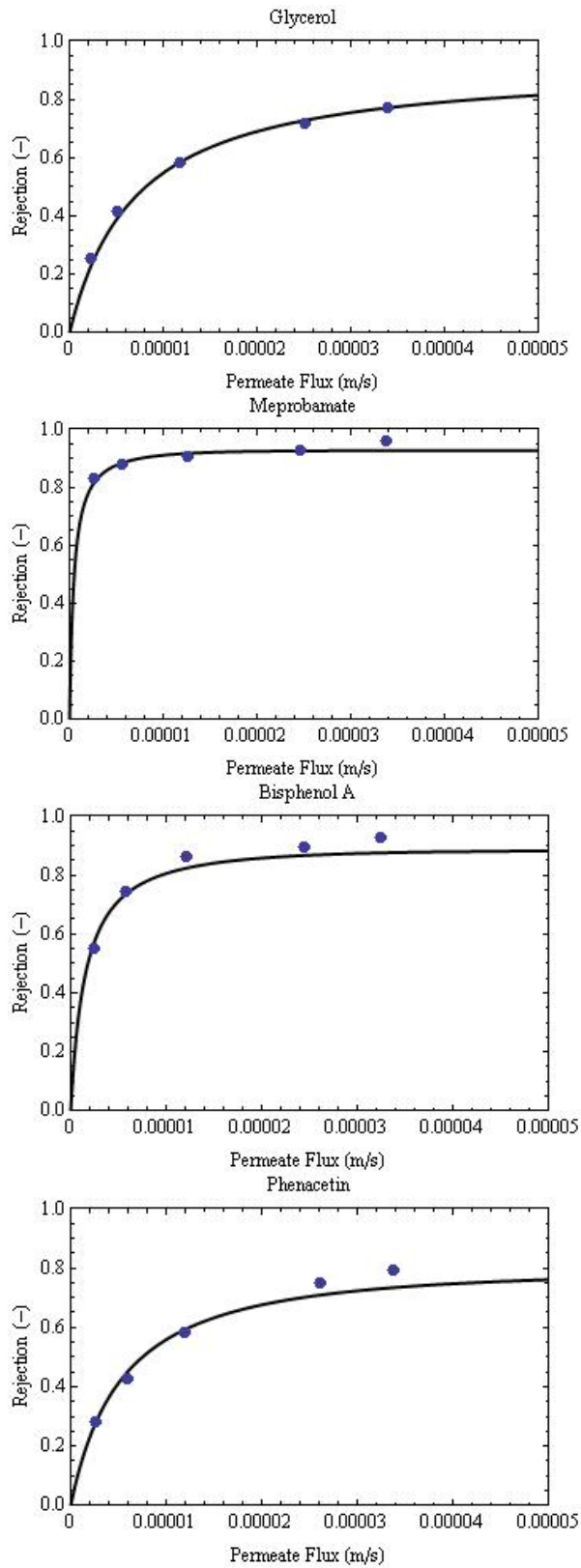


Figure 5.32. Sample hydrodynamic model fits of intrinsic rejection versus permeate flux data.

The resulting membrane pore radii from this process are presented in Figure 5.33 (left). As can be observed from Figure 5.33, the pore radius generally increased with increasing molecular size, although there are obvious outliers. On closer inspection, many of the outliers included compounds exhibiting solute–membrane interactions. Many of these outliers are aromatically based compounds with phenolic functional groups, including 1-naphthalenemethanol, resorcinol, acetaminophen, and isobutylparaben. Past research has demonstrated that these compounds interact with membrane materials and that rejection is not only a function of size. Therefore, the hydrodynamic model might not be appropriate for these compounds. Removing the outlier compounds resulted in a significant correlation between Stokes radius and pore radius (Figure 5.33). This finding indicates that, for the NF membrane evaluated, there is a distribution of pores and that the hydrodynamic approach using one pore radius will result in a poor fit of rejection for compounds with a large distribution of molecular size. The pore size distribution approach is evaluated further in the phenomenological modeling section.

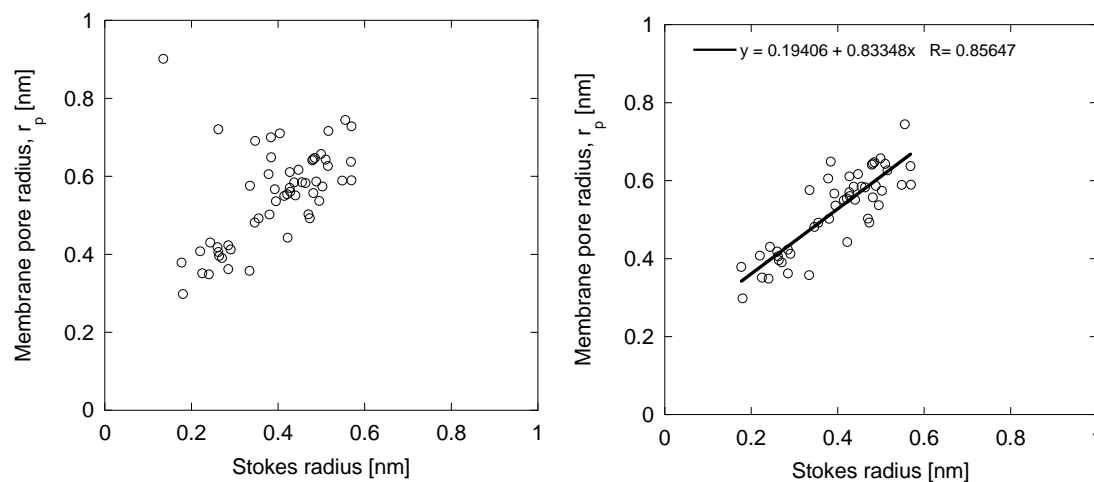


Figure 5.33. NF-270 membrane pore size determination using all nonionic organic solutes.

The hydrodynamic model using the Peclet number with the thickness-to-porosity ratio [δ/A_k , Equation 5.8] was also investigated. Using the Peclet number presented in Equation 5.7 resulted in a one-fitting-parameter model (λ), which did not always adequately describe the rejection versus permeate flux curve for each compound (Figure 5.34). The inclusion of δ/A_k improved model fits significantly (examples given in Figures 5.32 and 5.34); however, it resulted in an additional term that needs to be predetermined to predict the rejection of a “new” compound. Bowen and Mohammad (1998) demonstrated by using four nonionic sugar compounds that δ/A_k decreased with increasing molecular size as smaller molecules can take a more tortuous path through the membrane. An analysis of δ/A_k values obtained for all nonionic compounds did not support this finding, as δ/A_k did not correlate with the Stokes radius (Figure 5.35).

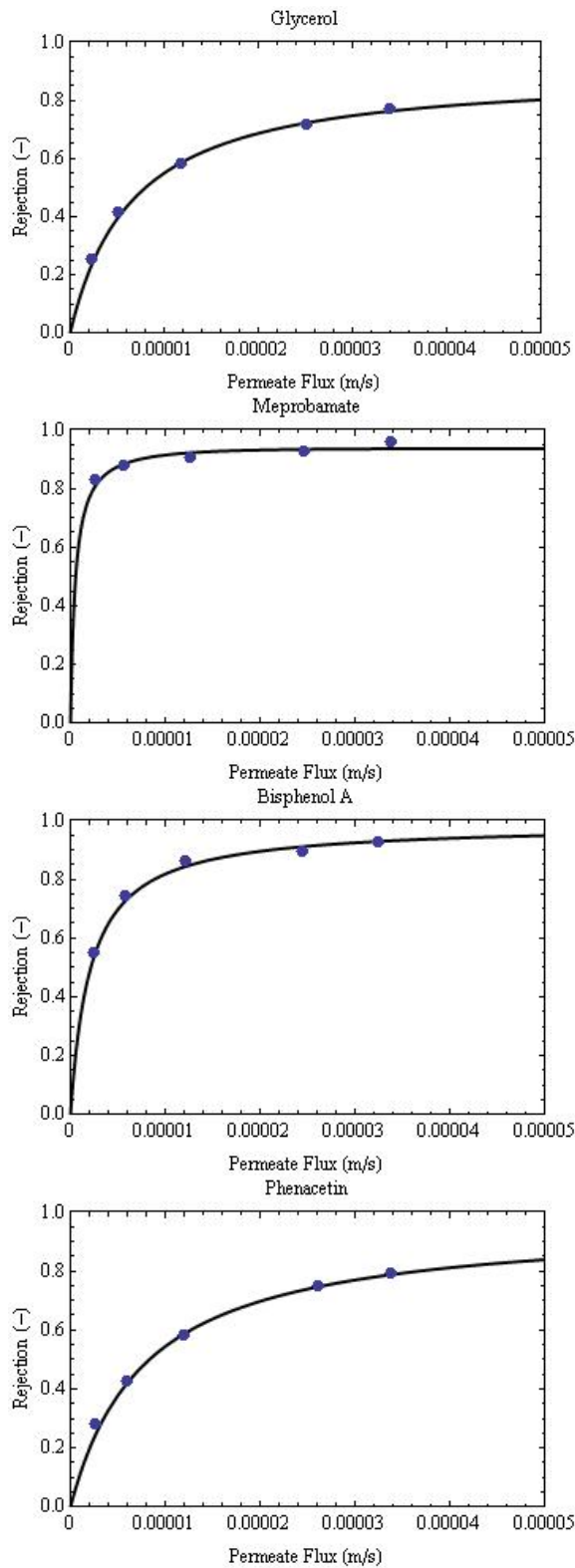


Figure 5.34. Sample hydrodynamic model fits of intrinsic rejection when incorporating δ/A_k into the Peclet number.

The advantage of the hydrodynamic model is that it incorporates a membrane pore radius and describes hindered transport through a theoretical pore structure. Theoretically, the pore radius of a membrane could be easily characterized by conducting rejection experiments with a few sugar and alcohol compounds. Describing the rejection of any nonionic solute would then require only a determination of a solute's Stokes radius. This work demonstrates, however, that the characterized membrane pore radius increases with increasing size of the characterization compound employed. This finding indicates that there is a significant pore size distribution and that using an average pore size results in poor model predictions for nonionic solutes. In addition, the model accounts only for steric effects on rejection and therefore cannot adequately describe the rejection of compounds that associate with the membrane.

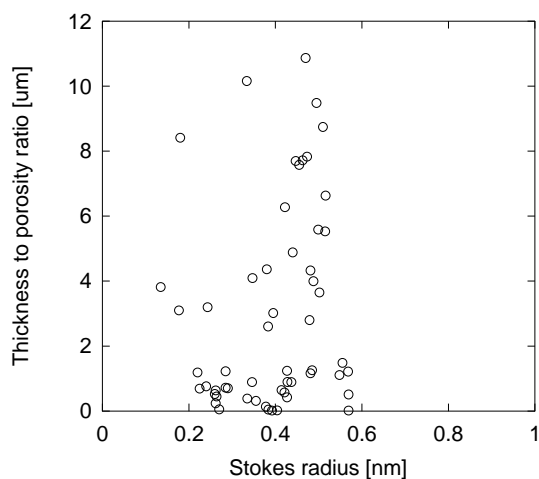


Figure 5.35. Thickness-to-porosity ratio (δ/A_k) versus Stokes radius for all nonionic solutes evaluated.

5.5 Solution–Diffusion Model

The theory of the solution–diffusion model is explained with further detail in Section 2.6.1. For a thorough review of the theoretical background of this model, the reader may refer to Wijmans and Baker (1995). To summarize, the major assumption implicit in this model is that the polymer matrix of the membrane is a solvent into which a molecule may partition. Once a compound has partitioned into this “solvent,” it will diffuse across the membrane, following a concentration gradient, according to Fick’s law. As a result, this model cannot be used to model compound behavior for membranes that contain pores within their structure. Pores provide an avenue for molecules to move across a membrane without partitioning into its polymer matrix, avoiding the type of behavior that the solution–diffusion model attempts to describe. ESPA2, an LPRO membrane, is thought to be relatively free of pores although the NF-270 membrane as an NF membrane likely contains a network of pores. Again, it is important that the polymer structure of membranes is not thoroughly understood and that the presence or absence of pores therefore is largely based on conjecture. What is clear is that the quantity of pores must be greater for an NF-270 membrane than for an ESPA2 membrane. Therefore, the solution–diffusion model is more appropriately applied to the ESPA2 membrane than to the NF-270 membrane.

5.5.1 Bench-Scale Modeling

We examine the solution–diffusion model first by using the bench-scale ESPA2 experimental data and the simplified model equation to develop a list of solute MTCs for all of the compounds. Equation 5.10 represents the simplified equation used for the solution–diffusion model and was adopted from Zhou’s doctoral dissertation focusing on modeling mass transfer through diffusion-controlled membranes (Zhou, 2004).

$$C_p = \frac{K_s C_f}{k_w (\Delta P - \Delta \pi) \left(\frac{2 - 2R}{2 - R} \right) + K_s} \quad (5.10)$$

The terms in Equation 5.10 are as follows:

C_p = Permeate concentration

C_f = Feed concentration

K_w = Water’s MTC

$(\Delta P - \Delta \pi)$ = Pressure drop across membrane

K_s = Solute MTC

R = Recovery

The first term in the denominator of this equation describes the permeate flux using k_w , $(\Delta P - \Delta \pi)$, and $\left(\frac{2 - 2R}{2 - R} \right)$, which is a manipulation empirically developed in studies cited in Zhou’s dissertation to incorporate the effects of recovery. For bench-scale modeling, this entire term is replaced by J_w , the permeate flux, which is a set-point that is recorded with each sample taken in the bench-scale experiments performed under this study. This simplification can be done because, by definition, $k_w (\Delta P - \Delta \pi)$ is equal to J_w and because the manipulation for recovery is negligible under bench-scale experimental conditions. The highest recovery value observed was 0.993 at 30 gfd.

Another alteration made to Equation 5.10 is the substitution of C_m for C_f . C_m is the membrane wall concentration determined with the film theory diffusion model, described in Section 2.6.1. This model takes into account hydrodynamic conditions and their effects on concentration polarization. The membrane wall concentration is more appropriate for the solution–diffusion model because it is the concentration that is actually “experienced” by the membrane at the feed water–membrane interface. With these alterations, the working equation simplifies to Equation 5.11.

$$C_p = \frac{K_s C_m}{J_w + K_s} \quad (5.11)$$

Manipulating this equation allowed K_s to be isolated from the other variables in Equation 5.12, which were known for each given data point.

$$K_s = \frac{J_w C_p}{C_M - C_p} \quad (5.12)$$

This new equation was incorporated into a program developed by using MATLAB technical computing software to calculate K_s values. With a total of 112 compounds, it was desirable to have a somewhat automated method of calculating the K_s values. For this, an Excel workbook was created that incorporated all of the necessary data to calculate K_s values for each compound. Each of the 112 compounds had its own worksheet within the workbook with columns for J_w , C_p , C_m , and rejection. The results for glutamic acid from this workbook are shown as an example in Table 5.12.

Table 5.12. Sample Data Table Used for Solution–Diffusion Modeling Program^a

J_w (gfd)	C_p (mg/L)	C_m (ng/L)	Intrinsic Rejection
2.92	1.4	16.97	0.915
2.92	1.3	16.98	0.922
7.63	1.2	17.30	0.928
7.63	1.1	17.30	0.934
10.53	0.8	18.69	0.957
10.53	0.7	18.71	0.965
10.53	0.3	18.15	0.984
10.53	0.4	18.14	0.980
19.08	0.6	19.64	0.970
19.08	0.6	19.65	0.971
27.72	0.4	21.58	0.982
27.72	0.5	21.56	0.978

^aData are from bench-scale experiments with glutamic acid and ESPA2 membranes.

In Table 5.12, each row represents a single data point from an experiment with glutamic acid and the ESPA2 membrane. The MATLAB program calculated a unique K_s value for each experimental data point and then averaged these values together to come up with a single MTC for each compound. The list of these MTCs is provided in Table 5.13

Table 5.13. Solution–Diffusion Model MTCs for All Compounds Processed with ESPA2 Membrane

Compound	K_s (m/s)	Compound	K_s (m/s)	Compound	K_s (m/s)	Compound	K_s (m/s)
Acetaminophen	1.74	Diclofenac	0.28	Methylparaben	5.85	Ranitidine	0.02
Acetic acid	2.07	Diethylphthalate	0.35	Methyl salicylate	1.85	Resorcinol	0.61
Alanine	3.57	Diethylstilbestrol	0.22	MTBE	0.06	Salbutamol	4.50
Amitriptyline	0.05	1,4-Dihydroxy-benzoic acid	1.13	Metoprolol	0.86	Salicylic acid	1.57
Arginine	0.61	Dilantin	0.73	1-Naphthalenemethanol	0.21	Serine	0.75
Atenolol	5.10	Diltiazem	0.07	Naproxen	0.42	Sucralose	1.20
Atrazine	0.54	Diphenhydramine	0.10	2-Naphthol	0.23	Sucrose	0.32
Baclofen	0.99	Enalapril maleate	0.00	<i>N</i> -Nitrosodibutylamine	0.40	Sulfacetamide	0.91
Benzoic acid	1.70	Ethanol	42.53	<i>N</i> -Nitrosodiethylamine	1.34	Sulfamethoxazole	0.78
Benzophenone	0.24	Fenofibrate	0.00	NDMA	15.14	Sulfadimethoxine	0.86
Benzyl acetate	0.48	Fluconazole	0.29	<i>N</i> -Nitrosodiphenylamine	0.15	Sulfadoxin	0.24
Benzyl alcohol	1.57	Fluoxetine	0.04	<i>N</i> -Nitrosodipropylamine	1.03	Sulfamerazine	1.09
Bisphenol A	0.77	2-Fluorophenol	2.89	NMEA	5.94	Sulfasalazine	0.15
1,4-Butanediol	1.82	Furosemide	0.62	<i>N</i> -Nitrosomorpholine	2.08	Tamoxifen	0.00
Butylparaben	0.24	Gemfibrozil	0.17	<i>N</i> -Nitrosopiperidine	1.48	TCCP	0.48
Caffeine	1.33	Glucose	0.38	NPYR	2.56	TCEP	0.85
Captopril	2.00	Glutamic acid	0.74	4- <i>n</i> -Nonylphenol	0.28	TDCPP	0.21
Carbamazepine	0.75	Glycerin	2.46	Norfluoxetine	0.04	Thiabendazole	0.57
Chloretracycline	1.36	Guanidine	3.66	Oxybenzone	0.27	Trazodone	1.33
Cimetidine	1.67	Ibuprofen	0.68	Pentoxifylline	0.94	Trichloroacetic acid	0.27
Ciprofloxacin	0.91	Isopropanol	1.72	Phenacetine	0.25	Triclocarban	0.11
Clofibric acid	0.81	Ketoconazole	1.03	Phenylalanine	3.66	Triclosan	0.30
Cysteine	0.30	Lysine	3.50	2-Phenylphenol	1.18	Triethylene glycol	1.12
DEET	0.70	Maleic acid	0.00	Primidone	1.21	Trimethoprim	1.65
Dibromoacetic acid	0.25	Methotrexate	0.56	Propylparaben	0.90	Tyrosine	1.44
Dichloroacetic acid	0.27			Propyphenazone	0.41	Uracil	3.30
2,4-Dichlorophenol	0.89			Pseudoephedrine	1.10	Urea	42.93
Desloratadine	0.20					Warfarin	0.08

After calculating the MTC, the MATLAB program generated a figure of rejection versus permeate flux for each of the compounds. These figures display all of the data points used in the calculation as circles and the model curve, predicting rejection with the calculated MTCs, as dots connected with a dashed line. Figure 5.36 provides three examples of predicted rejection for the compounds alanine, 1,4-butanediol, and NDMA. These figures are included here to demonstrate the approach that was used by the research team to visually understand the accuracy of the model for each of the compounds and to group them accordingly.

As with the phenomenological model, the degree to which the solution–diffusion model could estimate rejection varied by compound. Solutes that expressed flat or declining rejection-versus-flux curves were inaccurately modeled with the solution–diffusion method. Furthermore, many of the compound MTCs summarized in Table 5.13 were calculated to be near 0 (e.g., amitriptyline and triclocarban). Very low MTCs result when a compound is efficiently rejected by the ESPA2 membrane. With a cluster of MTCs that are approximately 0, correlations between quantitative molecular parameters and MTCs lose resolution. As a result, the approach taken to correlate descriptors with modeled MTC values was performed in groups.

By sorting through the model plots and visually examining each of figures (examples shown in Figure 5.36), it was possible to qualitatively group the compounds into categories according to the model’s accuracy. Categories for “modelability” of high, medium, and low were created for compounds whose models fit data accurately, moderately, and poorly, respectively. These groups served two purposes. One is to eliminate inaccurate MTCs from molecular descriptor correlation exercises. Second, it may be possible to determine if there are common descriptors among the compounds of each group. This understanding could provide a method of predicting the applicability of the solution–diffusion model for a given molecule.

Table 5.14 lists the compounds that were deemed to have high modelability with the solution–diffusion method. Next to the names of the compounds are several important molecular descriptors. There is a broad range of values for molecular weight and $\text{Log } K_{ow}$, and all classes are represented in this list. It seems that the most consistent trend is that, with only three exceptions, all of the compounds have “normal” interactions with the membrane. This finding demonstrates the shortcoming of the solution–diffusion model. As stated before, this model is developed to describe diffusion of a compound through a medium. If there are interactions (either repellent or attractive) between the molecule and the polymer matrix, then the compound is not able to freely dissolve and therefore the transport phenomenon pertinent to the compound–membrane couple is more complex than described by Fickian diffusion.

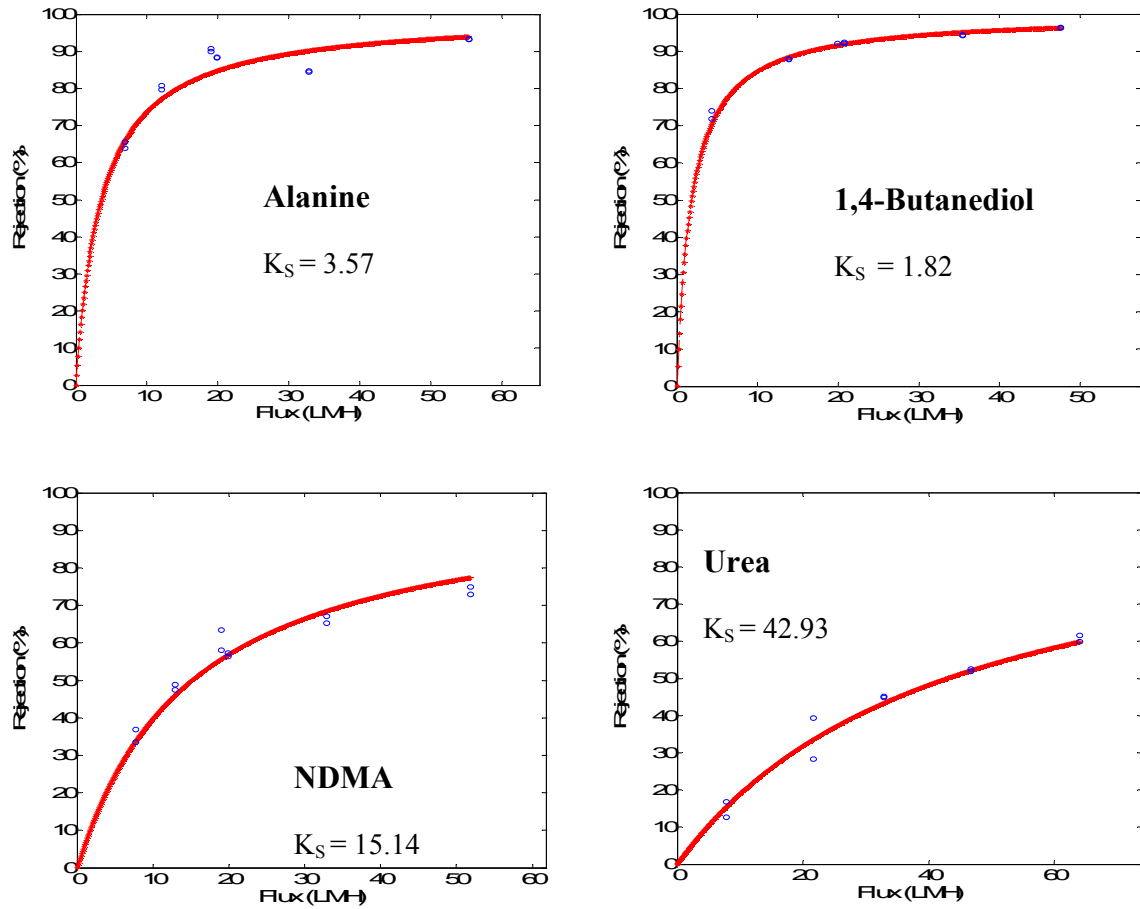


Figure 5.36. Plot produced by the MATLAB model for solution-diffusion, showing rejection versus flux in LMH for alanine, 1,4-butanediol, NDMA, and urea.

Table 5.14. List of Compounds that Demonstrate High “Modelability” with Solution–Diffusion Method

Compound Name	Class	Level of Interaction	Mol Wt (Da)	Log K_{ow}
1,4-Butanediol	HN	Normal	90.12	-1.02
Amitriptyline	HCP	Normal	277.41	1.57
Arginine	HCNP	Normal	174.2	-5.29
Baclofen	HCNP	Normal	213.67	-0.94
Benzyl alcohol	HN	Extreme	108.1	1.03
Butylparaben	HoN	Normal	194.23	3.46
Cysteine	HCNP	Normal	121.2	-2.27
Diethylphthalate	HHoN	Normal	222.2	2.7
Enalapril maleate	HCN	Normal	376.46	0.08
Ethanol	HN	Normal	46.1	-0.19
Fenofibrate	HoN	Normal	360.8	4.8
Fluoxetine	HoN	Normal	309.3	1.03
Glucose	HN	Normal	180.2	-3.17
Glycerin	HN	Normal	92.1	-2.32
Lysine	HCNP	Normal	146.2	-4.53
Maleic acid	HCN	Normal	116.07	-4.49
MTBE	HN	Normal	88.2	1.15
NDMA	HN	Normal	74.1	-0.64
Norfluoxetine	HCP	Normal	295.3	1.58
Pentoxifylline	HN	Normal	278.3	0.32
Phenacetine	HN	Normal	179.2	1.63
Ranitidine	HCP	Normal	314.4	-1.09
Resorcinol	HN	Moderate	110.1	0.76
Tamoxifen	HCP	Normal	371.52	5.33
Triethylene glycol	HN	Normal	150.2	-1.87
Uracil	HN	Moderate	112.1	-0.71
Urea	HN	Normal	60.1	1.69
Warfarin	HHoN	Normal	308.34	1.91

5.5.2 Correlating Mass Transfer Coefficients with Molecular Descriptors

In an attempt to create correlations between molecular descriptors and MTCs, a number of categories had to be considered. First, the category of “modelability” was used to eliminate compounds that could not be fit with the solution–diffusion equation. This group includes compounds that had declining and straight rejection-versus-flux curves. Using solute MTCs that did not effectively describe the rejection curves would only degrade correlations; therefore, these solutes were not included in the correlation exercises. By using the remaining compounds, different categories were included and excluded from correlations in an attempt to find strong correlations with a single descriptor. Examining only compounds that fit into a certain category is a process that would mimic the modeling of an untested compound with a decision tree. If one knows certain properties, including charge, Log K_{ow} , and size-related descriptors, a compound can be included in an appropriate model to determine its MTC.

As described in Section 5.3, which discusses molecular descriptor correlations with the phenomenological model variables, it is most useful to compare molecules within the same class as they are likely subject to the same rejection mechanisms. First, all neutral compounds that did not exhibit low “modelability” were examined as a group. This group includes HN, HHoN, and HoN compounds. The strongest correlation with a single parameter for neutral compounds was found to be the Wilke–Chang diffusion coefficient with an R^2 value of 0.60 (Figure 5.37). It is not surprising that the best correlation for MTC was with a coefficient developed specifically to model diffusion. However, the fact that even this coefficient correlated rather poorly with MTCs suggests that mechanisms other than diffusion are likely involved in transmembrane transport. When the same correlation was examined for the individual, neutral classes alone (i.e., HN, HoN, and HHoN) and for charged and negative compounds, the R^2 value decreased, indicating a weakening of the correlation.

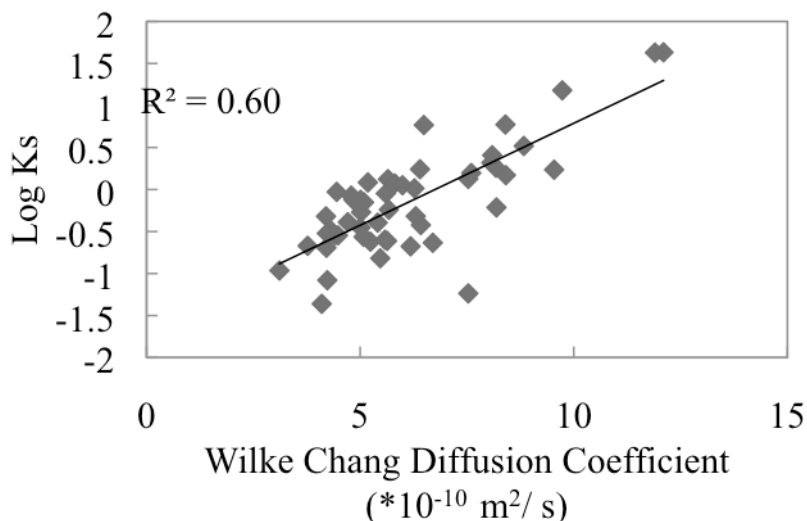


Figure 5.37. Correlation between Wilke–Chang diffusion coefficient and solution–diffusion MTCs (K_s) for neutral compounds.

The second best R^2 value to come from the modeling efforts was for a correlation with the Stokes radius and the MTC with an R^2 value of 0.50 (Figure 5.38). Diffusion is largely related to molecule size, so again the relative strength of this correlation, compared to other descriptors, is logical.

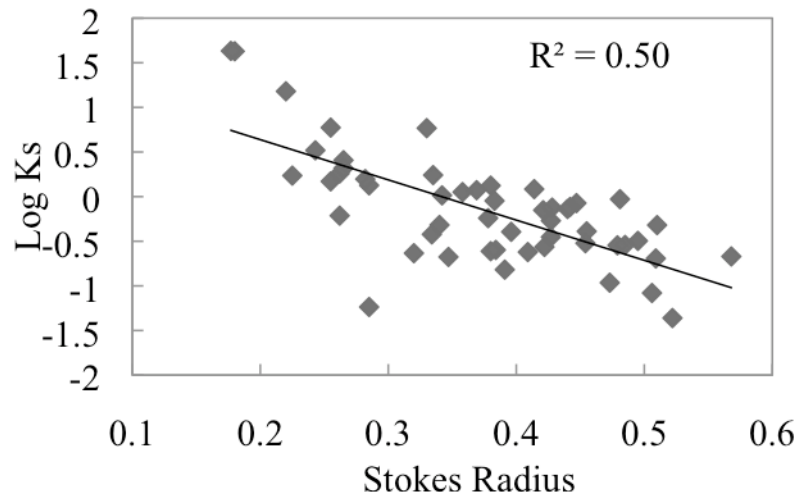


Figure 5.38. Correlation between Stokes radius (nm) and solution–diffusion MTCs (K_s) for neutral compounds.

5.5.3 Conclusions

Considering the theoretical concept of the solution–diffusion model, this model shouldn't be used to describe solute transport in NF and LPRO membranes for two main reasons. First, the fact that many NF membranes are thought to contain a network of pores, through which molecules can pass, undermines the concept that they dissolve into the membrane and diffuse across. Second, the solution–diffusion model does not take into account the possibility of membrane–solute interactions that alter the rate of diffusion. In essence, findings of this study suggest that the solution–diffusion model is too simple to incorporate the complex nature of membrane behavior with organic compounds. Furthermore, the model creates curves similar to those of the phenomenological model but has only one fitting parameter, although the phenomenological model has two. Stronger correlations were found with molecular descriptors for the phenomenological fitting parameters than for the solution–diffusion MTCs. For these reasons, the phenomenological model is deemed to be a superior method of modeling the rejection-versus-flux curves of organic compounds in NF membrane applications. Thus, the solution–diffusion model was not applied to model pilot- and full-scale systems used in this study.

5.6 Empirical Models—Rejection Diagram

In this section, the rejection diagram approach developed by Bellona et al. (2004) was investigated by utilizing the NF-270 membrane bench-scale rejection database. The model was updated by employing molecular descriptors that are relatively simple to calculate and by utilizing the hydrodynamic model to optimize the rejection ranges. The updated rejection diagram was also applied to the ESPA2 membrane bench-scale rejection database to evaluate applications to different membranes.

5.6.1 Optimization using the NF-270 Rejection Database

A decision diagram approach for predicting rejection developed by Bellona et al. (2004) was evaluated as a method to predict NF-270 membrane bench-scale rejection data qualitatively. A slightly modified version of the diagram presented in Section 2.6.7 was utilized with key

molecular descriptors and membrane properties to calculate rejection. A summary of predicted versus experimental data derived in this study is provided in Figure 5.39. Because of the nature of the approach, only ranges of rejection can be calculated for a given solute, which are represented by the error bars in Figure 5.39. More than half of the compounds in the database had experimental rejection values outside the range predicted by the diagram approach; therefore, the rejection diagram was updated to provide better model fits. Particularly, the diagram was improved by adding molecular descriptors more readily available than the Taft number, as it can be very difficult to obtain these values. In addition, the predicted ranges can be narrowed to better fit the data.

5.6.1.1 Updated Rejection Diagram

Considering the findings of this study, an attempt was made to improve the precision of the rejection diagram. Compounds with electrostatic interactions with the membrane are highly rejected; however, on the basis of observations from bench-scale experiments and previous research by Verliefe et al. (2007), positively charged compounds exhibit lower rejection than do negatively charged compounds; therefore, the rejection of charged solutes was split into negatively charged and positively charged. Negatively charged compounds were listed as exhibiting greater than 90% rejection, and positively charged compounds were listed as exhibiting greater than 75% rejection.

Compounds with adsorptive effects, decreasing rejection over time, exhibit two main properties: hydrophobic ($\text{Log } K_{ow} > 2$) or a proton donating group attached (-OH or $-\text{NH}_n$) to a benzene ring. The rejection diagram was updated not to include the Taft number based on the difficulty of calculating this descriptor. Considering the findings of this study, it was assumed if a compound has a proton donating group attached to a benzene ring or a $\text{Log } K_{ow}$ greater than 2, the compound will adsorb to the membrane. A compound with a proton donating group not attached to benzene or a $\text{Log } K_{ow} < 2$ will not adsorb to the membrane. It should be noted that the hydrophobic cutoff was changed from $\text{Log } K_{ow}$ of 3 to $\text{Log } K_{ow}$ of 2 because the vast number of compounds observed to adsorb to the membrane exhibited $\text{Log } K_{ow}$ values between 2 and 3 as reported by Braeken et al. (2005). Compounds with a proton donating group, hydroxyl group, or amine group attached to a six-ring aromatic structure can adsorb to the membrane surface through hydrogen bonding as reported by Williams et al. (1999). Compounds with adsorptive effects have lower-than-expected rejection because of steric exclusion.

The steric exclusion mechanism is split into two different pathways: one for compounds with adsorptive effects and one for compounds that have no interactions with the membrane. On the basis of the bench-scale database, steric interactions have some effect on the rejection of compounds that adsorb. Rejection of compounds with adsorptive effects is difficult to predict; therefore, the rejection ranges are very broad depending on a compound's size. Compounds with r_s/r_p or molecular weight/MWCO ratios of less than 0.9 will be poorly removed, qualified as less than 30% rejected. Compounds with r_s/r_p or molecular weight/MWCO ratios between 0.9 and 1.0 will have moderate removal, specified as 30 to 70% rejected and compounds with r_s/r_p or molecular weight/MWCO ratios greater than 1.0 will be highly removed, representing rejection greater than 70%.

To determine the r_s/r_p ratios for compounds that do not interact with the membrane, the hydrodynamic model was used (Bowen et al., 2004). The hydrodynamic model predicts rejection based solely on solute size (Stokes radius) and the pore size of the membrane. Rejection predicted by the hydrodynamic model is presented as a function of r_s/r_p in

Figure 5.40. From the hydrodynamic model, compounds with r_s/r_p ratios greater than 0.75 will be highly rejected (greater than 80% rejection). Compounds with r_s/r_p ratios between 0.6 and 0.75 exhibit moderate rejection (30 to 80%). This category is difficult to narrow down because of the steepness of the hydrodynamic curve between r_s/r_p ratios of 0.6 and 0.75. Compounds with r_s/r_p ratios of less than 0.6 exhibit poor rejection (less than 30%). Figure 5.41 presents the updated rejection diagram.

In Figure 5.42, predicted rejections from the updated rejection diagram using all compounds are presented. Only 11% of the experimental compounds were predicted out of range with the updated rejection diagram. Charged compounds had a few outliers. Four negatively charged compounds were predicted out of range but only by a few percentage points: 90% predicted rejection compared to 87 and 88% experimental rejection. Only two positively charged compounds were overpredicted; metformin and trimethoprim exhibited 60% and 71% rejection, respectively. Metformin and trimethoprim did exhibit a decrease in rejection over time; initially, metformin exhibited 74% rejection but then decreased after 18 h to 60%, although trimethoprim exhibited only a 7% decrease in rejection after 18 h. The decrease in rejection could be due to a concentration layer buildup at the membrane surface, resulting in lower observed rejection because rejection takes into account only feed and permeate concentration (Verliefde et al., 2007).

Only 7 of the 67 neutral compounds were predicted out of range: triethylene glycol, Nitrosodipropylamine (NDPA), NMEA, triclosan, acetaminophen, 2-phenylphenol, and bromoform. Triethylene glycol, NMEA, and acetaminophen were predicted out of range by only a few percentage points: 3, 6, and 1%, respectively. Bromoform was predicted to be poorly removed, less than 30%; however, the data supported that it was rejected by 41%. 2-Phenylphenol exhibited only 24% rejection, where predicted rejection was between 30 and 70%. NDPA and triclosan were greatly overpredicted, by 15 and 35%, respectively. Both of these compounds exhibited adsorptive effects that seem to be independent of steric interactions.

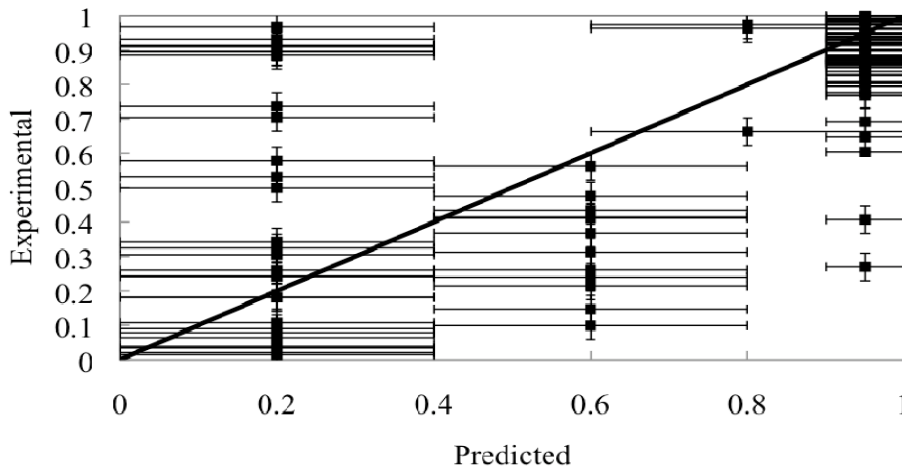


Figure 5.39. Experimental NF-270 rejection as a function of predicted rejection values based on the qualitative rejection diagram.

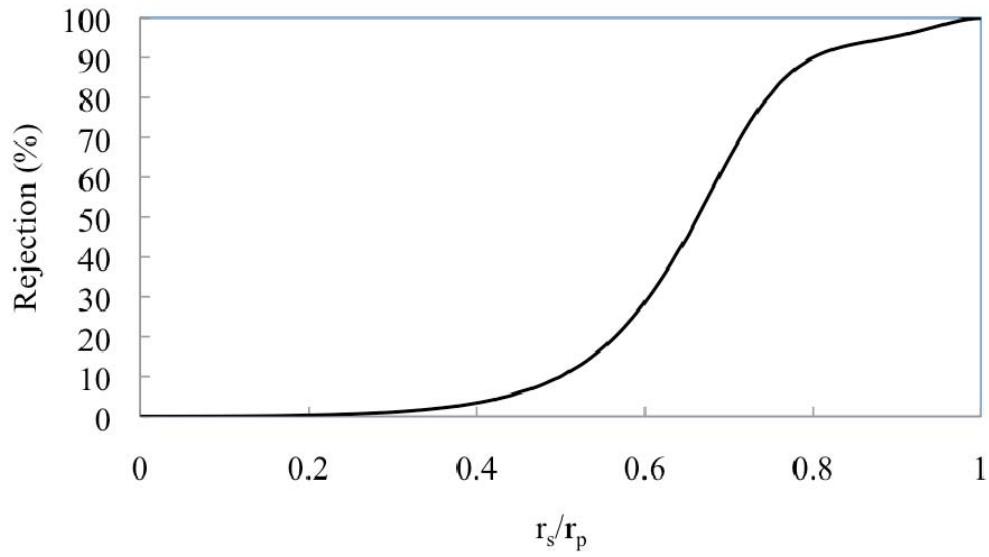


Figure 5.40. Experimental rejection data as a function of r_s/r_p compared to the hydrodynamic model.

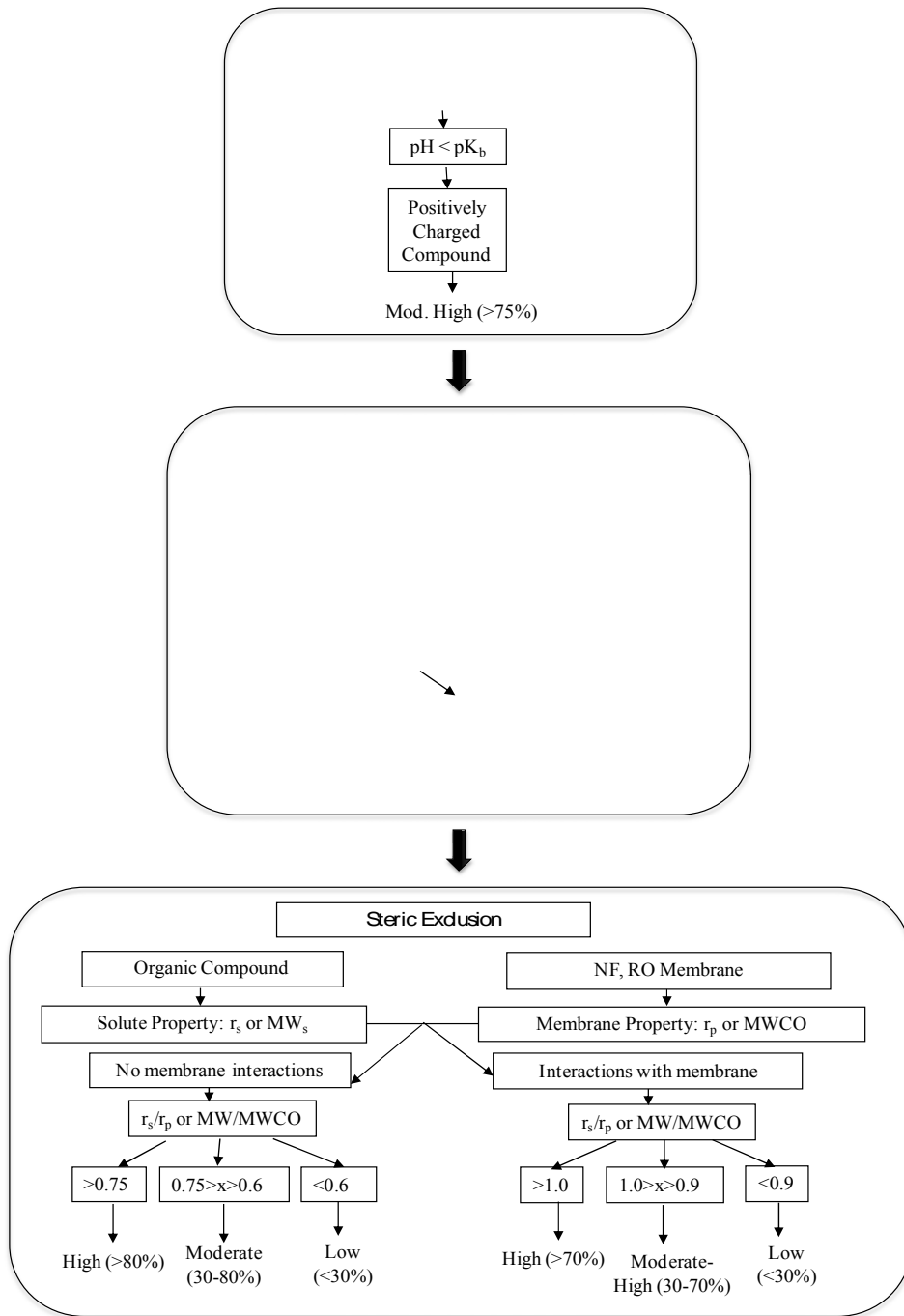


Figure 5.41. Modified solute rejection diagram.

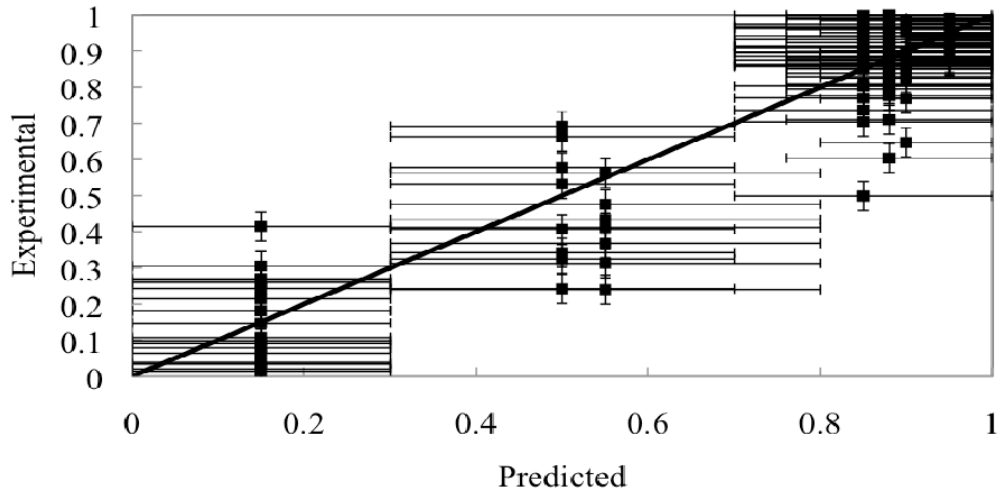


Figure 5.42. Experimental NF-270 membrane rejection as a function of rejection predicted by updated rejection diagram for compounds in Table 3.2.

5.6.2 Applying the Updated Rejection Diagram to ESPA2 Membrane Rejection Database

The updated rejection diagram was applied to all compounds (Table 3.2) in the ESPA2 membrane 12-gfd rejection database. The updated rejection diagram was able to successfully predict rejection for the ESPA2 membrane bench-scale data, and results are presented in Figure 5.43. Only 4 out of the 111 experimental compounds were predicted out of range with the updated rejection diagram. Ethanol, chloroform, and dichlorobromomethane were predicted out of range by only 5%. Isopropanol was underpredicted by 24%. This finding could be due to experimental error or due to isopropanol being close to the MWCO estimation.

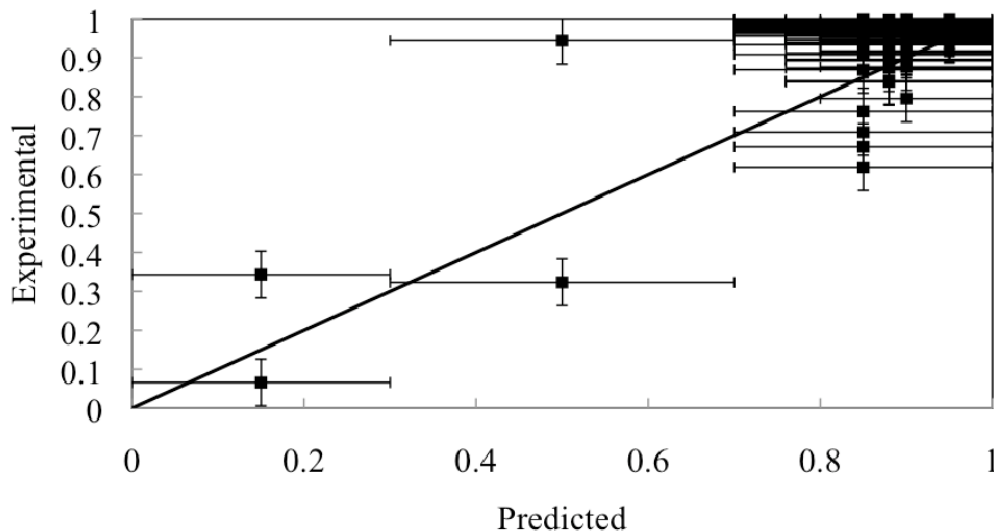


Figure 5.43. Experimental ESPA2 rejection compared to predicted rejection from updated rejection diagram.

Chapter 6

Validation of Rejection Models at Pilot Scale

6.1 Introduction

Although a significant amount of past work has been undertaken evaluating the rejection of organic solutes by various membranes at the bench scale, minimal work has been performed evaluating rejection at larger scales: specifically, on systems capable of achieving overall system recoveries of 60 to 85%. In addition, very little information exists on how bench-scale organic solute rejection trends relate to pilot- or full-scale trends and whether bench-scale rejection data can be used to model pilot- and full-scale rejection. The objective of this portion of the study was to compare the rejection of organic solutes at the bench and pilot scales with the ultimate goal of developing a modeling approach to describe rejection at the pilot and full scales. Different pilot-scale experiments using NF and RO membranes were conducted to support this task.

6.2 Pilot-Scale Rejection Experiments Using Nanofiltration Membranes and Rejection Modeling Using QSPR and Empirical Models

6.2.1 Comparing Bench- and Pilot-Scale Nanofiltration Testing

Pilot-scale experiments were conducted on a two-stage membrane unit employing 21 4040 spiral-wound NF-270 membranes treating microfiltered tertiary wastewater effluent provided by a full-scale water reclamation facility. The rejection data generated at pilot scale were used to evaluate models developed at bench scale including the QSPR models and the empirical rejection diagram.

For this comparison, the bench- and pilot-scale systems represent different configurations that are operated under different conditions. Bench-scale experimentation was conducted at a low feed flow rate (1.5 L/min) and very low recovery (1%), although pilot-scale testing was conducted at a high feed flow rate (83 L/min) and high recovery (85%). Bench-scale systems are flat-sheet systems with a small membrane area, whereas pilot-scale systems employed spiral-wound configurations with a large membrane area. To compare bench scale to pilot scale, rejection behavior of select solutes was first examined.

Bench-scale rejection data for caffeine and acetaminophen as a function of recovery and permeate flux are presented in Figure 6.1 for the NF-270 membrane. Small variations in recovery resulted in large changes in permeate flux rate at bench scale for caffeine and acetaminophen. As recovery changed between 0.1 and 1.4%, permeate flux increased from 5 to 60 gfd. Caffeine rejection stayed relatively constant (greater than 90%), whereas acetaminophen rejection increased from 40 to 70% over the permeate flux range. Observed rejection results for acetaminophen and caffeine as a function of recovery and permeate flux rate at pilot scale for the NF-270 membrane are presented in Figure 6.2. Differing from bench-scale behavior, larger variations of recovery resulted in small variations in permeate flux at pilot scale. At pilot scale, recovery increased from 60 to 85%, whereas permeate flux increased only from 9 to 13 gfd. Rejection

of caffeine and acetaminophen stayed relatively constant as recovery and permeate flux rate varied.

The bench- and pilot-scale rejection data for the NF-270 membrane are compared in Figure 6.3. Most compounds had equal or higher rejection at pilot scale than at bench scale. This finding could be due to potential fouling that occurred, given that the pilot-scale feed water was wastewater effluent. Comerton et al. (2008) also observed higher organic solute rejection with fouled membranes than with virgin membranes. At pilot scale, negatively charged compounds were greater than 90% removed and positively charged compounds were greater than 84% removed. This behavior was reported by Verliefde et al. (2007) and Bellona et al. (2008). Bench-scale data for ionic compounds were comparable; however, trimethoprim was rejected by only 71% at bench scale. Most neutral compounds exhibited higher rejection at pilot scale than at bench scale and were greater than 80% removed, except for propylparaben, bisphenol A, and triclosan. All three compounds exhibited adsorptive effects at bench scale.

Triclocarban, triclosan, and propylparaben also exhibited adsorptive effects at pilot scale for the NF-270 membrane. Initially high rejection (90%) was observed for triclocarban, whereas the compound adsorbed to the membrane, presented in Figure 6.4. As time progressed and as the membrane became saturated, permeation through the membrane occurred and rejection decreased drastically, resulting in only 44% rejection after 600 h. Triclosan and propylparaben exhibited the same behavior as triclocarban, with a 50% and 30% decrease after 600 h, respectively.

The bench- and pilot-scale rejection data are compared in Figure 6.5 for the ESPA2 membrane. Rejection of most compounds was similar except for acetaminophen, caffeine, propylparaben, and urea. On the basis of the size of acetaminophen (molecular weight of 151 g/mol), caffeine (molecular weight of 194 g/mol), and propylparaben (molecular weight of 180 g/mol) and the MWCO of the ESPA2 membrane (about 100 Da), acetaminophen, caffeine, and propylparaben should exhibit rejection greater than 90% based on steric exclusion (Agenson et al., 2003; Bellona et al., 2004; Kimura et al., 2004; Van der Bruggen et al., 1999). This unexpected observation at pilot scale could be due to experimental errors.

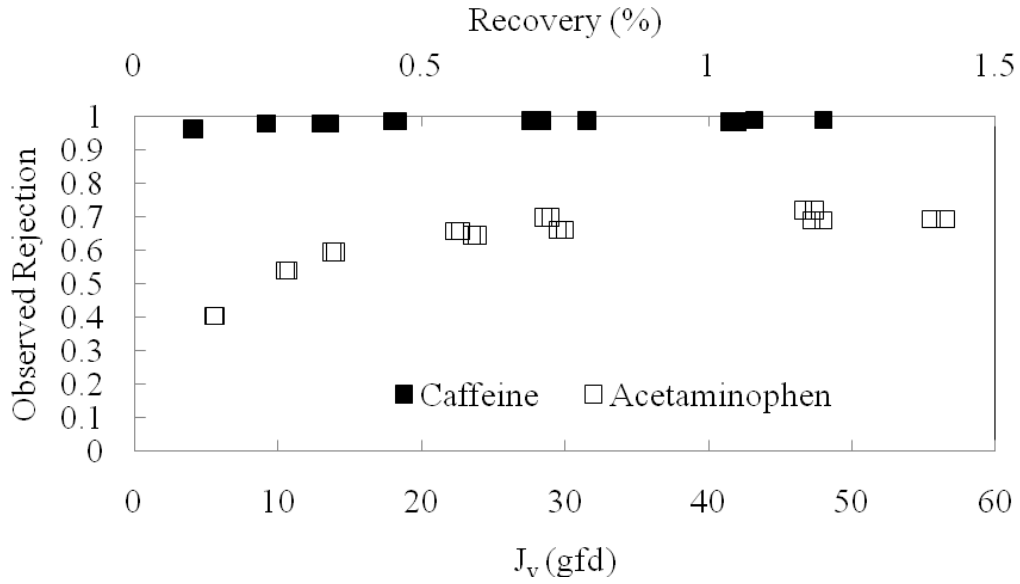


Figure 6.1. Bench-scale rejection for caffeine and acetaminophen as a function of permeate flux (primary x axis) and recovery (secondary x axis) for NF-270 membrane.

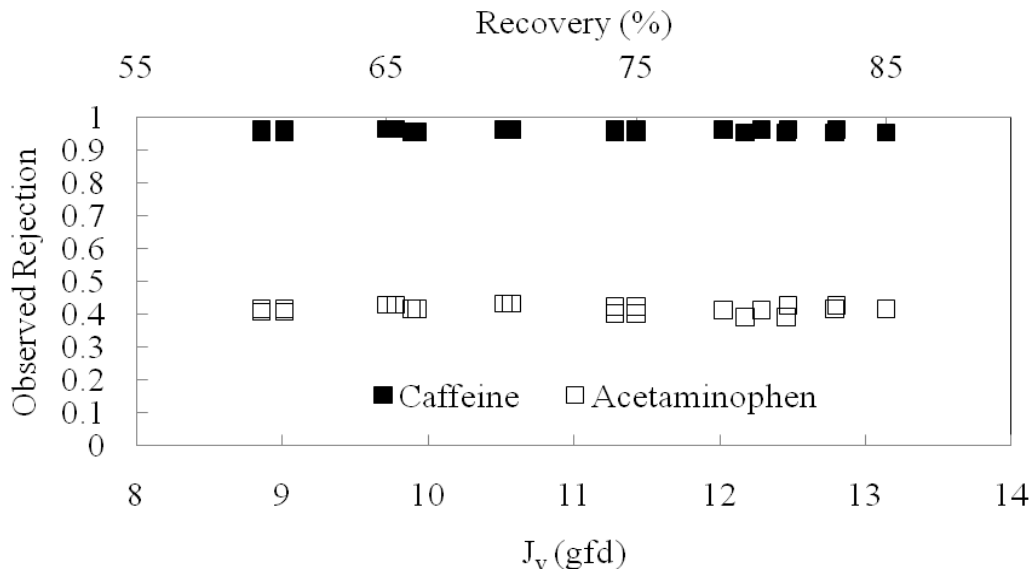


Figure 6.2. Pilot-scale rejection for caffeine and acetaminophen as a function of recovery (primary x axis) and permeate flux (secondary x axis) for NF-270 membrane.

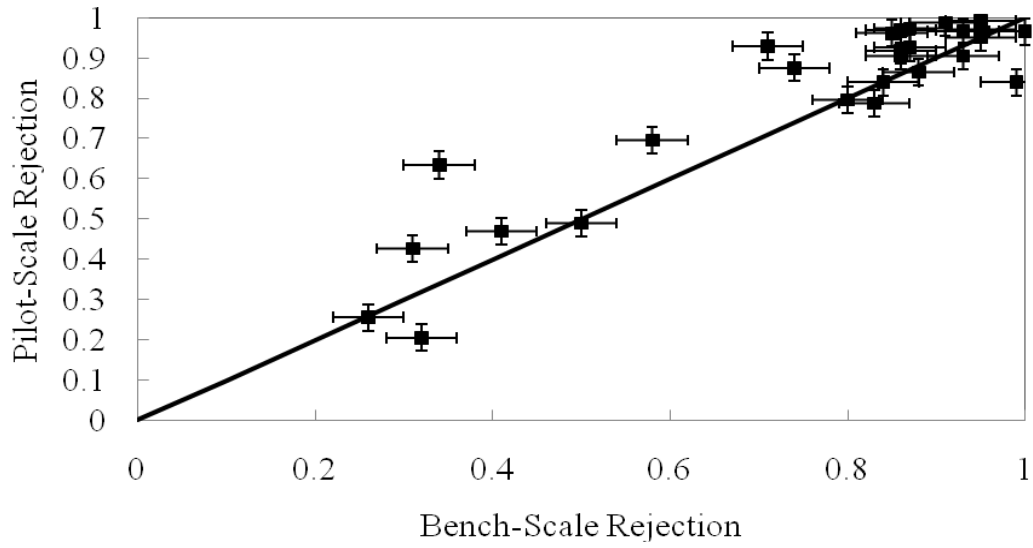


Figure 6.3. Pilot-scale rejection at 12 gfd compared to 12-gfd bench-scale rejection for NF-270 membrane.

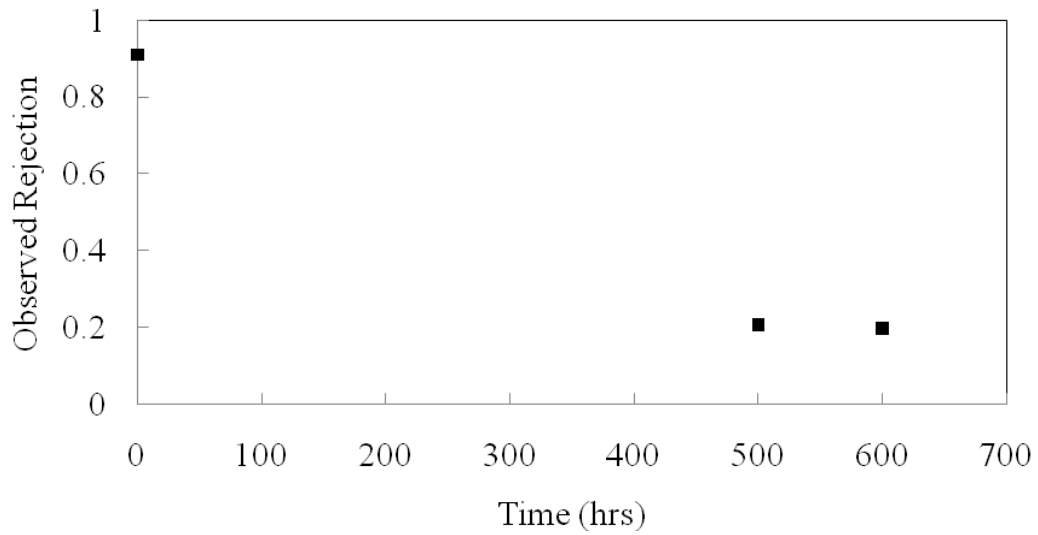


Figure 6.4. Observed rejection as function of time for triclorcarban at pilot scale for NF-270 membrane.

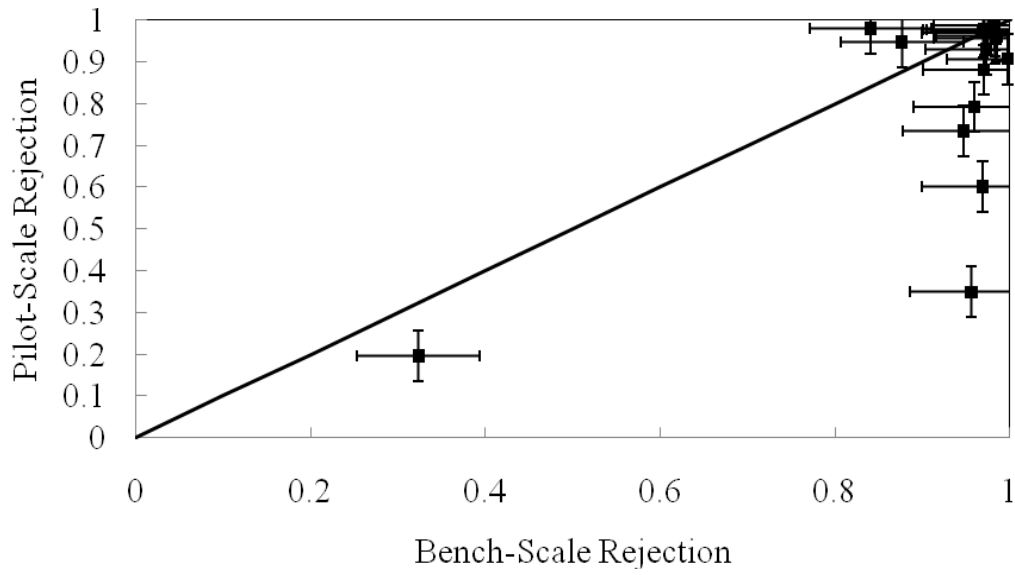


Figure 6.5. Pilot-scale rejection at 12 gfd compared to 12-gfd bench-scale rejection for ESPA2 membrane.

6.2.2 QSPR Model To Describe Pilot-Scale Nanofiltration Rejection Data

The QSPR model developed based upon the NF-270 membrane bench-scale data, restated in Equation 6.1, was applied to the NF-270 membrane pilot-scale data for neutral compounds. Rejection results of these experiments are presented in Figure 6.6.

$$Ref(\%) = 263.68Stokes + 0.4158FOSA + 7.694IP - 122.3 \quad (6.1)$$

This QSPR model yielded the highest R2 value and lowest RMSE value for the NF-270 membrane bench-scale database. During internal validation at bench scale, the QSPR model obtained the highest q2 value and was externally validated with bench-scale data yielding an R2 value of 0.75. Only three compounds were predicted within the confidence interval range seen in Table 6.1. Bisphenol A, carbamazepine, and dilantin rejection was underpredicted on the basis of relatively low FOSA values. Usually, compounds with low FOSA exhibit low rejection because of adsorptive effects; this was not the case for bisphenol A, carbamazepine, and dilantin. Propylparaben, triclosan, and triclocarban were overpredicted because these compounds exhibit extreme adsorptive effects, causing very low rejection (<50%). All of the compounds were predicted within 40%, with the majority predicted within 20%.

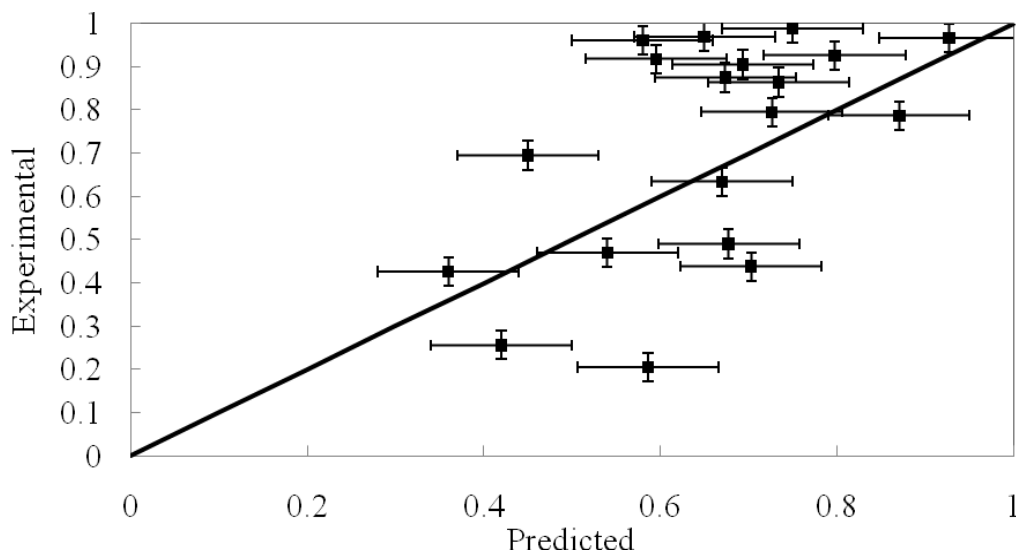


Figure 6.6. Developed QSPR (Stokes, FOSSA, IP) applied to neutral NF-270 membrane pilot-scale data.

Table 6.1. NF-270 Membrane Pilot-Scale Rejection, Predicted QSPR Rejection, and Percentage Difference from Experimental Pilot-Scale Data

Compound Name	Class	Pilot-Scale Avg 15-gfd Rejection	QSPR Predicted Rejection	Percentage Difference
Propylparaben	HHoN	0.21	0.59	38%
Atrazine	HHoN	0.80	0.73	-7%
Carbamazepine	HHoN	0.92	0.60	-32%
DEET	HHoN	0.86	0.73	-13%
Dilantin	HHoN	0.91	0.69	-21%
Thiabendazole	HHoN	0.70	0.45	-25%
Acetaminophen	HN	0.43	0.36	-7%
Caffeine	HN	0.96	0.58	-38%
Methylparaben	HN	0.26	0.42	16%
Phenacetine	HN	0.47	0.54	7%
Propylphenazone	HN	0.99	0.75	-24%
Primidone	HN	0.97	0.65	-32%
Meprobamate	HN	0.93	0.80	-13%
TCEP	HN	0.79	0.87	8%
Fluoxetine	HoN	0.97	0.93	-4%
Butylparaben	HoN	0.63	0.67	4%
Bisphenol A	HoN	0.88	0.67	-20%
Triclosan	HoN	0.49	0.68	19%
Triclocarban	HoN	0.44	0.70	26%

6.2.3 Application of the Empirical Rejection Diagram to the NF-270 Membrane

The rejection diagram developed with the NF-270 membrane bench-scale database provided an excellent fit for the pilot-scale data. The results after application of the rejection diagram to pilot-scale data are presented in Figure 6.7 and Table 6.2. The experimental and predicted rejections are listed in Table 6.2 with the respective rejection ranges and error percentages. Figure 6.7 presents the predicted rejection as it relates to the experimental rejection, with error bars representing the rejection range predicted. Overall, the rejection diagram was an excellent fit with only four compounds (TCEP, propylparaben, triclocarban, and triclosan) overpredicted. Propylparaben, triclocarban, and triclosan are very hydrophobic with Log K_{ow} values of 2.92, 5.75, and 5.17, respectively. These compounds had high initial rejection, triclocarban and triclosan experiencing greater than 90% rejection initially, and propylparaben experiencing greater than 50% rejection. After saturation of the membrane occurred, rejection of triclocarban and triclosan decreased to below 50% and rejection of propylparaben decreased to 21%. These compounds can be very difficult to predict because of the affinity for the membrane. Besides compounds with adsorptive properties, all other compounds were predicted within range. The model is simple to use and can predict rejection for most compounds, including ionic compounds.

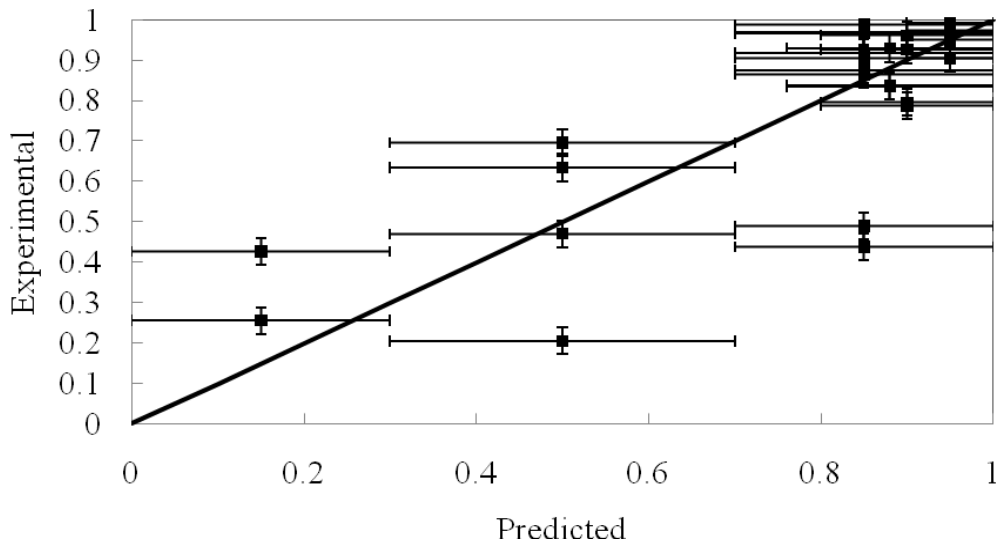


Figure 6.7. Rejection diagram applied to NF-270 membrane pilot-scale data.

Table 6.2. Pilot-Scale Rejection and Predicted Rejection from Rejection Diagram for Experimental NF-270 Pilot-Scale Data

Compound Name	Class	Pilot-Scale Avg 12-gfd Rejection	Rejection Diagram Predicted Rejection	Rejection Range (+/-)
Sulfamethoxazole	HCN	0.97	0.95	5%
Diclofenac	HCN	0.97	0.95	5%
Gemfibrozil	HCN	0.99	0.95	5%
Ibuprofen	HCN	0.97	0.95	5%
Ketoprofen	HCN	0.90	0.95	5%
Naproxen	HCN	0.95	0.95	5%
Atenolol	HCP	0.84	0.88	12%
Norfluoxetine	HCP	0.84	0.88	12%
Trimethoprim	HCP	0.93	0.88	12%
Propylparaben	HHoN	0.21	0.50	20%
Atrazine	HHoN	0.80	0.90	10%
Carbamazepine	HHoN	0.92	0.85	15%
DEET	HHoN	0.86	0.85	15%
Dilantin	HHoN	0.91	0.85	15%
Thiabendazole	HHoN	0.70	0.50	20%
Acetaminophen	HN	0.43	0.15	15%
Caffeine	HN	0.96	0.90	10%
Methylparaben	HN	0.26	0.15	15%
Phenacetine	HN	0.47	0.50	20%
Propylphenazone	HN	0.99	0.85	15%
Meprobamate	HN	0.93	0.90	10%
TCEP	HN	0.79	0.90	10%
Primidone	HN	0.97	0.85	15%
Butylparaben	HoN	0.63	0.50	20%
Fluoxetine	HoN	0.97	0.85	15%
Bisphenol A	HoN	0.88	0.85	15%

6.3 Pilot-Scale Rejection Experiments Using Nanofiltration Membranes and the Phenomenological Pilot-Scale Model

6.3.1 Introduction

A 16- to 28-gpm pilot-scale membrane system (two-stage system with 21 4040 membrane elements) was installed in a pilot laboratory at CSM to conduct controlled-rejection experiments. The pilot system was fed by using two 500-gal tanks and experiments were conducted in recycle mode where concentrate and permeate were returned to the feed water tank to extend the length of experiments. Additionally, the membrane system was also deployed at a water reclamation facility in California and was tested with microfiltered, tertiary-treated wastewater effluent (California Title 22). Two different but very similar NF membranes were tested: the NF membrane (Dow/Filmtec, termed NF-4040) was used for controlled pilot-scale experiments in the pilot laboratory and the NF-270 membrane (Dow/Filmtec) was used for pilot experiments at the water reclamation facility. Pilot experiments conducted in the laboratory were used to develop approaches for describing pilot-scale rejection data, whereas data generated at the water reclamation facility were used to validate the modeling approaches developed previously.

6.3.2 Model Theory

6.3.2.1 Differential Element Approach

Because pilot- and full-scale systems are operated at high recoveries and have large concentration gradients across a system, models developed for bench-scale systems, which are operated at extremely low recovery, are not directly applicable. To remedy this problem, the differential element approach (Sharma and Chellam, 2008) is a method that conceptually divides a membrane element or series of membrane elements into identical sub-elements that are treated as completely mixed reactors. Each sub-element is connected to its immediate neighbor by using appropriate flow and solute mass balances at steady state. The following equations are used for the differential element approach. The flow mass balance is given by

$$Q_f(j) = Q_f(1) - \sum_{k=1}^{j-1} Q_p(k) \quad (6.1)$$

where $Q_f(j)$ is the feed water flow rate of the current element, and $Q_f(1)$ and $Q_p(k)$ are the feed and permeate flow rate of the previously evaluated element. The solute mass balance is given by

$$C_f(j+1) = \frac{Q_f(j)C_f(j) - Q_p(j)C_p(j)}{Q_f(j+1)} \quad (6.2)$$

The permeate flow rate $Q_p(j)$ for each sub-element j can be calculated as

$$Q_p(j) = J_v(j) \frac{A}{n} = L_p [\Delta P - \pi(j)] \frac{A}{n} \quad (6.3)$$

where $J_v(j)$ is the local permeate flux for sub-element j , A is the active membrane area, n is the number of sub-elements, L_p is the membrane solvent permeability constant, ΔP is the hydraulic pressure across the membrane, and $\Delta\pi(j)$ is the osmotic pressure difference calculated on the basis of the Van't Hoff equation:

$$\Delta\pi(j) = 2RT[C_m(j) - C_p(j)] \quad (6.4)$$

or other empirical relationships between TDS and osmotic pressure. For experiments with extremely low feed concentrations, the effect of osmotic pressure on flux is expected to be small. The pressure drop is assumed to be linear across the membrane system, and the following equation can be used to calculate the driving force for permeate flow from each sub-element:

$$\Delta P(j) = \left((P(1) - (j - 0.5)) \frac{P(1) - P(j+1)}{n} \right) \quad (6.5)$$

The permeate $C_p(j)$ and feed concentrations for each sub-element can be related by using a one-dimensional film theory model as

$$\frac{C_p(j)}{C_f(j)} = \frac{\exp(J_v(j)/k(j))}{\frac{C_m(j) - C_p(j)}{C_p(j)} + \exp(J_v(j)/k(j))} \quad (6.6)$$

The expression

$$\frac{C_m(j) - C_p(j)}{C_p(j)} \quad (6.7)$$

can be calculated from membrane transport models including the solution–diffusion model, the hydrodynamic model, the ENP equation approach, and the phenomenological model. For these models, parameters related to the membrane and the solute are inputs and the differential element approach is used to model the concentration gradient through the system. For this study, the phenomenological model was used:

$$\frac{C_m - C_p}{C_p} = \sigma \frac{\left[1 - \exp\left(-\frac{1-\sigma}{P} J_v\right) \right]}{(1-\sigma)} \quad (6.8)$$

with the model parameters previously described. Once $C_p(j)$ for each sub-element is determined, the weighted average permeate concentration over the entire element can be calculated by using

$$C_p = \frac{\sum_{j=1}^n Q_p(j) C_p(j)}{\sum_{j=1}^n Q_p(j)} \quad (6.9)$$

6.3.2.2 Characterization of Hydrodynamic Conditions

In order to apply the differential element approach, a few requirements have to be fulfilled. First, the hydrodynamic conditions of the system need to be characterized, including an understanding of the cross-flow velocity across the system and the geometry of the feed-brine spacer and a way to calculate the MTC k in Equation 6.6. For this information, we followed the approach of Sharma and Chellam (2008), which was based on the approach of others working with large-scale membrane systems (Schock and Miquel, 1987; Geraldles and de Pinho, 2006). In order to calculate k , we used a commonly employed empirical mass transfer correlation presented as Equation 3.5 (see Chapter 3). To use the mass transfer correlation, the cross-flow velocity of element j is needed. It is calculated by

$$\frac{Q_f(j)}{A_c} \quad (6.10)$$

where $Q_f(j)$ is the feed flow rate of element j , and A_c is the channel area. The feed-brine channel and spacer of a membrane need to be characterized to calculate the hydraulic diameter (d_c) and the channel area (A_c). The hydraulic diameter (d_c) has been calculated by assuming the channel has a variable cross-section because of the spacer:

$$d_c = \frac{4\varepsilon}{\frac{2}{h} + (1 - \varepsilon)S_{V,SP}} \quad (6.11)$$

where ε is the spacer porosity, h is the channel height, and $S_{V,SP}$ is the specific surface of the spacer. The porosity of the spacer can be calculated by using the average filament thickness and mesh size of the spacer according to

$$\varepsilon = \frac{1 - V_{SP}}{V_{TOT}} \quad (6.12)$$

where V_{SP} is the volume of the spacer and V_{TOT} is the volume occupied by the spacer. The specific surface of the spacer ($S_{V,SP}$) is calculated by

$$S_{V,SP} = \frac{4}{\text{spacer - thickness}} \quad (6.13)$$

To get the information necessary to calculate the cross-flow velocity, it was necessary to sacrifice membrane elements and to measure channel dimensions and spacer characteristics. However, to calculate k in Equation 6.6 [given as $k(j)$], a relationship similar to that in Equation 3.5 is needed. The coefficients in Equation 3.5 have been reported to be dependent on the type and size of spiral-wound element, spacer type, and scale of membrane system (Sutzkover et al., 2000; Geraldles and de Pinho, 2006; Sharma and Sharma, 2008). Geraldles and de Pinho (2006) performed a study of spiral-wound NF-200 membrane elements, which were the previous generation of the NF-4040. Therefore, this mass transfer correlation was adopted for the determination of the mass transport coefficient [$k(j)$] for each element and is the same as in Equation 3.5.

6.3.2.3 Spreadsheet Model Development

An additional requirement for model development was to understand and model the permeate flux rate [$J_v(j)$] in any given element throughout the pilot-scale system. A database was constructed that included the inlet and outlet pressures of each individual pressure vessel and first- and second-stage permeate flux rates at each overall system feed flow rate and recovery set-point. Linear regressions between inlet pressure and outlet pressure and recovery for each pressure vessel at each feed flow rate evaluated were then constructed. The regression equations allowed for the calculation of the driving pressure throughout the system, given the recovery and the feed flow rate and, therefore, the permeate flux rate in the system's four stages if one used Equation 6.3 with the pressure data and L_p as a fitting parameter. To do this, the feed flow rate of the pilot-scale system was manipulated between 53 Lpm and 98 Lpm (14 and 26 gpm) and at each flow set-point, the recovery was manipulated. During this exercise, the inlet and outlet of each pressure vessel were measured and the flow rates across the system recorded. The membrane permeability constant was measured during bench-scale experiments by using the sacrificed membrane elements.

By using all of the gathered information and equations, an Excel-based differential element model was constructed that allowed for the evaluation of rejection over a range of recovery (50–90%) and feed flow rate (53 Lpm and 87 Lpm [14 and 26 gpm]). The model was calibrated with rejection data generated during this study, which is discussed in subsequent sections.

6.3.3 NF-4040 Bench-Scale Results and Model Evaluation

Feed water for the laboratory pilot-scale experiments was prepared by producing 1800 L of NF-4040 permeate from dechlorinated drinking water. This NF-4040 permeate was characterized by TOC analysis, electrical conductivity, ion chromatography, and inductively coupled plasma analysis and exhibited TOC concentrations of less than 0.3 ppm, low conductivity (<150 $\mu\text{S}/\text{cm}$), and a low concentration of ions (mainly sodium and chloride, <20 mg/L each). This feed water was spiked with the organic compound of interest at a nominal concentration of 700 ppb. The feed water temperature was set at 17 to 18 $^{\circ}\text{C}$, and if needed, pH was adjusted to approximately 6.3. Most of the organic solutes evaluated were analyzed by using HPLC-DAD analysis. Experiments were conducted over a range of recovery and subsequent permeate flux rate set-points. Most experiments were performed at a constant feed flow rate of 17 gpm with system recovery manipulated by increasing the system back-pressure. For these experiments, system recovery values between 50 and 85% were evaluated and the actual values depended on where the system was operating when samples were collected. Samples were collected from the various sampling ports directly into HPLC vials and subsequently were analyzed by the HPLC-DAD method. In order to cut down on the number of samples, a full sampling of the system was performed only at the lowest and highest recovery set-points. Full sampling (14 samples total) included collecting a feed sample, permeate samples from each pressure vessel, all concentrate streams, and combined permeate streams. Otherwise, samples were collected from the feed, concentrate (first and second stages), and permeate (first stage, second stage, combined) streams.

6.3.3.1 Rejection of Organic Solutes

Rejection data generated at bench scale for the organic solutes were fit with the phenomenological model by manipulating the reflection coefficient (σ) and the solute permeability coefficient (P). The phenomenological model satisfactorily described the rejection of all solutes at bench scale, and predicted values were generally within 5% of experimental values for all solutes evaluated. The rejection of acetaminophen, caffeine, and phenacetine with model fits is presented in Figure 6.8. For the NF membrane, rejection of the tested solutes at bench scale followed the decreasing trend of propyphenazone > DEET > caffeine > thiabendazole > acetaminophen. Rejection generally increased with increased molecular size as measured by the Stokes radius.

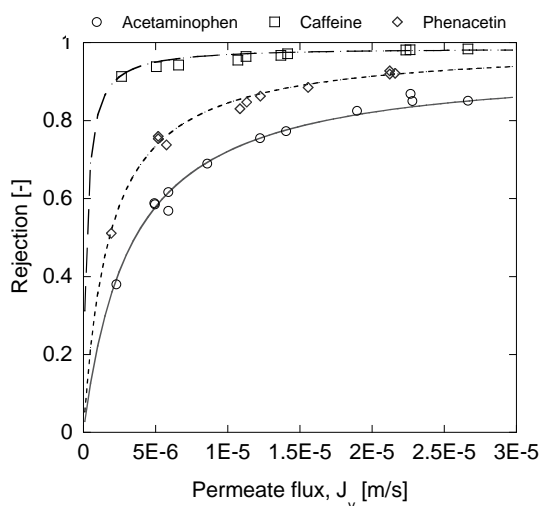


Figure 6.8. Intrinsic rejection and phenomenological model fits for acetaminophen (phenomenological model coefficients $\sigma = 0.921$, $P = 3.15E-6$ m/s), caffeine ($\sigma = 0.983$, $P = 2.13E-7$ m/s), and phenacetine ($\sigma = 0.989$, $P = 1.76E-6$ m/s).

6.3.3.2 Effect of Solute Concentration on Rejection and Model Parameters

Because solute concentrations change dramatically throughout a pilot- or full-scale treatment system, bench-scale experiments were conducted to evaluate the effect of solute concentration on rejection and the phenomenological model parameters. Acetaminophen and phenacetine experiments were conducted at three feed water concentrations: 300, 1000, and 1500 $\mu\text{g/L}$ (Figure 6.9). Feed water concentrations in the range of 300 to 1300 $\mu\text{g/L}$ were found to have an undetectable influence on rejection and phenomenological model coefficients. Past research has demonstrated that solutes with strong solute–membrane interactions have increased rejection with increased concentration because of the affinity of the solute for the membrane and the limited sites for adsorption (Ahmad and Tan, 2004; Matsuura and Sourirajan, 1971). It is worth noting that acetaminophen is a compound that could be expected to exhibit solute–membrane interaction effects, as it has a hydroxyl group attached to a benzene ring. As previously mentioned, the rejection of acetaminophen is difficult to predict because of lower-than-expected rejection on the basis of size; however, acetaminophen was not observed to exhibit solute–membrane interaction (i.e., decreased rejection over time and decreased rejection with increased permeate flux). Acetaminophen behavior is significantly different from other solutes with similar structure, i.e.,

methylparaben, benzylacetate, and methylsalicylate, which tend to sorb to membrane materials.

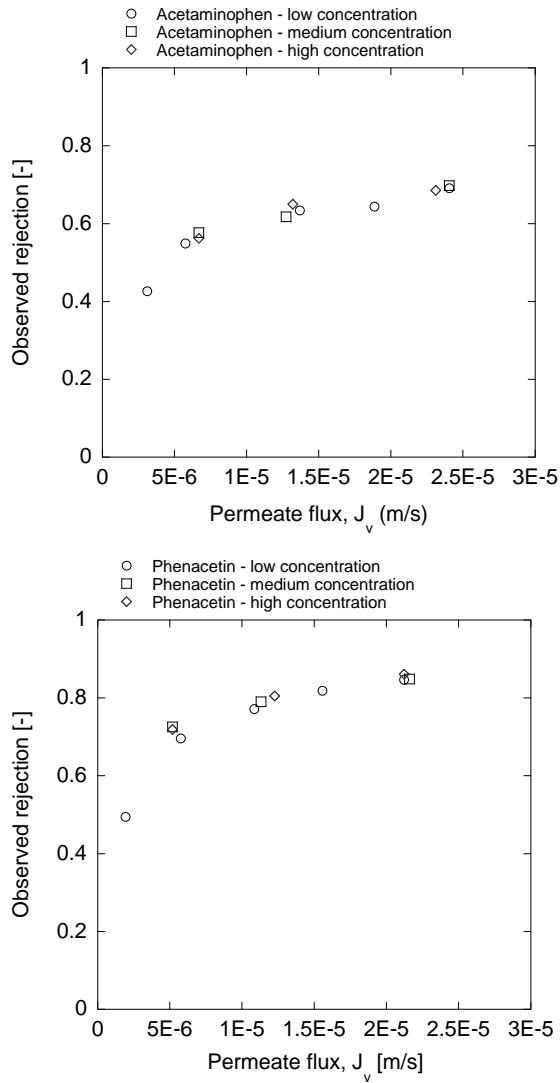


Figure 6.9. Observed rejection of acetaminophen (left) and phenacetine (right) versus permeate flux (J_v) at different feed water concentrations (low = 300 $\mu\text{g/L}$, medium = 1000 $\mu\text{g/L}$, high = 1500 $\mu\text{g/L}$).

6.3.3.3 Effect of Experimental Run Time on Rejection

Experiments were conducted to determine the effect of experimental run time on rejection, as past research has demonstrated that, for certain organic solutes, equilibrium takes up to several days to achieve (Kimura et al., 2003a; Hofman et al., 2007). Experiments with acetaminophen (Figure 6.10) and the other solutes revealed that rejection stabilized within 1 h and that minimal changes were observed over 20 h of continuous operation of bench-scale experiments.

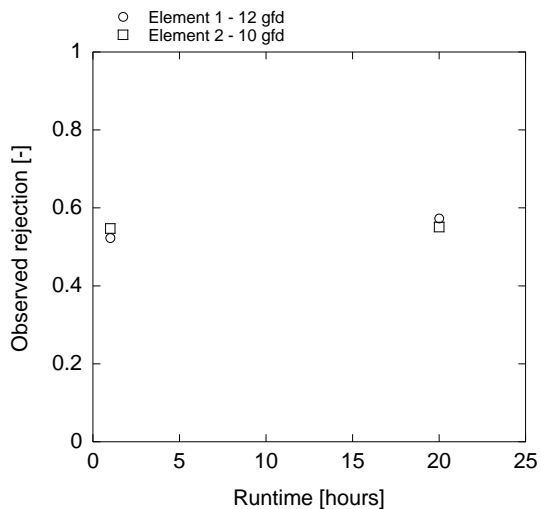


Figure 6.10. Bench-scale rejection of acetaminophen by membrane specimens extracted from two separate spiral-wound elements versus experimental run time.

6.3.3.4 Effect of Membrane Variability on Rejection and Model Parameters

The pilot-scale system consisted of 21 spiral-wound elements, whereas the bench-scale system requires only 139 cm² of membrane material. Therefore, three spiral-wound elements were sacrificed to evaluate the variability of membrane material on the rejection of acetaminophen and phenomenological model parameters (Figure 6.11).

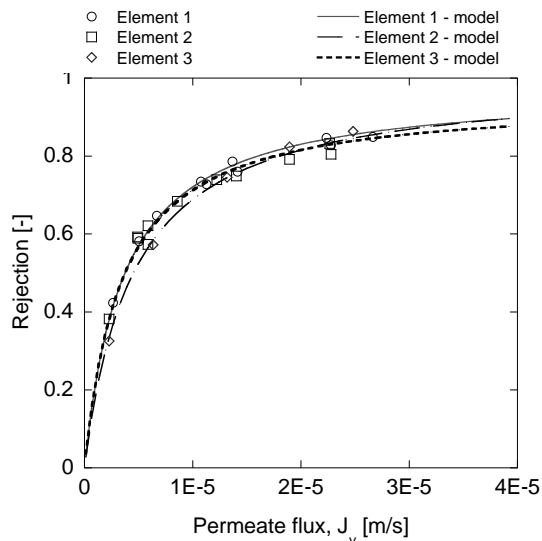


Figure 6.11. Acetaminophen rejection versus permeate flux rate for membranes extracted from three spiral-wound membrane elements.

Note: Each membrane element was evaluated in replicate. Model fits yielded the following parameters: element 1 ($\sigma = 0.96$, $P = 3.51\text{E-}6$ m/s), element 2 ($\sigma = 0.99$, $P = 4.50\text{E-}6$ m/s), and element 3 ($\sigma = 0.88$, $P = 2.92\text{E-}6$ m/s).

The rejection of acetaminophen was found to be fairly consistent among the membrane elements tested; however, model parameters differed more significantly with reflection coefficients differing by approximately 11% and the solute permeability differing by approximately 54%. The effect of the variability of model parameters on pilot-scale modeled results is presented in the next section.

6.3.4 Pilot-Scale Model Development

6.3.4.1 Observations from Pilot-Scale Experiments

Pilot-scale experiments with acetaminophen and caffeine were performed by adjusting the overall system recovery between set-points of 50% and 90%. Sampling was performed at locations across the pilot-scale unit to generate a data set that could be used to calibrate the pilot-scale model, which is discussed in detail in the next section.

Two separate recovery experiments were conducted: constant feed flow rate and variable permeate flux rate and variable feed flow rate and constant permeate flux rate. Past research examining pilot-scale membrane systems has reported a significant decrease in rejection with increasing system recovery (Hofman et al., 2007). However, rejection of both caffeine and acetaminophen for constant feed flow rate experiments was relatively constant over the range of recovery investigated (Figure 6.12). Rejection of both solutes, however, decreased with increasing recovery when the permeate flux rate was kept constant and when feed flow rate decreased.

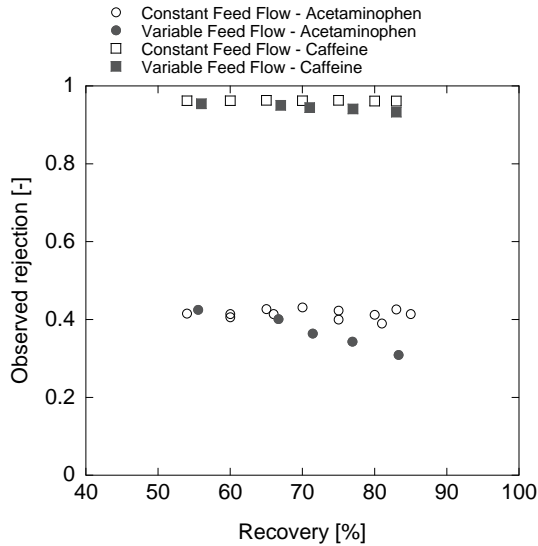


Figure 6.12. Rejection of acetaminophen and caffeine versus recovery for constant feed flow rate and variable feed flow rate experiments.

Notes: Constant feed flow rate experiments were performed at a feed flow rate of 64.4 Lpm (17 gpm) with a variable permeate flux rate to achieve recovery set-points between 50 and 90%. Variable feed flow rate experiments were performed at a feed flow rate of 68.1 Lpm (18 gpm), 56.8 (15), 53.0 (14), 49.2 (13), and 45.4 (12), with the permeate flow rate held constant at 37.9 Lpm (10 gpm).

During variable feed flow rate experiments, the cross-flow velocity was significantly reduced when recovery was increased, which led to concentration polarization. Because permeate flux was held constant, decreased rejection was observed. However, at a constant feed flow rate, the concentration polarization effect appeared to be offset by the increase in permeate flux as recovery increased, which resulted in relatively constant rejection versus recovery.

Caffeine concentrations across the pilot-scale membrane unit during constant feed flow rate experiments at 60 and 80% recovery are summarized in Figures 6.13 and 6.14. As was expected, caffeine concentrations increased significantly (~6 times) between the feed water and the second-stage concentrate during 80% recovery experiments (Figure 6.13). During both recovery experiments, combine permeate concentrations were observed to be very similar, although concentrate concentrations differed significantly. It appears that, although increased recovery resulted in higher concentration polarization within the system (i.e., cross-flow velocity decreased significantly), increasing recovery also raised permeate flux, which counteracted the effect of concentration polarization. As recovery rose, first-stage rejection increased because of higher permeate flux (Figure 6.14) and second-stage rejection decreased because of concentration polarization effects. Possibly by coincidence, these effects tended to cancel each other out and rejection was very stable as a function of recovery. These findings indicate that, for the system studied, recovery had a minimal impact on the rejection of nonionic organic solutes when the feed flow rate was kept constant and operated in a normal flow range for the elements.

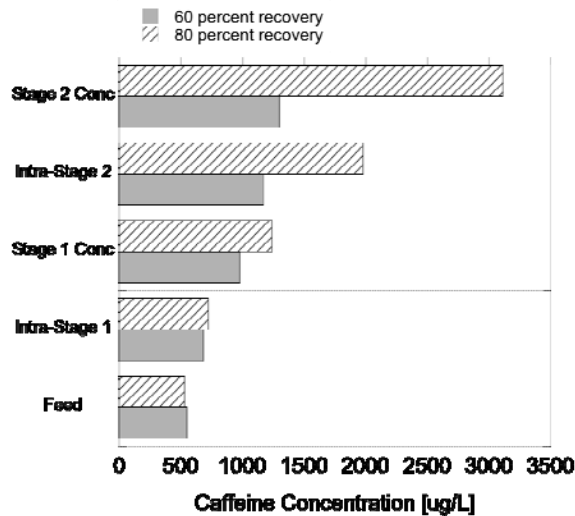


Figure 6.13. Caffeine concentrations in feed, intraconcentrate, and concentrate samples as a function of recovery

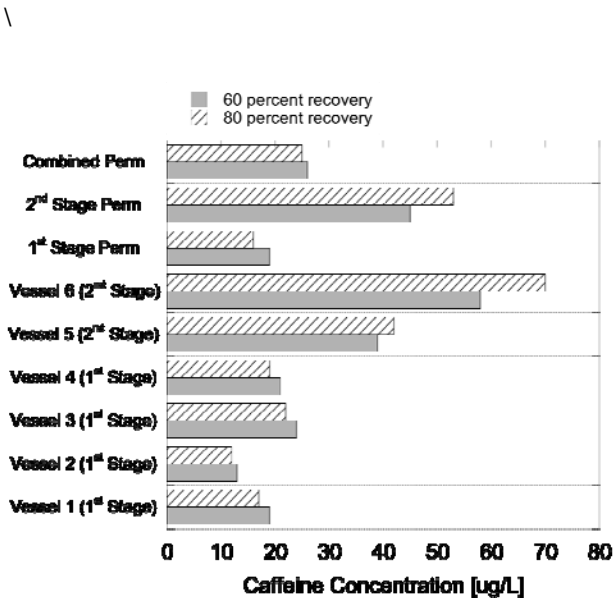


Figure 6.14. Caffeine concentrations in permeate as a function of recovery.

6.3.4.2 Pilot-Scale Model Calibration

As pointed out in the previous section, the hydrodynamics of the pilot-scale system resulted in relatively constant rejection over a wide range of recovery set-points, which is hypothesized to be caused by the contradictory effects of concentration polarization and permeate flux on rejection. On the basis of the caffeine concentration data presented in Figure 6.14, it appears that the second stage of the system played a large role in this phenomenon, as recovery had a large effect on second-stage concentrate concentrations, indicating that permeate flux rates changed significantly in the second stage as recovery increased. To effectively capture this finding in the model, caffeine data from two experiments were used to calibrate the model, specifically to ensure that model outputs of flow rates (e.g., permeate and

concentrate) and concentration fit with the experimental data. To meet this goal, it was necessary to use the membrane solvent permeability coefficient (L_p) as a fitting parameter so that the permeate flux rate of each stage of the system could be manipulated to achieve the correct flow rates, concentrations, and mass balances throughout the system.

A routine was performed to find the best model fit for caffeine rejection and caffeine concentrations across the system by manipulating the phenomenological model parameters (σ and P) and the membrane solvent permeability constant in each stage of the pilot-scale system. The results of this procedure are presented in Figure 6.15. The ideal model parameters for fitting caffeine rejection and describing the concentration and flow rate distribution across the system were $\sigma = 0.987$, $P = 6.24\text{E-}8 \text{ m-s}^{-1}$, first-stage $L_p = 1.15\text{E-}6 \text{ m}^3\text{-m}^{-2}\text{-s}^{-1}\text{-bar}^{-1}$, and second-stage $L_p = 9.9\text{E-}7 \text{ m}^3\text{-m}^{-2}\text{-s}^{-1}\text{-bar}^{-1}$. These L_p values used with the pressure data yielded model outputs of permeate flow and flux rates and permeate and concentrate concentrations that most satisfactorily fit the experimental data for caffeine (Figure 6.15).

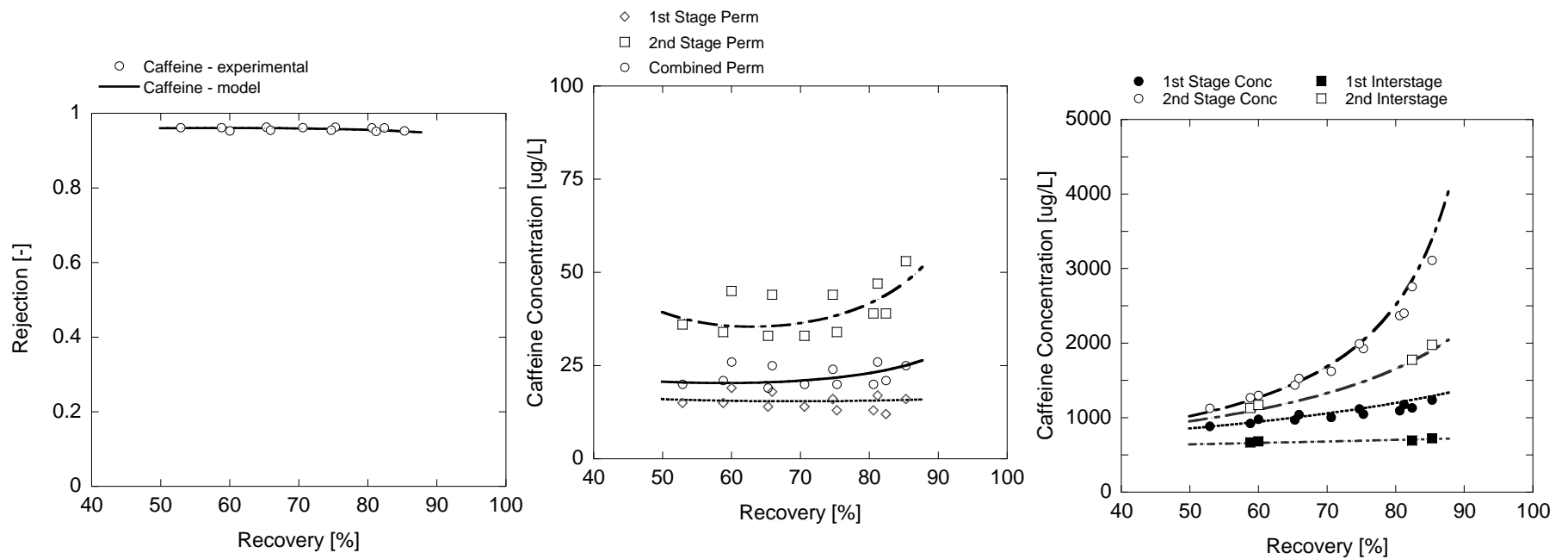


Figure 6.15. Left: Rejection of caffeine from two experiments with model fit (average feed concentration = 530 µg/L, $\sigma = 0.987$, $P = 6.24E-8$ m/s); middle: 1st-stage, 2nd-stage, and combined permeate concentrations with model fit; right: 1st intrastage, 1st-stage concentrate, 2nd intrastage, and 2nd-stage concentrate with model fit.

The model describes a decrease in the second-stage permeate concentration as recovery grew from approximately 50 to 70%, followed by an increase from 70 to approximately 89%. The initial decrease was due to the second-stage permeate flow and flux increasing enough to offset the effect of the mounting first-stage concentrate concentration and concentration polarization. Eventually, however, the concentration polarization effect in the second stage increased enough that the growth in rejection associated with higher permeate flux was not enough to maintain a constant second-stage permeate concentration. On the contrary, the first-stage permeate concentration stayed relatively constant, although the combined permeate increased marginally.

6.3.4.3 Rejection of Acetaminophen, Phenacetine, DEET, and Thiabendazole

Phenomenological model parameters determined from bench-scale experiments were used to model the rejection of acetaminophen, DEET, phenacetine, and thiabendazole at pilot scale. For acetaminophen, the highest and lowest reflection coefficient (σ) and solute permeability coefficient (P) as determined from bench-scale experiments with specimens taken from different elements were used for modeling. Acetaminophen rejection and permeate and concentrate concentrations with model fits are presented in Figure 6.16. The highest measured model coefficients determined during pilot scale provided the best model fit, with the lowest model parameters underpredicting rejection by approximately 10%. Unlike the case for caffeine, the rejection curve was more dependent upon recovery, exhibiting a 3 to 5% decline as recovery increased above 70%; however, the acetaminophen rejection figures appeared to decline slightly as well with increasing recovery. The second-stage permeate concentration was overpredicted by the model, which led to the combined permeate model output being greater than the experimental data. However, model output concentrate data were similar to measured data.

DEET rejection by the NF membrane was the highest of all solutes tested, approximately 98% for all recoveries investigated (Figure 6.17). Similar to acetaminophen, second-stage permeate concentrations were overpredicted, which led to the model rejection output being lower than the experimental values. It is worth noting that, because of high rejection, permeate concentrations of DEET were near the detection limit for the HPLC-DAD method. Phenacetine and thiabendazole pilot-scale data are summarized in Figures 6.18 and 6.19, respectively. For phenacetine, the first-stage permeate concentration was overpredicted, which led to an overprediction of rejection and of the concentrate concentrations. The thiabendazole model output was similar to that of phenacetine, with rejection and concentrate concentration overpredicted for all recoveries.

It is worth noting that, through the development of the pilot-scale model, numerous sources of error were identified because of the largeness of the system. The model was partially calibrated to mimic the operational set-points during experiments as measured by the SCADA system, flow meters, and pressure gauges. The pilot-scale unit's feed flow rate was controlled by a variable frequency drive that in turn was controlled by a proportional-integral-derivative loop, which caused fluctuations in the feed flow rate, permeate flow rate, recovery, and pressure. Therefore, defining the conditions under which each sample was collected was a difficult task and could be considered a good estimate. In addition, sample concentrations were subject to the same overall effect of variability inherent to the system. Finally, this approach used phenomenological model parameters determined through bench-scale testing with a membrane specimen with 0.15 ft² of area to describe the rejection of a membrane system with approximately 1722 ft² of membrane area. Variation in membrane properties can

have a large effect on phenomenological model parameters determined at bench scale and on overall rejection at the pilot and full scales. Therefore, model fits for DEET, phenacetine, and thiabendazole were deemed to be acceptable, and this approach was evaluated for describing and predicting the rejection of organic contaminants by the NF-270 membrane during a pilot-scale evaluation at a water reuse facility.

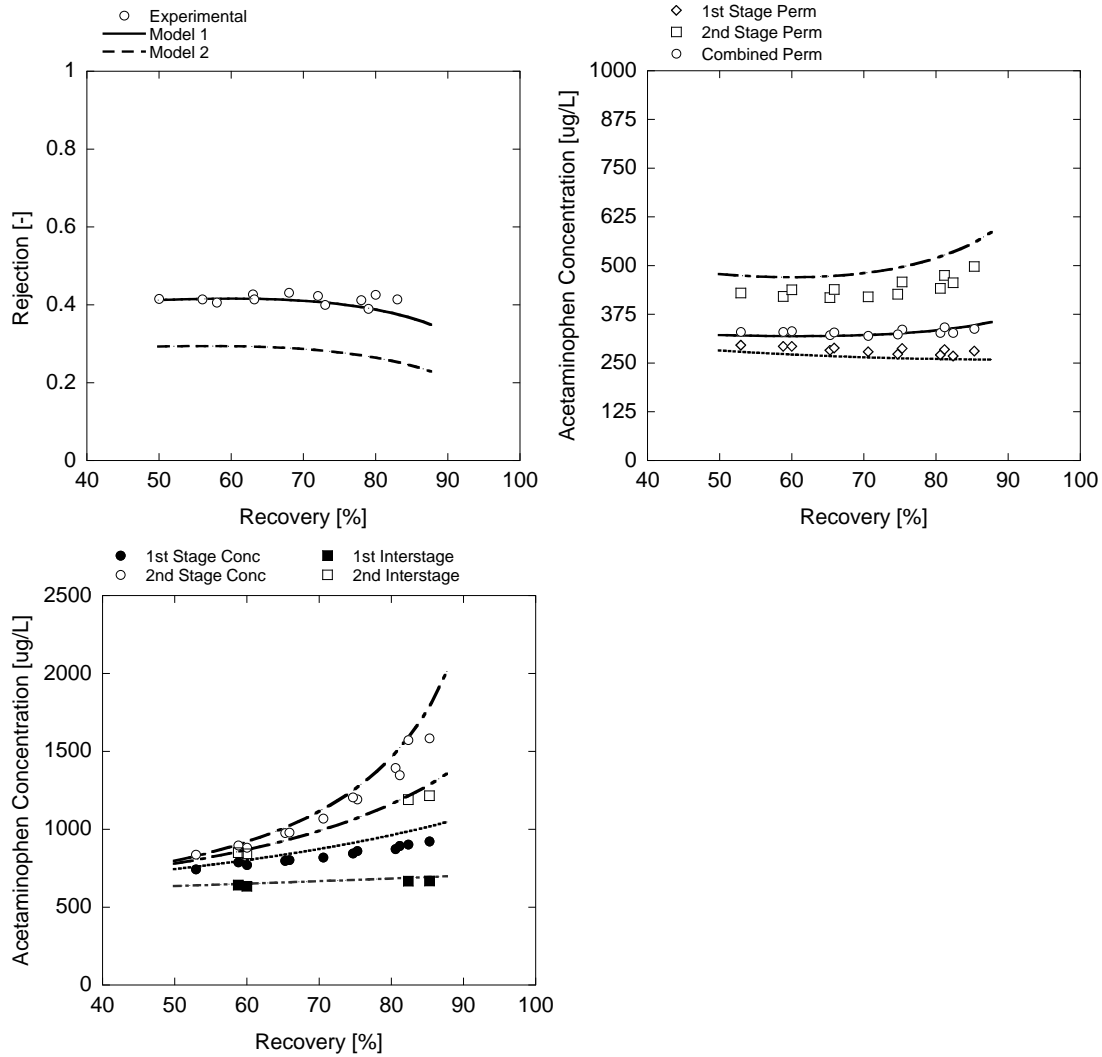


Figure 6.16. Left: Rejection of acetaminophen with model fit (feed concentration = 560 µg/L, solid rejection line: $\sigma = 0.99$, $P = 2.92E-6$ m/s, dashed rejection line: $\sigma = 0.88$, $P = 4.5E-6$ m/s); middle: 1st-stage, 2nd-stage, and combined permeate concentrations with model fit using $\sigma = 0.99$, $P = 2.92E-6$ m/s; right: 1st interstage, 1st-stage concentrate, 2nd interstage, and 2nd-stage concentrate with model fit using $\sigma = 0.99$, $P = 2.92E-6$ m/s.

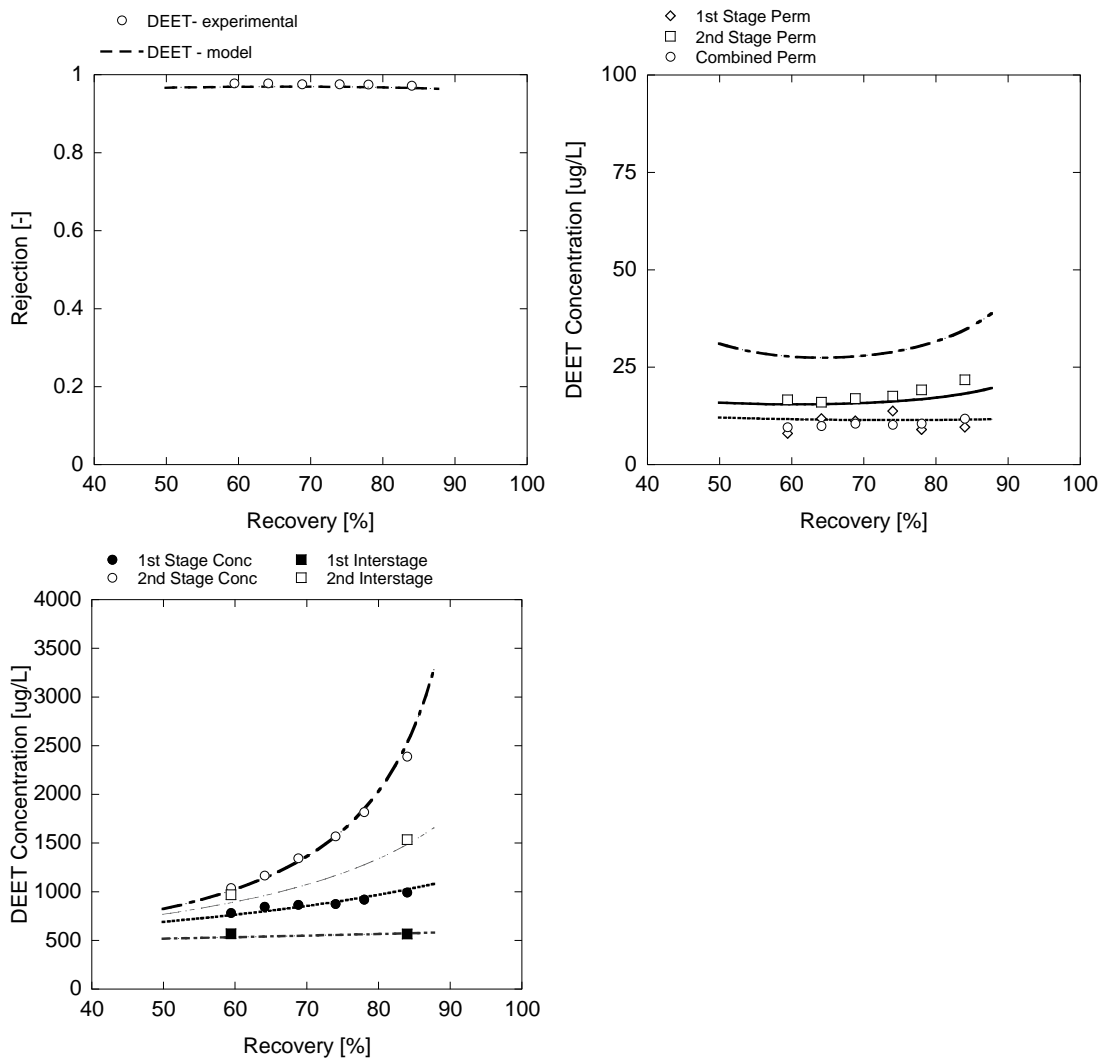


Figure 6.17. Left: Rejection of DEET with model fit (feed concentration = 430 µg/L, $\sigma = 0.99$, $P = 6.35E-8$ m/s); middle: 1st-stage, 2nd-stage, and combined permeate concentrations with model fit; right: 1st interstage, 1st-stage concentrate, 2nd interstage, and 2nd-stage concentrate with model fit.

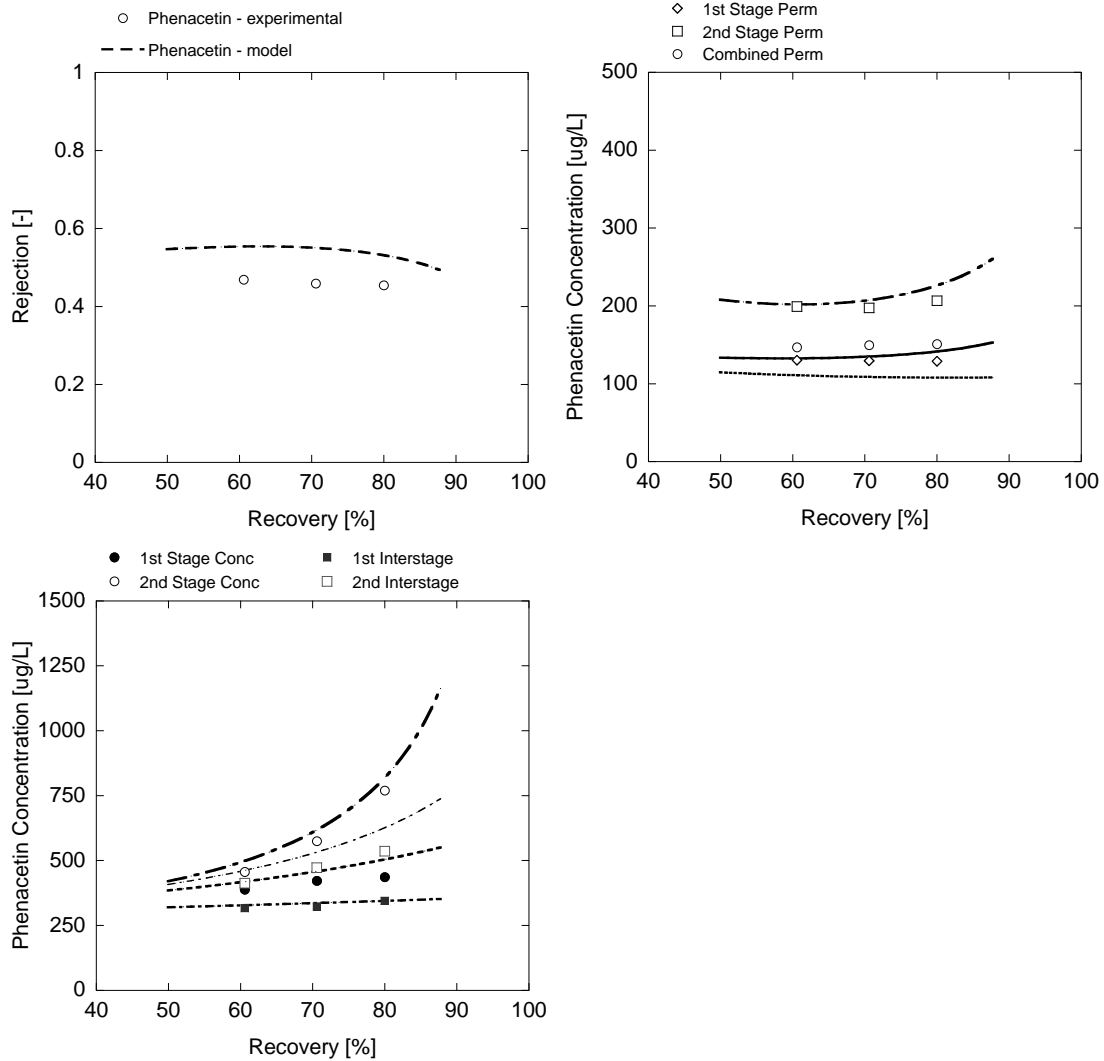


Figure 6.18. Top left: Rejection of phenacetine with model fit (feed concentration = 280 $\mu\text{g/L}$, $\sigma = 0.989$, $P = 1.75\text{E-}6$ m/s); top right: 1st-stage, 2nd-stage, and combined permeate concentrations with model fit; bottom left: 1st interstage, 1st-stage concentrate, 2nd interstage, and 2nd-stage concentrate with model fit.

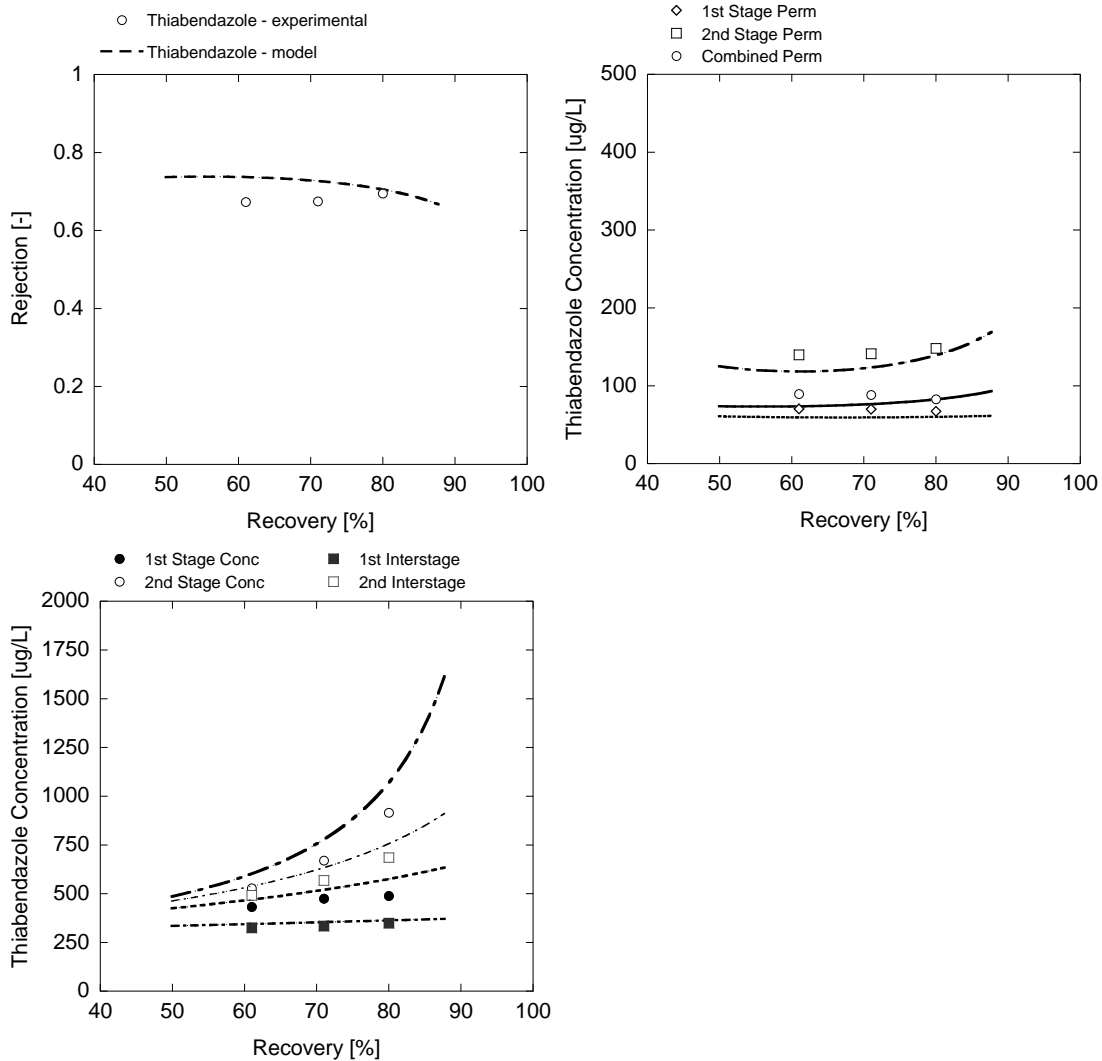


Figure 6.19. Top left: Rejection of thiabendazole with model fit (feed concentration = 270 $\mu\text{g/L}$, $\sigma = 0.909$, $P = 5.08\text{E-}7$ m/s); top right: 1st-stage, 2nd-stage, and combined permeate concentrations with model fit; bottom left: 1st interstage, 1st-stage concentrate, 2nd interstage, and 2nd-stage concentrate with model fit.

6.3.4.4 Effect of Feed Flow Rate on Rejection and Model Output

The model was built to incorporate different feed flow rates, and phenacetine samples were collected to evaluate the effect of feed flow rate on rejection (Figure 6.20). In general, reducing the feed flow rate decreased rejection as a result of concentration polarization because of reduced cross-flow velocity. Experimental phenacetine rejection generally displayed the same phenomenon, with 20-gpm experiments resulting in the highest rejection followed by 19 and 17 gpm. This result indicates that organic contaminant rejection can be increased by running membrane systems at a higher feed flow rate and permeate flux.

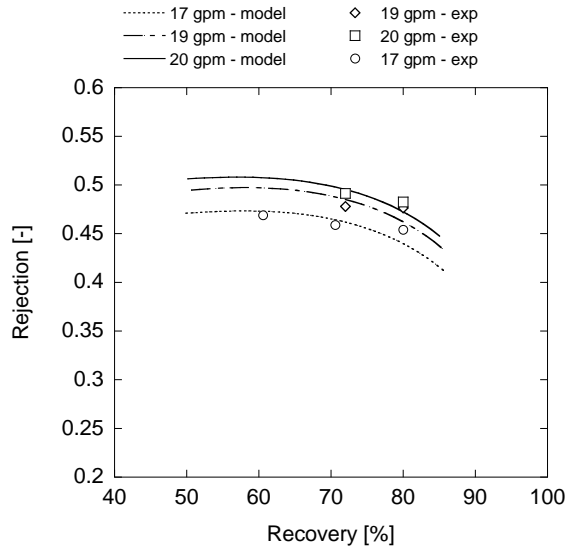


Figure 6.20. Rejection of phenacetine versus recovery at three feed flow rates.

6.3.5 Model Development and Validation—Pilot Testing of NF-270 Membrane

6.3.5.1 Observations

The NF-270 membrane was pilot tested for approximately 1500 h at a water reuse facility in Southern California for a separate WaterReuse Research Foundation project (WRRF-08-010). Feed water for water reuse facility pilot-scale experiments was microfiltered (pore size = 0.1 μm) tertiary-treated wastewater effluent that was pH adjusted to 6.3, with 2- to 3-mg/L antiscalant (King Lee Pretreat Plus) and 2- to 3-mg/L chloramine concentrations. A list of average concentrations of major bulk constituents in wastewater effluent feeding the pilot-scale system is presented in Table 6.3. Pilot testing was conducted for approximately 1500 h, during which several operational settings were evaluated and membrane cleanings were performed. Four organic contaminant sampling and analysis campaigns were performed during testing of the NF-270 membrane. During testing, samples were collected across the two-stage pilot-scale system and were analyzed by LC/MS-MS for the quantification of organic contaminants. Rejection was evaluated under different operational settings, including feed flow rate and recovery. Rejection data were used to validate modeling approaches developed during this study.

Table 6.3. Average Bulk Wastewater Quality for Major Constituents

Constituent	Average	StDev
Conductivity ($\mu\text{S}/\text{cm}$)	1023.2	96.4
UV-254 (cm^{-1})	0.13	0.01
Constituent	Average (mg/L)	StDev (mg/L)
DOC	6.4	0.9
NO ₃ -N	2.7	1.0
Alkalinity (as CaCO ₃)	216.0	21.0
Chloride	123.1	15.6
Calcium	54.2	9.4
Magnesium	14.5	4.0
Phosphate	0.4	0.4
Sodium	136.3	16.1
Silica	10.7	1.4

A summary of feed water concentrations of quantified organic contaminants over the course of pilot testing is provided in Figure 6.21. Concentrations of organic contaminants ranged from low nanograms per liter to low micrograms per liter with atenolol, TCEP, meprobamate, carbamazepine, DEET, sulfamethoxazole, triclocarban, and primidone displaying the greatest concentrations, respectively. Depending on when samples were collected, the concentration of certain compounds varied significantly.

A comparison of rejection of the various organic contaminants as a function of time is presented in Figure 6.22. During the first 500 h of operation, the NF-270 process was operated at a feed flow rate of 22 gpm and a recovery of 85%, resulting in a permeate flux of approximately 15 gfd. Under these conditions, operation was very stable, with almost no membrane fouling observed from operational data (e.g., specific flux decreased negligibly). Rejection determined after 24 and 500 h of operation was similar for most organic contaminants, with the major exception being triclocarban, which decreased significantly between 24 and 500 h. Triclocarban is a relatively hydrophobic ($\text{Log } K_{\text{ow}} = 4.74$) antibacterial compound that is replaced with chlorine atoms. The observed decrease in rejection is hypothesized to be due to adsorptive interactions with the membrane, which resulted in relatively high initial rejection that decreased after some time. The rejection of several compounds (naproxen, diclofenac, sulfamethoxazole, and dilantin) increased slightly (~10%) over time, although ibuprofen, TCEP, and DEET rejection decreased slightly (~10%) over time. As a comparison, the rejection of major cations and anions and of bulk organic carbon is presented in Figure 6.23. Slight differences (~10%) in rejection for 24 h and 500 h of operation were also observed for certain inorganic constituents. These small discrepancies cannot be explained with certainty; however, possible explanations include membrane fouling and compaction, analytical error, and changes in feed water composition. Whatever the explanation, these factors are extremely difficult to incorporate into modeling approaches and any predictive modeling approach should be considered an estimate of rejection.

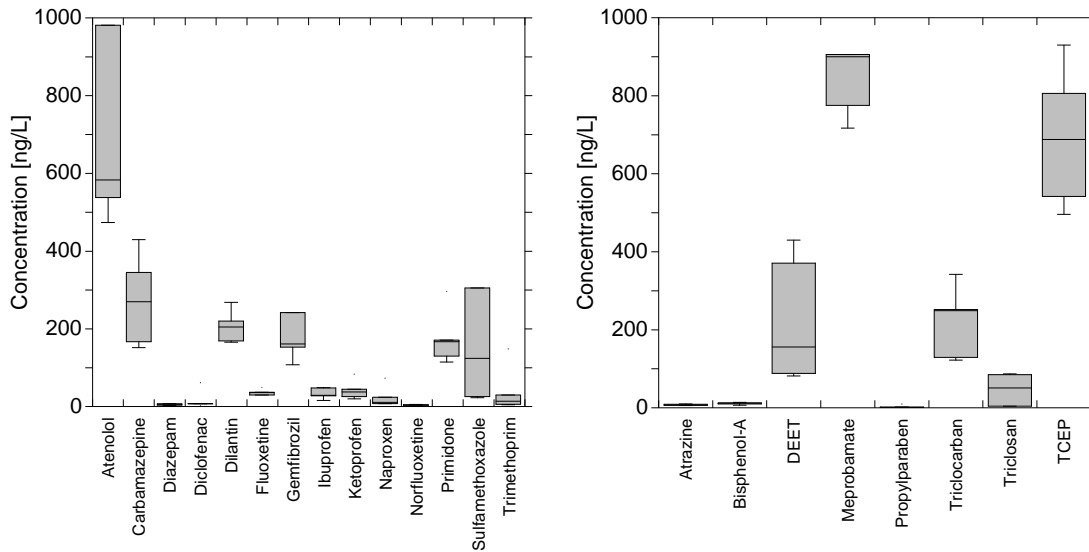


Figure 6.21. Ranges of pharmaceutically active compounds (left) and a pesticide (atrazine), personal care products (DEET, propylparaben, triclocarban, triclosan), a plasticizer (TCEP), and a pharmaceutically active compound (meprobamate).

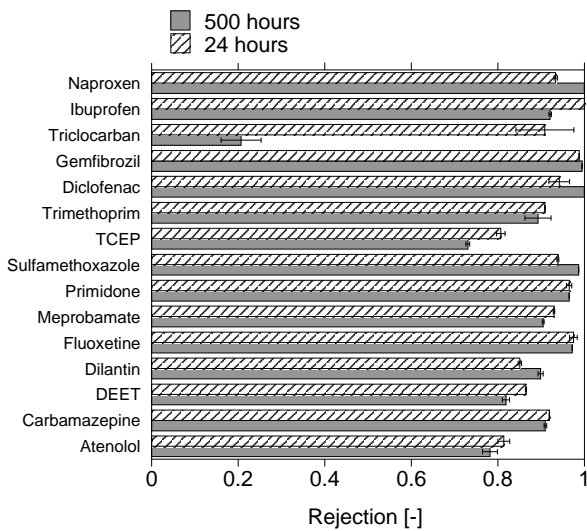


Figure 6.22. Rejection of organic contaminants by NF-270 (22-gpm feed flow rate, 85% recovery) over a period of 500 h.

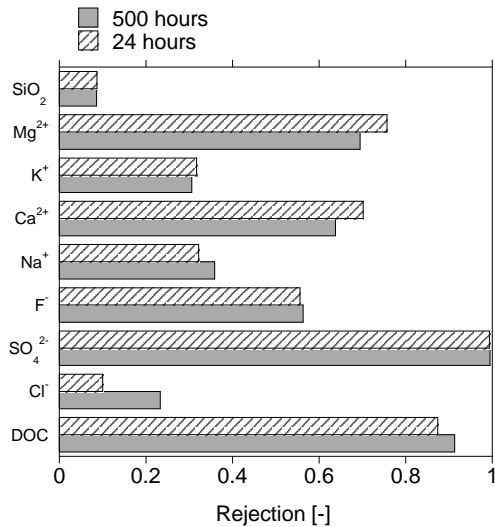


Figure 6.23. Rejection of inorganic constituents and bulk carbon by NF-270 (22-gpm feed flow rate, 85% recovery) over a period of 500 h.

6.3.5.2 Phenomenological Model

Bench-scale-derived phenomenological model coefficients were used to describe the rejection of organic contaminants at pilot scale. Similar to the NF-4040 pilot-scale modeling approach, the NF-270 membrane pilot-scale model was calibrated to describe pilot flow distributions at different recoveries and feed flow rates during treatment of wastewater effluent. This approach assumes that the feed water matrix has minimal effect upon rejection as bench-scale experiments were conducted with synthetic feed water (i.e., deionized water) and as the pilot system was fed with wastewater effluent. Given the many factors that could potentially affect rejection at pilot scale (e.g., analytical error, fouling, scaling, compaction, membrane variability, and variability in operational conditions), we believe that feed water matrix effects are likely insignificant. It is worth pointing out that feed water pH, which is likely to have the largest impact on rejection, particularly for ionic compounds, was 6.3 for both pilot- and bench-scale experiments.

Model calibration was first investigated by fitting rejection data and evaluating model outputs of permeate and concentrate concentrations. For this process, the average measured feed water concentration was used in the model (averaged over the three recovery sets of conditions evaluated). Examples of this exercise for meprobamate and carbamazepine are presented in Figures 6.24 and 6.25. For most compounds, measured concentrate and permeate concentrations were in agreement with the model output, although some discrepancies were observed (see Figures 6.24 and 6.25). These differences likely occurred because these contaminants were quantified at very low concentrations and because there were multiple steps in the LC/MS-MS method including SPE, leading to some analytical error. Care was taken to minimize and correct for any analytical error by using radiolabeled isotope standards for each compound evaluated.

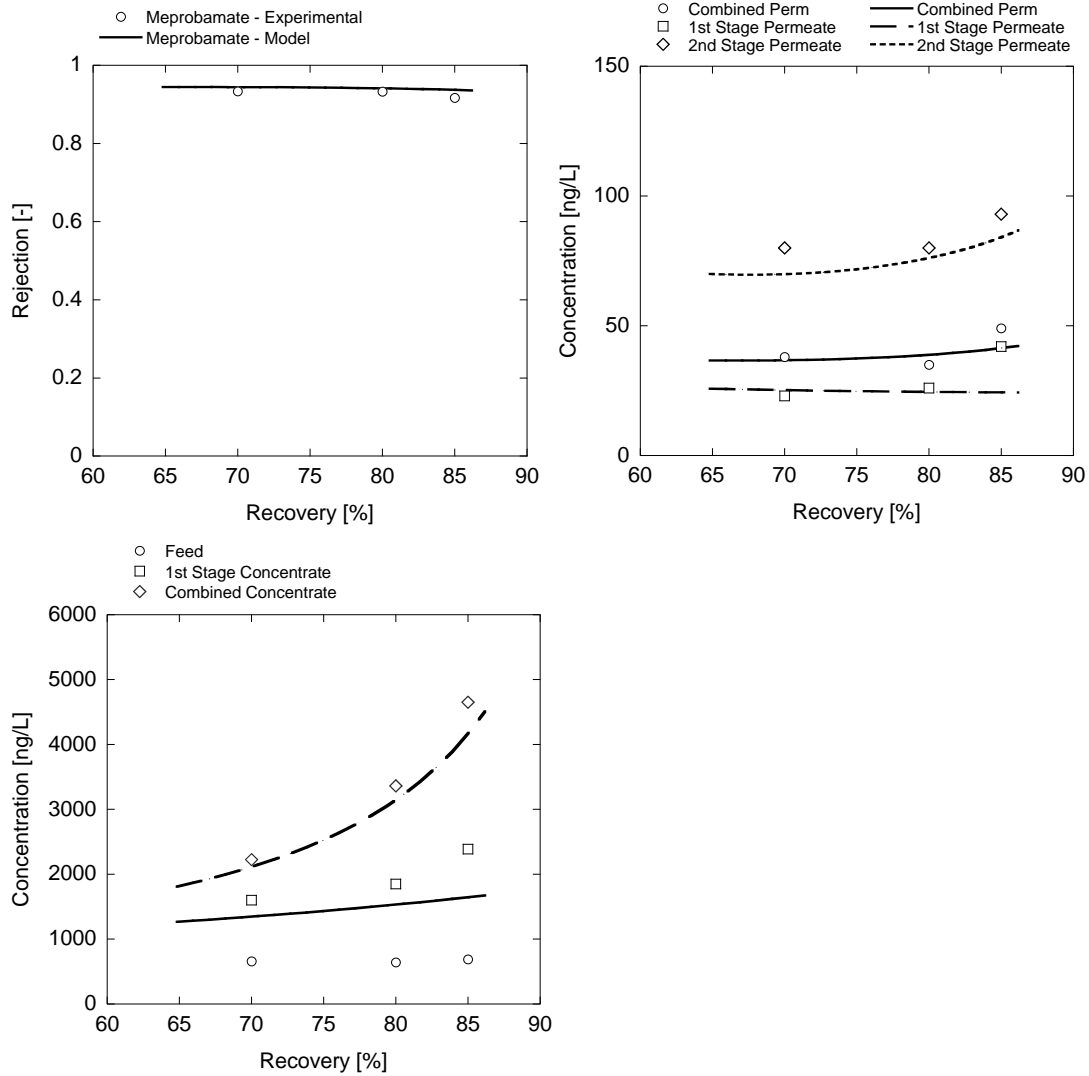


Figure 6.24. Meprobamate rejection (top left), permeate concentrations (top right, and concentrate concentrations (bottom left) as function of system recovery (20-gpm feed flow rate).

Note: Model fits calculated by using bench-scale-derived phenomenological model coefficients.

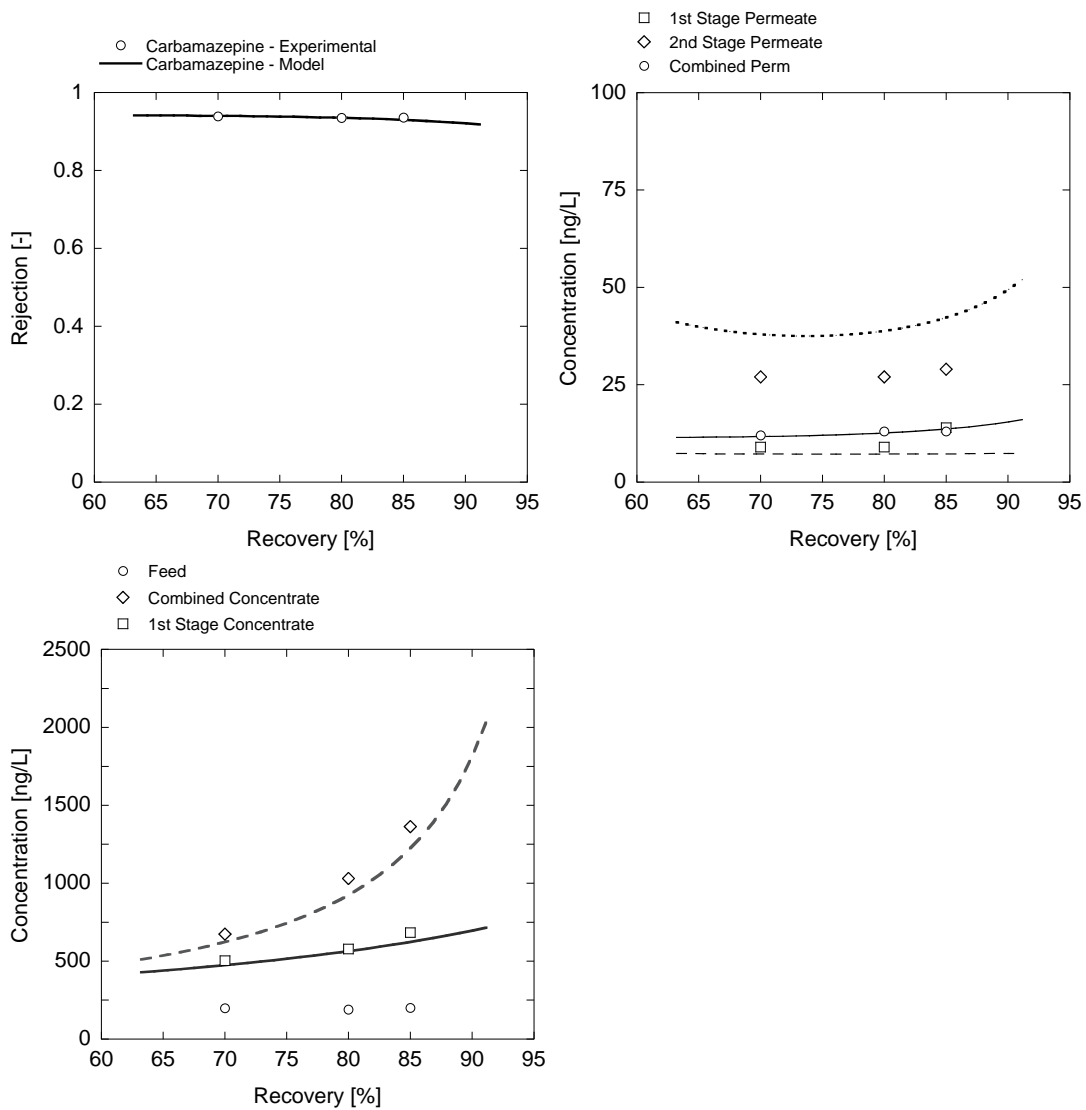


Figure 6.25. Carbamazepine rejection (top left), permeate concentrations (top right), and concentrate concentrations (bottom left) as function of system recovery (20-gpm feed flow rate).

Note: Model fits were calculated by using bench-scale-derived phenomenological model coefficients.

An example of model fits using bench-scale-derived phenomenological mode coefficients for the rejection of organic contaminants quantified in permeate and feed samples during the first 24 h of pilot-scale testing is presented in Figure 6.26 (left, data from two feed and two combined permeate samples). Although most of the ionic contaminants, with the exception of sulfamethoxazole, were well described by this approach, several of the nonionic organic contaminants were underpredicted by approximately 10% (e.g., meprobamate and primidone). Besides sulfamethoxazole, meprobamate, and primidone, modeled rejection at 85% recovery and a feed flow rate of 22 gpm was within 6% of experimental values. Unfortunately, compounds quantified in feed water that would be expected to have lower rejection values—such as acetaminophen, propylparaben, and caffeine—were excluded from this analysis because of analytical issues (e.g., low recovery of isotope standard). As a comparison, the average rejection values for the pilot system operating at 85% recovery and 22 gpm feed flow rate over the 1500 h of testing are provided in Figure 6.26 (right).

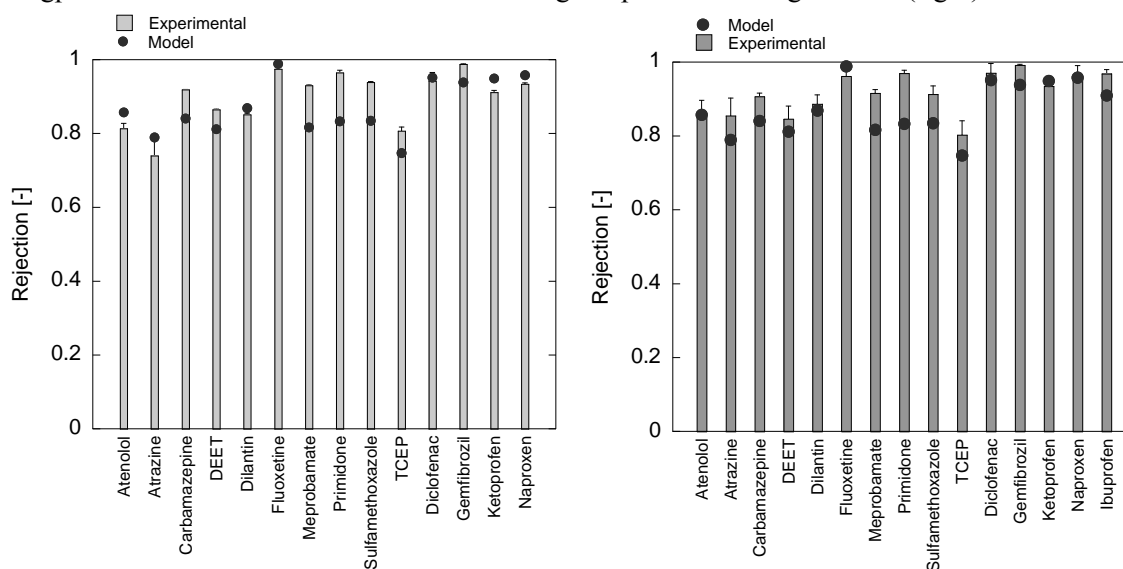


Figure 6.26. Rejection of organic contaminants quantified in feed and permeate samples after 24 h (left) and for three sampling campaigns performed over 1500 h of testing (right) of NF-270 membrane at 85% recovery and feed flow rate of 22 gpm.

Note: Model points represent rejection calculated with phenomenological coefficients derived from bench-scale experiments.

Because of the low concentrations of organic contaminants in feed and permeate samples, the relatively complex analytical method employed, and potential sources of error during experimentation, measured rejection could be variable depending on the compound evaluated. Measured rejection values for atenolol, ketoprofen, and TCEP over 1500 h of testing at a feed flow rate of 22 gpm with model fits are presented in Figure 6.27. At 85% recovery, atenolol and TCEP measured rejection varied by approximately 10%. Pilot-scale model fits, therefore, provide an estimation of rejection as the observed variability cannot be explained.

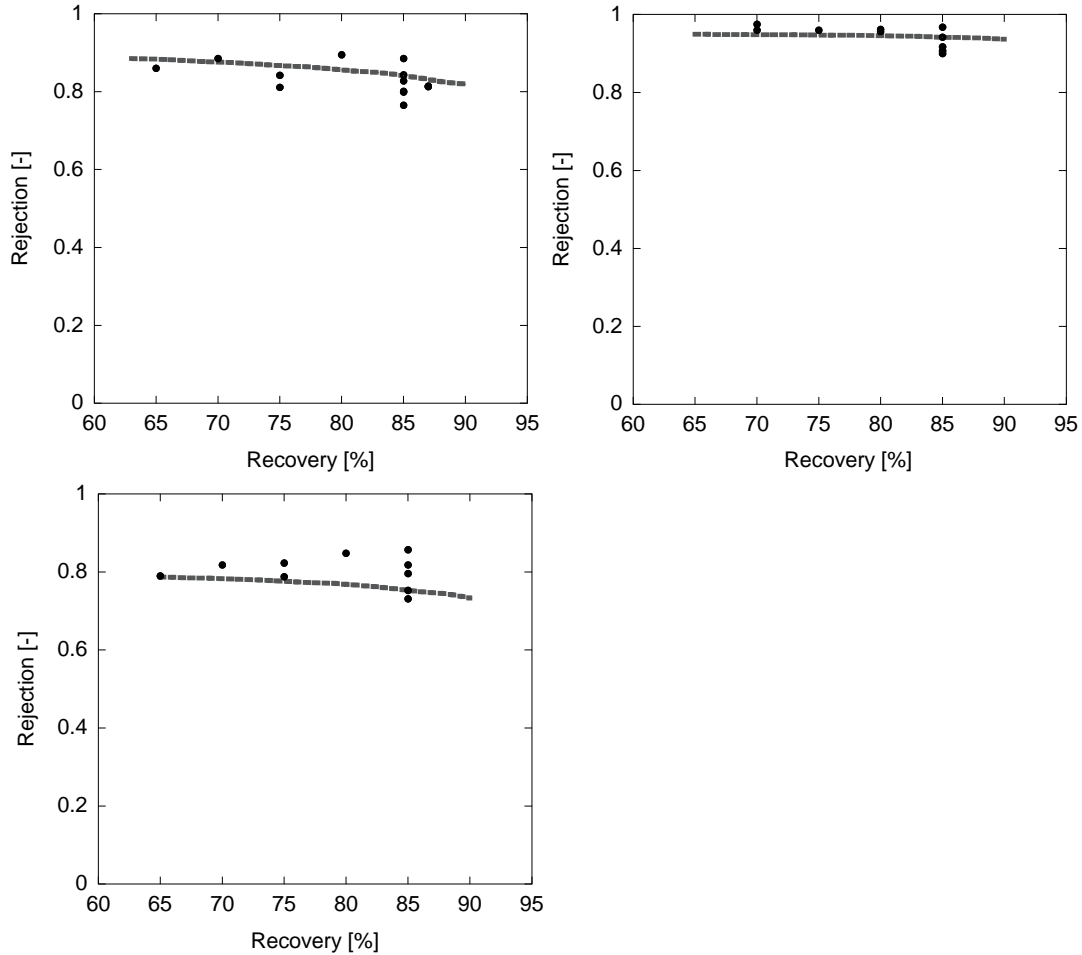


Figure 6.27. Rejection values for atenolol (top left), ketoprofen (top right), and TCEP (bottom) at 22 gpm feed flow rate.

Note: Values collected over several sampling campaigns.

The effect of the feed flow rate was also evaluated during pilot-scale testing, and rejection of organic contaminants at 22 and 16 gpm is presented in Figure 6.28. A significant decrease in rejection was observed for all organic contaminants, with the exception of triclorcarban, when the pilot-scale system was operated at 16 gpm. Modeled rejection examples at 16 and 22 gpm feed flow rates are presented in Figure 6.28. The reduction in the calculated cross-flow velocity by decreasing the feed flow rate from 22 to 16 gpm resulted in a theoretical drop in rejection of 3 to 7%, depending on the range of rejection. The rejection of several compounds, however, was observed to decrease by more than 10%, which was not described by the model. One possible explanation is that this experiment was done after approximately 1500 h of testing. Although the membrane had been cleaned prior to the experiment, membrane fouling can result in cake-enhanced concentration polarization, which would exacerbate the effect of cross-flow velocity on rejection. Typical membrane systems treating wastewater effluent are operated at approximately 10 to 12 fd permeate flux to avoid potential fouling issues. Operating at a recovery of 80 to 85%, while achieving 10 to 12 gfd permeate flux, requires a relatively low feed flow rate and, subsequently, a low cross-flow velocity. Because organic contaminant rejection in a two-stage system is negligibly affected

by recovery, operating a higher permeate flux and cross-flow velocity will likely result in increased rejection of organic contaminants.

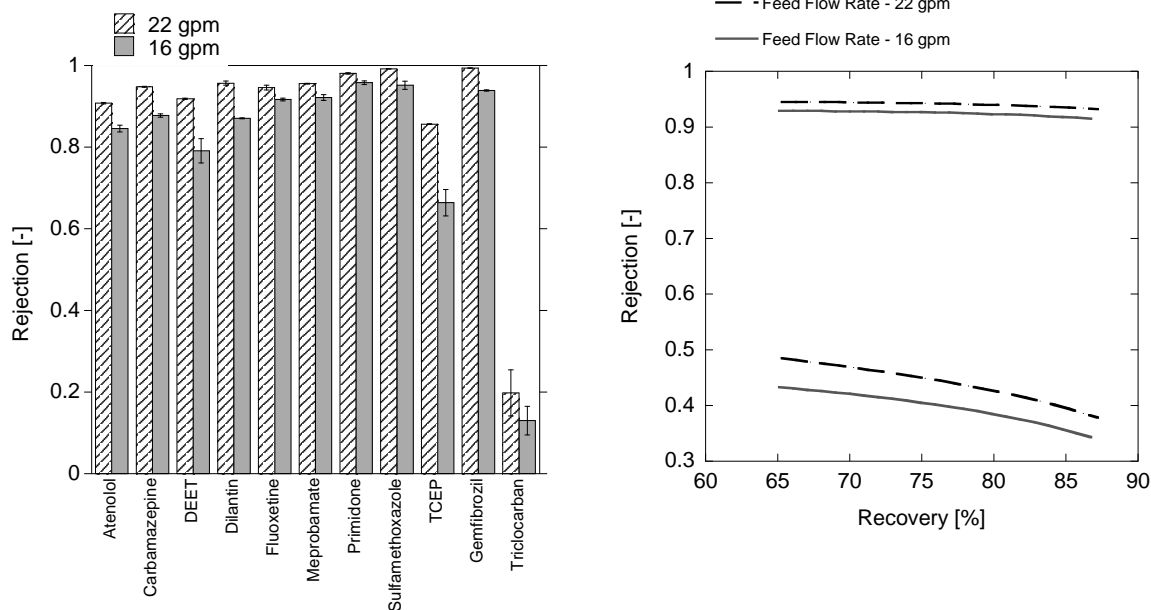


Figure 6.28. Rejection of contaminants at 16 and 22 gpm feed flow rate and 85% recovery during pilot-scale testing (left) and modeled rejection at 22 and 16 gpm (right).

6.3.6 Predicting Rejection Using Previously Developed QSPR Approach

The nonionic QSPR approach to predict $\text{Log } P_s$ and sigma was redeveloped by using several of the compounds quantified in the wastewater effluent as validation compounds. Carbamazepine, DEET, dilantin, meprobamate primidone, and TCEP were removed from the validation set, and the QSPR approaches developed previously were recalculated. The QSPR approach using Log solubility, second moment of the y axis charge density, and depth yielded a statistically significant correlation with experimental $\text{Log } P_s$ values ($R^2 = 0.88$). From the developed equation, the $\text{Log } P_s$ for carbamazepine (-6.46), DEET (-6.63), dilantin (-6.54), meprobamate (-6.16), primidone (-6.16), and TCEP (-6.56) was calculated. Sigma was calculated by using the monomodal pore size distribution presented in the previous chapter. An example using pilot-scale DEET data generated at a feed flow rate of 20 gpm is presented in Figure 6.29. Predicted rejection was in very good agreement with observed rejection, and permeate and concentrate concentrations were in general agreement with observed values.

The bench-scale phenomenological coefficients underpredicted the rejection of meprobamate and primidone, and these compounds' predicted $\text{Log } P_s$ values were very close to the bench-scale-derived values. Therefore, this approach underpredicted the rejection of primidone and meprobamate. Predicted rejection of carbamazepine and dilantin was within 5% of observed values at 70, 80, and 85%. TCEP rejection was overpredicted by approximately 5% at all recoveries evaluated.

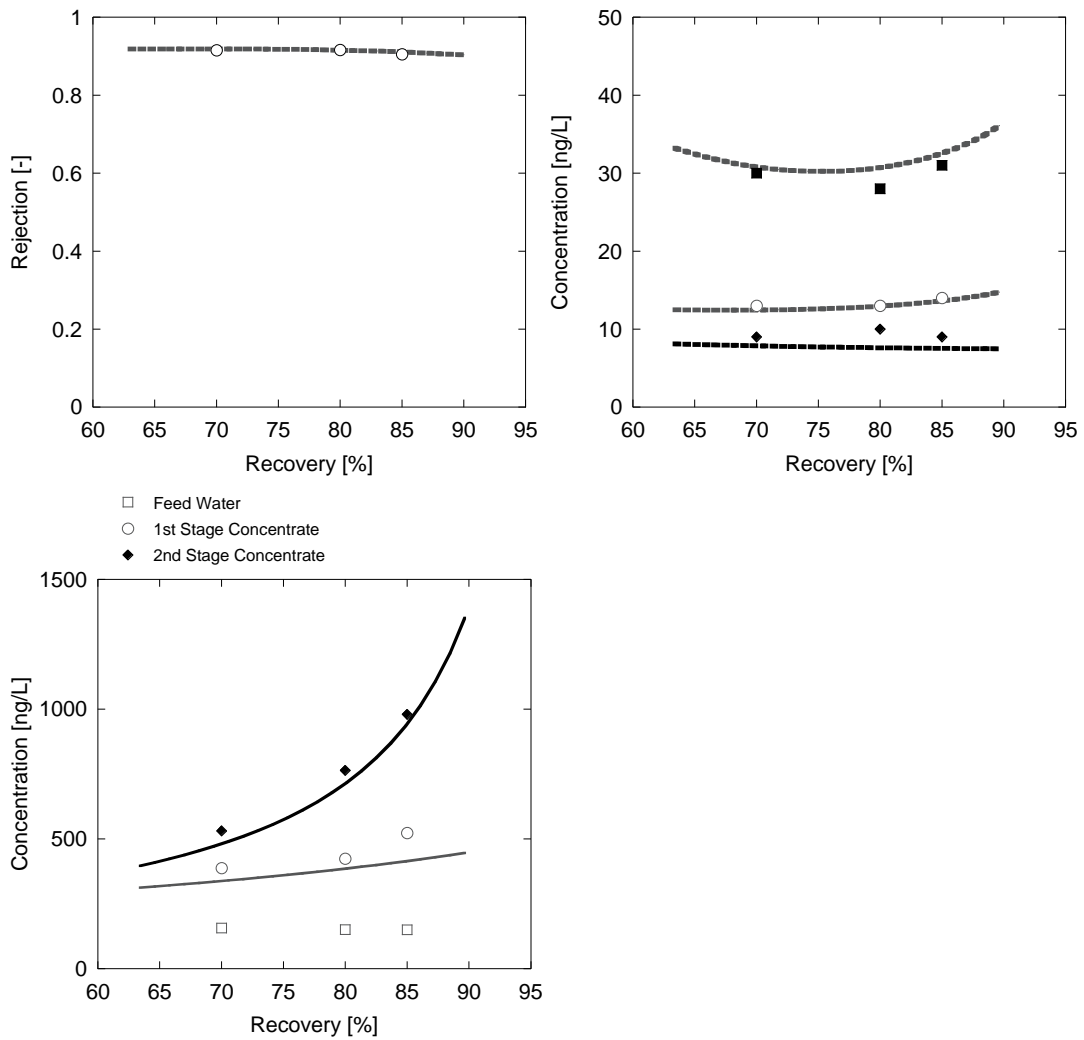


Figure 6.29. Observed and predicted DEET rejection values (top left) and observed and predicted permeate (right) and concentrate (bottom left) concentrations.

Note: Sigma was calculated as 0.99 and $\text{Log } P_s$ as -6.63 m/s.

6.4 Pilot-Scale Rejection Experiments Using the ESPA2 Reverse Osmosis Membrane

6.4.1 Experimental Conditions

Pilot-scale experiments were conducted with the pilot-scale RO system at CSM to develop a rejection data set for ESPA2 RO model validation. A multiday experiment was conducted by using synthetic feed water spiked with a suite of trace organic chemicals to assess the effect of operating conditions and experimental run time on rejection. Because of the MWCO of the ESPA2 membrane, it was anticipated that rejection would be greater than 90%; therefore, two sensitive LC/MS-MS methods (Chapter 3.2.5) were used for sample analysis. In addition to the low detection limit (< 50 ng/L), a large suite of compounds could be analyzed by using these methods.

For the pilot-scale experiment, approximately 450 gal of tap water was added to one of the two 500-gal tanks feeding the pilot-scale system. The water was first dechlorinated (with sodium metabisulfite) and then was filtered with the ESPA2 membrane. During the filtration step, the concentrate stream was wasted and the permeate stream collected in a second 500-gal tank and subsequently spiked with 34 compounds. The compounds that were tested by using the ESPA2 membrane pilot-scale experiment are listed in Table 3.4.

During all experiments, the feed flow rate was set at 20 gpm and temperature was maintained at approximately 18 °C. Three recovery set-points were evaluated over the 1st day of experimentation: the first sample was collected at a recovery of 85% (average permeate flux of 13.7 gfd), the second at 75% recovery (12.1 gfd), and the third at 60% recovery (9.7 gfd).

Once a recovery set-point was achieved, the system was allowed to run for 2 h before sampling took place. After collection of samples for the three recovery set-points, the recovery was again adjusted to 85% and was allowed to operate for 3 days. During this time, three more sampling events took place at approximately 24-h intervals. Before sampling occurred, feed water temperature, pH, and pressures and flow rates were recorded. Flow rates monitored included feed, combined permeate, first-stage permeate, second-stage permeate, first-stage concentrate, and combined concentrate. Samples were collected from each of these streams, and three 2-mL aliquots were collected in HPLC vials, while one 1-L bottle was filled with each of the permeate samples.

Following the completion of the multiday experiment, two additional, single-compound experiments were performed with glycerol and urea at concentrations high enough to be detected by using the HPLC method described in Section 3.2.3. The rejection of urea was tested for five different recovery set-points ranging between 65 and 85%, with feed flow rates of 22 and 16 gpm. Rejection of glycerol was examined for the same range of recoveries but was tested only at a feed flow rate of 22 gpm. Each experimental set-point was allowed to equilibrate for 1 h before sampling took place. The same set of samples was taken during these experiments as during the multiday experiment described earlier. Results from these experiments are presented in the following sections.

6.4.2 Analytical Results

As anticipated, a number of the compounds evaluated exhibited very high rejection by the ESPA2 membrane and were not detected in permeate samples by using the LC/MS-MS method. Compounds that were detected at levels above detection limits in more than one permeate sample are listed in Table 6.4. Methylparaben was detected in all samples but is omitted from many figures and analyses because of questionable analytical data. In the first four sample events methylparaben permeate and concentrate concentrations were each higher than the feed concentrations. This observation may be the result of the compound partitioning into the membrane.

There are several reasons that some compounds were not detected in any of the experimental samples. One reason is that, for compounds that are known to partition into membranes, such as various hormones, there may have been a large amount of mass that partitioned onto the membrane surface or into its polymer matrix. The pilot-scale system contains approximately 1785 sq ft of membrane surface area, and it is feasible that enough mass partitioned into the membrane material to decrease the feed concentration to levels below detection limits. Another possible explanation for not detecting certain compounds in the samples is the criterion for determining the detection limit. A signal-to-noise ratio of 30 was used to define the detection limit. Compounds with signal-to-noise ratios less than 30 were not quantified. For some compounds, the signal-to-noise ratio was much higher than for others and certain compounds with low signals were difficult to quantify. \

Table 6.4. Compounds Detected in All Samples from Pilot-Scale Experiment with ESPA2 Membranes by Using LC/MS-MS Method

Compounds Detected in All Samples		
Acetaminophen	Caffeine	Methylparaben
Atrazine	Cimetidine	Propylparaben
Atenolol	DEET	Sulfamethoxazole

Feed concentrations over the course of the experiment were evaluated to determine the loss of compound mass. Figure 6.30 presents the feed water concentrations for the nine compounds that were detected in all samples over the 4 days that the experiment took place. A noticeable decline was observed during the 1st day, after which the concentration stabilized for atenolol, trimethoprim, propylparaben, and cimetidine. An explanation for this trend is that a loss of mass onto and into the membrane polymer occurred relatively quickly until a level of saturation was reached. This theory would explain the early, rapid concentration decline and the subsequent period of relative stability. Atrazine, acetaminophen, caffeine, DEET, and sulfamethoxazole all remained relatively stable during the entire course of the experiment, although DEET exhibited a decrease on the last day of the experiment.

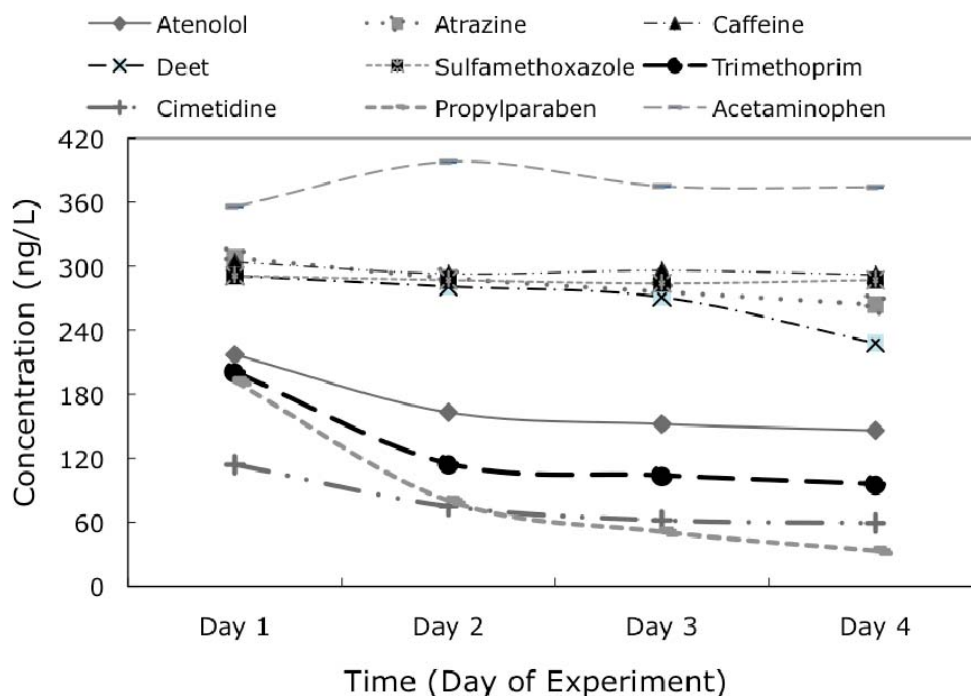


Figure 6.30. Feed water concentrations of nine compounds detected over the course of the multiday, pilot-scale experiment.

The main goal of the experiment was to develop a data set depicting compound rejection over a range of recoveries for as many compounds as possible. This data set could then be used to develop methods to scale up bench-scale models to larger systems such as pilot- and full-scale membrane treatment trains. Figures 6.31 and 6.32 present the rejection-versus-recovery curve for the five well-removed and four poorly removed compounds, respectively. For this section, well-removed compounds are those that had 85% rejection or higher in all samples. Poorly removed compounds are those that had at least one sample with a rejection level below that threshold.

Compounds that were well removed include atenolol, atrazine, DEET, sulfamethoxazole, and trimethoprim. The lowest molecular weight among these compounds was 191 g/mol for DEET. The rest of the compounds ranged from approximately 216 to 290 g/mol. Given that the MWCO for the ESPA2 membrane is between 70 and 100 g/mol, the most important rejection mechanism for each of these compounds is steric exclusion. The removal of these compounds varied between approximately 86% and 99%. Consistent among all the compounds is the lack of rejection variation across the range of recovery examined in this experiment. The data points for each individual compound remain within a 2 to 3% range. This observation is not surprising, given the limited range of flux in this experiment. In bench-scale experiments, flux typically spanned a range of 6 to 30 gfd, although the range was only 9.7 to 13.7 gfd in the pilot-scale experiment. Compounds that were poorly removed include caffeine, cimetidine, propylparaben, and acetaminophen. The rejection of these compounds as a function of recovery is presented in Figure 6.32.

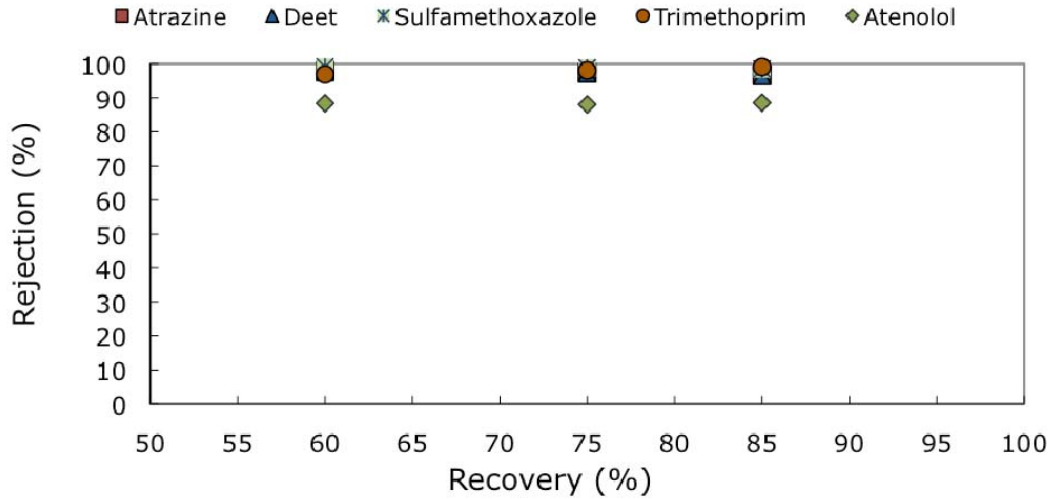


Figure 6.31. Rejection versus recovery for well-removed compounds in ESPA2 membrane pilot-scale experiment.

Cimetidine exhibited a gradual increase in rejection as recovery increased; however, this pattern is probably due to analytical error. Figure 6.32 presents the first-stage, second-stage, and combined permeate concentrations of cimetidine for the three recovery set-points. As expected, for a given recovery, the first-stage permeate concentration is lower than that of the second stage. The combined permeate concentration theoretically must fall between these two values, and because the flow rate is higher in the first stage than in the second stage, the combined permeate concentration should fall closer in value to that of the first stage. In Figure 6.33, it is clear that only the recovery of 60% behaves in this expected way. Therefore, an analytical error is likely associated with both the 75 and 85% recovery data.

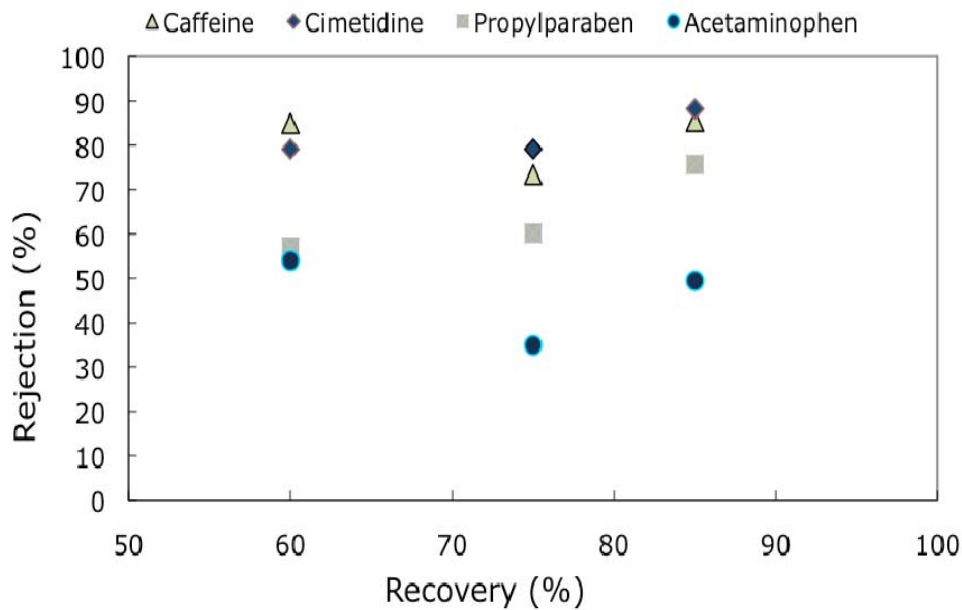


Figure 6.32. Rejection versus recovery for poorly removed compounds in ESPA2 membrane pilot-scale experiment.

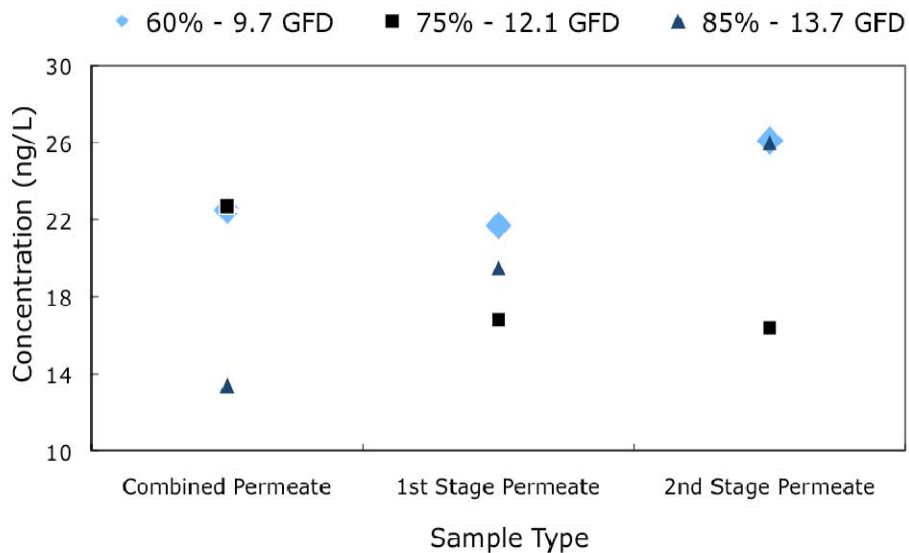


Figure 6.33. 1st-stage, 2nd-stage, and combined permeate concentrations of cimetidine for the three recovery set-points tested in the pilot-scale experiment with ESPA2 membranes.

Propylparaben permeate concentrations are presented in Figure 6.34. These data are consistent with the anticipated trend described in the previous paragraph. Also, a mass balance calculation performed during data analysis demonstrated that a weighted average of the combined concentrate and permeate concentrations correlated well with the measured

feed concentrations, indicating that the data are reliable. These two observations suggest that the trend observed for propylparaben of increasing rejection with increasing flux is accurate.

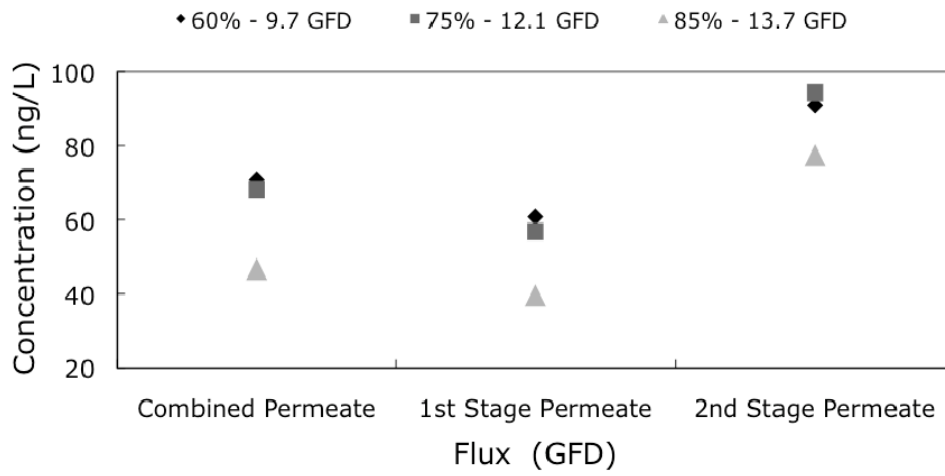


Figure 6.34. 1st-stage, 2nd-stage, and combined permeate propylparaben concentrations for the three recovery set-points tested in the pilot-scale experiment with ESPA2 membranes.

Acetaminophen and caffeine both have their lowest rejection at a flux of 75% and similar rejection levels at 60 and 85%. It is unclear what caused the rejection to “dip” at the middle recovery point for each of these two compounds. Most compounds exhibit increased removal with increasing recovery. For some compounds, however, a decline in removal followed by an incline after a certain level of recovery has been observed but is unprecedented and therefore is probably linked to analytical error.

Data from the experiments with urea and glycerol are presented in Figures 6.35 and 6.36, respectively. Both of these compounds exhibited stable rejection across the range of recoveries tested in the experiments. Approximately 20 to 25% of urea was rejected by the ESPA2 membranes in the pilot-scale experiment, whereas glycerol was removed at percentages between 90 and 95%. Analytical results from these two experiments are more reliable than those from the multiday experiment as they were spiked at elevated levels and then measured by using the HPLC method, which is a much simpler method. Because this method involves fewer steps, it may introduce less error. These data are useful for scaling up models developed at the bench scale in order to obtain pilot-scale data for two compounds that are consistently present in the permeate of installations that employ the ESPA2 RO membrane.

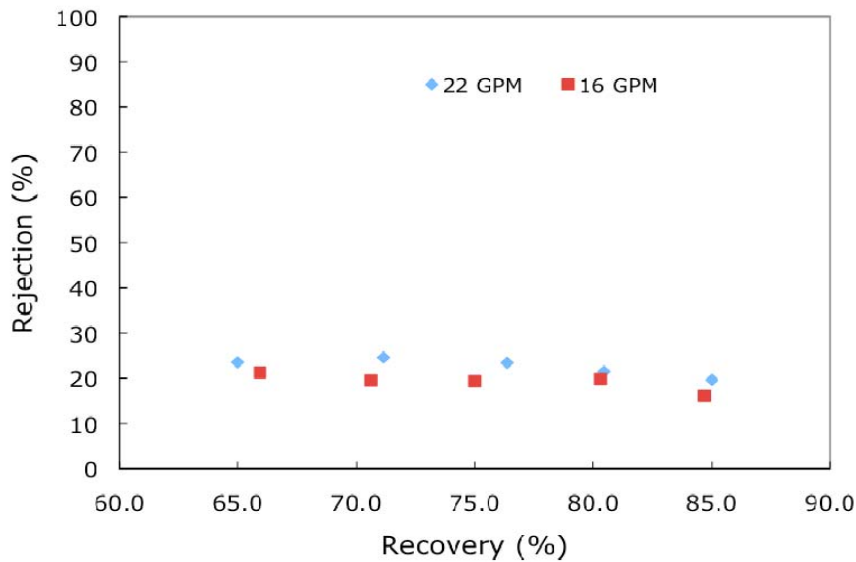


Figure 6.35. Rejection versus recovery for urea in ESPA2 membrane pilot-scale experiment.

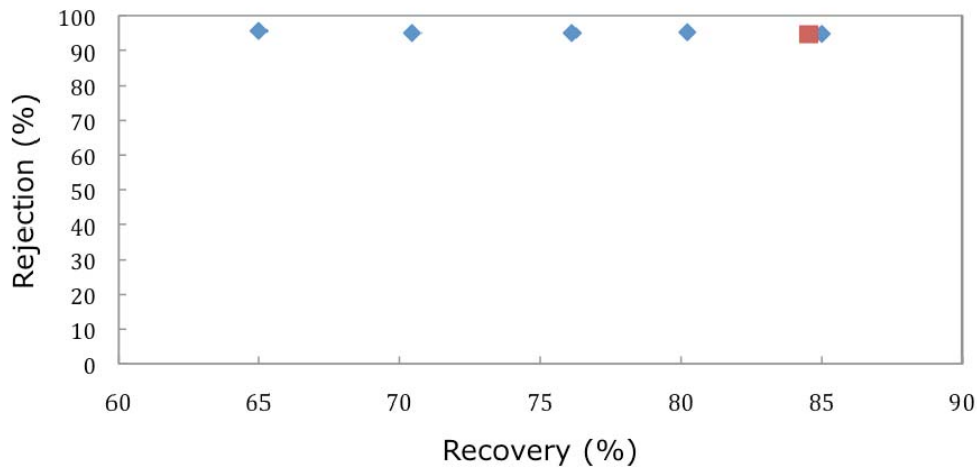


Figure 6.36. Rejection versus recovery for glycerol in ESPA2 membrane pilot-scale experiment.

6.4.3 QSPR Model ESPA2 Membrane

The QSPR model developed for the ESPA2 membrane, restated in Equation 6.14, yielded an R^2 of 0.75 and RMSE of 0.346 and was applied to the ESPA2 pilot-scale data, presented in Figure 6.37.

$$\text{Ref}(\log \text{Removal}) = -1.11e^{-8} \text{FOSA} + 6.207E_{\text{HOMO}} + 4.72e^{-8} \text{SASA} + 1.333 \quad (6.14)$$

The model was internally validated, yielding a q^2 of 0.66, and externally validated, yielding an R^2 of 0.74. Almost half of the compounds were predicted out of range (Table 6.5). Some

outliers could be due to experimental error such as acetaminophen and caffeine having relatively low rejection.

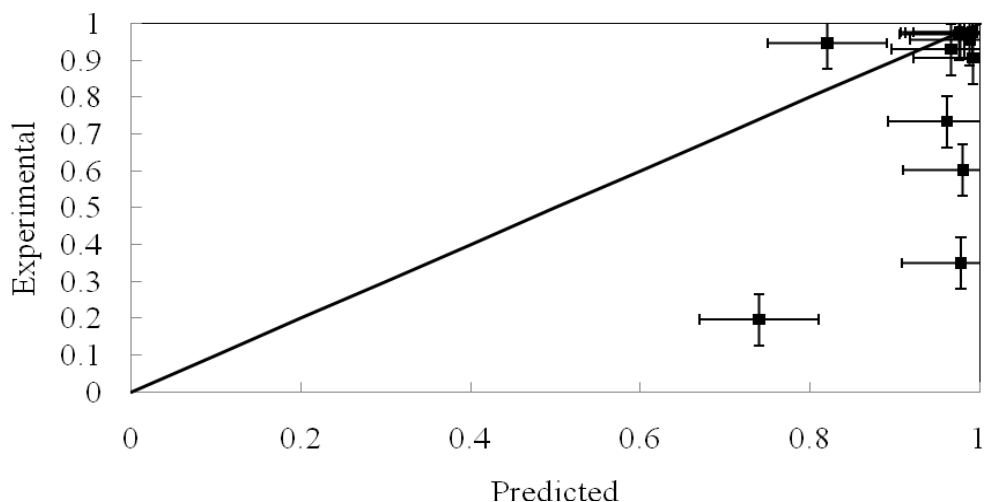


Figure 6.37. Experimental rejection for the ESPA2 membrane pilot scale compared to predicted rejection using the QSPR.

Table 6.5. ESPA2 Pilot-Scale Rejection, Predicted QSPR Rejection, and Percentage Difference from Experimental Pilot-Scale Data

Compound Name	Class	Pilot-Scale Avg 12-gfd Rejection	QSPR Predicted Rejection	% Difference
Atrazine	HHoN	0.98	0.98	1%
Carbamazepine	HHoN	0.98	0.99	1%
DEET	HHoN	0.98	0.98	0%
Propylparaben	HHoN	0.60	0.98	38%
Acetaminophen	HN	0.35	0.98	63%
Caffeine	HN	0.73	0.96	23%
Primidone	HN	0.97	0.98	1%
TCPP	HN	0.96	0.99	3%
TCEP	HN	0.93	0.97	4%
Glycerol	HN	0.95	0.82	-13%
Urea	HN	0.20	0.74	54%
Triclosan	HoN	0.91	0.99	9%

On the basis of the size of acetaminophen (molecular weight of 151 g/mol) and caffeine (molecular weight of 194) and the MWCO of the ESPA2 membrane (about 100 g/mol), acetaminophen and caffeine should exhibit rejection greater than 90%. Propylparaben (molecular weight of 180 g/mol) also exhibited lower-than-expected rejection based on steric interactions. Urea was also overpredicted because of its high FOSA value; however, the molecular weight of urea is below the MWCO so the low rejection was expected. This

observation was also seen at bench scale, indicating that it could be a limitation of the QSPR model.

6.4.4. Application of the Rejection Diagram to the ESPA2 Membrane

The rejection diagram provided a moderate fit for the ESPA2 pilot-scale data. The application of the rejection diagram at pilot scale is presented in Figure 6.38 and Table 6.7. The experimental and predicted rejections are listed in Table 6.6 with the respective rejection ranges and error percentages. Figure 6.38 presents the predicted rejection as it relates to the experimental rejection with error bars representing the rejection range predicted.

Propylparaben, acetaminophen, caffeine, and urea were predicted out of range. Experimental rejection values for propylparaben, acetaminophen, and caffeine were lower than expected on the basis of their size possibly because of experimental error. Urea was overpredicted by 10%. All other compounds tested at pilot scale were predicted within range. The model is simple to use and can predict rejection for most compounds for the ESPA2 membrane.

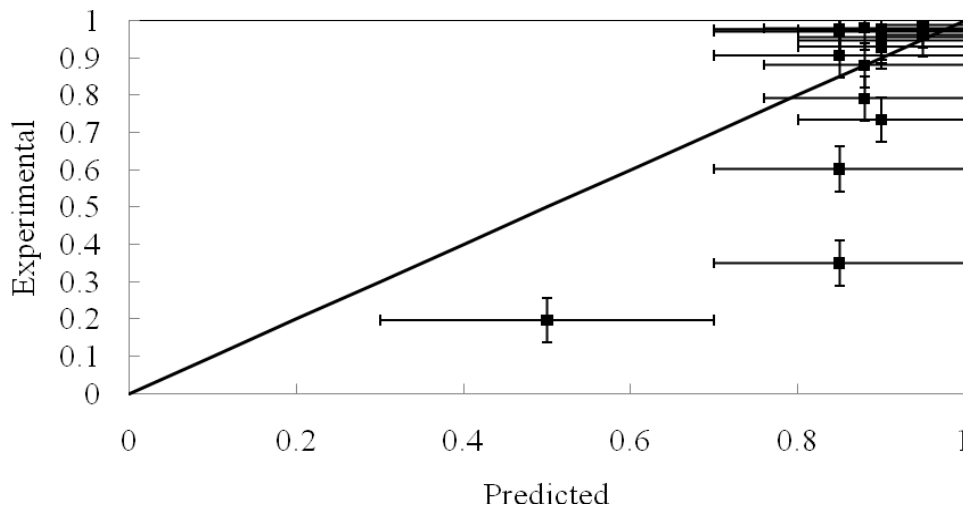


Figure 6.38. ESPA2 membrane pilot-scale rejection compared to the rejection predicted from the updated rejection diagram.

Table 6.6. Bench- and Pilot-Scale Rejection, Predicted Rejection from Rejection Diagram, and Percentage Difference from Experimental Pilot-Scale Data for ESPA2 Membrane

Compound Name	Class	Pilot-Scale Avg 12-gfd Rejection	Rejection Diagram Predicted Rejection	Rejection Range (+/-)	%Difference
Sulfamethoxazole	HCN	0.99	0.95	5%	-4%
Gemfibrozil	HCN	0.96	0.95	5%	-1%
Atenolol	HCP	0.88	0.88	12%	0%
Cimetidine	HCP	0.79	0.88	12%	9%
Trimethoprim	HCP	0.98	0.88	12%	-10%
Carbamazepine	HHoN	0.98	0.85	15%	-13%
DEET	HHoN	0.98	0.85	15%	-13%
Propylparaben	HHoN	0.60	0.85	15%	25%
Atrazine	HHoN	0.98	0.90	10%	-8%
Urea	HN	0.20	0.50	20%	30%
Primidone	HN	0.97	0.85	15%	-12%
Acetaminophen	HN	0.35	0.85	15%	50%
Caffeine	HN	0.73	0.90	10%	17%
TCPP	HN	0.96	0.90	10%	-6%
TCEP	HN	0.93	0.90	10%	-3%
Glycerol	HN	0.95	0.90	10%	-5%
Triclosan	HoN	0.91	0.85	15%	-6%

6.4.5 Phenomenological Model for the ESPA2 Membrane

Bench-scale-derived phenomenological model coefficients were input into the differential element model calibrated for the ESPA2 membrane to describe the rejection of organic solutes as a function of recovery at pilot scale. Several examples of this modeling approach are presented in Figure 6.39. Of the solutes presented, the worst model fit was found for the rejection of acetaminophen, which was significantly overpredicted. Model fits for the other solutes examined were in the range of experimental rejection values; however, atrazine and sulfamethoxazole were underpredicted by approximately 2 to 5% by using this approach. Similar results were observed for NF-270 membrane pilot-scale results; that is, the pilot model underestimated the experimental rejection for several compounds.

One limitation of the phenomenological model is that, in the range of permeate flux evaluated, rejection is strongly dependent on the solute permeability coefficient (P). This parameter can be difficult to fully evaluate because it requires the determination of rejection at very low permeate flux. Although bench-scale ESPA2 membrane experiments included two flux set-points below 10 gfd (i.e., 3 and 7 gfd), the shape of the rejection curve could not always be fully characterized at low permeate flux. Compounds with high rejection (e.g., atrazine and sulfamethoxazole) have relatively flat rejection-versus-flux curves, which make

model fitting, especially at low permeate flux, a challenge. The major issue associated with characterizing rejection at low permeate flux is the time it takes to process an acceptable amount of permeate before a sample is taken for analysis. For the SEPA cells used, achieving a permeate flux of 3 gfd requires a permeate flow rate of approximately 1 mL/min. Approximately 250 mL of permeate was processed through the membrane before samples were collected for analysis and required approximately 4 h at a permeate flux of 3 gfd.

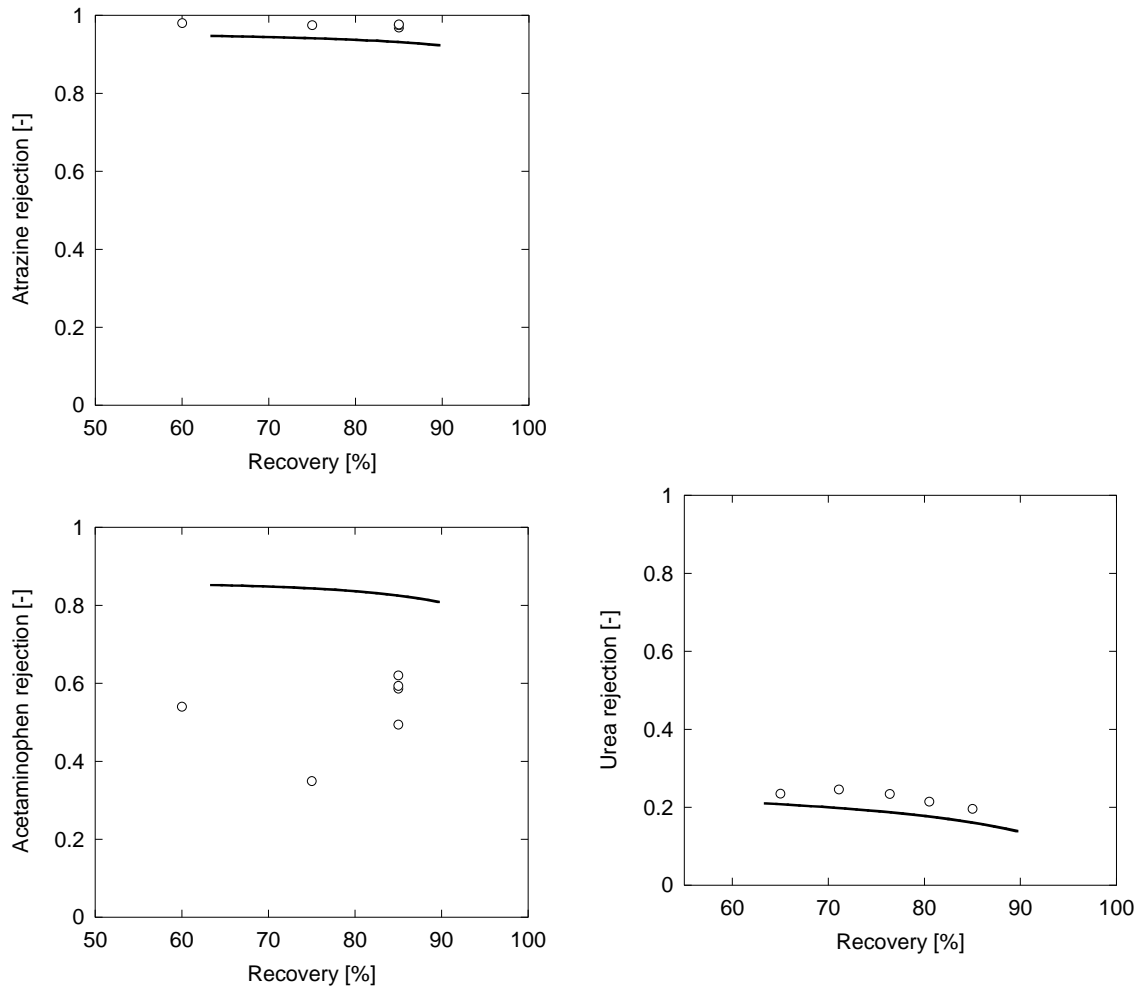


Figure 6.39. Pilot-scale rejection of organic solutes with phenomenological model fits using coefficients derived from bench-scale experiments

Chapter 7

Validation of Rejection Models at Full Scale

7.1 Full-Scale Sampling Campaign

A full-scale sampling campaign was performed at the Orange County Water District (OCWD)'s Ground Water Replenishment (GWR) System to quantify the removal of organic contaminants by the ESPA2 membrane and to develop a data set for model validation at full scale. Samples were collected from the feed water, interstage permeate, and concentrate (waste stream) streams (Stages 1 and 2), combined permeate stream, and combined concentrate stream. For data set development purposes, samples were collected over a range of recovery set-points. The team had initially planned to sample at recoveries of 65, 75, and 85%. Unfortunately, the full-scale system could not be manipulated below 76% recovery. The team evaluated 76, 78, and 84% recoveries during the sampling event.

The concentrations of the organic contaminants that were quantified in the GWR RO feed water are presented in Figure 7.1. Out of the target analytes, only two solutes, bisphenol A and octylphenol, could not be quantified in the RO feed water. Concentrations of the quantified organic contaminants varied from the low nanograms per liter level to low micrograms per liter. It is important that the error bars in Figure 7.1 are calculated from the concentration variation in triplicate samples.

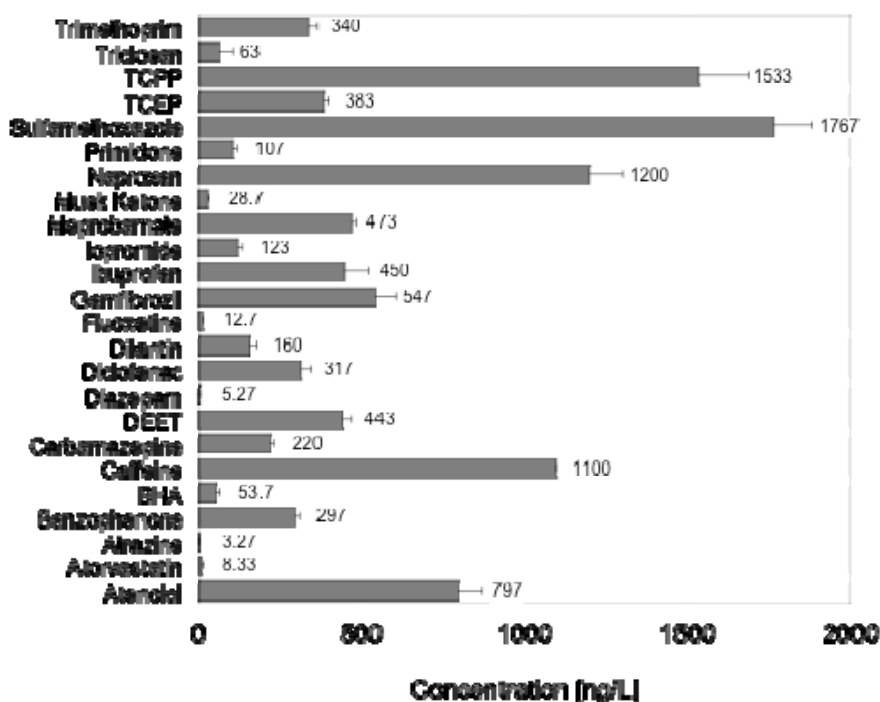


Figure 7.1. Feed concentration of organic compounds quantified in OCWD's RO feed water (error bars calculated from triplicate samples).

Note: BHA = bisphenol A

Overall rejection values for the compounds quantified in the RO feed water for each recovery set-point are presented in Table 7.1. For many of the compounds, rejection was close to 100% as the compound could not be quantified in the combined permeate samples. Very low concentrations of DEET, atenolol, trimethoprim, meprobamate, gemfibrozil, ibuprofen, naproxen, sulfamethoxazole, and fluoxetine were quantified in one or more combined permeate samples, resulting in rejection greater than 99%. The high rejection for these compounds was expected because of electrostatic interactions for the ionic compounds and steric interactions for the nonionic compounds, given that the nonionic compounds had a molecular weight greater than the MWCO for the ESPA2 membrane (100 Da) (Agenson et al., 2003; Bellona et al., 2004; Kimura et al., 2004; Van der Bruggen et al., 1999; Verliefe et al., 2007; Ozaki and Li, 2002).

Table 7.1. Rejection Values for Sampling Campaign Performed at OCWD’s Full-Scale RO Facility

Compound	Rejection: 76% Recovery	Rejection: 78% Recovery	Rejection: 84% Recovery	Type	Mol Wt	Log D (6)
Benzophenone	0.673	0.729	0.732	Neutral	182.2	3.18
DEET	0.997	0.997	0.997	Neutral	191.3	1.96
Caffeine	1.000	1.000	1.000	Neutral	194.2	-0.13
Ibuprofen	0.997	0.996	1.000	Negative	206.3	2.12
Atrazine	1.000	1.000	1.000	Neutral	215.7	2.63
Meprobamate	0.999	0.999	0.999	Neutral	218.3	0.70
Primidone	1.000	1.000	1.000	Neutral	218.3	0.40
Naproxen	0.999	0.999	1.000	Negative	230.3	1.81
Carbamazepine	1.000	1.000	1.000	Neutral	236.3	2.67
Gemfibrozil	0.999	1.000	0.999	Negative	250.3	3.12
Dilantin	1.000	1.000	1.000	Neutral	252.3	2.52
Sulfamethoxazole	1.000	0.999	0.999	Positive	253.3	0.49
Atenolol	0.998	0.998	0.998	Positive	266.3	-2.73
Diazepam	1.000	1.000	1.000	Negative	284.8	2.96
TCEP	1.000	1.000	1.000	Neutral	285.5	0.48
Triclosan	0.976	0.431	0.919	Neutral	289.5	5.17
Trimethoprim	0.998	0.998	0.998	Positive	290.3	-0.42
Musk ketone	1.000	1.000	1.000	Neutral	294.3	3.86
Diclofenac	1.000	1.000	1.000	Negative	295.1	2.23
Fluoxetine	1.000	0.959	1.000	Neutral	309.3	1.03
TCCP	1.000	1.000	1.000	Neutral	327.6	1.53
Bisphenol A	1.000	1.000	1.000	Neutral	360.5	3.50
Atorvastatin	1.000	1.000	1.000	Negative	558.6	2.41
Iopromide	1.000	1.000	1.000	Neutral	791.1	-2.95

Benzophenone was only moderately (60–80%) rejected by the ESPA2 membrane. Benzophenone has a molecular weight (182 g/mol) greater than the MWCO of the ESPA2 membrane and therefore should exhibit greater rejection than 60 to 80% on the basis of steric exclusion. However, benzophenone is relatively hydrophobic (Log D of 3.18) and does exhibit adsorptive properties that were observed at bench scale for the NF-270 membrane, which could cause a decrease in observed rejection. Compound rejection remained constant over the recovery range that was investigated for most compounds except for triclosan.

Triclosan exhibited 97% and 91% rejection for recovery set-points of 76 and 84%, respectively; however, for 78% recovery, triclosan was rejected by only 43%. This large decrease in rejection could be due to experimental error or to the adsorptive effects of triclosan that were observed at bench scale.

On the basis of these and past results, the ESPA2 membrane reduces concentration of the compounds in the feed water to levels in the combined permeate that are at or below the detection level of the LC/MS-MS method. Although many of the compounds were below the detection limit in the combined permeate samples, sampling across the full-scale RO train allowed for the evaluation of permeate concentrations and rejection values for each stage of the system. An example of the first-stage, second-stage, third-stage, and combined permeate concentrations at 84% recovery is presented in Figure 7.2. In general, concentrations in the first-stage permeate are very low, usually below the detection level of the LC/MS-MS method. As the water leaves the first stage, however, the feed water becomes more concentrated and the permeate flux decreases, which yields higher second- and third-stage permeate concentrations. Because the permeate flow from the first stage is greater than that of the second and third stages and because the concentration is so low, the combined permeate is often also very low. Sampling the full system, therefore, offers a few advantages over sampling only the feed and combined permeate streams: namely, that the data can be used for modeling purposes and that the contribution of mass from each stage into the final permeate can be quantified.

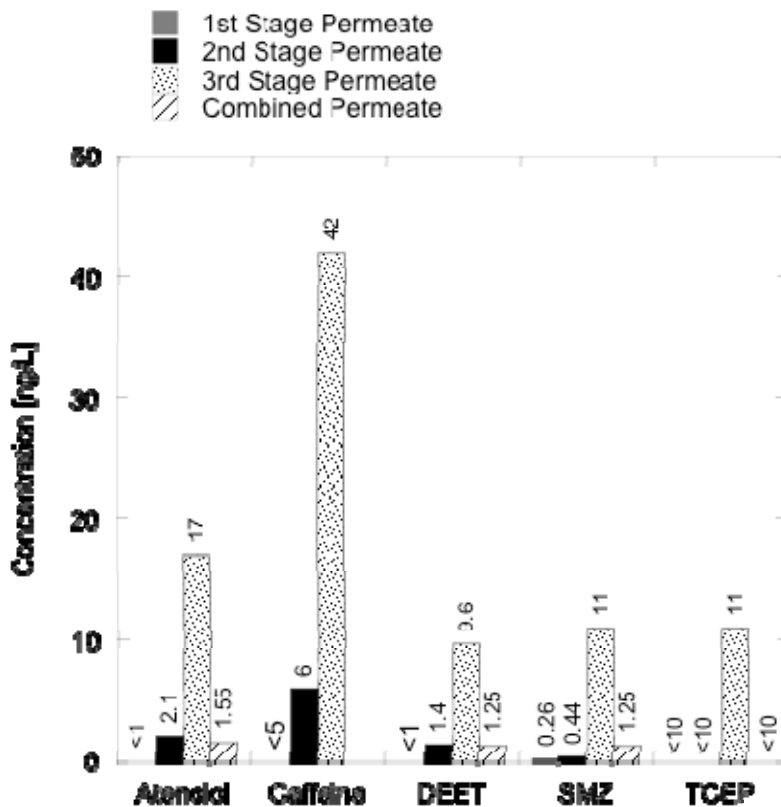


Figure 7.2. ESPA2 membrane permeate concentrations for five compounds

Note: SMZ = sulfamethoxazole

7.2 Quantitative Structure Property Relationship Model

The QSPR developed at bench scale for the ESPA2 membrane was applied to the compounds investigated at full scale. The QSPR model, restated in Equation 7.1, yielded an R^2 of 0.75 and RMSE of 0.346 at bench scale.

$$Ref(\log Removal) = -1.11e^{-3}FOSA + 6.207E_{HOMO} + 4.72e^{-3}SASA + 1.333 \quad (7.1)$$

The predicted rejection is compared to rejection results from full scale at 84% recovery and 12 gfd, presented in Figure 7.3 and Table 7.2. The error bars in Figure 7.3 are the experimental deviation in the y direction and the model confidence intervals in the x direction. All compounds except benzophenone were predicted within the confidence interval range. During bench-scale testing with the NF-270 membrane, benzophenone exhibited adsorptive interactions with the membrane causing a decrease in rejection over time. This behavior was not observed at bench scale with the ESPA2 membrane, possibly because of the brevity of the experiments. The initial saturation of the compound onto the ESPA2 membrane before adsorption would occur could require a longer period than needed for saturation onto the NF-270 membrane. Because full-scale operations are continuous, the membranes were fully saturated at the time of sampling; therefore, benzophenone was partitioning into the permeate stream, resulting in lower rejection than expected based on the size of the compound.

All compounds investigated at full scale, with the exception of benzophenone, were predicted within range. This finding indicates that a QSPR model developed at bench scale can be used to predict the rejection at full-scale operations by using the ESPA2 membrane. Rejection can be predicted only by obtaining the FOSA, SASA, and E_{HOMO} values for a given compound.

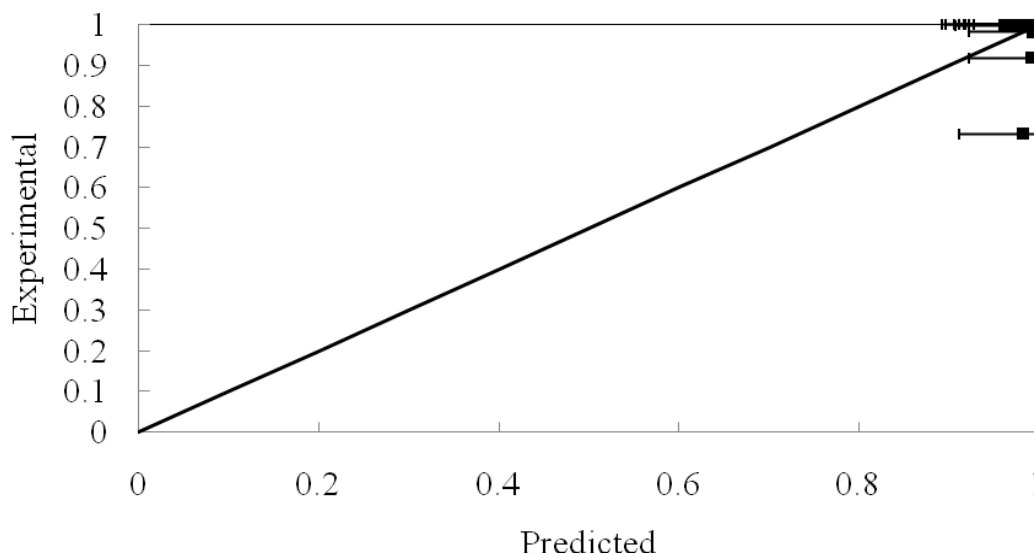


Figure 7.3. Experimental full-scale ESPA2 membrane rejection compared to QSPR predicted rejection.

Table 7.2. ESPA2 Membrane Full-Scale Rejection, Predicted QSPR Rejection, and Percentage Difference from Experimental Full-Scale Data

Compound Name	Class	Full-Scale Avg 12-gfd Rejection	QSPR Predicted Rejection	Percentage Difference
Atrazine	HHoN	1.00	0.98	-2%
Carbamazepine	HHoN	1.00	0.99	-1%
DEET	HHoN	1.00	0.98	-2%
Dilantin	HHoN	1.00	0.99	-1%
Caffeine	HN	1.00	0.96	-4%
Primidone	HN	1.00	0.98	-2%
TCPP	HN	1.00	0.99	-1%
TCEP	HN	1.00	0.97	-3%
Benzophenone	HoN	0.73	0.98	25%
Bisphenol A	HoN	0.98	0.99	1%
Fluoxetine	HoN	1.00	1.00	0%
Triclosan	HoN	0.92	0.99	7%

7.3 Phenomenological Model

An approach was developed to model rejection data obtained through a sampling campaign at a water reuse facility employing the ESPA2 membrane. Samples for organic contaminant analysis were collected across the full-scale system operating at 76, 78, and 84% recovery. In order to span a relatively broad range of recoveries (76–85%), the feed flow rate had to be reduced below the normal set-point. As a result, samples were collected across the system at system recoveries of 84, 78, and 76% by decreasing the feed flow rate.

The full-scale facility does not monitor permeate or concentrate flow rates for individual stages in the three-stage system. Thus, to model overall rejection, it was necessary to estimate flow rates from individual stages by using Hydranautics' membrane system design tool (IMS Design). The system configuration, measured permeate flow rate, and recovery were input into IMS Design, and the permeate flow rate for each stage was determined at the three recoveries evaluated. To more accurately characterize the permeate flux of each stage, experimentally determined feed water quality data (e.g., inorganic ions and pH) was input into IMS Design. Once the permeate flow rate was determined, the permeate flux was calculated for each stage. A simple mass balance model was developed that used the phenomenological model to calculate rejection for each stage. Unlike the pilot model previously discussed, an average permeate flux rate was used for each stage rather than breaking each stage into smaller elements. Additionally, concentration polarization was not considered in the modeling approach as the hydrodynamic conditions could not be assessed.

With the exception of benzophenone and triclosan, rejection of all of the compounds quantified in the feed water was greater than 99%. Fitting the phenomenological/mass balance model to rejection data for these compounds required sigma values greater than 0.99 and permeability coefficients (P) significant less than 10^{-8} m/s. Bench-scale experimentally derived permeability coefficients for the ESPA2 membrane were generally in the range of 10^{-7} to 10^{-8} m/s, which would have resulted in an underestimation of rejection. This finding

implies that, although bench-scale rejection experiments could be used to estimate the rejection of organic contaminants at a larger-scale membrane system (i.e., pilot-scale system) employing virgin or rather unfouled membrane elements, this approach would underestimate the rejection of a system employing membranes that had been in operation for a long time. Although this situation cannot be explained with certainty, membrane compaction and fouling could be potential explanations.

For the modeling exercise, the phenomenological model parameters were manipulated to fit experimental rejection although also approximating experimentally determined permeate and concentrate concentrations. Examples of model fits using this approach are presented in Figures 7.4 through 7.7 for atenolol, DEET, benzophenone, and meprobamate, respectively. This simple approach was effective for describing concentration gradients across the membrane system and could be used to model rejection if phenomenological coefficients are known. It is worth noting that, although it can be a significant challenge to quantify organic contaminants in a wastewater matrix at the parts-per-trillion level and permeate samples at very low concentrations, analytical data generally agreed with mass balance calculations. Through this approach, the actual presence of organic contaminants in permeate samples (versus false positives from contamination) could be evaluated with greater levels of confidence than by just measuring feed and combined permeate samples. In addition, by sampling across a membrane system, especially the latter stage's permeate concentrations, an estimation of a solute's combined permeate concentration can be provided. For example, combined permeate concentrations of the chlorinated flame retardant TCEP were below quantification level; however, third-stage permeate concentrations were used in conjunction with feed and concentrate concentrations, and model results indicate that this compound would be present in the combined permeate stream at 3 to 4 ng/L (Figure 7.8).

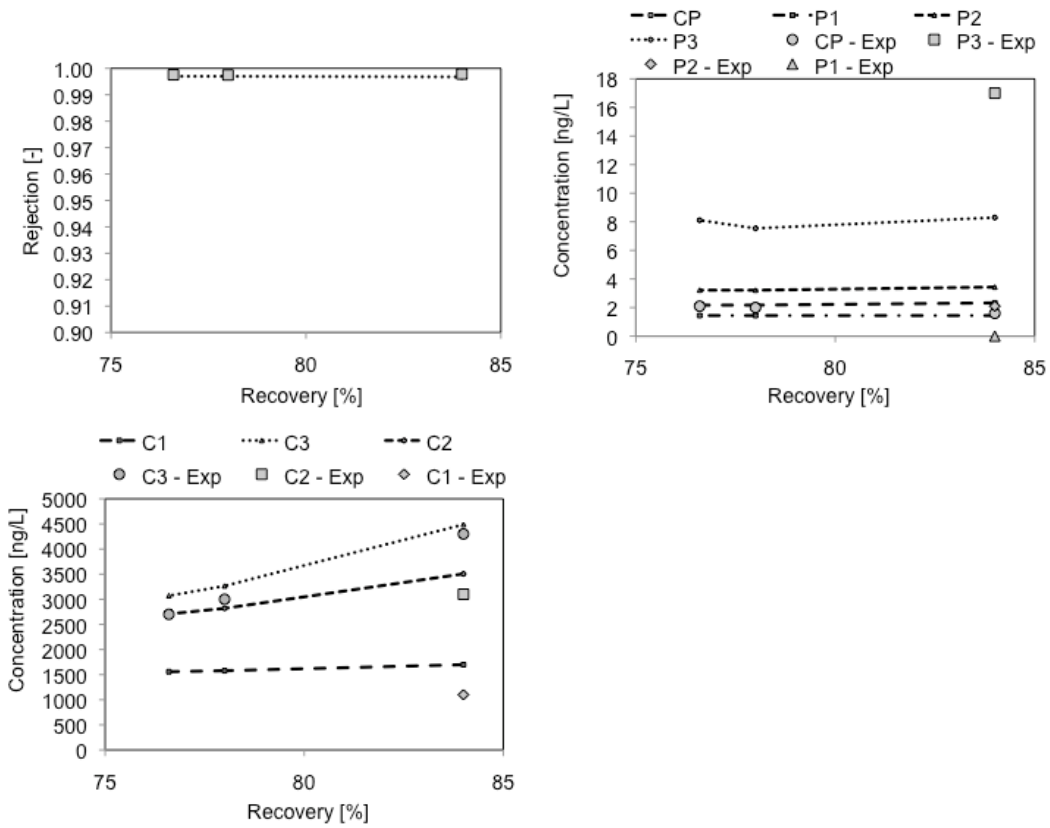


Figure 7.4. Rejection of atenolol (top left), atenolol permeate concentrations (top right), and concentrate concentrations (bottom left).

Note: For phenomenological model fits, sigma was 0.998 and P was $2E-9$ m/s.

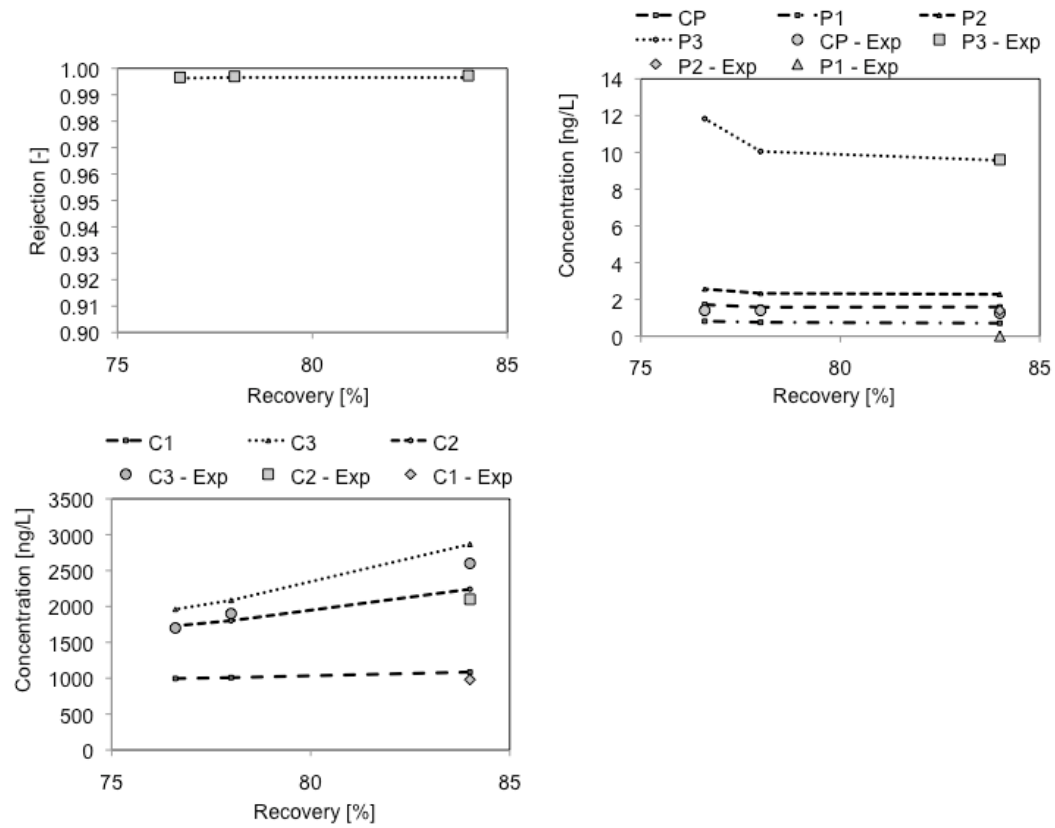


Figure 7.5. Rejection of DEET (top left), DEET permeate concentrations (top right), and concentrate concentrations (bottom left).

Note: For phenomenological model fits, sigma was 0.998 and P was 7E-9 m/s.

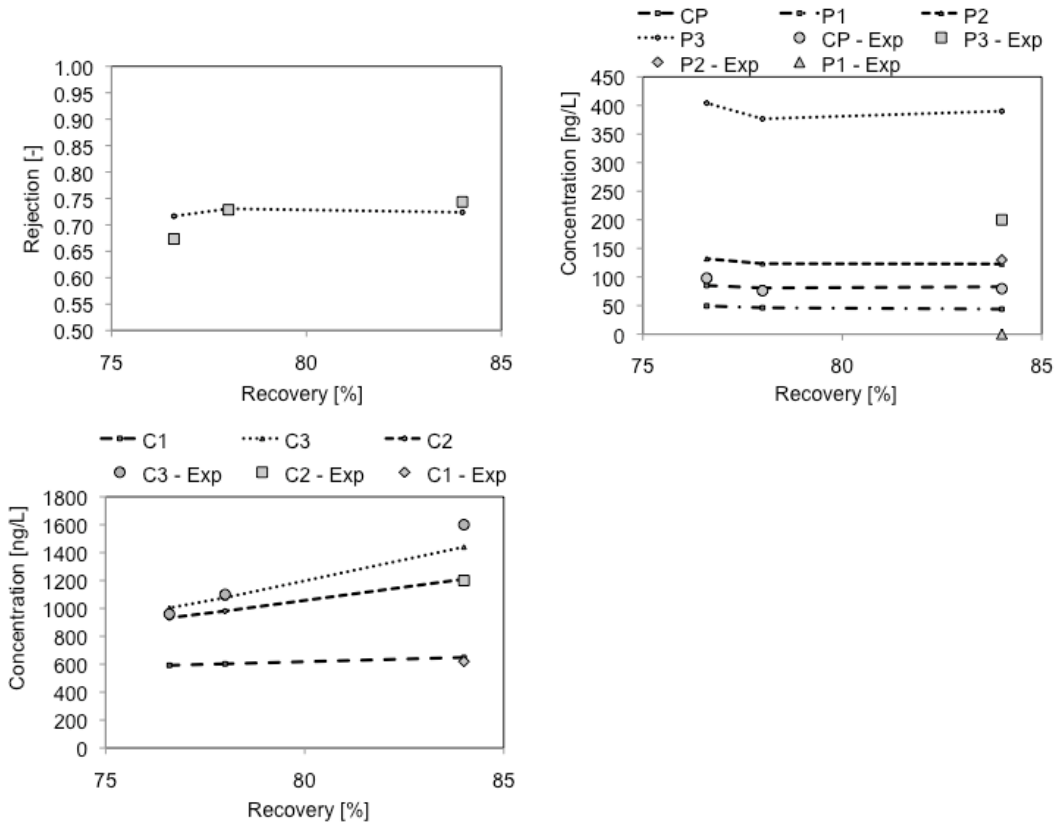


Figure 7.6. Rejection of benzophenone (top left), benzophenone permeate concentrations (top right), and concentrate concentrations (bottom left).

Note: For phenomenological model fits, sigma was 0.9 and P was $7E-7$ m/s.

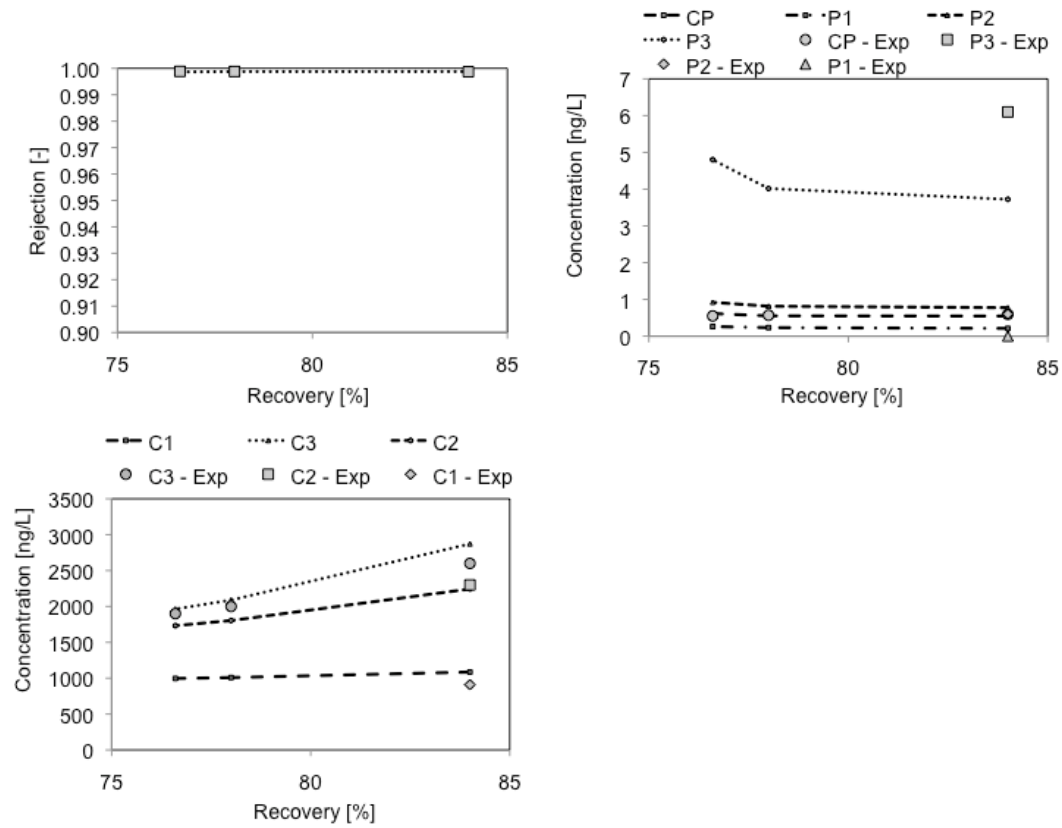


Figure 7.7. Rejection of meprobamate (top left), meprobamate permeate concentrations (top right), and concentrate concentrations (bottom left).

Note: For phenomenological model fits, sigma was 0.9999 and P was $3E-9$ m/s.

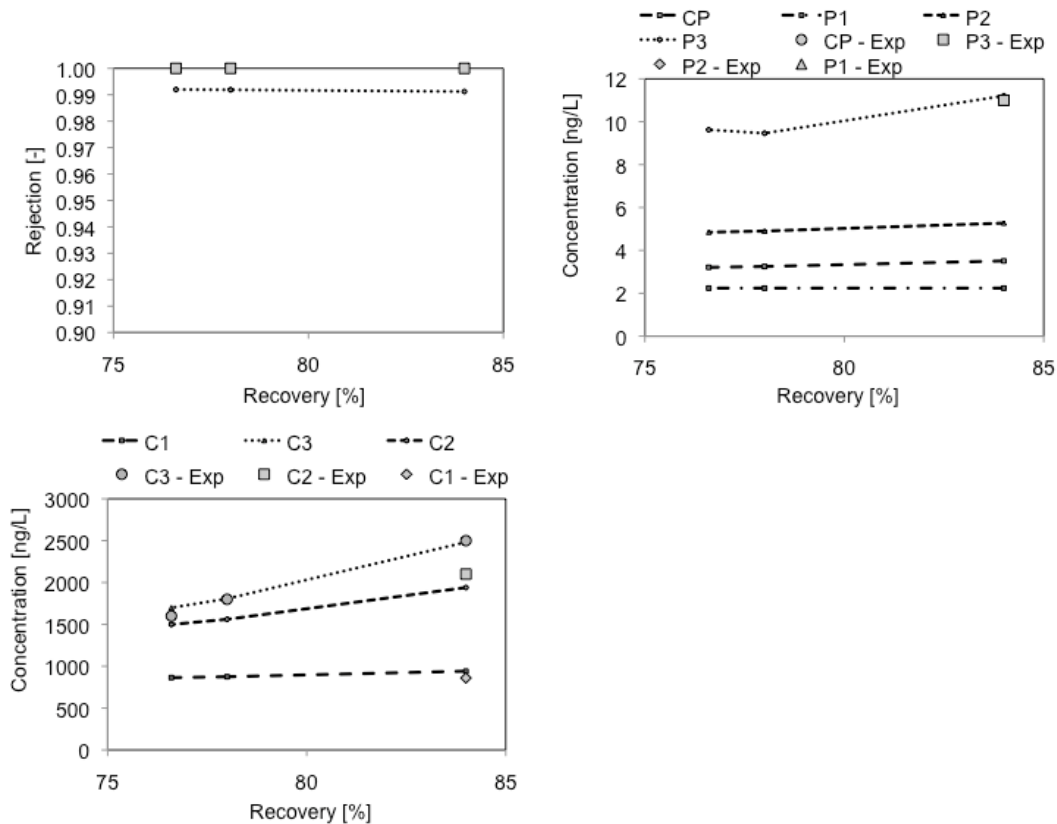


Figure 7.8. Rejection of TCEP (top left), TCEP permeate concentrations (top right), and concentrate concentrations (bottom left).

Note: For phenomenological model fits, sigma was 0.994 and P was $3E-9$ m/s.

One of the main reasons why the development of modeling approaches to describe the rejection of organic contaminants has been of such interest over the past decade is the occurrence and subsequent poor removal of NDMA during water reuse applications. Although NDMA was not one of the analytes measured during the sampling campaigns, the research team has evaluated the rejection of NDMA at other full-scale water recycling facilities employing the ESPA2 membrane (Bellona et al., 2008). Bench-scale NDMA rejection data fit with the phenomenological model resulted in a reflection coefficient of 0.89 and a permeability coefficient of $3.3E-6$ m/s. Placing these values in the full-scale phenomenological/mass balance model resulted in a predicted full-scale rejection of approximately 40%. Past NDMA sampling results from a water reuse facility demonstrated ESPA2 membrane rejection of NDMA at approximately 30% (Bellona et al., 2008).

7.4 Rejection Diagram

The rejection diagram updated with bench-scale NF-270 membrane data was applied to compounds investigated at full scale. The rejection diagram provided an excellent fit for the ESPA2 membrane full-scale data. The application of the rejection diagram at full scale is presented in Figure 7.9 and Table 7.3. Figure 7.9 compares the predicted rejection with experimental full-scale rejection, with error bars representing the predicted rejection ranges.

All compounds investigated at full scale were predicted within the rejection ranges, even benzophenone, which was inaccurately predicted at full scale with the QSPR model. This finding indicates that the rejection diagram is an effective way to predict rejection. The model is simple to use and can predict rejection within a range for bench, pilot, and full scales for two different membranes.

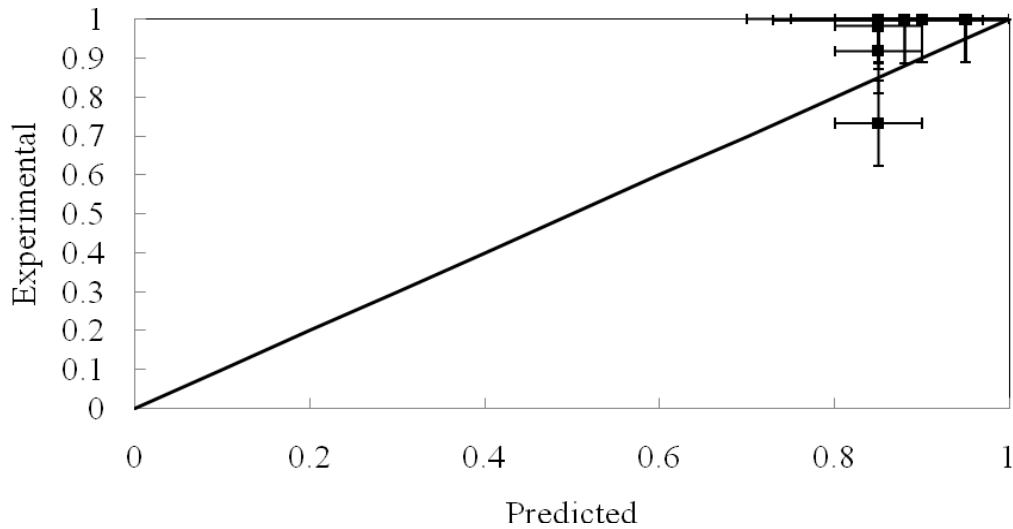


Figure 7.9. Experimental ESPA2 full-scale rejection compared to rejection predicted by updated rejection diagram.

Table 7.3. ESPA2 Membrane Full-Scale Rejection, Rejection Predicted from Rejection Diagram, Predicted Rejection Ranges, and Percentage Difference from Experimental Full-Scale Data

Compound Name	Class	Full-Scale Avg 12-gfd Rejection	Rejection Diagram Predicted Rejection	Rejection Range (+/-)	Percentage Difference
Diclofenac	HCN	1.000	0.95	5%	-5%
Gemfibrozil	HCN	0.999	0.95	5%	-5%
Ibuprofen	HCN	1.000	0.95	5%	-5%
Naproxen	HCN	1.000	0.95	5%	-5%
Sulfamethoxazole	HCN	0.999	0.95	5%	-5%
Atenolol	HCP	0.998	0.88	12%	-12%
Trimethoprim	HCP	0.998	0.88	12%	-12%
Carbamazepine	HHoN	1.000	0.85	15%	-15%
DEET	HHoN	0.997	0.85	15%	-15%
Dilantin	HHoN	1.000	0.85	15%	-15%
Atrazine	HHoN	1.000	0.90	10%	-10%
Primidone	HN	1.000	0.85	15%	-15%
Caffeine	HN	1.000	0.90	10%	-10%
TCP	HN	1.000	0.90	10%	-10%
TCEP	HN	1.000	0.90	10%	-10%
Benzophenone	HoN	0.732	0.85	15%	12%
Bisphenol A	HoN	0.983	0.85	15%	-13%
Fluoxetine	HoN	1.000	0.85	15%	-15%
Triclosan	HoN	0.919	0.85	15%	-7%

Chapter 8

Conclusions and Recommendations

8.1 Conclusions

8.1.1 Summary of Project Results

The objectives of this study were (a) to evaluate molecular modeling approaches for trace organic solutes in high-pressure membrane applications and to determine method-independent and reliable molecular descriptors for the development of QSPR models, (b) to identify, develop, and optimize membrane modeling strategies and to develop models that can be employed to predict the rejection of trace organic solutes, and lastly (c) to evaluate the efficiency with which membranes employed at full scale remove trace organic chemicals and to successfully predict the removal rates with the developed model(s).

8.1.2 Literature Review

A comprehensive literature review was conducted to identify the major factors affecting the rejection of organic solutes by NF and RO membranes, potentially viable modeling approaches, and to summarize past modeling efforts. Major findings from the literature review included the following:

- The rejection of organic solutes depends on three primary mechanisms: size exclusion, electrostatic exclusion, and solute–membrane interactions.
- Operational conditions such as fouling, permeate flux, concentration polarization, and recovery can have a significant impact on rejection.
- Achieving equilibrium rejection conditions for solutes with membrane interactions can take hours to days.
- The overall effect of membrane fouling on the rejection of organic solutes is not well understood.
- Feed water matrix and temperature can impact rejection; however, pH appears to be the most important factor as it affects the speciation of solutes with acidic and basic functional groups, as well as affecting membrane surface charge.
- Ionic organic solutes are generally well removed by NF and RO membranes regardless of size.
- Nonionic solutes with solute–membrane interactions are likely to have incomplete removal.
- Molecular size is a dominant factor in the rejection of nonionic solutes; however, size is less important for solutes with membrane interactions.
- Limited work has been performed to predict which compounds will have strong solute–membrane interactions on the basis of molecular descriptors.
- Pertinent modeling approaches include mass transfer equations, QSPR models, and empirical models.

- Mass transfer models are advantageous because they integrate operational conditions and to a limited degree solute and membrane properties.
- QSPR models are advantageous because solute properties are easily incorporated; however, it can be difficult to incorporate operating conditions and membrane properties.
- Empirical models are advantageous because they are simple to use.
- Models that rely solely on solute size often overpredict rejection because solute–membrane interactions are not included.
- In concept, the solution–diffusion model is advantageous because only one solute input parameter is required. The phenomenological model is advantageous because of the “black box” nature of the model and the possibility of correlating solute properties to the input parameters.
- Considering the complexity and numerical effort of several modeling approaches, including the DSPM and the SFPM, these models may not be applicable to large-scale membrane systems treating multicomponent aqueous solutions.
- The differential element approach combined with the phenomenological model can be applied to a full-scale system and could potentially include both operational conditions and solute and membrane properties.
- Adjustments to any model need to be made to account for fouling and for changes in temperature and feed water chemistry. In addition, experimental replication is needed to account for differences between different types of membranes.

Information gained through the literature review was used to develop a representative list of organic solutes for experimentation, an experimental protocol for measuring rejection, and a list of pertinent modeling strategies for NF and RO membranes.

8.1.3 Organic Solute Selection

For this study, 270 organic solutes were initially selected for model development and model validation. The list of compounds was compiled from a variety of sources and yielded a relatively diverse set of organic solutes on the basis of properties (e.g., size, charge, hydrophobicity/hydrophilicity, etc.), relevance to membrane treatment (e.g., functional groups affecting rejection and likelihood of permeation), and environmental relevance (e.g., EPA Candidate Contaminant List, recent advancements in emerging contaminant research, human health, and environmental relevance). After removal of compounds that caused analytical and experimental issues (e.g., high volatilization, instability, and poor solubility), a shorter list of 137 compounds (shown in Appendix A) was generated for model development and validation. Care was taken that the reduced list of solutes for experimentation retained the diversity of the full list although covering the different rejection mechanisms. Compounds were categorized by expected rejection mechanism based on charge and hydrophobicity. Six different categories were developed: HN (less than 0.01% charged at pH 6.5; $\text{Log } K_{ow} < 2$), HHoN (less than 0.01% charged at pH 6.5; $\text{Log } K_{ow} > 2$ and $\text{Log } K_{ow} < 3$), HoN (less than 0.01% charged at pH 6.5; $\text{Log } K_{ow} > 3$), HCN (greater than 50% negatively charged at pH 6.5), HCP (greater than 50% positively charged at pH 6.5), and HCNP (having both positive and negative charge at pH 6.5).

For each rejection mechanism subgroup, principal component analysis and *k*-means clustering/discriminate analysis was performed to further group similar compounds based on molecular properties calculated and compiled from various sources (e.g., Syracuse Research Corporation, ACD Labs, Schrödinger [software package], and Hyperchem). For HN, HHoN, HoN, HCN, and HCP compounds, five groups were developed, although for HCNP, three groups were developed. Random selection was then used to select at least 33% of the compounds from each grouping (all compounds were selected from groups with only two compounds, 66% were selected from groups with three compounds, 50% of compounds were selected from groups with four compounds).

This selection process yielded a group of 134 compounds for model development and validation (Table 3.2). On the basis of further analysis, this final list of compounds retained much of the diversity of the full list based on the criteria outlined previously (e.g., properties, rejection mechanisms, classes of compounds, environmental relevance, etc.). The list was then randomized with the 33 top compounds selected for the validation set and the remaining 101 selected for the model development set.

8.1.4 Bench-Scale Experimentation

Several criteria were used to develop an experimental protocol to measure organic solute rejection at bench scale under conditions that allowed the development of a rejection database for the select solutes. This database provided the basis for subsequent rejection model developments. These criteria included as follows:

- The application of many identified modeling approaches requires relationships that describe solute rejection as a function of permeate flux.
- Permeate flux should span a broad range and include fluxes relevant to full-scale applications.
- During conduct of these experiments, concentration polarization should be minimized.
- Rejection measurement should be conducted under steady-state or quasi-steady-state conditions to capture solutes with membrane interactions.
- Replicate experiments should be conducted with different membrane coupons to capture potential membrane variability.

Three bench-scale cross-flow SEPA testing systems were developed that included computerized control and data logging of temperature, permeate flow rate, and flux. For each compound, replicate experiments were conducted by using flat-sheet membrane material cut from a spiral-wound element. During experimentation, concentration polarization was minimized by maintaining recovery below 1.5%. Short-term rejection was evaluated at five permeate flux set-points spanning a range from 3 to 60 gfd. Longer-term rejection to study potential interactions between solutes and membranes was evaluated by operating the SEPA system at flux of 12 gfd for approximately 24 h. Feed and permeate samples were collected in replicate, and solute concentration quantified by a variety of analytical methods, including TOC analysis, RID, LC DAD, GC-ECD, and LC/MS-MS. By characterization of the hydrodynamic conditions of the testing system, intrinsic rejection (i.e., rejection in the absence of concentration polarization) was calculated for each compound by using feed and permeate concentrations. The rejection-versus-flux data were used to populate a database

consisting of rejection data and solute properties, which subsequently was used for model development.

Because of the large number of experiments planned, two different membranes were employed during the study. The NF-270 membrane from Dow/Filmtec was selected as a representative NF membrane because this membrane had been used in previous pilot-scale studies using reclaimed water and exhibited excellent rejection performance for organic solutes, low fouling propensities, and a significantly higher specific flux than conventional RO membranes (Bellona and Drewes, 2007; Bellona et al., 2008). The ESPA2 membrane from Hydranautics was selected as a representative LPRO membrane because this membrane is employed at several full-scale water reclamation facilities.

During the course of this study, an enormous number of data was generated through the execution of the experimental protocol. The major findings from the bench-scale rejection experiments were

- The NF-270 membrane exhibited variable rejection depending on the properties of the organic solute and the permeate flux evaluated. Rejection was highly dependent on permeate flux and generally increased with increasing flux.
- Rejection by the ESPA2 membrane was less variable across the range of permeate flux evaluated and for the organic solutes evaluated.
- Both the NF-270 and ESPA2 membranes provide very good (generally greater than 90%) rejection of ionic organic solutes at the pH evaluated (6.3).
- Positively charged organic solutes were, in general, rejected to a lesser degree than were negatively charged organic solutes.
- Solutes with significant membrane interactions exhibited decreasing rejection with increasing permeate flux and a decrease in rejection during short-term and 24-h rejection tests.
- Approximately 15% of the solutes evaluated exhibited solute–membrane interactions during use of the NF-270 membrane. The effect of solute–membrane interaction on rejection was not as pronounced for the ESPA2 membrane.
- During experimentation, numerous solutes were problematic because of degradation or hydrolysis and because of low solubility.
- Variability between replicate experiments was generally very low.
- Comparison of past results indicated that the source of membrane material can have a significant impact on rejection experiments. For example, rejection results from using free membrane samples from manufacturers could be significantly different from those for the same membrane material cut from spiral-wound elements.
- Conducting recycle mode experiments with solutes exhibiting very strong solute–membrane interactions (e.g., THMs) proved difficult. These compounds tended to absorb into the membrane, resulting in reduced feed concentrations that made it difficult to accurately calculate rejection.

8.1.5 Bench-Scale Modeling

Numerous possible modeling approaches for describing solute mass transfer through high-pressure membranes were identified. Several approaches were characterized as impractical for describing rejection at larger-scale membrane applications, including the DSPM and the SFPM. Modeling approaches evaluated during this study included QSPRs, empirical models, the hydrodynamic model, the phenomenological model, and the solution–diffusion model. The major findings from the model development portion of the study included as follows:

- The experimental protocol yielded a robust data set that could be used to evaluate different modeling approaches.
- The hydrodynamic model was found to poorly predict the rejection of a wide variety of nonionic organic solutes, presumably because of either the difficulty of selecting an adequate size parameter or because of the importance of additional solute properties not considered in the model. In addition, this model is applicable only to NF membranes and nonionic solutes.
- The phenomenological model was a simple, yet effective, approach for describing the rejection of a broad range of organic solutes as a function of permeate flux for both membranes evaluated. Additionally, statistically significant QSPRs were developed between model coefficients and solute properties to predict rejection.
- The solution–diffusion model was an effective approach to describe rejection by the ESPA2 membrane; however, the model offered little advantage over the phenomenological model.
- Rejection data for solutes with membrane interactions could not be fit with transport models evaluated during the course of the study. The SFPM can describe the behavior of these compounds (i.e., decreasing rejection with increasing flux); however, it is difficult to apply to a broad range of solutes because of the second-order nonlinear differential equation for solute velocity.
- QSPR modeling approaches were developed that could describe the rejection of solutes with and without solute–membrane interactions at a permeate flux of 12 gfd. In addition, multiple linear regression, PLS, and recursive partitioning analysis were useful for determining the dominant solute properties affecting rejection.
- The statistical significance of developed QSPR models was greatly increased by using 24-h rejection data. This finding indicates that it is important to run “long-term” experiments to adequately characterize rejection.
- The dominant solute descriptors affecting the rejection of nonionic solutes were found to be size descriptors (e.g., Stokes radius, SASA, and volume), surface area descriptors (i.e., FOSA and PISA), and electronic descriptors (i.e., E_{HOMO} , E_{LUMO} , IP, and polarization).
- Developing QSPRs for the entire compound list proved to be difficult, and no accurate approach was developed. In addition, the development of effective (on the basis of accuracy and statistical significance) QSPRs for ionic compounds was not achievable because of an inadequate descriptor for charge. Recursive partitioning can be used to develop a statistical approach to predict rejection; however, it requires a large number of solute descriptors that may not be available.
- The rejection diagram approach, which is similar to recursive partitioning, was redeveloped based on findings from bench-scale experimentation. This approach is likely the most useful for estimating rejection as it includes basic solute descriptors

that are readily available. An analysis of the redeveloped rejection diagrams demonstrated that they can predict, within a range, the rejection of a wide variety of organic solutes.

8.1.6 Pilot-Scale Model Development

A significant portion of this study evaluated rejection at pilot scale under carefully controlled laboratory experiments and in the field at a water reclamation facility. This approach provided valuable information on comparing and upscaling bench-scale experimental rejection results to larger membrane systems. The major findings from this portion of the study included as follows:

- System recovery has a minor influence on the rejection of organic solutes in the range of 50 to 90%.
- Rejection can be increased by operating at higher cross-flow velocity (i.e., greater feed flow rate) and permeate flux.
- Comparing bench-scale rejection to pilot- or full-scale rejection is difficult as bench-scale systems are operated at low recovery and as permeate flux can vary widely, although the opposite holds true for large-scale systems in the field.
- Bench-scale rejection results can be used to describe the rejection at large scale; however, the hydrodynamic conditions and flux and concentration gradients for a large-scale system need to be characterized.
- The differential element approach combined with the phenomenological model was an effective modeling approach to describe rejection at pilot scale. Bench-scale-derived phenomenological model coefficients could be used to estimate pilot-scale permeate concentrations and rejection.
- QSPRs and the rejection diagram approach developed with bench-scale rejection data could estimate rejection at pilot scale.

8.1.7 Full-Scale Rejection and Model Development

A full-scale sampling campaign was conducted at a water reclamation facility employing the ESPA2 membrane at full scale to evaluate the rejection of a wide variety of organic contaminants under realistic conditions and to develop a data set for model validation. The findings from this portion of the study included as follows:

- Rejection of the vast majority of the contaminants quantified in the feed water was greater than 99%.
- Several solutes identified as having solute–membrane interactions were only incompletely rejected, including triclosan and benzophenone.
- Rejection observed at full scale was greater than observed at bench scale. This finding could be due to the membrane compaction and establishment of a fouling layer, as the ESPA2 membrane had been operating for a significant length of time when sampling occurred.
- Phenomenological model coefficients derived at bench scale for the ESPA2 membrane would underestimate the rejection observed from the full-scale data because the beneficial role of the fouling layer was not considered.

- Similarly, QSPRs and the rejection diagrams developed by using bench-scale data underpredicted the rejection of organic solutes at full scale.

8.2 Recommendations

Different modeling approaches were evaluated during the course of the study to develop a broadly applicable model to predict the rejection of trace organic chemicals by NF and RO membranes. Although modeling approaches were developed that can estimate rejection at bench-, pilot-, and full-scale installations, developing accurate models for the thousands of potential organic contaminants is difficult for a number of previously discussed reasons. The research team found that bench-scale results can be used to describe the rejection of organic solutes at larger scales; however, changes in membrane performance over time from compaction, fouling, and aging are difficult to incorporate into modeling approaches. If one puts these issues aside, there are different modeling approaches that can be adopted based on the level of effort required for development. They are listed in order of increasing complexity:

- The rejection diagram is a simple and effective approach for describing the range of rejection for a wide variety of organic solutes as it requires few, easily determined, solute descriptors. The rejection diagrams were developed and tested during the course of this study for one RO-type membrane and one NF-type membrane..
- A utility looking to develop a transport model to describe the rejection of organic solutes would be advised to sacrifice an (fouled) element from its system and to run experiments (rejection as a function of permeate flux) with organic solutes spanning a range of size, charge, and hydrophobicity. For nonionic solutes, simple correlations can be developed between the reflection coefficient and permeability coefficient and a solute size descriptor. For ionic compounds, the measured range of reflection and permeability coefficients should be sufficient to estimate the range of rejection for these compounds. A simple mass balance model can be developed for a full-scale membrane system by using bench-scale-derived phenomenological coefficients.
- The major issue with QSPR models is that they are dependent upon the conditions used to develop the rejection data and require a large number of rejection data to generate statistically significant correlations. The solute selection method employed during this study proved to be a good approach for selecting solutes for QSPR development.

8.3 Future Research Needs

A number of research questions were raised during the completion of this study that should be studied further to understand the transport of organic compounds through NF and RO membranes. These include the following:

- Understanding the solute properties that result in adsorption and partitioning through membrane materials and developing modeling approaches for these compounds.
- Quantifying the time it takes to reach rejection equilibrium conditions for a broad range of solutes with strong membrane interactions.
- Quantifying the effect of membrane compaction and fouling on the rejection of organic solutes.

- Identifying membrane-specific descriptors that affect solute mass transport.
- Integrating membrane-specific descriptors into rejection models.

References

- Agenson, K. O.; Oh, J.-H.; Urase, T. Retention of a wide variety of organic pollutants by different nanofiltration/reverse osmosis membranes: controlling parameters of process. *J. Membr. Sci.* **2003**, *225*, 91–103.
- Ahmad, A. K.; Tan, K.Y. Reverse osmosis of binary organic solute mixtures in the presence of strong solute-membrane affinity. *Desalination* **2004**, *165*, 193–199.
- Akthakul, A.; McDonald, W. F.; Mayes, A. M. Noncircular pores on the surface of asymmetric polymer membranes: evidence of pore formation via spinodal demixing. *J. Membr. Sci.* **2002**, *208*, 147–155.
- Alexander, K. L.; Alt, S.; Owens, E.; Patel, M. V.; McGovern, L. Low Fouling Reverse Osmosis Membranes: Evidence to the Contrary on Microfiltered Secondary Effluent. In *Proceedings of the American Water Works Association Membrane Technology Conference*, Atlanta, GA, 2003.
- American Water Works Association Membrane Technology Research Committee. Recent advances and research needs in membrane fouling—committee report. *J.—Am. Water Works Assoc.* **2005**, *97*, 79–89.
- Ariza, M. J.; Canas, A.; Malfeito, J.; Benavente, J. Effect of pH on electrokinetic and electrochemical parameters of both sub-layers of composite polyamide/polysulfone membranes. *Desalination* **2002**, *148*, 377–382.
- AWWA. *M46: Reverse Osmosis and Nanofiltration*, 2nd ed.; American Water Works Association: Denver, CO, 2007.
- Balanec, B.; Gesan-Guiziou, G.; Chaufer, B.; Rabiller-Baudry, M.; Daufin, G. Treatment of dairy process waters by membrane operations for water reuse and milk constituents concentration. *Desalination* **2002**, *147*, 89–94.
- Bandini, S.; Vezzani, D. Nanofiltration modeling: the role for dielectric exclusion in membrane characterization. *Chem. Eng. Sci.* **2003**, *58*, 3303–3326.
- Bartels, C.; Franks, R.; Furukawa, R.; Murkute, P.; Papukchiev, U. Integrated Membrane System for Low Fouling RO Desalting of Municipal Wastewater. <http://tinyurl.com/8zvvgzv> (accessed Sept 2012), 2008.
- Belfroid, A. C.; Van der Horst, A.; Vethaak, A. D.; Schäfer, A. J.; Rijs, G. B. J.; Wegener, J.; Confino, W. P. Analysis and occurrence of estrogenic hormones and their glucuronides in surface water and waste water in The Netherlands. *Sci. Total Environ.* **1999**, *225*, 101–108.
- Bellona, C. Employing Nanofiltration and Ultra-Low Pressure Reverse Osmosis for Drinking Water Augmentation: Efficiency of Operation and Removal of Emerging Organic Contaminants. Ph.D. Dissertation, Colorado School of Mines, Golden, CO, 2007.
- Bellona, C.; Drewes, J. E. The role of membrane surface charge and solute physico-chemical properties in the rejection of organic acids by NF membranes. *J. Membr. Sci.* **2005**, *249*, 227–234.
- Bellona, C.; Drewes, J. E. Viability of a low pressure nanofilter in treating recycled water for water reuse applications—a pilot-scale study. *Water Res.* **2007**, *41*, 3948–3958.

- Bellona, C.; Drewes, J.; Xu, P.; Amy, G. Factors affecting the rejection of organic solutes during NF/RO treatment—a literature review. *Water Res.* **2004**, *38*, 2795–2809.
- Bellona, C.; Drewes, J. E.; Oelker, G.; Luna, J.; Filteau, G.; Amy, G. Comparing reverse osmosis and nanofiltration for water reclamation. *J. Am. Water Works Assoc.* **2008**, *100*, 102–116.
- Ben-David, A.; Oren, Y.; Freger, V. Thermodynamic factors in partitioning and rejection of organic compounds by polyamide composite membranes. *Environ. Sci. Technol.* **2006a**, *40*, 7023–7028.
- Ben-David, A.; Bason, S.; Jopp, J.; Oren, Y.; Freger, V. Partitioning of organic solutes between water and polyamide layer of RO and NF membranes: correlation to rejection. *J. Membr. Sci.* **2006b**, *281*, 480–490.
- Berg, P.; Hagemeyer, G.; Gimbel, R. Removal of pesticides and other micro-pollutants by nanofiltration. *Desalination* **1997**, *113*, 205–208.
- Bouranene, S.; Szymczyk, A.; Fievet, P.; Vidonne, A. Influence of inorganic electrolytes on the retention of polyethyleneglycol by a nanofiltration ceramic membrane. *J. Membr. Sci.* **2007**, *290*, 216–221.
- Boussahel, R.; Montiel, A.; Baudu, M. Effects of organic and inorganic matter on pesticide rejection by nanofiltration. *Desalination* **2002**, *145*, 109–114.
- Bowen, W. R.; Mohammad, A. W. Diafiltration by nanofiltration: prediction and optimization. *AIChE J.* **1998**, *44*, 1799–1811.
- Bowen, W. R.; Mukhtar, H. Characterization and prediction of separation performance of nanofiltration membranes. *J. Membr. Sci.* **1996**, *112*, 263–274.
- Bowen, W. R.; Welfoot, J. S. Predictive modeling of nanofiltration: membrane specification and process optimization. *Desalination* **2002**, *147*, 197–203.
- Bowen, W. R.; Hilal, N.; Lovitt, R. W.; Williams, P. M. Atomic force microscope studies of membranes: surface pore structures of cyclopore and anopore membranes. *J. Membr. Sci.* **1996**, *110*, 233–238.
- Bowen, W. R.; Mohammad, A. W.; Hidal, N. Characterization of nanofiltration membranes for predictive purposes—use of salts, uncharged solutes and atomic force microscopy. *J. Membr. Sci.* **1997**, *126*, 91–105.
- Bowen, W. R.; Welfoot, J. S.; Williams, M. Linearized transport model for nanofiltration: development and assessment. *AIChE J.* **2002**, *48*, 760–771.
- Bowen, W. R.; Cassey, B.; Jones, P.; Oatley, D. L. Modelling the performance of membrane nanofiltration—application to an industrially relevant separation. *J. Membr. Sci.* **2004**, *242*, 211–220.
- Braeken, L.; Ramaekers, R.; Zhang, Y.; Maes, G.; Van der Bruggen, B.; Vandecasteele, C. Influence of hydrophobicity on retention in nanofiltration of aqueous solutions containing organic compounds. *J. Membr. Sci.* **2005**, *252*, 195–203.
- Braeken, L.; Van der Bruggen, B.; Vandecasteele, C. Flux decline in nanofiltration due to adsorption of dissolved organic compounds: model prediction of time dependency. *J. Phys. Chem. B* **2006**, *110*, 2957–2962.
- Braghetta, A.; Digiano, F. A.; Ball, W. P. Nanofiltration of natural organic matter: pH and ionic strength effects. *J. Environ. Eng.* **1997**, *123*, 628–640.

- Bruchet, A.; Prompsy, C.; Filippi, G.; Souali, A. A broad spectrum analytical scheme for the screening of endocrine disruptors (Eds), pharmaceuticals and personal care products in wastewaters and natural waters. *Water Sci. Technol.* **2002**, *46*, 97–104.
- Bruni, L.; Bandini, S. The role of the electrolyte on the mechanism of charge formation in polyamide nanofiltration membranes. *J. Membr. Sci.* **2008**, *308*, 136–151.
- Carballa, M.; Omil, F.; Lema, J. M.; Llupart, M.; Garcia-Jares, C.; Rodriguez, I.; Gomez, M.; Ternes, T. Behavior of pharmaceuticals, cosmetics and hormones in a sewage treatment plant. *Water Res.* **2004**, *38*, 2918–2926.
- Chang, S.; Waite, T. D.; Schafer, A. I.; Fane, A. G. Adsorption of trace steroid estrogens to hydrophobic hollow fiber membranes. *Desalination* **2002**, *146*, 381–386.
- Chellam, S.; Taylor, J. S. Simplified analysis of contaminant rejection during ground and surface water nanofiltration under the information collection rule. *Water Res.* **2001**, *35*, 2460–2474.
- Childress, A. E.; Elimelech, M. Relating nanofiltration membrane performance to membrane charge (electrokinetic) characteristics. *Environ. Sci. Technol.* **2000**, *34*, 3710–3716.
- Cho, J.; Amy, G.; Pellegrino, J. Membrane filtration of natural organic matter: initial comparison of rejection and flux decline characteristics with ultrafiltration and nanofiltration membranes. *Water Res.* **1999**, *33*, 2517–2526.
- Cho, J.; Amy, G.; Pellegrino, J. Membrane filtration of natural organic matter: comparison of flux decline, NOM rejection, and foulants during filtration with three UF membranes. *Desalination* **2000**, *127*, 283–298.
- Chung, T.-S.; Qin, J.-J.; Huan, A.; Toh, K.-C. Visualization of the effect of shear rate on the outer surface morphology of ultrafiltration membranes by AFM. *J. Membr. Sci.* **2002**, *196*, 251–266.
- Clesceri, L. S.; Greenberg, A. E.; Eaton, A. D., Eds. *Standard Methods for the Examination of Water and Wastewater*, 20th ed.; American Public Health Association: Washington, DC, 1998.
- Cleveland, C. T.; Seacord, T. F.; Zander, A. K. Standardized membrane pore size characterization by polyethylene glycol rejection. *J. Environ. Eng.* **2002**, *128*, 399–407.
- Cussler, E. L. *Diffusion: Mass transfer in fluid systems*. Cambridge University Press: Cambridge, UK, 1997.
- Deen, W. M. Hindered transport of large molecules in liquid-filled pores. *AIChE J.* **1987**, *33*, 1409.
- Delgado, J. M. Molecular diffusion coefficients of organic compounds in water at different temperatures. *J. of Phase Equilibria and Diffusion* **2007**, *28* (5), 427–432.
- Deshmukh, S. S.; Childress, A. E. Zeta potential of commercial RO membranes: influence of source water type and chemistry. *Desalination* **2001**, *140*, 87–95.
- DiGiano, F. A.; Arweiler, S.; Riddick, J. A., Jr. Alternative tests for evaluating NF fouling. *J.—Am. Water Works Assoc.* **2000**, *92*, 103–115.

- DiGiano, F. A.; Roudman, A.; Arnold, M.; Freeman, B. D.; Preston, J.; Nagai, K.; DeSimone, J. M. *Laboratory Tests of New Membrane Materials*; AWWA Research Foundation: Denver, CO, 2001.
- Donnan, F. G. The theory of membrane equilibria. *Chem. Rev.* **1924**, *1*, 73–90.
- Dresner, L. Some remarks on the intergration of the extended Nernst-Planck equation in the hyperfiltration of multicomponent solutions. *Desalination* **1971**, *10*, 27–46.
- Drewes, J. E.; Fox, P.; Reinhard, M. Removal of organics in indirect potable reuse systems: A comparison of efficiencies of long-term soil-aquifer treatment (SAT) and best available technologies (BAT). <http://www.nwri-usa.org/pdfs/NWRIRemovalOfOrganicsInIndirectPotableReuseSystems.pdf> (accessed Oct 2012), 2001.
- Drewes, J. E.; Reinhard, M.; Fox, P. Comparing microfiltration–reverse osmosis and soil–aquifer treatment for indirect potable reuse. *Water Res.* **2003**, *37*, 3612–3621.
- Drewes, J. E.; Bellona, C.; Oedekoven, M.; Xu, P.; Kim, T.-U.; Amy, G. Rejection of wastewater-derived micropollutants in high-pressure membrane applications leading to indirect potable reuse. *Environ. Prog.* **2005**, *24*, 400–409.
- Drewes, J. E.; Bellona, C.; Xu, P.; Amy, G.; Filteau, G.; Oelker, G. *Comparing nanofiltration to reverse osmosis for treating recycled water*. AwwaRF Project #3012 Final Report. AwwaRF: Denver, CO, 2008.
- Duranceau, S. J.; Taylor, J. S.; Mulford, L. A. SOC removal in a membrane softening process. *J.—Am. Water Works Assoc.* **1992**, *84*, 68–78.
- Eriksson, L.; Jaworska, J.; Worth, A. P.; Cronin, M. T. D.; McDowell, R. M.; Gramatica, P. Methods for reliability and uncertainty assessment and for applicability evaluations of classification- and regression-based QSARs. *Environ. Health Perspect.* **2003**, *111* (10), 1361–1375.
- Freger, V.; Arnot, A. C.; Howell, J. A. Separation of concentrated organic/inorganic salt mixtures by nanofiltration. *J. Membr. Sci.* **2000**, *178*, 185–193.
- Fritzsche, A. K.; Arevalo, A. R.; Connolly, A. F.; Moore, M. D.; Elings, V.; Wu, C. M. The structure and morphology of the skin of polyethersulfone ultrafiltration membranes: a comparative atomic force microscope and scanning electron microscope study. *J. Appl. Polym. Sci.* **1992**, *45*, 1945.
- Gallenkemper, M.; Wintgens, T.; Melin, T. Nanofiltration of endocrine disrupting compounds. <http://www.iwaponline.com/ws/00305/ws003050321.htm> (accessed Oct 2012), 2002.
- Geens, J.; Van der Bruggen, B.; Vandecasteele, C. Transport model for solvent permeation through nanofiltration membranes. *Sep. Purif. Technol.* **2006**, *48*, 255–263.
- Geraldes, V.; de Pinho, M. N. Mass transfer coefficient determination method for high-recovery pressure-driven membrane modules. *Desalination* **2006**, *195*, 69–77.
- Gwon, E.; Yu, M.; Oh, H.; Ylee, Y. Fouling characteristics of NF and RO operated for removal of dissolved matter from groundwater. *Water Res.* **2003**, *37*, 2989–2997.
- Hagmeyer, G.; Gimbel, R. Modeling the salt rejection of nanofiltration membranes for ternary ion mixtures and for single salts at different pH values. *Desalination* **1998**, *117*, 247–256.

- Hirose, M.; Ito, H.; Kamiyama, Y. Effect of skin layer surface structures on the flux behavior of RO membrane. *J. Membr. Sci.* **1996**, *121*, 209.
- Ho, C. C.; Zydney, A. L. Effect of membrane morphology on the initial rate of protein fouling during microfiltration. *J. Membr. Sci.* **1999**, *155*, 261–267.
- Hofman, J. A. M. H.; Gijbetsen, A. J.; Cornelissen, E. *Nanofiltration retention models for organic contaminants*; Water Research Foundation Project No. 2945; WRF: Denver, CO, 2007.
- Hong, S.; Elimelech, M. Chemical and physical aspects of natural organic matter (NOM) fouling of nanofiltration membranes. *J. Membr. Sci.* **1997**, *132*, 159–181.
- Hu, J. Y.; Ong, S. L.; Shan, J. H.; Kang, J. B.; Ng, W. J. Treatability of organic fractions derived from secondary effluent by reverse osmosis membrane. *Water Res.* **2003**, *37*, 4801–4809.
- Hu, J. Y.; Jin, X.; Ong, S. L. Rejection of estrone by nanofiltration: influence of solution chemistry. *J. Membr. Sci.* **2007**, *302*, 188–196.
- Jain, S.; Gupta, S. K. Analysis of modified surface force pore flow model with concentration polarization and comparison with Spiegler-Kedem model in reverse osmosis systems. *J. Membr. Sci.* **2004**, *232*, 45–62.
- Jarusutthirak, C.; Amy, G.; Croue, J.-P. Fouling characteristics of wastewater effluent organic matter (EfOM) isolates on NF and UF membranes. *Desalination* **2002**, *145*, 247–255.
- Jin, X.; Hu, J.; Ong, S. L. Influence of dissolved organic matter on estrone removal by NF membranes and the role of their structures. *Water Res.* **2007**, *41*, 3077–3088.
- Kargol, A. A mechanistic model of transport processes in porous membranes generated by osmotic and hydrostatic pressure. *J. Membr. Sci.* **2001**, *191*, 61–69.
- Kedem, O.; Katchalsky, A. Thermodynamic analysis of the permeability of biological membranes to non-electrolytes. *Biochim. Biophys. Acta* **1958**, *27*, 229–246.
- Kim, J. Y.; Lee, H. K.; Kim, S. C. Surface structure and phase separation mechanism of polysulfone membranes by atomic force microscopy. *J. Membr. Sci.* **1999**, *163*, 159.
- Kim, D. H.; Kim, K. W.; Kim, J. Y.; Oh, H.; Cho, J. Removal and transport mechanisms (diffusion vs. convection) of arsenic in membrane (UF and NF) processes. <http://tinyurl.com/9rgx53p> (accessed Oct 2012), 2002.
- Kim, T.-U.; Drewes, J. E.; Summers, R. S.; Amy, G. L. Solute transport model for trace organic neutral and charged compounds through nanofiltration and reverse osmosis membranes. *Water Res.* **2007**, *41*, 3977–3988.
- Kim, J.-H.; Park, P.-K.; Lee, C.-H.; Kwon, H.-H. Surface modification of nanofiltration membranes to improve the removal of organic micro-pollutants (EDCs and PhACs) in drinking water treatment: Graft polymerization and cross-linking followed by functional group substitution. *J. Membr. Sci.* **2008**, *381* (2), 190–198.
- Kimura, K.; Amy, G.; Drewes, J. E.; Watanabe, Y. Adsorption of hydrophobic compounds onto NF/RO membranes: An artifact leading to overestimation of rejection. *J. Membr. Sci.* **2003a**, *221*, 89–101.

- Kimura, K.; Amy, G.; Drewes, J. E.; Heberer, T.; Kim, T.-U.; Watanabe, Y. Rejection of organic micropollutants (disinfection by-products, endocrine disrupting compounds, and pharmaceutically active compounds) by NF/RO membranes. *J. Membr. Sci.* **2003b**, *227*, 113–121.
- Kimura, K.; Toshima, S.; Amy, G.; Watanabe, Y. Rejection of neutral endocrine disrupting compounds (EDCs) and pharmaceutically active compounds (PhACs) by RO membranes. *J. Membr. Sci.* **2004**, *245*, 71–78.
- Kiso, Y. Factors affecting adsorption of organic solutes on cellulose in an aqueous solution system. *Chromatographia* **2001**, *22*, 55–58.
- Kiso, Y.; Kitao, T.; Kiyokatsu, J.; Miyagi, M. The effects of molecular width on permeation of organic solute through cellulose acetate reverse osmosis membrane. *J. Membr. Sci.* **1992**, *74*, 95–103.
- Kiso, Y.; Li, H.; Kitao, T. Pesticide separation by nanofiltration membranes. *J. Jpn. Soc. Water Environ.* **1996**, *10*, 648.
- Kiso, Y.; Nishimura, Y.; Kitao, T.; Nishimura, K. Rejection properties of non-phenylic pesticides with nanofiltration membranes. *J. Membr. Sci.* **2000**, *171*, 229–237.
- Kiso, Y.; Sugiura, Y.; Kitao, T.; Nishimura, K. Effects of hydrophobicity and molecular size on rejection of aromatic pesticides with nanofiltration membranes. *J. Membr. Sci.* **2001a**, *192*, 1–10.
- Kiso, Y.; Kon, T.; Kitao, T.; Nishimura, K. Rejection properties of alkyl phthalates with nanofiltration membranes. *J. Membr. Sci.* **2001b**, *182*, 205–214.
- Košutić, K.; Kunst, B. Removal of organics from aqueous solutions by commercial RO and NF membranes of characterized porosities. *Desalination* **2002**, *142*, 47–56.
- Košutić, K.; Kaštelan-Kunst, L.; Kunst, B. Porosity of some commercial reverse osmosis and nanofiltration polyamide thin-film composite membranes. *J. Membr. Sci.* **2000**, *168*, 101–108.
- Košutić, K.; Dolar, D.; Kunst, B. On experimental parameters characterizing the reverse osmosis and nanofiltration membranes' active layer. *J. Membr. Sci.* **2006**, *282*, 109–114.
- Košutić, K.; Dolar, D.; Asperger, D.; Kunst, B. Removal of antibiotics from a model wastewater by RO/NF membranes. *Sep. Purif. Technol.* **2007**, *53*, 244–249.
- Kwak, S.-Y.; Ihm, D. W. Use of atomic force microscopy and solid-state NMR spectroscopy to characterize structure-property-performance correlation in high-flux reverse osmosis (RO) membranes. *J. Membr. Sci.* **1999**, *158*, 143–153.
- Lee, S.; Lueptow, R. M. Membrane rejection of nitrogen compounds. *Environ. Sci. Technol.* **2001**, *35*, 3008–3018.
- Lee, S.; Park, G.; Amy, G.; Hong, S.-K.; Moon, S.-H.; Lee, D.-H.; Cho, J. Determination of membrane pore size distribution using the fractional rejection of nonionic and charged macromolecules. *J. Membr. Sci.* **2002**, *201*, 191–201.
- Levine, B. B.; Madireddi, K.; Lazarova, V.; Stenstrom, M. K.; Suffet, M. Treatment of trace organic compounds by membrane processes: at the Lake Arrowhead water reuse pilot plant. *Water Sci. Technol.* **1999**, *40*, 293–302.

- Libotean, D.; Giralt, J.; Giralt, F.; Rallo, R.; Wolfe, T.; Cohen, Y. Neural network approach for modeling the performance of reverse osmosis membrane desalting. *J. Membr. Sci.* **2009**, *326*, 408–419.
- Libotean, D.; Giralt, J.; Rallo, R.; Cohen, Y.; Giralt, F.; Ridgeway, H. F.; Rodriguez, G.; Phipps, D. Organic passage through RO membranes. *J. Membr. Sci.* **2008**, *313*, 23–42.
- Liikanen, R.; Miettinen, I.; Laukkanen, R. Selection of NF membranes to improve quality of chemically treated surface water. *Water Res.* **2003**, *37*, 864–872.
- Lopez-Ramirez, J. A.; Coello Oviedo, M. D.; Quiroga Alonso, J. M. Comparative studies of reverse osmosis membranes for wastewater reclamation. *Desalination* **2006**, *191*, 137–147.
- Majewska-Nowak, K.; Kabsch-Korbutowicz, M.; Dodź, M.; Winnicki, T. The influence of organic carbon concentration on atrazine removal by UF membranes. *Desalination* **2002**, *147*, 117–122.
- Marts, M. The effects of membrane fouling on surface properties and rejection of organic solutes. Master's thesis, Colorado School of Mines, Golden, CO, 2008.
- Mason, E. A.; Lonsdale, H. K. Statistical-mechanical theory of membrane transport. *J. Membr. Sci.* **1990**, *51*, 1–81.
- Masselin, I.; Chasseray, X.; Chevalier, M.-R.; Lainé, J.-M.; Lemordant, D. Determination of the porosity to thickness ratio $A_k/\Delta x$ for UF and MF membranes by diffusion experiments. *J. Membr. Sci.* **2000**, *172*, 125–133.
- Matsuura, T.; Sourirajan, S. Physiochemical criteria for reverse osmosis separation of alcohols, phenols, and monocarboxylic acids in aqueous solutions using porous cellulose acetate membranes. *J. Appl. Polym. Sci.* **1971**, *15*, 2905–2927.
- McCallum, A.; Hyung, H.; Do, T. A.; Huang, C.-H.; Kim, J.-H. Adsorption, desorption, and steady-state removal of 17 β -estradiol by nanofiltration membranes. *J. Membr. Sci.* **2008**, *319*, 38–43.
- Mehdizadeh, H.; Dickson, J. Modelling of temperature effects on the performance of reverse osmosis membranes, *Chemical Engineering Communications* **1991**, *103*, 99.
- Mohammad, A.; Ali, N. Understanding the steric and charge contributions in NF membranes using increasing MWCO polyamide membranes. *Desalination* **2002**, *147*, 205–212.
- Mulford, L. A.; Taylor, J. S.; Linton, D. G.; Nickerson, D. M.; Chellam, S. Predicting Membrane System Water Quality using an Integrated Diffusion Model. http://www.techstreet.com/standards/awwa/mtc53689?product_id=888710 (accessed Oct 2012), 2001.
- Murthy, Z. V. P.; Gupta, S. K. Estimation of mass transfer coefficient using a combined nonlinear membrane transport and film theory model. *Desalination* **1995**, *109*, 39–49.
- Ng, H. Y.; Elimelech, M. Influence of colloidal fouling on rejection of trace organic contaminants by reverse osmosis. *J. Membr. Sci.* **2004**, *244*, 215–226.
- Nghiem, L. D.; Coleman, P. J. NF/RO filtration of the hydrophobic ionogenic compound triclosan: transport mechanisms and the influence of membrane fouling. *Sep. Purif. Technol.* **2008**, *62*, 709–716.

- Nghiem, L. D.; Schäfer, A. I. Adsorption and transport of trace contaminant estrone in NF/RO membranes. *Environ. Eng. Sci.* **2002**, *19*, 441–451.
- Nghiem, L. D.; Schäfer, A. I.; Waite, T. D. Adsorptive interactions between membranes and trace contaminants. *Desalination* **2002a**, *147*, 269–274.
- Nghiem, L. D.; Schäfer, A. I.; Waite, T. D. Adsorption of estrone on nanofiltration and reverse osmosis membranes in water and wastewater treatment. *Water Sci. Technol.* **2002b**, *46*, 265–272.
- Nghiem, L. D.; Schäfer, A. I.; Elimelech, M. Removal of natural hormones by nanofiltration membranes: Measurement, modeling, and mechanisms. *Environ. Sci. Technol.* **2004**, *38*, 1888–1896.
- Nghiem, L. D.; Schäfer, A. I.; Elimelech, M. Pharmaceutical retention mechanisms by nanofiltration membranes. *Environ. Sci. Technol.* **2005**, *39*, 7698–7705.
- Nghiem, L. D.; Schäfer, A.; Elimelech, M. Role of electrostatic interactions in the retention of pharmaceutically active contaminants by a loose nanofiltration membrane. *Journal of Membrane Science*, **2006**, *286* (1–2), 52–59.
- Nghiem, L.; Espendiller, C.; Braun, G. Influence of organic and colloidal fouling on the removal of sulphamethoxazole by nanofiltration membranes. *Water Sci. Technol.* **2008**, *58*, 163–169.
- Nghiem, L. D.; Tadkaew, N.; Sivakumar, M. Removal of trace organic contaminants by submerged membrane bioreactors. *Desalination*. **2009**, *236*, 127–134.
- Niemi, H.; Palosaari, S. Calculation of permeate flux and rejection in simulation of ultrafiltration and reverse osmosis processes. *J. Membr. Sci.* **1993**, *84*, 123–137.
- Oedekoven, M. The application of the Spiegler-Kedem approach for modeling the rejection of organic solute rejection by NF and RO membranes. Master's thesis, Colorado School of Mines, Golden, CO, 2005.
- Ozaki, H.; Li, H. Rejection of organic compounds by ultra-low pressure reverse osmosis membrane. *Water Res.* **2002**, *36*, 123–130.
- Ozaki, H.; Sharma, K.; Saktaywin, W. Performance of an ultra-low-pressure reverse osmosis membrane (ULPROM) for separating heavy metal: Effects of interference parameters. *Desalination* **2002**, *144*, 287–294.
- Peng, W.; Escobar, I. C.; White, D. B. Effects of water chemistries and properties of membrane on the performance and fouling—A model development study. *J. Membr. Sci.* **2004**, *238*, 33–46.
- Plakas, K. V.; Karabelas, A. J.; Wintgens, T.; Melin, T. A study of selected herbicides retention by nanofiltration membranes—The role of organic fouling. *J. Membr. Sci.* **2006**, *284*, 291–300.
- Radjenovic, J.; Petrovic, M.; Ventura, F.; Barcelo, D. Rejection of pharmaceuticals in nanofiltration and reverse osmosis membrane drinking water treatment. *Water Res.* **2008**, *42*, 3601–3610.
- Reinhard, M.; Goodman, N. L.; McCarty, P. L.; Argo, D. G. Removing trace organics by reverse osmosis using cellulose acetate and polyamide membranes. *J.—Am. Water Works Assoc.* **1986**, *78*, 163–174.

- Rodriguez, G.; Buonora, S.; Knoell, T.; Phipps, D., Jr.; Ridgway, H. Final Report: Rejection of Pharmaceuticals by Reverse Osmosis Membranes: Quantitative Structure Activity Relationship (QSAR) Analysis. NWRI Project 01-EC-002. <http://www.ocwd.com/fv-853> (accessed Oct 2012), 2004.
- Santos, J. L. C.; de Beukelaar, P.; Vankelecom, I. F. J.; Velizarov, S.; Crespo, J. G. Effect of solute geometry and orientation on the rejection of uncharged compounds by nanofiltration. *Sep. Purif. Technol.* **2006**, *50*, 122–131.
- Schaep, J.; Vandecasteele, C.; Mohammad, A. W.; Bowen, W. R. Analysis of the salt retention of nanofiltration membranes using the Donnan-steric partitioning model. *Sep. Sci. Technol.* **1999**, *34*, 3009–3030.
- Schäfer, A. I.; Waite, T. D. Trace contaminant removal using hybrid processes in water recycling. In *Chemical Water and Wastewater Treatment*; Hahn, H. H.; Hoffman, E.; Odegaard, H.; Eds.; IWA Publishing: London, 2002; Vol. VII, pp. 319–330.
- Schäfer, A. I.; Mauch, R.; Waite, T. D.; Fane, A. G. Charge effects in the fractionation of natural organics using ultrafiltration. *Environ. Sci. Technol.* **2002a**, *36*, 2572–2580.
- Schäfer, A. I.; Mastrup, M.; Lund-Jensen, R. Particle interactions and removal of trace contaminants from water and wastewaters. *Desalination* **2002b**, *147*, 243–250.
- Schäfer, A. I.; Nghiem, L. D.; Waite, T. D. Removal of natural hormone estrone for aqueous solutions using nanofiltration and reverse osmosis. *Environ. Sci. Technol.* **2003**, *37*, 182–188.
- Schäfer, A. I.; Fane, A. G.; Waite, T. D.; Eds. *Nanofiltration: Principles and applications*; Elsevier Advanced Technology Publishing: Oxford, England, 2005.
- Schock, G.; Miquel, A. Mass transfer and pressure loss in spiral-wound modules. *Desalination* **1987**, *64*, 339–352.
- Schutte, C. F. The rejection of specific organic compounds by reverse osmosis membranes. *Desalination* **2003**, *158*, 285–294.
- Seidel, A.; Waypa, J. J.; Elimelech, M. Role of charge (Donnan) exclusion in removal of arsenic from water by a negatively charged porous nanofiltration membrane. *Environ. Eng. Sci.* **2001**, *18*, 105–113.
- Serrano, D. A.; Wio, H. S. Separation factor of membranes used for isotopic separation by gaseous diffusion: pore morphology influence and effect of cracks. *J. Membr. Sci.* **2002**, *204*, 5–25.
- Sharma, R. R.; Chellam, S. Temperature effects on the morphology of porous thin film composite nanofiltration membranes. *Environ. Sci. Technol.* **2005**, *39*, 5022–5030.
- Sharma, R. R.; Chellam, S. Solute rejection by porous thin film composite nanofiltration membranes at high feed water recoveries. *J. Colloid and Interface Science* **2008**, *328*, 353–366.
- Shetty, G. R.; Chellam, S. Predicting membrane fouling during municipal drinking water nanofiltration using artificial neural networks. *J. Membr. Sci.* **2003**, *217*, 69–86.
- Shim, Y.; Lee, H.-G.; Lee, S.; Moon, S.-H.; Cho, J. Effects of NOM and ionic species on membrane surface charge. *Environ. Sci. Technol.* **2002**, *36*, 3864–3871.

- Singh, S.; Khulbe, K. C.; Matsuura, T.; Ramamurthy, P. Membrane characterization by solute transport and atomic force microscopy. *J. Membr. Sci.* **1998**, *142*, 111–127.
- Snyder, S.; Adham, S.; Redding, A. M.; Cannon, F. S.; DeCarolis, J.; Oppenheimer, J.; Wert, E. C.; Yoon, Y. Role of membranes and activated carbon in the removal of endocrine disruptors and pharmaceuticals. *Desalination* **2007**, *202*, 56–181.
- Sorin, A.; Favre-Reguillon, A.; Pellet-Rostaing, S.; Bernier, G.; Lemaire, M. Polycarboxylic acids rejection by charged nanofiltration membrane. *J. Membr. Sci.* **2006**, *279*, 446–452.
- Speth, T. F.; Summers, R. S.; Gusses, A. M. Nanofiltration foulants from a treated surface water. *Environ. Sci. Technol.* **1998**, *32*, 3612–3617.
- Speth, T. F.; Gusses, A. M.; Summers, R. S. Evaluation of nanofiltration pretreatments for flux loss control. *Desalination* **2000**, *130*, 31–44.
- Spiegler, K. S.; Kedem, O. Thermodynamics of hyperfiltration (reverse osmosis): criteria for efficient membranes. *Desalination* **1966**, *1*, 311–326.
- Stamatialis, D. F.; Dias, C. R.; de Pinho, M. N. Atomic force microscopy of dense and asymmetric cellulose-based membranes. *J. Membr. Sci.* **1999**, *160*, 235–242.
- Steinle-Darling, E.; Reinhard, M. Nanofiltration for trace organic contaminant removal: structure, solution, and membrane fouling effects on the rejection of perfluorochemicals. *Environmental Sci. Technol.* **2008**, *42* (14), 5292–5297.
- Steinle-Darling, E.; Litwiller, E.; Reinhard, M. Effects of sorption on the rejection of trace organic contaminants during nanofiltration. *Environ. Sci. Technol.* **2010**, *44*, 2592–2598.
- Straatsma, J.; Bargeman, G.; van der Horst, H. C.; Wesselingh, J. A. Can nanofiltration be fully predicted by a model? *J. Membr. Sci.* **2002**, *198*, 273–284.
- Sutzkover, I.; Hasson, D.; Semiat, R. Simple technique for measuring the concentration polarization level in a reverse osmosis system. *Desalination* **2000**, *131*, 117–127.
- Tan, J. M. A.; Matsuura, T. Effect of non-solvent additive on the surface morphology and the gas separation performance of poly(2,6-dimethyl-1,4-phenylene) oxide membranes. *J. Membr. Sci.* **1999**, *160*, 7.
- Tanninen, J.; Nystrom, M. Separation of ions in acidic conditions using NF. *Desalination* **2002**, *147*, 295–299.
- Taylor, J. S.; Jacobs, E. P. Reverse osmosis and nanofiltration. In *Water Treatment Membrane Processes*, Mallevalle, J., Odendaal, P. E., Wiesner, M. R., Eds.; McGraw-Hill: New York, 1996; pp. 4.1–4.20.
- Taylor, J. S.; Chen, S.-S.; Mulford, L. A.; Norris, C. D. *Flat sheet, bench and pilot testing for pesticide removal using reverse osmosis*. AWWA Research Foundation: Denver, CO. 2000.
- Timmer, J. M. K. Properties of nanofiltration membranes; model development and industrial application. Doctoral dissertation, Technische Universiteit Eindhoven, Eindhoven, The Netherlands, 2001.
- Tödthheide, V.; Laufenberg, G.; Kunz, B. Waste water treatment using reverse osmosis: real osmotic pressure and chemical functionality as influencing parameters on the

- retention of carboxylic acids in multi-component systems. *Desalination* **1997**, *110*, 213–222.
- Tsuru, T.; Nakao, S.-I.; Kimura, S. Calculation of ion rejection by extended Nernst-Planck equation with charged reverse osmosis membranes for single and mixed electrolyte solutions. *J. Chem. Eng. Jpn.* **1991a**, *24*, 511–517.
- Tsuru, T.; Urairi, M.; Nakao, S.-I.; Kimura, S. Reverse osmosis of single and mixed electrolytes with charged membranes: experiment and analysis. *J. Chem. Eng. Jpn.* **1991b**, *24*, 518–524.
- Tu, S.-C.; Ravindran, V.; Den, W.; Pirbazari, M. Predictive membrane transport model for nanofiltration processes in water treatment. *AIChE J.* **2001**, *47*, 1346–1362.
- Urase, T.; Sato, K. The effect of deterioration of nanofiltration membrane on retention of pharmaceuticals. *Desalination* **2007**, *202*, 385–391.
- Van der Bruggen, B.; Vandecasteele, C. Flux decline during nanofiltration of organic components in aqueous solution. *Environ. Sci. Technol.* **2001**, *35*, 3535–3540.
- Van der Bruggen, B.; Vandecasteele, C. Modeling of the retention of uncharged molecules with nanofiltration. *Water Res.* **2002**, *36*, 1360–1368.
- Van der Bruggen, B.; Schaep, J.; Maes, W.; Wilms, D.; Vandecasteele, C. Nanofiltration as a treatment method for the removal of pesticides from ground waters. *Desalination* **1998**, *117*, 139.
- Van der Bruggen, B.; Schaep, J.; Wilms, D.; Vandecasteele, C. Influence of molecular size, polarity and charge on the retention of organic molecules by nanofiltration. *J. Membr. Sci.* **1999**, *156*, 29–41.
- Van der Bruggen, B.; Everaert, K.; Wilms, D.; Vandecasteele, C. Application of nanofiltration for removal of pesticides, nitrate and hardness from ground water: rejection properties and economic evaluation. *J. Membr. Sci.* **2001**, *193*, 239–248.
- Van der Bruggen, B.; Braeken, L.; Vandecasteele, C. Evaluation of parameters describing flux decline in nanofiltration of aqueous solutions containing organic compounds. *Desalination* **2002**, *147*, 281–288.
- Van der Bruggen, B.; Manttari, M.; Nystrom, M. Drawbacks of applying nanofiltration and how to avoid them: a review. *Sep. Purif. Technol.* **2008**, *63*, 251–263.
- Vanderford, B. J.; Pearson, R. A.; Rexing, D. J.; Snyder, S. A. Analysis of endocrine disruptors, pharmaceuticals, and personal care products in water using liquid chromatography/tandem mass spectrometry. *Anal. Chem.* **2003**, *75*, 6265–6274.
- Vanderford, B. J.; Snyder, S. A. Analysis of pharmaceuticals in water by isotope dilution liquid chromatography/tandem mass spectrometry. *Environ. Sci. Technol.* **2006**, *40*, 7312–7320.
- Verliefde, A.; Cornelissen, E.; Amy, G.; Van der Bruggen, B.; van Dijk, H. Priority organic micropollutants in water sources in Flanders and the Netherlands and assessment of removal possibilities with nanofiltration. *Environ. Pollut.* **2007**, *46*, 281–289.

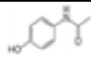
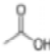
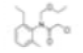
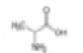

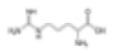
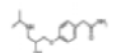
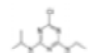

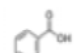
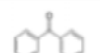
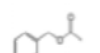
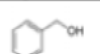



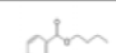
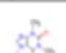
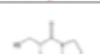

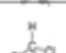
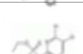
- Verma, R. O.; Hansch, C. Matrix metalloproteinases (MMPs): Chemical-biological functions and QSAR. *Bioorganic & Medicinal Chemistry* **2007**, *15*, 2223–2268.
- Vezzani, D.; Bandini, S. Donnan equilibrium and dielectric exclusion for characterization of nanofiltration membranes. *Desalination* **2002**, *149*, 477–483.
- Wang, X.-L.; Tsuru, T.; Nakao, S.-I.; Kimura, S. The electrostatic and steric-hindrance model for the transport of charged solutes through nanofiltration membranes. *J. Membr. Sci.* **1997**, *135*, 19–32.
- Wang, X.-L.; Wang, W.-N.; Wang, D.-X. Experimental investigation on separation performance of nanofiltration membranes for inorganic electrolyte solutions. *Desalination* **2002**, *145*, 115–122.
- Wendler, B.; Goers, B.; Wozny, G. Nanofiltration of solutions containing surfactants—Prediction of flux decline and mass transfer. *Desalination* **2002**, *147*, 217–222.
- Wijmans, J. G.; Baker, R. W. The solution–diffusion model: A review. *J. Membr. Sci.* **1995**, *107*, 1–21.
- Williams, M. E.; Hestekin, J. A.; Smothers, C. N.; Bhattacharyya, D. Separation of organic pollutants by reverse osmosis and nanofiltration membranes: Mathematical models and experimental verification. *Ind. Eng. Chem. Res.* **1999**, *38*, 3683–3695.
- Wintgens, T.; Gallenkemper, M.; Melin, T. Occurrence and removal of endocrine disrupters in landfill leachate treatment plants. *Water Sci. Technol.* **2003**, *48*, 127–134.
- Wold, S. PLS for multivariate linear modeling. In *Chemometric methods in molecular design: Methods and principles in medicinal chemistry*; van de Waterbeemd, H., Ed. VCH: New York, 1995; pp 195–218.
- Xu, Y.; Lebrun, R. E. Investigation of the solute separation by charged nanofiltration membrane: Effect of pH, ionic strength and solute type. *J. Membr. Sci.* **1999**, *158*, 93–104.
- Xu, P.; Drewes, J. E.; Bellona, C.; Amy, G.; Kim, T.-U.; Adam, M.; Heberer, T. Rejection of emerging organic micropollutants in nanofiltration/reverse osmosis membrane application. *Water Environ. Res.* **2005**, *17*, 40–48.
- Xu, P.; Drewes, J. E.; Kim, T.-U.; Bellona, C.; Amy, G. Effect of membrane fouling on transport of organic contaminants in NF/RO membrane applications. *J. Membr. Sci.* **2006**, *279*, 165–175.
- Yangali-Quintanilla, V.; Sadmani, A.; McConville, M.; Kennedy, M.; Amy, G. A QSAR model for predicting rejection of emerging contaminants (pharmaceuticals, endocrine disruptors) by nanofiltration membranes. *Water Res.* **2010** *44* (2), 373–384..
- Yoon, Y.; Lueptow, R. M. Removal of organic compounds by NF and RO membranes. *J. Membr. Sci.* **2005**, *261*, 76–86.
- Yoon, S.-H.; Lee, C.-H.; Kim, K.-J.; Fane, A. G. Effect of calcium ion on the fouling of nanofilter by humic acid in drinking water production. *Water Res.* **1998**, *32*, 2180–2186.
- Yoon, Y.; Amy, G.; Cho, J.; Her, N.; Pellegrino, J. Transport of perchlorate (ClO₄⁻) through NF and UF membranes. *Desalination* **2002**, *147*, 11–17.
- Zhao, Y. Modeling of membrane solute mass transfer in NF/RO membrane systems. Doctoral thesis, University of Central Florida, Orlando, FL, 2004.

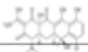

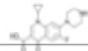
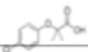
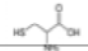


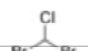
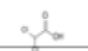


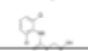
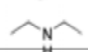
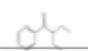
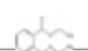
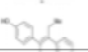
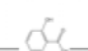

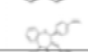

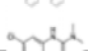
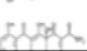
- Zhao, W.; Song, L. Experimental study of water and salt fluxes through reverse osmosis membranes. *Environ Sci. Technol.* **2005**, *39*, 3382–3387.
- Zhao, Y.; Taylor, J. S. Modeling membrane performance over time. *J.—Am. Water Works Assoc.* **2004**, *96*, 90–97.
- Zhao, Y.; Taylor, J.; Hong, S. Combined influence of membrane surface properties and feed water qualities on RO/NF mass transfer: A pilot study. *Water Res.* **2005**, *39*, 1233–1244.
- Zheng, F.; Zhang, Z.; Li, C.; Yuan, Q. A comparative study of suitability on different molecular size descriptors with the consideration of molecular geometry in nanofiltration. *J. Membr. Sci.* **2009**, *332*, 13–23.

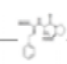
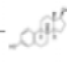
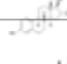
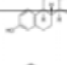

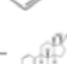
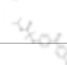
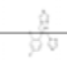
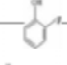
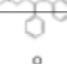
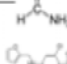
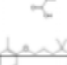

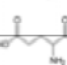
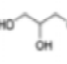
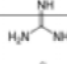
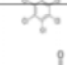
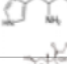
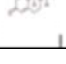



Appendix A

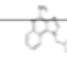
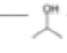

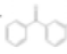
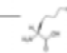


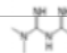
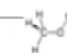
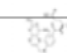
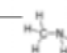
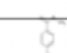
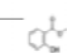
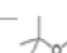
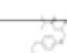
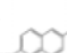

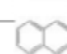


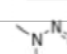
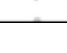
Supplemental Information



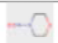



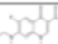
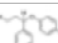
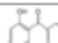




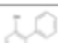
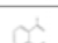
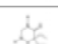

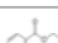

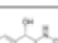


Table A.1. Compounds Selected For Study. 1Data from Chemfinder/SRC Physprop; 2Data from ACD Software (v. 8.14)

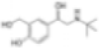
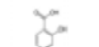
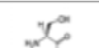

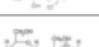
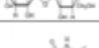
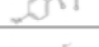
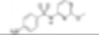
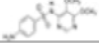
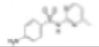
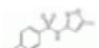


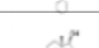
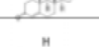

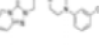
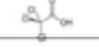

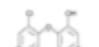


Compound	CAS Number	Structure	Molecular Weight ¹ (g/mol)	Class	log Kow ¹	log D ²					Analysis Method
						pH 4	pH 6	pH 7	pH 8	pH 9	
Acetaminophen	103-90-2		151.20	HN	0.46	0.34	0.34	0.34	0.33	0.28	LC-MS-MS
Acetic Acid	64-19-7		60.10	HCN	-0.17	-0.35	-1.52	-2.48	-3.38	-3.90	TOC
Acetochlor	34256-82-1		269.80	HoN	3.03	2.92	2.92	2.92	2.92	2.92	GC-ECD
Alanine	56-41-7		89.10	HCNP	NA	-3.18	-3.18	-3.18	-3.19	-3.27	TOC
Amitriptyline	50-48-6		277.41	HCP	4.92	1.31	1.57	2.28	3.21	3.78	LC-MS-MS
Arginine	74-79-3		174.20	HCNP	-4.20	-5.30	-5.29	-5.28	-5.20	-4.84	TOC
Atenolol	29122-68-7		266.30	HCP	0.16	-3.00	-2.73	-2.02	-1.09	-0.29	HPLC-DAD LC-MS-MS
Atrazine	1912-24-9		215.70	HHoN	2.61	2.60	2.63	2.63	2.63	2.63	HPLC-DAD LC-MS-MS
Baclofen	1134-47-0		213.67	HCNP	-0.96	-1.15	-0.94	-0.94	-0.94	-0.96	HPLC-DAD
Benzoic Acid	65-85-0		122.12	HCN	1.87	1.68	1.03	0.11	-0.74	-1.17	HPLC-DAD
Benzophenone	119-61-9		182.20	HoN	3.18	3.18	3.18	3.18	3.18	3.18	HPLC-DAD LC-MS-MS
Benzyl Acetate	140-11-4		150.18	HN	1.96	1.93	1.93	1.93	1.93	1.93	HPLC-DAD
Benzyl Alcohol	100-51-6		108.10	HN	1.10	1.03	1.03	1.03	1.03	1.03	HPLC-DAD
Bisphenol-A	80-05-7		228.30	HoN	3.32	3.43	3.43	3.43	3.43	3.39	HPLC-DAD LC-MS-MS
Bromoform	75-25-2		252.70	HHoN	2.40	2.29	2.29	2.29	2.29	2.29	GC-ECD
1,4-Butanediol	110-63-4		90.12	HN	-0.83	-1.02	-1.02	-1.02	-1.02	-1.02	HPLC-RID
Butylparaben	94-26-8		194.23	HoN	3.57	3.46	3.46	3.43	3.25	2.61	HPLC-DAD
Caffeine	58-08-2		194.20	HN	-0.07	-0.13	-0.13	-0.13	-0.13	-0.13	HPLC-DAD LC-MS-MS
Captopril	62571-86-2		217.30	HCN	0.34	-0.21	-2.02	-2.90	-3.38	-3.51	TOC
Carbamazepine	298-46-4		236.30	HHoN	2.45	2.67	2.67	2.67	2.67	2.67	LC-MS-MS
Chloroform	67-66-3		119.40	HN	1.97	1.76	1.76	1.76	1.76	1.76	GC-ECD
Chlorpyrifos	2921-88-2		350.60	HoN	4.96	4.77	4.77	4.77	4.77	4.77	GC-ECD

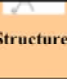
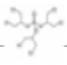
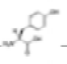
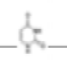

Compound	CAS Number	Structure	Molecular Weight ¹ (g/mol)	Class	log Kow ¹	log D ¹					Analysis Method
						pH 4	pH 6	pH 7	pH 8	pH 9	
Chlortetracycline	57-62-5		478.90	HN	-0.62	-3.18	-2.87	-3.11	-3.81	-4.55	HPLC-DAD
Cimetidine	51481-61-9		252.30	HCP	0.40	-2.39	-1.28	-0.45	-0.02	0.06	HPLC-DAD
Ciprofloxacin	85721-33-1		331.30	HCN	0.28	-1.75	-1.07	-0.85	-0.95	-1.47	HPLC-DAD
Clofibrilic Acid	882-09-7		214.60	HCN	2.60	1.85	-0.04	-0.76	-0.99	-1.02	HPLC-DAD
Cysteine	52-90-4		121.30	HCNP	-2.50	-2.27	-2.27	-2.32	-2.61	-3.10	TOC
Desloratadine	100643-71-8		310.83	HoN	NA	-0.80	0.08	0.78	1.73	2.66	HPLC-DAD
Dibromoacetic Acid	631-64-1		217.85	HN	NA	-0.85	-2.03	-2.09	-2.10	-2.10	GC-HAA
Dibromochloromethane	124-48-1		208.30	HHoN	2.16	2.20	2.20	2.20	2.20	2.20	GC-ECD
Dichloroacetic Acid	79-43-6		128.90	HCN	0.92	-2.06	-3.15	-3.20	-3.21	-3.21	GC-HAA
Dichlorobromomethane	75-27-4		163.80	HHoN	2.00	2.02	2.02	2.02	2.02	2.02	GC-ECD
2,4-Dichlorophenol	120-83-2		163.00	HoN	3.06	2.99	2.99	2.96	2.72	2.00	HPLC-DAD
Diclofenac	15307-86-5		295.10	HCN	4.50	3.84	2.23	1.28	0.57	0.34	HPLC-DAD LC-MS-MS
Diethylamine	109-89-7		73.14	HCP	0.58	-2.47	-2.46	-2.38	-1.97	-1.12	TOC
Diethyl-m-toulamide (DEET)	134-62-3		191.30	HHoN	2.20	1.96	1.96	1.96	1.96	1.96	HPLC-DAD LC-MS-MS
Diethylphthalate	84-66-2		222.20	HHoN	2.42	2.70	2.70	2.70	2.70	2.70	HPLC-DAD
Diethylstilbestrol	56-53-1		268.40	HoN	5.10	5.93	5.93	5.93	5.93	5.93	HPLC-DAD
1,4-Dihydroxybenzoic Acid	99-10-5		154.10	HCN	0.86	0.80	-0.89	-1.67	-1.98	-2.06	HPLC-DAD
Dilantin	57-41-0		252.30	HHoN	2.47	2.52	2.52	2.50	2.36	1.79	LC-MS-MS
Diltiazem	42399-41-7		414.50	HCP	NA	0.54	0.92	1.72	2.65	3.36	HPLC-DAD
Diphenhydramine	58-73-1		255.40	HCP	3.27	0.57	1.07	1.92	2.84	3.46	LC-MS-MS
Diuron	330-54-1		233.10	HHoN	2.70	2.78	2.78	2.78	2.78	2.78	GC-ECD
Doxycycline	564-25-0		444.45	HCNP	-0.02	-3.39	-3.06	-3.17	-3.74	-4.67	HPLC-DAD

Compound	CAS Number	Structure	Molecular Weight ¹ (g/mol)	Class	log Kow ¹	log D ²					Analysis Method
						pH 4	pH 6	pH 7	pH 8	pH 9	
Enalapril	75847-73-3		376.46	HCN	0.07	0.67	0.08	-0.72	-1.21	-1.31	HPLC-DAD
17β Estradiol	50-28-2		272.40	HoN	4.01	4.13	4.13	4.13	4.13	4.11	LC-MS-MS
Estriol	50-27-1		288.40	HHoN	2.45	2.94	2.94	2.94	2.94	2.92	LC-MS-MS
Estrone	53-16-7		270.40	HoN	3.13	3.69	3.69	3.69	3.68	3.66	LC-MS-MS
Ethanol	64-17-5		46.10	HN	-0.31	-0.19	-0.19	-0.19	-0.19	-0.19	HPLC-RID
Ethylbenzene	100-41-4		106.20	HoN	3.15	3.21	3.21	3.21	3.21	3.21	HPLC-DAD
Ethynyl Estradiol	57-63-6		296.40	HoN	3.67	4.52	4.52	4.52	4.52	4.49	LC-MS-MS
Fenofibrate	49562-28-9		360.80	HoN	5.20	4.80	4.80	4.80	4.80	4.80	HPLC-DAD
Fluconazole	86386-73-4		306.27	HN	NA	-0.05	-0.04	-0.04	-0.04	-0.04	HPLC-DAD
2-Fluorophenol	367-12-4		112.10	HN	1.71	1.71	1.71	1.70	1.63	1.24	HPLC-DAD
Fluoxetine	54910-89-3		309.30	HoN	4.05	0.99	1.03	1.31	2.06	3.00	LC-MS-MS
Formamide	75-12-7		45.00	HN	-1.51	-1.51	-1.51	-1.51	-1.51	-1.51	HPLC-RID
Furosemide	54-31-9		330.70	HN	2.03	2.00	0.26	-0.09	-0.15	-0.21	HPLC-DAD
Gemfibrozil	25812-30-0		250.30	HCN	4.80	4.32	3.12	2.15	1.26	0.76	HPLC-DAD LC-MS-MS
Glucose	50-99-7		180.20	HN	-3.24	-3.17	-3.17	-3.17	-3.17	-3.17	HPLC-RID
L-Glutamic Acid	56-86-0		147.10	HCN	-3.70	-4.03	-4.81	-4.92	-4.94	-5.00	TOC
Glycerol (Glycerin)	56-81-5		92.10	HN	-1.76	-2.32	-2.32	-2.32	-2.32	-2.32	HPLC-RID
Guanidine	113-00-8		59.10	HCP	-1.63	-3.81	-3.81	-3.81	-3.81	-3.81	TOC
Hexachlorobenzene	118-74-1		284.80	HoN	5.73	4.89	4.89	4.89	4.89	4.89	GC-ECD
Histidine	71-00-1		155.20	HCN	-3.32	-4.76	-4.48	-4.00	-3.81	-3.87	HPLC-DAD
Hydrocortisone (Cortisol)	50-23-7		362.70	HN	1.61	1.43	1.43	1.43	1.43	1.43	HPLC-DAD
Ibuprofen	15687-27-1		206.30	HCN	3.97	3.58	2.12	1.16	0.36	0.03	HPLC-DAD LC-MS-MS

Compound	CAS Number	Structure	Molecular Weight ¹ (g/mol)	Class	log Kow ¹	log D ²					Analysis Method
						pH 4	pH 6	pH 7	pH 8	pH 9	
Imiquimod	99011-02-6		240.30	HCP	NA	0.98	1.76	2.63	3.26	3.43	HPLC-DAD
Isopropanol	67-63-0		60.10	HN	0.05	0.16	0.16	0.16	0.16	0.16	HPLC-RID
Ketoconazole	65277-42-1		531.44	HCP	4.35	0.21	2.51	3.29	3.51	3.54	HPLC-DAD
Ketoprofen	22071-15-4		254.30	HCN	3.12	2.61	1.04	0.09	-0.64	-0.90	HPLC-DAD LC-MS-MS
Lysine	56-87-1		146.20	HCNP	-3.05	-4.55	-4.53	-4.52	-4.41	-3.99	TOC
Maleic Acid	110-16-7		116.07	HCN	-0.48	-2.08	-4.49	-5.11	-5.19	-5.20	HPLC-DAD
Meprobamate	57-53-4		218.30	HN	0.70	0.70	0.70	0.70	0.70	0.70	LC-MS-MS
Metformin	657-24-9		129.20	HCP	-2.64	-4.32	-4.31	-4.31	-4.31	-4.31	LC-MS-MS
Methanol	67-56-1		32.00	HN	-0.77	-0.72	-0.72	-0.72	-0.72	-0.72	HPLC-RID
Methotrexate	59-05-2		454.45	HCN	-1.85	-2.79	-4.39	-4.90	-4.98	-4.99	HPLC-DAD
Methylamine	74-89-5		31.10	HCP	-0.57	-3.76	-3.75	-3.66	-3.19	-2.32	TOC
Methylparaben	99-76-3		152.15	HN	1.96	1.86	1.86	1.84	1.69	1.09	LC-MS-MS
Methyl Salicylate	119-36-8		152.15	HHoN	2.55	2.23	2.23	2.23	2.23	2.16	HPLC-DAD
Methyl-tert-butyl-ether (MTBE)	1634-04-4		88.20	HN	0.94	1.15	1.15	1.15	1.15	1.15	HPLC-RID
Metoprolol	37350-58-6		267.40	HCP	1.90	-1.31	-1.04	-0.33	0.60	1.40	HPLC-DAD
Naproxen	22204-53-1		230.30	HCN	3.18	2.94	1.81	0.85	-0.06	-0.61	HPLC-DAD LC-MS-MS
1-Naphthalenemethanol	4780-79-4		158.20	HHoN	2.37	2.26	2.26	2.26	2.26	2.26	HPLC-DAD
2-Naphthol	135-19-3		144.20	HHoN	2.70	2.71	2.71	2.71	2.70	2.61	HPLC-DAD
n-Nitrosodibutylamine	924-16-3		158.20	HHoN	2.63	2.55	2.55	2.55	2.55	2.55	LC-MS-MS
n-Nitrosodiethylamine	55-18-5		102.10	HN	0.48	0.42	0.42	0.42	0.42	0.42	LC-MS-MS
n-Nitrosodimethylamine	62-75-9		74.10	HN	-0.57	-0.64	-0.64	-0.64	-0.64	-0.64	LC-MS-MS
n-Nitrosodiphenylamine	86-30-6		198.23	HoN	3.13	3.13	3.13	3.13	3.13	3.13	LC-MS-MS

Compound	CAS Number	Structure	Molecular Weight ¹ (g/mol)	Class	log Kow ¹	log D ¹					Analysis Method
						pH 4	pH 6	pH 7	pH 8	pH 9	
n-Nitrosodipropylamine	621-64-7		130.20	HN	1.36	1.49	1.49	1.49	1.49	1.49	LC-MS-MS
n-Nitrosomethylethylamine	10595-95-6		88.11	HN	0.04	0.01	0.01	0.01	0.01	0.01	LC-MS-MS
n-Nitrosomorpholine	59-89-2		116.10	HN	-0.44	-0.55	-0.55	-0.55	-0.55	-0.55	LC-MS-MS
n-Nitrosopiperidine	100-75-4		114.10	HN	0.36	0.41	0.41	0.41	0.41	0.41	LC-MS-MS
n-Nitrosopyrrolidine	930-55-2		100.10	HN	-0.20	-0.15	-0.15	-0.15	-0.15	-0.15	LC-MS-MS
4-Nonylphenol	104-40-5		220.40	HoN	5.76	6.19	6.19	6.19	6.19	6.16	LC-MS-MS
Norflloxacin	70458-96-7		319.30	HCNP	-1.03	-1.59	-0.90	-0.68	-0.78	-1.30	HPLC-DAD LC-MS-MS
Norfluoxetine	126924-38-7		295.30	HCP	NA	3.38	3.38	3.38	3.38	3.38	LC-MS-MS
Oxybenzone	131-57-7		228.30	HoN	3.80	3.64	3.63	3.53	3.07	2.19	LC-MS-MS
Oxytetracycline	79-57-2		460.44	HN	-0.90	-4.35	-4.03	-4.18	-4.87	-5.75	HPLC-DAD
Pentoxifylline	6493-05-6		278.30	HN	0.29	0.32	0.32	0.32	0.32	0.32	HPLC-DAD
Phenacetin	62-44-2		179.20	HN	1.60	1.63	1.63	1.63	1.63	1.63	HPLC-DAD
Phenylalanine	63-91-2		165.19	HCN	-1.38	-2.27	-2.26	-2.27	-2.29	-2.30	HPLC-DAD
2-Phenylphenol	90-43-7		170.21	HoN	3.09	2.94	2.94	2.94	2.94	2.94	HPLC-DAD
o-Phthalaldehyde	643-79-8		134.13	HN	1.43	0.39	0.39	0.39	0.39	0.39	HPLC-DAD
Primidone	125-33-7		218.30	HN	0.91	0.40	0.40	0.40	0.40	0.40	HPLC-DAD LC-MS-MS
Progesterone	57-83-0		314.40	HoN	3.90	4.04	4.04	4.04	4.04	4.04	LC-MS-MS
Propylparaben	94-13-3		180.21	HHoN	3.04	2.93	2.92	2.90	2.72	2.09	HPLC-DAD LC-MS-MS
Propyphenazone	479-92-5		230.30	HN	1.94	1.74	1.74	1.74	1.74	1.74	HPLC-DAD
Pseudoephedrine	90-82-4		165.20	HCP	0.89	-2.04	-1.86	-1.25	-0.33	0.52	HPLC-DAD
Ranitidine	66357-35-5		314.40	HCP	0.27	-1.86	-1.09	-0.18	0.68	1.13	HPLC-DAD
Resorcinol	108-46-3		110.10	HN	0.80	0.76	0.76	0.76	0.75	0.69	HPLC-DAD

Compound	CAS Number	Structure	Molecular Weight ¹ (g/mol)	Class	log Kow ¹	log D ²					Analysis Method
						pH 4	pH 6	pH 7	pH 8	pH 9	
Salbutamol	18559-94-9		239.32	HCP	0.64	-3.08	-2.84	-2.15	-1.23	-0.46	HPLC-DAD
Salicylic Acid	69-72-7		138.10	HCN	2.30	-4.08	-4.08	-4.08	-4.11	-4.31	HPLC-DAD
Serine	56-45-1		105.10	HCNP	-3.10	-4.08	-4.08	-4.08	-4.11	-4.31	TOC
Sucralose	56038-13-2		397.64	HN	-1.00	0.23	0.23	0.23	0.23	0.23	LC-MS-MS
Sucrose	57-50-1		342.30	HN	-3.70	-3.48	-3.48	-3.48	-3.48	-3.48	HPLC-RID
Sulfacetamide	144-80-9		214.20	HCN	-0.96	-0.97	-1.48	-2.27	-2.81	-2.95	HPLC-DAD
Sulfadimethoxine	122-11-2		310.30	HCN	1.63	1.48	1.28	0.66	-0.10	-0.45	HPLC-DAD
Sulfadoxine	2447-57-6		310.33	HCN	0.70	0.34	0.11	-0.53	-1.28	-1.60	HPLC-DAD
Sulfamerazine	127-79-7		264.31	HCN	0.14	0.34	0.30	0.03	-0.68	-1.37	HPLC-DAD
Sulfamethoxazole	723-46-6		253.30	HCP	0.90	0.88	0.49	-0.27	-0.90	-1.09	LC-MS-MS
Sulfasalazine	599-79-1		398.40	HCN	3.81	2.03	0.35	0.07	0.02	-0.07	HPLC-DAD
Tamoxifen	10540-29-1		371.52	HCP	6.30	4.79	5.33	6.20	7.11	7.71	HPLC-DAD
Testosterone	58-22-0		288.40	HoN	3.32	3.47	3.47	3.47	3.47	3.47	LC-MS-MS
Thiabendazole	148-79-8		201.25	HHoN	2.47	2.22	2.47	2.47	2.47	2.46	HPLC-DAD
Trazodone	19794-93-5		371.86	HCP	3.21	-0.93	0.85	1.47	1.64	1.66	HPLC-DAD
Trichloroacetic Acid	76-03-9		163.40	HCN	1.33	-1.85	-2.08	-2.08	-2.08	-2.08	GC-HAA
Triclocarbon	101-20-2		315.58	HoN	4.90	5.74	5.74	5.74	5.74	5.74	LC-MS-MS
Triclosan	3380-34-5		289.50	HoN	4.76	5.17	5.17	5.11	4.76	3.95	HPLC-DAD LC-MS-MS
Triethylene Glycol	112-27-6		150.20	HN	-1.98	-1.87	-1.87	-1.87	-1.87	-1.87	HPLC-RID
Trimethoprim	738-70-5		290.30	HCP	0.91	-1.63	-0.42	0.38	0.73	0.79	LC-MS-MS
Tris(2-chloroethyl)phosphate (TCEP)	115-96-8		285.50	HN	1.44	0.48	0.48	0.48	0.48	0.48	LC-MS-MS
Tris(1-chloro-2-propyl)-phosphate (TCPP)	13674-84-5		327.60	HN	2.60	1.53	1.53	1.53	1.53	1.53	LC-MS-MS

Compound	CAS Number	Structure	Molecular Weight ¹ (g/mol)	Class	log Kow ¹	log D ²					Analysis Method
						pH 4	pH 6	pH 7	pH 8	pH 9	
Tris(1,3-dichloro-2-propyl)phosphate (TDCPP)	13674-87-8		430.90	HoN	3.65	1.79	1.79	1.79	1.79	1.79	LC-MS-MS
Tyrosine	60-18-4		181.19	HHoN	-2.26	-2.92	-2.92	-2.92	-2.92	-2.92	HPLC-DAD
Uracil	66-22-8		112.10	HN	-1.07	-0.71	-0.71	-0.71	-0.73	-0.92	HPLC-DAD
Urea	57-13-6		60.10	HN	-2.10	1.69	1.69	1.69	1.69	1.69	HPLC-RID
Warfarin	81-81-2		308.34	HHoN	2.70	3.30	1.91	0.96	0.22	-0.04	HPLC-DAD

Appendix B

Equations Employed

Ionic Strength:

$$I = \frac{1}{2} \sum_{i=1}^n c_i z_i^2 \quad (\text{B.1})$$

Where I is the ionic strength, c_i is the molar concentration in moles per liter, and z_i is the charge of the solute

Permeate Flux:

$$J_v = \frac{Q_p}{A} \quad (\text{B.2})$$

Where J_v is the permeate flux, Q_p is the volumetric permeate flow rate, and A is the cross-sectional area of the membrane.

Recovery:

$$\text{Recovery (\%)} = \frac{Q_p}{Q_f} \times 100 \quad (\text{B.3})$$

Where Q_p is the volumetric permeate flow rate and Q_f is the volumetric feed flow rate.

Sherwood Number:

$$Sh = \frac{k d_H}{D_i} = a Re^b Sc^c \quad (\text{B.4})$$

Where Sh is the Sherwood number, k is the MTC, d_H is the hydraulic diameter, D_i is the diffusion coefficient of the solute, Re is the Reynolds number, Sc is the Schmidt number, and a , b , and c were found experimentally to be 0.42, 0.5, and 0.33, respectively.

$$Re = \frac{\rho V d_H}{\mu} \quad (\text{B.5})$$

Where ρ is density, V is cross-flow velocity, and μ is viscosity.

$$Sc = \frac{\mu}{\rho D_i} \quad (\text{B.6})$$

$$d_H = \frac{4s}{2/h_{sp} + (1-s)S_{v,sp}} \quad (\text{B.7})$$

Where h_{sp} is the height of the feed space, $S_{v,sp}$ is defined by Equation A-9, and e is the porosity of the feed spacer (Schock and Miquel, 1987).

$$V = \frac{Q_F}{bh_{sp}s} \quad (\text{B.8})$$

Where b is the channel width (Schock and Miquel, 1987).

$$S_{v,sp} = \frac{4}{d} \quad (\text{B.9})$$

Where d is the membrane thickness (Schock and Miquel, 1987).

Wilke–Chang Correlation for Determining the Solute Diffusion Coefficient:

$$D_i = \frac{6.4 \times 10^{-8} (\phi M)^{0.8} T}{\eta V_s^{0.6}} \quad (\text{B.10})$$

Where ϕ is an association factor for hydrogen bonding (set at 2.26 for water as the solvent), M is the molecular weight of the solvent (grams/mole), T is temperature, h is kinematic viscosity, and V_s is the molar volume of the solute.

LaBas molecular volume:

$$V_s = \sum_i n_i \Delta V'_{B,i} \quad (\text{B.11})$$

Where $V'_{B,i}$ are the molar volumes increments assigned to each substituent group. A list of molar volumes assigned to various substituent groups is presented in Table B.1.

Table B.1. LaBas Molar Volume Increments (Hofman et al., 2007)

Atom	DV' _{B,i} (10 ⁶ m ³ /mol)	Atom	DV' _{B,i} (10 ⁶ m ³ /mol)
C	14.8	Br	27.0
H	3.7	Cl in R-CHCl-R'	24.6
O (except as below)	7.4	Cl in RCl	21.6
Carbonyl	7.4	F	8.7
Aldehyde, ketone	7.4	I	37.0
Methyl ether	9.9	S	25.6
Ethyl ester	9.9	P	27.0
Higher esters	9.9	Ring	
Higher ethers	9.9	3-membered	-6.0
Acids (-OH)	11.0	4-membered	-8.6
Joined to S, P, N	8.3	5-membered	-11.5
N Double bonded	15.6	6-membered	-15.0
Primary amine	10.5	Naphthalene	-30.0
Secondary amine	12.0	Anthracene	-47.5

Stokes–Einstein equation for determining Stokes radius:

$$r_s = \frac{k_B T}{6\pi\eta D_t} \quad (\text{B.12})$$

Where k_B is Boltzman constant (J/K).

Appendix C

Quality Control of Bench-Scale Experimentation

Quality control experiments were carried out to ensure minimal variability during bench-scale testing. These experiments examined the effects of solutes tested alone or in a mixture or at high or low feed concentration or when methanol was used as a cosolvent. The variability between membranes was also examined. The experiments were conducted at bench scale with the same procedure described in Chapter 3.3.1.1.

Single Solute versus Mixture. With the large number of compounds to be tested and experiments and analytical tests being very time-consuming, testing each compound individually was not possible. Therefore, solutes were tested in batches of three to five compounds at a time as long as analytical tests allowed for quantification. A few compounds were tested individually to confirm little or no variability. All compounds tested exhibited little or no variability in results. Caffeine tested individually and in a mixture with 2-naphthol and resorcinol showed almost no variation in rejection under the same operating conditions as illustrated in Figure C.1.

Feed Water Concentration. Some analytical methods required different feed water concentrations. Before experiments began, a series of tests using different feed concentrations was performed to observe the effect of solute concentration on rejection. All compounds tested exhibited little or no variability. Caffeine was tested with a feed water concentration of 700 $\mu\text{g/L}$ and 5 mg/L and exhibited little or no variability (Figure C.2).

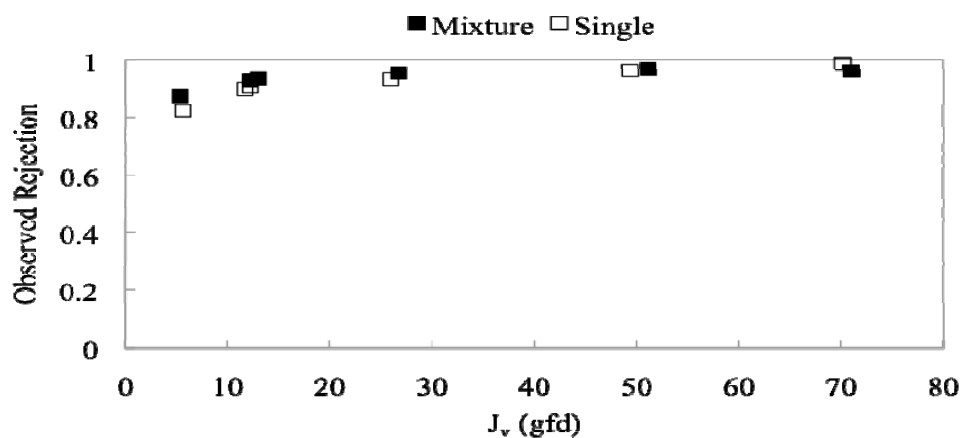


Figure C.1. Experiment with caffeine to test the effect of other solutes on rejection under the same operating conditions. The mixture consisted of caffeine with 2-naphthol and resorcinol.

Membrane Variability. Previous studies reported variability between membrane specimens with respect to solute rejection (Hofman et al., 2007). Rejection can vary between flat-sheet and spiral-wound membranes and also within a spiral-wound membrane. These variations are most likely due to imperfections during the membrane casting process. This variability was tested by using flat-sheet and spiral-wound membrane specimens with different compounds. The results from an experiment with caffeine, presented in Figure C.3, illustrate the greatest difference in results, with as much as 6% difference in rejection for the same permeate flux. Duplicate experiments on different membrane specimens were carried out in order to account for this variability.

Methanol as a Cosolvent. Some compounds are very hydrophobic and therefore have very low solubilities. These compounds needed a cosolvent in order to prepare the spike solution for experimentation. Preliminary experiments were conducted to test the effects of using methanol as a cosolvent with a variety of compounds. Two different experiments were conducted: one where a compound was dissolved in 100% methanol and another where a compound was dissolved in 100% deionized water. Little variability was observed whether methanol or deionized water was used as the solvent for 2-naphthol (Figure C.4).

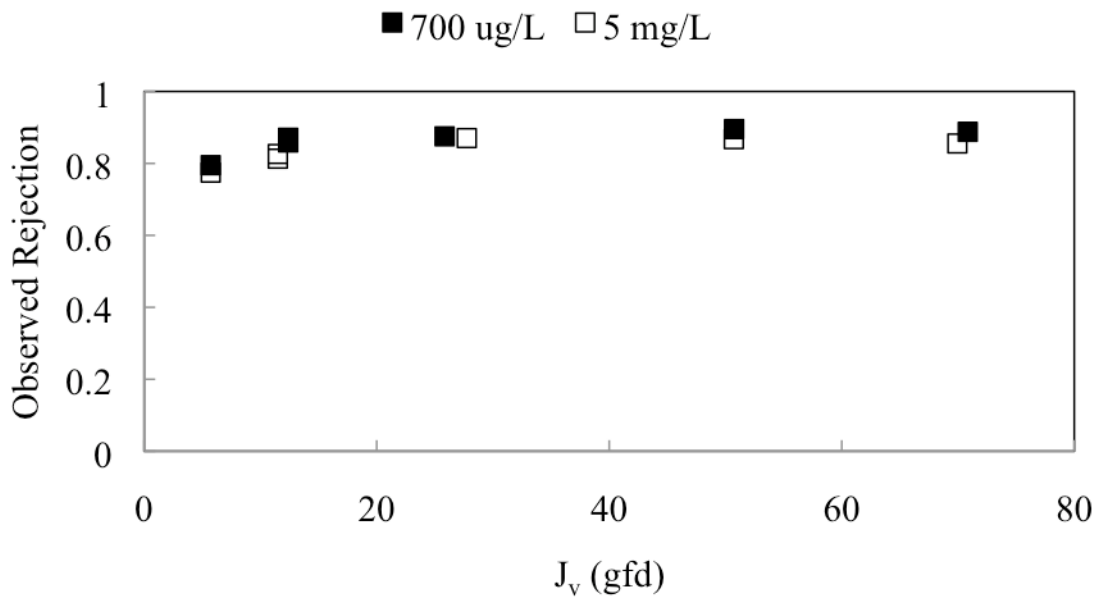


Figure C.2. Experiment with caffeine testing the variability in rejection with high concentration and low concentration under the same operating conditions.

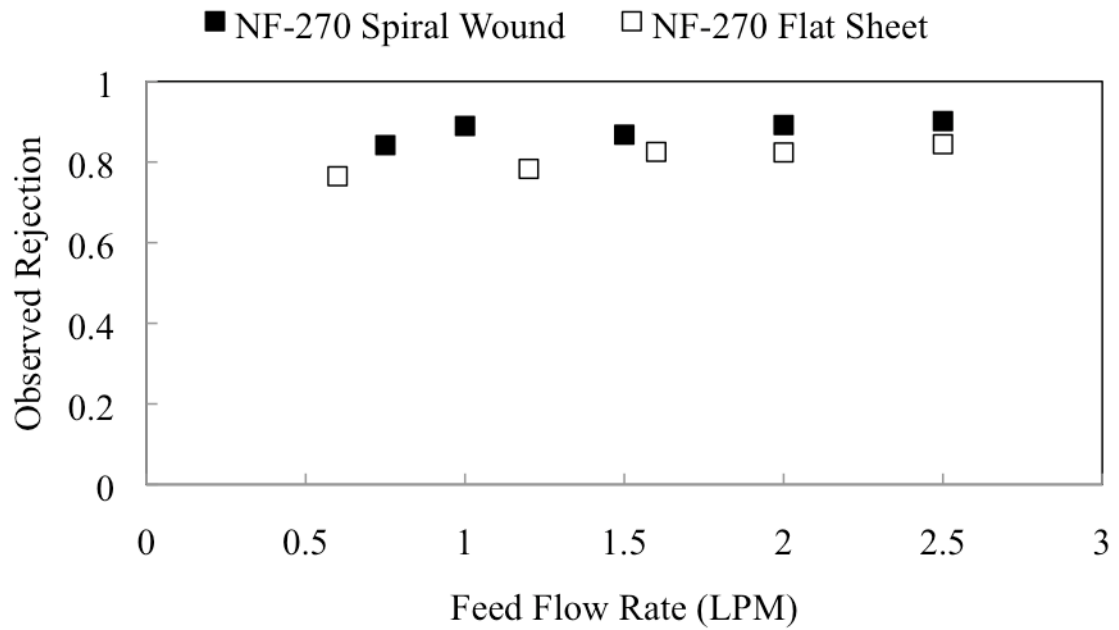


Figure C.3. Experiment with caffeine testing the variability between membrane specimens from a spiral-wound element and flat sheets under the same operating conditions.

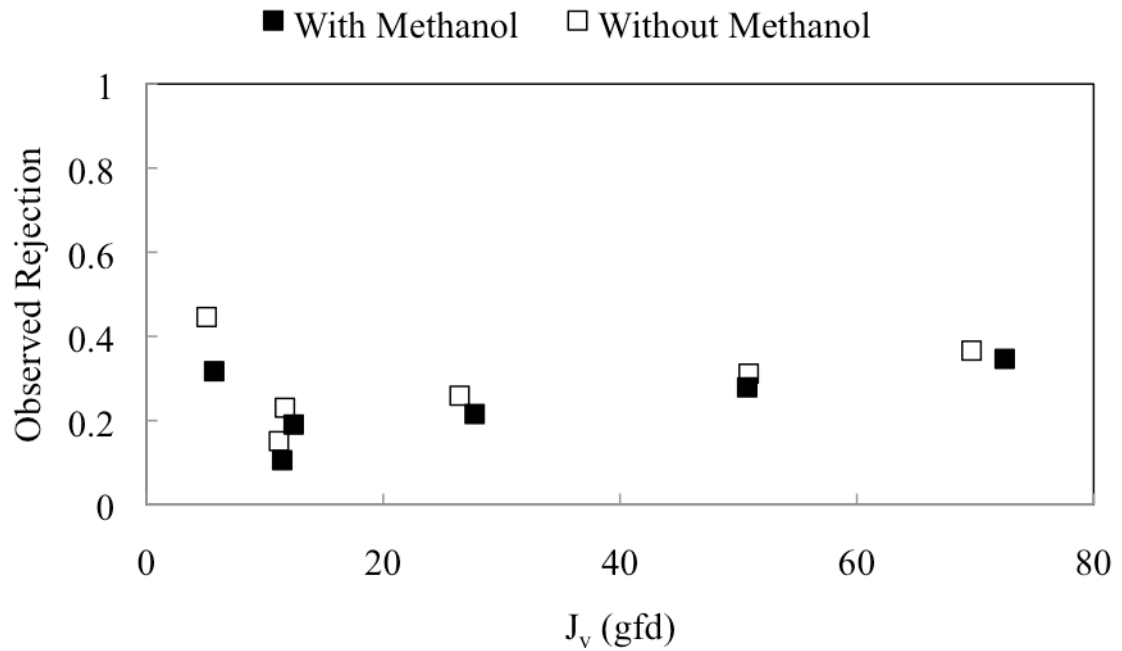


Figure C.4. Experiment with 2-naphthol testing the effects of using methanol as a solvent in order to increase solubility of the compound.

Appendix D

Correlation Matrix for Descriptors

Table D.1. Correlation Matrix for All the Descriptors Examined

	MW	Length	Width	Depth	EqWidth	Vol (Å ³)	Area (Å ²)	Hyd Energy	Polarization	LaBas Mol Vol	W-C Diff
MW	1.00	0.68	0.75	0.72	0.85	0.93	0.63	0.05	0.92	0.95	-0.83
Length (nm)	0.68	1.00	0.52	0.57	0.62	0.86	0.65	-0.05	0.83	0.83	-0.84
Width (nm)	0.75	0.52	1.00	0.52	0.88	0.80	0.58	0.05	0.78	0.78	-0.75
Depth (nm)	0.72	0.57	0.52	1.00	0.86	0.76	0.53	0.07	0.74	0.78	-0.66
EqWidth (nm)	0.85	0.62	0.88	0.86	1.00	0.89	0.64	0.07	0.87	0.90	-0.81
Vol (Å ³)	0.93	0.86	0.80	0.76	0.89	1.00	0.74	0.03	0.98	0.99	-0.90
Area (Å ²)	0.63	0.65	0.58	0.53	0.64	0.74	1.00	0.25	0.61	0.68	-0.62
Hydration E	0.05	-0.05	0.05	0.07	0.07	0.03	0.25	1.00	0.00	0.03	-0.04
Polarization (Å ³)	0.92	0.83	0.78	0.74	0.87	0.98	0.61	0.00	1.00	0.98	-0.90
LaBas Mol Vol	0.95	0.83	0.78	0.78	0.90	0.99	0.68	0.03	0.98	1.00	-0.89
W-C Diff Coeff	-0.83	-0.84	-0.75	-0.66	-0.81	-0.90	-0.62	-0.04	-0.90	-0.89	1.00
Stokes radius	0.93	0.85	0.78	0.77	0.89	0.99	0.68	0.03	0.98	0.99	-0.93
Log D (6)	0.32	0.44	0.33	0.11	0.26	0.42	0.39	0.38	0.48	0.38	-0.42
Vol (cm ³ /mol)	0.91	0.84	0.78	0.77	0.89	0.98	0.71	0.12	0.97	0.98	-0.89
Polar SA (Å ²)	0.43	0.25	0.33	0.40	0.42	0.37	0.07	-0.58	0.33	0.40	-0.32
Dipole	0.13	0.08	0.32	0.26	0.34	0.15	0.00	0.20	0.16	0.17	-0.18
SASA	0.89	0.89	0.78	0.76	0.88	0.97	0.69	0.04	0.96	0.97	-0.92
FOSA	0.21	0.42	0.14	0.58	0.41	0.39	0.49	0.11	0.29	0.38	-0.32
FISA	0.10	0.12	0.08	0.21	0.17	0.11	-0.17	-0.71	0.10	0.13	-0.10
PISA	0.23	0.40	0.35	-0.03	0.19	0.30	-0.05	-0.01	0.42	0.29	-0.39
WPSA	0.48	-0.05	0.27	0.11	0.22	0.25	0.42	0.43	0.19	0.26	-0.16
	MW	Length	Width	Depth	EqWidth	Vol (Å ³)	Area (Å ²)	Hyd Energy	Polarization	LaBas Mol Vol	W-C Diff
Vol	0.91	0.86	0.79	0.78	0.90	0.99	0.68	0.03	0.98	0.99	-0.91
glob	-0.66	-0.84	-0.59	-0.56	-0.66	-0.78	-0.64	-0.10	-0.74	-0.77	0.81
QPpolrz	0.88	0.84	0.80	0.70	0.86	0.96	0.61	0.09	0.99	0.96	-0.90
QPlogPC16	0.92	0.79	0.81	0.68	0.86	0.95	0.57	-0.11	0.96	0.95	-0.89
QPlogPoct	0.80	0.62	0.64	0.68	0.76	0.79	0.35	-0.41	0.79	0.81	-0.71
QPlogPw	0.38	0.24	0.24	0.38	0.36	0.32	-0.07	-0.67	0.33	0.36	-0.29
QPlogPo/w	0.55	0.55	0.52	0.28	0.47	0.62	0.58	0.50	0.64	0.59	-0.57
QPlogS	-0.79	-0.75	-0.70	-0.52	-0.70	-0.85	-0.65	-0.23	-0.87	-0.83	0.80
CIQlogS	-0.83	-0.66	-0.74	-0.52	-0.73	-0.85	-0.69	-0.23	-0.85	-0.83	0.72
IP (eV)	-0.20	-0.41	-0.43	-0.07	-0.29	-0.35	-0.11	0.11	-0.44	-0.32	0.47
EA (eV)	0.49	0.28	0.48	0.11	0.34	0.40	0.21	0.36	0.45	0.39	-0.54
E _{HOMO}	0.07	0.42	0.26	0.07	0.19	0.26	0.02	-0.24	0.35	0.24	-0.41
E _{LUMO}	-0.04	-0.06	-0.10	0.05	-0.03	-0.03	0.09	-0.38	-0.11	-0.02	0.24
Pot Energy	0.49	0.45	0.28	0.51	0.45	0.51	0.06	-0.32	0.60	0.53	-0.48

Table D.2.

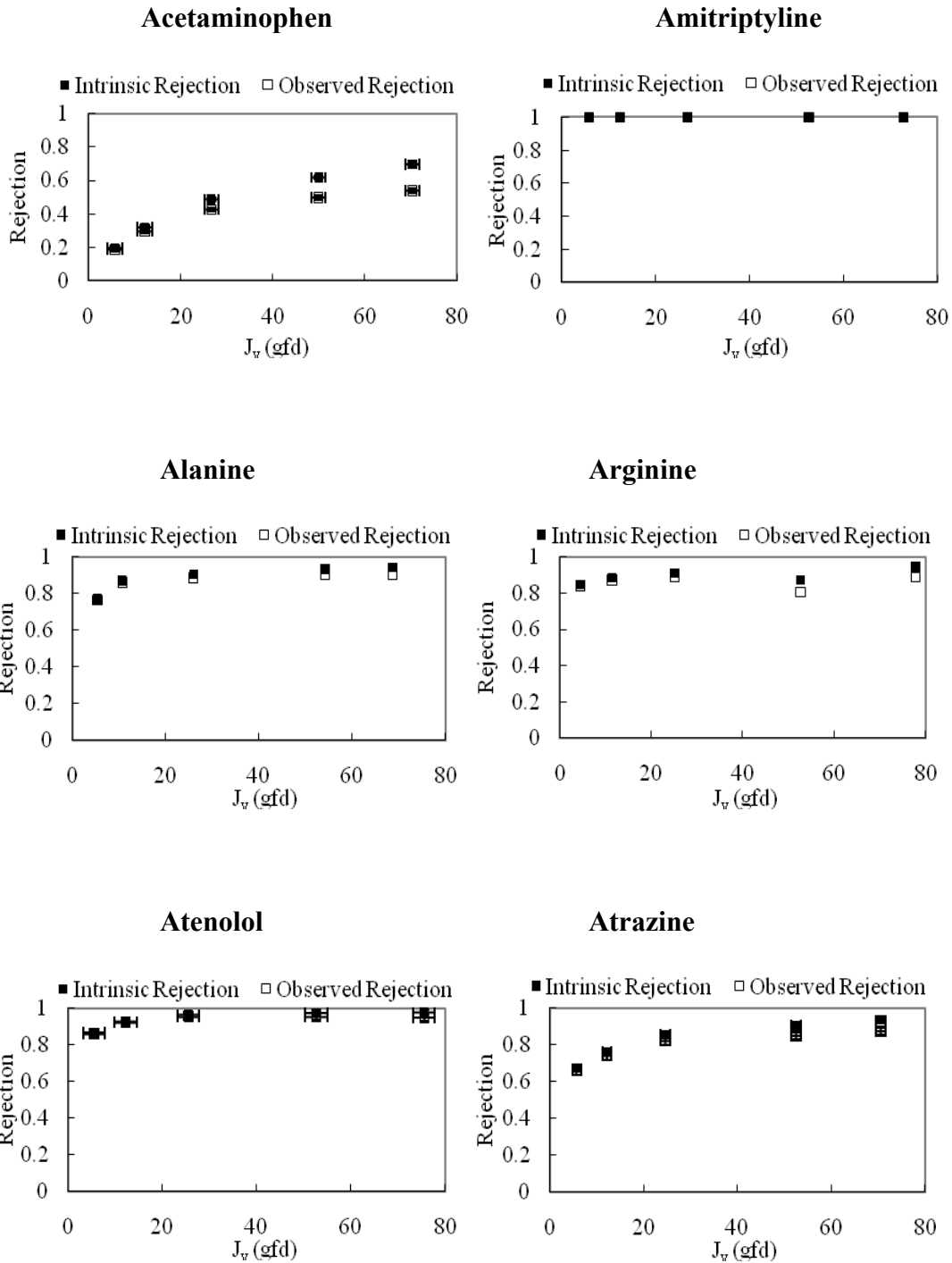
	Stokes	Log D (6)	Vol (cm ³ /mol)	Polar SA	Dipole	SASA	FOSA	FISA	PISA	WPSA	Vol	glob
MW	0.93	0.32	0.91	0.43	0.13	0.89	0.21	0.10	0.23	0.48	0.91	-0.66
Length (nm)	0.85	0.44	0.84	0.25	0.08	0.89	0.42	0.12	0.40	-0.05	0.86	-0.84
Width (nm)	0.78	0.33	0.78	0.33	0.32	0.78	0.14	0.08	0.35	0.27	0.79	-0.59
Depth (nm)	0.77	0.11	0.77	0.40	0.26	0.76	0.58	0.21	-0.03	0.11	0.78	-0.56
EqWidth (nm)	0.89	0.26	0.89	0.42	0.34	0.88	0.41	0.17	0.19	0.22	0.90	-0.66
Vol (A3)	0.99	0.42	0.98	0.37	0.15	0.97	0.39	0.11	0.30	0.25	0.99	-0.78
Area (A2)	0.68	0.39	0.71	0.07	0.00	0.69	0.49	-0.17	-0.05	0.42	0.68	-0.64
Hydration E	0.03	0.38	0.12	-0.58	0.20	0.04	0.11	-0.71	-0.01	0.43	0.03	-0.10
Polarization (A3)	0.98	0.48	0.97	0.33	0.16	0.96	0.29	0.10	0.42	0.19	0.98	-0.74
LaBas Mol Vol	0.99	0.38	0.98	0.40	0.17	0.97	0.38	0.13	0.29	0.26	0.99	-0.77
W-C Diff Coeff	-0.93	-0.42	-0.89	-0.32	-0.18	-0.92	-0.32	-0.10	-0.39	-0.16	-0.91	0.81
Stokes radius	1.00	0.40	0.98	0.39	0.18	0.98	0.38	0.13	0.32	0.23	0.99	-0.80
Log D (6)	0.40	1.00	0.46	-0.45	-0.08	0.41	-0.04	-0.45	0.52	0.17	0.39	-0.40
Vol (cm3/mol)	0.98	0.46	1.00	0.27	0.18	0.97	0.40	0.03	0.32	0.25	0.98	-0.78
Polar SA (A2)	0.39	-0.45	0.27	1.00	0.29	0.37	0.17	0.84	-0.18	-0.09	0.39	-0.23
Dipole	0.18	-0.08	0.18	0.29	1.00	0.22	0.11	0.31	0.10	-0.21	0.21	-0.21
SASA	0.98	0.41	0.97	0.37	0.22	1.00	0.39	0.12	0.37	0.18	0.99	-0.88
FOSA	0.38	-0.04	0.40	0.17	0.11	0.39	1.00	0.11	-0.49	-0.22	0.40	-0.31
FISA	0.13	-0.45	0.03	0.84	0.31	0.12	0.11	1.00	-0.17	-0.44	0.14	-0.04
PISA	0.32	0.52	0.32	-0.18	0.10	0.37	-0.49	-0.17	1.00	-0.13	0.34	-0.42
WPSA	0.23	0.17	0.25	-0.09	-0.21	0.18	-0.22	-0.44	-0.13	1.00	0.19	-0.12
Vol	0.99	0.39	0.98	0.39	0.21	0.99	0.40	0.14	0.34	0.19	1.00	-0.82
glob	-0.80	-0.40	-0.78	-0.23	-0.21	-0.88	-0.31	-0.04	-0.42	-0.12	-0.82	1.00
QPpolrz	0.96	0.52	0.96	0.24	0.21	0.96	0.27	0.03	0.50	0.17	0.97	-0.79
QPlogPC16	0.95	0.39	0.92	0.47	0.18	0.94	0.14	0.23	0.46	0.23	0.95	-0.75
QPlogPoct	0.80	0.00	0.73	0.81	0.24	0.78	0.23	0.61	0.16	0.05	0.80	-0.56
QPlogPw	0.35	-0.41	0.24	0.93	0.22	0.32	0.06	0.84	-0.05	-0.18	0.35	-0.16
QPlogPo/w	0.59	0.80	0.67	-0.44	-0.13	0.60	0.02	-0.61	0.53	0.44	0.59	-0.57
	Stokes	Log D (6)	Vol (cm ³ /mol)	Polar SA	Dipole	SASA	FOSA	FISA	PISA	WPSA	Vol	glob
QPlogS	-0.84	-0.70	-0.86	0.01	0.03	-0.85	-0.13	0.22	-0.51	-0.37	-0.84	0.77
CIQPlogS	-0.82	-0.62	-0.85	-0.01	0.05	-0.79	-0.09	0.23	-0.40	-0.51	-0.81	0.62
IP (eV)	-0.36	-0.57	-0.35	0.11	-0.03	-0.40	0.02	0.09	-0.62	0.26	-0.37	0.41
EA (eV)	0.43	0.47	0.41	-0.07	0.27	0.43	-0.22	-0.22	0.47	0.35	0.41	-0.39
E _{HOMO}	0.29	0.45	0.26	-0.06	0.06	0.35	0.07	0.07	0.58	-0.49	0.31	-0.40
E _{LUMO}	-0.07	-0.28	-0.05	0.24	-0.39	-0.08	0.14	0.20	-0.38	0.08	-0.07	0.10
Pot Energy	0.53	0.10	0.48	0.41	0.12	0.47	0.27	0.43	0.16	-0.28	0.52	-0.19

Table D.3.

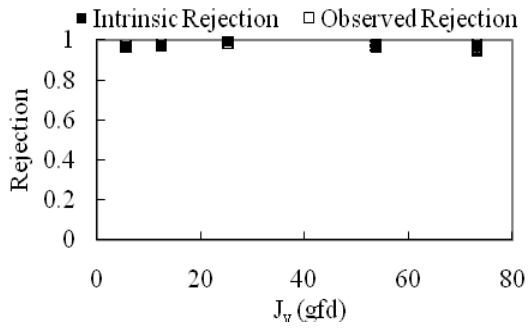
	Qppolrz	QPlogPC16	QPlogPoct	QPlogPw	QPlogPo/w	QPlogS	CIQPlogS	IP	EA	E _{HOMO}	E _{LUMO}	Pot Energy
MW	0.88	0.92	0.80	0.38	0.55	-0.79	-0.83	-0.20	0.49	0.07	-0.04	0.49
Length (nm)	0.84	0.79	0.62	0.24	0.55	-0.75	-0.66	-0.41	0.28	0.42	-0.06	0.45
Width (nm)	0.80	0.81	0.64	0.24	0.52	-0.70	-0.74	-0.43	0.48	0.26	-0.10	0.28
Depth (nm)	0.70	0.68	0.68	0.38	0.28	-0.52	-0.52	-0.07	0.11	0.07	0.05	0.51
EqWidth (nm)	0.86	0.86	0.76	0.36	0.47	-0.70	-0.73	-0.29	0.34	0.19	-0.03	0.45
Vol (Å ³)	0.96	0.95	0.79	0.32	0.62	-0.85	-0.85	-0.35	0.40	0.26	-0.03	0.51
Area (Å ²)	0.61	0.57	0.35	-0.07	0.58	-0.65	-0.69	-0.11	0.21	0.02	0.09	0.06
Hydration E	0.09	-0.11	-0.41	-0.67	0.50	-0.23	-0.23	0.11	0.36	-0.24	-0.38	-0.32
Polarization (Å ³)	0.99	0.96	0.79	0.33	0.64	-0.87	-0.85	-0.44	0.45	0.35	-0.11	0.60
LaBas Mol Vol	0.96	0.95	0.81	0.36	0.59	-0.83	-0.83	-0.32	0.39	0.24	-0.02	0.53
W-C Diff Coeff	-0.90	-0.89	-0.71	-0.29	-0.57	0.80	0.72	0.47	-0.54	-0.41	0.24	-0.48
Stokes radius	0.96	0.95	0.80	0.35	0.59	-0.84	-0.82	-0.36	0.43	0.29	-0.07	0.53
Log D (6)	0.52	0.39	0.00	-0.41	0.80	-0.70	-0.62	-0.57	0.47	0.45	-0.28	0.10
Vol (cm ³ /mol)	0.96	0.92	0.73	0.24	0.67	-0.86	-0.85	-0.35	0.41	0.26	-0.05	0.48
Polar SA (Å ²)	0.24	0.47	0.81	0.93	-0.44	0.01	-0.01	0.11	-0.07	-0.06	0.24	0.41
Dipole	0.21	0.18	0.24	0.22	-0.13	0.03	0.05	-0.03	0.27	0.06	-0.39	0.12
SASA	0.96	0.94	0.78	0.32	0.60	-0.85	-0.79	-0.40	0.43	0.35	-0.08	0.47
FOSA	0.27	0.14	0.23	0.06	0.02	-0.13	-0.09	0.02	-0.22	0.07	0.14	0.27
FISA	0.03	0.23	0.61	0.84	-0.61	0.22	0.23	0.09	-0.22	0.07	0.20	0.43
PISA	0.50	0.46	0.16	-0.05	0.53	-0.51	-0.40	-0.62	0.47	0.58	-0.38	0.16
WPSA	0.17	0.23	0.05	-0.18	0.44	-0.37	-0.51	0.26	0.35	-0.49	0.08	-0.28
Vol	0.97	0.95	0.80	0.35	0.59	-0.84	-0.81	-0.37	0.41	0.31	-0.07	0.52
Glob	-0.79	-0.75	-0.56	-0.16	-0.57	0.77	0.62	0.41	-0.39	-0.40	0.10	-0.19
Qppolrz	1.00	0.94	0.72	0.24	0.69	-0.89	-0.85	-0.50	0.50	0.41	-0.18	0.53
QPlogPC16	0.94	1.00	0.86	0.47	0.54	-0.83	-0.81	-0.40	0.46	0.31	-0.06	0.54
QPlogPoct	0.72	0.86	1.00	0.82	0.09	-0.50	-0.49	-0.19	0.18	0.17	0.15	0.65
QPlogPw	0.24	0.47	0.82	1.00	-0.46	0.04	0.04	0.03	-0.12	0.01	0.27	0.52
QPlogPo/w	0.69	0.54	0.09	-0.46	1.00	-0.89	-0.86	-0.42	0.52	0.27	-0.21	0.04
QPlogS	-0.89	-0.83	-0.50	0.04	-0.89	1.00	0.94	0.45	-0.51	-0.33	0.12	-0.33
	Qppolrz	QPlogPC16	QPlogPoct	QPlogPw	QPlogPo/w	QPlogS	CIQPlogS	IP	EA	E _{HOMO}	E _{LUMO}	Pot Energy
CIQPlogS	-0.85	-0.81	-0.49	0.04	-0.86	0.94	1.00	0.32	-0.45	-0.15	0.03	-0.26
IP (eV)	-0.50	-0.40	-0.19	0.03	-0.42	0.45	0.32	1.00	-0.44	-0.90	0.31	-0.24
EA (eV)	0.50	0.46	0.18	-0.12	0.52	-0.51	-0.45	-0.44	1.00	0.25	-0.71	0.13
E _{HOMO}	0.41	0.31	0.17	0.01	0.27	-0.33	-0.15	-0.90	0.25	1.00	-0.25	0.27
E _{LUMO}	-0.18	-0.06	0.15	0.27	-0.21	0.12	0.03	0.31	-0.71	-0.25	1.00	-0.17
Pot Energy	0.53	0.54	0.65	0.52	0.04	-0.33	-0.26	-0.24	0.13	0.27	-0.17	1.00

Appendix E

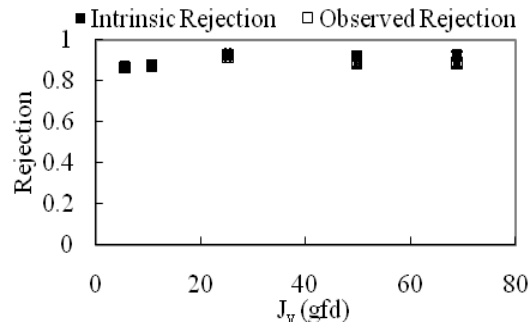
NF-270 Membrane Experimental Bench-Scale Rejection Diagrams



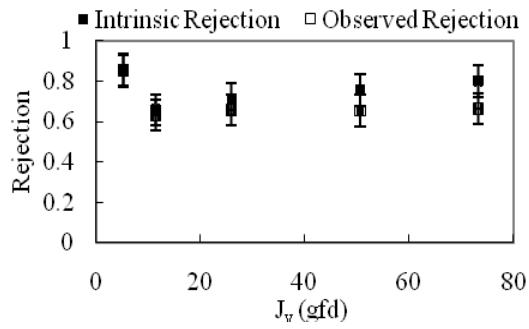
Baclofen



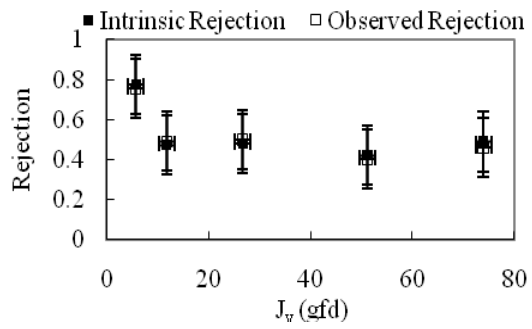
Benzoic Acid



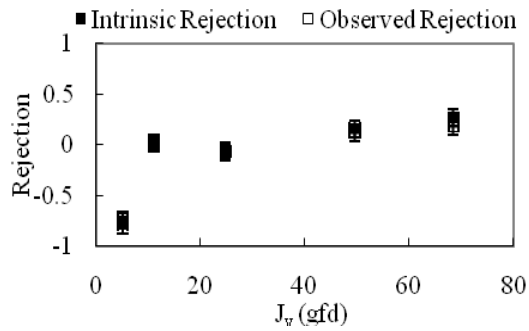
Benzophenone



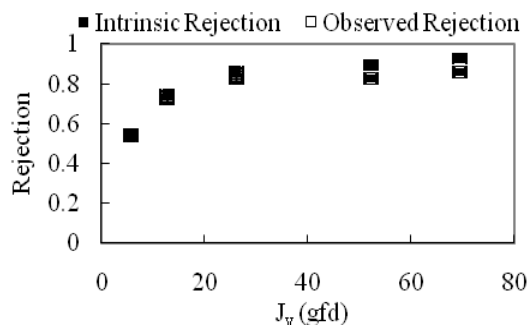
Benzyl Acetate



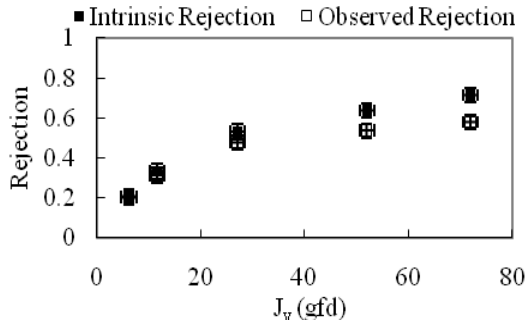
Benzyl Alcohol



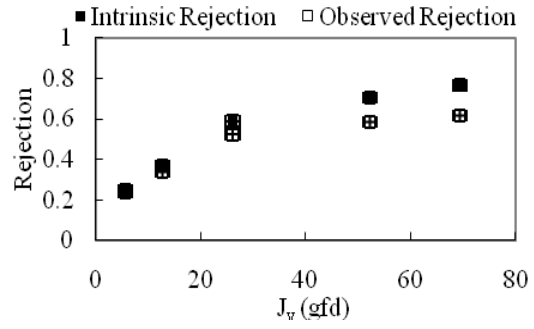
Bisphenol A



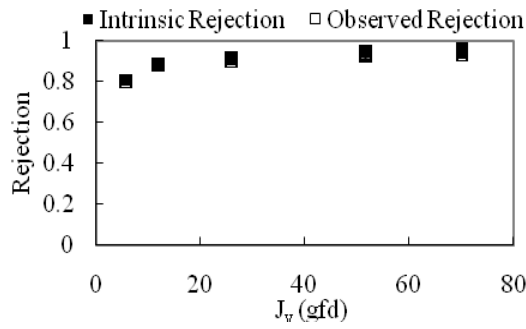
1,4-Butanediol



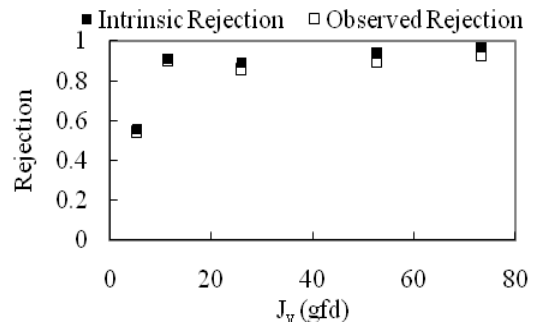
Isobutylparaben



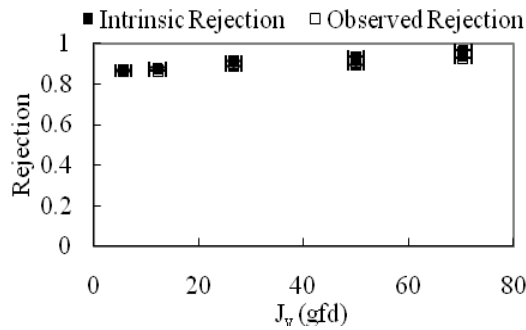
Caffeine



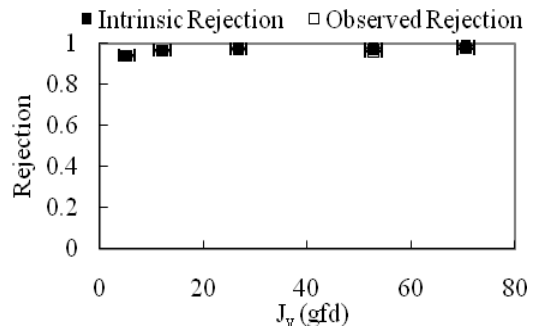
Captopril



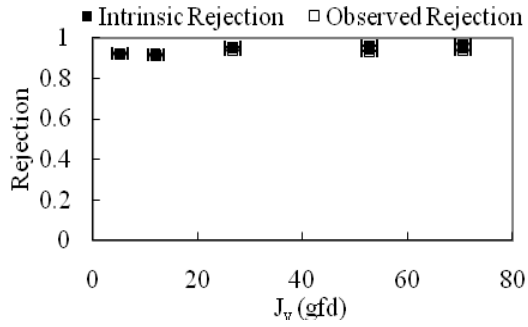
Carbamazepine



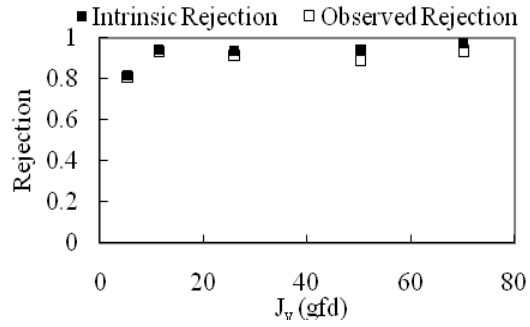
Ciprofloxacin



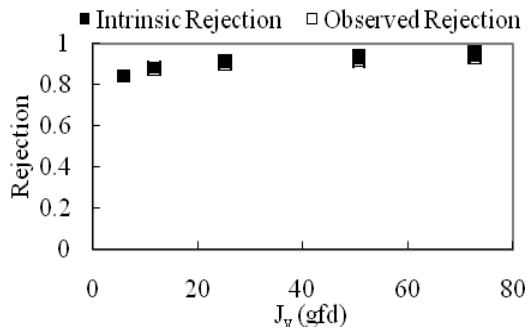
Clofibric Acid



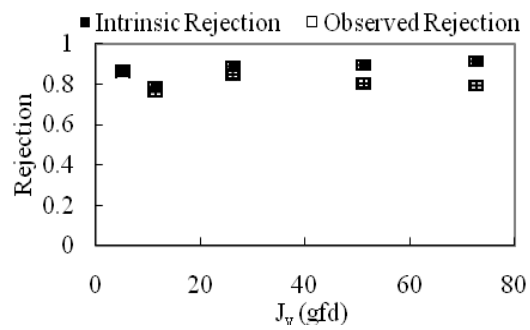
Cysteine



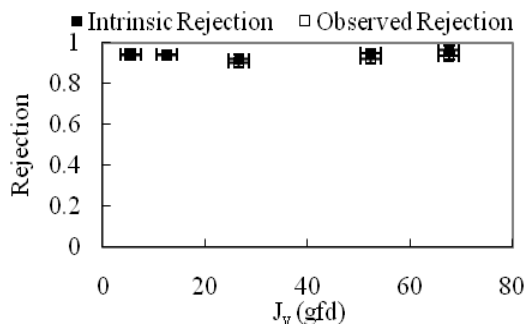
DEET



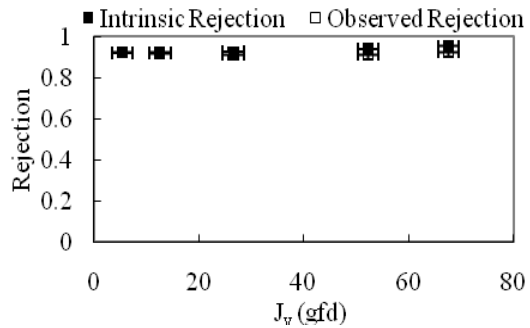
Desloratadine



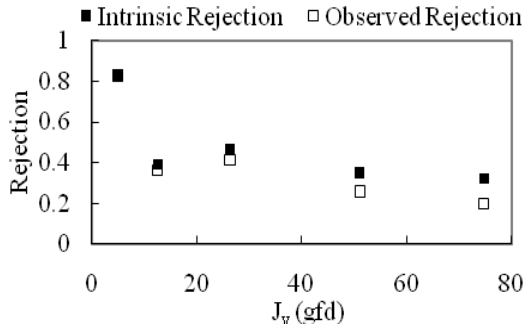
Dibromoacetic Acid



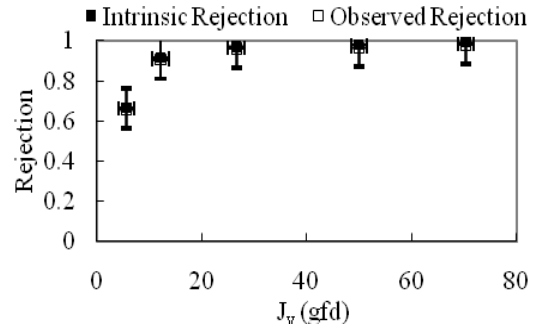
Dichloroacetic Acid



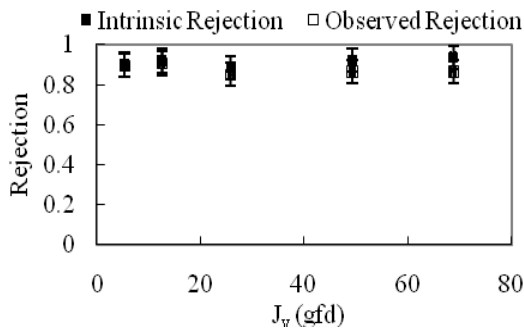
2,4-Dichlorophenol



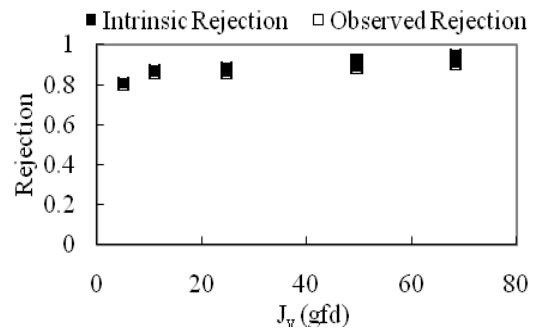
Diclofenac



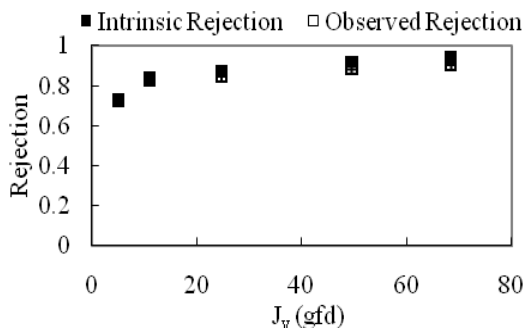
Diethylstilbestrol



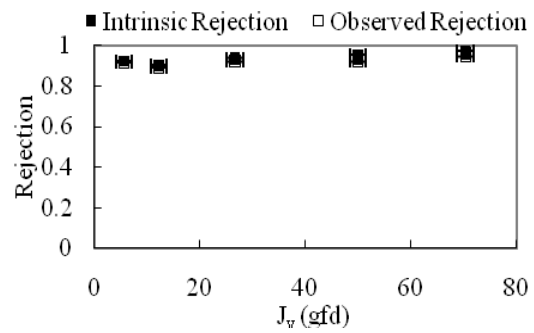
Diethylphthalate



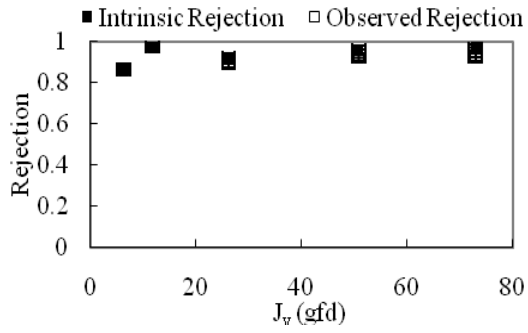
1,4-Dihydrobenzoic Acid



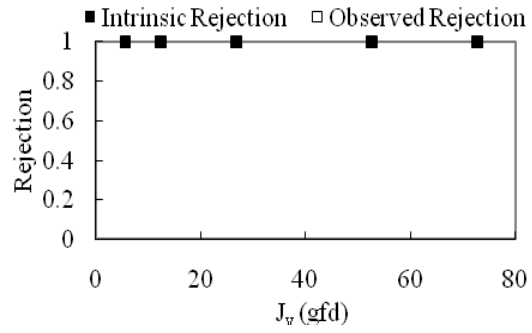
Dilantin



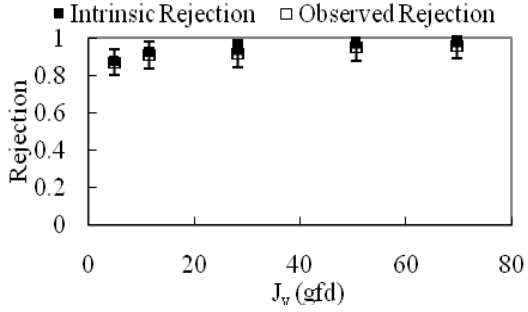
Diltiazem



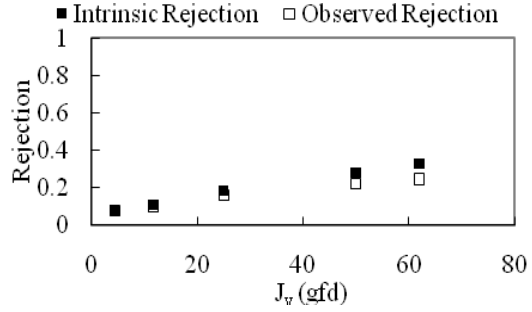
Diphenhydramine



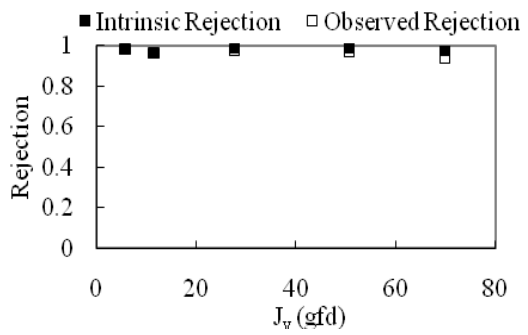
Enalapril



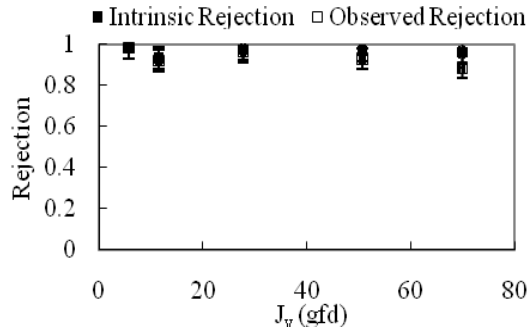
Ethanol



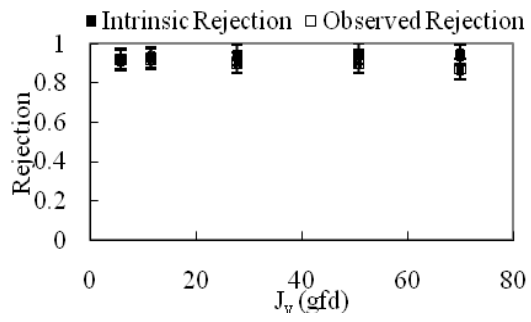
Ethinylestradiol



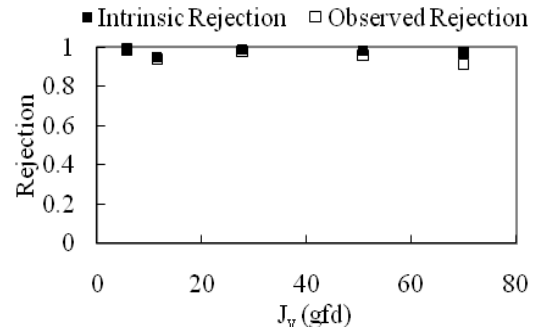
17 β -Estradiol



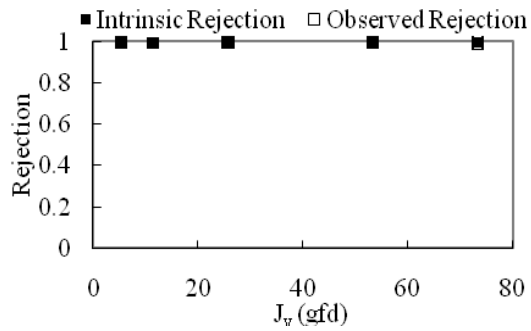
Estriol



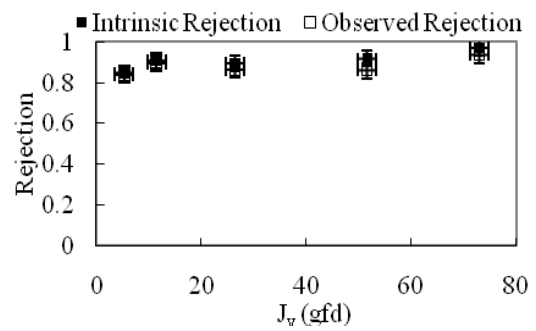
Estrone



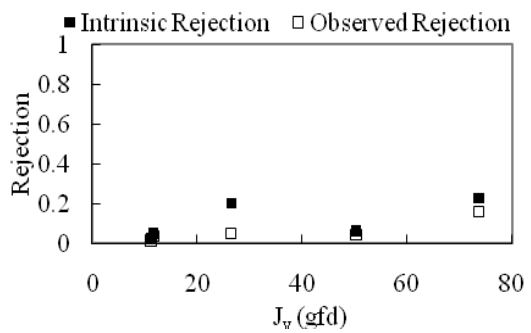
Fenofibrate



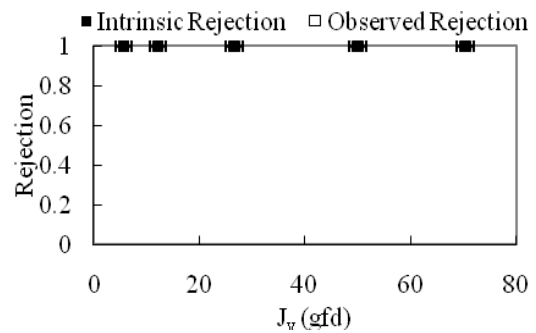
Fluconazole



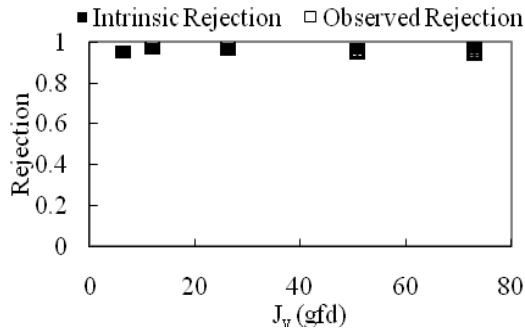
2-Fluorophenol



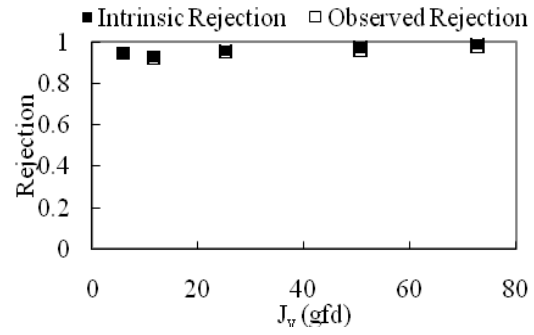
Fluoxetine



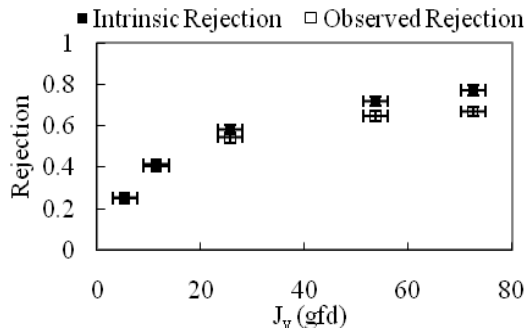
Furosemide



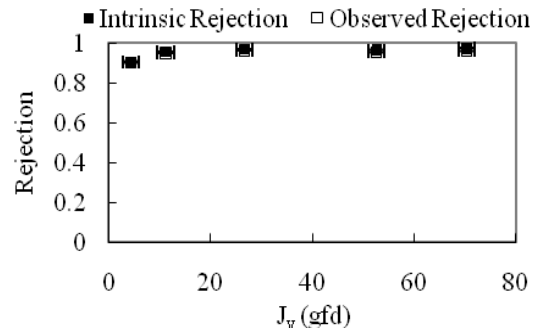
Gemfibrozil



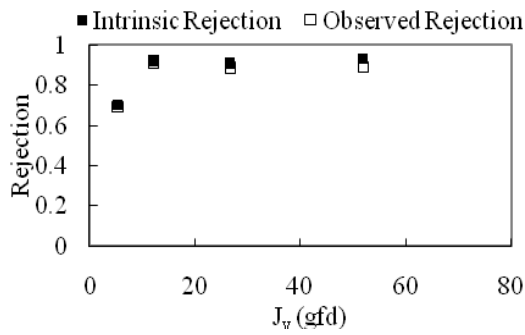
Glycerol



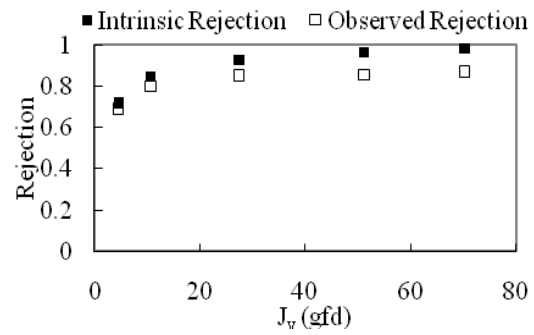
Glucose



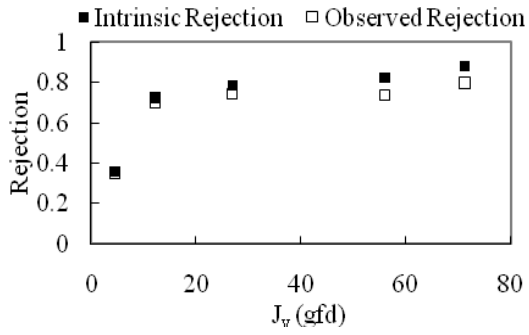
Glutamic Acid



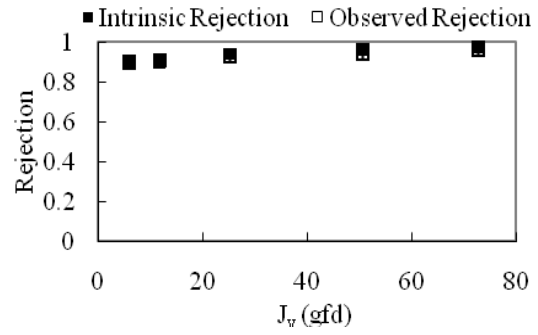
Guanidine



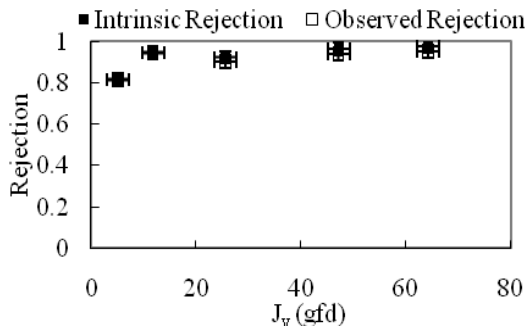
Histidine



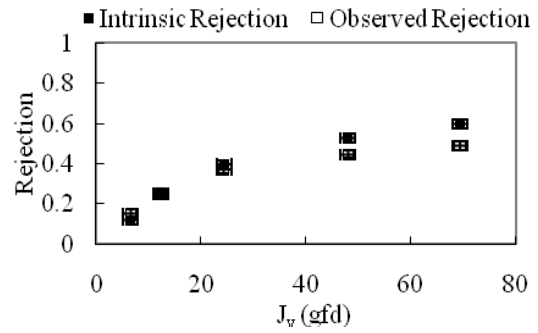
Ibuprofen



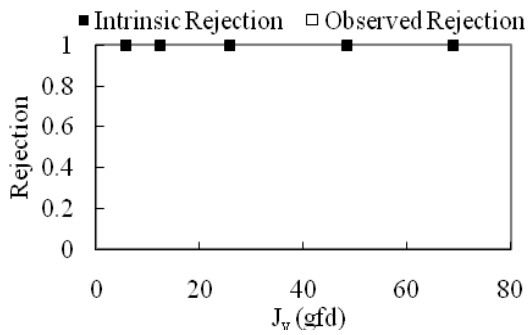
Imiquimod



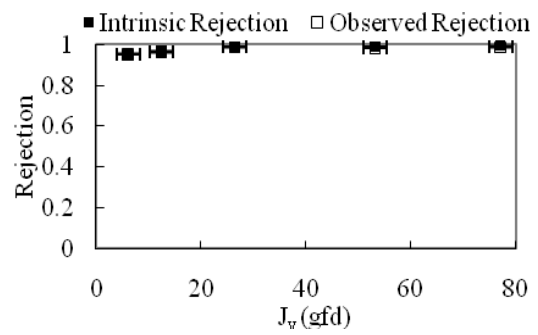
Isopropanol



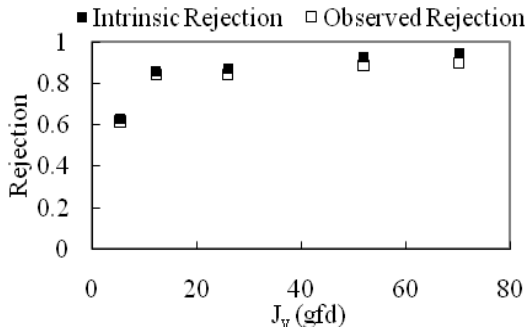
Ketoconazole



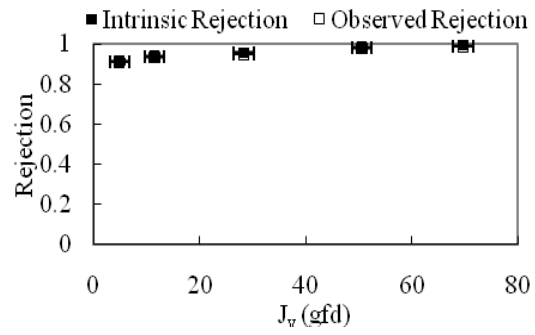
Ketoprofen



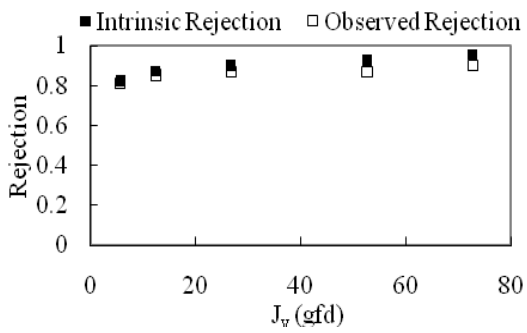
Lysine



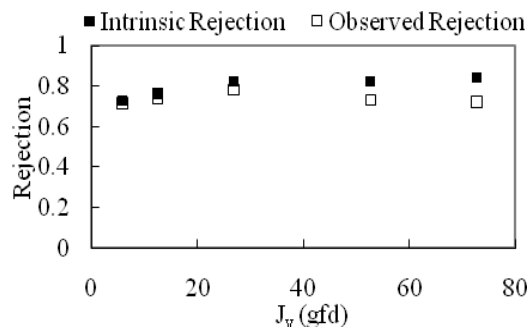
Maleic Acid



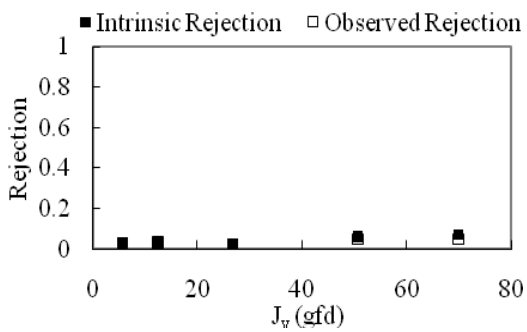
Meprobamate



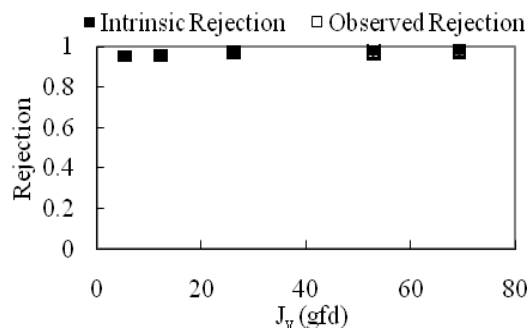
Metformin



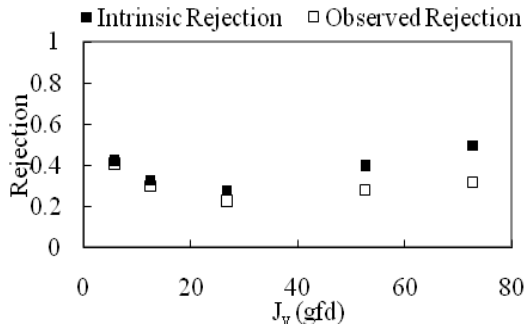
Methanol



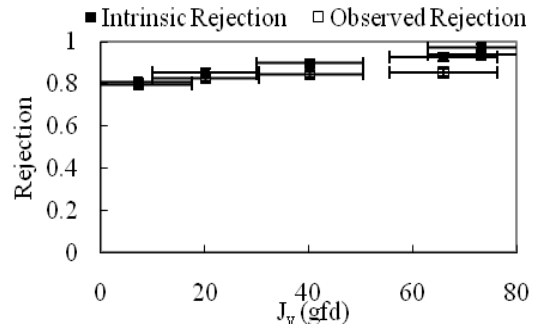
Methotrexate



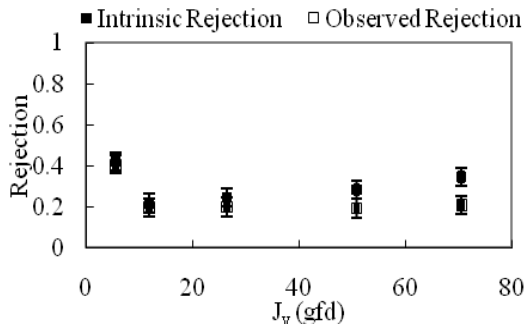
Methylparaben



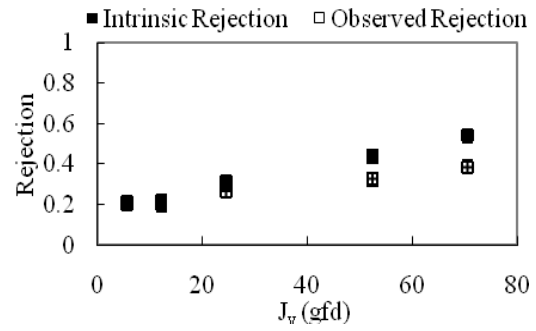
Metoprolol



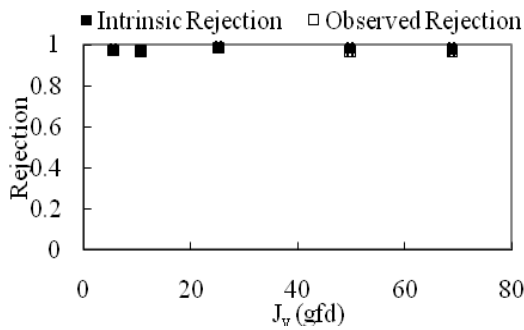
2-Naphthol



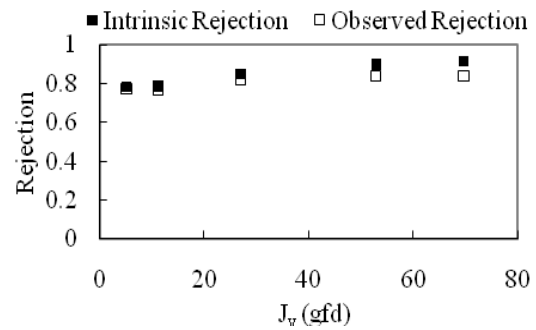
1-Naphthalene-Methanol



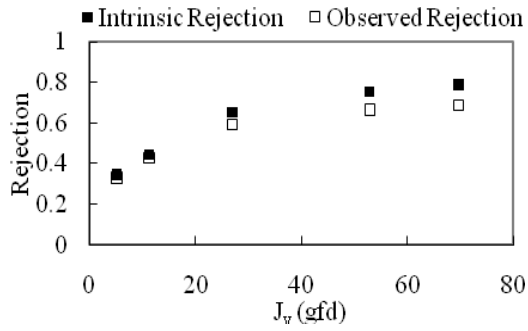
Naproxen



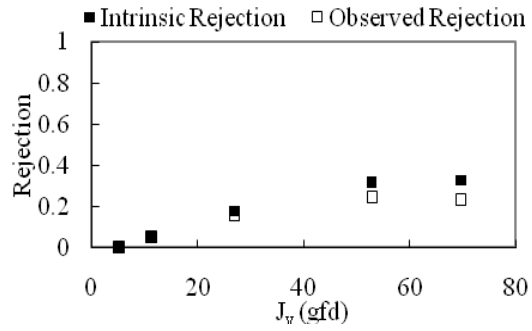
N-Nitrosodibutylamine



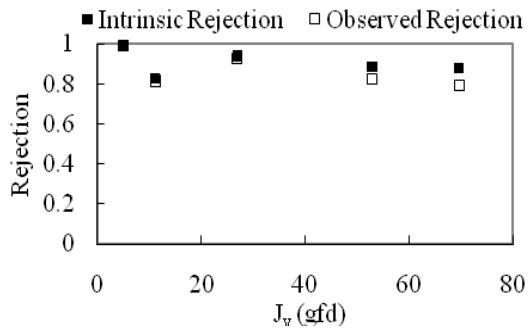
NDEA



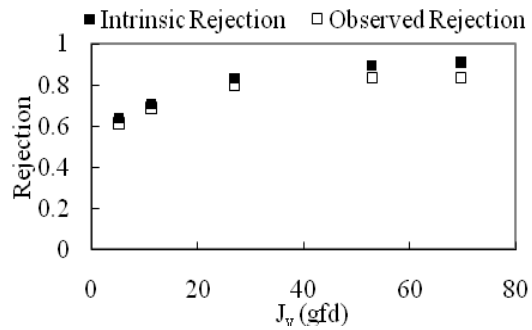
NDMA



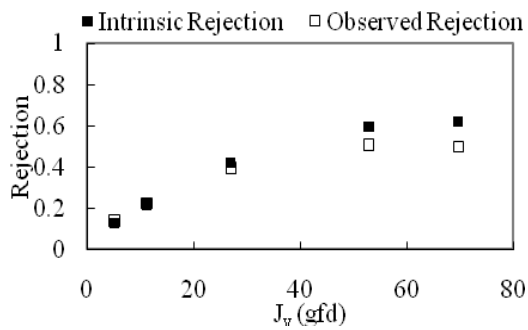
N-Nitrosodiphenylamine



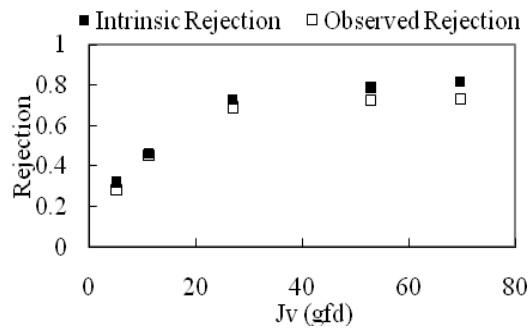
N-Nitrosodipropylamine



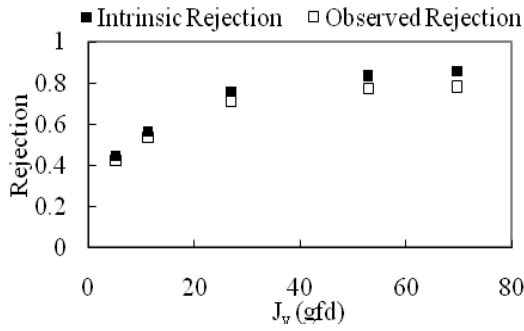
NMEA



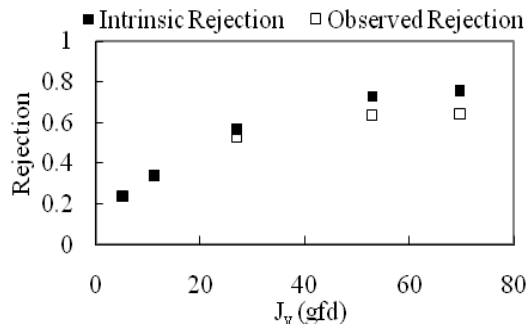
N-Nitrosomorpholine



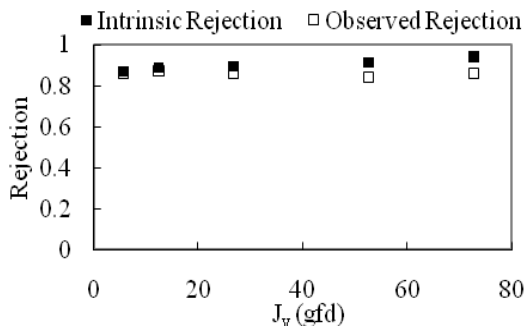
N-Nitrosopiperidine



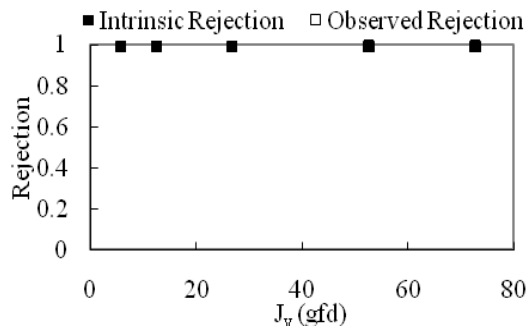
NPYR



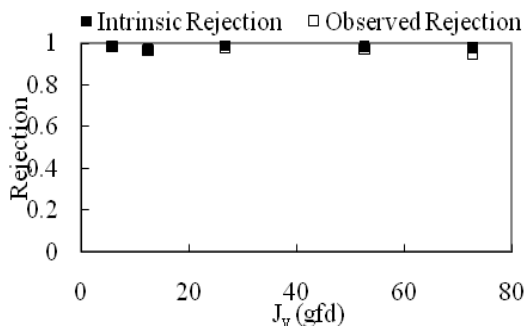
4-n-Nonylphenol



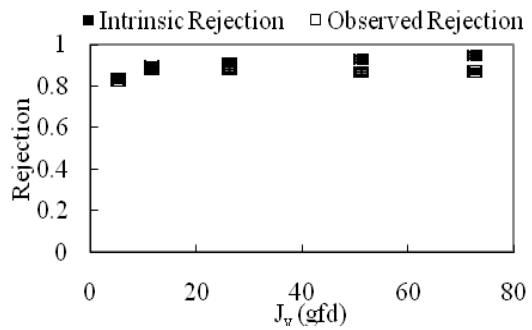
Norfluoxetine



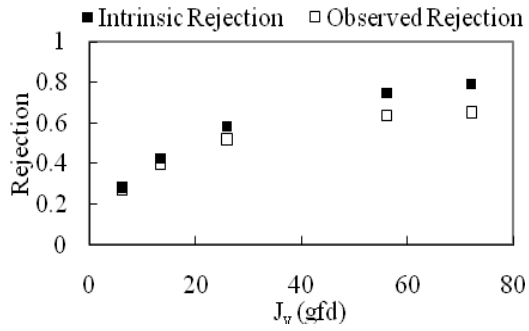
Oxybenzone



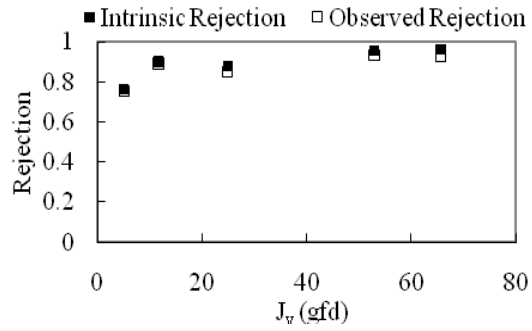
Pentoxifylline



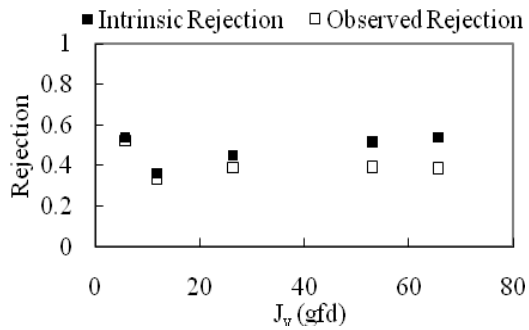
Phenacetine



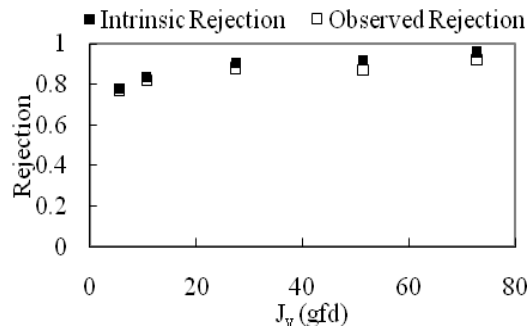
Phenylalanine



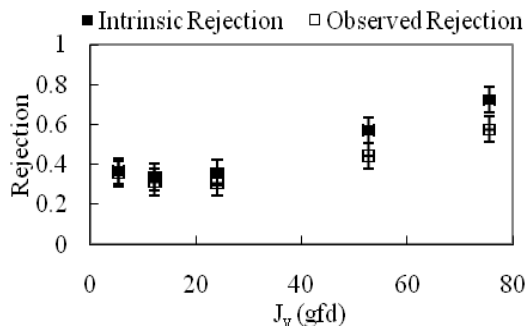
2-Phenylphenol



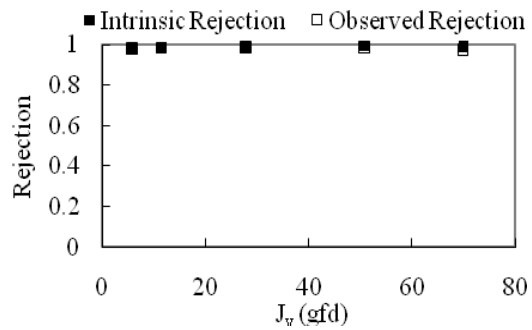
Primidone



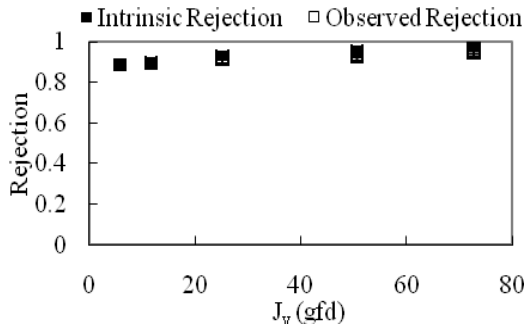
Propylparaben



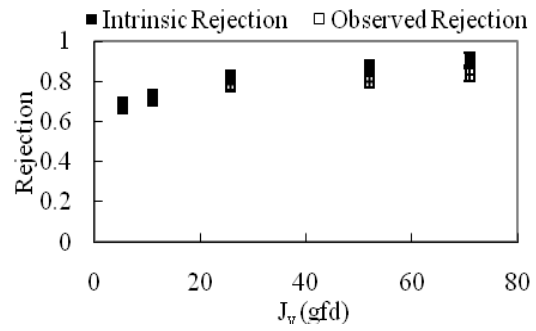
Progesterone



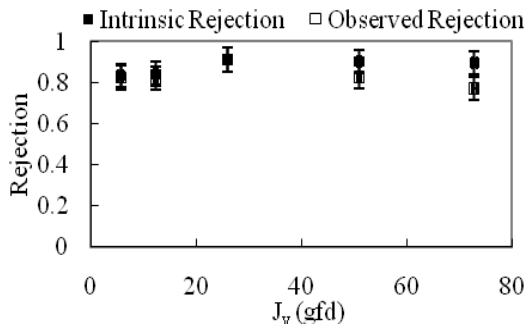
Propyphenazone



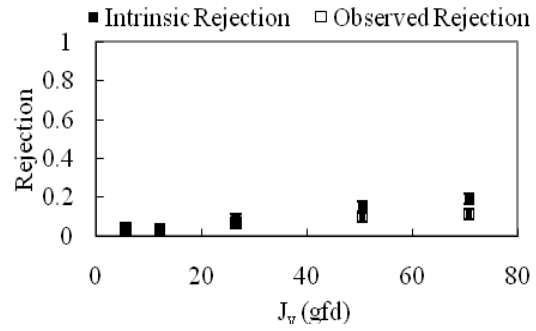
Pseudoephedrine



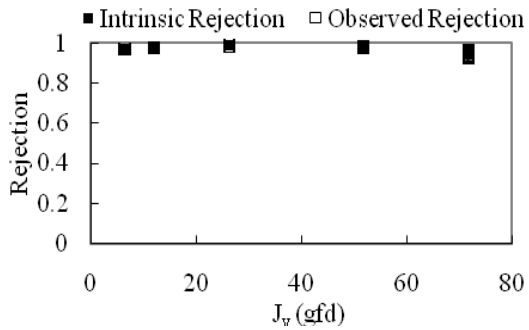
Ranitidine



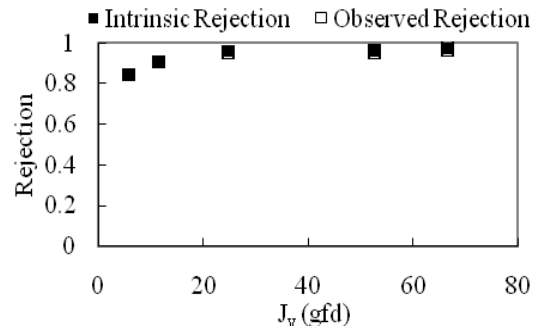
Resorcinol



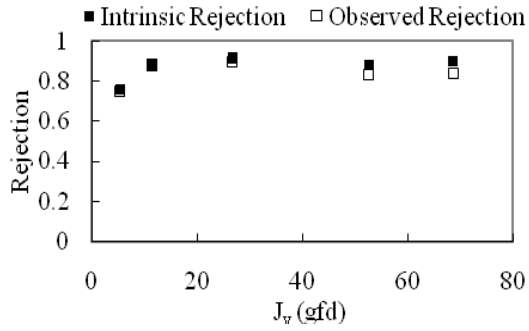
Salbutamol



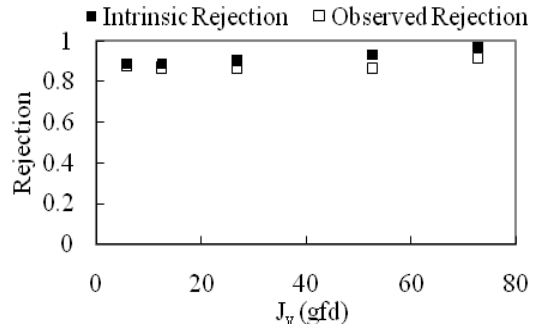
Salicylic Acid



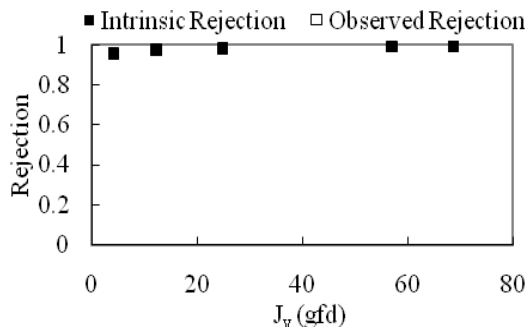
Serine



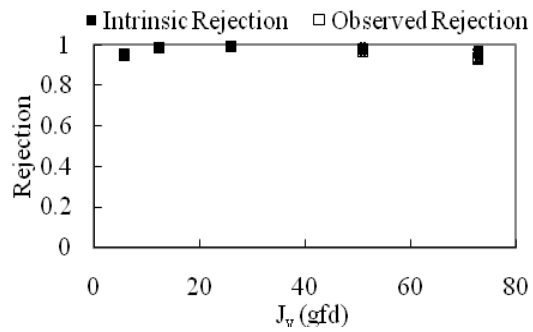
Sucralose



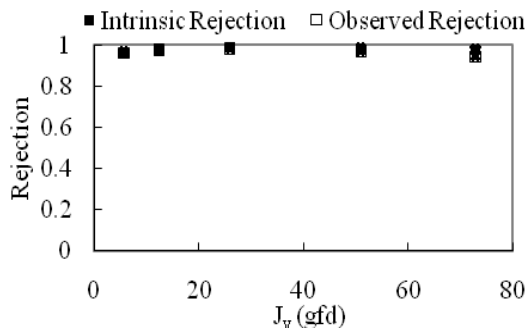
Sucrose



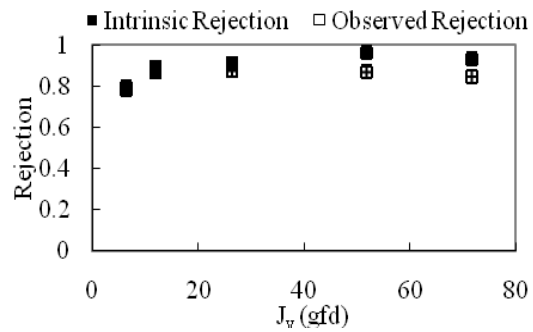
Sulfacetamide



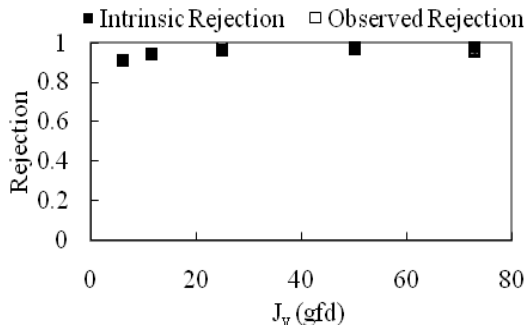
Sulfadimethoxine



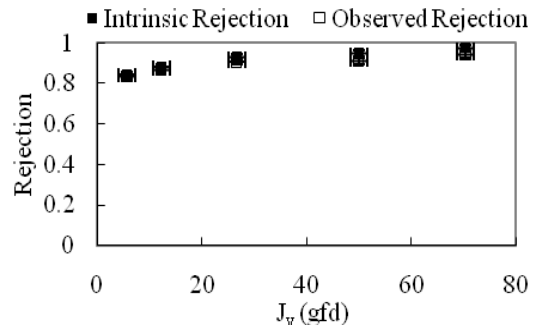
Sulfadoxin



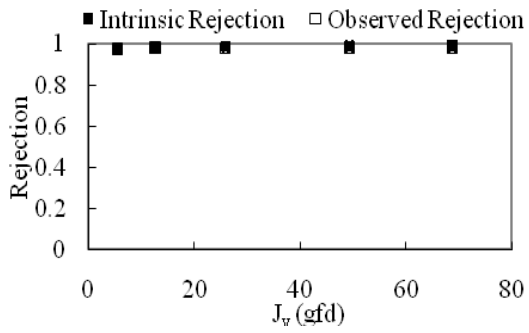
Sulfamerazine



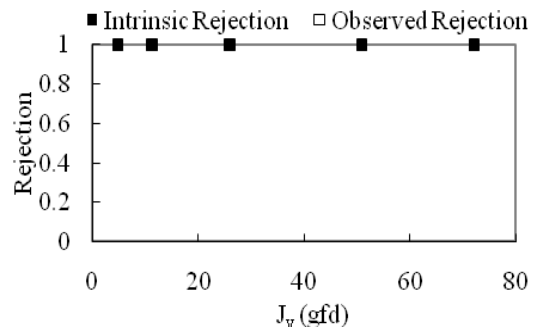
Sulfamethoxazole



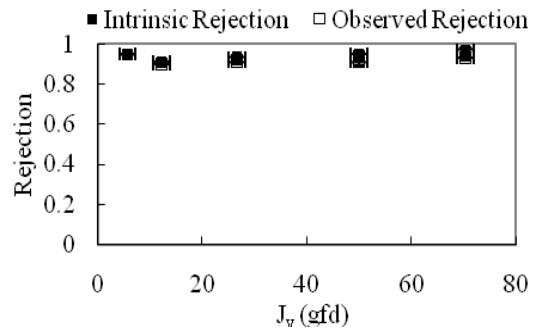
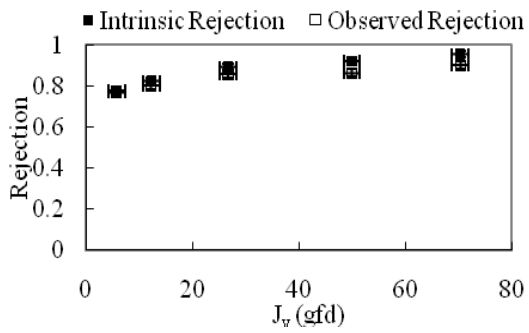
Sulfasalazine



Tamoxifen

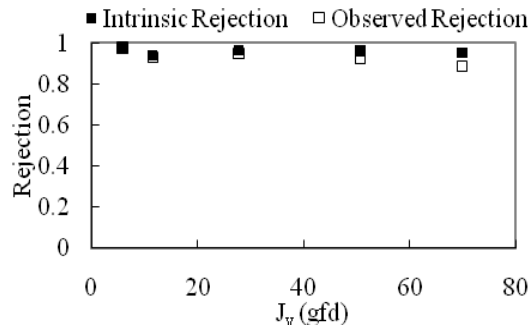
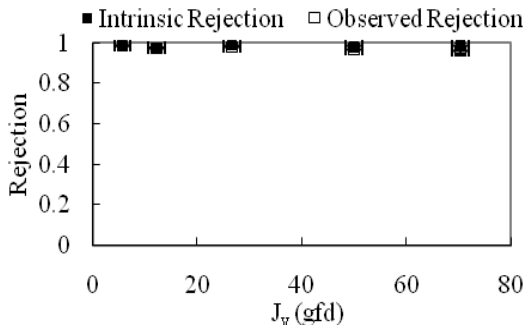


TCEP TCP



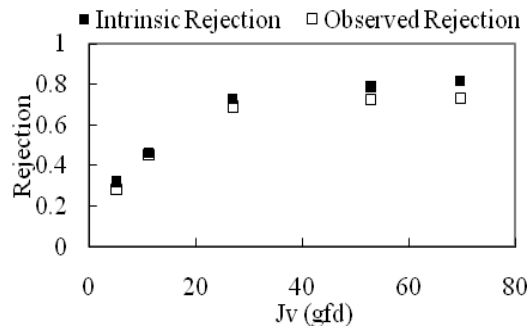
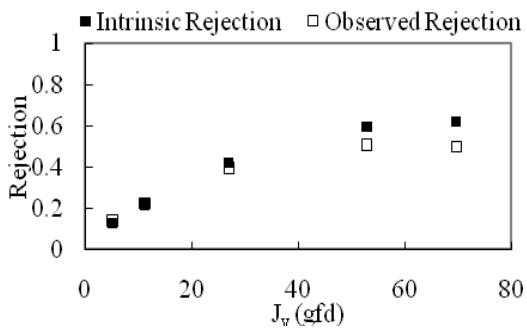
TDCPP

Testosterone



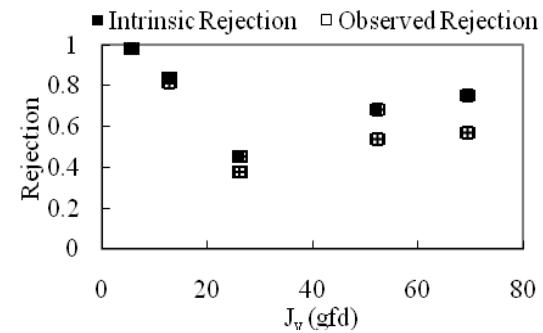
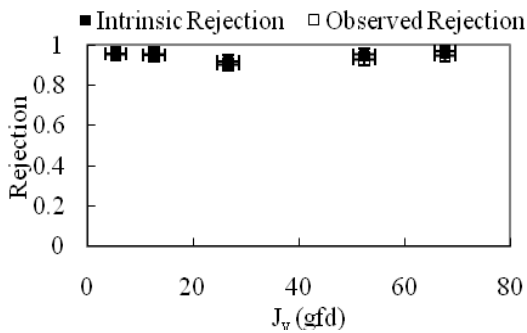
Thiabendazole

Trazodone

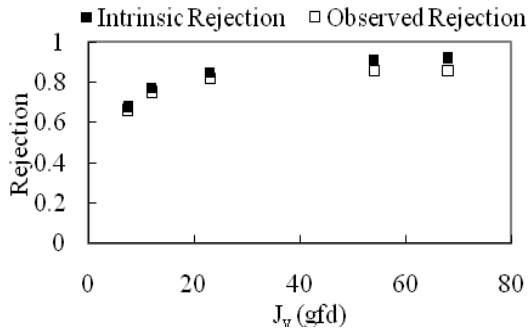


Trichloroacetic Acid

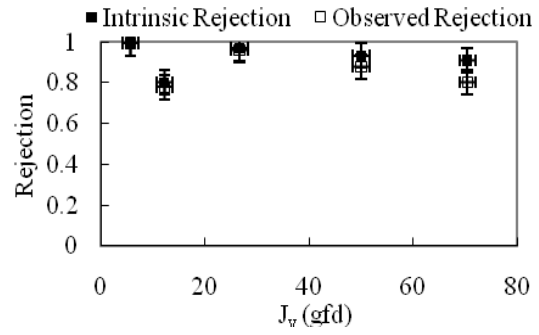
Triclosan



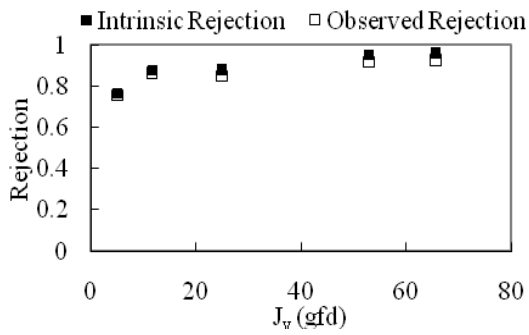
Triethylene Glycol



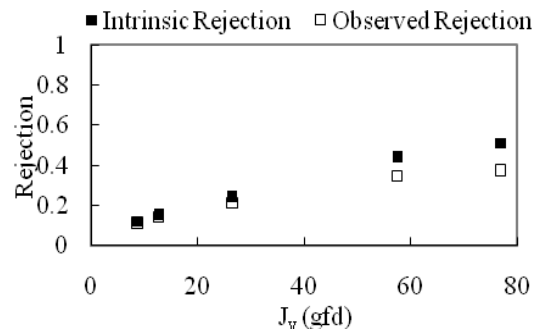
Trimethoprim



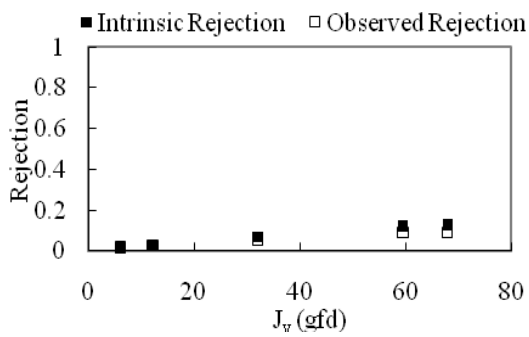
Tyrosine



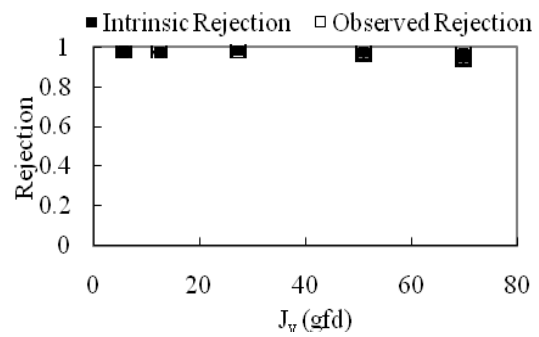
Uracil



Urea

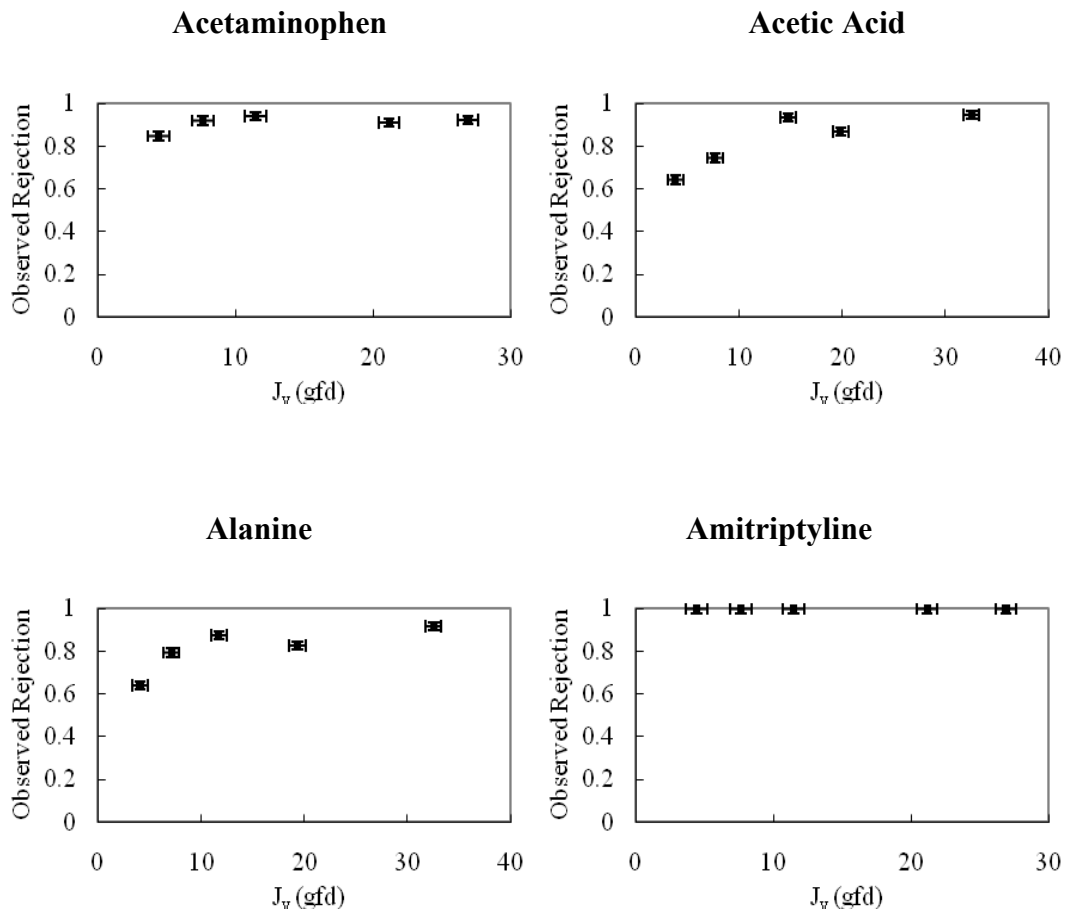


Warfarin

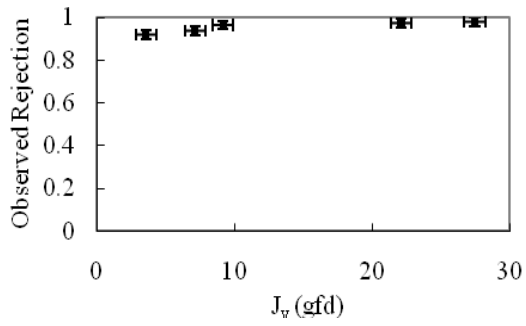


Appendix F

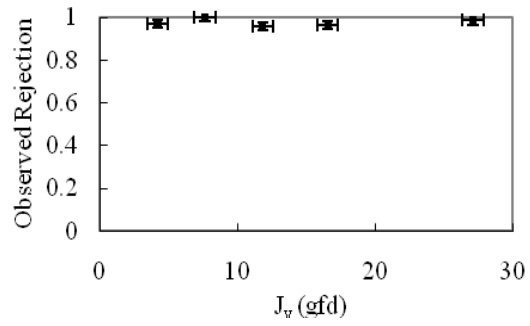
ESPA2 Membrane Experimental Bench-Scale Rejection Diagrams



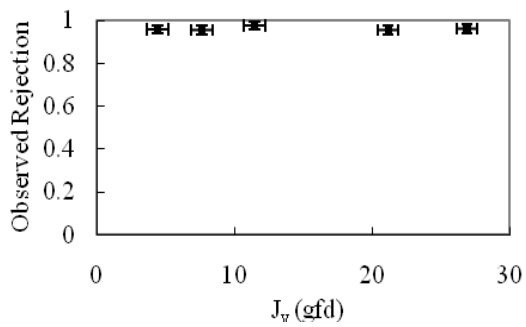
Arginine



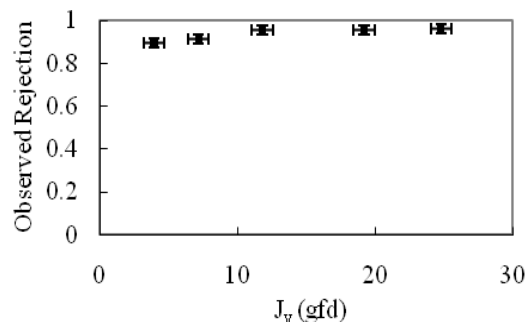
Atenolol



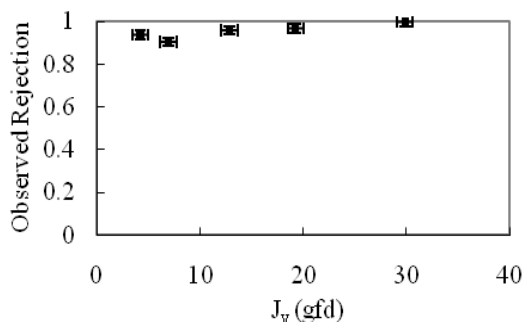
Atrazine



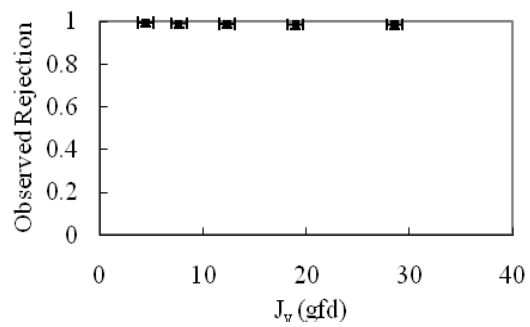
Baclofen



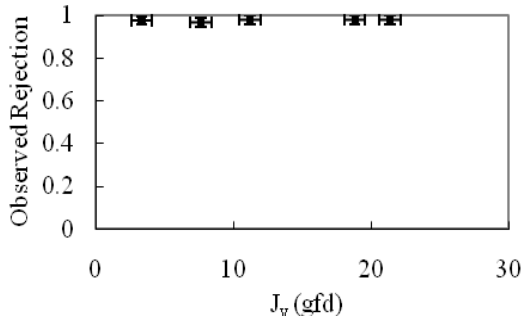
Benzoic Acid



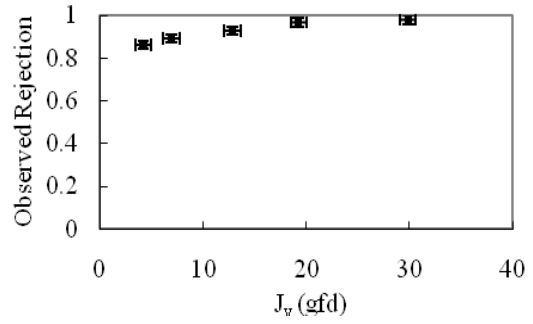
Benzophenone



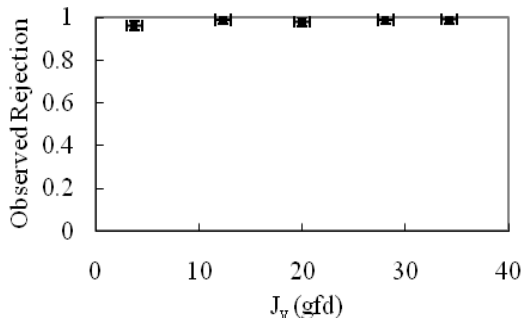
Benzyl Acetate



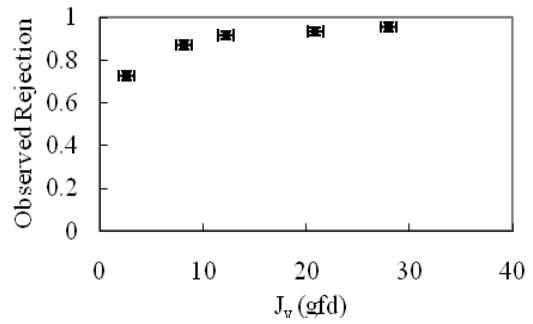
Benzyl Alcohol



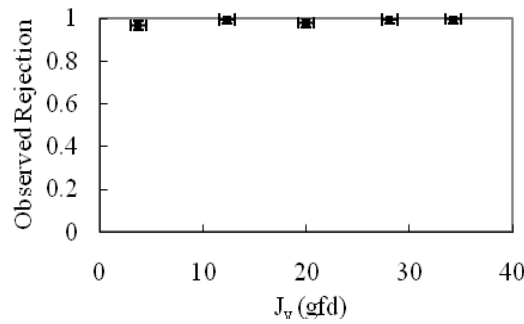
Bisphenol A



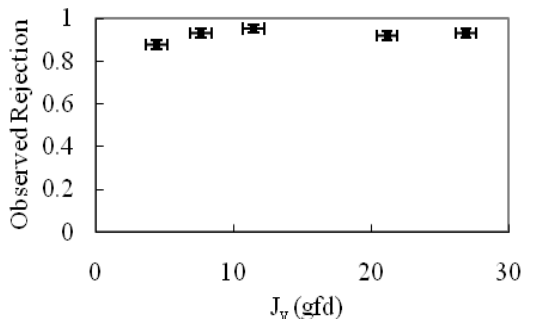
1,1-Butanediol



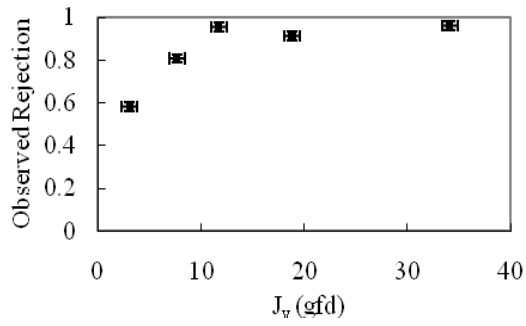
Butylparaben



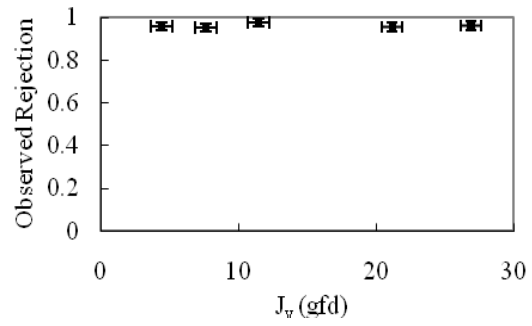
Caffeine



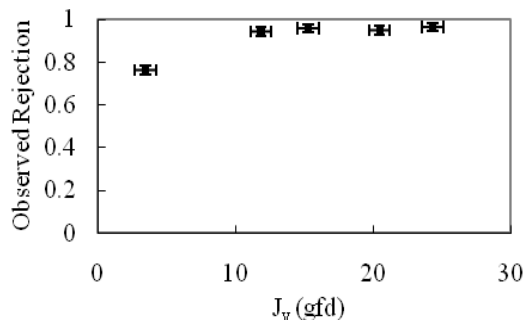
Captopril



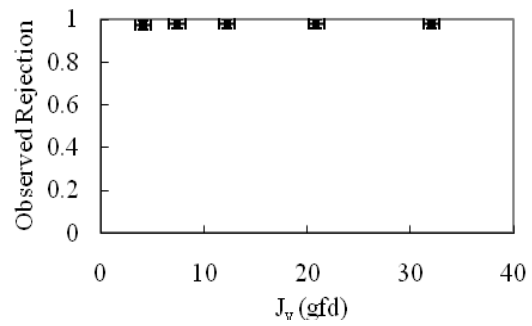
Carbamazapine



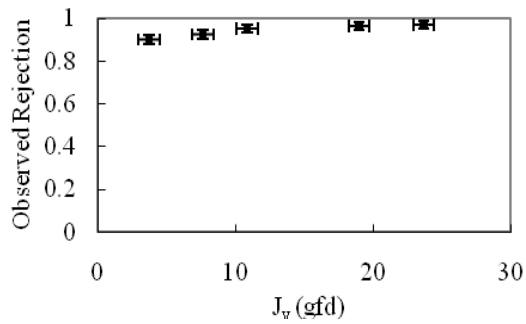
Cimetidine



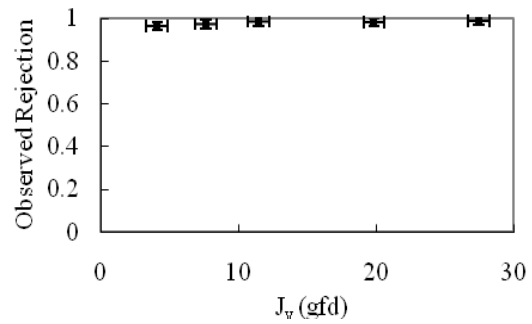
Ciprofloxacin



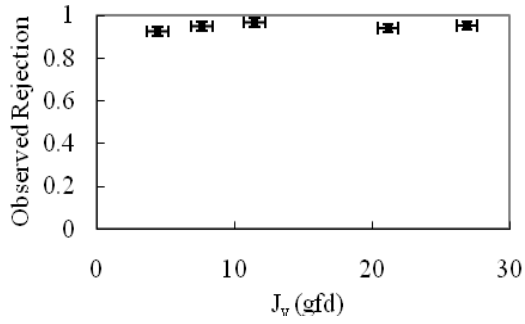
Clofibric Acid



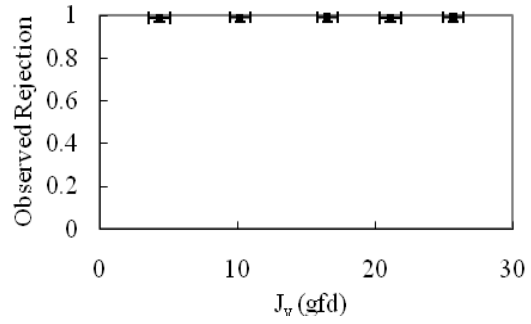
Cysteine



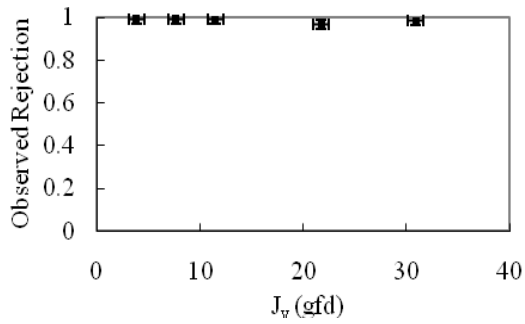
DEET



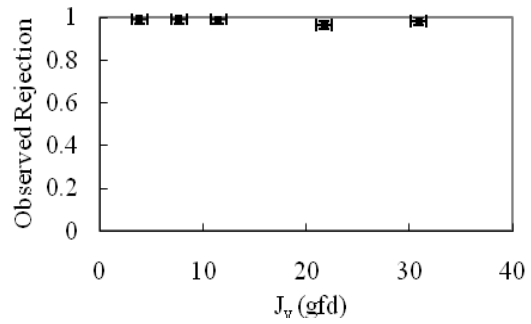
Desloratdine



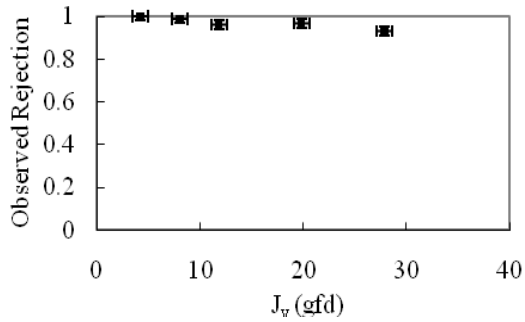
Dibromoacetic Acid



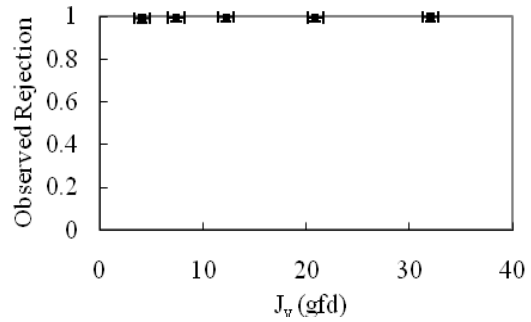
Dichloroacetic Acid



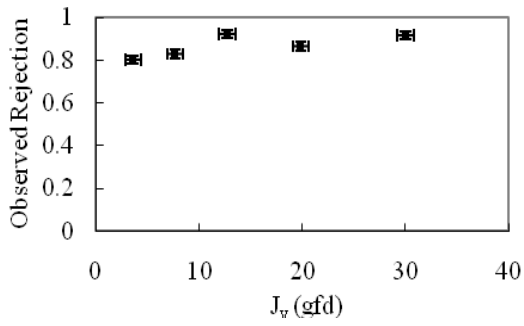
2,4-Dichlorophenol



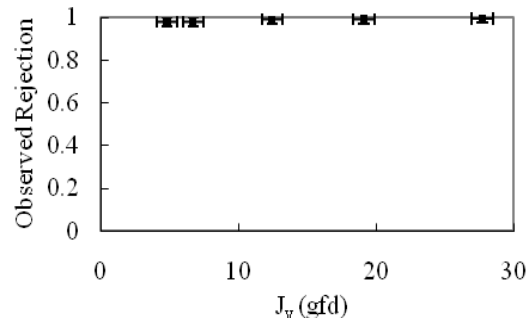
Diclofenac



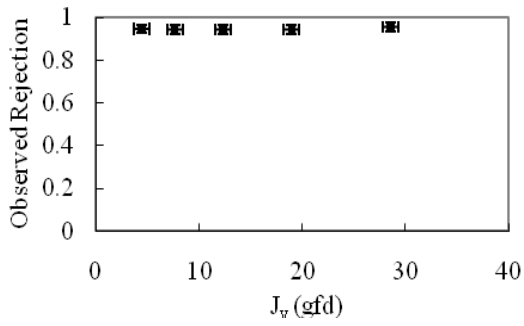
Diethylamine



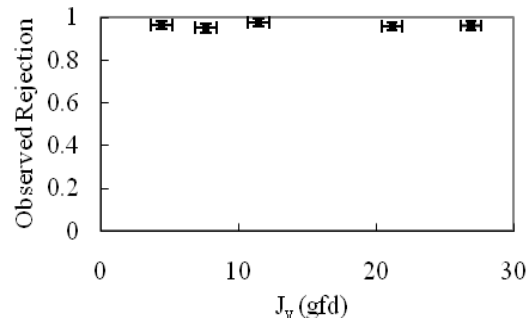
Diethylphthalate



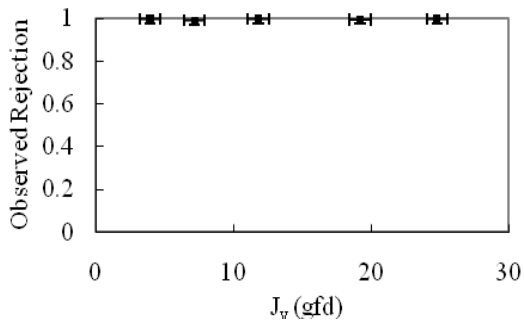
1,4-Dihydroxybenzoic Acid



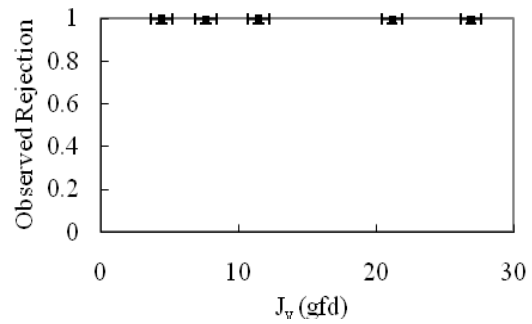
Dilantin

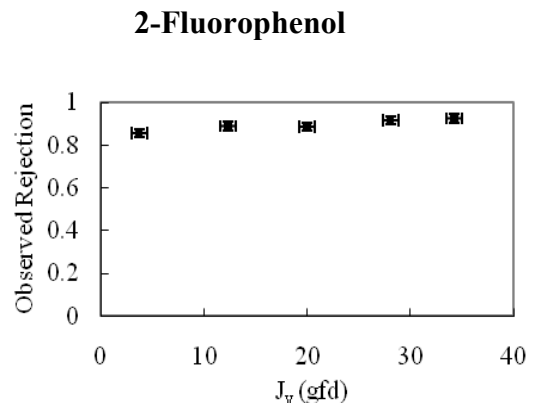
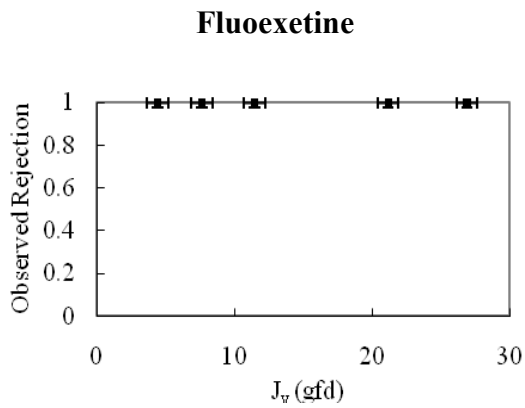
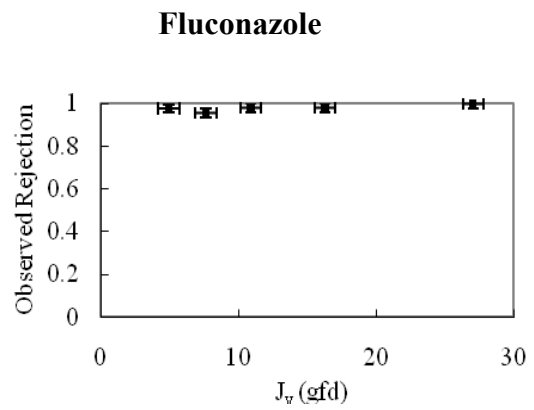
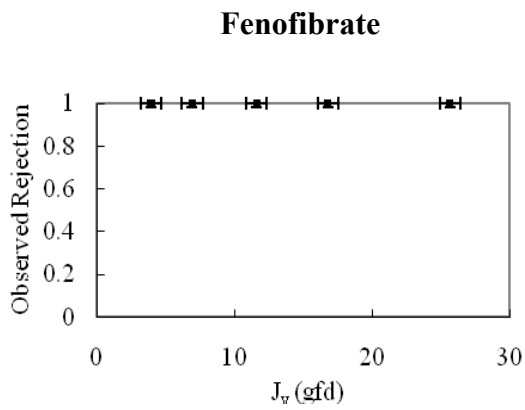
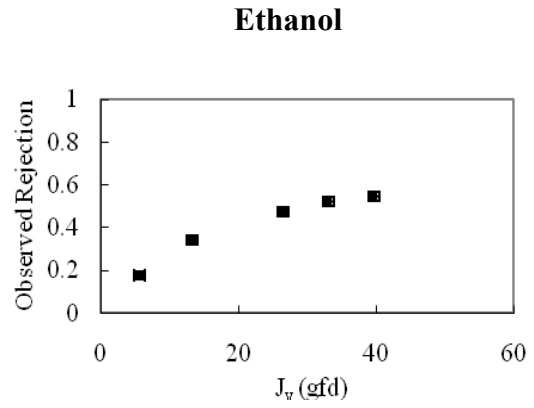
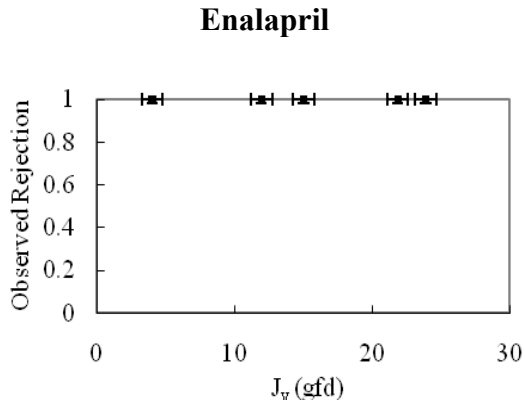


Diltiazem

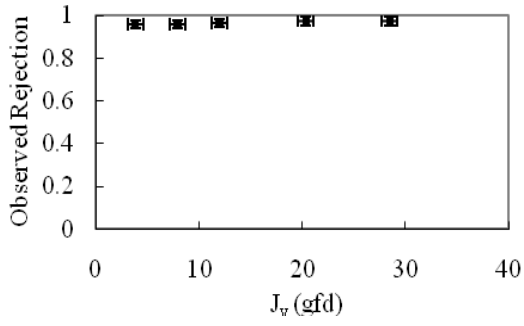


Diphenhydramine

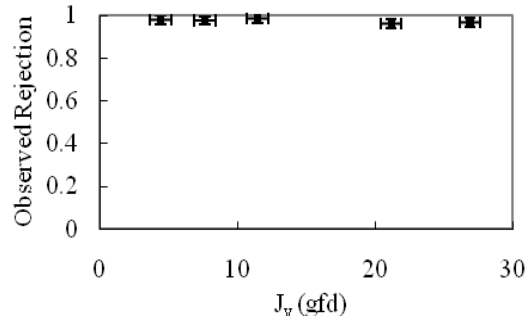




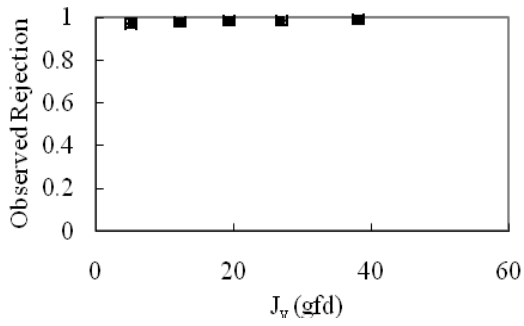
Furosemide



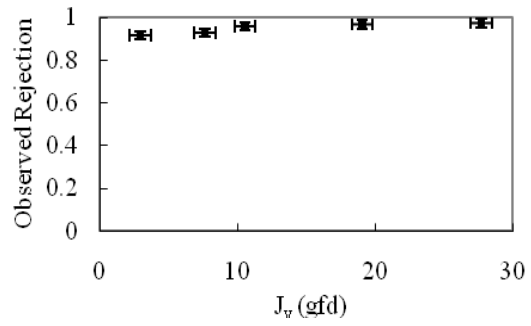
Gemfibrozil



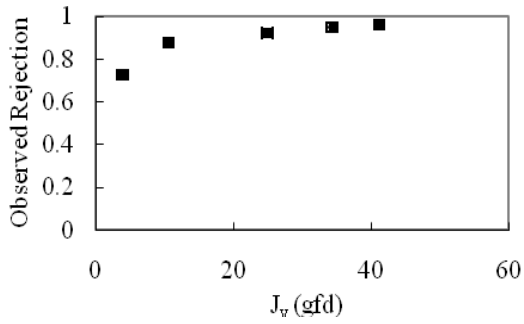
Glucose



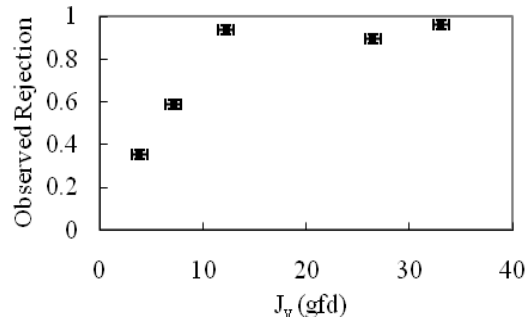
Glutamic Acid



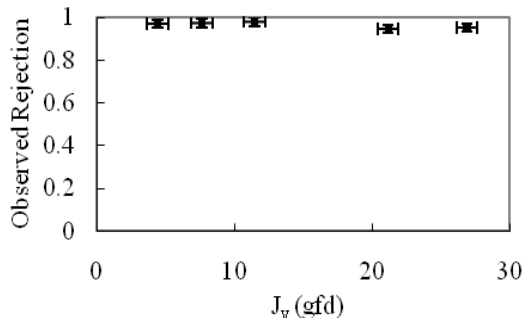
Glycerol



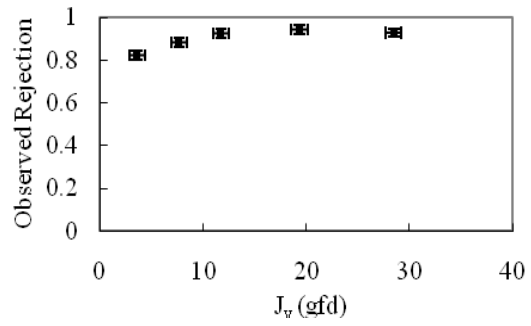
Guanidine



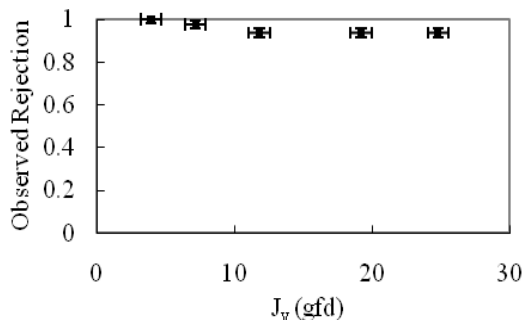
Ibuprofen



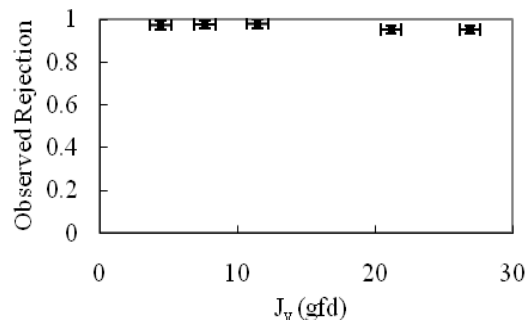
Isopropanol



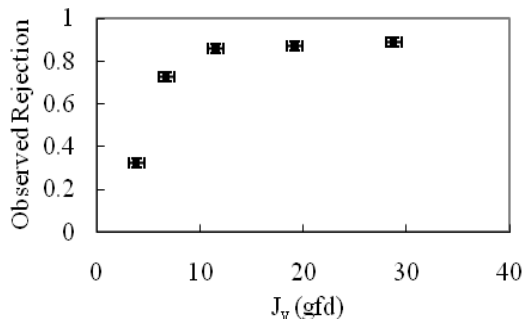
Ketoconazole



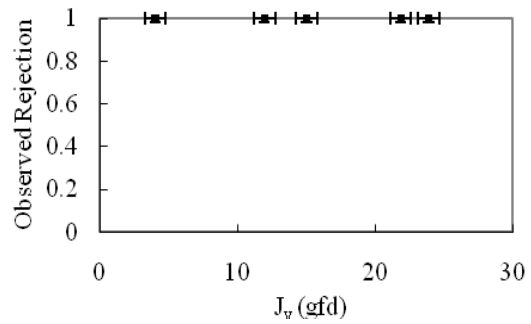
Ketoprofen



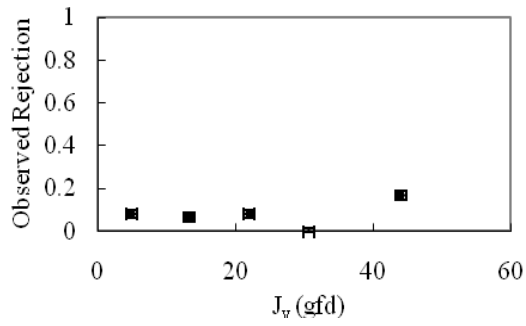
Lysine



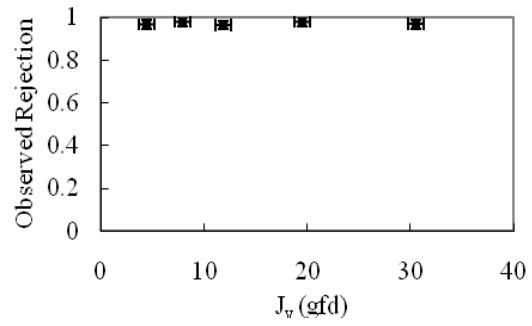
Maleic Acid



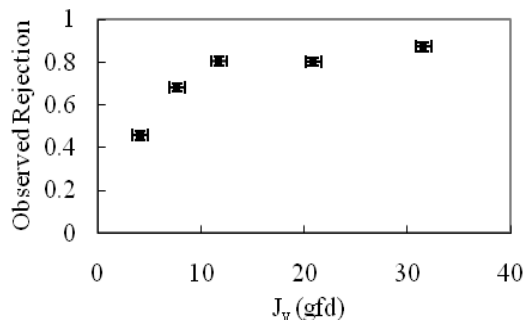
Methanol



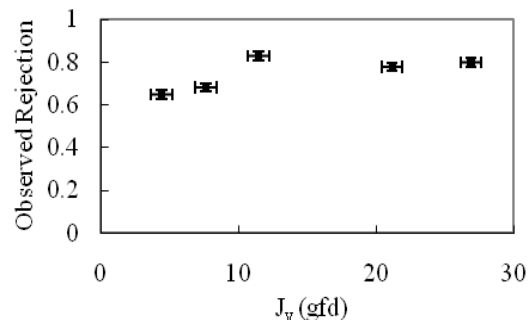
Methotrexate



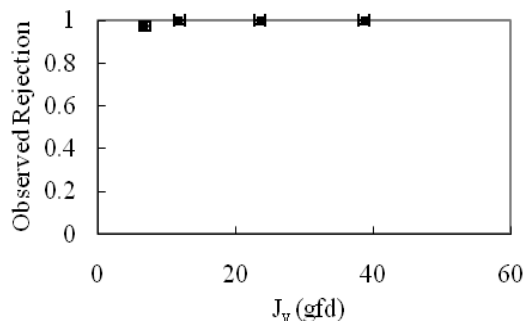
Methylamine



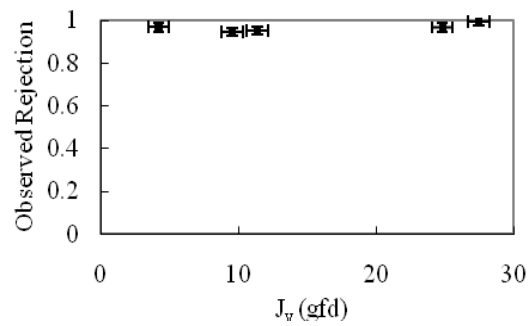
Methylparaben



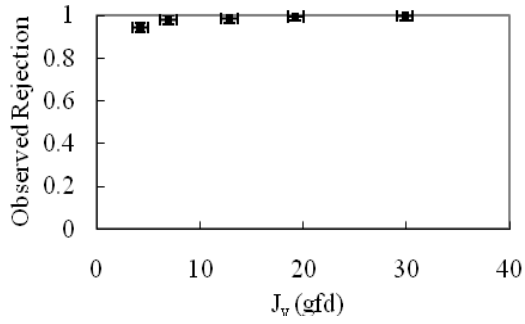
MTBE



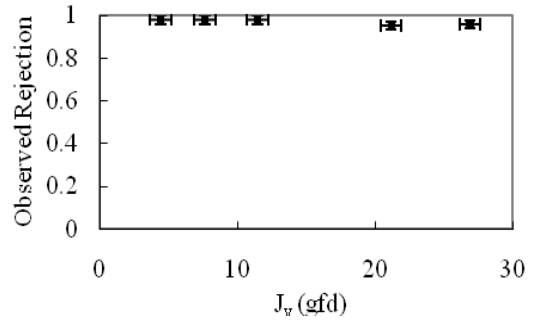
Metoprolol



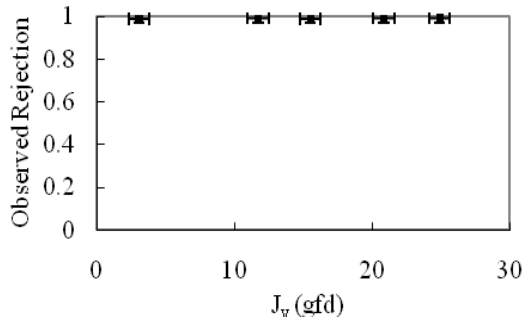
1-Naphthalenemethanol



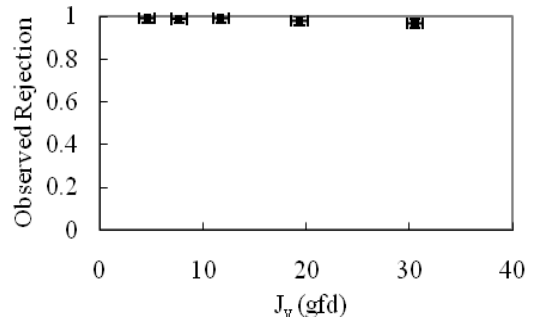
Naproxen



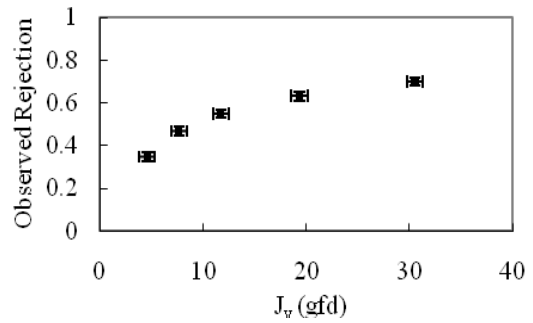
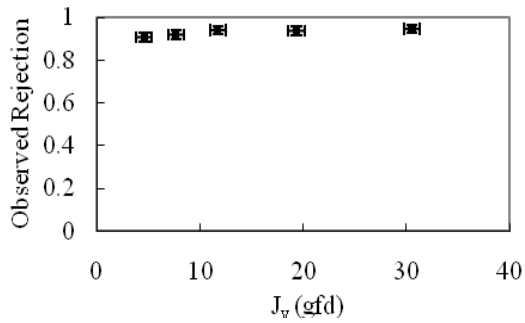
2-Naphthol



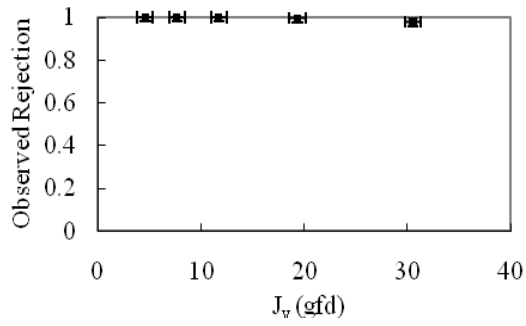
N-Nitrosodibutylamine



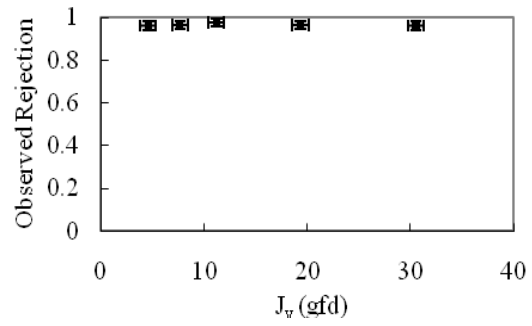
NDEA NDMA



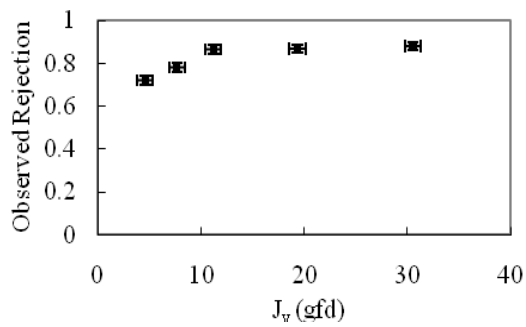
***N*-Nitrosodiphenylamine**



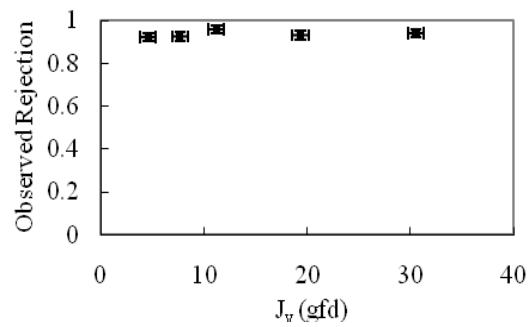
***N*-Nitrosodipropylamine**



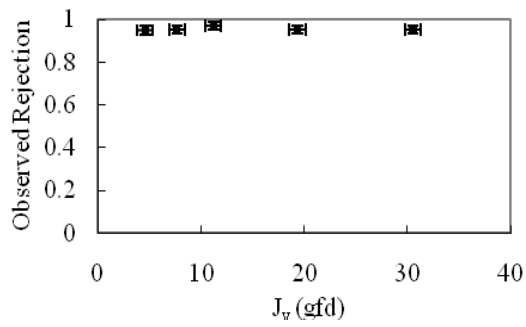
NMEA



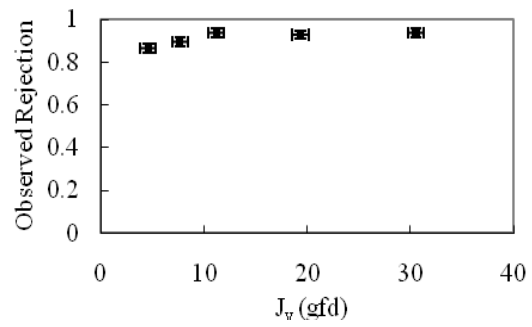
***N*-Nitrosomorpholine**



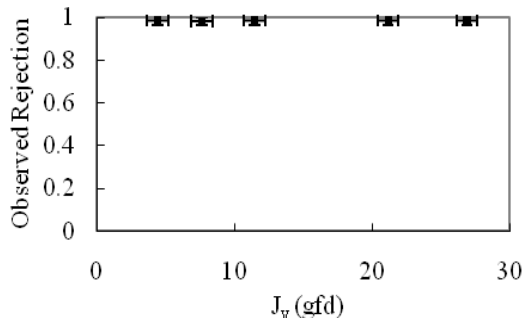
***N*-Nitrosopiperidine**



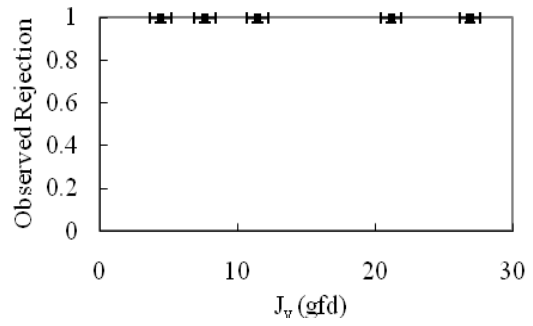
NPYR



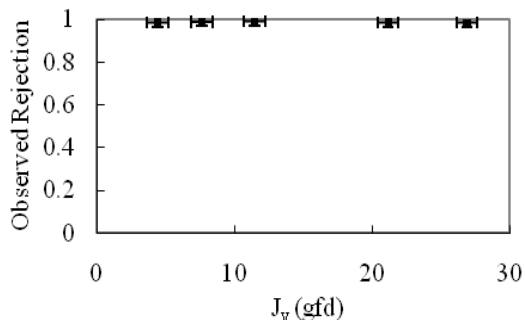
4-*n*-Nonylphenol



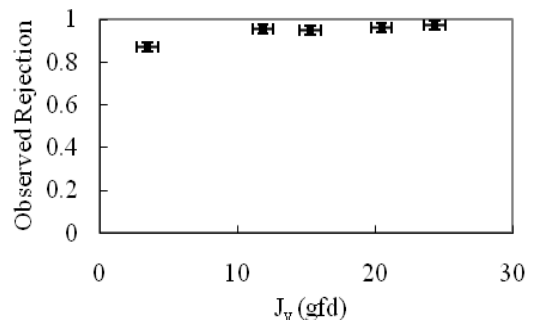
Norfluoxetine



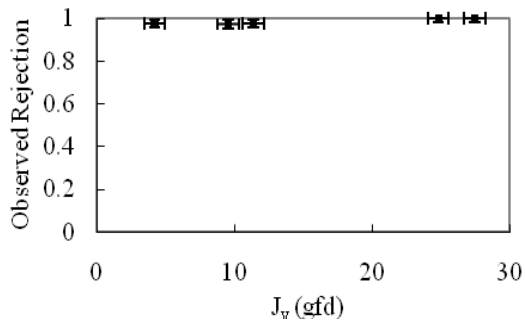
Oxybenzone



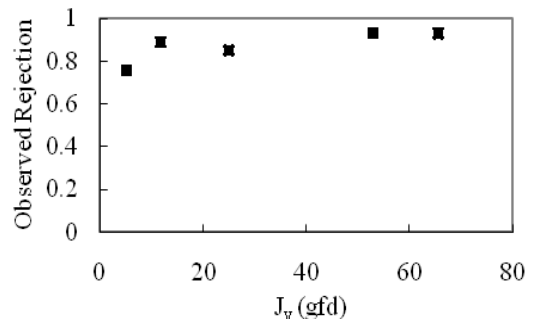
Pentoxifylline



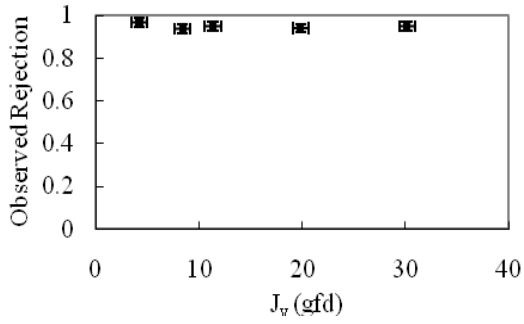
Phenacetine



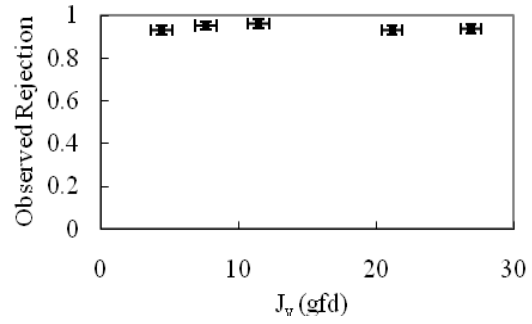
Phenylalanine



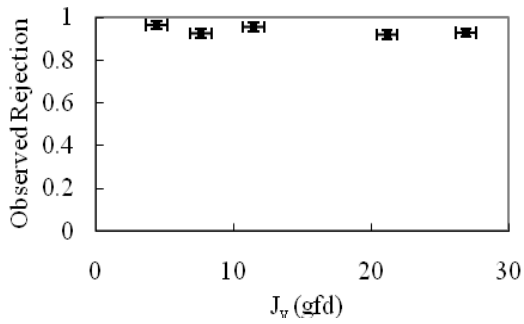
2-Phenylphenol



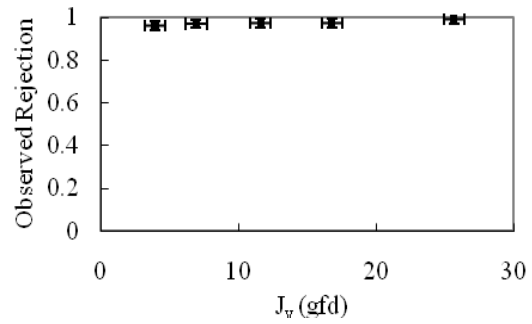
Primidone



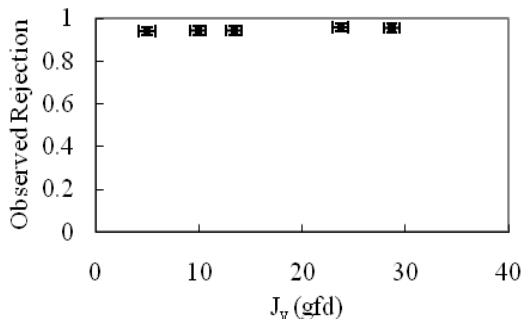
Propylparaben



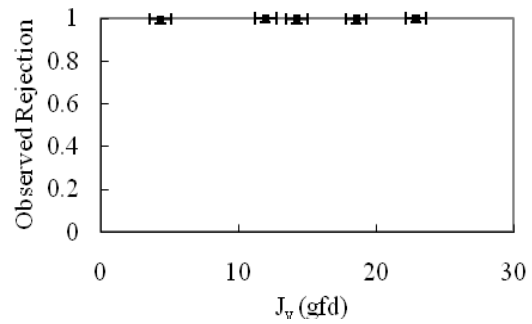
Propyphenazone



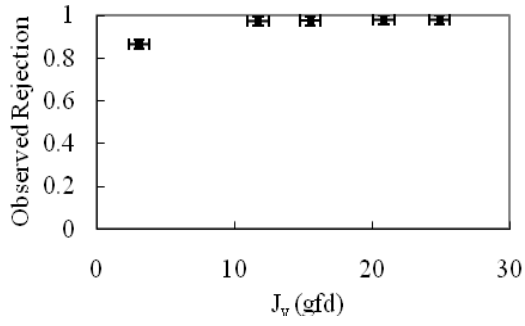
Pseudoephedrine



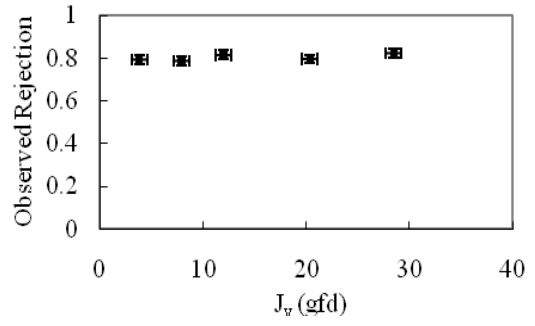
Ranitidine



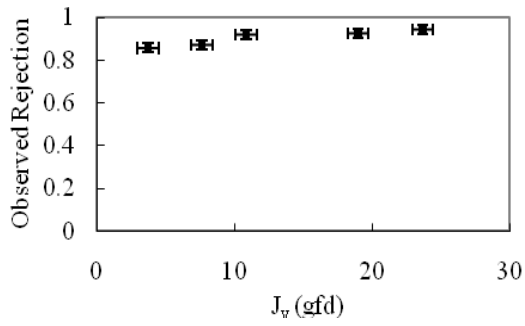
Resorcinol



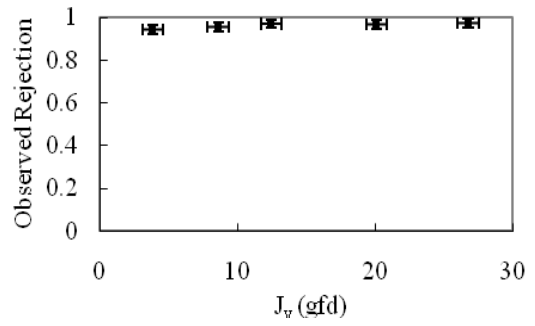
Salbutamol



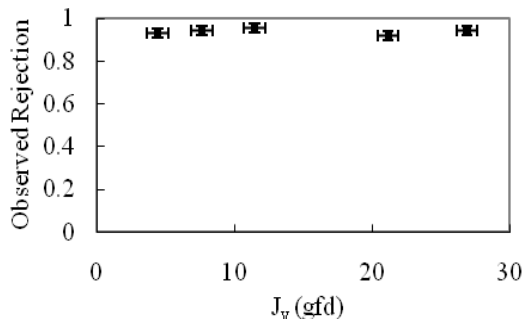
Salicylic Acid



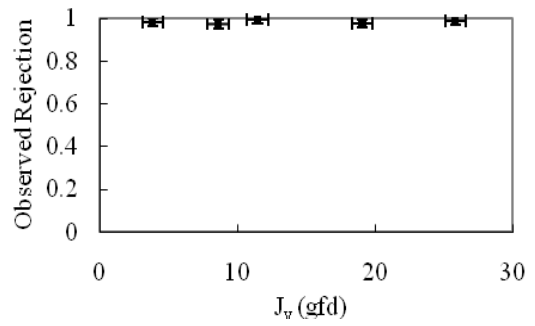
Serine



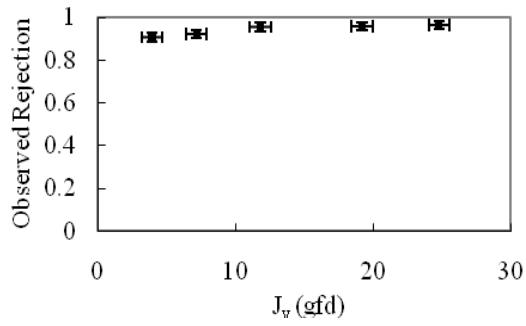
Sucralose



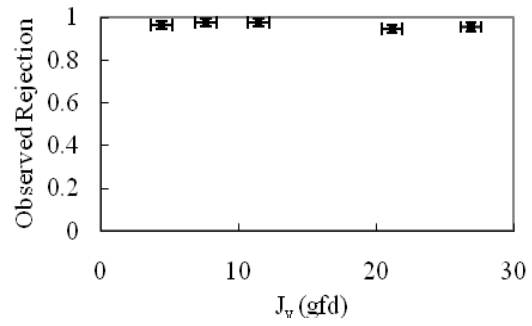
Sucrose



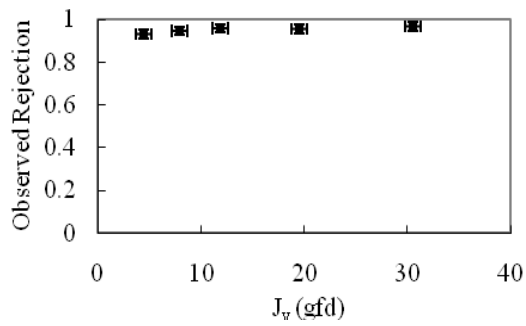
Sulfacetamide



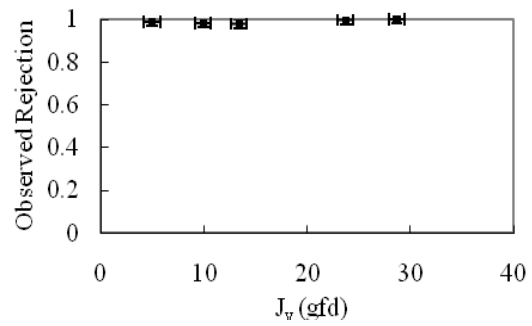
Sulfamethoxazole



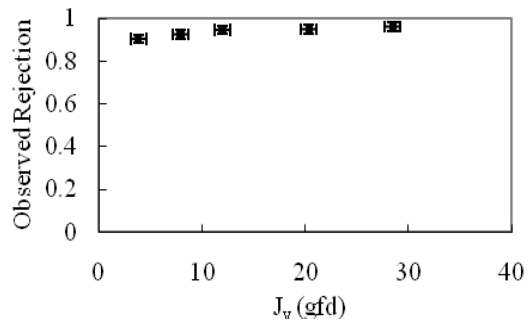
Sulfadimethoxine



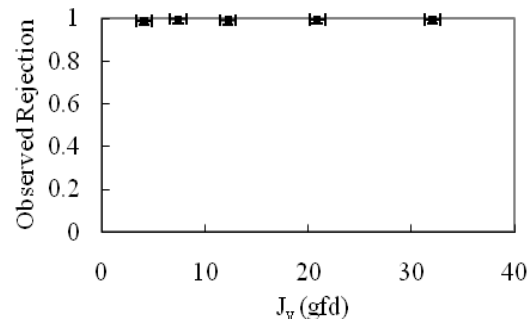
Sulfadoxine



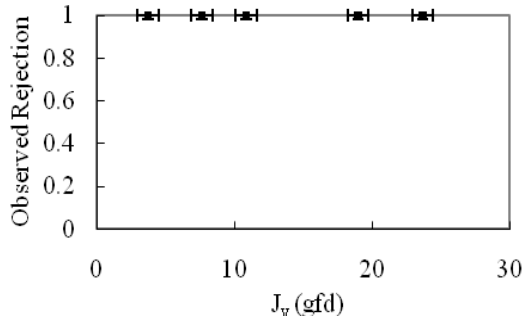
Sulfamerazine



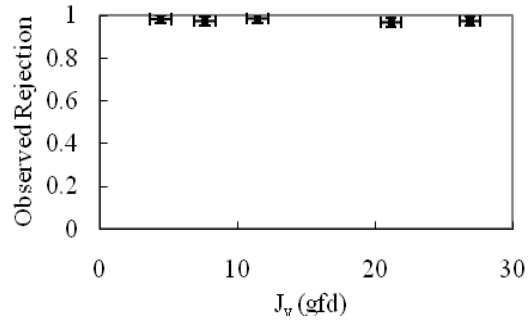
Sulfasalazine



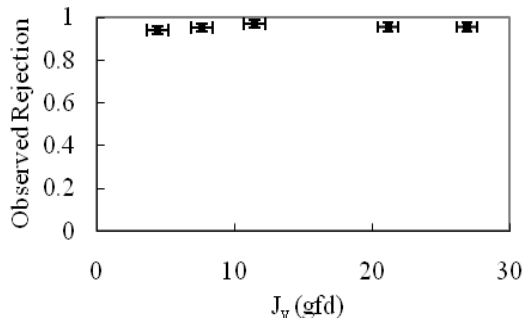
Tamoxifen



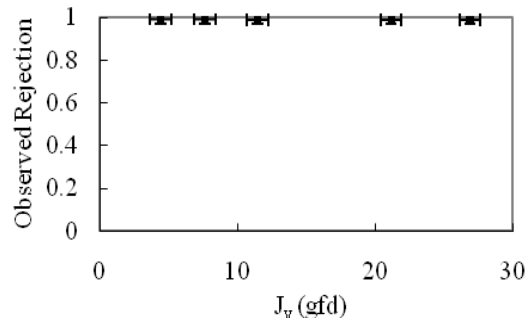
TCPP



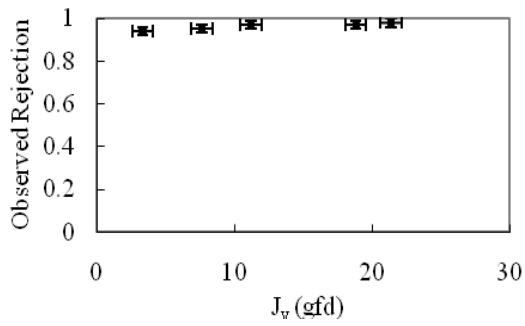
TCEP



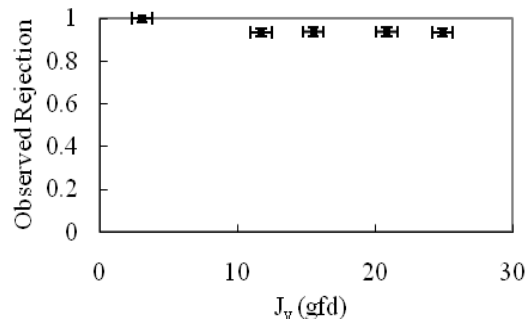
TDCPP



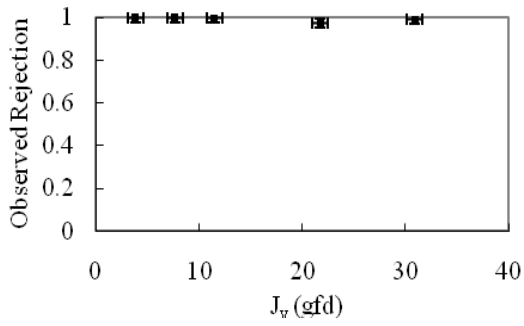
Thiabendazole



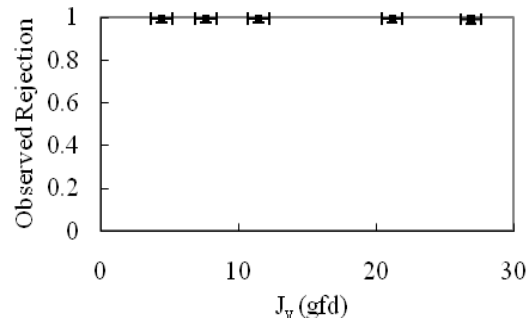
Trazodone



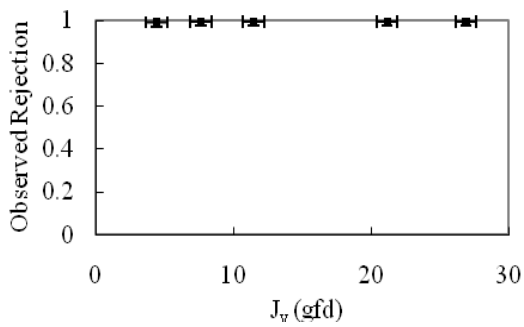
Trichloroacetic Acid



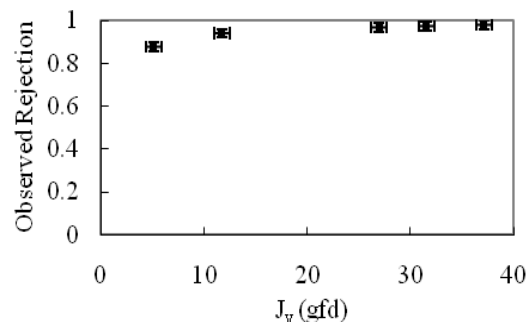
Triclorcarban



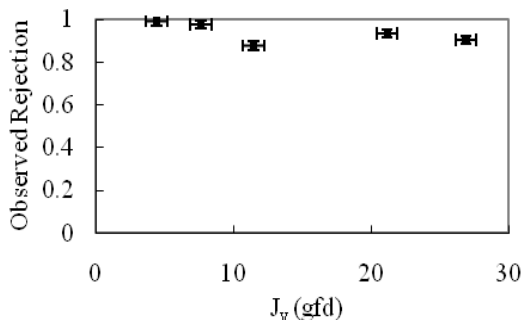
Triclosan



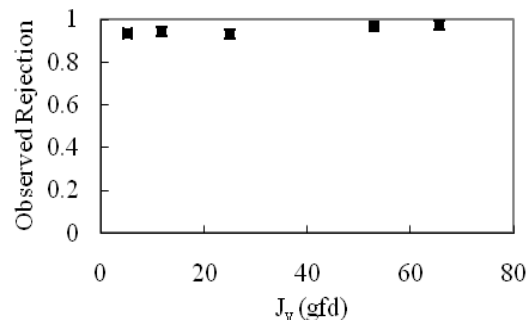
Triethylene Glycol



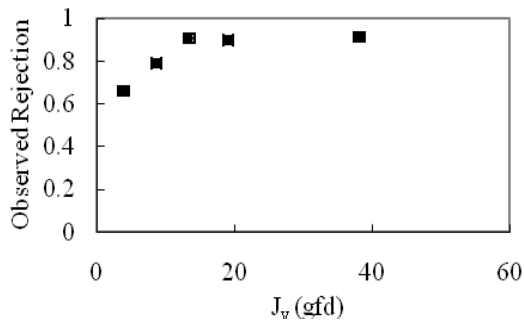
Trimethoprim



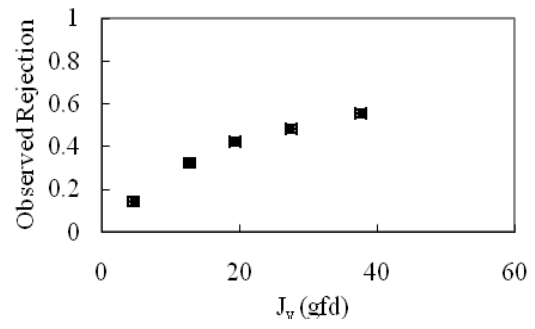
Tyrosine



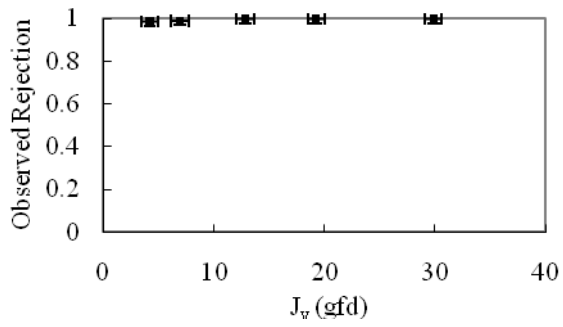
Uracil



Urea



Warfarin



Practical Solutions for Water Scarcity



1199 North Fairfax Street, Suite 410

Alexandria, VA 22314 USA

(703) 548-0880

Fax (703) 548-5085

E-mail: Foundation@WateReuse.org

www.WateReuse.org/Foundation